

PATHWAYS TO FUNCTIONALIZED SILOXANES FROM POLYHEDRAL
OLIGOMERIC SILSESQUIOXANES

By

Badru-Deen Barry

A DISSERTATION

Submitted to
Michigan State University
in partial fulfillment of the requirements
for the degree of

Chemistry—Doctor of Philosophy

2021

ABSTRACT

PATHWAYS TO FUNCTIONALIZED SILOXANES FROM POLYHEDRAL OLIGOMERIC SILSESQUIOXANES

By

Badru-Deen Barry

This dissertation is an account of my efforts toward developing strategies for the synthesis of novel functionalized polyhedral oligomeric silsesquioxanes (POSS). These organic/inorganic nanomaterials date back to 1946 and the pioneering work of Scott's synthesis of octamethylsilsesquioxane. POSS cages constitute a framework of silicon-oxygen polyhedron with reactive or inert organic coroneae. These hybrid nanostructures are versatile precursors that find applications in polymer chemistry, catalysis, engineering, medicine, and electronics. Their properties are partly dictated by the peripheral organic groups. They are generally benign and easily processible into composite materials with high thermal degradation temperatures, low dielectric constants and superior mechanical properties. These features of POSS compounds have prompted growing interest in their exploration, particularly their use as models for the synthesis of the next generation hybrid nanocomposites.

POSS molecules come in different cage sizes with condensed and incompletely condensed structures. The completely condensed analogues are denoted as T_n , where n = number of silicon atoms in the cage and $n \geq 6$. Whereas the cubic/condensed silsesquioxanes were the initially discovered compounds, most explorations today are focused on the incompletely condensed di-, tri-, and tetra-functional scaffolds because of the ability to derivatize them into more functional materials for a myriad of applications. Even with the partially condensed structures, current research focus on this family of

compounds has been dominated by the highly symmetric tetrafunctional octasilsesquioxane otherwise known as the double-decker oligomeric silsesquioxane. This functional POSS precursor has enormous potential for the synthesis of nanosized hybrid clusters with defined shape, structure, and physicochemical properties.

In this study, efforts have been made to disclose strategies for the synthesis of asymmetrically functionalized double-decker shaped silsesquioxanes that can serve as nano-linkers to two dissimilar polymer matrices. The conversion of dead-end silsesquioxanes into more functional cage precursors, and surface transformation of cubic and functionalized DDSQs into modifiable precursors for the synthesis of well-defined 3D networks well among my aims. POSS cages used in these investigations were obtained either from commercially available cages or cage-like precursors or were synthesized from monomeric trialkoxy- (or trichloro-)silanes by hydrolytic condensation. Products obtained from this study could open an avenue for the exploration of new structure/property relationships and provide a unique way by which cages can be used as linkers to form both linear POSS/polymer and 3D networks. This research promises to open a new research direction for the synthesis of novel materials that combine three unconventional materials into hybrid POSS/polymer composites. With the asymmetric POSS cage as the building block, unprecedented properties may emerge from the synergy of these building blocks.

To my parents, wife and two daughters

ACKNOWLEDGEMENTS

My inclination for a doctoral degree had been an inimitable aspiration in my life. Even though the path to this goal was hectic, the vision is materialized with the inspirations, guidance, and mentorship of an adorable class of people that merit commendations. The contributions of these eminent scientists, professors and scholars, research colleagues and friends made this struggle worth undertaking. To this end, I would like to acknowledge the following people for their diverse roles in helping me transform this dream into reality.

First and foremost, I am grateful to the Michigan State University for offering me the opportunity to pursue my graduate studies and to the Chemistry department particularly for the tutelage and research exposure that have positively impacted my life, both from an academic and multicultural viewpoint. I would also want to thank the Office of Naval Research (ONS) for funding part of this study under grant number N00014-16-2109.

My special thanks go to my advisor Dr Robert E. Maleczka Jr. and collaborator, Dr Andre Lee of the Department of Chemical Engineering and Material Science, MSU, for their outstanding mentorship, tenacity, and courage in aiding me through my graduate studies. Accomplishing this goal would have been impossible had it not been for their priceless support. They did not only accept me into their joint research group, but they also gave their support, priceless and insightful comments, criticisms, guidance, and motivations that has transformed me into a better researcher and chemist. They encouraged me to explore various areas of my research and shaped my faculty by

critiquing my work from experimental details to quality of work and results. Having them as my supervisors was truly intriguing and phenomenal and for which reason, I consider them as the finest elites I have ever been fortunate to work with. To these two professors, I am truly grateful.

Next, I would like to extend my sincere gratitude to my committee for their boundless contributions. Dr. James Ned Jackson, Dr. Kevin D. Walker, and Dr. Aaron L. Odom have been very supportive in my struggle. Their commitment to attend to my concerns and proffer suggestions whenever I am challenged with research problems is amazing. Having them on my committee was a thing to my advantage and is part of the reasons that irrefutably made my research objectives to be attained.

I was also blessed to have come across special friends and lab mates in the Maleczka and Lee research groups during my graduate studies. From the moments we shared our research pains to taking a break from lab activities by playing board games on weekends are memories that will ever linger in my mind. My appreciation therefore goes to both past and present lab mates including Susanne Miller, Chachurika Jayasundara, Jonathan E. Dannatt, David F Vogelsang, Fangyi Shen, Jose Montero, Emmanuel Maloba, Aditya Patil, Arzoo Chhabra, Thomas Oleskey, and Austin K. King. Together we created an ambiance of a healthy workplace that served as a panacea to soothing our research and academic struggles.

On the technical wing, I am heavily indebted to three prominent scholars in the Chemistry Department at MSU - Dr. Dan Holmes, Dr. Xie Li (both of the NMR facility) and Dr. Richard Staples (X-Ray Crystallographer). These gentlemen always had their offices open to me to answer to some of my questions based on NMR and X-ray crystallography.

Further, I am grateful to all the secretaries from the Chair's office to those in the graduate office for their invaluable and timely duties in keeping all graduate students abreast with news, events and needs of the graduate school. To Heidi, Tiphani, Anna, Mary and Brenda, I say thank you for your assistance since my entry into graduate school to date. You guys have been amazing.

Most importantly, my experience in the graduate school started with the inspiration of two distinguished country mates of mine - Dr Patrick K. Lukulay and Dr Thomas B. R. Yormah. The success of this work owes its genesis to these gentlemen whom for the most times in their lives are invigorated to promote education in their country. These people would be always remembered for providing me this opportunity to pursue graduate studies at the Michigan State University and for giving me all necessary support that made my career a reality. To these two influential people, I say kudos.

Lastly, I cannot end this section without recognizing the loving support and courage demonstrated by my wife and two kids. We came and we conquered together. I am therefore most pleased with my wife and two daughters for their motivation and fortitude during this struggle. Their roles have been truly supportive and irreplaceable. Thank you all for been with me in thick and thin.

TABLE OF CONTENTS

LIST OF TABLES.....	xii
LIST OF FIGURES.....	xiv
LIST OF SCHEMES.....	xxiv
CHAPTER 1.0	1
1.1 Introduction	1
1.2 Background.....	1
1.2.1 Silsesquioxanes.....	1
1.2.2 Classification and Nomenclature of Silsesquioxanes.....	1
1.2.2.1 Classification	1
1.2.2.2 Nomenclature	2
1.3 Polyhedral Oligomeric Silsesquioxanes (POSS)	4
1.3.1 Synthesis of Polyhedral Oligomeric Silsesquioxanes (POSS)	6
1.4 Incompletely Condensed Polyhedral Oligomeric Silsesquioxanes	7
1.5 Synthesis of Condensed Difunctional Double-Decker Shaped Silsesquioxanes..	10
1.6 Motivation and Research Goals	11
1.7 Dissertation Summary	13
REFERENCES.....	15
CHAPTER 2.0: Synthesis of Asymmetrically Functionalized Double-Decker Shaped Silsesquioxanes	23
2.1 Introduction	24
2.2 Results and Discussions	29
2.2.1 Solubility of DDSQ(OH) ₄ in Various Organic Solvents.....	31
2.2.2 Optimization of the Selective Borylation for the Generation of (p- MeOC ₆ H ₄ B)DDSQ(OH) ₂ 3	32
2.2.3 Substrate Scope for Asymmetrically Functionalized Double-Decker Shaped Silsesquioxanes.....	34
2.2.4 Structural Analysis of Asymmetric DDSQs (6) by Si-NMR.....	36
2.3 Conclusions	50
2.4 Experimental Details	51
2.4.1. General Information	51
2.4.1.1 General Experimental Procedure for the Synthesis of DDSQ Boronate Esters	53
2.4.1.2 Deborylation of DDSQ Bis-boronate Ester with Pinacol.....	54
2.4.1.3 General Procedure for Solubility Test for DDSQ(OH) ₄ in Different Organic Solvents.....	54
2.4.1.4 General Experimental Procedures for the Multi-step Synthesis of Asymmetrically Functionalized DDSQs	55
2.4.1.4.1 Mono-borylation of DDSQ(OH) ₄ with p-MeOC ₆ H ₄ B(OH) ₂ (Step 1)....	55

2.4.1.4.2 General Procedure for the First Silylation of Mono-borylated DDSQ(OH) ₂ (3) - (Step 2)	56
2.4.1.4.3 General Procedure for the Deborylation of a Mixture of (p-MeOC ₆ H ₄ B)- DDSQSiR ¹ R ² and (p-MeOC ₆ H ₄ B) ₂ DDSQ (Step 3)	57
2.4.1.4.4 General Procedure for the Second Silylation of Monosilylated DDSQ (5)	58
2.4.2 Synthetic Scope for Asymmetrically Functionalized Double-Decker Shaped Silsesquioxanes.....	59
APPENDIX	60
REFERENCES.....	125

CHAPTER 3.0: Synthesis of Incompletely Condensed Asymmetrically Functionalized Double-Decker Shaped Silsesquioxane Disilanols ‘Bird Nest-Shaped Silsesquioxanes’

3.1 INTRODUCTION.....	129
3.2 Modifications of Incompletely Condensed POSS Cages.....	131
3.2.1 Tetrafunctional Polyhedral Oligomeric Silsesquioxanes and their Derivatives	133
3.2.2 Asymmetrically Functionalized DDSQs	135
3.3 Results and Discussions	140
3.3.1 Optimization of (p-MeOC ₆ H ₄ B) ₂ DDSQ(OH) ₂ (3)	140
3.3.2 Substrate Scope	141
3.3.3 Transformation of Monosilylated DDSQ diol into Condensed Asymmetric DDSQs (7)	143
3.3.4 Spectral Data for Asymmetric R ¹ R ² DDSQ(OH) ₂	144
3.3.5 Structural Characterization by ²⁹ Si NMR Spectroscopy.....	149
3.3.6 NMR and Mass Spectral Data for Condensed Asymmetric D ₂ T ₈ Silsesquioxanes.....	159
3.3.7 Structural Characterization of Completely Condensed Asymmetric D ₂ T ₈ Silsesquioxanes by ²⁹ Si NMR Spectroscopy	163
3.4 Conclusion	170
3.5 Experimental Details	170
3.5.1 Materials and Methods	170
3.5.2 General Experimental Procedure for the Synthesis of DDSQ Bis-boronate Ester (2).....	172
3.5.3 Partial Deborylation of DDSQ Bis-boronate Ester with Pinacol	173
3.5.4 General Experimental Procedure for the Multi-step Synthesis of monosilylated DDSQ diol.....	175
3.6 Synthetic Modifications of Monosilylated DDSQ diols (5) into Fully Condensed Asymmetric DDSQs of the D ₂ T ₈ type (7)	178
APPENDIX	179
REFERENCES.....	224

Chapter 4.0: Base-Promoted Hydrolysis of Dodecaphenyl Silsesquioxane into Partially Condensed Octaphenyl Silsesquioxane.....

4.1 Abstract.....	230
-------------------	-----

4.2 Introduction	231
4.3 Research Hypothesis	233
4.4 Proposed Reaction Mechanism for the Formation of Double-decker Octaphenyl silsesquioxanetetraol (5)	234
4.4.1 Hydrolysis of $\text{Ph}_{12}\text{T}_{12}$ (1) into $[(\text{PhSiO})_8(\text{O})_2(\text{OTMS})_4]$ (3)	235
4.4.2 Time-course Study for the Hydrolysis of 1 into 3	237
4.4.3 Synthesis of $[(\text{PhSiO})_8(\text{O})_2(\text{OH})_4]$ (5) from $\text{Ph}_{12}\text{T}_{12}$ (1)	240
4.4.4 Condition Screening Results for the Synthesis of $(\text{PhSiO})_8(\text{O})_2(\text{OH})_4$ 5 from $\text{Ph}_{12}\text{T}_{12}$ (1)	241
4.5 Single Crystal X-ray Structures	242
4.6 Experimental Section	246
4.6.1 Materials and Methods	246
4.6.1.1 Synthesis of 5,11,14,17-tetrakis(trimethylsilyl)octaphenyltetracyclo[7.3.3. 3 ^{3;7}]octasilsesquioxane (3) from Dodecaphenyl T_{12} [$\text{Ph}_{12}\text{T}_{12}$] (1)	248
4.6.1.2. Time-course Study for the Hydrolysis of 1 followed by TMS Capping to Afford 3	250
4.6.1.3 Synthesis of 5,11,14,17-Tetra(hydro)octaphenyltetracyclo[7.3.3.3 ^{3;7}] octasilsesquioxane $[(\text{PhSiO})_8(\text{O})_2(\text{OH})_4]$ 5 from Dodecaphenyl Silsesquioxane $[\text{Ph}_{12}\text{T}_{12}]$ 1	251
4.6.1.4 Screening Conditions for the Synthesis of $(\text{PhSiO})_8(\text{O})_2(\text{OH})_4$ 3 from 1	252
APPENDIX	253
REFERENCES	294
 Chapter 5.0: De novo construction of Double-Decker Shaped Silsesquioxanes with Modifiable Surface Functionalities	298
5.1 Introduction	298
5.1.1 Styrenyl functionalized Polyhedral Oligomeric Silsesquioxanes	300
5.1.2 Corner-capping $\text{DDSQ}(\text{OH})_4$ with styrenyl and styryl groups	304
5.1.3 Styryl functionalized Polyhedral Oligomeric Silsesquioxanes	306
5.1.4 p-Bromophenyl functionalized Polyhedral Oligomeric Silsesquioxanes	308
5.2 Experimental Section	313
5.2.1 Materials and Methods	313
5.2.1.1 Synthesis of dichloro(methyl)(4-vinylphenyl)silane (2) from 4- bromostyrene (1)	315
5.2.1.2 Synthesis of $[(\text{styryl})(\text{Me})_2\text{DDSQ}]$ from $\text{DDSQ}(\text{OH})_4$ (3) and styryl $(\text{Me})\text{SiCl}_2$ (2)	316
5.2.2 Synthesis of T_n styryl Silsesquioxanes	317
5.2.3 Synthesis of 5,11,14,17-tetrakis((trimethylsilyl)oxy)-1,3,5,7,9,11,14,17-octakis (4-vinylphenyl)-2,4,6,8,10,12,13,15,16,18-decaoxa-1,3,5,7,9,11,14,17-octasilatricyc- lo[7.3.3.3 ^{3;7}]octadecane (9)	319
5.2.4 Synthesis of 2,4,6,8-tetrakis(4-bromophenyl)-2,4,6,8-tetrakis((trimethylsilyl)- oxy)-1,3,5,7,2,4,6,8-tetraoxatetrasiloxane	321
5.2.5 Borylation of $[4\text{-BrC}_6\text{H}_4\text{Si}(\text{OTMS})]_4$	322
5.2.6 Synthesis of tetra-n-butylammonium octa(4-bromophenyl)octasilsesqui- oxane fluoride	323

5.2.7 Synthesis of 1,3,5,7,9,11,14,17-octakis(4-bromophenyl)-5,11,14,17-tetrakis((tr-imethylsilyl)oxy)-2,4,6,8,10,12,13,15,16,18-decaoxa-1,3,5,7,9,11,14,17-octasilatricy- clo[7.3.3.3 ^{3,7}]octadecane	325
APPENDIX	327
REFERENCES.....	348
CHAPTER 6: Conclusions and Future Direction	355
6.1 Conclusions	355
6.2 Future Directions.....	356

LIST OF TABLES

Table 2-1: Full Protection of DDSQ(OH) ₄ 1 with p-substituted Phenylboronic Acid	29
Table 2-2: Crystal Structures of Bis-boronated DDSQ Esters 2 (Displacement ellipsoid contour probability drawn at 50%)	30
Table 2-3: Solubility Tests for DDSQ(OH) ₄ (1) in Organic Solvents.....	32
Table 2-4: Optimization of Monoboronate Ester Formation	33
Table 2-5: Scope for Asymmetrically Functionalized DDSQs	34
Table 2-6: Crystal Data and Structure Refinement for Compounds 2A - 2C	105
Table 2-7: Bond Lengths in Å for CCDC 1843217	106
Table 2-8: Bond Angles in ° for CCDC 1843217	108
Table 2-9: Hydrogen Fractional Atomic Coordinates (×10 ⁴) and Equivalent Isotropic Displacement Parameters (Å ² ×10 ³) for CCDC 1843217. U _{eq} is defined as 1/3 of the trace of the orthogonalised U _{ij}	110
Table 2-10: Bond Lengths in Å for CDCC 1823844	112
Table 2-11: Bond Angles in ° for CDCC 1823844.....	114
Table 2-12: Hydrogen Fractional Atomic Coordinates (×10 ⁴) and Equivalent Isotropic Displacement Parameters (Å ² ×10 ³) for CCDC 1823844. U _{eq} is defined as 1/3 of the trace of the orthogonalised U _{ij}	116
Table 2-13: Bond Lengths in Å for CCDC 1850462	118
Table 2-14: Bond Angles in ° for CCDC 1850462.....	120
Table 2-15: Hydrogen Fractional Atomic Coordinates (×10 ⁴) and Equivalent Isotropic Displacement Parameters (Å ² ×10 ³) for CCDC 1850462. U _{eq} is defined as 1/3 of the trace of the orthogonalised U _{ij}	123
Table 3-1: Optimization for the partial deborylation of (p-MeOC ₆ H ₄ B) ₂ DDSQ (2) for the synthesis of monoborylated DDSQ diol (3)	140
Table 3-2: Substrate scope for the synthesis of asymmetric monosilylated DDSQ(OH) ₂ (5).....	142
Table 3-3: Post Functionalization of asymmetric monosilylated DDSQ(OH) ₂ (5) into Completely Condensed Asymmetric DDSQs of the D ₂ T ₈ Type	143

Table 3-4: Crystal Data and Structure Refinement for Asymmetric DDSQ Diols 5a , 5b , 5e and 5f	206
Table 3-5: Crystal Data and Structure Refinement for Asymmetric DDSQ 7a	223
Table 4-1: LCMS-G2-XS QToF time course analysis of data for selected intermediates obtained from the hydrolysis of 1 followed by silylation with TMSCl.....	237
Table 4-2: Relative intensity of Species in Table 4.1 expressed as a percentage	238
Table 4-3: Synthesis of [(PhSiO) ₈ (O) ₂ (OTMS) ₄] (3) from Ph ₁₂ T ₁₂ (1).....	239
Table 4-4: Hydrolysis of 12 with Acetic Acid ^a	241
Table 4-5: Crystal and Experimental Data for 5,11,14,17-tetrakis(trimethylsilyl)-octaphenyltetracyclo[7.3.3.-3 ^{3,7}]octasilsesquioxane (3) (CCDC 299794 ^a).....	285
Table 4-6: Crystal and Experimental Data for 5,11,14,17-tetra(hydro)octaphenyltetracyclo[7.3.3.-3 ^{3,7}]octasilsesquioxane (C ₄₈ H ₄₄ O ₁₄ Si ₈) (5)	286
Table 4-7: Bond Lengths in Å for 5,11,14,17-tetra(hydro)octaphenyltetracyclo[7.3.3.-3 ^{3,7}]octasilsesquioxane (5).....	287
Table 4-8: Bond Angles in ° for 5,11,14,17-tetra(hydro)octaphenyltetracyclo[7.3.3.-3 ^{3,7}]octasilsesquioxane (5).....	289
Table 4-9: Hydrogen Fractional Atomic Coordinates (×10 ⁴) and Equivalent Isotropic Displacement Parameters (Å ² ×10 ³) for 5,11,14,17-tetra(hydro)octaphenyltetracyclo[7.3.3.-3 ^{3,7}]octasilsesquioxane (5). U _{eq} is defined as 1/3 of the trace of the orthogonalised U _{ij}	292
Table 4-10: Hydrogen Bond information for 5,11,14,17-tetra(hydro)octaphenyltetracyclo[7.3.3.-3 ^{3,7}]octasilsesquioxane (5)	293
Table 5-1: Crystal and Experimental Data for 9,19-dimethyl-1,3,5,7,11,13,15,17-octaphenyl-9,19-bis(4-vinylphenyl)-2,4,6,8,10,12,14,16,18,20,21,22,23,24-tetradeca-1,3,5,7,9,11,13,15,17,19-decasilapentacyclo[11.7.1.13,11.15,17.17,15]tetracosane (4)	344
Table 5-2: Crystal and Experimental Data for 2,4,6,8-tetrakis(4-bromophenyl)-2,4,6,8-tetrakis((trimethylsilyl)oxy)-1,3,5,7,2,4,6,8-tetraoxatetrasilocane ⁶⁵⁻⁶⁷	346

LIST OF FIGURES

Figure 1-1: Different architectures of $(\text{RSiO}_{3/2})_n$	2
Figure 1-2: Systematic/trivial nomenclature of Silsesquioxanes.....	3
Figure 1-3: Cubic octameric silsesquioxane	5
Figure 1-4: Methacrylate heptaphenylPOSS	5
Figure 1-5: Incompletely condensed POSS frameworks ²⁵⁻²⁷	7
Figure 1-6: Octaphenyl tetrasilanolPOSS $[\text{DDSQ}(\text{OH})_4]$	9
Figure 2-1: Double-decker oligomeric silsesquioxane tetraol (1) and (b) R_7 -trisilanol POSS	25
Figure 2-2: Designed Graphical Pathway to Asymmetrically Functionalized DDSQs...	31
Figure 2-3: Stacked ^{29}Si NMR of AB 6a , AA 7a and BB 8a	37
Figure 2-4: Stacked ^{29}Si NMR of AB 6b , AA 7b and BB 8b	39
Figure 2-5: Stacked ^{29}Si NMR of AB 6c , Symmetric AA 7c and BB 8c	41
Figure 2-6: Stacked ^{29}Si NMR of AB 6d , AA 7d and BB 8d	42
Figure 2-7: Stacked ^{29}Si NMR of AB 6f , AA 7f and BB 8f	44
Figure 2-8: Stacked ^{29}Si NMR of AB 6g , AA 7g and BB 8g	45
Figure 2-9: Stacked ^{29}Si NMR of AB 6h , AA 7h and BB 8h	47
Figure 2-10: Stacked ^{29}Si NMR of AB 6i and AA 7i	49
Figure 2-11: ^1H NMR (500 MHz, CDCl_3) of $(p\text{-MeOC}_6\text{H}_4\text{B})_2\text{DDSQ}$ 2a	71
Figure 2-12: ^{11}B NMR (160 MHz, CDCl_3) of $(p\text{-MeOC}_6\text{H}_4\text{B})_2\text{DDSQ}$ 2a	72
Figure 2-13: ^{13}C NMR (126 MHz, CDCl_3) of $(p\text{-MeOC}_6\text{H}_4\text{B})_2\text{DDSQ}$ 2a	72
Figure 2-14: ^{29}Si NMR (99 MHz, CDCl_3) of $(p\text{-MeOC}_6\text{H}_4\text{B})_2\text{DDSQ}$ 2a	73
Figure 2-15: ^1H NMR (500 MHz, CDCl_3) of $(\text{C}_6\text{H}_4\text{B})_2\text{DDSQ}$ 2b	74
Figure 2-16: ^{11}B NMR (160 MHz, CDCl_3) of $(\text{C}_6\text{H}_4\text{B})_2\text{DDSQ}$ 2b	75

Figure 2-17: ^{13}C NMR (126 MHz, CDCl_3) of $(\text{C}_6\text{H}_4\text{B})_2\text{DDSQ } 2\text{b}$	75
Figure 2-18: ^{29}Si NMR (99 MHz, CDCl_3) of $(\text{C}_6\text{H}_4\text{B})_2\text{DDSQ } 2\text{b}$	76
Figure 2-19: ^1H NMR (500 MHz, CDCl_3) of $(\text{p-MeC}_6\text{H}_4\text{B})_2\text{DDSQ } 2\text{c}$	77
Figure 2-20: ^{11}B NMR (160 MHz, CDCl_3) of $(\text{p-MeC}_6\text{H}_4\text{B})_2\text{DDSQ } 2\text{c}$	78
Figure 2-21: ^{13}C NMR (126 MHz, CDCl_3) of $(\text{pMeC}_6\text{H}_4\text{B})_2\text{DDSQ } 2\text{c}$	78
Figure 2-22: ^{29}Si NMR (99 MHz, CDCl_3) of $(\text{C}_6\text{H}_4\text{B})_2\text{DDSQ } 2\text{c}$	79
Figure 2-23: ^1H NMR (500 MHz, CDCl_3) of AB 6a	80
Figure 2-24: ^{13}C NMR (126 MHz, CDCl_3) of AB 6a	81
Figure 2-25: ^{29}Si NMR (99 MHz, CDCl_3) of AB 6a	81
Figure 2-26: ^1H NMR (500 MHz, CDCl_3) of AB 6b	82
Figure 2-27: ^{13}C NMR (126 MHz, CDCl_3) of AB 6b	83
Figure 2-28: ^{29}Si NMR (99 MHz, CDCl_3) of AB 6b	83
Figure 2-29: ^1H NMR (500 MHz, CDCl_3) of AB 6c	84
Figure 2-30: ^{13}C NMR (126 MHz, CDCl_3) of AB 6c	85
Figure 2-31: ^{29}Si NMR (99 MHz, CDCl_3) of AB 6c	85
Figure 2-32: ^1H NMR (500 MHz, CDCl_3) of AB 6d	86
Figure 2-33: ^{13}C NMR (126 MHz, CDCl_3) of AB 6d	87
Figure 2-34: ^{29}Si NMR (99 MHz, CDCl_3) of AB 6d	87
Figure 2-35: ^1H NMR (500 MHz, CDCl_3) of AB 6f	88
Figure 2-36: ^{13}C NMR (126 MHz, CDCl_3) of AB 6e	89
Figure 2-37: ^{29}Si NMR (99 MHz, CDCl_3) of AB 6f	89
Figure 2-38: ^1H NMR (500 MHz, CDCl_3) of AB 6g	90
Figure 2-39: ^{13}C NMR (126 MHz, CDCl_3) of AB 6g	91
Figure 2-40: ^{29}Si NMR (99 MHz, CDCl_3) of AB 6g	91
Figure 2-41: ^1H NMR (500 MHz, CDCl_3) of AB 6h	92

Figure 2-42: ^{13}C NMR (126 MHz, CDCl_3) of AB 6h	93
Figure 2-43: ^{29}Si NMR (99 MHz, CDCl_3) of AB 6h	93
Figure 2-44: ^1H NMR (500 MHz, CDCl_3) of AB 6i	94
Figure 2-45: ^{13}C NMR (126 MHz, CDCl_3) of AB 6i	95
Figure 2-46: ^{29}Si NMR (99 MHz, CDCl_3) of AB 6i	95
Figure 2-47: Mass Spec of AB 6a	96
Figure 2-48: Mass Spec of AB 6b	97
Figure 2-49: Mass Spec of AB 6c	98
Figure 2-50: Mass Spec of AB 6d	99
Figure 2-51: Mass Spec of AB 6f	100
Figure 2-52: Mass Spec of AB 6g	101
Figure 2-53: Mass Spec of AB 6h	102
Figure 2-54: Mass Spec of AB 6i	103
Figure 3-1: Representative Incompletely Condensed Silsesquioxanes.....	129
Figure 3-2: Tetrafunctional Polyhedral Oligomeric Silsesquioxanes	134
Figure 3-3: Monborylated $\text{DDSQ}(\text{OH})_2$	138
Figure 3-4: Stacked ^{29}Si NMR of AB diol 5a and AA 6a	150
Figure 3-5: Stacked ^{29}Si NMR of AB diol 5b and AA 6b	151
Figure 3-6: Stacked ^{29}Si NMR of AB diol 5c and AA 6c	152
Figure 3-7: Stacked ^{29}Si NMR of AB diol 5d and AA 6d	153
Figure 3-8: Stacked ^{29}Si NMR of AB diol 5e and AA 6e	154
Figure 3-9: Stacked ^{29}Si NMR of AB diol 5f and AA 6f	155
Figure 3-10: Stacked ^{29}Si NMR of AB diol 5g and AA 6g	156
Figure 3-11: ^{29}Si NMR of AB diol 5h	158
Figure 3-12: ^{29}Si NMR of 7a stacked with its symmetric AA and BB	163

Figure 3-13: Stacked ^{29}Si NMR of AA, AB and BB (7b)	165
Figure 3-14: Stacked ^{29}Si NMR of AA and BB (7c)	167
Figure 3-15: Stacked ^{29}Si NMR of AA, AB(7d) and BB	169
Figure 3-16: ^1H NMR of 2a (CDCl_3 + 1%TMS, 500 MHz).....	180
Figure 3-17: ^{13}C NMR of 2a (CDCl_3 + 1%TMS, 126 MHz)	181
Figure 3-18: ^{11}B NMR of 2a (CDCl_3 + 1%TMS, 160 MHz)	181
Figure 3-19: ^{29}Si NMR of 2a (CDCl_3 + 1%TMS, 99 MHz).....	182
Figure 3-20: ^1H NMR of 5a (CDCl_3 + 1%TMS, 500 MHz).....	183
Figure 3-21: ^{13}C NMR of 5a (CDCl_3 + 1%TMS, 126 MHz)	184
Figure 3-22: ^{29}Si NMR of 5a (CDCl_3 + 1%TMS, 99 MHz).....	184
Figure 3-23: Mass spec of 5a	185
Figure 3-24: ^1H NMR of 5b (CDCl_3 + 1%TMS, 500 MHz)	186
Figure 3-25: ^{13}C NMR of 5b (CDCl_3 + 1%TMS, 126 MHz)	187
Figure 3-26: ^{29}Si NMR of 5b (CDCl_3 + 1%TMS, 99 MHz)	187
Figure 3-27: Mass spec of 5b	188
Figure 3-28: ^1H NMR of 5c (CDCl_3 + 1%TMS, 500 MHz).....	189
Figure 3-29: ^{13}C NMR of 5c (CDCl_3 + 1%TMS, 126 MHz)	190
Figure 3-30: ^{29}Si NMR of 5c (CDCl_3 + 1%TMS, 99 MHz).....	190
Figure 3-31: Mass spec of 5c	191
Figure 3-32: ^1H NMR of 5d (CDCl_3 + 1%TMS, 500 MHz)	192
Figure 3-33: ^{13}C NMR of 5d (CDCl_3 + 1%TMS, 126 MHz)	193
Figure 3-34: ^{29}Si NMR of 5d (CDCl_3 + 1%TMS, 99 MHz)	193
Figure 3-35: Mass spec of 5d	194
Figure 3-36: ^1H NMR of 5e (CDCl_3 + 1%TMS, 500 MHz).....	195
Figure 3-37: ^{13}C NMR of 5e (CDCl_3 + 1%TMS, 126 MHz)	196

Figure 3-38: ^{29}Si NMR of 5e (CDCl_3 + 1%TMS, 99 MHz).....	196
Figure 3-39: Mass spec of 5e	197
Figure 3-40: ^1H NMR of 5f (CDCl_3 + 1%TMS, 500 MHz)	198
Figure 3-41: ^{13}C NMR of 5f (CDCl_3 + 1%TMS, 126 MHz)	199
Figure 3-42: ^{29}Si NMR of 5f (CDCl_3 + 1%TMS, 99 MHz)	199
Figure 3-43: Mass spec of 5f	200
Figure 3-44: ^1H NMR of 5g (CDCl_3 + 1%TMS, 500 MHz)	201
Figure 3-45: ^{13}C NMR of 5g (CDCl_3 + 1%TMS, 126 MHz)	202
Figure 3-46: ^{29}Si NMR of 5g (CDCl_3 + 1%TMS, 99 MHz)	202
Figure 3-47: ^1H NMR of 5h (CDCl_3 + 1%TMS, 500 MHz)	203
Figure 3-48: ^{13}C NMR of 5h (CDCl_3 + 1%TMS, 126 MHz)	204
Figure 3-49: ^{29}Si NMR of 5h (CDCl_3 + 1%TMS, 99 MHz)	204
Figure 3-50: Mass spec of 5h	205
Figure 3-51: Single Crystal Structure of 5a (Displacement ellipsoid contour probability drawn at 50%)	207
Figure 3-52: The following hydrogen bonding interactions with a maximum D-D distance of 2.9 Å and a minimum angle of 120 ° are present in 5a : O4–O10: 2.767 Å, O10–O4_1: 2.738 Å.....	207
Figure 3-53: Single Crystal Structure of 5b (Displacement ellipsoid contour probability drawn at 50%)	208
Figure 3-54: The following hydrogen bonding interactions with a maximum D-D distance of 3.1 Å and a minimum angle of 110 ° are present in REN1220D: O13–O14_1: 2.741 Å, O14–O13: 2.767 Å	208
Figure 3-55: Single Crystal Structure of 5e (Displacement ellipsoid contour probability drawn at 50%)	209
Figure 3-56: The following hydrogen bonding interactions with a maximum D-D distance of 2.9 Å and a minimum angle of 120 ° are present in 5e : O1–O2_1: 2.721 Å, O2–O1: 2.724 Å.....	209
Figure 3-57: Single Crystal Structure of 5f (Displacement ellipsoid contour probability drawn at 50%)	210

Figure 3-58: The following hydrogen bonding interactions with a maximum D-D distance of 2.9 Å and a minimum angle of 120 ° are present in REM221BB: O4–O10: 2.777 Å, O10–O4_1: 2.787 Å	210
Figure 3-59: ¹ H NMR (CDCl ₃ + 1%TMS, 500 MHz).....	211
Figure 3-60: ¹³ C NMR (CDCl ₃ + 1%TMS, 126 MHz)	212
Figure 3-61: ²⁹ Si NMR (CDCl ₃ + 1%TMS, 99 MHz).....	212
Figure 3-62: Mass spec of 7a	213
Figure 3-63: ¹ H NMR (CDCl ₃ + 1%TMS, 500 MHz).....	214
Figure 3-64: ¹³ C NMR (CDCl ₃ + 1%TMS, 126 MHz)	215
Figure 3-65: ²⁹ Si NMR (CDCl ₃ + 1%TMS, 99 MHz).....	215
Figure 3-66: Mass spec of 7b	216
Figure 3-67: ¹ H NMR (CDCl ₃ + 1%TMS, 500 MHz).....	217
Figure 3-68: ¹³ C NMR (CDCl ₃ + 1%TMS, 126 MHz)	218
Figure 3-69: ²⁹ Si NMR (CDCl ₃ + 1%TMS, 99 MHz).....	218
Figure 3-70: Mass spec of 7c	219
Figure 3-71: ¹ H NMR (CDCl ₃ + 1%TMS, 500 MHz).....	220
Figure 3-72: ¹³ C NMR (CDCl ₃ + 1%TMS, 126 MHz)	221
Figure 3-73: ²⁹ Si NMR (CDCl ₃ + 1%TMS, 99 MHz).....	221
Figure 3-74: Single Crystal Structure of 7a (Displacement ellipsoid contour probability drawn at 50%)	222
Figure 4-1: Structures of cage-like Silsesquioxanes - dodecaphenylT ₁₂ (1), octaphenylT ₈ (2), tetrakis(trimethylsilyl)octaphenylT ₈ (3), and heptaphenylT ₇ triol (4)	231
Figure 4-2: Graph of relative intensity (%) vs hydrolysis time.....	238
Figure 4-3: Compound 3 showing two molecules of THF solvent per molecule of interest (Displacement ellipsoid contour probability drawn at 50%)	243
Figure 4-4: Single molecule of 3 in the asymmetric unit, which is represented by the reported sum (Z is 4 and Z' is 1).....	243
Figure 4-5: Packing diagram of 3	243

Figure 4-6: Compound 5 with two THF molecules co-crystallized per molecule of interest (Displacement ellipsoid contour probability drawn at 50%)	244
Figure 4-7: Single molecule of 5 in the asymmetric unit, which is represented by the reported sum formula (Z is 2 and Z' is 1).....	244
Figure 4-8: Hydrogen bonding interactions in 5	245
Figure 4-9: Packing diagram of 5,11,14,17-tetra(hydro)octaphenyltetracyclo[7.3.3.-3 ^{3;7}]octasilsesquioxane (5)	246
Figure 4-10: 5,11,14,17-tetra(sodio)octaphenyltetracyclo[7.3.3.3 ^{3;7}]octasilsesquioxanolate (12)	249
Figure 4-11: ¹ H NMR of 3 (500 MHz, CDCl ₃)	254
Figure 4-12: ¹³ C NMR of 3 (126 MHz, CDCl ₃)	255
Figure 4-13: ²⁹ Si NMR of 3 (99 MHz, CDCl ₃)	255
Figure 4-14: ¹ H NMR of 5 (500 MHz, CDCl ₃)	256
Figure 4-15: ¹³ C NMR of 5 (126 MHz, CDCl ₃)	256
Figure 4-16: ²⁹ Si NMR of 5 (99 MHz, CDCl ₃)	257
Figure 4-17: ¹ H NMR of 3 – 16h (500 MHz, CDCl ₃)	258
Figure 4-18: ²⁹ Si NMR of 3 – 16h (99 MHz, CDCl ₃).....	259
Figure 4-19: ¹ H NMR of 3 – 24h (500 MHz, CDCl ₃)	260
Figure 4-20: ²⁹ Si NMR 3 – 24h (99 MHz, CDCl ₃)	261
Figure 4-21: ¹ H NMR 3 – 36h (500 MHz, CDCl ₃)	262
Figure 4-22: ²⁹ Si NMR 3 – 36h (99 MHz, CDCl ₃)	263
Figure 4-23: ¹ H NMR 3 – 48h (500 MHz, CDCl ₃)	264
Figure 4-24: ²⁹ Si NMR 3 – 48h (99 MHz, CDCl ₃)	265
Figure 4-25: ¹ H NMR 3 – 72h (500 MHz, CDCl ₃)	266
Figure 4-26: ²⁹ Si NMR 3 – 72h (99 MHz, CDCl ₃)	267
Figure 4-27: Stacked ¹ H NMR of 5,11,14,17-tetrakis(trimethylsilyl)octaphenyltetracyclo[7.3.3.-3 ^{3;7}]octasilsesquioxane (3) from 16 to 72 Hydrolysis of 1 (500 MHz, CDCl ₃) ...	268

Figure 4-28: Stacked ^{29}Si NMR of 5,11,14,17-tetrakis(trimethylsilyl)octaphenyltetracyclo[7.3.3.-3 ^{3,7}]octasilsesquioxane (3) from 16 to 72 Hydrolysis of 1 (99 MHz, CDCl_3)	269
Figure 4-29: ^1H NMR of commercial 1 (500 MHz, Toluene- d_8).....	270
Figure 4-30: ^{29}Si NMR of commercial 1 (99 MHz, CDCl_3)	271
Figure 4-31: ^1H NMR of recovered 1 (500 MHz, Toluene- d_8)	272
Figure 4-32: ^{29}Si NMR of recovered 1 (99 MHz, CDCl_3).....	273
Figure 4-33: Stacked ^1H NMR of Commercial $\text{Ph}_{12}\text{T}_{12}$ (1) and Recovered $\text{Ph}_{12}\text{T}_{12}$ (1) (500 MHz, Toluene- d_8)	274
Figure 4-34: Stacked ^{29}Si NMR of Commercial $\text{Ph}_{12}\text{T}_{12}$ (1) and Recovered $\text{Ph}_{12}\text{T}_{12}$ (1) (99 MHz, CDCl_3).....	275
Figure 4-35: Stacked ^1H NMR of Resinous product from the acid hydrolysis of intermediate salt (12) (500 MHz, CDCl_3)	276
Figure 4-36: Stacked ^{29}Si NMR of Resinous product from the acid hydrolysis of intermediate salt 12 (99 MHz, CDCl_3)	277
Figure 4-37: DOESY NMR Spectra of resinous product (500 MHz, CDCl_3)	278
Figure 4-38: DOSY Spectra for 5,11,14,17-tetrakis(trimethylsilyl)octaphenyltetracyclo[7.3.3.-3 ^{3,7}]octasilsesquioxane (3) (500 MHz, CDCl_3).....	279
Figure 4-39: Commercial $\text{Ph}_{12}\text{T}_{12}$ (1).....	280
Figure 4-40: 5,11,14,17-tetrakis(trimethylsilyl)octaphenyltetracyclo[7.3.3.-3 ^{3,7}]octasilsesquioxane (3) from 16 h hydrolyzed 12	280
Figure 4-41: 5,11,14,17-tetrakis(trimethylsilyl)octaphenyltetracyclo[7.3.3.-3 ^{3,7}]octasilsesquioxane (3) from 24 h hydrolyzed 12	281
Figure 4-42: 5,11,14,17-tetrakis(trimethylsilyl)octaphenyltetracyclo[7.3.3.-3 ^{3,7}]octasilsesquioxane (3) from 36 h hydrolyzed 12	281
Figure 4-43: 5,11,14,17-tetrakis(trimethylsilyl)octaphenyltetracyclo[7.3.3.-3 ^{3,7}]octasilsesquioxane (3) from 48 h hydrolyzed 12	282
Figure 4-44: 5,11,14,17-tetrakis(trimethylsilyl)octaphenyltetracyclo[7.3.3.-3 ^{3,7}]octasilsesquioxane (3) from 72 h hydrolyzed 12	282
Figure 4-45: MS Spectra for 0 – 2 h hydrolyzed 12	283
Figure 4-46: MS Spectra for 4 – 8 h hydrolyzed 12	283

Figure 4-47: MS Spectra for 36 – 72 h hydrolyzed 12	284
Figure 4-48: Mass Spectral Data for Resinous Mixture	284
Figure 5-1: GC/MS – styrene	328
Figure 5-2: ^1H NMR of 2 (CDCl_3 + 1%TMS, 500 MHz).....	328
Figure 5-3: ^{13}C NMR of 2 (CDCl_3 + 1%TMS, 126 MHz)	329
Figure 5-4: ^{29}Si NMR of 2 (99 MHz, CDCl_3)	329
Figure 5-5: ^1H NMR of 4 (CDCl_3 + 1%TMS, 500 MHz).....	330
Figure 5-6: ^{29}Si NMR of 4 (99 MHz, CDCl_3)	331
Figure 5-7: Mass spec of 4	331
Figure 5-8: ^1H NMR of 6 (CDCl_3 + 1%TMS, 500 MHz).....	332
Figure 5-9: ^{13}C NMR of 6 (CDCl_3 + 1%TMS, 126 MHz)	332
Figure 5-10: ^{29}Si NMR of 6 (99 MHz, CDCl_3)	333
Figure 5-11: Mass spec of 6	333
Figure 5-12: ^1H NMR of 7 (CDCl_3 + 1%TMS, 500 MHz).....	334
Figure 5-13: ^{13}C NMR of 7 (CDCl_3 + 1%TMS, 126 MHz)	334
Figure 5-14: ^{29}Si NMR of 7 (99 MHz, CDCl_3)	335
Figure 5-15: Mass spec of 7	335
Figure 5-16: ^1H NMR of 12 (CDCl_3 + 1%TMS, 500 MHz).....	336
Figure 5-17: ^{13}C NMR of 12 (CDCl_3 + 1%TMS, 126 MHz)	337
Figure 5-18: ^{29}Si NMR of 12 (99 MHz, CDCl_3)	337
Figure 5-19: ^1H NMR of 13 (CDCl_3 + 1%TMS, 500 MHz).....	338
Figure 5-20: ^{11}B NMR of 13 (CDCl_3 + 1%TMS, 160 MHz)	338
Figure 5-21: ^{29}Si NMR of 13 (99 MHz, CDCl_3)	339
Figure 5-22: ^1H NMR of 14 (Acetone- d_6 , 500 MHz).....	339
Figure 5-23: ^{13}C NMR of 14 (126 MHz, Acetone- d_6)	340

Figure 5-24: ^{19}F NMR of 14 (Acetone- d_6 , 471 MHz).....	340
Figure 5-25: ^{29}Si NMR of 14 (Acetone- d_6 , 99 MHz).....	341
Figure 5-26: ^1H NMR of 14 (CDCl_3 + 1%TMS, 500 MHz).....	342
Figure 5-27: ^{13}C NMR of 14 (CDCl_3 + 1%TMS, 500 MHz)	342
Figure 5-28: ^{29}Si NMR of 14 (CDCl_3 + 1%TMS, 99 MHz).....	343
Figure 5-29: Crystal Structure of 4	344
Figure 5-30: Packing diagram of 9,19-dimethyl-1,3,5,7,11,13,15,17-octaphenyl-9,19-bis(4-vinylphenyl)-2,4,6,8,10,12,14,16,18,20,21,22,23,24-tetradecaoxa-1,3,5,7,9,11,13,15,17, 19-decasilapentacyclo[11.7.1.13,11.15,17.17,15]tetracosane (4) (Displacement ellipsoid contour probability drawn at 50%)	345
Figure 5-31: Crystal Structure of 12	346
Figure 5-32: Packing diagram of 2,4,6,8-tetrakis(4-bromophenyl)-2,4,6,8-tetrakis((trimethylsilyl)oxy)-1,3,5,7,2,4,6,8-tetraoxatetrasilocane	347

LIST OF SCHEMES

Scheme 1-1: Hydrolytic Polycondensation of RSiX_3	6
Scheme 1-2: Acid/base promoted cleavage of Completely Condensed Silsesquioxanes	6
Scheme 1-3: Hydrolysis and condensation of RSiX_3	7
Scheme 1-4: Corner-capping trisilanol POSS with trifunctional monomers	9
Scheme 1-5: Hydrolytic condensation of phenyltrimethoxysilane	10
Scheme 1-6: Condensation of $\text{DDSQ}(\text{ONa})_4$ with Me_2SiCl_2	11
Scheme 1-7: Condensation of $\text{DDSQ}(\text{OH})_4$ with $\text{R}^1\text{R}^2\text{SiCl}_2$, where $\text{R}^1 \neq \text{R}^2$	11
Scheme 2-1: Styryl-POSS macromonomer synthesis and its polymerization ¹²	24
Scheme 2-2: Synthesis of organic–inorganic polyimide with DDSQ in the main chain ²³	25
Scheme 2-3: Ruthenium catalyzed silylative coupling of divinyl-substituted silsesquioxanes DDSQ-2ViSi with two different styrenes	26
Scheme 2-4: Side capping of DDSQ tetraol with two different chlorosilanes.....	27
Scheme 2-5: (A) Bis-protection of $\text{DDSQ}(\text{OH})_4$ (1) with a boronic acid, (B) bis-deprotection of 2 with pinacol, and (C) stability of boronic acid protecting group under standard silylation conditions	28
Scheme 2-6: Monoborylation of $\text{DDSQ}(\text{OH})_4$ 1 with $p\text{-MeO-C}_6\text{H}_4\text{B}(\text{OH})_2$	28
Scheme 2-7: Synthesis of DDSQ Bis-boronate Esters 2	53
Scheme 2-8: Deborylation of $(p\text{-MeOC}_6\text{H}_4\text{B})_2\text{DDSQ}$ with Pinacol.....	54
Scheme 2-9: Monoborylation of $\text{DDSQ}(\text{OH})_4$ 1 with $p\text{-MeO-C}_6\text{H}_4\text{B}(\text{OH})_2$	55
Scheme 2-10: Silylation of Mono-borylated Product, $(p\text{-MeOC}_6\text{H}_4\text{B})\text{DDSQ}(\text{OH})_2$ with $\text{R}^1\text{R}^2\text{SiCl}_2$	56
Scheme 2-11: Deborylation of $(p\text{-MeOC}_6\text{H}_4\text{B})\text{DDSQSIR}^1\text{R}^2$ and $(p\text{-MeOC}_6\text{H}_4\text{B})_2\text{DDSQ}$ with Pinacol	57

Scheme 2-12: Second Silylation of Monosilylated Precursor, $R^1R^2SiDDSQ(OH)_2$	58
Scheme 2-13: Substrate Scope of the Multistep Pathway for the Synthesis of Asymmetrically Functionalized DDSQ.....	59
Scheme 3-1: Hydrolysis of cyclopentyltrichlorosilane into heptacyclopentyl POSS trisilanol.....	130
Scheme 3-2: Selective cleavage of completely condensed octacyclohexyl silsesquioxane for the synthesis of octacyclohexyl POSS disilanol (Path A) and heptacyclohexyl POSS trisilanol (Path B)	130
Scheme 3-3: Condensation of $DDSQ(OH)_4$ with diphenyldichlorosilane	131
Scheme 3-4: Condensation of $DDSQ(OH)_4$ with 3-cyanopropyl(methyl)dichlorosilane	132
Scheme 3-5: Synthesis of difunctional POSS, phenyl ₇ anilinePOSS from heptaphenylPOSS trisilanol.....	132
Scheme 3-6: Condensation of trisilanol POSS for the synthesis of metallasilsesquioxane	133
Scheme 3-7: Functionalization of POSS endo disilanol with $MeHSiCl_2$ and subsequent hydrosilylation	133
Scheme 3-8: Known routes into asymmetrically functionalized DDSQs.....	137
Scheme 3-9: Synthetic route into $R^1R^2SiDDSQ(OH)_2$ (5).....	139
Scheme 3-10: Optimal deborylation of 2 with pinacol for the synthesis of 3	140
Scheme 3-11: Synthesis of asymmetrically functionalized $R^1R^2SiDDSQ(OH)_2$ (5)	141
Scheme 3-12: Synthesis of 9,19-bis(4-methoxyphenyl)-1,3,5,7,11,13,15,17-octaphenyl-2,4,6,8,10,12,14,16,18,20,21,22,23,24-tetradeca-1,3,5,7,11,13,15,17-octasila-9,19-diborapentacyclo[11.7.1.13,11.15,17.17,15]tetracosane (2)	172
Scheme 3-13: Complete Deborylation of (p-MeOC ₆ H ₄ B) ₂ DDSQ (2) with Pinacol	173
Scheme 3-14: Partial Deborylation of (p-MeOC ₆ H ₄ B) ₂ DDSQ (2) with Pinacol	173
Scheme 3-15: Synthesis of asymmetrically functionalized monosilylated $DDSQ(OH)_2$	175
Scheme 3-16: Synthesis of completely condensed asymmetrically functionalized D ₂ T ₈	178

Scheme 4-1: Prior strategies for the partial cleavage of completely condensed (a) octaphenylT ₈ , (b) hexacyclohexylT ₆	232
Scheme 4-2: Hydrolysis of Ph ₁₂ T ₁₂ (1) for the synthesis of 5,11,14,17-tetrakis(trimethylsilyl)octaphenyltetracyclo[7.3.3.3 ^{3,7}]octasilsesquioxane (3)	233
Scheme 4-3: Base cleavage of 1 with NaOH followed by acid hydrolysis of intermediate 12 with AcOH to give 5	234
Scheme 4-4: Proposed route to 5 from 1	234
Scheme 4-5: Synthesis of 5,11,14,17-tetrakis(trimethylsilyl)octaphenyltetracyclo- [7.3.3.-3 ^{3,7}]octasilsesquioxane [(PhSiO) ₈ (O) ₂ (OTMS) ₄] (3) from Ph ₁₂ T ₁₂ (1)	235
Scheme 4-6: Time-course analysis for the synthesis of 3 from 1	237
Scheme 4-7: Synthesis of 5 from 1	240
Scheme 4-8: Optimal Conditions for the Synthesis of (PhSiO) ₈ (O) ₂ (OH) ₄ (5)	241
Scheme 4-9: Hydrolysis of Ph ₁₂ T ₁₂ (1) for the synthesis of 15,11,14,17-tetrakis(trimethylsilyl)octaphenyltetracyclo[7.3.3.3 ^{3,7}]octasilsesquioxane (3)	248
Scheme 4-10: Time-course study for the synthesis of 3 from 1	250
Scheme 4-11: Base hydrolysis of [Ph ₁₂ T ₁₂] 1 for the synthesis of [(PhSiO) ₈ (O) ₂ (OH) ₄] 5	251
Scheme 4-12: Optimization for the synthesis of (PhSiO) ₈ (O) ₂ (OH) ₄ (5)	252
Scheme 5-1: Silylative coupling and cross metathesis of octavinylT ₈ with styrenes... 300	
Scheme 5-2: Hydrosilylation of POSS-OSi(Me) ₂ H with ethynylbenzene	301
Scheme 5-3: Elaboration of OctavinylT ₈ for the synthesis of a variety of different POSS	302
Scheme 5-4: Fluoride catalyzed rearrangement of polysilsesquioxanes to mixed T ₁₀ and T ₁₂ isomers	303
Scheme 5-5: Metathesis of mixed VinylT ₁₀ and VinylT ₁₂ for the synthesis of styrenylT _{10/12} cages	304
Scheme 5-6: Synthesis of 3,13-dianilino DDSQ from phenyltrimethoxysilane	305
Scheme 5-7: Synthesis of asymmetric styrenylDDSQs from the silylative coupling of divinylDDSQ with substituted styrenes	306

Scheme 5-8: Synthesis of [(styryl(Me)) ₂ DDSQ]	306
Scheme 5-9: Route to styryl-functionalized T _n cage silsesquioxanes	307
Scheme 5-10: Synthesis of styryl-functionalised T ₈ -F Cage	307
Scheme 5-11: Synthesis of Brominated Octaphenylsilsesquioxanes (Br _x OPS), x = the average number of bromines per molecule	309
Scheme 5-12: Selective self-catalyzed bromination of octa(phenyl)silsesquioxane (OPS) for the selective synthesis of octabrominated OPS	309
Scheme 5-13: Synthesis of octa(dibromophenyl)silsesquioxane	310
Scheme 5-14: Synthesis of sodium cyclotetrasiloxanates from para-substituted phenyltriethoxysilane	310
Scheme 5-15: Synthesis of sodium and potassium cyclosiloxanates based on trisiloxanolate cycles with vinyl and alkyl substituents	311
Scheme 5-16: Synthesis of Br-T ₈ from all-cis-Br-T ₄ -tetraol	312
Scheme 5-17: Synthesis of tetra-n-butylammonium octa(para-bromophenyl)octasilsesquioxane fluoride	312
Scheme 5-18: Synthesis of dichloro(methyl)(4-vinylphenyl)silane (2) via Grignard	315
Scheme 5-19: Capping of DDSQ(OH) ₄ (3) with dichloro(methyl)(4-vinylphenyl)silane (2)	316
Scheme 5-20: Synthesis of sty ₈ T ₈ (6), sty ₁₀ T ₁₀ (7) and sty ₁₂ T ₁₂ (8) from styryltrimethoxysilane (5)	317
Scheme 5-21: Hydrolysis of sty ₈ T ₈ with sodium hydroxide	319
Scheme 5-22: Synthesis of 2,4,6,8-tetrakis(4-bromophenyl)-2,4,6,8-tetrakis((trimethylsilyl)oxy)-1,3,5,7,2,4,6,8-tetraoxatetrasilocane (12) from the sodium hydroxide hydrolysis of 4-bromophenyltrimethoxysilane (10)	321
Scheme 5-23: Synthesis of 2,4,6,8-tetrakis(4-(4,4,5,5-tetramethyl-1,3,2-dioxaborolan-2-yl)phenyl)-2,4,6,8-tetrakis((trimethylsilyl)oxy)-1,3,5,7,2,4,6,8-tetraoxatetrasilocane	322
Scheme 5-24: Synthesis of fluoride ion entrapped octa(4-bromophenyl)octasilsesquioxane (14)	323
Scheme 5-25: Cleavage of 14 for the synthesis of 1,3,5,7,9,11,14,17-octakis(4-bromophenyl)-5,11,14,17-tetrakis((trimethylsilyl)oxy)-2,4,6,8,10,12,13,15,16,18-decaoxa-1,3,5,7,9,11,14,17-octasilatricyclo[7.3.3.3.7]octadecane (15)	325

KEY TO ABBREVIATIONS

AA = Symmetric double-decker shaped silsesquioxane

AB = Asymmetric double-decker shaped silsesquioxane

ACN = acetonitrile

APCI = Atmospheric Pressure Chemical Ionization

Ar = Argon

BB = Symmetric double-decker shaped silsesquioxane

Bpin = 4,4,5,5-Tetramethyl-1,3,2-dioxaborolane

B₂pin₂ = bis(pinacolato)diboron

bpy = 2,2'-bipyridine

CDCl₃ = deuterated chloroform

CHB = C–H activation borylation

C_{hex} = cyclohexyl

°C = Degrees Celsius

COD cyclooctadiene

DCM = dichloromethane

DDSQ = Double Decker Oligomeric Silsesquioxane

DDSQ(OH)₄ = Tetrasilanol double-decker shaped silsesquioxane

DDSQ(ONa)₄ = Tetrasodium double-decker shaped silsesquioxane

DSC = Differential Scanning Calorimetry

DPS = Diphenyl-functionalized Silsesquioxane

dtbpy = 4,4'-di-tert-butyl-2,2'-bipyridine

EtOAc = ethyl acetate

FC = Fractional crystallization

GC-MS Gas chromatography – Mass spectroscopy

h = hour

ICBM = Intercontinental Ballistic Missile

Ir = iridium

LC/MS = Liquid Chromatography-Mass Spectrometry

m = multiplet peak in NMR spectrum

M⁺ = molecular ion peak in mass spectrum

m/z = mass divided by charge of an ion

Me = methyl

mg = milligrams

MHz = mega hertz

mL = milliliter

mmol = millimole

mp = melting point

N₂ = nitrogen

MS = Mass Spectrometry

MW = Molecular Weight

NASA = National Aeronautics and Space Administration

NMR = Nuclear Magnetic Resonance Spectroscopy

OIBS = Octa-isobutyl Silsesquioxane

OIBS-EDN = Octa-isobutyl Silsesquioxane Endo-disilanol

OPS = Octaphenyl Silsesquioxane

ORTEP = Oak Ridge Thermal Ellipsoid Plot

Ph = Phenyl

PFG = Pulse-Field Gradient

POSS = Polyhedral Oligomeric Silsesquioxane

ppm = parts per million

rt = room temperature

s = singlet peak in NMR spectrum

T₄ = Tetraphenylsilsesquioxane

T₆ = Hexaphenylsilsesquioxane

T₈ = Octaphenylsilsesquioxane

T₁₀ = Decaphenylsilsesquioxane

T₁₂ = Dodecaphenylsilsesquioxane

THF = tetrahydrofuran

T_d = Decomposition temperature

T_g = Glass Transition Temperature

T_m = Melting temperature

TGA = Thermogravimetric Analysis

TLC = Thin layer chromatography

TMS = tetramethylsilane

TPS = Thermal Protection System

CHAPTER 1.0

1.1 Introduction

This chapter presents some background information on the growth of silsesquioxane chemistry, particularly previous literature related to the work described in this study. The chapter also reviews recent developments in this chemistry, pinpointing the motivations that led to our overall goal and objectives.

1.2 Background

1.2.1 Silsesquioxanes

Silsesquioxanes are a diverse class of organosilicon compounds with the empirical formula $\text{RSiO}_{3/2}$; where R can be hydrogen, alkyl or aryl group. The term is a portmanteau of three Latin syllables; 'sil' for silicon, 'sesqui' for three-halves typifying a Si:O ratio of 1:1.5 per unit molecule and 'oxane' for oxygen.¹ The compounds contain several well-defined 3D structures with tunable physical and chemical properties. The arrangement of the Si–O–Si framework, analogous to that of the silica architecture, makes silsesquioxanes model nanofillers and polymer modifiers.^{2–4}

1.2.2 Classification and Nomenclature of Silsesquioxanes

1.2.2.1 Classification

Early classification of silsesquioxanes was based on their structures. Following the first isolation of some volatile silsesquioxanes from the co-hydrolysis products of Me_2SiCl_2 and MeSiCl_3 by Scott in 1945,⁵ and the confirmation of their polyhedral nature by Barry and Gilkey,⁶ several other studies corroborated the fact that the condensation of trifunctional organosilanes produces a range of products with general formula, $(\text{RSiO}_{3/2})_n$. The resulting frameworks can be (i) random silsesquioxanes having no regular

arrangement of the Si-O-Si linkages, (ii) ladder structures where two siloxane chains are oxygen-linked at regular intervals with no polyhedra, (iii) fully condensed cages that are completely closed structures, or (iv) incompletely condensed cages that can serve as precursors to completely condensed structures.¹³ The random and ladder structures constitute the polysilsesquioxanes (also known as T-resins) and the closed and partial cage structures the polyhedral oligomeric silsesquioxane (POSS) (**Figure 1-1**).

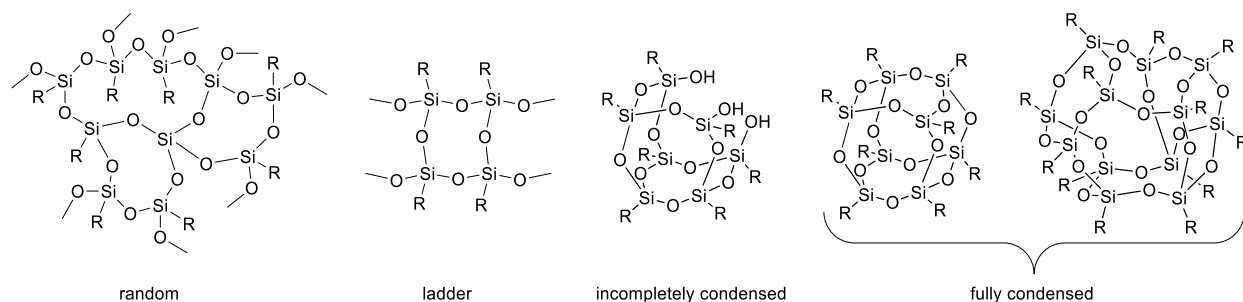


Figure 1-1: Different architectures of $(\text{RSiO}_{3/2})_n$

However, unlike the polysilsesquioxanes that lack regularity, the well-defined rigid frameworks of the polyhedral oligomeric silsesquioxanes make them a more interesting class of silsesquioxanes for the synthesis of new materials. The surge in research interest is particularly skewed towards the cubic T_8 architecture due to its high symmetry and stability.

1.2.2.2 Nomenclature

Silsesquioxanes are generally named using either the IUPAC system of nomenclature or the systematic (otherwise known as the trivial) nomenclature. The latter is more conveniently adopted because it describes only the number of silsesquioxane units, $\text{SiO}_{3/2}$ in a molecule and the type of R group(s) on the silicon vertices unlike the IUPAC systems which requires details that makes the process cumbersome.^{1,7} For instance, the compound $(\text{iBuSiO}_{3/2})_8$ is octaisobutylsilsesquioxane based on the

systematic name, and 1,3,5,7,9,11,13,15-octaisobutyl-2,4,6,8,10,12,14,16,17,18,19,20-dodecaoxa-1,3,5,7,9,11,13,15-octasilapentacyclo[9.5.1.13,9.15,15.17,13] icosane, based on the IUPAC system. For cases where the number of substituents is less than the number of silsesquioxane units, $R_{n-1}R'(SiO_{3/2})_n$, as in $(CH_3)_7\text{vinyl}(SiO_{3/2})_8$, the systematic and IUPAC names become heptamethylvinylsilsesquioxane and 1,3,5,7,9,11,13-heptamethyl-15-vinyl-2,4,6,8,10,12,14,16,17,18,19,20-dodecaoxa-1,3,5,7,9,11,13,15-octasilapentacyclo [9.5.-1.13,9.15,15.17,13]icosane respectively.

A more convenient nomenclature also used to overcome the difficulty with the IUPAC system is to adopt the nomenclature as in siloxane chemistry. Here upper-case letters and numerical subscripts are used to describe the type of silicon atoms found in the polyhedra and in some cases, a superscript to denote the substituent on the silicon vertices. Based on this system, the letters M, D, T and Q are used as shorthand notations for the number of oxygen atoms bound to a silicon. Thus, silicon sites in POSS molecules are classified as an M-siloxane if the silicon atom is bound to one oxygen (R_3SiO), D-siloxane when the silicon is bound to two oxygens (R_2SiO_2), T-siloxane when it is bound to 3 oxygens ($RSiO_3$) and Q-siloxane when it is bound to 4 oxygen atoms (SiO_4) (**Figure 1-2**).⁸



Figure 1-2: Systematic/trivial nomenclature of Silsesquioxanes

Applying this system to the examples above, $(^i\text{Bu}SiO_{3/2})_8$ becomes $^i\text{Bu}_8\text{T}_8$ or T_8^iBu and $(CH_3)_7\text{vinyl}(SiO_{3/2})_8$ becomes $\text{Me}_7\text{T}_7(\text{CH}_2=\text{CH})\text{T}$ or $\text{T}_7\text{MeT}_{\text{vi}}$

1.3 Polyhedral Oligomeric Silsesquioxanes (POSS)

Polyhedral Oligomeric Silsesquioxanes are a class of hybrid organic-inorganic nanoparticles with the basic molecular composition of $(\text{RSiO}_{3/2})_n$, where R is hydrogen or an organic group and $n = 6, 8, 10, 12, \dots$. Structurally, the compounds are made of several fused rings of Si-O-Si frameworks having each silicon atom bound to an organic group and three oxygens to form an Si-O based polyhedron.⁹ They are considered as the smallest particles of silica (nanostructural dimension of 1 – 3 nm in diameter) with tunable ability to offer material properties that are typical to both the core inorganic siloxane and the peripheral organic units.^{9–11} Consequently, both the composite rigidity and stability that comes from the inorganic core, and the toughness and processability from the organic coronae are tenable from a single material. The organic groups in the structure can be derivatized into more functional materials and used as binders or linkers to polymer matrices. The presence of various types of functionalities on the POSS core allows their easy incorporation onto surfaces to obtain composite materials with unique properties.^{12,13} Thus, the hybrid nature of these nanoparticles provides the property synergy that are intermediate to those of classical ceramics and polymers resulting in the generation of advanced engineering materials. Polyhedral oligomeric silsesquioxanes are therefore important building blocks for the design of new materials in polymer chemistry, material science, medicine, catalysis, and engineering. Depending on the value of n , there can be several different well-defined 3D structures of known silsesquioxanes, the most explored being the cubic silsesquioxane with an n value of 8 (**Figure 1-3**).¹²

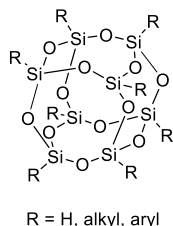
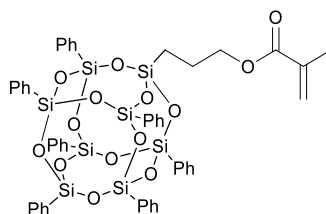


Figure 1-3: Cubic octameric silsesquioxane

Like other completely condensed POSS cages, octameric silsesquioxanes have a unique rigid silica core bearing eight organic functional groups anchored on the silicon vertices. They have an internal diameter of 0.53 nm, a sphere-like organic-inorganic molecular diameter of 1-2 nm and a volume that is less than 2 nm³.¹² These cage derivatives are highly symmetrical and easy to handle and modify. They are synthesized from the hydrolysis and condensation reactions of various trifunctional silanes.^{3,8,12,14-16} However, cubic octafunctional POSS with mixed functionalities have also been obtained from the corner capping of various trisilanol POSS cages. Such POSS cages display different substitution patterns with different groups on the vertices as in the case of methacrylate heptaphenyl POSS derivative below (**Figure 1-4**).¹⁷



methacrylate heptaphenylPOSS

Figure 1-4: Methacrylate heptaphenylPOSS

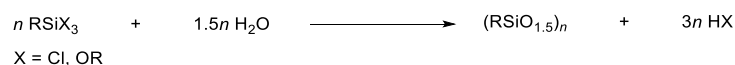
POSS molecules are easy to disperse into polymer matrices.¹⁷ The incorporation of POSS into polymer matrices causes significant property enhancement due to the strong interactions between the polymer chain and the nanoparticle. The strong nano

effects impacted by the POSS cage restricts the segmental motion of the polymer and hence leads to significant property enhancement in the composite. POSS/Polymer nanocomposites are obtained from either physical blending or chemical copolymerization courtesy of the reactive functional groups on both the polymer and POSS.

1.3.1 Synthesis of Polyhedral Oligomeric Silsesquioxanes (POSS)

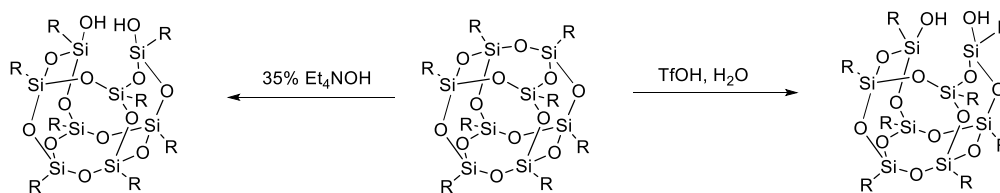
POSS compounds have been synthesized from the hydrolytic polycondensation of trifunctional organosilicon monomers, RSiX_3 , where R is a stable organic group and X, a very reactive halogen or alkoxide group (**Scheme 1-1**).^{15,16,18–23}

Scheme 1-1: Hydrolytic Polycondensation of RSiX_3



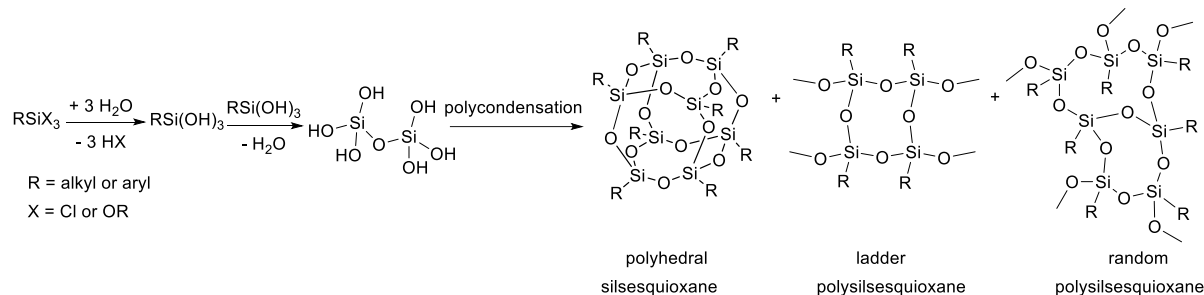
Whereas this approach affords both completely and incompletely condensed POSS cages, a higher yielding route specific to partially condensed products involves the base/acid promoted cleavage of fully condensed POSS (**Scheme 1-2**).^{24–27}

Scheme 1-2: Acid/base promoted cleavage of Completely Condensed Silsesquioxanes



Formation of silsesquioxanes from the hydrolysis of trichloro/trialkoxysilanes is a consecutive two-step process involving (i) the rapid hydrolysis of the trifunctional monomer into trisilanol, followed by (ii) polycondensations yielding different silsesquioxane frameworks (**Scheme 1-3**).

Scheme 1-3: Hydrolysis and condensation of RSiX_3



Formation of various architectures is condition dependent and as a complicated process, reaction parameters such as initial monomer concentration, the nature of solvent, the nature of the R and X substituents, and the amount of water to be added requires careful considerations. For instance, the type of X group used can influence the reaction kinetics and polycondensations conducted at higher temperatures favors the formation of completely condensed cages over other frameworks.

1.4 Incompletely Condensed Polyhedral Oligomeric Silsesquioxanes

Incompletely condensed polyhedral oligomeric silsesquioxanes are important building blocks for the synthesis of silsesquioxane-containing polymers, silica-supported catalyst, electronic materials, and network solids.^{21,28–38} Since the first synthesis and isolation of heptacyclohexyl trisilanolPOSS by Brown and Vogt in 1965,¹⁹ there has been a rapidly expanding library of different partially condensed POSS cages including the difunctional, trifunctional or tetrafunctional silsesquioxanes (**Figure 1-5**).

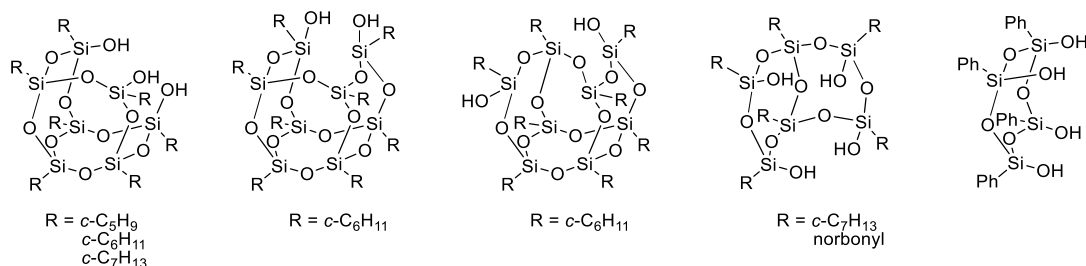


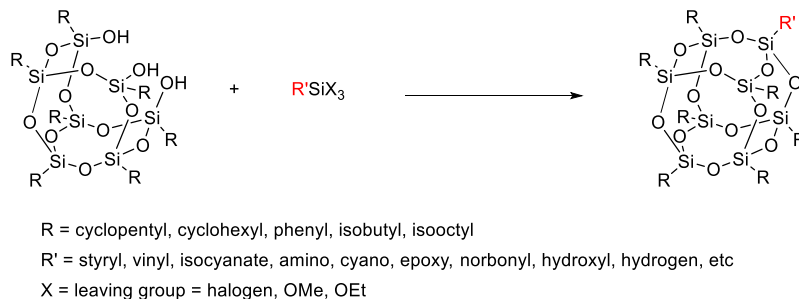
Figure 1-5: Incompletely condensed POSS frameworks²⁵⁻²⁷

Majority of the work in this field is credited to the Feher group for their tremendous efforts in developing procedures to access various types of partially condensed POSS cages.

This class of silsesquioxanes has been accessed from both the hydrolytic condensation of functional organosilicon monomer^{19,21,30,39–41} and via the controlled partial hydrolysis of fully condensed POSS frameworks.³⁰ However, whereas the former approach affords complex resins and/or polyhedral oligosilsesquioxanes (i.e., $[\text{RSiO}_{3/2}]_n$), in addition to the incompletely-condensed frameworks, the latter using fully condensed POSS precursors offers a better route that is devoid of the undesired T-gels. The poorer yields obtained from monomeric chloro/alkoxy-silanes is a result of the formation of unstable intermediates that are very difficult to isolate from the crude. In addition, the synthetic procedures for the hydrolytic condensations of cyclohexyltrichlorosilane, cyclopentyltrichlorosilane and cycloheptyltrichlorosilane require long gestation periods that may vary from one partially condensed POSS to another.³⁹

Compared to other 3D macromolecular systems like fullerenes and carboranes, incompletely condensed POSS cages are easier to functionalize and incorporate into polymer systems due to their solubility and the flexibility of the core siloxane cage.^{42–44} Modification of various trifunctional precursors has been achieved via corner-capping reactions with functionalized trichloro- or trialkoxy-silanes.^{4,21,45,46} The process involves condensation of the terminal silanols or other reactive functionalities on the open end of the cage with chloro- or alkoxysilanes to yield completely condensed monofunctional POSS compounds (**Scheme 1-4**).

Scheme 1-4: Corner-capping trisilanol POSS with trifunctional monomers



Monofunctionalized POSS cages have found huge applications as important synthetic precursors for the synthesis of POSS/polymer composites with high shear storage modulus (E'), high glass transition (T_g), melting (T_m), and decomposition (T_d) temperatures.^{31,47–49}

Lately, a special type of polyhedral oligomeric silsesquioxane with a unique symmetry, the so-called double-decker oligomeric silsesquioxane (DDSQ) has emerged as an even more interesting nanobuilding block precursor. This partially condensed cage bearing four dangling reactive groups symmetrically aligned in the molecule was discovered by Yoshida and coworkers in 2004.⁵⁰ Modifications of their strategy leading to better yields of this compound were later reported by the Kawakami group.^{24,51} This unique open POSS cage has two parallel cyclic siloxane rings arranged in planes that are linked by two oxygen atoms with phenyl coronae and four silanols (**Figure 1-6**).

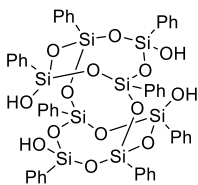
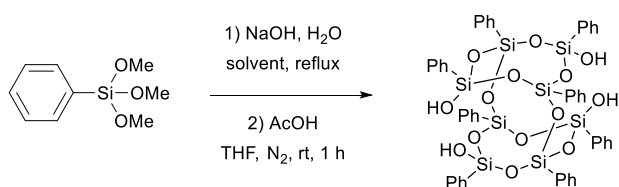


Figure 1-6: Octaphenyl tetrasilanol POSS [DDSQ(OH)₄]

The position of the silanols offers this compound the added advantages of not only broadening the applications of POSS cages but also the ability to better impact the

physico-chemical properties including material flammability, viscosity, oxidative resistance, and thermal stability of polymers.^{28,52–58} The two reactive ends of the $\text{DDSQ}(\text{OH})_4$ can be derivatized via condensation reactions with various chlorosilanes into open DDSQ cages with four M-silicons and eight-silicons ($\text{M}_4\text{T}_8 = \text{DDSQ-4OSi}$) or condensed siloxanes with ten silicons, eight of which are T, and two D ($\text{D}_2\text{T}_8 = \text{DDSQ-2Si}$).^{59,60} Functionalized DDSQs of such frameworks are easy to incorporate into linear polymer backbones as in ‘beads-on-chain’. However, compared to monofunctionalized POSS which can only be pendant to polymer matrices, the ability of the functionalized DDSQs to link two or more polymer matrices makes their design better nano-precursors that can enhance the composite material properties by effectively retarding the backbone motion of polymers.^{57,61–63} Double-decker oligomeric silsesquioxane is synthesized from the hydrolysis of phenyltrimethoxysilane with sodium hydroxide and water in refluxing isopropanol followed by acid workup (**Scheme 1-5**).^{50,51}

Scheme 1-5: Hydrolytic condensation of phenyltrimethoxysilane



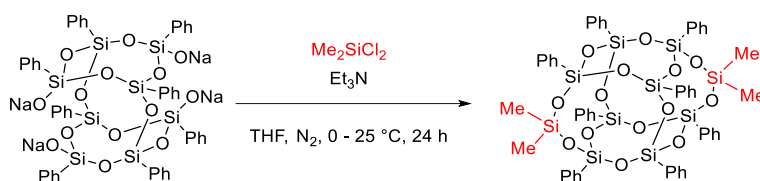
Functionalization of the open ends with suitable chlorosilanes can afford closed POSS derivatives that are ideal comonomers for incorporation into polymer matrices.

1.5 Synthesis of Condensed Difunctional Double-Decker Shaped Silsesquioxanes

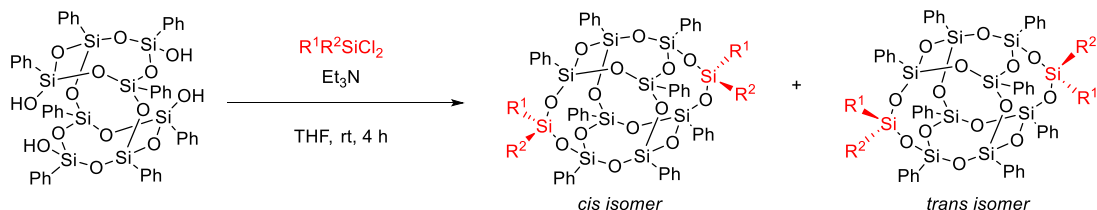
Condensation of $\text{DDSQ}(\text{OH})_4$ with mono-, di- or tri-functional capping agents in the presence of Et_3N can afford either open DDSQs of the M_4T_8 framework or closed derivatives of the D_2T_8 architecture. Based on the reagent used for capping, the

functionalized DDSQs can either be a single compound or one that is made up of a mixture of geometric isomers (cis and trans). Formation of a single compound can result if, for instance, the bridging dichlorosilane has identical R substituents (R_2SiCl_2) (**Scheme 1-6**)⁵¹ whereas geometric isomers are obtained with difunctional chlorosilanes with two different R groups (**Scheme 1-7**).⁶⁴

Scheme 1-6: Condensation of $DDSQ(ONa)_4$ with Me_2SiCl_2



Scheme 1-7: Condensation of $DDSQ(OH)_4$ with $R^1R^2SiCl_2$, where $R^1 \neq R^2$



Isolation of the cis/trans isomers had been a challenge until recently when various groups used both fractional crystallization (FC) and liquid chromatographic techniques.^{54,65–67} Interestingly, the structural differences between the geometric isomers (cis- and trans-forms) impacts differences on the physico-chemical properties of the POSS/polymer composite.⁵²

1.6 Motivation and Research Goals

Since the discovery of polyhedral oligomeric silsesquioxanes, much of the research focus had been on derivatizations leading to bifunctional nano-precursors that are integrated into polymer matrices.^{54,55,57,62,68–71} For this specific purpose, investigations on the applications of completely condensed POSS systems, the partially condensed

POSS trisilanols ($\text{RSiO}_{1.5})_7(\text{OH})_3$, and the double-decker shaped tetrasilanol $\text{DDSQ}(\text{OH})_4$ have predominated in research laboratories and industries. This is so because of their nanometric dimensions which upon incorporation into polymer systems retard the chain mobility and hence boost their physico-chemical and mechanical properties. These structures have been functionalized with a range of groups via corner capping, side-capping, and derivatization of the organic peripherals on the silicon atoms.^{12,24,45} Functionalized double-decker shaped silsesquioxanes with the $\text{DDSQ-2(R}^1\text{R}^2)$ architecture are particularly used as model building blocks for the synthesis of linear POSS/polymer composites.^{55,56,69,70,72–74} Their integration into polymer systems results in composites with enhanced physico-chemical properties including the glass transition temperature (T_g), dielectric properties and chemical resistance. However, these compounds have also been used to a limited extent as amphiphilic molecules,⁷⁵ and as support for heterogeneous catalysts.⁷⁶

In contrast, the synthesis and study of products resulting from the side-capping of incompletely condensed $\text{DDSQ}(\text{OH})_4$ cages with two different polymerizable groups (A/B systems) has remained a challenge. To this end, my dissertation is devoted to uncovering strategies and methods for the synthesis of novel POSS nano-precursors. Specifically, my research aims to synthesize symmetric and asymmetrically functionalized double-decker shaped silsesquioxanes with capping agents bearing Si, B, or C atoms. My goals are:

(i) Synthesis and characterization of asymmetrically functionalized DDSQs that can link two dissimilar polymer matrices.

- (ii) Study of the fissure patterns of dodecaphenylsilsesquioxane ($\text{Ph}_{12}\text{T}_{12}$) as an alternative route for the synthesis of 'Octaphenyl Double-Decker shaped Silsesquioxane.
- (iii) Development of protocol(s) for the synthesis of DDSQs with cage substituents that can be synthetically modified.

1.7 Dissertation Summary

This dissertation is a collection of our strides towards developing protocols for the synthesis of novel functionalized Polyhedral Oligomeric Silsesquioxanes (POSS) as promising materials with scientific and engineering benefits. Special attention is focused on transforming cubic and/or $\text{DDSQ}(\text{OH})_4$ precursors into unique derivatives via complete or partial condensation approaches. Alternative approaches to access the highly desirable and expensive octaphenyl tetrasilanolPOSS precursors were also explored using cheaper starting materials. Chapter 1 gives a compendium of some relevant background to this research that enables the identification of explorable gaps as outlined in our research aim and objectives. Chapter 2 presents a synthetic route for the synthesis of asymmetrically functionalized double-decker shaped silsesquioxanes that has the potential to bridge two dissimilar polymer matrices. Chapter 3 discloses our efforts toward developing a general route into a crucial intermediate that is ideal for the efficient synthesis of condensed asymmetrically functionalized DDSQs and as a ligand for solid support. Chapter 4 outlines an economically viable route into the most coveted and costly $\text{DDSQ}(\text{OH})_4$ using the dead-end cubic dodecasilsesquioxane ($\text{Ph}_{12}\text{T}_{12}$) as a precursor. Chapter 5 reveals our preliminary attempts to expand the library of symmetrical incompletely condensed octa-functional double-decker shaped silsesquioxanes bearing unhindered styryl or p-bromophenyl substituents on the silicon vertices. Chapter 6, the

final chapter of this dissertation, sums up the findings in this study and outlines recommendations for future studies based on our results.

REFERENCES

REFERENCES

- (1) Voronkov M.G., Lavrent'yev V.I. Polyhedral oligosilsesquioxanes and their homo derivatives. In: Inorganic Ring Systems. *Topics in Current Chemistry*, **1982**, 102. Springer, Berlin, Heidelberg.
- (2) Li, G., Wang, L., Ni, H. et al. Polyhedral Oligomeric Silsesquioxane (POSS) Polymers and Copolymers: A Review. *J. Inorg. Organomet. Polym.* **2001**, 11, 123–154.
- (3) Li, G.; Pittman, C. U. Polyhedral Oligomeric Silsesquioxane (POSS) Polymers, Copolymers, and Resin Nanocomposites. *Macromolecules Containing Metal and Metal-Like Elements*; John A Wiley & Sons: Hoboken, NJ, **2005**; 79– 131.
- (4) Phillips, S. H.; Haddad, T. S.; Tomczak, S. J. Developments in Nanoscience: Polyhedral Oligomeric Silsesquioxane (POSS) – *Polym. / Curr. Opin. Solid State Mater. Sci.* **2004**, 8, 21–29.
- (5) Scott, D. W. Thermal Rearrangement of Branched-Chain Methylpolysiloxanes. *J. Am. Chem. Soc.* **1946**, 68, 356–358.
- (6) Barry, A. J.; Daudt, W. H.; Domicone, J. J.; Gilkey, J. W. Crystalline Organosilsesquioxanes. *J. Am. Chem. Soc.* **1955**, 77, 4248–4252.
- (7) Cordes, D. B.; Lickiss, P. D. ChemInform Abstract: Preparation and Characterization of Polyhedral Oligosilsesquioxanes. *ChemInform.* **2013**, 47–133.
- (8) Jennings, A. R.; Iacono, S. T.; Mabry, J. M. Polyhedral Silsesquioxanes. In *Handbook of Sol-Gel Science and Technology: Processing, Characterization and Applications*; Klein, L., Aparicio, M., Jitianu, A., Eds.; *Springer International Publishing: Cham*, **2018**; 3153–3176.
- (9) Hartmann-Thompson, C. Applications of Polyhedral Oligomeric Silsesquioxanes; *Springer Science & Business Media*, **2011**, 247–325.
- (10) Dudziec, B.; Żak, P.; Marciniak, B. Synthetic Routes to Silsesquioxane-Based Systems as Photoactive Materials and Their Precursors. *Polym.* **2019**, 504.
- (11) Kuo, S.-W.; Chang, F.-C. POSS Related Polymer Nanocomposites. *Prog. Polym. Sci.* **2011**, 36, 1649–1696.

- (12) Cordes, D. B.; Lickiss, P. D.; Rataboul, F. Recent Developments in the Chemistry of Cubic Polyhedral Oligosilsesquioxanes. *Chem. Rev.* **2010**, *110*, 2081–2173.
- (13) Laine, R. M. Nanobuilding Blocks Based on the $[\text{OSiO}_{1.5}]_x$ ($x = 6, 8, 10$) Octasilsesquioxanes. *J. Mater. Chem.* **2005**, *15*, 3725–3744.
- (14) Feher, F. J.; Wyndham, K. D.; Soulivong, D.; Nguyen, F. Syntheses of Highly Functionalized Cube-Octameric Polyhedral Oligosilsesquioxanes ($\text{R}_8\text{Si}_8\text{O}_{12}$). *J. Chem. Soc., Dalton Trans.*, **1999**, 1491–1498.
- (15) Bassindale, A. R.; Gentle, T. E. Siloxane and Hydrocarbon Octopus Molecules with Silsesquioxane Cores. *J. Mater. Chem.* **1993**, 1319–1325.
- (16) Agaskar, P. A. New Synthetic Route to the Hydridospherosiloxanes $\text{O}_h\text{-H}_8\text{Si}_8\text{O}_{12}$ and $\text{D}_{5h}\text{-H}_{10}\text{Si}_{10}\text{O}_{15}$. *Inorg. Chem.* **1991**, *30*, 2707–2708.
- (17) Scheschkewitz, D. Functional Molecular Silicon Compounds I: Regular Oxidation States; *Springer*, **2014**.
- (18) Lickiss, P. D.; Rataboul, F. Fully Condensed Polyhedral Oligosilsesquioxanes (POSS): From Synthesis to Application. *Adv. Organomet. Chem.* **2008**, *57*, 1.
- (19) Brown, J. F.; Vogt, L. H. The Polycondensation of Cyclohexylsilanetriol. *J. Am. Chem. Soc.* **1965**, 4313–4317.
- (20) Behbehani, H.; Brisdon, B. J.; Mahon, M. F.; Molloy, K. C. The Structure of Hexa(cyclohexylsilsesquioxane), $(\text{C}_6\text{H}_{11})_6\text{Si}_6\text{O}_9$. *J. Organometal. Chem.* **1994**, *469*, 19–23.
- (21) Feher, F. J.; Newman, D. A.; Walzer, J. F. Silsesquioxanes as Models for Silica Surfaces. *J. Am. Chem. Soc.* **1989**, *111*, 1741–1748.
- (22) Bassindale, A. R.; Chen, H.; Liu, Z.; MacKinnon, I. A.; Parker, D. J.; Taylor, P. G.; Yang, Y.; Light, M. E.; Horton, P. N.; Hursthouse, M. B. A Higher Yielding Route to Octasilsesquioxane Cages Using Tetrabutylammonium Fluoride, Part 2: Further Synthetic Advances, Mechanistic Investigations and X-Ray Crystal Structure Studies into the Factors That Determine Cage Geometry in the Solid State. *J. Organometal. Chem.* **2004**, *689*, 3287–3300.
- (23) Bassindale, A. R.; Parker, D. J.; Pourny, M.; Taylor, P. G.; Horton, P. N.; Hursthouse, M. B. Fluoride Ion Entrapment in Octasilsesquioxane Cages as Models for Ion Entrapment in Zeolites. Further Examples, X-Ray Crystal Structure Studies, and

Investigations into How and Why They May Be Formed. *Organometallics*. **2004**, 23, 4400–4405.

(24) Li, Z.; Kawakami, Y. Formation of Incompletely Condensed Oligosilsesquioxanes by Hydrolysis of Completely Condensed POSS via Reshuffling. *Chem. Lett.* **2008**, 37, 804–805.

(25) Feher, F. J.; Terroba, R.; Jin, R.-Z. Controlled Partial Hydrolysis of Spherosilicate Frameworks: Syntheses of Endo-[(Me₃SiO)₆Si₆O₇(OH)₄] and Endo-[(Me₃SiO)₆Si₆O₇OSiMe₂(CH=CH₂)₄] from [(Me₃SiO)₆Si₆O₉]. *Chem. Commun.* **1999**, 2513–2514.

(26) Feher, F. J.; Terroba, R.; Ziller, J. W. A New Route to Incompletely-Condensed Silsesquioxanes: Base-Mediated Cleavage of Polyhedral Oligosilsesquioxanes. *Chem. Commun.* **1999**, 2309–2310.

(27) Feher, F. J.; Terroba, R.; Ziller, J. W. Base-Catalyzed Cleavage and Homologation of Polyhedral Oligosilsesquioxanes. *Chem. Commun.* **1999**, 2153–2154.

(28) Wu, S.; Hayakawa, T.; Kikuchi, R.; Grunzinger, S. J.; Kakimoto, M.-A.; Oikawa, H. Synthesis and Characterization of Semiaromatic Polyimides Containing POSS in Main Chain Derived from Double-Decker-Shaped Silsesquioxane. *Macromolecules* **2007**, 40, 5698–5705.

(29) Ohno, K.; Sugiyama, S.; Koh, K.; Tsujii, Y.; Fukuda, T.; Yamahiro, M.; Oikawa, H.; Yamamoto, Y.; Ootake, N.; Watanabe, K. Living Radical Polymerization by Polyhedral Oligomeric Silsesquioxane-Holding Initiators: Precision Synthesis of Tadpole-Shaped Organic/Inorganic Hybrid Polymers. *Macromolecules* **2004**, 37, 8517–8522.

(30) Feher, F. J.; Soulivong, D.; Lewis, G. T. Facile Framework Cleavage Reactions of a Completely Condensed Silsesquioxane Framework. *J. Am. Chem. Soc.* **1997**, 119, 11323–11324.

(31) Lichtenhan, J.; Otonari, Y. A.; Carr, M. J. Linear Hybrid Polymer Building Blocks: Methacrylate-Functionalized Polyhedral Oligomeric Silsesquioxane Monomers and Polymers. *Macromolecules* **1995**, 28, 8435–8437.

(32) Feher, F. J.; Budzichowski, T. A.; Weller, K. J. Polyhedral Aluminosilsesquioxanes: Soluble Organic Analogs of Aluminosilicates. *J. Am. Chem. Soc.* **1989**, 111, 7288–7289.

(33) Chandrasekhar, V.; Murugavel, R.; Voigt, A.; Roesky, H. W.; Schmidt, H.-G.; Noltemeyer, M. Cyclic and Polyhedral Aluminosiloxanes with Al₂Si₂O₄, Al₄Si₂O₆, and Al₄Si₄O₁₂ Frameworks: X-Ray Crystal Structures of [(2,4,6-Me₃C₆H₂)N(SiMe₃)Si(OAlⁱBu-

$(\text{OAl}(\text{iBu})_2\text{O})_2$ and $[(2,6\text{-Me}_2\text{C}_6\text{H}_3)\text{N}(\text{SiMe}_3)\text{SiO}_3\text{Al-C}_4\text{H}_8\text{O}_2]_4$. *Organometallics* **1996**, *15*, 918–922.

(34) Feher, F. J.; Walzer, J. F.; Blanski, R. L. Olefin Polymerization by Vanadium-Containing Polyhedral Oligometallasilasesquioxanes. *J. Am. Chem. Soc.* **1991**, *113*, 3618–3619.

(35) Feher, F. J.; Blanski, R. L. Polyhedral Oligometallasilasesquioxanes as Models for Silica-Supported Catalysts: Chromium Attached to Two Vicinal Siloxy Groups. *J. Chem. Soc., Chem. Commun.* **1990**, 1614–1616.

(36) Buys, I. E.; Hambley, T. W.; Houlton, D. J.; Maschmeyer, T.; Masters, A. F.; Smith, A. K. Models of Surface-Confined Metallocene Derivatives. *J. Mol. Catal.* **1994**, *86*, 309–318.

(37) Ruffieux, V.; Schmid, G.; Braunstein, P.; Rosé, J.; Braunstein, P.; Rosé, J. Oligosilasesquioxane-8-OSS-Ethyldiphenylphosphine: A New Functional Oligosilasesquioxane Ligand. *J. Chem. Eur.* **1997**, *3*, 900–903.

(38) Abbenhuis, H. C. L.; van Herwijnen, H. W. G.; van Santen, R. A. Macromolecular Materials in Heterogeneous Catalysis: An Aluminium Silasesquioxane Gel as Active Catalyst in Diels–Alder Reactions of Enones. *Chem. Commun.* **1996**, 1941–1942.

(39) Feher, F. J.; Budzichowski, T. A.; Blanski, R. L.; Weller, K. J.; Ziller, J. W. Facile Syntheses of New Incompletely Condensed Polyhedral Oligosilasesquioxanes: $[(\text{C-C}_5\text{H}_9)_7\text{Si}_7\text{O}_9(\text{OH})_3]$, $[(\text{C-C}_7\text{H}_{13})_7\text{Si}_7\text{O}_9(\text{OH})_3]$, and $[(\text{C-C}_7\text{H}_{13})_6\text{Si}_6\text{O}_7(\text{OH})_4]$. *Organometallics* **1991**, *10*, 2526–2528.

(40) Delmas, L. C.; Horton, P. N.; White, A. J. P.; Coles, S. J.; Lickiss, P. D.; Davies, R. P. Siloxane-Based Linkers in the Construction of Hydrogen Bonded Assemblies and Porous 3D MOFs. *Chem. Commun.* **2017**, *53*, 12524–12527.

(41) Voronkov, M. G.; Lavrent'yev, V. I. Polyhedral Oligosilasesquioxanes and Their Homo Derivatives. In *Inorganic Ring Systems*; Springer Berlin Heidelberg, **1982**; 199–236.

(42) Rossow T., Seiffert S. Supramolecular Polymer Networks: Preparation, Properties, and Potential. In: Seiffert S. (eds) *Supramolecular Polymer Networks and Gels. Adv. Polym. Sci.* **2015**, *268*, 1–46. Springer, Cham.

(43) Kahn, A.; Koch, N.; Gao, W. *J Polym Sci Part B: Polym Phys* **2003**, *41*, 2529–2548, Wiley Periodicals.

- (44) Kannan, R. Y.; Salacinski, H. J.; Sales, K. M.; Butler, P. E.; Seifalian, A. M. The Endothelialization of Polyhedral Oligomeric Silsesquioxane Nanocomposites: An In Vitro Study. *Cell Biochem Biophys* **2006**, *45*, 129–136.
- (45) Feher, F. J.; Phillips, S. H.; Ziller, J. W. Facile and Remarkably Selective Substitution Reactions Involving Framework Silicon Atoms in Silsesquioxane Frameworks. *J. Am. Chem. Soc.* **1997**, *119*, 3397–3398.
- (46) Li, G.; Wang, L.; Ni, H.; Pittman, C. U., Jr. J. Inorg. Organomet. *Polym.* **2001**, *11*, 123–154.
- (47) Mather, P. T.; Jeon, H. G.; Romo-Uribe, A.; Haddad, T. S.; Lichtenhan, J. D. Mechanical Relaxation and Microstructure of Poly(norbornyl-POSS) Copolymers. *Macromolecules*. **1999**, *32*, 1194–1203.
- (48) Xu, H.; Kuo, S.-W.; Lee, J.-S.; Chang, F.-C. Glass Transition Temperatures of Poly(hydroxystyrene-Co-Vinylpyrrolidone-Co-Isobutylstyryl Polyhedral Oligosilsesquioxanes). *Polymer* **2002**, *43*, 5117–5124.
- (49) Milliman, H. W.; Ishida, H.; Schiraldi, D. A. Structure Property Relationships and the Role of Processing in the Reinforcement of Nylon 6-POSS Blends. *Macromolecules* **2012**, *45*, 4650–4657.
- (50) Morimoto, Y.; Watanabe, K.; Ootake, N.; Inagaki, J. I.; Yoshida, K.; Ohguma, K. Silsesquioxane Derivatives and Process for Production Thereof. 20040249103A1. December **2004**.
- (51) Lee, D. W.; Kawakami, Y. Incompletely Condensed Silsesquioxanes: Formation and Reactivity. *Polym. J.* **2007**, *39*, 230–238.
- (52) Schoen, B. W. Aminophenyl Double Decker Silsesquioxanes: Spectroscopic Elucidation, Physical and Thermal Characterization, and Their Applications. Ph. D. ProQuest Dissertations Publishing, **2013**. 35993163599316.
- (53) Ervithayasuporn, V.; Sodkhomkhum, R.; Teerawatananond, T.; Phurat, C.; Phinyocheep, P.; Somsook, E.; Osotchan, T. Unprecedented Formation Of cis- And trans- Di[(3-Chloropropyl)isopropoxysilyl]-Bridged Double-Decker Octaphenylsilsesquioxanes. *Eur. J. Inorg. Chem.* **2013**, 3292–3296.
- (54) Hoque, M. A.; Kakihana, Y.; Shinke, S.; Kawakami, Y. Polysiloxanes with Periodically Distributed Isomeric Double-Decker Silsesquioxane in the Main Chain. *Macromolecules* **2009**, *42*, 3309–3315.

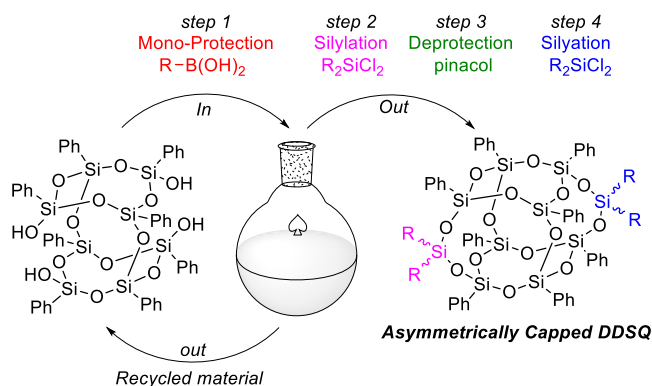
- (55) Cao, J.; Fan, H.; Li, B.-G.; Zhu, S. Synthesis and Evaluation of Double-Decker Silsesquioxanes as Modifying Agent for Epoxy Resin. *Polymer*, **2017**, 124, 157–167.
- (56) Xu, S.; Zhao, B.; Wei, K.; Zheng, S. Organic-Inorganic Polyurethanes with Double Decker Silsesquioxanes in the Main Chains: Morphologies, Surface Hydrophobicity, and Shape Memory Properties. *J. Polym. Sci. Part B: Polym. Phys.* **2018**, 893–906.
- (57) Liu, N.; Wei, K.; Wang, L.; Zheng, S. Organic–inorganic Polyimides with Double Decker Silsesquioxane in the Main Chains. *Polym. Chem.* **2016**, 7, 1158–1167.
- (58) Wei, K.; Wang, L.; Zheng, S. Organic–inorganic Polyurethanes with 3,13-Dihydroxypropyloctaphenyl Double-Decker Silsesquioxane Chain Extender. *Polym. Chem.* **2013**, 4, 1491–1501.
- (59) Morimoto, Y.; Watanabe, K.; Ootake, N. Silsesquioxane Derivative and Process for Producing the Same, US7319129B2, **2008**.
- (60) Dudziec, B.; Marciniak, B. Double-Decker Silsesquioxanes: Current Chemistry and Applications. *Curr. Org. Chem.* **2017**, 21, 2794–2813.
- (61) Wei, K.; Wang, L.; Li, L.; Zheng, S. Synthesis and Characterization of Bead-like Poly(N -Isopropylacrylamide) Copolymers with Double Decker Silsesquioxane in the Main Chains. *Polym. Chem.* **2015**, 6, 256–269.
- (62) Wu, S.; Hayakawa, T.; Kakimoto, M.-A.; Oikawa, H. Synthesis and Characterization of Organosoluble Aromatic Polyimides Containing POSS in Main Chain Derived from Double-Decker-Shaped Silsesquioxane. *Macromolecules* **2008**, 41, 3481–3487.
- (63) Hao, J.; Wei, Y.; Chen, B.; Mu, J. Polymerization of Polyhedral Oligomeric Silsesquioxane (POSS) with Perfluoro-Monomers and a Kinetic Study. *RSC Adv.* **2017**, 7, 10700–10706.
- (64) Schoen, B. W.; Holmes, D.; Lee, A. Identification and Quantification of Cis and Trans Isomers in Aminophenyl Double-Decker Silsesquioxanes Using ^1H - ^{29}Si gHMBC NMR. *Magn. Reson. Chem.* **2013**, 51, 490–496.
- (65) Walczak, M.; Januszewski, R.; Majchrzak, M.; Kubicki, M.; Dudziec, B.; Marciniak, B. Unusual Cis and Trans Architecture of Dihydrofunctional Double-Decker Shaped Silsesquioxane and Synthesis of Its Ethyl Bridged π -Conjugated Arene Derivatives. *New J. Chem.* **2017**, 41, 3290–3296.

- (66) Schoen, B. W.; Lira, C. T.; Lee, A. Separation and Solubility of Cis and Trans Isomers in Nanostructured Double-Decker Silsesquioxanes. *J. Chem. Eng. Data* **2014**, *59*, 1483–1493.
- (67) Vogelsang, D. F.; Maleczka, R. E.; Lee, A. HPLC Characterization of Cis and Trans Mixtures of Double-Decker Shaped Silsesquioxanes. *Silicon Chem.* **2019**, *11*, 5–13.
- (68) Seino, M.; Hayakawa, T.; Ishida, Y.; Kakimoto, M.-A.; Watanabe, K.; Oikawa, H. Hydrosilylation Polymerization of Double-Decker-Shaped Silsesquioxane Having Hydrosilane with Diynes. *Macromolecules* **2006**, *39*, 3473–3475.
- (69) Hoque, M. A.; Kawakami, Y. Synthesis of Polysilsesquioxanes with Double-Decker Silsesquioxane Repeating Units. *J. Sci. Res.* **2016**, *8*, 217–227.
- (70) Žak, P.; Dudziec, B.; Dutkiewicz, M.; Ludwiczak, M.; Marciniec, B.; Nowicki, M. A New Class of Stereoregular Vinylene-Arylene Copolymers with Double-Decker Silsesquioxane in the Main Chain. *J. Polym. Sci. Part A: Polym. Chem.* **2016**, *54*, 1044–1055.
- (71) Moore, L. M. J.; Zavala, J. J.; Lamb, J. T.; Reams, J. T.; Yandek, G. R.; Guenther, A. J.; Haddad, T. S.; Ghiassi, K. B. Bis-Phenylethynyl Polyhedral Oligomeric Silsesquioxanes: New High-Temperature, Processable Thermosetting Materials. *RSC Adv.* **2018**, *8*, 27400–27405.
- (72) Seurer, B.; Vij, V.; Haddad, T.; Mabry, J. M.; Lee, A. Thermal Transitions and Reaction Kinetics of Polyhedral Silsesquioxane Containing Phenylethynyl- phthalimides. *Macromolecules* **2010**, *43*, 9337–9347.
- (73) Jiang, Q.; Zhang, W.; Hao, J.; Wei, Y.; Mu, J.; Jiang, Z. A Unique “cage–cage” Shaped Hydrophobic Fluoropolymer Film Derived from a Novel Double-Decker Structural POSS with a Low Dielectric Constant. *J. Mater. Chem.* **2015**, *3*, 11729–11734.
- (74) Liu, N.; Li, L.; Wang, L.; Zheng, S. Organic-Inorganic Polybenzoxazine Copolymers with Double Decker Silsesquioxanes in the Main Chains: Synthesis and Thermally Activated Ring-Opening Polymerization Behavior. *Polymer* **2017**, *109*, 254–265.
- (75) Kucuk, A. C.; Matsui, J.; Miyashita, T. Langmuir–Blodgett Films Composed of Amphiphilic Double-Decker Shaped Polyhedral Oligomeric Silsesquioxanes. *J. Colloid Interface Sci.* **2011**, *355*, 106–114.
- (76) Díaz, U.; Brunel, D.; Corma, A. Catalysis Using Multifunctional Organosiliceous Hybrid Materials. *Chem. Soc. Rev.* **2013**, *42*, 4083–4097.

CHAPTER 2.0: Synthesis of Asymmetrically Functionalized Double-Decker

Shaped Silsesquioxanes

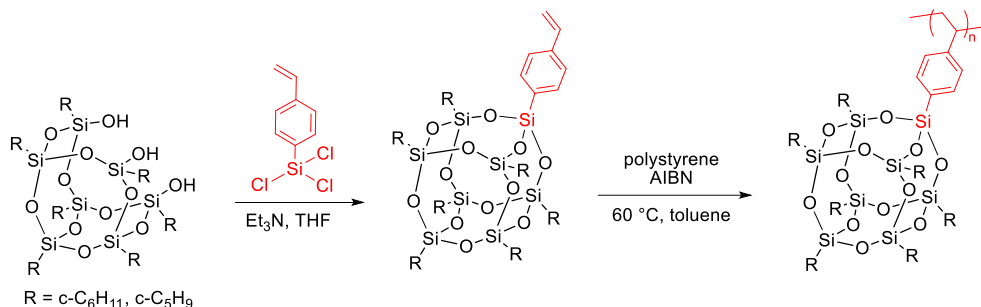
Parts of this chapter are published under the title “A general diversity-oriented synthesis of asymmetric double-decker shaped silsesquioxanes” with the following citation: Barry, B.-D.; Dannatt, J. E.; King, A. K.; Lee, A.; Maleczka Jr., R. E. *Chem. Commun.*, **2019**, 55, 8623–8626.



2.1 Introduction

Silsesquioxanes have attracted significant research interest for the synthesis of materials with properties that meet medicinal, synthetic, industrial and materials science demands.^{1–4} Over the years, explorations in this field have been dominated by the manipulation of cubic-like silsesquioxanes for the synthesis of hybrid polymers.^{2,5–7} This is due to the well-defined spatial dimensions, the presence of seven relatively inert peripheral organic moieties to accommodate solubility and processability, and one polymerizable reactive organic group.^{8–14} Such silsesquioxane frameworks are accessed by corner-capping incompletely condensed R_7 -trisilanol POSS with R' -trichlorosilanes.^{12–16} The resulting condensed structure bears a polymerizable R' group that can be incorporated as a pendant nanostructure to a linear polymer chain.

Scheme 2-1: Styryl-POSS macromonomer synthesis and its polymerization¹²



After the first synthesis of DDSQ-tetraol (1),^{17,18} two reactive edges could be accessed via the condensation of 1 with various chlorosilane capping agents.^{8,19,20}

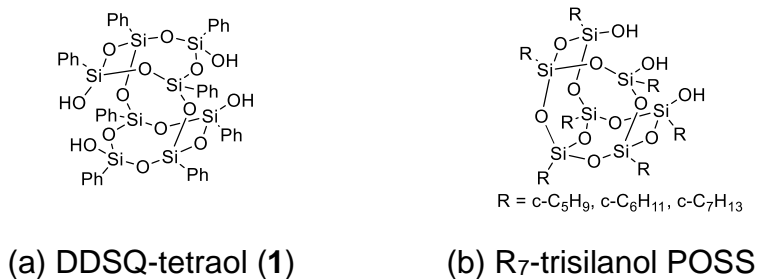
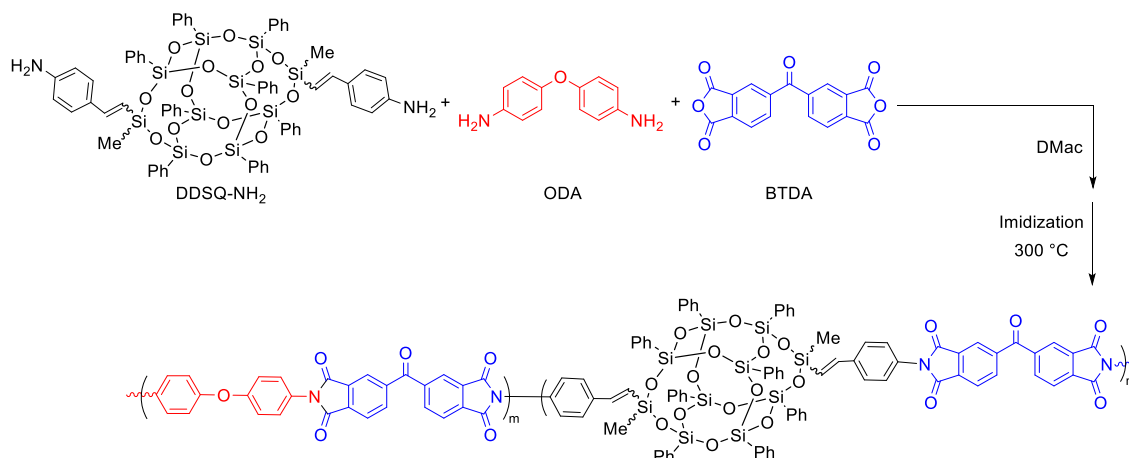


Figure 2-1: Double-decker oligomeric silsesquioxane tetraol (1) and (b) R₇-trisilanol POSS

Unlike the monofunctionalized POSS where the nano-precursor acts as a pendant, this framework allows incorporation into a linear polymer backbone (**Scheme 2-2**).^{21–24} Incorporating silsesquioxanes in this manner may provide more effective retardation to the backbone motion of a linear polymer, which in turn could allow a more efficient approach to property enhancement.^{23–26}

Scheme 2-2: Synthesis of organic–inorganic polyimide with DDSQ in the main chain²³

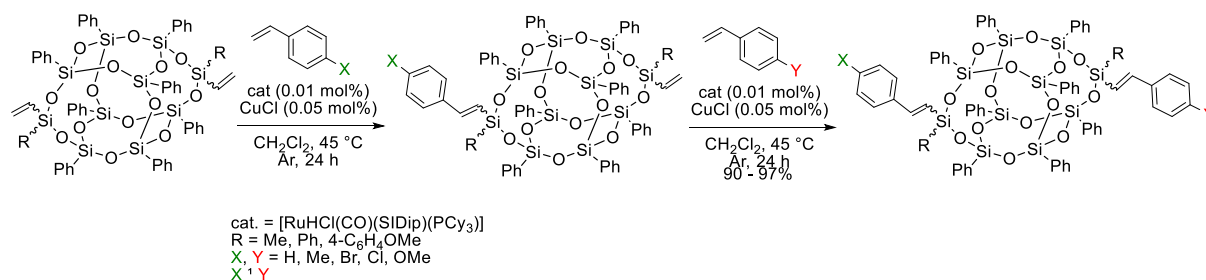


It is noteworthy, however, that in all the cases above the two lengths of polymer bridged by the silsesquioxane linker are from the same monomer. This results from the fact that DDSQ tetraol is symmetrically capped. We believe that silsesquioxanes bridging two distinct polymers will offer an interesting new class of materials. To produce and explore such materials requires the symmetry in **1** to be broken. Certainly, synthetically

accessing such asymmetric DDSQ systems presents a significant challenge due to the nanometer scale distance between capping sites.

Recently, two routes to asymmetric DDSQs have been reported. In 2018 the Zak and Marciniec team developed an olefin metathesis catalyst able to selectively couple one vinyl group on a symmetrically capped divinyl-substituted DDSQ with various styrene derivatives.²⁷ After this mono-functionalization, a second styrene derivative was added to afford an asymmetric AB system (**Scheme 2-3**).

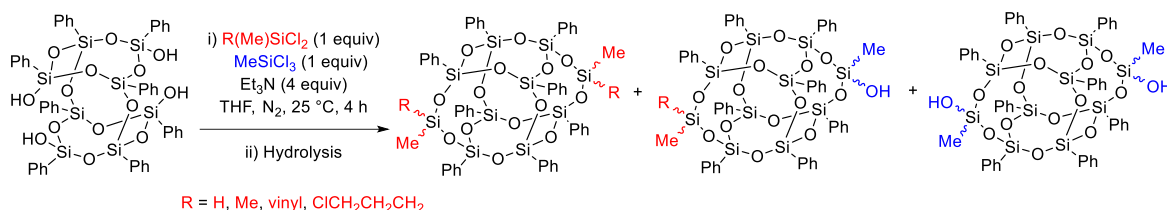
Scheme 2-3: Ruthenium catalyzed silylative coupling of divinyl-substituted silsesquioxanes DDSQ-2ViSi with two different styrenes



While this ground-breaking work effectively provided an AB system, major limitations include the necessity of the vinyl and styryl coupling partners, the requirement of ruthenium-based catalyst and lack of a reason for asymmetry. A more general synthetic route must be one that is amenable to a broader range of functionalities. Thus, in our previous attempt to develop a methodology that supports a diverse array of functional groups we explored the capping of DDSQ tetraol with a premixture of two chlorosilanes.²⁸ In that study, we demonstrated that the AB system could be isolated if one of the chlorosilanes is a trichloromethylsilane. The latter upon workup, provided a silane and the

resultant polarity difference between the symmetric by-products and the desired asymmetric system enabling separation by HPLC (**Scheme 2-4**).

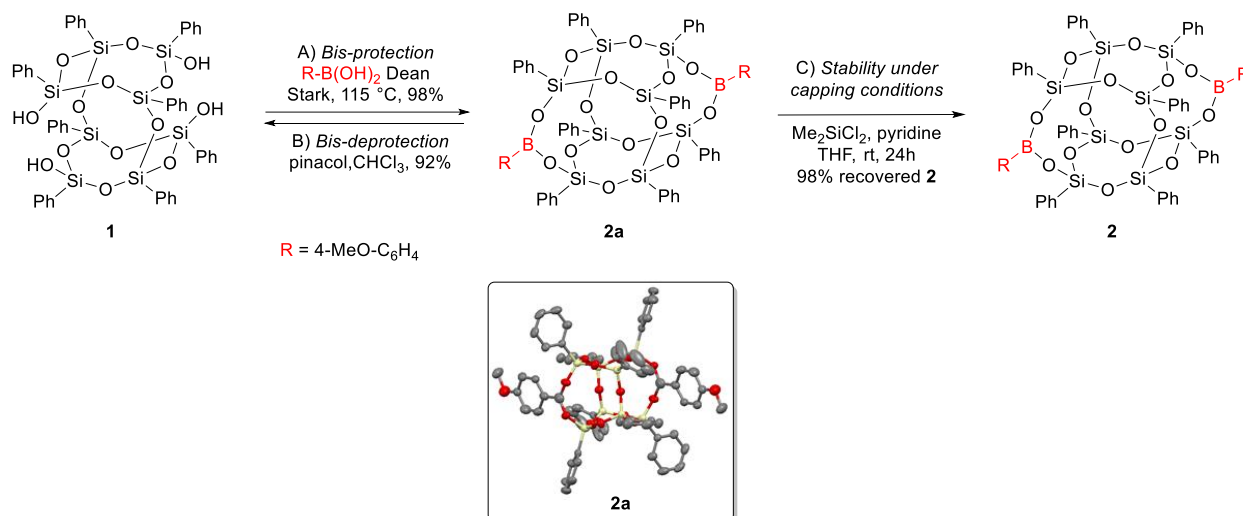
Scheme 2-4: Side capping of DDSQ tetraol with two different chlorosilanes



Again, this technique was limited in that it requires HPLC and is thus scale limited, it generated significant symmetric by-product waste, and it required differences in polarity between the by-products and desired asymmetric material.

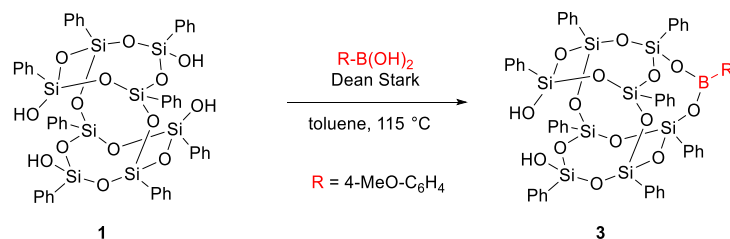
To improve on current methodologies, we sought a synthetic route where all chlorosilane capping agents are tolerated, excess DDSQ tetraol can be recovered then recycled, and symmetric by-products are minimized. To this end, a protecting group strategy was envisioned. If **1** could be mono protected by masking two silanol groups, silylation of the free silanol edge, followed by deprotection and capping with another chlorosilane would afford the desired asymmetric material. To achieve this goal, we first had to identify an effective protecting group. The desired protecting group would be able to protect two silanols simultaneously, be easily installed and removed without impacting the DDSQ framework and tolerate standard capping conditions (**Scheme 2-5**).

Scheme 2-5: (A) Bis-protection of DDSQ(OH)₄ (**1**) with a boronic acid, (B) bis-deprotection of **2** with pinacol, and (C) stability of boronic acid protecting group under standard silylation conditions



Once this is achieved, we can next seek optimal conditions that could lead to the mono-protected **1** (**Scheme 2-6**).

Scheme 2-6: Monoborylation of DDSQ(OH)₄ **1** with p-MeO-C₆H₄B(OH)₂



2.2 Results and Discussions

All reactions were followed using ^1H , ^{11}B , ^{13}C and ^{29}Si spectroscopy and the final asymmetric products were purified by flash chromatography. The isolated compounds were all characterized by ^1H , ^{11}B , ^{13}C and ^{29}Si NMR spectroscopy (**Appendix**). The asymmetrically functionalized DDSQs **6** were obtained almost exclusively with minor symmetric AA **7** and BB **8** by-products. The asymmetric products (**6**) are denoted AB implying that these products are composed of one of each of the A and B capping silyl groups. In addition to the spectral data, single X-ray crystal structures were obtained for all bis-borylated DDSQs (**Appendix**).

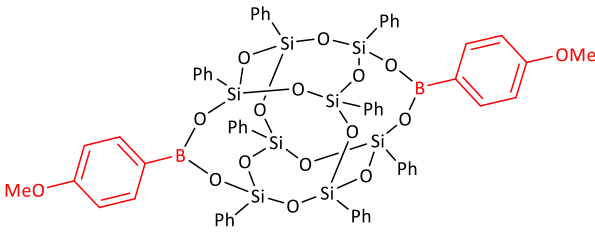

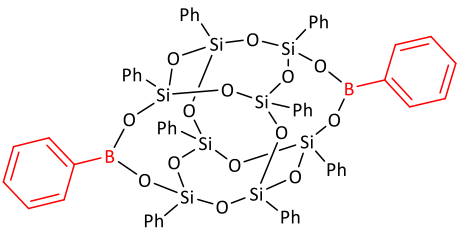
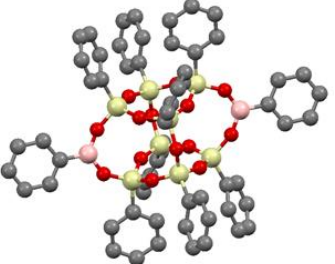
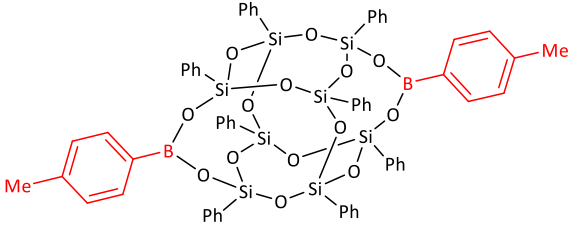

Table 2-1: Full Protection of DDSQ(OH)₄ **1** with p-substituted Phenylboronic Acid

Entry	RB(OH) ₂	Product 2	Isolated Yield (%)
1	<i>p</i> -MeO-C ₆ H ₄ B(OH) ₂	2a	98
2	C ₆ H ₄ B(OH) ₂	2b	95
3	<i>p</i> -Me-C ₆ H ₄ B(OH) ₂	2c	96

^aExperimental conditions: DDSQ tetraol **1** (2 mmol), RB(OH)₂ (5 mmol), toluene (40 mL), N₂, 115 °C, 24h

After initial evaluation it was found that **1** could be bis-protected with a variety of boronic acids under Dean-Stark conditions in high isolated yields. Among the boronic acids explored, 4-methoxyphenylboronic acid allowed simple spectroscopic analysis due to its distinct methoxy protons while also affording the highest yield of 98% (**entry 1**). Recrystallization of the bis-boronate DDSQ esters from DCM/hexane (1:3) provided single crystals suitable for X-ray analysis (**Table 2-2**).

Table 2-2: Crystal Structures of Bis-boronated DDSQ Esters **2** (Displacement ellipsoid contour probability drawn at 50%)

Entry	DDSQ Bis-Boronate Ester 2	Crystal Structure
1	 <p style="text-align: center;">2a</p>	 <p style="text-align: center;">2a</p>
2	 <p style="text-align: center;">2b</p>	 <p style="text-align: center;">2b</p>
3	 <p style="text-align: center;">2c</p>	 <p style="text-align: center;">2c</p>

2a: CCDC 1843217; **2b:** CCDC 1823844; **2c:** 1850462

Deborylation of **2** was achieved by stirring with pinacol providing a high yield of pure **1** (**Scheme 2-5B**). To our knowledge, this is the first report of a boronic acid used as a protecting group for silanols; however, borosiloxane cages have been reported.²¹ Excitingly, compound **2** was stable under the capping reaction conditions with one alteration. Using pyridine as opposed to the more common triethylamine provided a nearly quantitative recovery of bis-protected material (**Scheme 2-5C**). In our hands, pyridine had

no adverse effects on the capping of **1**. However, even with this development, it is worth mentioning that borylation of **1** for the synthesis of **3** afforded a mixture of borylated cages (**Scheme 2-9**) that were difficult to isolate in their pure forms. As a result, a pictorial outline (**Figure 2-2**) was designed for the multistep synthesis of the asymmetric compounds. The route consists of four (4) steps, viz: (i) Selective protection with boronic acid; (ii) First silylation with 'A' di-chlorosilane; (iii) Deprotection with pinacol and (iv) Second silylation with 'B' di-chlorosilane.

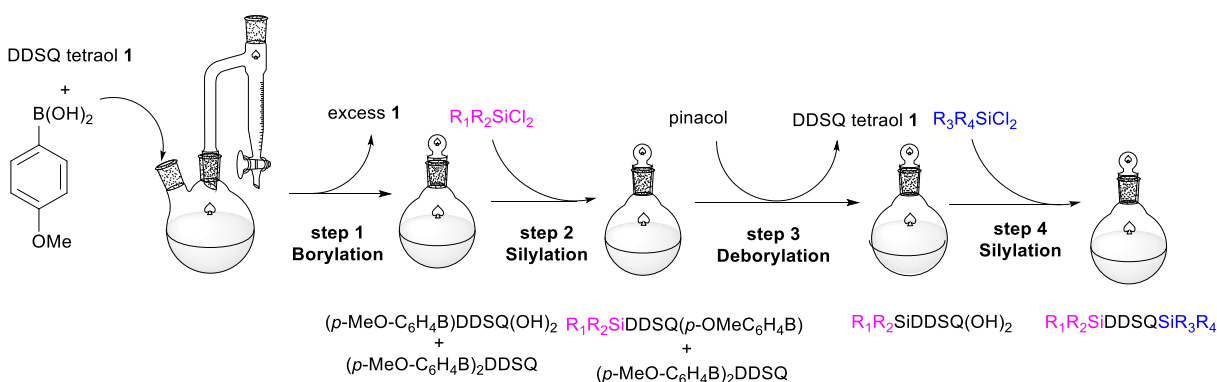


Figure 2-2: Designed Graphical Pathway to Asymmetrically Functionalized DDSQs

For this pathway to be effective by minimizing the generation of undesired symmetric products, the unreacted **1** in steps 1 and 3 must be quantitatively recovered.

2.2.1 Solubility of DDSQ(OH)_4 in Various Organic Solvents

DDSQ(OH)_4 **1** is least soluble in toluene (**Table 2-3, entry 3**) followed by chloroform (**Table 2-3, entry 2**) and is most soluble in acetone (**Table 2-3, entry 7**). However, because of the challenges to remove toluene from the reaction mixture owing to its high boiling point (111 °C), chloroform was chosen as the solvent for the deborylation in step 3. Unreacted **1** was efficiently recovered in both steps 1 and 3 by filtration due to the poor solubility of **1** in chloroform.

Table 2-3: Solubility Tests for DDSQ(OH)₄ (**1**) in Organic Solvents

Entry	solvent	wt. of empty vial (g)	wt. of vial + dry content	Solubility (g/10 mL)
1	CH ₂ Cl ₂	13.2020	13.2270	0.0250
2	CHCl ₃	13.1936	13.1994	0.0058
3	toluene	13.1035	13.1073	0.0038
4	DMF	13. 2058	13.3058	0.2000
5	EtOH	13.2432	13.3169	0.0737
6	MeOH	13.0843	13.0964	0.0121
7	acetone	13.0840	13.2640	0.1800

Reaction Conditions: DDSQ tetraol (0.2 g), solvent (10 mL), stir 2 min.

2.2.2 Optimization of the Selective Borylation for the Generation of (p-MeOC₆H₄B)DDSQ(OH)₂ **3**

With a suitable protecting group determined, optimal conditions leading to mono-protected **3** were sought (**Table 2-4**). Although all conditions screened could not exclusively afford mono-protected **1**, it was found that addition of 1 equivalent of p-MeO-C₆H₄B(OH)₂ under Dean-Stark conditions for 2 h afforded 42% recovered **1** and 58% of an inseparable mixture which by ¹H and ²⁹Si NMR spectroscopy consisted of mono-borylated **3** and bis-borylated **2** in a ratio of 1:3 (**Scheme 2-9**). While the ratio of compound **3** to compound **2** is not optimal, it was reasoned this mixture could be carried forward without significant loss of material as compound **2** could be recovered as starting material, **1**, after global deprotection (**Scheme 2-9**). Note that in both steps 1 and 3 (**Scheme 2-9**) compound **1** is recovered by filtration, which is enabled by its poor solubility in chloroform.

Table 2-4: Optimization of Monoboronate Ester Formation

Entry	p-MeOC ₆ H ₄ B(OH) ₂ (<i>'x'</i> equiv.)	Time (<i>'y'</i> h)	Rec'd DDSQ tetraol ^b (g)	Filtrate mass ^c (g)	mass loss ^d (g)	NMR ratio ^e mono:bis
1	0.1	1	0.47	0.08	0.00	2:1
2	0.2	1	0.43	0.11	0.01	2:1
3	0.3	1	0.41	0.14	0.00	1:1
4	0.4	1	0.36	0.19	0.00	1:2
5	0.5	1	0.34	0.20	0.01	1:2
6	0.5	2	0.26	0.29	0.00	2:5
7	0.5	4	0.27	0.27	0.01	1:4
8	0.5	8	0.27	0.28	0.00	1:3
9	0.5	18	0.21	0.34	0.00	2:5
10	0.5	24	0.17	0.38	0.00	1:4
11	1.0	1	0.31	0.24	0.00	1:7
12	1.0	2	0.22	0.31	0.02	1:11

^aExperimental conditions: DDSQ(OH)₄ **1** (0.53g, 0.51mmol), p-methoxyphenylboronic acid (*'x'* mmol), toluene (10 mL) nitrogen, 115 °C, *'y'* h. ^bRecovered DDSQ(OH)₄ **1** in grams; ^cMass of filtrate in grams; ^dLoss in mass of starting DDSQ(OH)₄ **1** in grams; ^eRatio of mono- to bis-borylated product based on crude ²⁹Si NMR.

2.2.3 Substrate Scope for Asymmetrically Functionalized Double-Decker Shaped Silsesquioxanes

Table 2-5: Scope for Asymmetrically Functionalized DDSQs

Entry	Asymmetric Product 6 ^a AB (6)	AA (7) By-products ^b	BB(8)	Recovered 1
1) $R_1 = \text{Me}$ $R_2 = \text{Me}$ $R_3 = \text{Me}$ $R_4 = \text{H}$	6a : 79% (22%)	7a : 2%	8a : 0%	62%
2) $R_1 = \text{Me}$ $R_2 = \text{Me}$ $R_3 = \text{Me}$ $R_4 = \text{OH}$	6b : 61% (16%)	7b : 4%	8b : 0%	66%
3) ^c $R_1 = \text{Me}$ $R_2 = \text{H}$ $R_3 = \text{Me}$ $R_4 = (3\text{-CNPr})$	6c : 52% (14%)	7c : 5%	8c : 6%	69%
4) $R_1 = \text{Me}$ $R_2 = \text{Me}$ $R_3 = \text{Me}$ $R_4 = (3\text{-CNPr})$	6d : 81% (21%)	7d : 4%	8d : 6%	71%
5) $R_1 = \text{Me}$ $R_2 = (3\text{-CNPr})$ $R_3 = \text{Me}$ $R_4 = \text{Me}$	6e : 74% (19%)	7e : 4%	8e : 5%	68%
6) ^c $R_1 = \text{Me}$ $R_2 = \text{vinyl}$ $R_3 = \text{Me}$ $R_4 = (3\text{-CNPr})$	6f : 65% (17%)	7f : 3%	8f : 6%	61%
7) ^c $R_1 = \text{Me}$ $R_2 = \text{vinyl}$ $R_3 = \text{Me}$ $R_4 = \text{H}$	6g : 50% (13%)	7g : 3%	8g : 2%	60%
8) ^c $R_1 = \text{Me}$ $R_2 = \text{H}$ $R_3 = \text{vinyl}$ $R_4 = \text{OH}$	6h : 68% (18%)	7h : 3%	8h : 0%	63%
9) ^c $R_1 = \text{Me}$ $R_2 = \text{vinyl}$ $R_3 = \text{isopropyl}$ $R_4 = \text{OH}$	6i : 56% (15%)	7i : 4%	8i : 0%	70%

^aYields reported are based on the calculated amount of compound **3** generated in step 1. Yields in parenthesis are based on the total amount of compounds **2** and **3** generated in step 1. ^bYields for **7** and **8** are based on the total amount of compounds **2** and **3** generated in step 1. The percentage of recovered **1** includes material from steps 1 and 3. ^cIsolated as a cis/trans mixture.

In our efforts to explore the scope of this multistep route, the reactions were scaled to DDSQ(OH)₄ **1** (1.96 mmol, 2 g), p-MeO-C₆H₄B(OH)₂ (1 equiv), chlorosilane (1 equiv based on **3**), pyridine (2 equiv based on **3**), and pinacol (1 equiv based on original p-MeO-C₆H₄B(OH)₂ added. With this route, the identity of the chlorosilanes used in steps 2 and 4 (**Scheme 2-13**) is unrestricted unlike prior synthetic routes.^{27,28} Overall, moderate to

high isolated yields were achieved with an average relative isolated yield of 65%. The high recovery of **1** is a key element of this strategy; namely the recyclability of compound **2** back to **1**. Symmetric by-products will only arise from inefficiencies in removing **1** in steps 1 and 3. Besides, the ^{29}Si NMR data is more informative. Spectra of compounds **6a–6i** exhibited six or eight characteristic peaks depending on if cis/trans isomers were present, and the high-resolution mass spectrometry are in excellent agreement with calculated theoretical molecular exact masses (**Appendix**). While some of the AB cages contain moieties that can serve as polymer end-cap groups (**6a**, **6b**, **6d**, **6e**, and **6i**), others possess moieties that enable them to bridge two distinct polymers (**6c**, **6f**, and **6g**). Asymmetric product **6h** is quite unique in that it bears three reactive polymerizable groups. Reversing the order in which chlorosilanes were added had little effect on isolated yields and had no observed effect on the amounts of symmetric by-products isolated (**6d** and **6e**). This experiment suggests the symmetric by-products can only be attributed to the small amounts of **1** passing through the filtration in steps 1 and 3 and is independent of the capping agent used. The variation of isolated symmetric materials throughout (**Table 2-5**) is attributed to the ability of the symmetric material to pass through the flash chromatography after the final step. It was observed that asymmetric products with a significant difference in polarity at the capping site afforded better yields of the isolated asymmetric products (**6b**, **6d**, **6e**, **6g**, and **6h**). This is not surprising as the success in separating the mixture by column chromatography relies on the interaction of the various components in the mixture with the stationary phase and the eluting solvent (mobile phase). It is also noteworthy that in **Table 2-5** (entries 2, 8, and 9) the corresponding symmetric by-product **8** was not isolated. This is likely because these symmetric products

are quite polar and thus will only slowly pass through the silica column. The symmetric product **8a** (entry 1), on the other hand, should readily pass through the silica. We expect in this case the mass of generated symmetric material may be low enough that it is difficult to detect.

2.2.4 Structural Analysis of Asymmetric DDSQs (6) by Si-NMR

In addition to literature reports and other spectroscopic data, the structures of the asymmetrically functionalized DDSQs were resolved by matching with spectra of symmetric products obtained from using the same capping agents as in the asymmetric products. The silicon atoms in each structure are numbered for clarity, with those in the same chemical environment bearing the same number.

6a: (1r,3R,11s,13S)-9,9,19-trimethyl-1,3,5,7,11,13,15,17-octaphenyl-2,4,6,8,10,12,14,16,18,20,21,22,23,24-tetradeca-oxa-1,3,5,7,9,11,13,15,17,19-decasilapentacyclo[11.7.1.13,11.15,17.17,15]tetracosane.

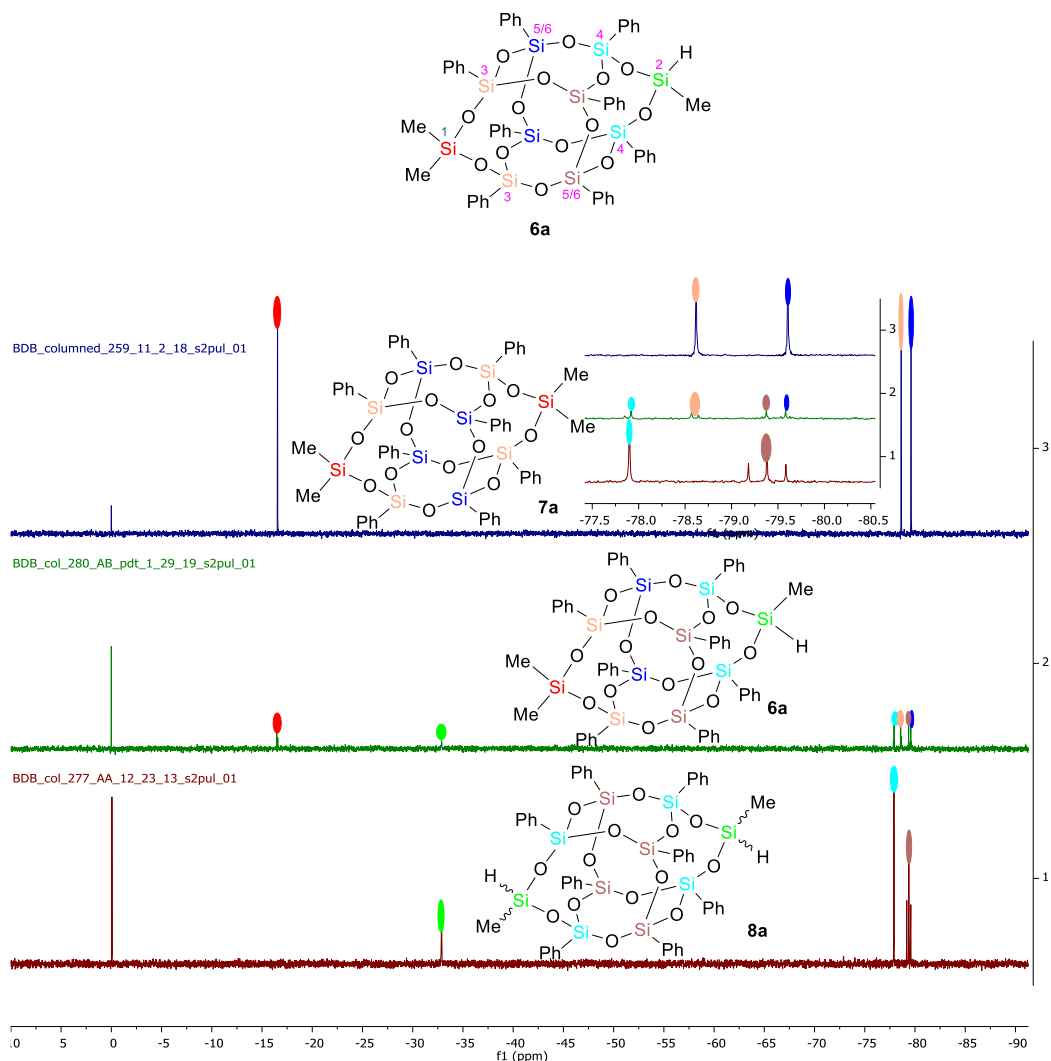


Figure 2-3: Stacked ^{29}Si NMR of AB **6a**, AA **7a** and BB **8a**

Spectra for **6a** $\text{C}_{51}\text{H}_{50}\text{Si}_{10}\text{O}_{14}$ reveals six (6) peaks characteristic of the chemically different Si atoms present in the structure. Figure 2-3 above shows a stacked spectrum of the symmetric tetramethyl capped cage (top), asymmetric AB **6a** (middle) and symmetric dimethyl dihydrido-capped DDSQ (bottom). Si#1 is the D-silicon with two Me substituents bridging one side of the DDSQ and shows up at -16.48 ppm. Si#2 is the other D-silicon with a methyl and hydrogen substituent capping the other end of the cage and

peaks at -32.87 ppm. The remaining Si atoms are T-silicons and as expected, have their chemical shifts in the T-silicon range (-77.8 to -79.8 ppm). Thus, by matching with the symmetric AA and BB cages, it can be delineated that the signal at -77.89 ppm denotes the two silicon atoms (Si#3) close to Si#2, and that at -78.61 ppm designate the two silicon atoms (Si#4) next to Si#1. The remaining signals between -79.28 to -79.74 represent the internal silicon (Si#5 and Si#6) that can interchange chemical shift values illustrating the different configurations of AB **6a** based on the orientation of the substituents on Si#1 and Si#2.

6b: (1*r*,3*R*,11*s*,13*S*)-9,19,19-trimethyl-1,3,5,7,11,13,15,17-octaphenyl-2,4,6,8,10,12,14,16,18,20,21,22,23,24-tetradeca-oxa-1,3,5,7,9,11,13,15,17,19-decasilapentacyclo[11.7.1.13,11.15,17.17,15]tetracosan-9-ol.

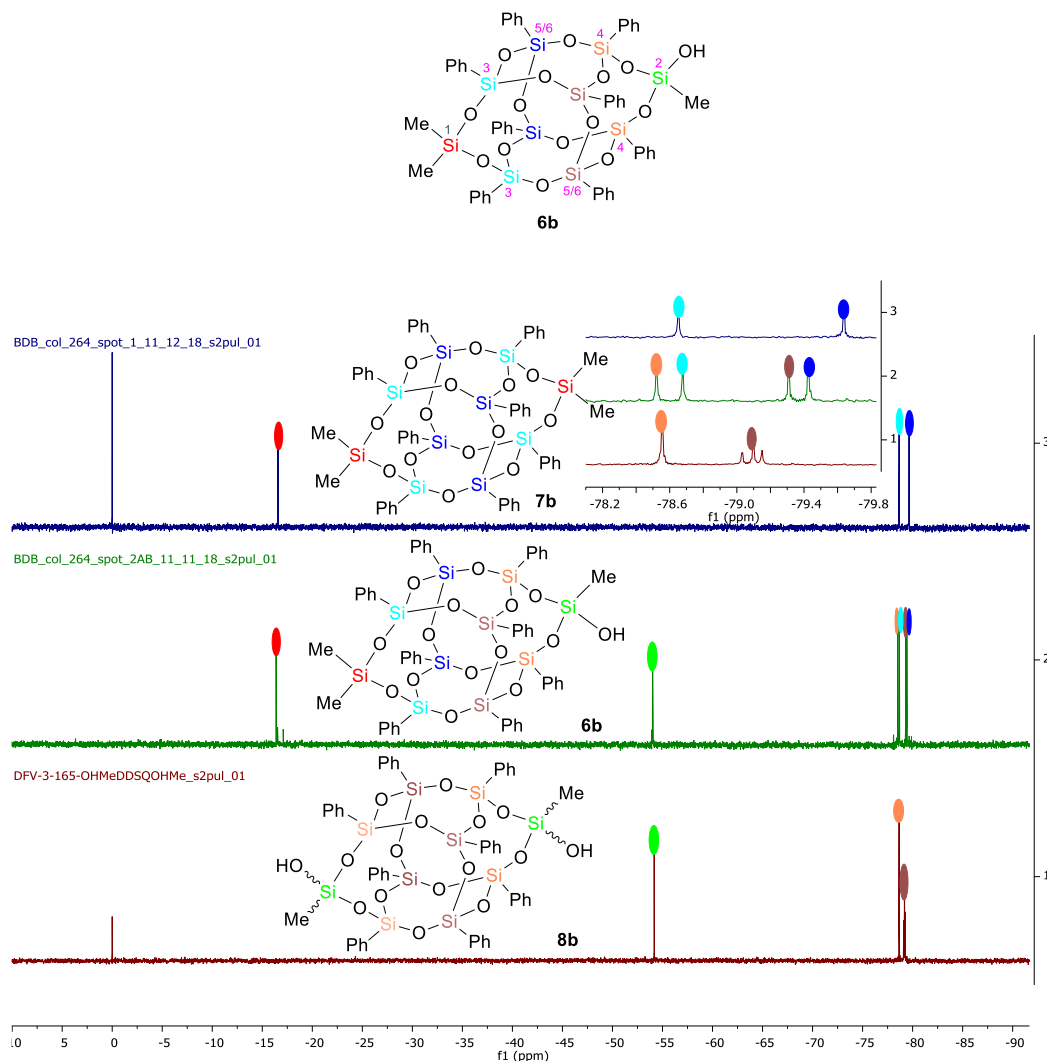


Figure 2-4: Stacked ^{29}Si NMR of AB **6b**, AA **7b** and BB **8b**

The ^{29}Si -NMR for AB **6b** $\text{C}_{51}\text{H}_{50}\text{Si}_{10}\text{O}_{15}$ shows six (6) peaks (**Figure 2-4**). The spectrum itself is stacked with that for the symmetric tetramethyl- AA **7b** and symmetric dimethyl-dihydroxyl-capped cages BB **8b**. The silicon atom having two methyl groups (Si#1), the only D-silicon in the structure, bridges one side of the DDSQ and appears upfield at -16.38 ppm. The other bridging group is a T-silicon bearing a free hydroxyl group (Si#2) gives a peak at -54.01 ppm (a region that is symbolic of Si atoms bearing

OH groups). The spectrum also indicates that the compound was isolated in its cis/trans form and thus, the environments of the remaining Si atoms can change depending on the orientation of the substituents on the capping chlorosilane, hence accounting for the remaining Si peaks in the -78.00 to -79.50 ppm region. The peak at -78.52 ppm represent the two T-silicon atoms (Si#3) bound to the $\text{Me}_2\text{SiO}_2^-$ group. That at -78.68 ppm (Si#4) denotes the other two T-silicon atoms linked to the $\text{Me}(\text{OH})\text{SiO}_2^-$ group. The remaining four Si-atoms (Si#5/6) are the four internal silicons that can assume two different environments based on the orientation of the substituents on Si#1 and Si#2. The cis configuration has the Me and OH groups on Si#1 and Si#2 on the same face.

6c: 4-((1*r*,3*R*,11*s*,13*S*)-9,19-dimethyl-1,3,5,7,11,13,15,17-octaphenyl-2,4,6,8,10,12,14,16,18,20,21,22,23,24-tetradecaoxa-1,3,5,7,9,11,13,15,17,19-decasilapentacyclo-[11.7.1.1.3,11.15,17.17,15]tetracosan-9-yl)butanenitrile.

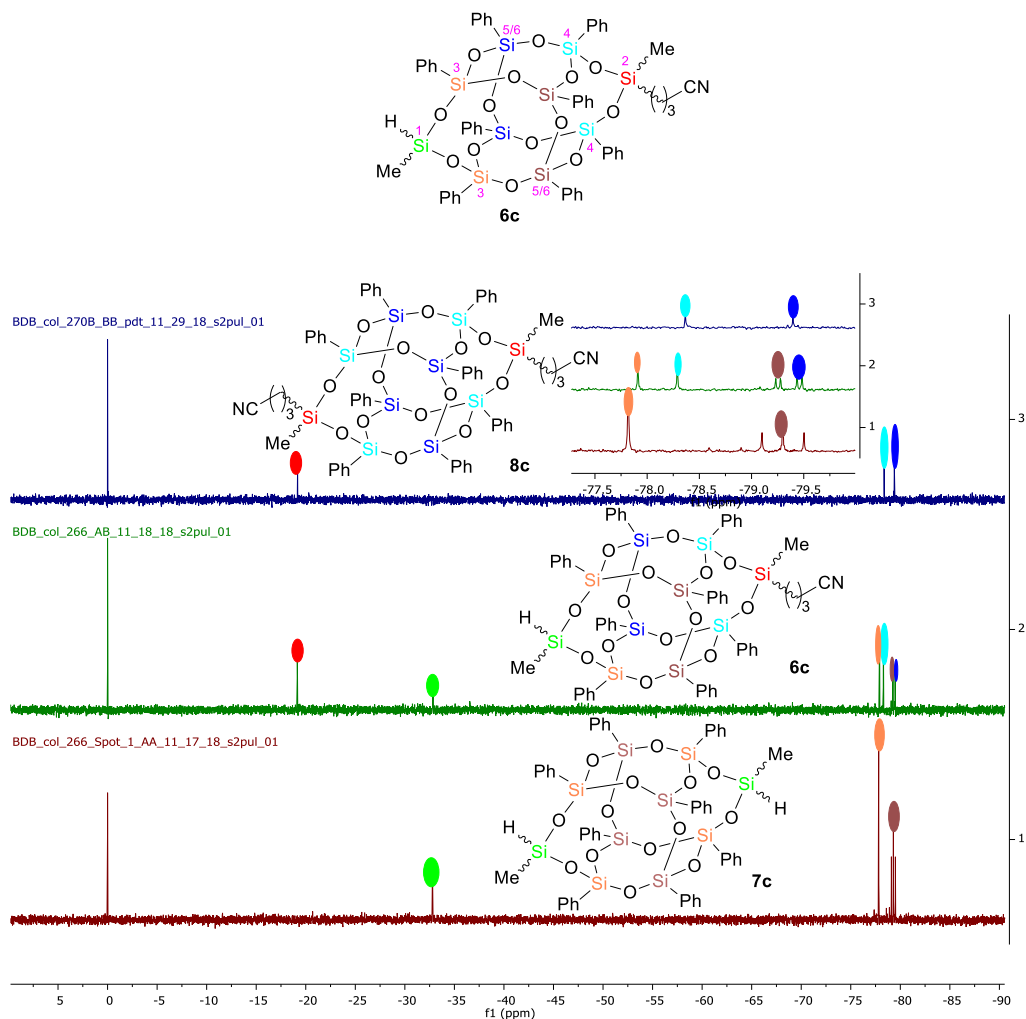


Figure 2-5: Stacked ^{29}Si NMR of AB **6c**, Symmetric AA **7c** and BB **8c**

AB **6c** $\text{C}_{54}\text{H}_{53}\text{Si}_{10}\text{NO}_{14}$ also has six (6) peaks, showing the different types of silicon atoms in the structure (**Figure 2-5**). AB **6c** (middle) is stacked with the symmetric AA (bottom) and BB (top) cages. For **6c**, the spectra show two D-silicons (Si#1 and Si#2), both appearing in the D-silicon region as expected. The silicon bonded to an Me and H groups (Si#1), appears upfield at -32.86 ppm and the other with the Me and 3-CNPr group (Si#2) appears downfield at -19.16 ppm. The spectra also illustrate that the compounds were isolated in their cis/trans forms. The environments of the remaining Si atoms can

thus change based on the orientation of the substituents on the capping chlorosilane as is shown by the signals between the -77.00 to -79.50 ppm region. Thus, the peak at -77.92 ppm (2Si) denotes Si#3, -78.30 ppm (2Si) Si#4, -79.24 ppm (1Si), signals at -79.29 ppm (1Si), -79.45 ppm (1Si), and -79.49 ppm (1Si) denotes one of each of the four internal silicons (Si#5 or Si#6 with cis/trans configuration),

6d: 4-((1r,3R,11s,13S)-9,19,19-trimethyl-1,3,5,7,11,13,15,17-octaphenyl-2,4,6,8,10,12,14,16,18,20,21,22,23,24-tetradeca-oxa-1,3,5,7,9,11,13,15,17,19-decasilapentacyclo[11.7.1.13,11.15,17.17,15] tetracosan-9-yl)butanenitrile.

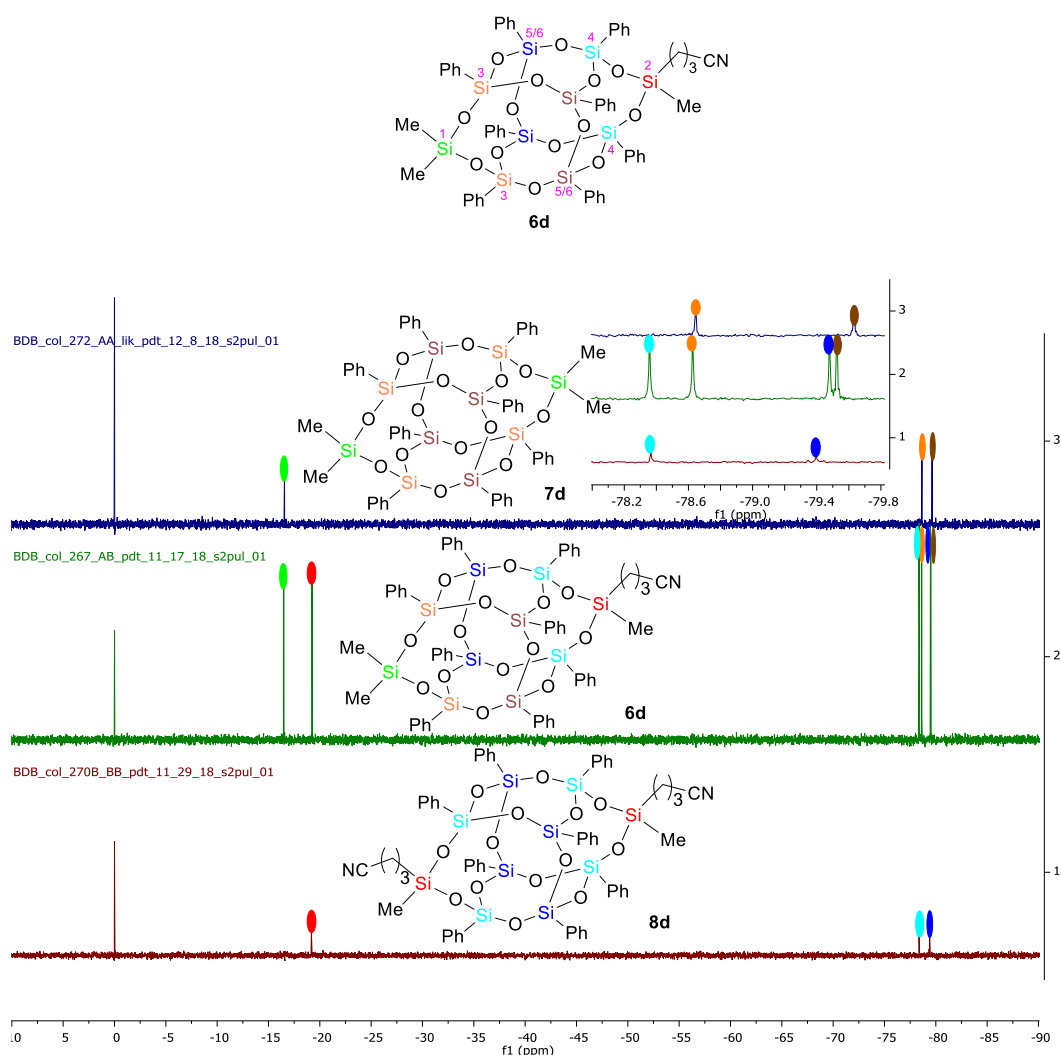


Figure 2-6: Stacked ^{29}Si NMR of AB 6d, AA 7d and BB 8d

Spectra for AB **6d** $C_{55}H_{55}Si_{10}NO_{14}$ displays six (6) peaks for the six different Si atoms present in the structure. AB **7d** (middle) is stacked with the symmetric AA **7d** (bottom) and BB **8d** (top) cages (**Figure 2-6**). Like is seen in its structure, the spectra shows two D-silicons (Si#1 and Si#2), found in the expected ppm range of -16.48 for the $Me_2SiO_2^-$ silicon (Si#1) and -19.24 for the $(Me)(3-CNPr)SiO_2^-$ (Si#2). Because the environments of the remaining Si atoms are affected by the orientation of the substituents on Si#1 and Si#2 and based on the stacked spectra above, the T-silicons in the structure are distributed thus: Signal at -78.36 ppm for the two Si#4 closest to Si#2, -78.63 ppm for the two Si#3 next to Si#1, -79.48 ppm for the internal silicons (Si#5 or Si#6) with a cis configuration for the Me groups on both Si#1 and Si#2, and -79.53 ppm for the internal silicons (Si#5 or Si#6) when substituents on Si#1 and Si#3 are trans. It must be mentioned that AB **6d** and AB **6e** are the same compounds that resulted by reversing the order of addition of the chlorosilanes to DDSQ tetraol. Whilst, the addition order was Me_2SiCl_2 first and then $Me(3CNPr)SiCl_2$ for **6d**, that for **6e** was the reverse.

6f: 4-((1s,3R,11r,13S)-9,19-dimethyl-1,3,5,7,11,13,15,17-octaphenyl-19-vinyl-2,4,6,8,10,12,14,16,18,20,21,22,23,24-tetradeca-oxa-1,3,5,7,9,11,13,15,17,19-decasilapentacyclo [11.7.1.13,11.15, 17.17,15]tetracosan-9-yl)butanenitrile.

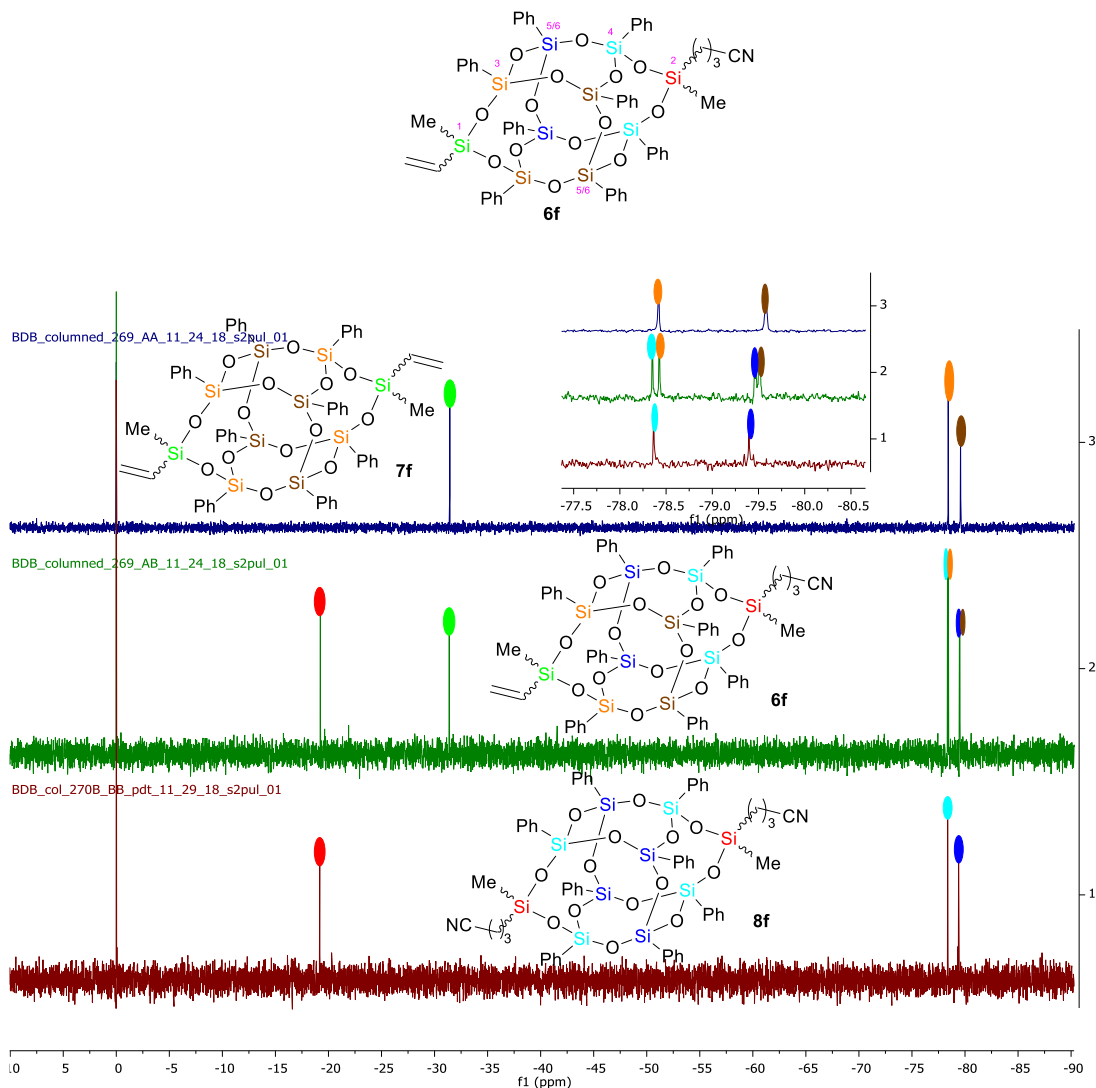


Figure 2-7: Stacked ^{29}Si NMR of AB **6f**, AA **7f** and BB **8f**

Spectra for AB **6f** $\text{C}_{56}\text{H}_{55}\text{Si}_{10}\text{NO}_{14}$ also shows six (6) peaks as seen in its stacked ^{29}Si -NMR with that of symmetric AA **7f** (top) and BB **8f** (bottom) cages (**Figure 2-7**). Here also, AB **6f** has two D-silicon peaks at -19.23 and -31.38 ppm in line with $(\text{C}_2\text{H}_3)(\text{Me})\text{SiO}_2$ - (Si#1) and $(\text{Me})(3\text{-CNPr})\text{SiO}_2$ - (Si#2) respectively. All the T-silicons in the structure are found in the -78.35 to -79.51 ppm range. By matching with spectra for **7f** and **8f** cages, -

78.35 ppm peak denotes the two Si#4 close to Si#2 and -78.43 ppm the two Si#3 atoms nearest to Si#1. Signals at -79.47 and -79.51 are symbolic of the four internal silicon atoms (Si#5 and Si#6) that can assume complementary signals based on the orientation of the substituents on Si#1/Si#2 (cis/trans). Clearly, the signal at -79.47 ppm is for the cis configuration of the Me groups on Si#1 and Si#2 and the -79.51 the trans configuration.

6g: (1r,3R,11s,13S)-9,19-dimethyl-1,3,5,7,11,13,15,17-octaphenyl-9-vinyl-2,4,6,8,10,12,14,16,18,20,21,22,23,24-tetradeca-oxa-1,3,5,7,9,11,13,15,17,19-decasilapentacyclo[11.7.1.13,11.15,17.17,15]tetracosane

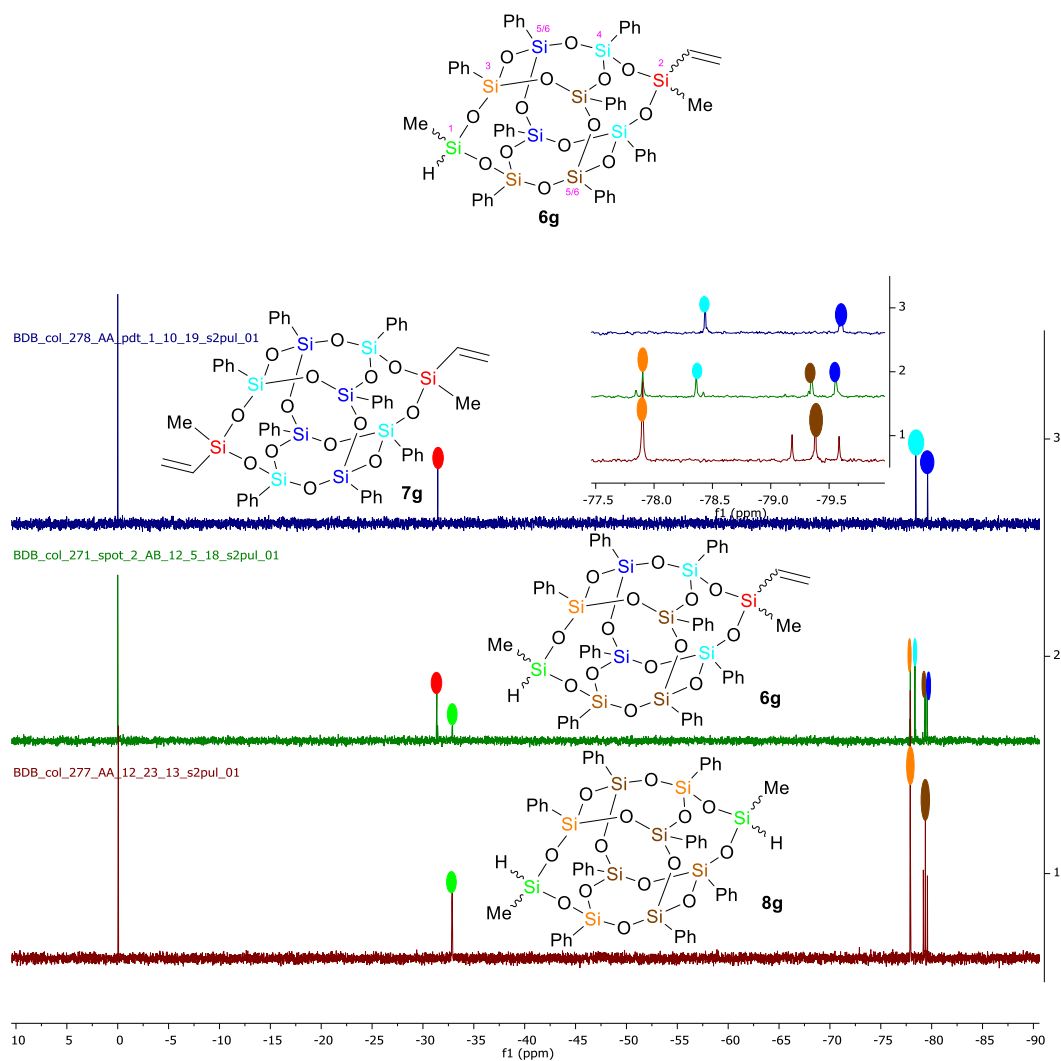


Figure 2-8: Stacked ^{29}Si NMR of AB **6g, AA **7g** and BB **8g****

Spectra for AB **6f** $C_{52}H_{50}Si_{10}O_{14}$ similarly displays six (6) peaks. AB **6f** (middle) is stacked with the symmetric AA (top) and BB (bottom) cages (**Figure 2-8**). The two D-silicon atoms in the structure give peaks at -31.37 and -32.91 ppm denoting one Si each for Si#1 having a Me and H substituents and Si#2 bearing a Me and vinyl substituents respectively. The T-silicons in the structure are found upfield between -77.90 and -79.56 ppm. These peaks are assigned to the T-silicons by matching with the spectra for **7g** and **8g**. Thus, the -77.90 ppm peak stems from the two Si#3 close to Si#1 and the -78.36 ppm peak the two Si#4 nearest to Si#2. Similarly, signals at -79.35 and -79.56 ppm are consistent with the four internal silicon atoms (Si#5 and Si#6) that can assume complementary signals based on the orientation of the substituents on Si#1/Si#2 (cis/trans). The signal at -79.35 ppm is for the cis configuration of the Me groups on Si#1 and Si#2 and the peak at -79.56, the trans configuration. It is worth mentioning that the divinylDDSQ cage (top) was isolated as the trans isomer only as is disclosed by the single peak at -79.56 ppm.

6h: (1*r*,3*R*,11*s*,13*S*)-19-methyl-1,3,5,7,11,13,15,17-octaphenyl-9-vinyl-2,4,6,8,10,12,14,16,18,20,21,22,23,24-tetradeca-1,3,5,7,9,11,13,15,17,19-decasilapentacyclo-[11.7.1. 13,11.15,17.17,15]tetracosan-9-ol.

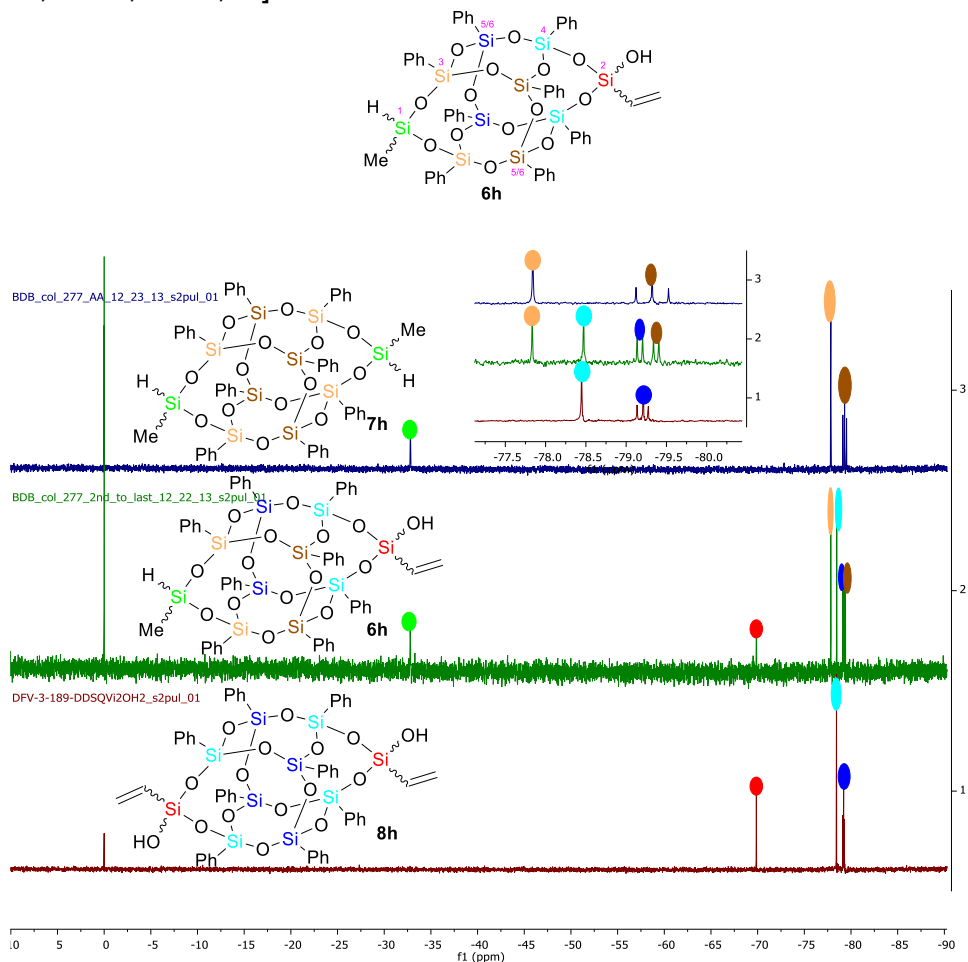


Figure 2-9: Stacked ^{29}Si NMR of AB **6h**, AA **7h** and BB **8h**

Unlike the spectra for AB **6a** to AB **6g**, those for AB **6h** (**Figure 2-9**) $\text{C}_{51}\text{H}_{48}\text{Si}_{10}\text{O}_{15}$ and AB **6i** (**Figure 2-10**) $\text{C}_{54}\text{H}_{54}\text{Si}_{10}\text{O}_{15}$ are quite unique. They display eight peaks instead of six and were isolated as geometric isomers (*cis/trans* forms). This is expected because the substituents on Si#1 and Si#2 are all different from one another and hence, make their internal silicons (Si#5 and Si#6) even more chemically different. As always, asymmetric **6h** (middle) is stacked with **7h** (top) and **8h** (bottom). The structure of AB **6h** has one distinct D-silicon capping one end of the DDSQ with a shift at -32.80 ppm that is consistent for Si#1. The second bridging Si on the other end of the cage, a T-silicon (Si#2)

appearing at -69.88 ppm is consistent for the region of T-silicons bearing a hydroxyl group. All other T-silicons in the structure appeared upfield between -77.86 and -79.43 ppm. These peaks are assigned to the T-silicons by matching with spectra for the AA and BB cages. Clearly, the -77.86 ppm peak denotes the two Si#3 close to Si#1 and the peak at -78.49 ppm, the two Si#4 nearest to Si#2. The remaining signals [-79.16 (1Si), -79.23 (1Si), -79.36 (1Si), -79.43 (1Si)] ppm are characteristic of each of the internal silicons (two Si#5 and two Si#6) which can assume complimentary signals based on the orientation of the substituents on Si#1/Si#2 (cis/trans).

6i: (1r,3R,11s,13S)-9-isopropyl-19-methyl-1,3,5,7,11,13,15,17-octaphenyl-19-vinyl-2,4,6,8,10,12,14,16,18,20,21,22,23,24-tetradeca-oxa-1,3,5,7,9,11,13,15,17,19-decasila-pentacyclo[11.7.1.13, 11.15,17.17,15]tetracosan-9-ol.

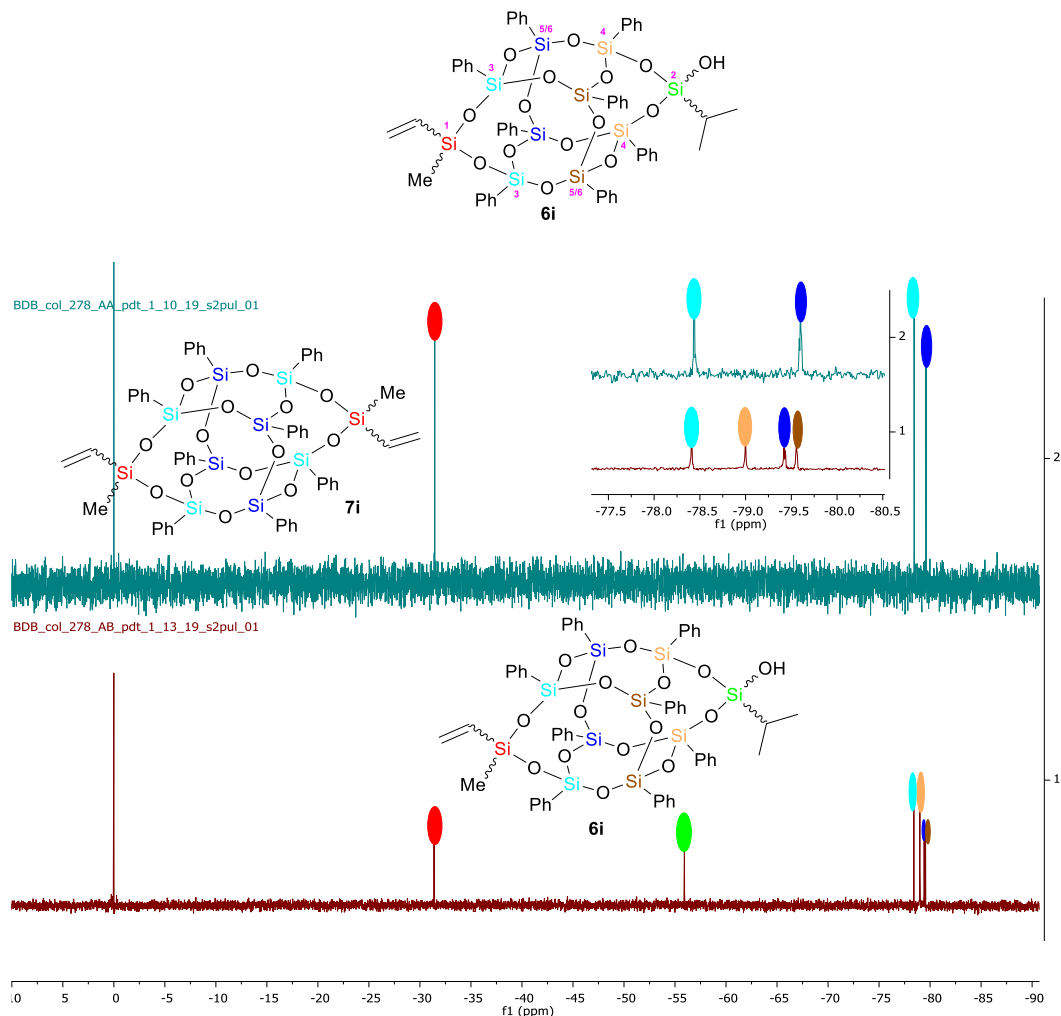


Figure 2-10: Stacked ^{29}Si NMR of AB **6i** and AA **7i**

Spectra for AB **6i** discloses 8 signals in line with the different kinds of silicon atoms in its structure (**Figure 2-10**). Asymmetric AB **6i** (bottom) is stacked with the symmetric AA (top). The isopropyltrichlorosilane capped DDSQ (BB cages) was not isolated, hence its absence from the stacked spectra. Like in AB **6h**, the structure of AB **6i** has one distinct D-silicon with a shift at -31.34 ppm typical of D-silicons with Me and vinyl substituents (Si#1). The other DDSQ bridging silicon is Si#2, a T-silicon having an isopropyl and OH

substituents exhibiting a peak at -55.89 ppm (Si#2); the expected range for T-silicons with one free hydroxyl group. The remaining silicons in the structure are all T-silicons showing up in the -78.36 to -79.51 ppm range. These peaks are assigned to the various T-silicons by matching. Thus, the signal at -78.36 ppm represents the two Si#3 close to Si#1 bearing the Me and vinyl substituents and the one at -78.98 ppm designates the two Si#4 close to Si#2. Signals at -79.38, -79.51 ppm each denotes two of the internal silicons (Si#5 and Si#6) that can interchange values based on the orientation of the substituents on Si#1/Si#2 (cis/trans).

2.3 Conclusions

In conclusion, a strategically novel synthesis of nano-sized, asymmetrically functionalized double-decker shaped silsesquioxanes (DDSQ) is reported. The technique relied on the protection of two silanol groups on DDSQ tetraol (**1**) using boronic acid. Importantly, the protocol discloses the effectiveness of pyridine as a base, which unlike the more commonly used triethylamine is inert to the boron protected cage. Additionally, pinacol chemoselectively demasks the boron protecting group without compromising the cage architecture. The protocol is general, robust and allows the assemblage of a wide range of functionalized asymmetrically functionalized DDSQs. Eight asymmetric compounds were synthesized and characterized as pure compounds by ^1H , ^{13}C , and ^{29}Si NMR and mass spectroscopy. Over 50% of the starting DDSQ tetraol (**1**) that could have otherwise contributed toward the synthesis of unwanted side products is recovered with a high purity and can be used in another cycle of synthesis. Efforts to use these compounds as nano-linkers to two different block copolymers are underway in our lab.

2.4 Experimental Details

2.4.1. General Information

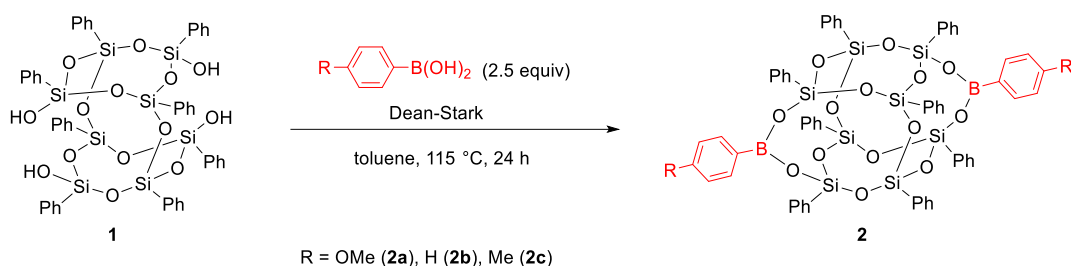
All manipulations were done under a nitrogen atmosphere using standard Schlenk techniques except otherwise stated. Tetrasilanol POSS (DDSQ tetraol) or $(\text{C}_6\text{H}_5)_8\text{Si}_8\text{O}_{10}(\text{OH})_4$ or $\text{DDSQ}(\text{OH})_4$ was purchased from Hybrid Plastics. Dimethyldichlorosilane, methyldichlorosilane, vinylmethyldichlorosilane, 3-chloropropylmethyldichlorosilane, 3-chloropropylmethyldichlorosilane, vinyltrichlorosilane, isopropyltrichlorosilane, and isobutyltrichlorosilane were purchased from Gelest. Methyltrichlorosilane $(\text{CH}_3)\text{SiCl}_3$ was purchased from Sigma-Aldrich. Triethylamine (Et_3N) was purchased from Avantor and distilled over calcium hydride before use. Deuterated chloroform with 1% (v/v) TMS and tetrahydrofuran- d_8 were purchased from Cambridge isotopes laboratories. Dichloromethane, trichloromethane, tetrahydrofuran, ethyl acetate, acetone, acetonitrile, methanol, isopropanol, 2,4,6-trimethylpyridine, and anhydrous magnesium sulfate were purchased from Aldrich. THF was distilled over benzophenone and sodium metal at a temperature of 50 °C under nitrogen. Toluene was distilled over calcium hydride at a temperature of 120 °C. The other solvents were used as purchased without further purification. Glassware was oven-dried and solvents such as tetrahydrofuran (THF) and toluene were freshly distilled prior to use. All ^1H , ^{11}B , ^{13}C and ^{29}Si NMR were acquired on an Agilent DirectDrive2 500 MHz NMR spectrometer equipped with a OneProbe operating at 500 MHz for ^1H NMR, 160 MHz for ^{11}B NMR, 126 MHz for ^{13}C NMR, and 99 MHz for ^{29}Si NMR CDCl_3 or deuterated THF and recorded at 25 °C. ^1H -NMR spectra were recorded with 8-32 scans, a relaxation delay of 1s, and a pulse angle of 45° and referenced to the residual protonated solvent in CDCl_3 (7.24 ppm).

¹³C-NMR spectra were collected with 254 scans, a relaxation delay of 0.1 s, and a pulse angle 45°. ²⁹Si NMR spectra were recorded with either 256 or 512 scans, a relaxation delay of 12 s and a pulse angle of 45°. Column chromatography was performed on EMD Millipore silica gel 60 columns of 40–63 Å silica, 230–400 mesh. Thin-layer chromatography (TLC) was performed on plates of EMD 250-µm silica 60-F254. High resolution mass spectroscopy was performed with APCI mass spectra recorded on a Finnigan LCQ Deca (ThermoQuest) technologies with LC/MS/MS (quadrupole/time-of-flight) and Waters Xevo G2-XS UPLC/MS/MS inert XL MSD with SIS Direct Insertion Probe. Melting points for all products were measured with a Thomas HOOVER capillary uni-melt melting point apparatus and are uncorrected. X-ray diffraction measurements were performed on a Stoe IPDS2 or a Bruker-AXS SMART APEX 2 CCD diffractometer using graphite-monochromated MoK α radiation. The structures were solved using direct methods (SHELXL-97) and refined by fullmatrix least-squares techniques against F² (SHELXL-97). Cell parameters were retrieved using the SAINT (Bruker, V8.34A, S3 after 2013) software and refined using SAINT (Bruker, V8.34A, after 2013) on 5941 reflections, 47 % of the observed reflections. Data reduction was performed using the SAINT (Bruker, V8.34A, after 2013) software which corrects for Lorentz polarization.

The yields reported are calculated by two methods. The first is based on the amount of compound **3** after step 1 in Scheme 2-13. This yield shows the overall efficiency of the route from the monoprotected material to the desired asymmetric product. The second method is based on the combined amounts of compounds **2** and **3** generated in step 1 of the same scheme for the yields of the symmetric products.

2.4.1.1 General Experimental Procedure for the Synthesis of DDSQ Boronate Esters

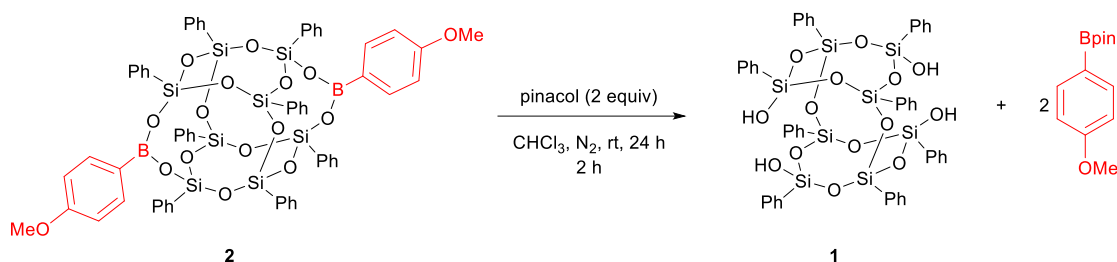
Scheme 2-7: Synthesis of DDSQ Bis-boronate Esters 2



An oven-dried 100 mL round bottom flask equipped with a magnetic stir bar was charged with DDSQ tetraol **1** (1.96 mmol, 2.1 g) and p-substituted phenylboronic acid (2.5 equiv, 5 mmol). The flask was fitted with a Dean-Stark apparatus and filled with nitrogen atmosphere. Toluene (40 mL) was added, and the mixture stirred over a pre-heated oil bath at a temperature of 115 °C for 24 h or until full conversion of the DDSQ tetraol **1** was detected by TLC. The solvent was evaporated under reduced pressure to afford a white solid. Isopropanol (20 mL) was added to the flask bearing a magnetic stir bar and the mixture heated at 40 °C for 20 minutes. The mixture was cooled to room temperature and filtered through a fine filter frit. The residue was washed with isopropanol (2 x 10 mL) and dried at reduced pressure to afford a pure white solid of the bis-protected cage (**Table 2-1**). From this product, fine crystals appropriate for crystallographic analysis were obtained from a mixture of DCM/hexanes (1:3) of the Bis-boronate esters **2** (**Table 2-2**). The solid was characterized by ^1H , ^{13}C , ^{11}B , ^{29}Si NMR X-ray crystallography and LCMS measurements. The structures investigated in this study are listed in Figure 2-1 and Table 2-2. NMR, mass spectral and crystallographic data are shown in **Appendix**.

2.4.1.2 Deborylation of DDSQ Bis-boronate Ester with Pinacol

Scheme 2-8: Deborylation of (p-MeOC₆H₄B)₂DDSQ with Pinacol



An oven-dried 50 mL round bottom flask bearing a magnetic stir bar was charged with p-MeO-C₆H₄B)₂DDSQ (**2**) (0.65 g, 0.5 mmol) and pinacol (0.1182 g, 1 mmol, 2 equiv). The flask was placed under a nitrogen atmosphere and CHCl₃ (10 mL) added to it. The reaction mixture was stirred at room temperature for 24 h. The heterogenous mixture was then filtered through a Buchner funnel using an aspirator. The residue was washed with 2 x 10 mL CHCl₃, transferred to a beaker, and dried in an oven at 80 °C for 5 h. The solid **1** (0.46 mmol, 92%) was analyzed by ¹H, ¹³C, ¹¹B and ²⁹Si NMR. NMR data for the products are shown in **Appendix**.

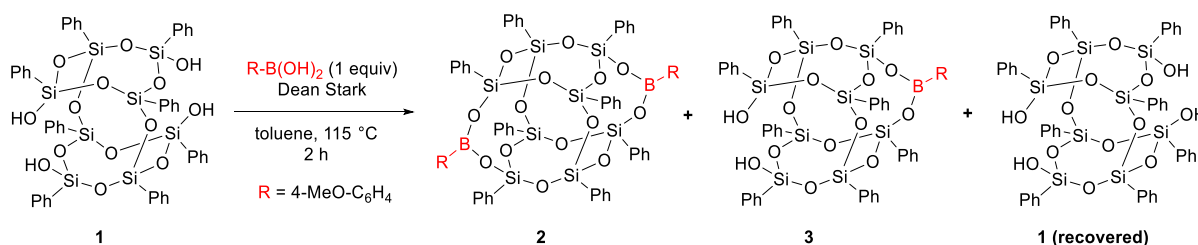
2.4.1.3 General Procedure for Solubility Test for DDSQ(OH)₄ in Different Organic Solvents

Into a 20 mL vial bearing a stir bar was added 0.2 g of DDSQ tetraol (**1**) and the solvent (10 mL). The vial was sealed with a cap and the reaction mixture stirred at room temperature for 2 minutes. The mixture was suction filtered through a fine frit filter funnel. The filtrate was transferred to an oven-dried pre-weighed 20 mL vial and the solvent evaporated with a rotary evaporator. The vial was cooled to room temperature and the weight determined (**Table 2-3**).

2.4.1.4 General Experimental Procedures for the Multi-step Synthesis of Asymmetrically Functionalized DDSQs

2.4.1.4.1 Mono-borylation of DDSQ(OH)₄ with p-MeOC₆H₄B(OH)₂ (Step 1)

Scheme 2-9: Monoborylation of DDSQ(OH)₄ **1** with p-MeO-C₆H₄B(OH)₂



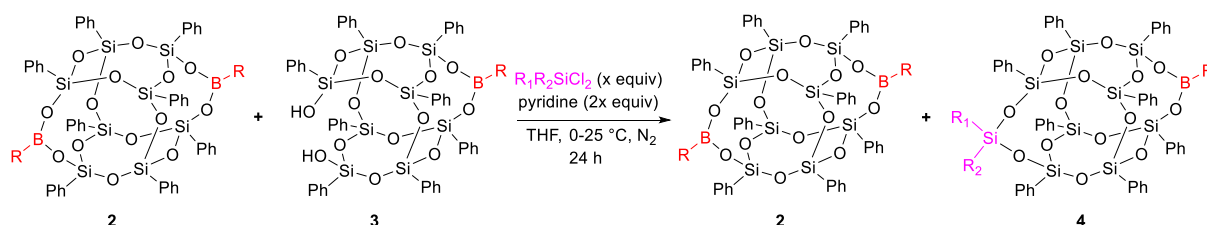
An oven-dried 100 mL round bottom flask equipped with a magnetic stir bar was charged with DDSQ(OH)₄ **1** (1.96 mmol, 2.1g) and p-methoxyphenylboronic acid (1 equiv, 1.96 mmol, 0.30 g). The flask was fitted with a Dean-Stark apparatus and filled with a nitrogen atmosphere. Toluene (40 mL) was added, and the mixture stirred in a pre-heated oil bath at 115 °C. After 2 h, the resulting heterogeneous mixture was cooled to room temperature and suction filtered using a fine-fritted funnel and filter flask to isolate the unreacted DDSQ(OH)₄. The residue was washed with toluene (2 x 10 mL) and filtered. The combined filtrate was evaporated under reduced pressure to afford a white solid. This solid is a mixture of both the mono- and bis-borylated cage and trace amounts of DDSQ(OH)₄. Chloroform (20 mL) was added to dissolve the solid in the flask. The contents were cooled in a refrigerator at -5 °C for 1 h and suction filtered using a fine-fritted funnel and a Buchner flask. The filtrate was dried by rotary evaporation to give a white solid. This dissolution in chloroform, refrigeration and filtration processes were repeated two times and the filtrate dried each time by rotary evaporation to give a white solid consisting of the bis- and mono-borylated cages in an average ratio of 3:1. The

resulting crude product was analyzed by ^1H , ^{11}B , and ^{29}Si NMR spectroscopy. It must be mentioned that all attempts to isolate the pure mono-borylated cage were unsuccessful.

2.4.1.4.2 General Procedure for the First Silylation of Mono-borylated DDSQ(OH)₂

(3) - (Step 2)

Scheme 2-10: Silylation of Mono-borylated Product, (p-MeOC₆H₄B)DDSQ(OH)₂ with $\text{R}^1\text{R}^2\text{SiCl}_2$



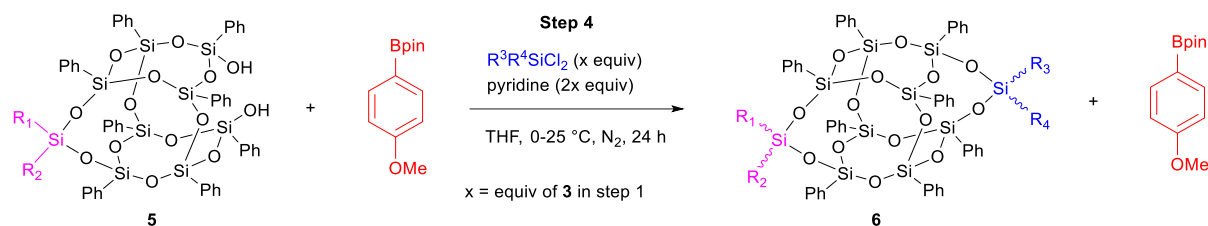
After isolating the recovered **1** by filtration, the crude product mixture (**Scheme 2-9**) was charged into a pre-dried 100 mL round bottom flask bearing a magnetic stir bar and sealed with a septum. The flask was purged with dry nitrogen for 30 min and THF (20 mL) added to it. The flask was immersed into an ice bath and the contents stirred vigorously under nitrogen for 1 h. $\text{R}^1\text{R}^2\text{SiCl}_2$ (x mmol, 1 equiv. based on the mono-borylated cage) in 5 mL THF was added first followed by dropwise addition of pyridine (2x mmol, 2 equiv. based on the mono-borylated cage) over a period of 10 minutes. The reaction mixture was stirred at 0 °C for 4 h and at room temperature for 20 h. The suspension was filtered through a glass frit, the residue washed with THF (3 x 5 mL) and the solvent together with other volatiles removed from the filtrate by rotary evaporation to afford a white solid. This crude solid is a mixture of the bis-boronate DDSQ ester and the silylated mono-boronate DDSQ ester that forms the substrate for the next step. Reaction was followed by both ^1H and ^{29}Si NMR.

Scheme 2-11: Deborylation of (p-MeOC₆H₄B)DDSQSiR¹R² and (p-MeOC₆H₄B)₂DDSQ with Pinacol

The crude product mixture (**Scheme 2-10**) was charged into a pre-dried 100 mL round bottom flask bearing a magnetic stir bar, pinacol (2 mmol) and chloroform (10 mL) were added to the flask under nitrogen and the reaction mixture stirred vigorously at room temperature for 24 h. The crude mixture was initially completely soluble in chloroform, but gradually turned to a colloidal solution over time. After 24 h, the resulting white suspension was filtered with a fine-fritted filter funnel and a Buchner flask. The white powdered residue was washed with chloroform (3 x 5 mL), filtered, dried in an oven at 80 °C for 5 h and characterized by ^1H and ^{29}Si NMR spectroscopy. The solvent and other volatiles were removed from the filtrate by rotary evaporation to afford a white solid/oily liquid which was similarly characterized by ^1H , ^{11}B , ^{13}C and ^{29}Si NMR spectroscopy. The solid from the crude filtrate which is mostly the monosilylated $\text{DDSQ}(\text{OH})_2$ and $p\text{-MeOC}_6\text{H}_4\text{Bpin}$ was used as starting material for the next silylation.

2.4.1.4.4 General Procedure for the Second Silylation of Monosilylated DDSQ (5)

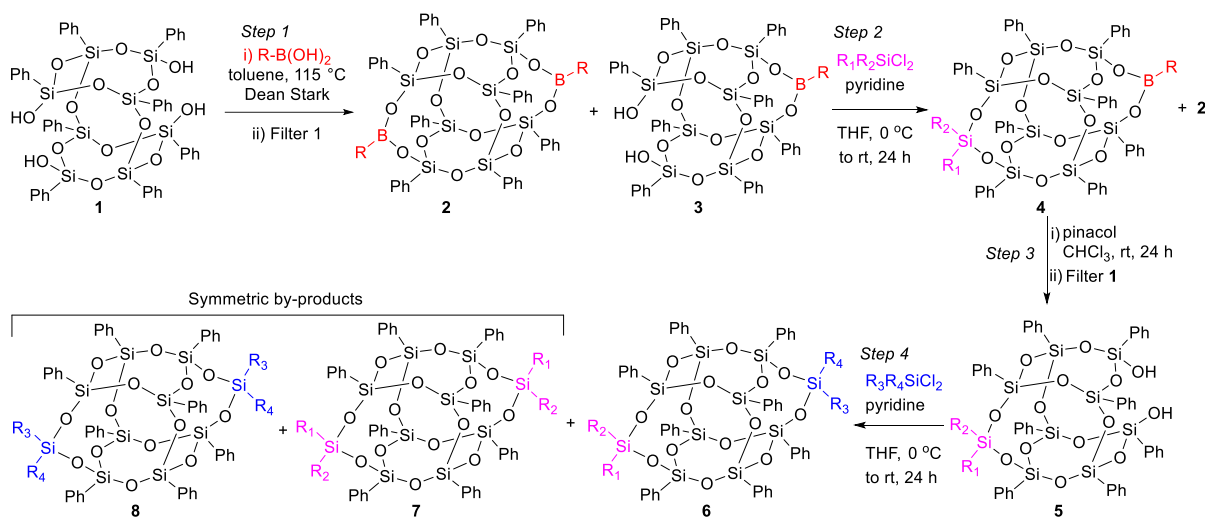
Scheme 2-12: Second Silylation of Monosilylated Precursor, $R^1R^2SiDDSQ(OH)_2$



The crude product mixture after isolating the DDSQ tetraol **1** (**Scheme 2-11**) was charged into an oven-dried 100 mL round bottom flask bearing a magnetic stir bar and a septum. The flask was purged with dry nitrogen for 30 min and THF (20 mL) added to it. The flask was immersed into an ice bath and the mixture stirred vigorously under nitrogen for 1 h. A suitable mono or di-substituted chlorosilane bearing R groups different from the former, $R^3R^4SiCl_2$ ('x' equiv as in Step 1) in 5 mL THF was added followed by dropwise addition of pyridine ('2x' equiv) over a period of 10 minutes. The reaction mixture was stirred at 0 °C for 4 h and at room temperature for 20 h. The suspension was filtered through a glass frit funnel, the residue washed with THF (3 x 5 mL) and the solvent together with other volatiles removed from the filtrate by rotary evaporation to afford a white solid/oil. This crude solid/oil is mostly the asymmetrically functionalized DDSQ cage and p-MeOC₆H₄Bpin. Reaction was followed by both ¹H and ²⁹Si NMR. All products were purified by flash column chromatography (ethylacetate:hexanes = 1:9 and in some cases ethylacetate:hexane = 1:16) and analyzed by ¹H, ¹³C, ²⁹Si and LCMS measurement. The chromatographed products were washed with hexanes to remove the p-MeOC₆H₄Bpin. The asymmetrically functionalized DDSQs synthesized in this study are listed in Table 2-5 and the NMR data in **Appendix**. Copies of NMR and mass spectra are given in **Appendix**.

2.4.2 Synthetic Scope for Asymmetrically Functionalized Double-Decker Shaped Silsesquioxanes

Scheme 2-13: Substrate Scope of the Multistep Pathway for the Synthesis of Asymmetrically Functionalized DDSQ



To demonstrate the synthetic scope, the asymmetric products (**Table 2-4**) were synthesized following the route described above (**Scheme 2-13**). Two yields are reported for the asymmetric material. The first yield is based on the amount of compound **3** after step 1. This yield shows the overall efficiency of the route from the monoprotected material to the desired asymmetric product. The yield in parenthesis and the yields of symmetric by-products are based on the combined amounts of compounds **2** and **3** generated in step 1. Finally, the reported yield for compound **1** is based on the amount of material recovered in steps 1 and 3.

APPENDIX

NMR and Mass Spectral Data of Isolated Products Bis-borylated DDSQ (2)

9,19-bis(4-methoxyphenyl)-1,3,5,7,11,13,15,17-octaphenyl-2,4,6,8,10,12,14,16,18,20,21,22,23,24-tetradecaoxa-1,3,5,7,11,13,15,17-octasila-9,19-diborapentacyclo[11.

7.1.13,11.15,17.17,15]tetracosane (2a) {(p-MeOC₆H₄B)₂DDSQ}

This product was isolated as a white crystalline solid in 2.50 g, 1.92 mmol (98%). mp 293 – 295 °C

¹H NMR (500 MHz, CDCl₃) δ (ppm) 7.74 – 7.61 (m, 8H), 7.60 – 7.54 (m, 4H), 7.53 – 7.15 (m, 32H), 6.75 – 6.64 (m, 4H), 3.71 (s, 6H).

¹¹B NMR (160 MHz, CDCl₃) δ (ppm) 29.9

¹³C NMR (126 MHz, CDCl₃) δ (ppm) 138.12, 134.55, 134.52, 129.40, 128.59, 128.37, 128.34, 128.33, 128.14, 128.10, 125.69, 21.75.

²⁹Si NMR (99 MHz, CDCl₃) δ (ppm) -78.62, -80.38.

1,3,5,7,9,11,13,15,17,19-decaphenyl-2,4,6,8,10,12,14,16,18,20,21,22,23,24-tetradecaoxa-1,3,5,7,11,13,15,17-octasila-9,19-diborapentacyclo[11.7.1.13,11.15,17.17,15]

tetracosane (2b) {(C₆H₅B)₂DDSQ}

This product was isolated as a white crystalline solid in 2.31 g, 1.86 mmol (95%). mp 279 – 281 °C

¹H NMR (500 MHz, CDCl₃) δ (ppm) 7.67 – 7.61 (m, 10H), 7.54 – 7.11 (m, 41H).

¹³C NMR (126 MHz, CDCl₃) δ (ppm) 135.80, 134.15, 134.13, 131.41, 131.26, 130.69, 130.59, 130.30, 127.97, 127.73, 127.54.

¹¹B NMR (160 MHz, CDCl₃) δ (ppm) 29.57

²⁹Si NMR (99 MHz, CDCl₃) δ (ppm) -78.62, -80.33.

1,3,5,7,11,13,15,17-octaphenyl-9,19-di-*p*-tolyl-2,4,6,8,10,12,14,16,18,20,21,22,23,24, tetradecaoxa-1,3,5,7,11,13,15,17-octasila-9,19-diborapentacyclo[11.7.1.13,11.15, 17.17,15]tetracosane (**2c**) {(*p*-tolylC₆H₄B)₂DDSQ}

This product was isolated as a white crystalline solid in 2.39 g, 1.88 mmol (96%). mp 289 – 291 °C

¹H NMR (500 MHz, CDCl₃) δ (ppm) 7.75 – 7.57 (m, 8H), 7.52 (d, J = 7.6 Hz, 4H), 7.50 – 7.18 (m, 32H), 6.99 (d, J = 7.7 Hz, 4H), 2.28 (s, 6H).

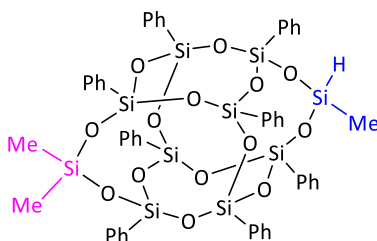
¹¹B NMR (160 MHz, CDCl₃) δ (ppm) 21.35

¹³C NMR (126 MHz, CDCl₃) δ (ppm) 141.61, 135.91, 134.14, 131.37, 130.62, 130.35, 128.35, 127.68, 21.62.

²⁹Si NMR (99 MHz, CDCl₃) δ (ppm) -78.67, -80.39.

Asymmetrically Functionalized DDSQs (6)

(1*r*,3*R*,11*s*,13*S*)-9,9,19-trimethyl-1,3,5,7,11,13,15,17-octaphenyl-2,4,6,8,10,12,14,16, 18,20,21,22,23,24-tetradecaoxa-1,3,5,7,9,11,13,15,17,19-decasilapentacyclo[11.7.1. 13,11.15,17.17,15]tetracosane. (**6a**)



Formula: C₅₁H₅₀O₁₄Si₁₀

This product was isolated as a white solid in 0.31 g, 0.27 mmol (79%). mp 266-268 °C

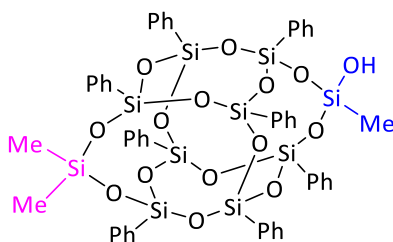
^1H NMR (500 MHz, CDCl_3) δ 7.57 – 7.16 (m, 40H), 4.98 (p, J = 1.5 Hz, 1H), 0.37 (t, J = 1.4 Hz, 3H), 0.30 (d, J = 1.2 Hz, 6H).

^{13}C NMR (126 MHz, CDCl_3) δ (ppm) δ 134.08, 133.93, 131.66, 127.83, 0.63, 0.56

^{29}Si NMR (99 MHz, CDCl_3) δ (ppm) -16.47 (1Si), -32.90 (1Si), -77.91 (2Si), -78.56 (2Si), -79.37 (2Si), -79.57 (2Si).

LC/MS QToF: exact mass for $\text{C}_{51}\text{H}_{51}\text{O}_{15}\text{Si}_{10}$ $[\text{M}+\text{H}]^+$ calculated m/z 1167.0966 found m/z 1167.0891

(1*r*,3*R*,11*s*,13*S*)-9,19,19-trimethyl-1,3,5,7,11,13,15,17-octaphenyl-2,4,6,8,10,12,14,16,18,20,21,22,23,24-tetradeca-oxo-1,3,5,7,9,11,13,15,17,19-decasilapentacyclo[11.7.1.13,11.15,17.17,15]tetracosan-9-ol. (**6b**)



Formula: $\text{C}_{51}\text{H}_{50}\text{O}_{15}\text{Si}_{10}$

This product was isolated as a white solid in 0.23 g, 0.19 mmol (61%). mp 256-258 °C

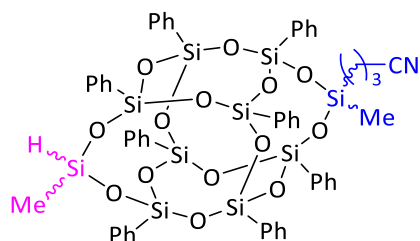
^1H NMR (500 MHz, CDCl_3) δ 7.57 – 7.16 (m, 40H), 0.35 (s, 3H), 0.30 (s, 6H).

^{13}C NMR (126 MHz, CDCl_3) δ 134.05, 131.99, 130.40, 127.83, 0.53, -3.90.

^{29}Si NMR (99 MHz, CDCl_3) δ -16.40 (1Si), -54.01 (1Si), -78.54 (2Si), -78.70 (2Si), -79.33 (2Si), -79.45 (2Si).

LC/MS QToF: exact mass for $\text{C}_{51}\text{H}_{51}\text{O}_{15}\text{Si}_{10}$ $[\text{M}+\text{H}]^+$ calculated m/z 1182.0842 found m/z 1183.0823

4-((1*r*,3*R*,11*s*,13*S*)-9,19-dimethyl-1,3,5,7,11,13,15,17-octaphenyl-2,4,6,8,10,12,14,16,18,20,21,22,23,24-tetradeca-1,3,5,7,9,11,13,15,17,19-decasilapentacyclo[11.7.1.13, 11.15,17.17,15]tetracosan-9-yl)butanenitrile. (**6c**)



Formula: C₅₄H₅₃NO₁₄Si₁₀

This product was isolated as a white solid in 0.21 g, 0.17 mmol (52%). mp 204 - 206

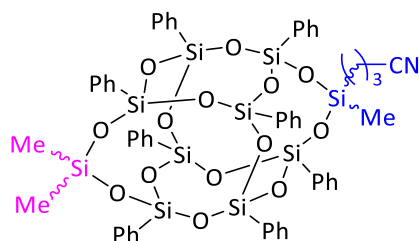
¹H NMR (500 MHz, CDCl₃) δ (ppm) 7.55 – 7.18 (m, 40H), 4.98 (s, 1H), 2.17 (t, J = 7.0 Hz, 2H), 1.76 – 1.69 (m, 2H), 0.88 – 0.85 (m, 2H), 0.37 (s, 3H), 0.33 (s, 3H).

¹³C NMR (126 MHz, CDCl₃) δ (ppm) 133.80, 131.60, 130.52, 127.84, 119.47, 29.70, 20.02, 19.43, 16.14.

²⁹Si NMR (99 MHz, CDCl₃) δ (ppm) -19.16 (1Si), -32.86 (1Si), -77.92 (2Si), -78.30 (2Si), -79.24 (1Si), -79.29 (1Si), -79.45 (1Si), -79.49 (1Si).

LC/MS QTof: exact mass for for C₅₄H₅₃KNO₁₄Si₁₀ [M+K]⁺calculated m/z 1258.0790 found m/z 1259.0798

4-((1*r*,3*R*,11*s*,13*S*)-9,19,19-trimethyl-1,3,5,7,11,13,15,17-octaphenyl-2,4,6,8,10,12,14,16,18,20,21,22,23,24-tetradecaoxa-1,3,5,7,9,11,13,15,17,19-decasilapentacyclo[11.7.1.13,11.15,17.17,15]tetracosan-9-yl)butanenitrile. (**6d**)



Formula: C₅₅H₅₅NO₁₄Si₁₀

This product was isolated as a white solid in 0.32 g, 0.26 mmol (81%). mp 218 – 220

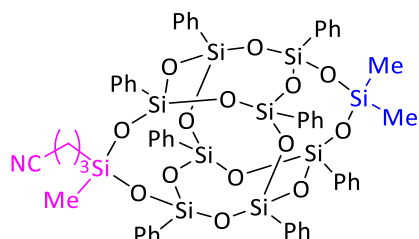
¹H NMR (500 MHz, CDCl₃) δ (ppm) 7.54 – 7.17 (m, 40H), 2.17 (t, J = 7.0 Hz, 2H), 1.77 – 1.68 (m, 2H), 0.88 – 0.82 (m, 2H), 0.32 (s, 3H), 0.30 (s, 6H).

¹³C NMR (126 MHz, CDCl₃) δ (ppm) 134.00, 133.99, 133.90, 133.82, 131.96, 131.67, 130.85, 130.53, 130.47, 130.39, 130.37, 127.90, 127.79, 127.74, 127.67, 20.03, 19.44, 16.14, 0.52, -0.89.

²⁹Si NMR (99 MHz, CDCl₃) δ (ppm) -16.48 (1Si), -19.24 (1Si), -78.36 (2Si), -78.63 (2Si), -79.48 (2Si), -79.53 (2Si).

LC/MS QTof: exact mass for for C₅₅H₅₅KNO₁₄Si₁₀ [M+K]⁺ calculated m/z 1272.0947 found m/z 1273.0958

4-((1*r*,3*R*,11*s*,13*S*)-9,19,19-trimethyl-1,3,5,7,11,13,15,17-octaphenyl-2,4,6,8,10,12,14,16,18,20,21,22,23,24-tetradeca-1,3,5,7,9,11,13,15,17,19-decasilapentacyclo[11.7.1.13,11.15,17.17,15]tetracosan-9-yl)butanenitrile. (**6e**)



Formula: C₅₅H₅₅NO₁₄Si₁₀

This product was isolated as a white solid in 0.31 g, 0.25 mmol (74%). mp 218 – 220

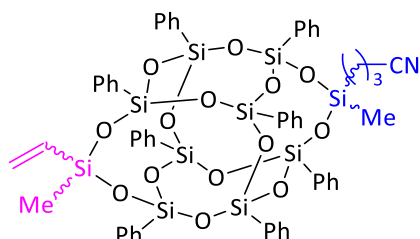
¹H NMR (500 MHz, CDCl₃) δ (ppm) 7.59 – 7.15 (m, 40H), 2.17 (t, J = 7.0 Hz, 2H), 1.76 – 1.69 (m, 2H), 0.86 (dd, J = 7.4, 4.0 Hz, 2H), 0.32 (s, 3H), 0.30 (6H).

¹³C NMR (126 MHz, CDCl₃) δ (ppm) 134.02, 131.98, 130.90, 130.40, 127.70, 119.50, 29.72, 19.46, 16.16, 14.16.

²⁹Si NMR (99 MHz, CDCl₃) δ (ppm) -16.48 (1Si), -19.24 (1Si), -78.36 (2Si), -78.63 (2Si), -79.48 (2Si), -79.53 (2Si).

LC/MS QTof: exact mass for C₅₅H₅₅KNO₁₄Si₁₀ [M+K]⁺ calculated m/z 1272.0947 found m/z 1273.0958

4-((1*s*,3*R*,11*r*,13*S*)-9,19-dimethyl-1,3,5,7,11,13,15,17-octaphenyl-19-vinyl-2,4,6,8,10,12,14,16,18,20,21,22,23,24-tetradecaoxa-1,3,5,7,9,11,13,15,17,19-decasilapentacyclo[11.7.1.13,11.15,17.17,15]tetracosan-9-yl)butanenitrile. (**6f**)



Formula: C₅₆H₅₅NO₁₄Si₁₀

This product was isolated as a white solid in 0.28 g, 0.22 mmol (65%). mp 220-222

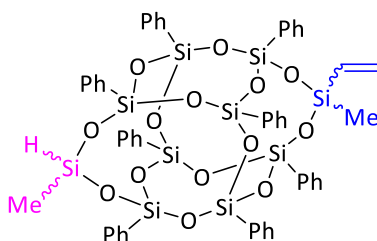
¹H NMR (500 MHz, CDCl₃) δ (ppm) 7.54 – 7.18 (m, 40H), 6.13 (d, J = 20.2 Hz, 1H), 5.96 (d, J = 16.4 Hz, 2H), 2.17 (t, J = 7.0 Hz, 2H), 1.72 (dt, J = 16.6, 7.3 Hz, 2H), 0.87 (d, J = 5.5 Hz, 2H), 0.37 (s, 3H), 0.32 (s, 3H).

¹³C NMR (126 MHz, CDCl₃) δ (ppm) 134.02, 133.83, 131.66, 130.42, 127.92, 127.80, 119.49, 29.71, 19.45, 16.15, 14.14, -1.16.

²⁹Si NMR (99 MHz, CDCl₃) δ (ppm) -19.23 (1Si), -31.38 (1Si), -78.35 (2Si), -78.43 (2Si), -79.47 (2Si) (d, J = 1.2 Hz), -79.51 (2Si) (d, J = 1.5 Hz).

LC/MS QToF: exact mass for C₅₆H₅₅KNO₁₄Si₁₀ [M+K]⁺ calculated m/z 1284.0947 found m/z 1285.0961

(1*r*,3*R*,11*s*,13*S*)-9,19-dimethyl-1,3,5,7,11,13,15,17-octaphenyl-9-vinyl-2,4,6,8,10,12,14,16,18,20,21,22,23,24-tetradeca-1,3,5,7,9,11,13,15,17,19-decasilapentacyclo[11.7.1.1.13,11.15,17.17,15]tetracosane. (**6g**)



Formula: C₅₂H₅₀O₁₄Si₁₀

This product was isolated as a white solid in 0.19 g, 0.16 mmol (50%). mp 235-237 °C

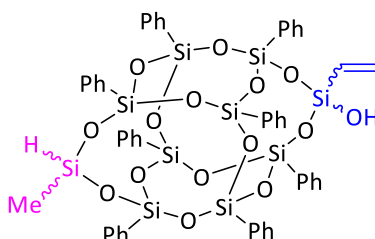
¹H NMR (500 MHz, CDCl₃) δ (ppm) 7.59 – 7.14 (m, 40H), 6.15 (dd, J = 20.2, 15.0 Hz, 1H), 6.02 – 5.90 (m, 2H), 4.98 (s, 1H), 0.37 (s, 6H).

¹³C NMR (126 MHz, CDCl₃) δ (ppm) 133.95, 131.88, 131.64, 130.40, 127.80, 127.63, -1.15.

²⁹Si NMR (99 MHz, CDCl₃) δ (ppm) -31.37 (1Si), -32.91 (1Si), -77.90 (2Si), -78.36 (2Si), -79.35 (2Si), -79.56 (2Si).

LC/MS QTof: exact mass for C₅₂H₅₁Si₁₀NO₁₄ [M+H]⁺ calculated m/z 1179.0966 found m/z 1181.0642

(1*r*,3*R*,11*s*,13*S*)-19-methyl-1,3,5,7,11,13,15,17-octaphenyl-9-vinyl-2,4,6,8,10,12,14,16,18,20,21,22,23,24-tetradeca-oxa-1,3,5,7,9,11,13,15,17,19-decasilapentacyclo[11.7.1.13, 11.15,17.17,15]tetracosan-9-ol. (**6h**)



Formula: C₅₁H₄₈O₁₅Si₁₀

This product was isolated as a white solid in 0.27 g, 0.23 mmol (68%). Mp 235-237 °C

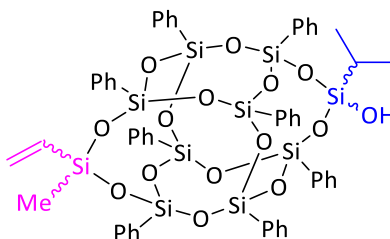
¹H NMR (500 MHz, CDCl₃) δ (ppm) 7.61 – 7.13 (m, 40H), 6.11 – 6.06 (m, 2H), 5.82 (m, 1H), 4.99 – 4.97 (m, 1H), 0.37 (d, J = 1.6 Hz, 3H).

¹³C NMR (126 MHz, CDCl₃) δ (ppm) 136.90, 134.08, 133.98, 131.52, 130.51, 127.84, 14.14.

²⁹Si NMR (99 MHz, CDCl₃) δ (ppm) -32.80 (1Si), -69.88 (1Si), -77.86 (2Si), -78.49 (2Si), -79.16 (1Si), -79.23 (1Si), -79.36 (1Si), -79.43 (1Si).

LC/MS QTof: exact mass for C₅₁H₄₉Si₁₀O₁₅ [M+H]⁺ calculated m/z 1181.0759 found m/z 1181.0642

(1*r*,3*R*,11*s*,13*S*)-9-isopropyl-19-methyl-1,3,5,7,11,13,15,17-octaphenyl-19-vinyl-2,4,6,8,10,12,14,16,18,20,21,22,23,24-tetradeca-oxa-1,3,5,7,9,11,13,15,17,19-decasilapentacyclo[11.7.1.13,11.15,17.17,15]tetracosan-9-ol. (**6i**)



Formula: C₅₄H₅₄O₁₅Si₁₀

This product was isolated as a white solid in 0.22 g, 0.18 mmol (56%). mp 228-230 °C

¹H NMR (500 MHz, CDCl₃) δ (ppm) 7.65 – 7.10 (m, 40H), 6.15 (m, 1H), 6.02 – 5.91 (m, 2H), 1.05 (d, J = 2.1 Hz, 6H), 0.38 – 0.33 (m, 3H).

¹³C NMR (126 MHz, CDCl₃) δ (ppm) 134.07, 131.82, 131.53, 130.39, 127.81, 127.62, 16.90, 12.01, -1.18.

²⁹Si NMR (99 MHz, CDCl₃) δ (ppm) -31.34 (1Si), -55.89 (1Si), -78.36 (2Si), -78.96 (2Si), -79.38 (2Si), -79.51 (2Si).

Copies of NMR Spectra

Bis-Boronate Esters (2)

9,19-bis(4-methoxyphenyl)-1,3,5,7,11,13,15,17-octaphenyl-2,4,6,8,10,12,14,16,18,-
20,21,22,23,24-tetradecaoxa-1,3,5,7,11,13,15,17-octasila-9,19-diborapentacyclo[11.
7.1.13,11.15,17.17,15]tetracosane (**2a**)

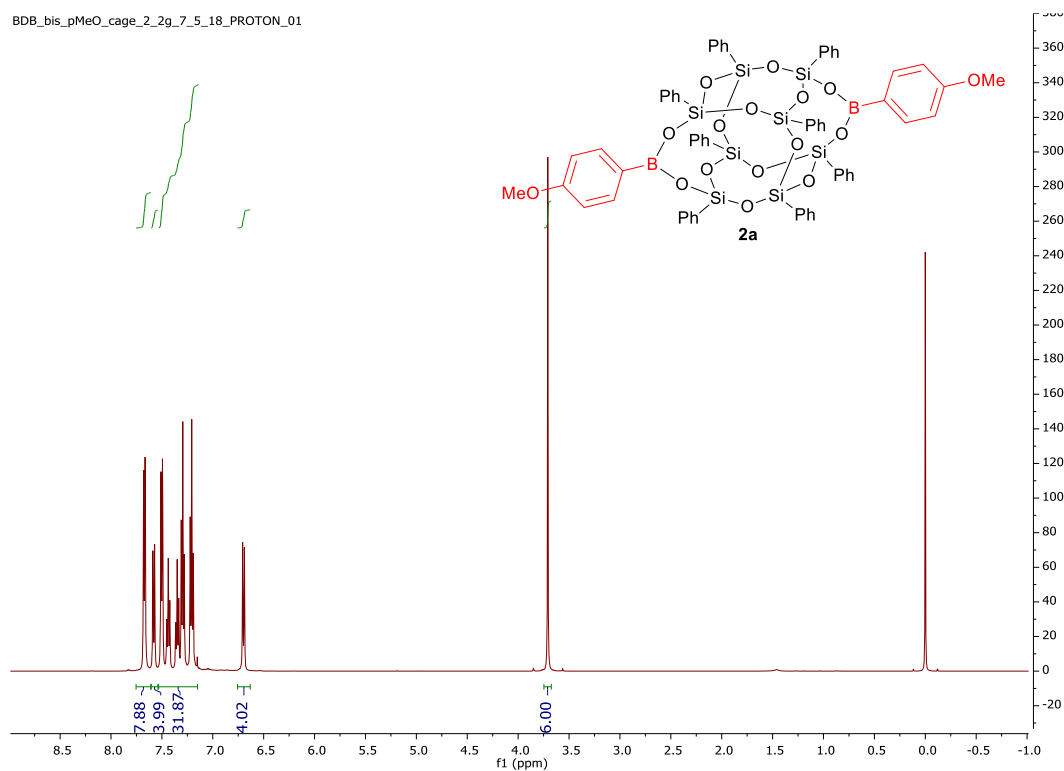


Figure 2-11: ¹H NMR (500 MHz, CDCl₃) of (p-MeOC₆H₄B)₂DDSQ **2a**

BDB_T8OH_2_5eq_pMeOPhB_OH_2_12_1_17_s2pul_02

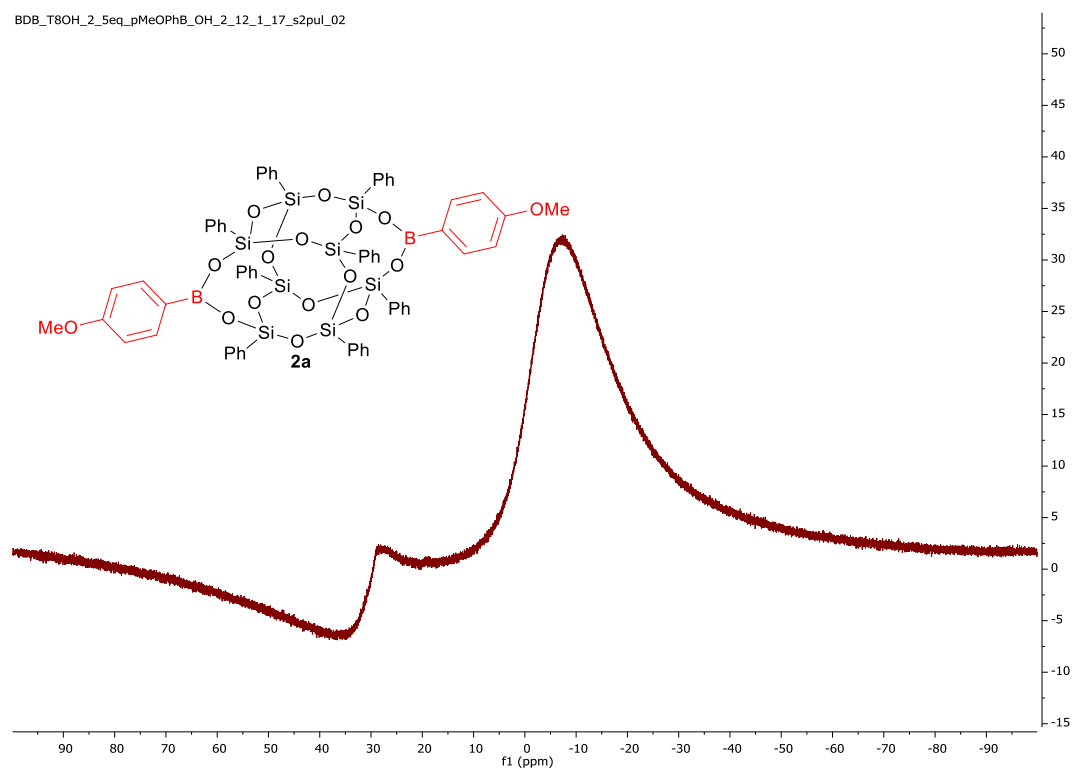


Figure 2-12: ^{11}B NMR (160 MHz, CDCl_3) of (p-MeOC₆H₄B)₂DDSQ **2a**

BDB_591_bis_cage_crystals_2_1_21_CARBON_01

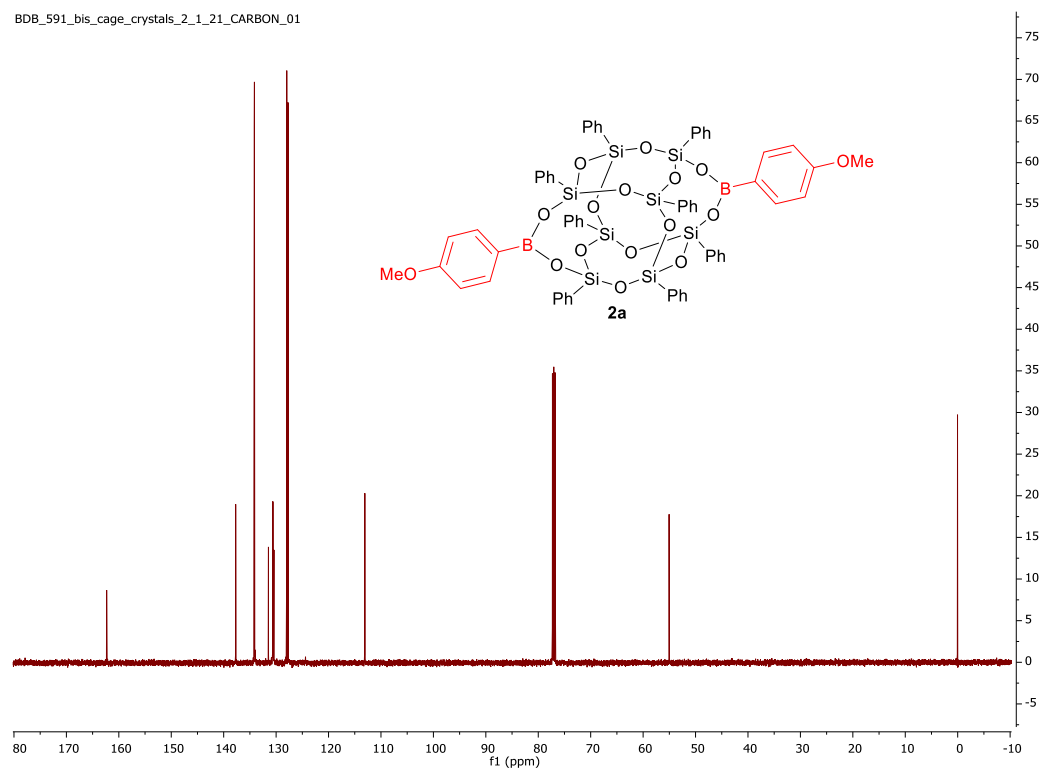


Figure 2-13: ^{13}C NMR (126 MHz, CDCl_3) of (p-MeOC₆H₄B)₂DDSQ **2a**

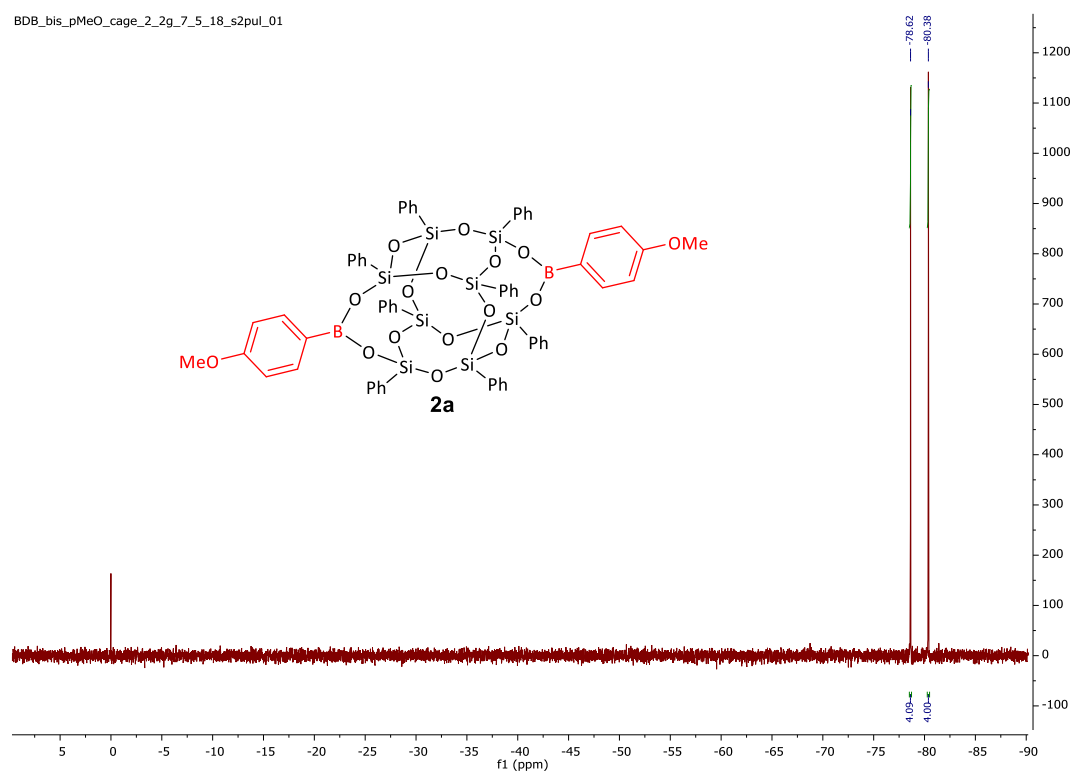


Figure 2-14: ^{29}Si NMR (99 MHz, CDCl_3) of (p-MeOC $_6$ H $_4$ B) $_2$ DDSQ **2a**

1,3,5,7,9,11,13,15,17,19-decaphenyl-2,4,6,8,10,12,14,16,18,20,21,22,23,24-tetra
decaoxa-1,3,5,7,11,13,15,17-octasila-9,19-diborapentacyclo[11.7.1.13,11.15,17.17,
15]tetracosane (**2b**)

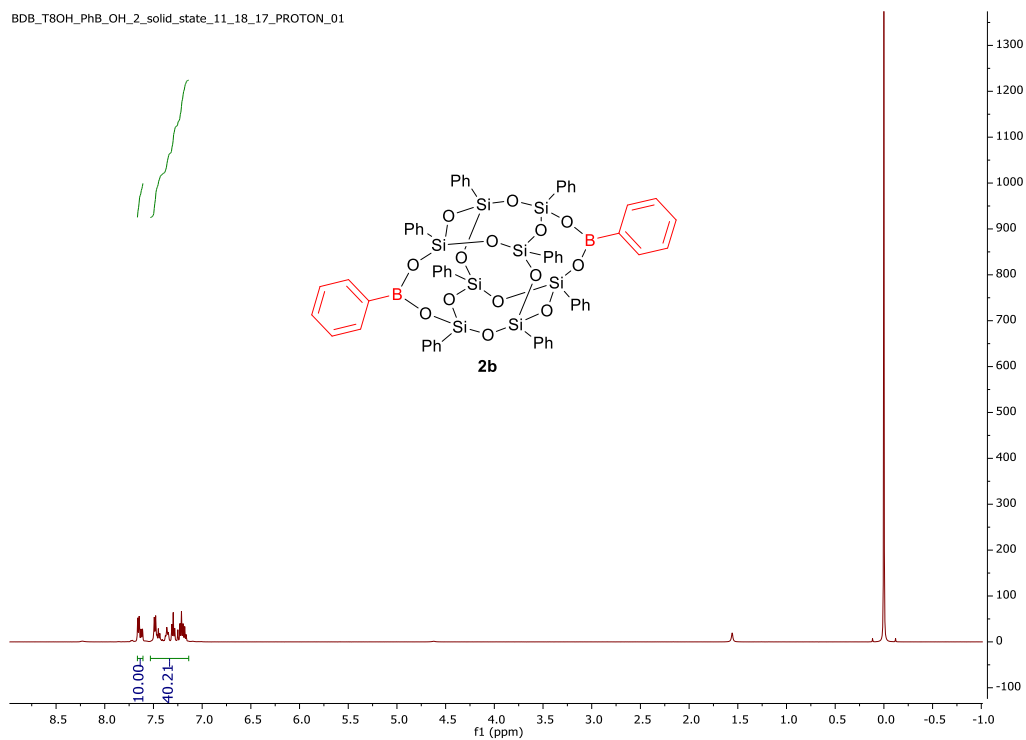


Figure 2-15: ^1H NMR (500 MHz, CDCl_3) of $(\text{C}_6\text{H}_4\text{B})_2\text{DDSQ}$ **2b**

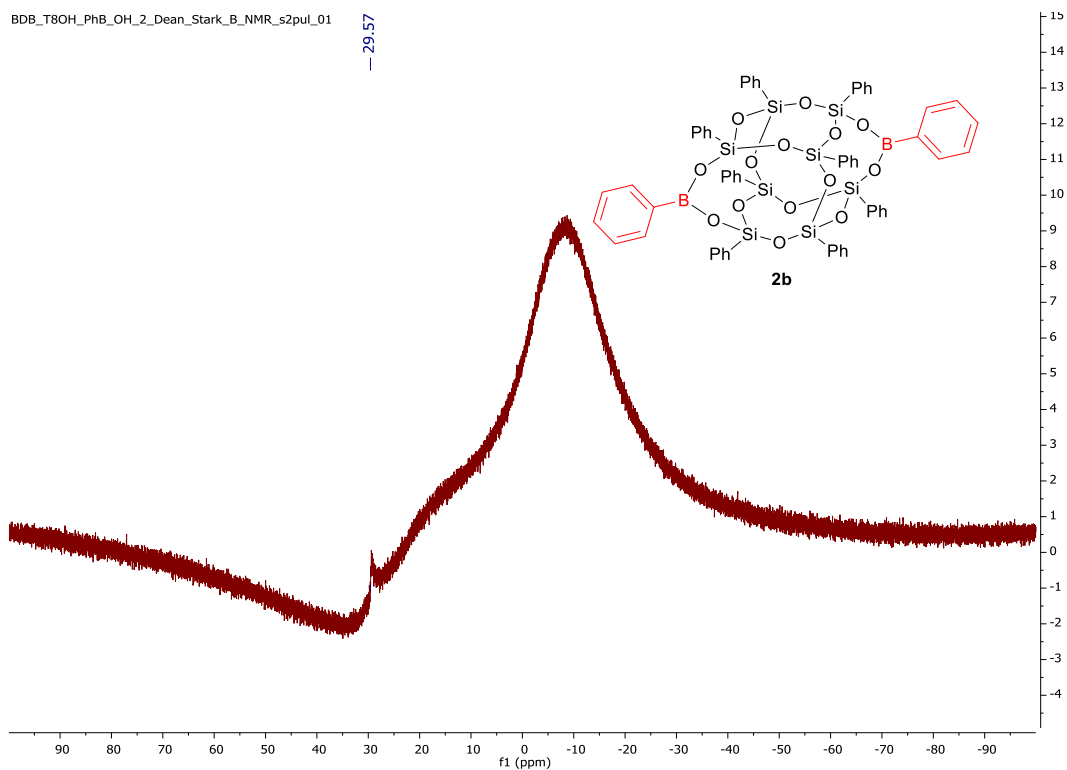


Figure 2-16: ^{11}B NMR (160 MHz, CDCl_3) of $(\text{C}_6\text{H}_4\text{B})_2\text{DDSQ}$ **2b**

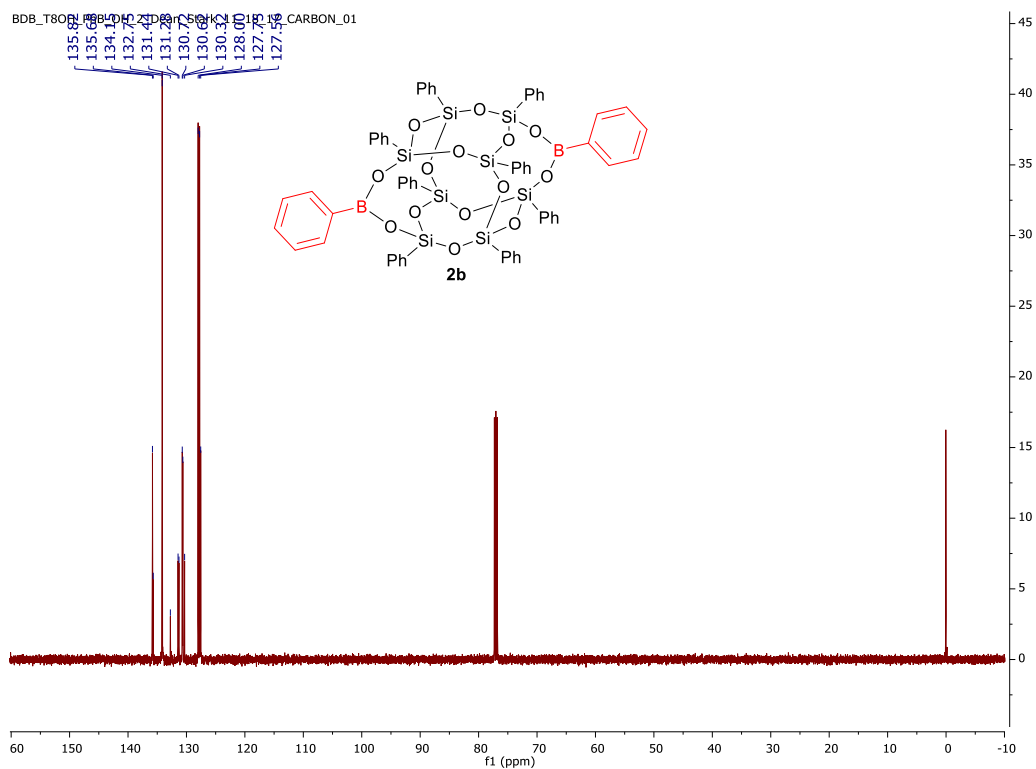


Figure 2-17: ^{13}C NMR (126 MHz, CDCl_3) of $(\text{C}_6\text{H}_4\text{B})_2\text{DDSQ}$ **2b**

BDB_T8OH_PhB_OH_2_Dean_Stark_11_18_17_s2pul_01

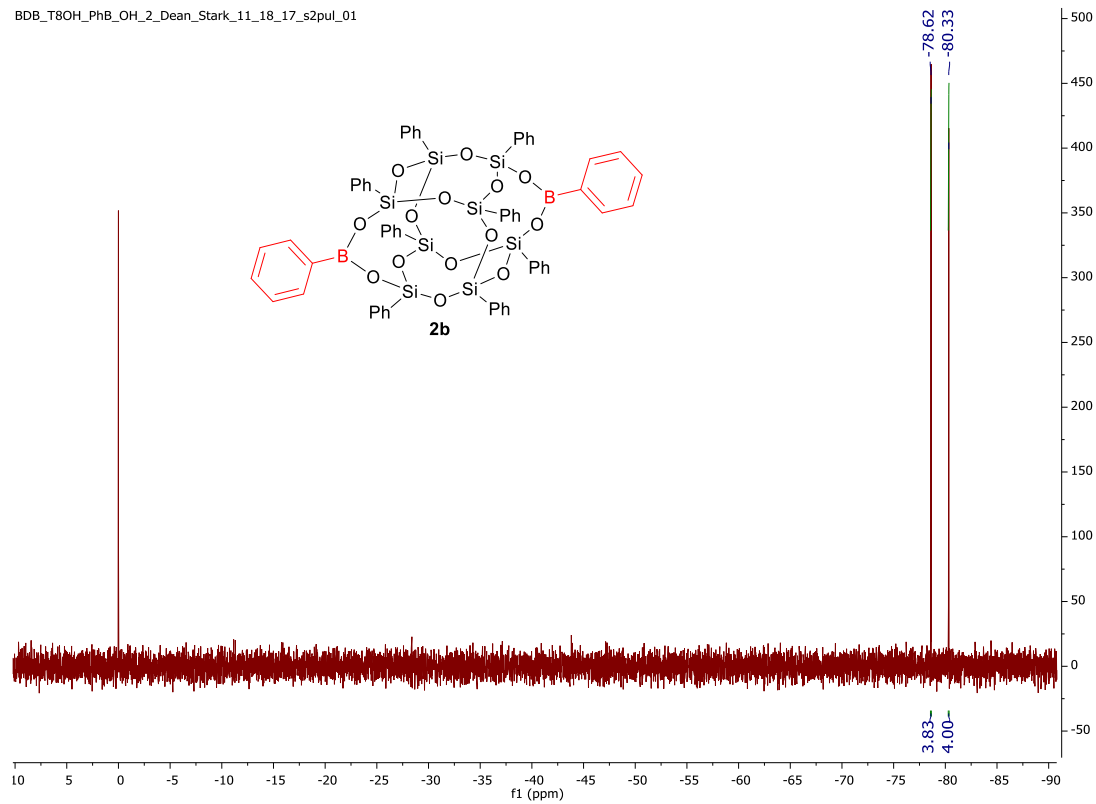


Figure 2-18: ^{29}Si NMR (99 MHz, CDCl_3) of $(\text{C}_6\text{H}_4\text{B})_2\text{DDSQ}$ **2b**

1,3,5,7,11,13,15,17-octaphenyl-9,19-di-*p*-tolyl-2,4,6,8,10,12,14,16,18,20,21,22,23,24-tetradecaoxa-1,3,5,7,11,13,15,17-octasila-9,19-diborapentacyclo[11.7.1.13,11.15,17.17,15]tetracosane (**2c**)

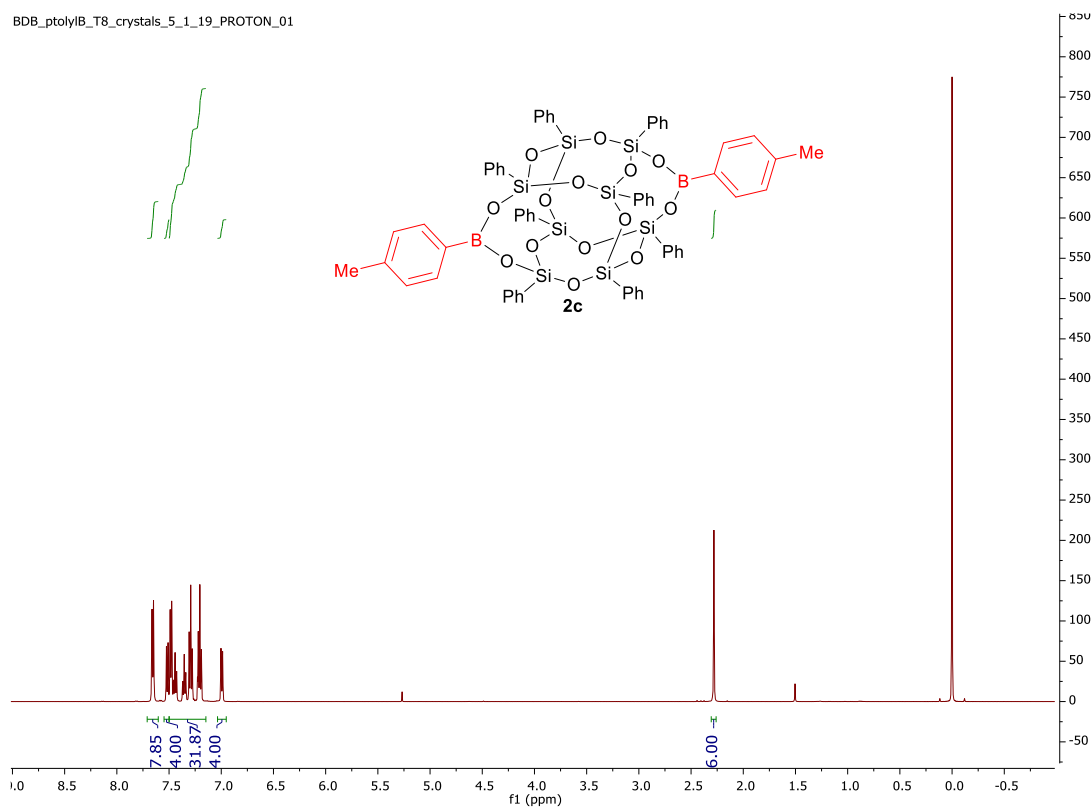


Figure 2-19: ^1H NMR (500 MHz, CDCl_3) of (*p*- $\text{MeC}_6\text{H}_4\text{B}$)₂DDSQ **2c**

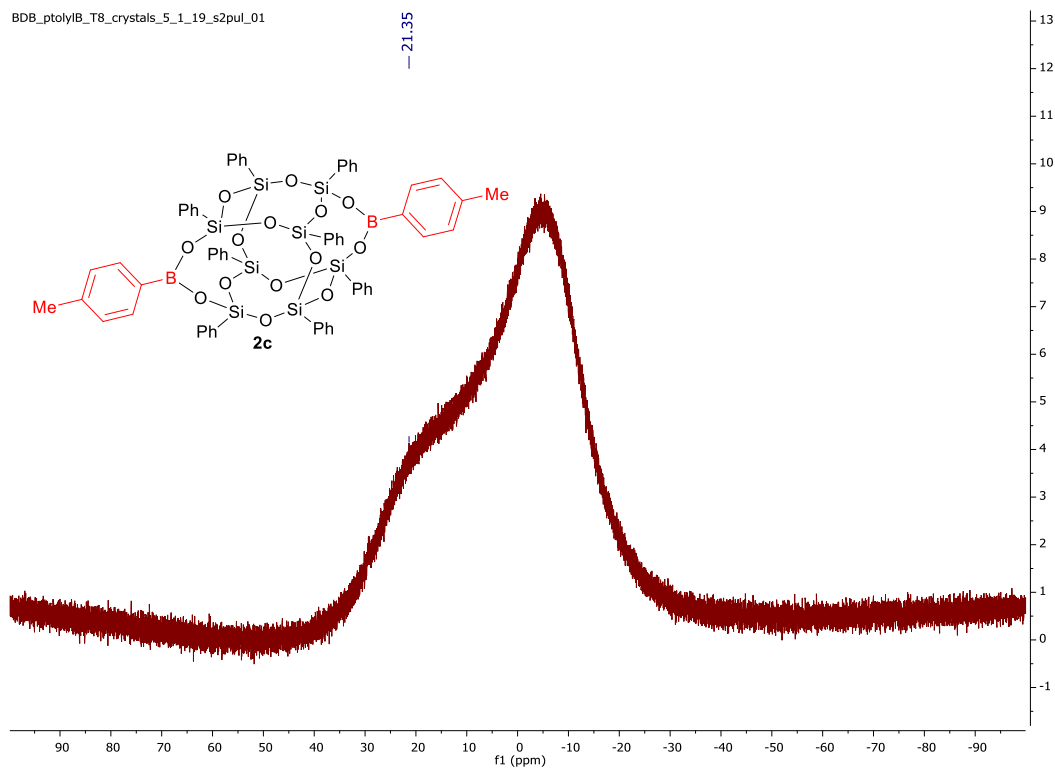


Figure 2-20: ^{11}B NMR (160 MHz, CDCl_3) of $(p\text{-MeC}_6\text{H}_4\text{B})_2\text{DDSQ}$ **2c**

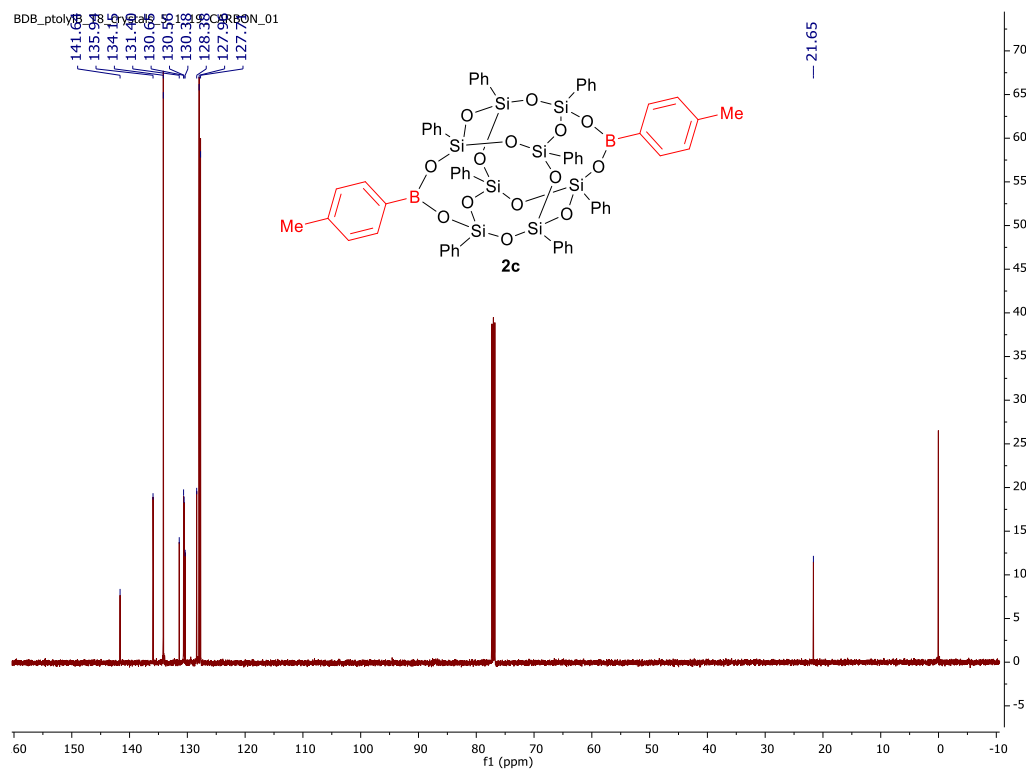


Figure 2-21: ^{13}C NMR (126 MHz, CDCl_3) of $(p\text{MeC}_6\text{H}_4\text{B})_2\text{DDSQ}$ **2c**

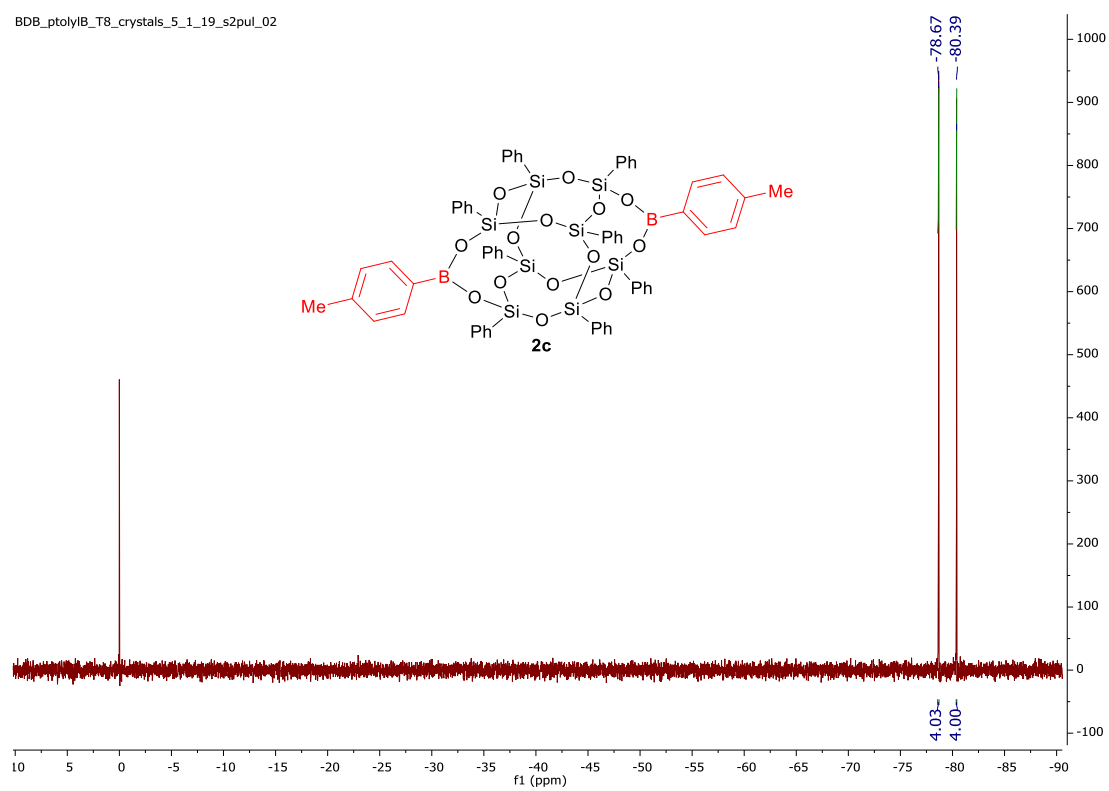


Figure 2-22: ^{29}Si NMR (99 MHz, CDCl_3) of $(\text{C}_6\text{H}_4\text{B})_2\text{DDSQ}$ **2c**

Asymmetrically Functionalized Products (6)

(1*r*,3*R*,11*s*,13*S*)-9,9,19-trimethyl-1,3,5,7,11,13,15,17-octaphenyl-2,4,6,8,10,12,14,16,18,20,21,22,23,24-tetradecaoxa-1,3,5,7,9,11,13,15,17,19-decasilapentacyclo[11.7.1.1.3.11.15, 17.17,15]tetracosane (**6a**)

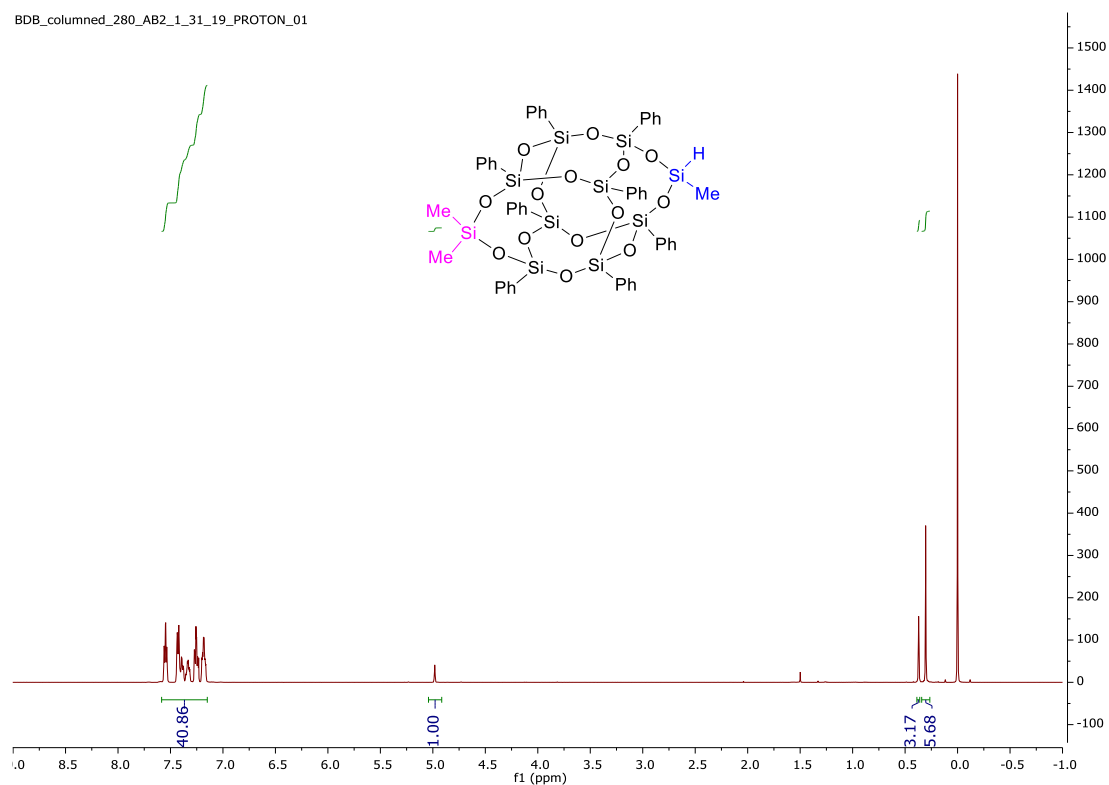


Figure 2-23: ¹H NMR (500 MHz, CDCl₃) of AB **6a**

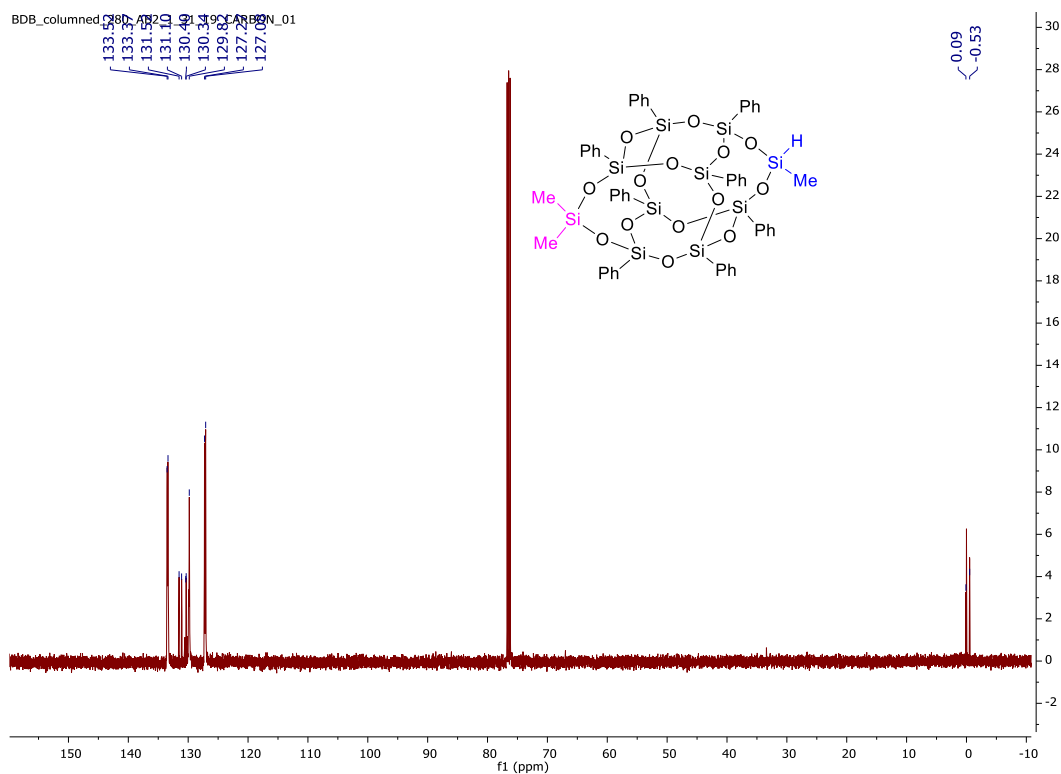


Figure 2-24: ^{13}C NMR (126 MHz, CDCl_3) of AB 6a

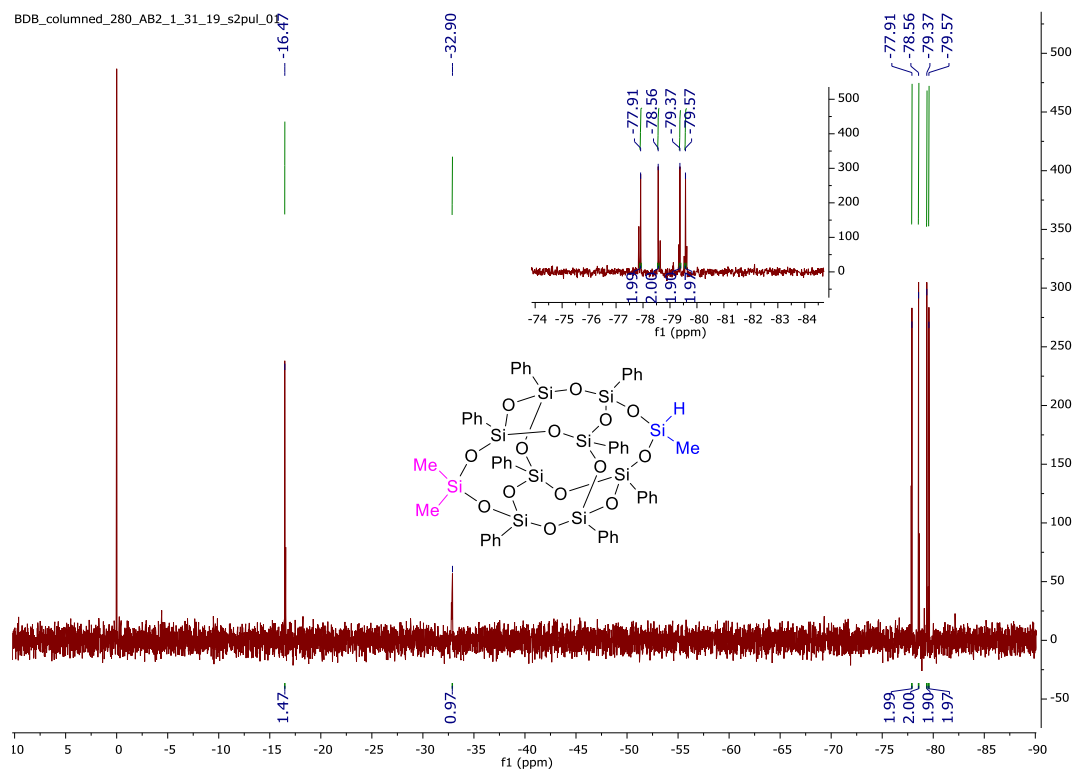


Figure 2-25: ^{29}Si NMR (99 MHz, CDCl_3) of AB 6a

(1*r*,3*R*,11*s*,13*S*)-9,19,19-trimethyl-1,3,5,7,11,13,15,17-octaphenyl-2,4,6,8,10,12,14, 16, 18,20,21,22,23,24-tetradeca-oxa-1,3,5,7,9,11,13,15,17,19-decasilapentacyclo [11.7.1. 13,11.15,17.17,15]tetracosan-9-ol (**6b**)

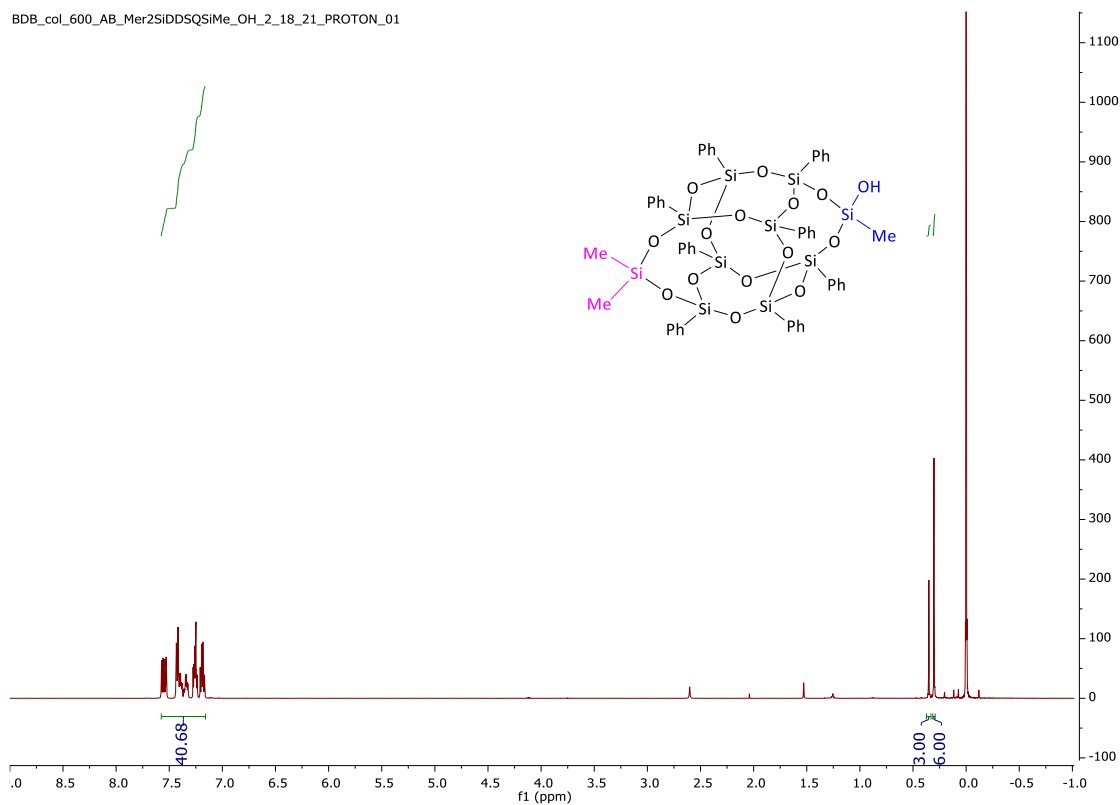


Figure 2-26: ^1H NMR (500 MHz, CDCl_3) of AB **6b**

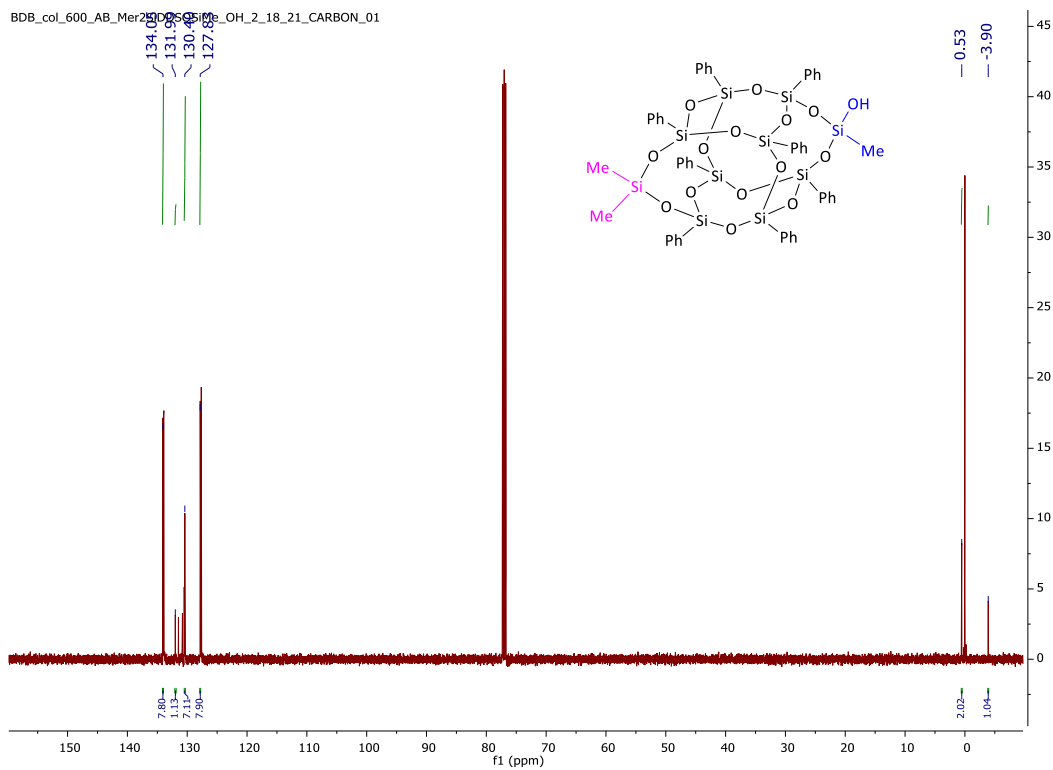


Figure 2-27: ^{13}C NMR (126 MHz, CDCl_3) of AB 6b

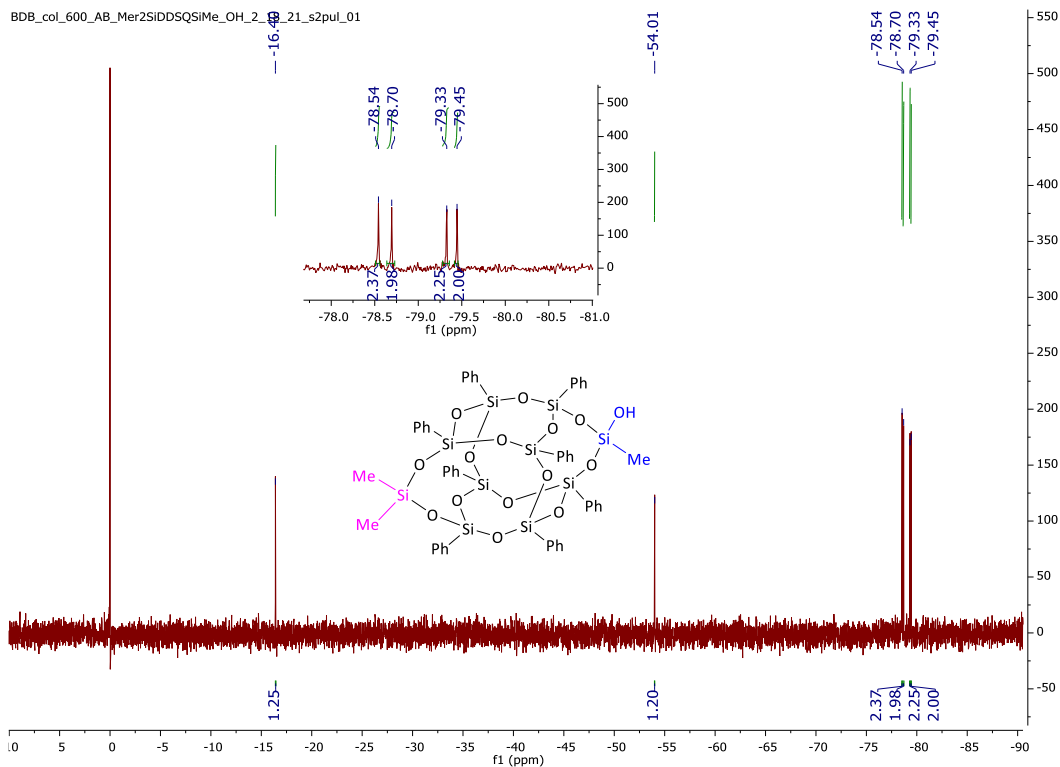


Figure 2-28: ^{29}Si NMR (99 MHz, CDCl_3) of AB 6b

4-((1*r*,3*R*,11*s*,13*S*)-9,19-dimethyl-1,3,5,7,11,13,15,17-octaphenyl-2,4,6,8,10,12,14,16,18,20,21,22,23,24-tetradecaoxa-1,3,5,7,9,11,13,15,17,19-decasilapentacyclo[11.7.1.13,11.15,17.17,15]tetracosan-9-yl)butanenitrile (**6c**)

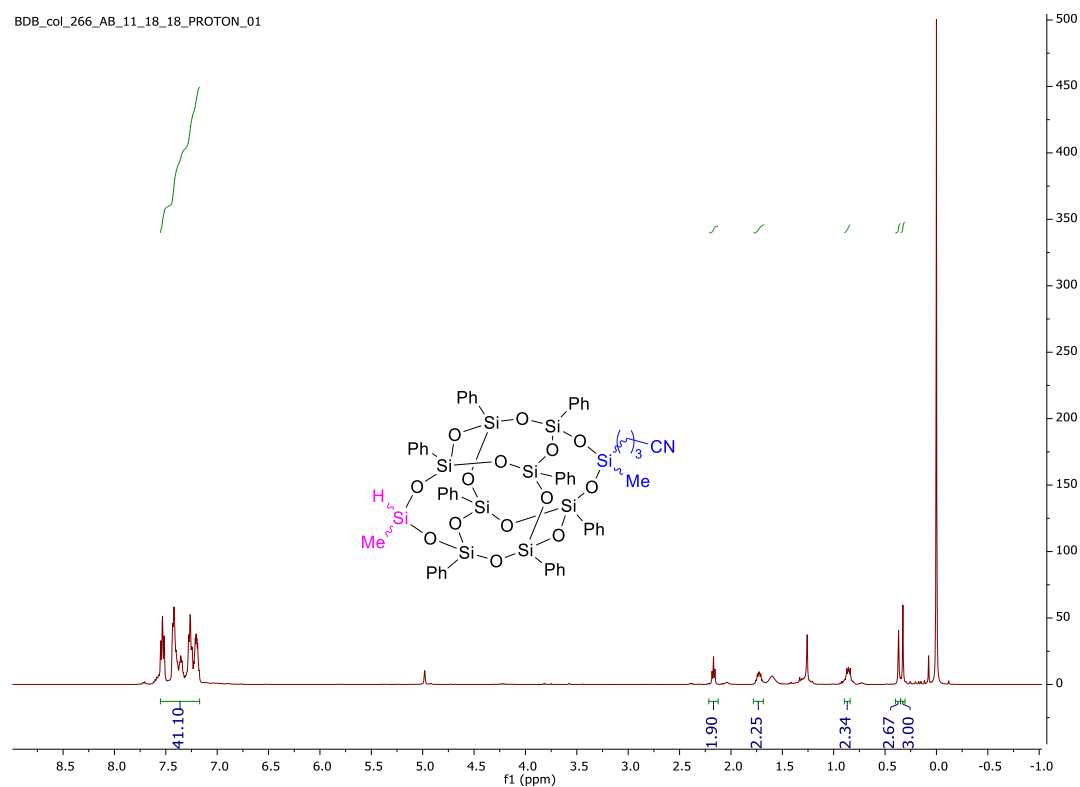


Figure 2-29: ¹H NMR (500 MHz, CDCl₃) of **AB 6c**

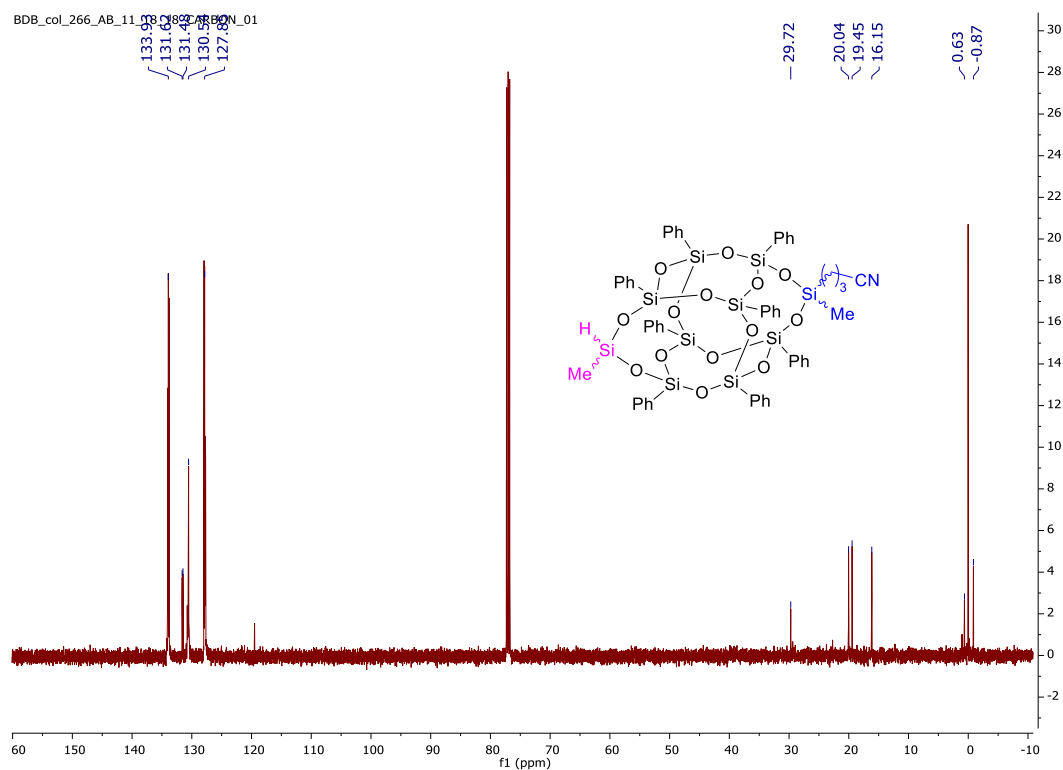


Figure 2-30: ^{13}C NMR (126 MHz, CDCl_3) of AB 6c

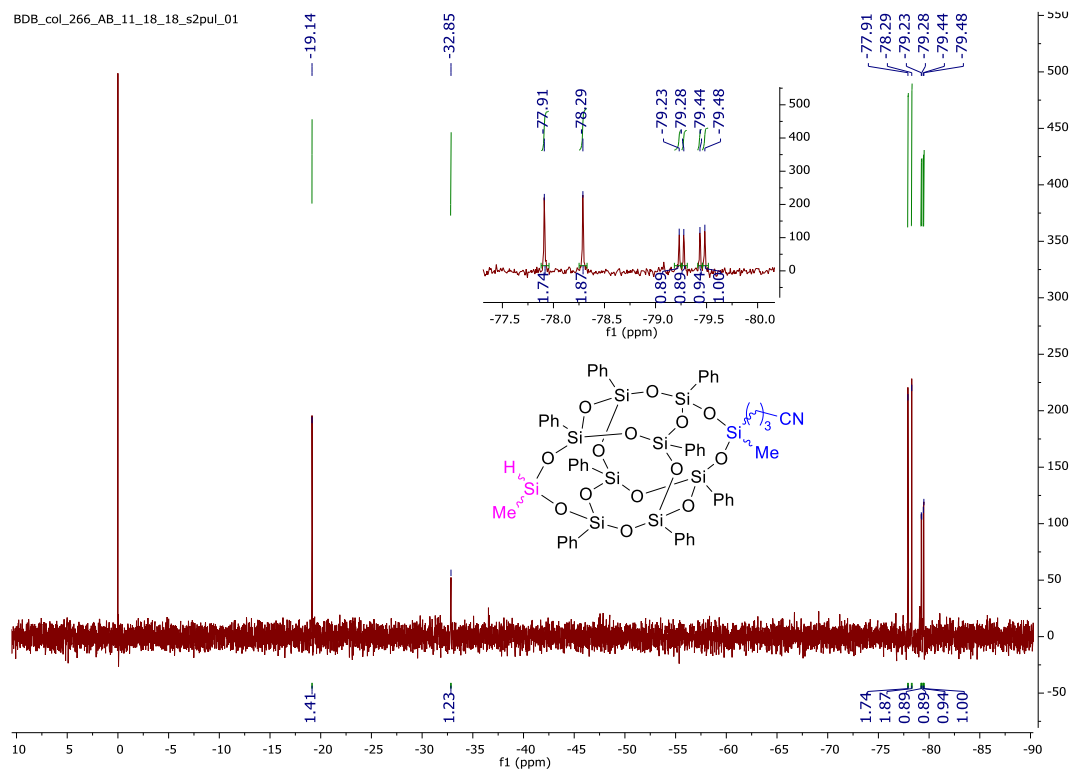


Figure 2-31: ^{29}Si NMR (99 MHz, CDCl_3) of AB 6c

4-((1*r*,3*R*,11*s*,13*S*)-9,19,19-trimethyl-1,3,5,7,11,13,15,17-octaphenyl-2,4,6,8,10,12,14,16,18,20,21,22,23,24-tetradecaoxa-1,3,5,7,9,11,13,15,17,19-decasilapentacyclo[11.7.1.13,11.15,17.17,15]tetracosan-9-yl)butanenitrile (**6d**)

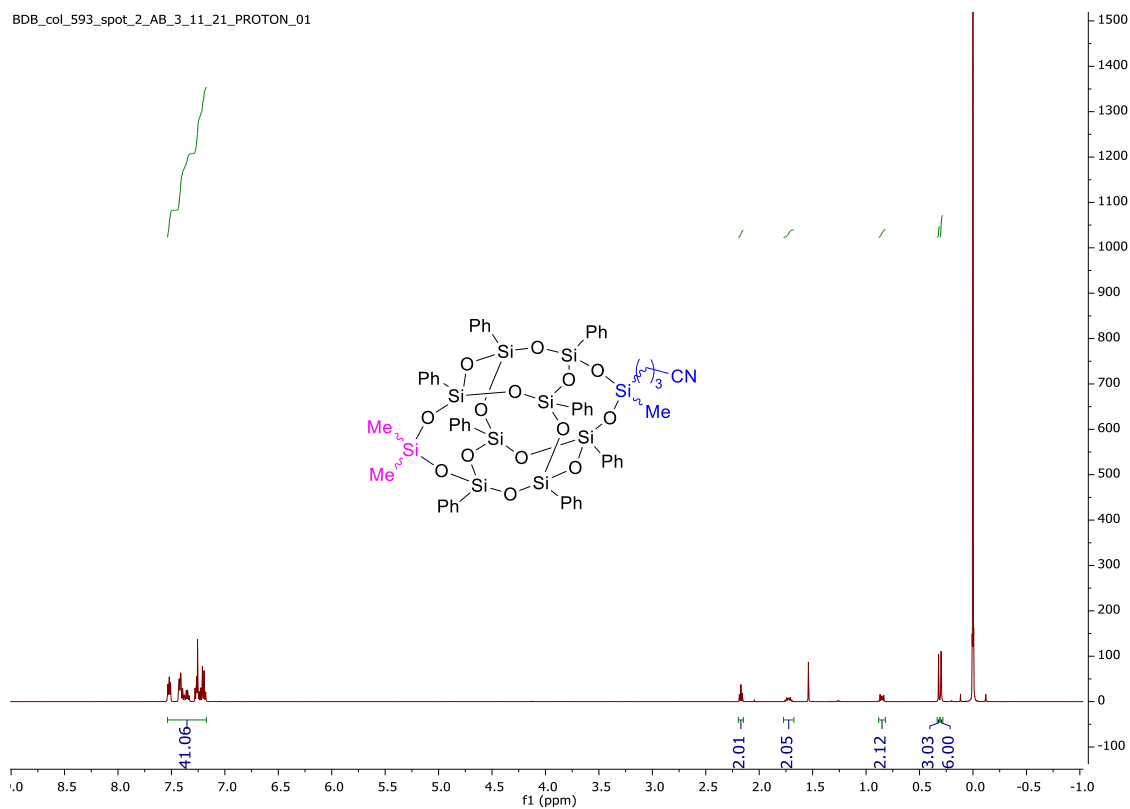


Figure 2-32: ^1H NMR (500 MHz, CDCl_3) of **AB 6d**

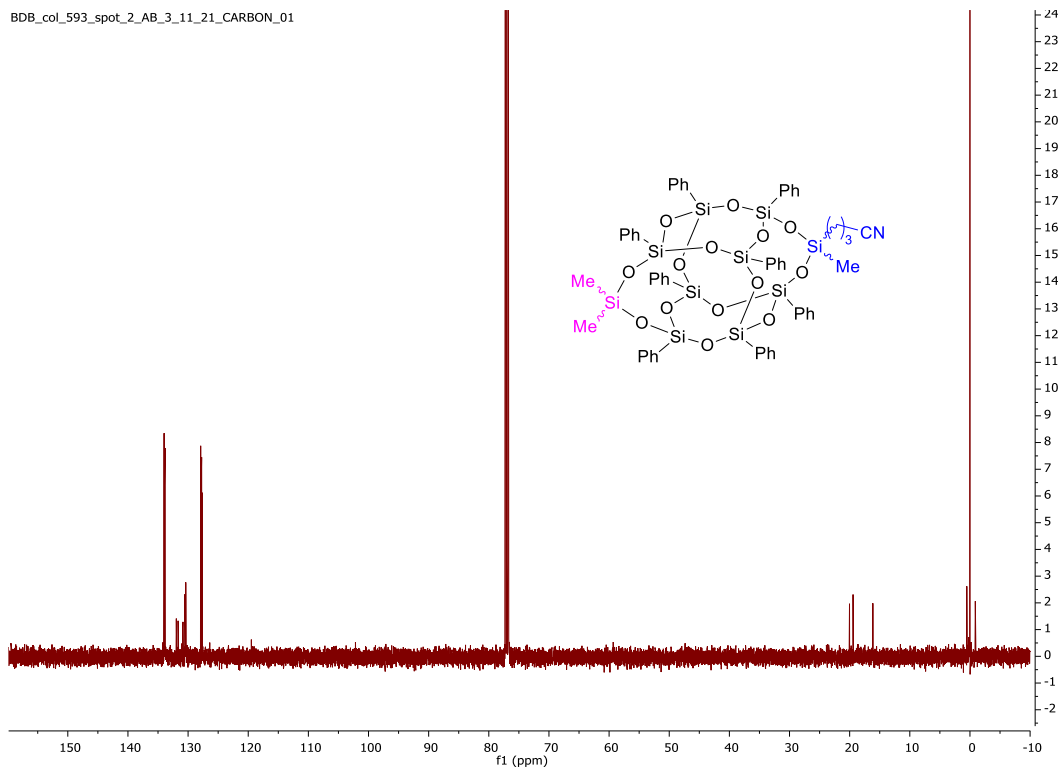


Figure 2-33: ^{13}C NMR (126 MHz, CDCl_3) of AB 6d

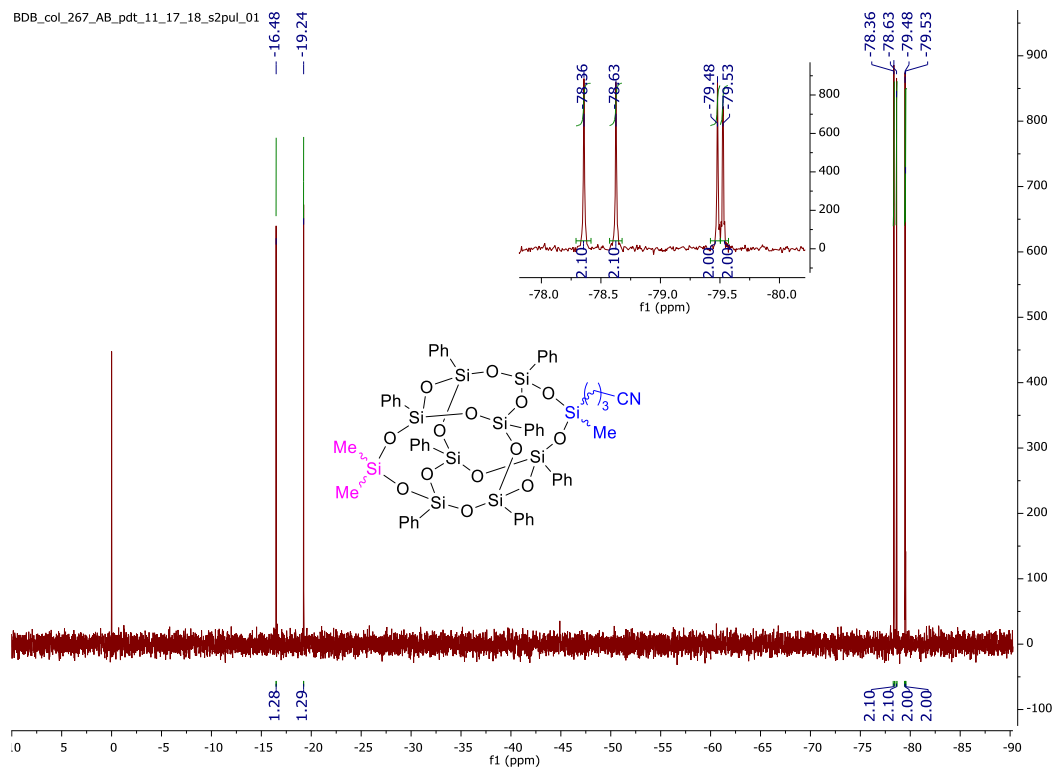


Figure 2-34: ^{29}Si NMR (99 MHz, CDCl_3) of AB 6d

4-((1*s*,3*R*,11*r*,13*S*)-9,19-dimethyl-1,3,5,7,11,13,15,17-octaphenyl-19-vinyl-2,4,6,8,10,12,14,16,18,20,21,22,23,24-tetradecaoxa-1,3,5,7,9,11,13,15,17,19-decasilapentacyclo[11.7.1.13,11.15,17.17,15]tetracosan-9-yl)butanenitrile (**6f**)

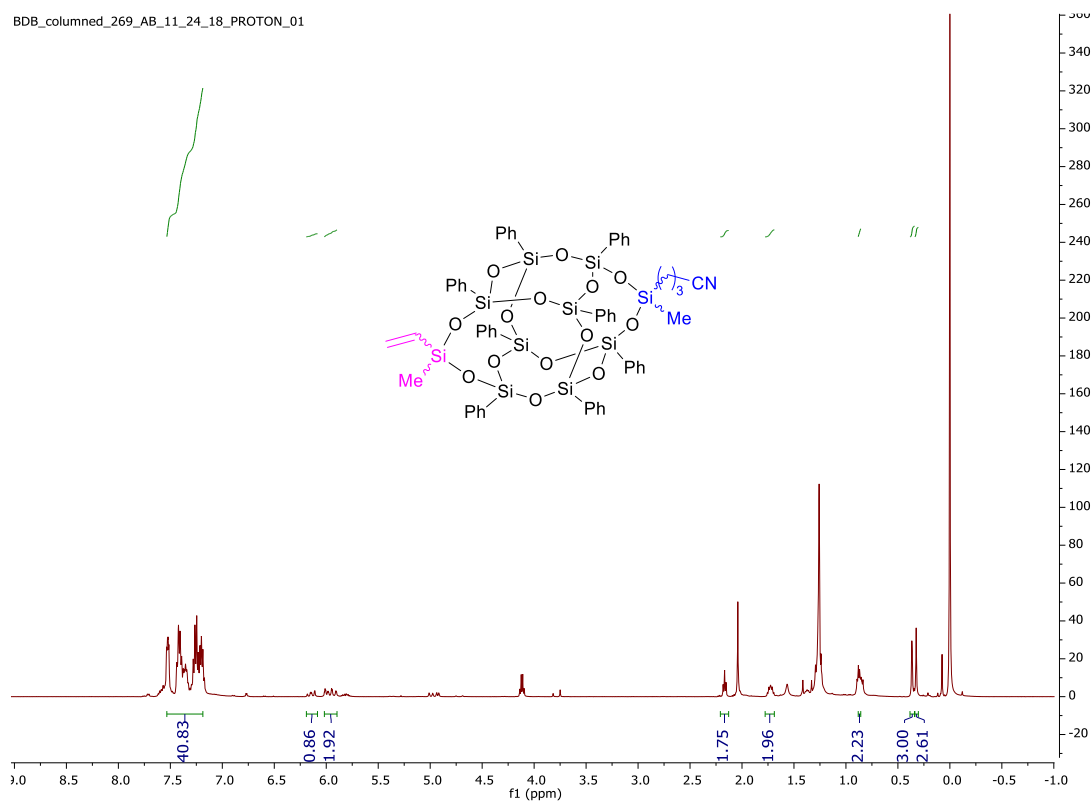


Figure 2-35: ¹H NMR (500 MHz, CDCl₃) of AB **6f**

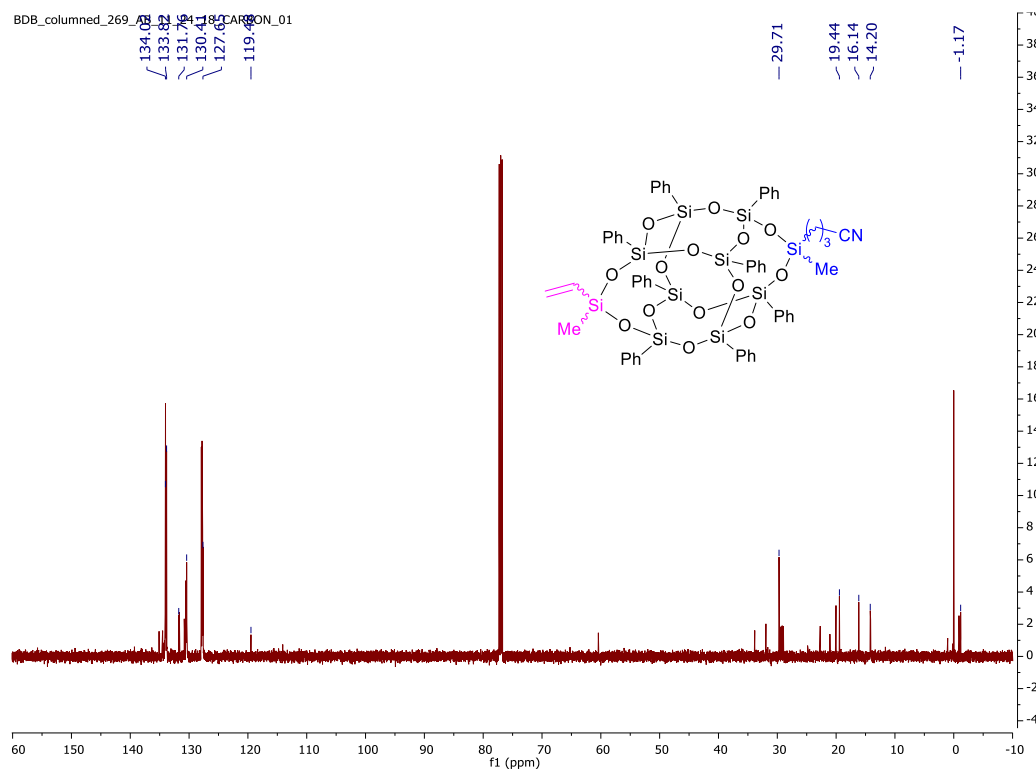


Figure 2-36: ^{13}C NMR (126 MHz, CDCl_3) of AB 6e

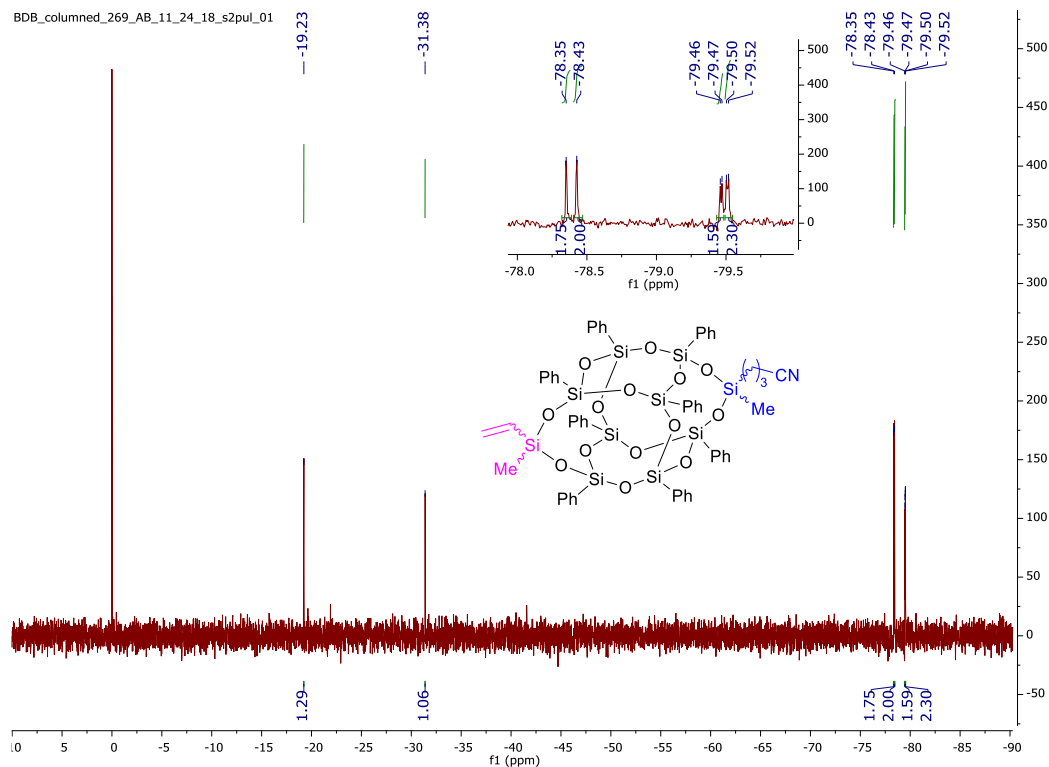


Figure 2-37: ^{29}Si NMR (99 MHz, CDCl_3) of AB 6f

(1*r*,3*R*,11*s*,13*S*)-9,19-dimethyl-1,3,5,7,11,13,15,17-octaphenyl-9-vinyl-2,4,6,8,10,12,14,16,18,20,21,22,23,24-tetradeca-oxa-1,3,5,7,9,11,13,15,17,19-decasilapentacyclo[11.7.1.13,11.15,17.17,15]tetracosane (**6g**)

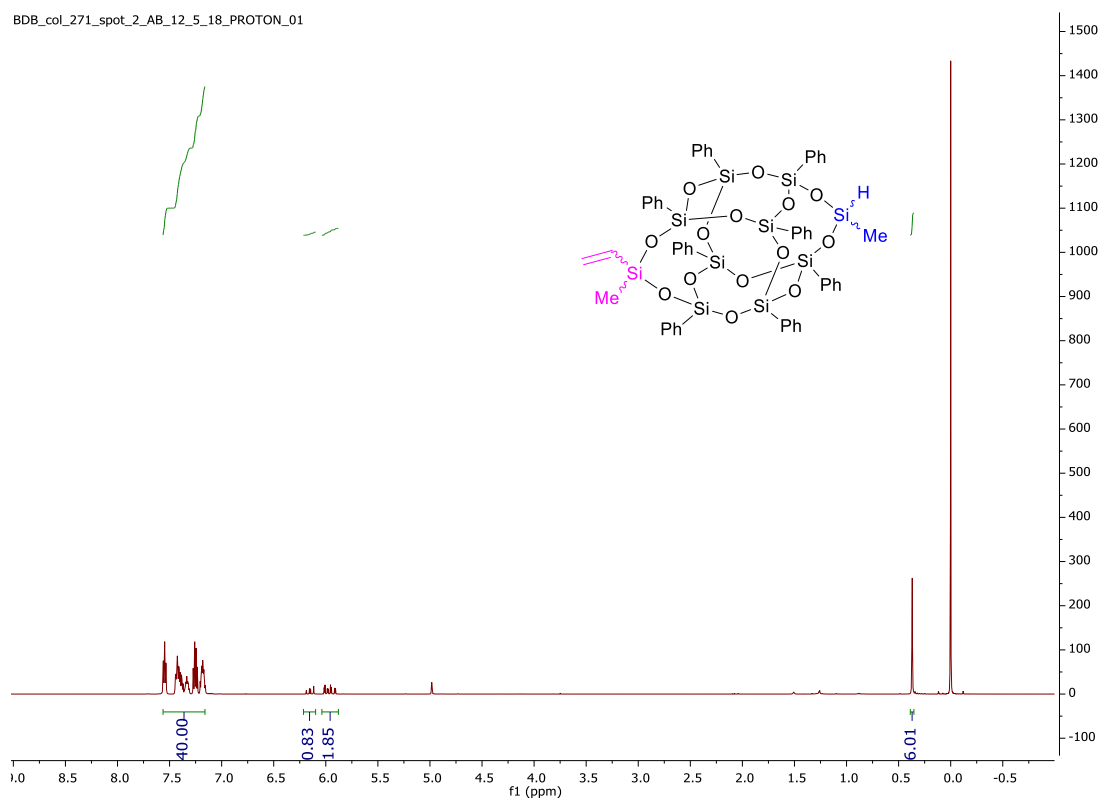


Figure 2-38: ^1H NMR (500 MHz, CDCl_3) of AB **6g**

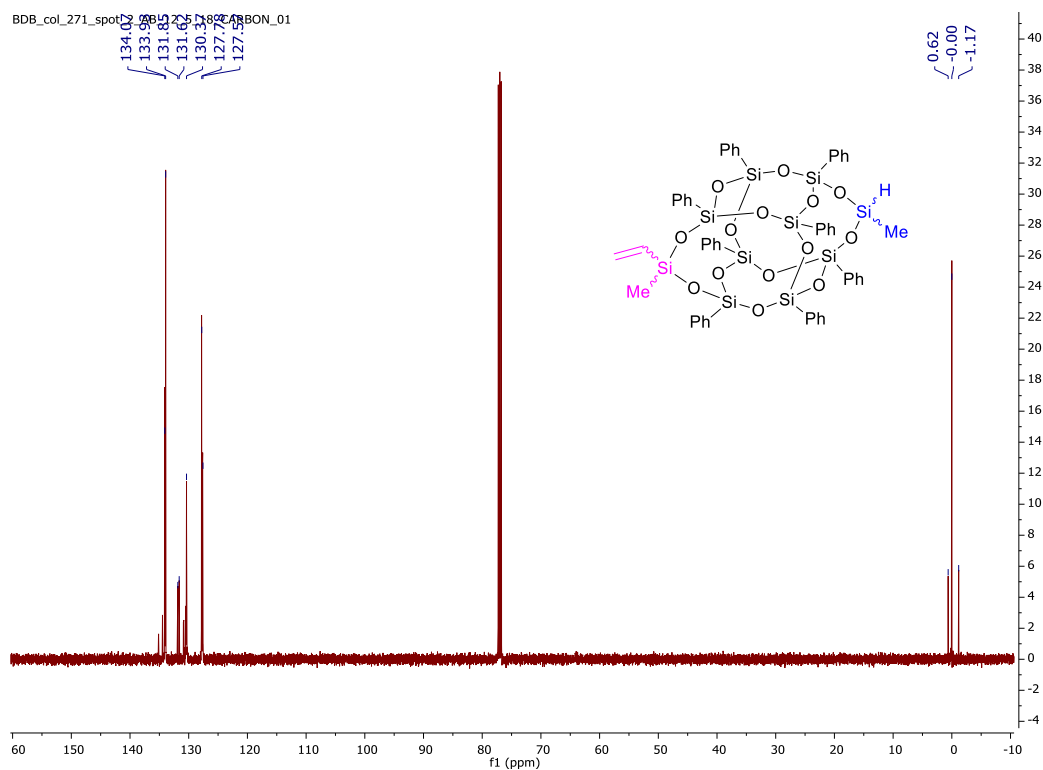


Figure 2-39: ^{13}C NMR (126 MHz, CDCl_3) of AB 6g

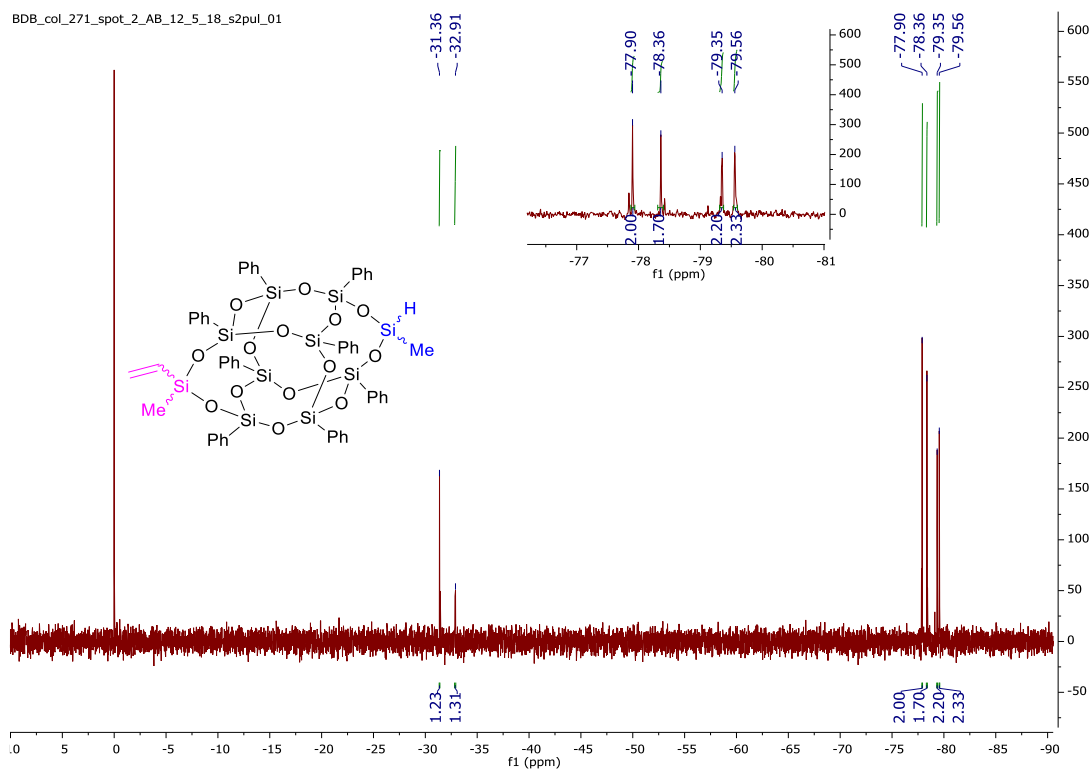


Figure 2-40: ^{29}Si NMR (99 MHz, CDCl_3) of AB 6g

(1*r*,3*R*,11*s*,13*S*)-19-methyl-1,3,5,7,11,13,15,17-octaphenyl-9-vinyl-2,4,6,8,10,12,14,16,18,20,21,22,23,24-tetradecaoxa-1,3,5,7,9,11,13,15,17,19-decasilapentacyclo[11.7.1.13, 11.15,17.17,15]tetracosan-9-ol (**6h**)

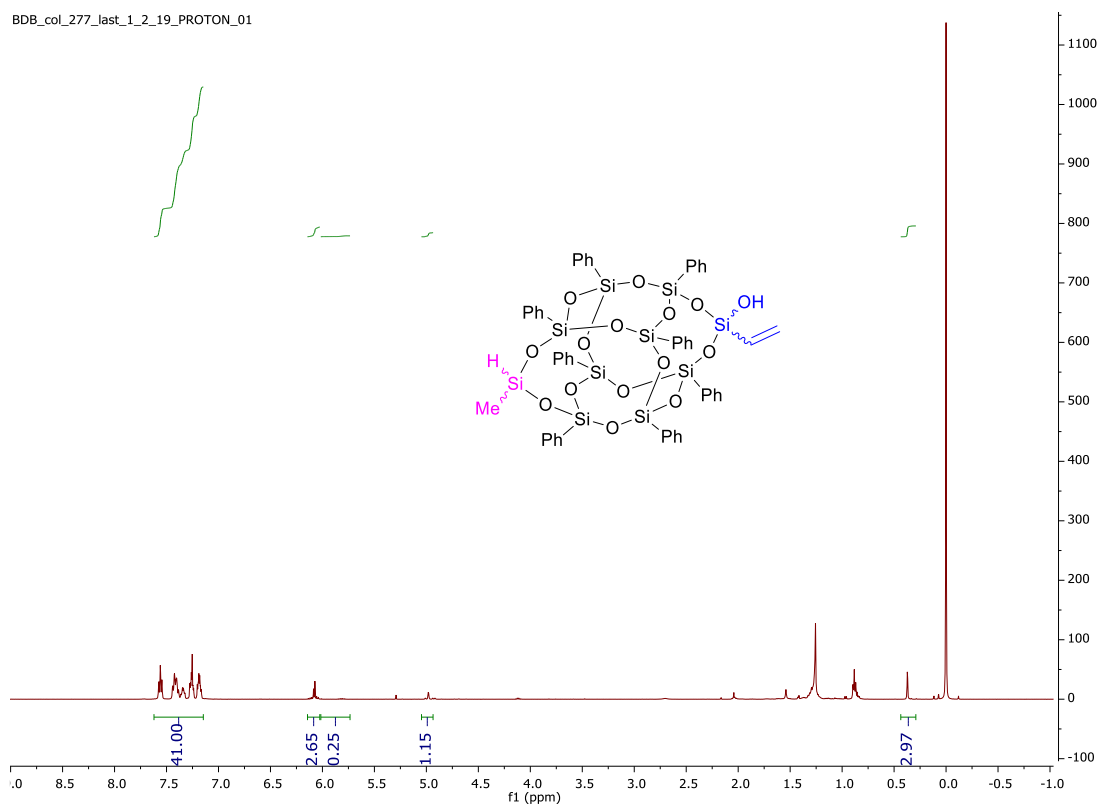


Figure 2-41: ^1H NMR (500 MHz, CDCl_3) of AB **6h**

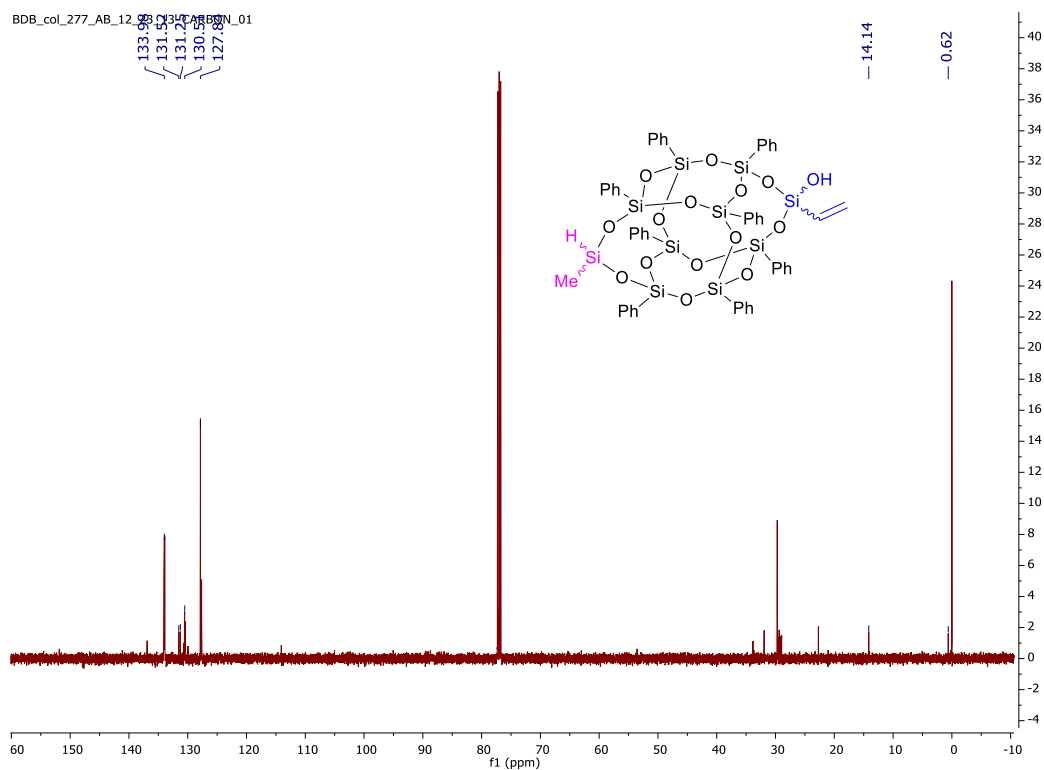


Figure 2-42: ^{13}C NMR (126 MHz, CDCl_3) of AB 6h

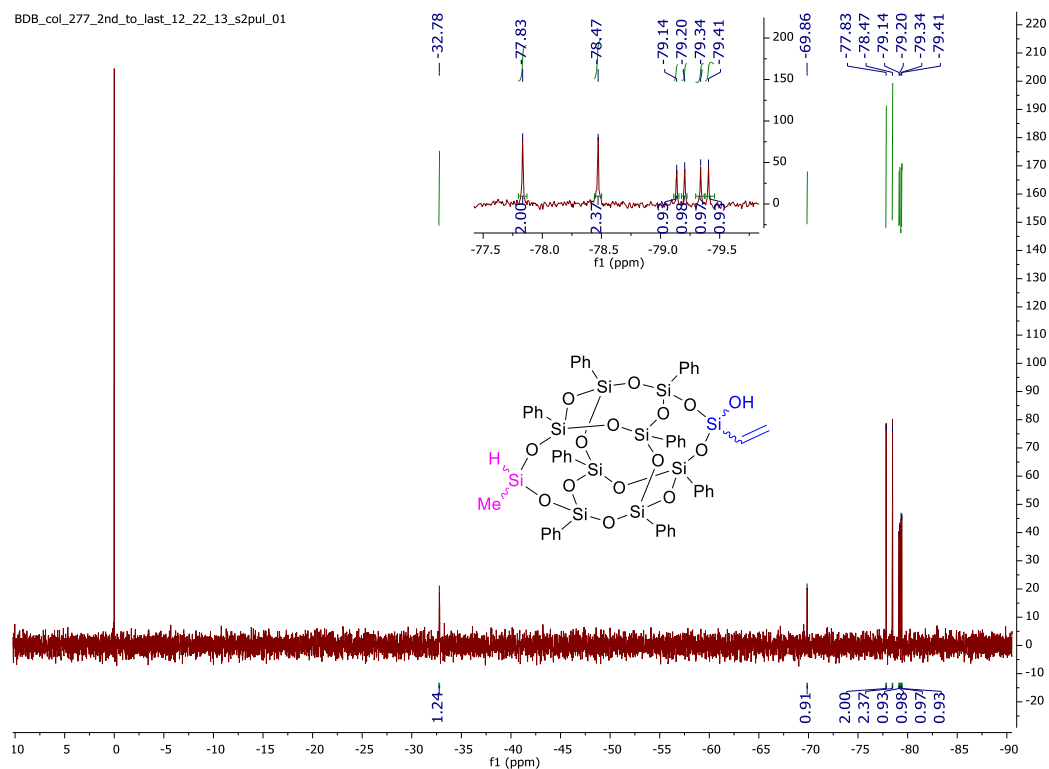


Figure 2-43: ^{29}Si NMR (99 MHz, CDCl_3) of AB 6h

(1*r*,3*R*,11*s*,13*S*)-9-isopropyl-19-methyl-1,3,5,7,11,13,15,17-octaphenyl-19-vinyl-2,4,6,8,10,12,14,16,18,20,21,22,23,24-tetradeca-oxa-1,3,5,7,9,11,13,15,17,19-decasilapentacyclo[11.7.1.13, 11.15,17.17,15]tetracosan-9-ol (**6i**)

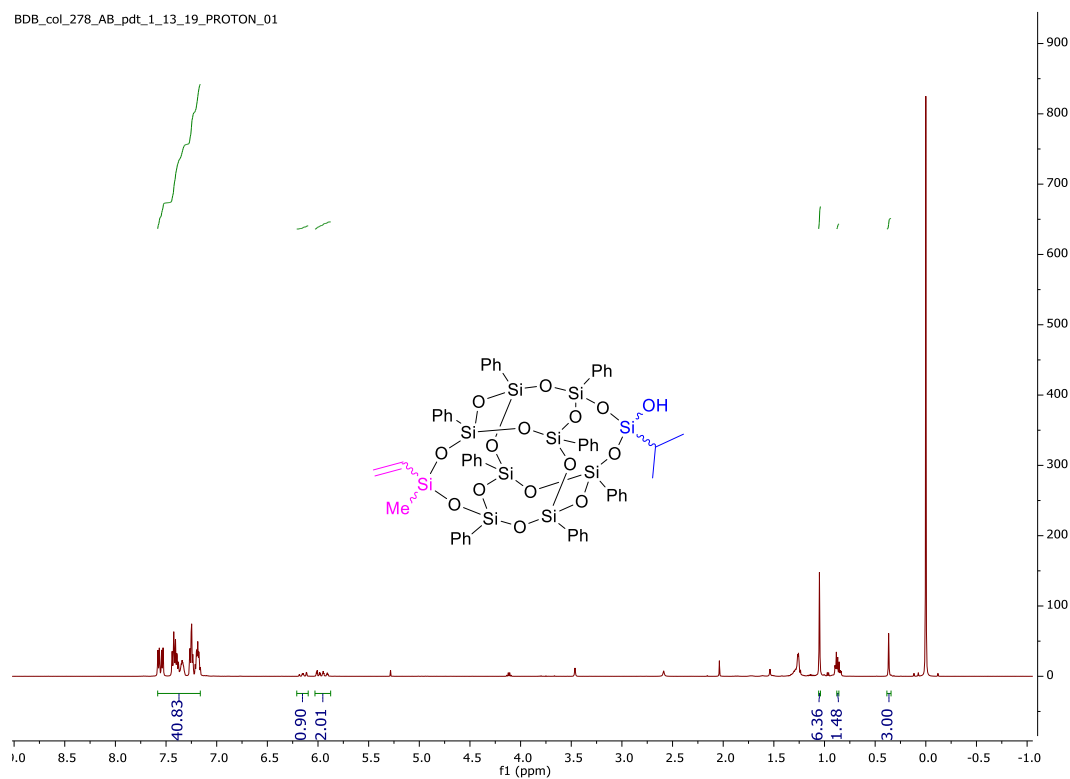


Figure 2-44: ¹H NMR (500 MHz, CDCl₃) of AB **6i**

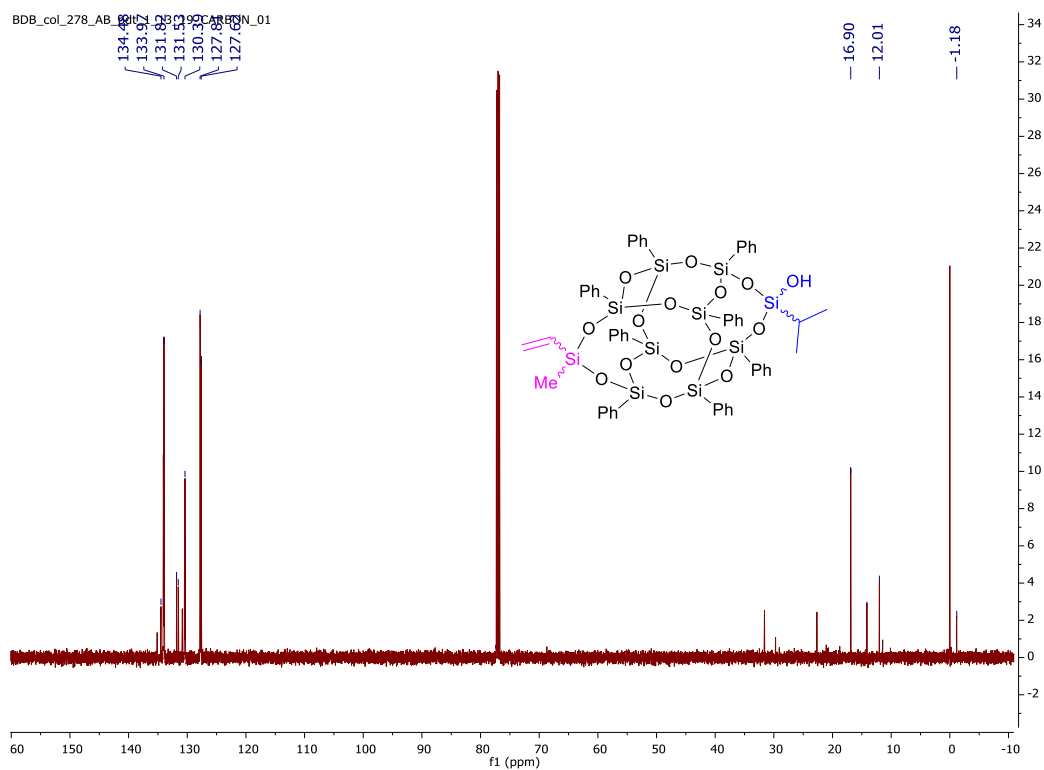


Figure 2-45: ^{13}C NMR (126 MHz, CDCl_3) of AB 6i

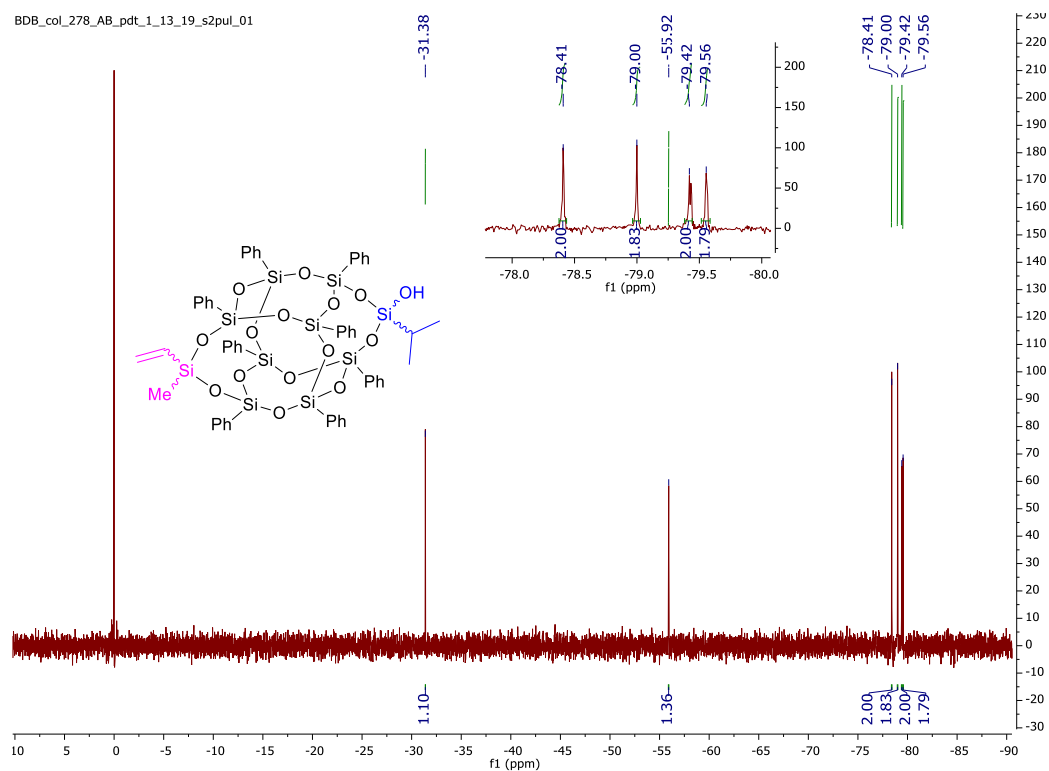


Figure 2-46: ^{29}Si NMR (99 MHz, CDCl_3) of AB 6i

Copies of Mass Spectra of Asymmetrically Functionalized DDSQs (6)

(1*r*,3*R*,11*s*,13*S*)-9,9,19-trimethyl-1,3,5,7,11,13,15,17-octaphenyl-2,4,6,8,10,12,14,16,18,20,21,22,23,24-tetradecaoxa-1,3,5,7,9,11,13,15,17,19-decasilapentacyclo[11.7.1.1.3, 11.15,17.17,15]tetracosane (**6a**)

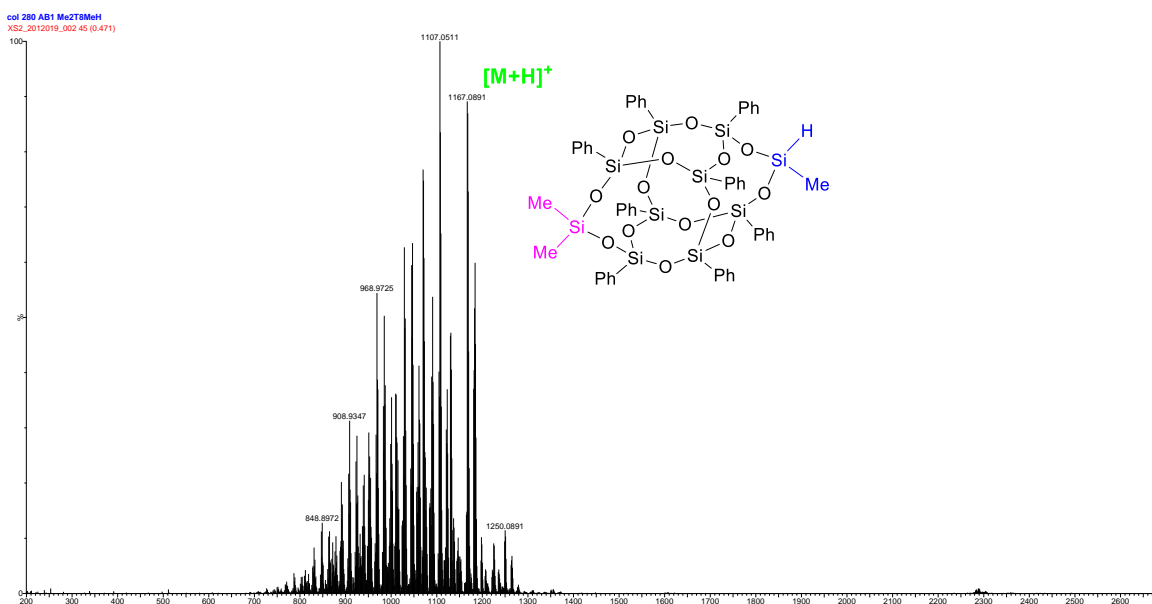


Figure 2-47: Mass Spec of AB 6a

(1*r*,3*R*,11*s*,13*S*)-9,19,19-trimethyl-1,3,5,7,11,13,15,17-octaphenyl-2,4,6,8,10,12,14, 16, 18,20,21,22,23,24-tetradeca-oxa-1,3,5,7,9,11,13,15,17,19-decasilapentacyclo
[11.7.1.13,11.15,17.17,15]tetracosan-9-ol (**6b**)

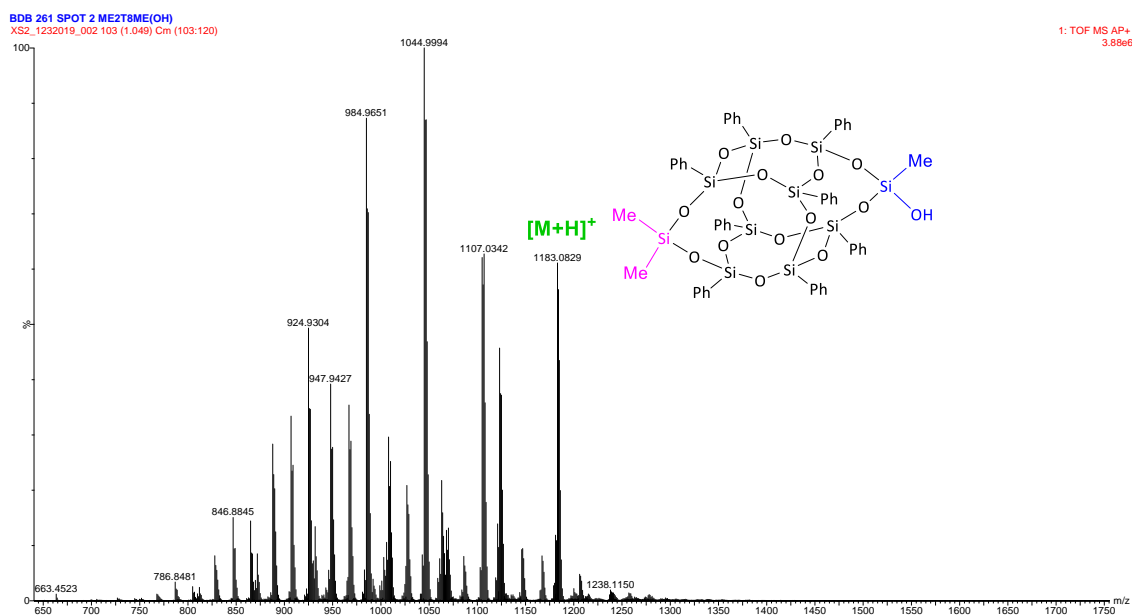


Figure 2-48: Mass Spec of AB 6b

4-((1*r*,3*R*,11*s*,13*S*)-9,19-dimethyl-1,3,5,7,11,13,15,17-octaphenyl-2,4,6,8,10,12,14, 16, 18,20,21,22,23,24-tetradecaoxa-1,3,5,7,9,11,13,15,17,19-decasilapentacyclo
[11.7.1.13,11.15,17.17,15]tetracosan-9-yl)butanenitrile (**6c**)

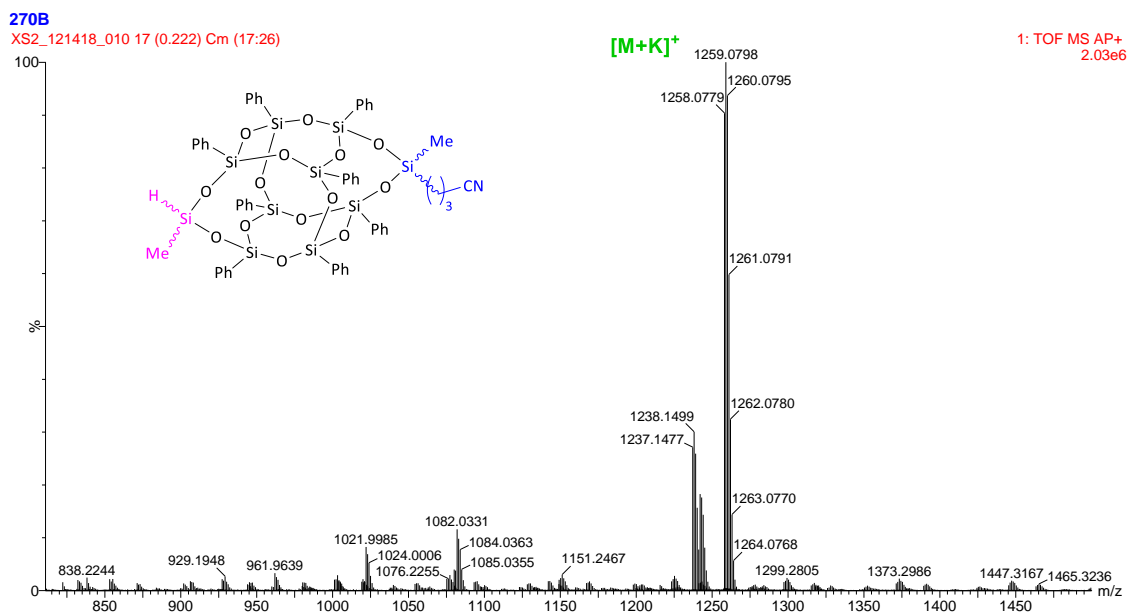


Figure 2-49: Mass Spec of AB 6c

4-((1*r*,3*R*,11*s*,13*S*)-9,19,19-trimethyl-1,3,5,7,11,13,15,17-octaphenyl-2,4,6,8,10,12,14,16,18,20,21,22,23,24-tetradecaoxa-1,3,5,7,9,11,13,15,17,19-decasilapentacyclo[11.7.1.13,11.15,17.17,15]tetracosan-9-yl)butanenitrile (**6d**)

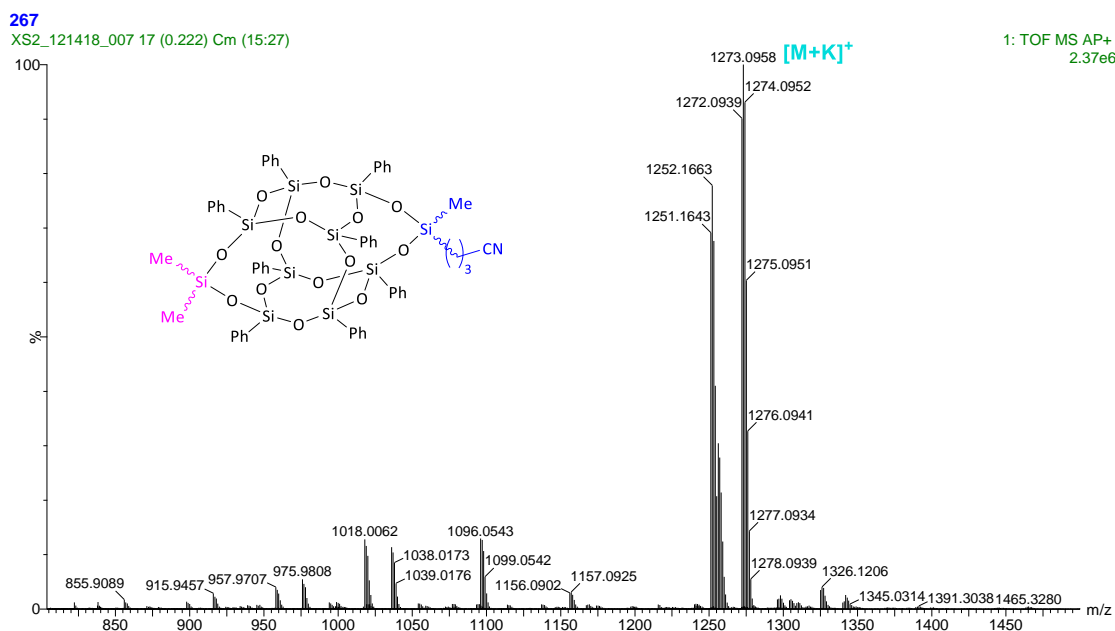


Figure 2-50: Mass Spec of AB 6d

4-((1*s*,3*R*,11*r*,13*S*)-9,19-dimethyl-1,3,5,7,11,13,15,17-octaphenyl-19-vinyl-2,4,6,8,10,12,14,16,18,20,21,22,23,24-tetradecaoxa-1,3,5,7,9,11,13,15,17,19-decasilapentacyclo[11.7.1.13,11.15,17.17,15]tetracosan-9-yl)butanenitrile (**6f**)

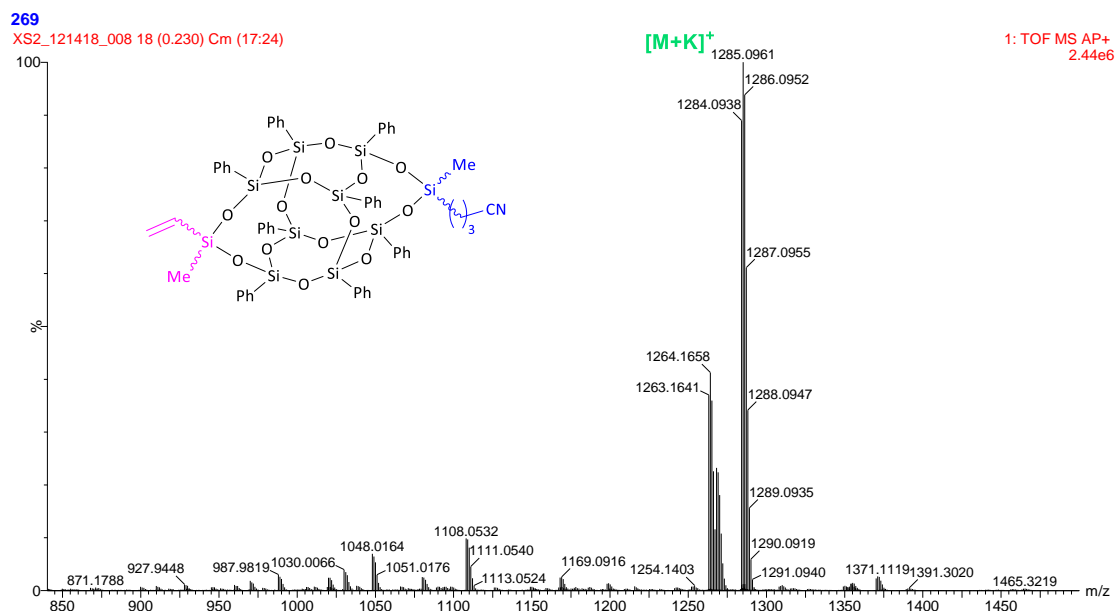


Figure 2-51: Mass Spec of AB 6f

(1*r*,3*R*,11*s*,13*S*)-9,19-dimethyl-1,3,5,7,11,13,15,17-octaphenyl-9-vinyl-2,4,6,8,10,12,14,16,18,20,21,22,23,24-tetradeca-oxa-1,3,5,7,9,11,13,15,17,19-decasilapentacyclo[11.7.1.13,11.15,17.17,15]tetracosane (**6g**)

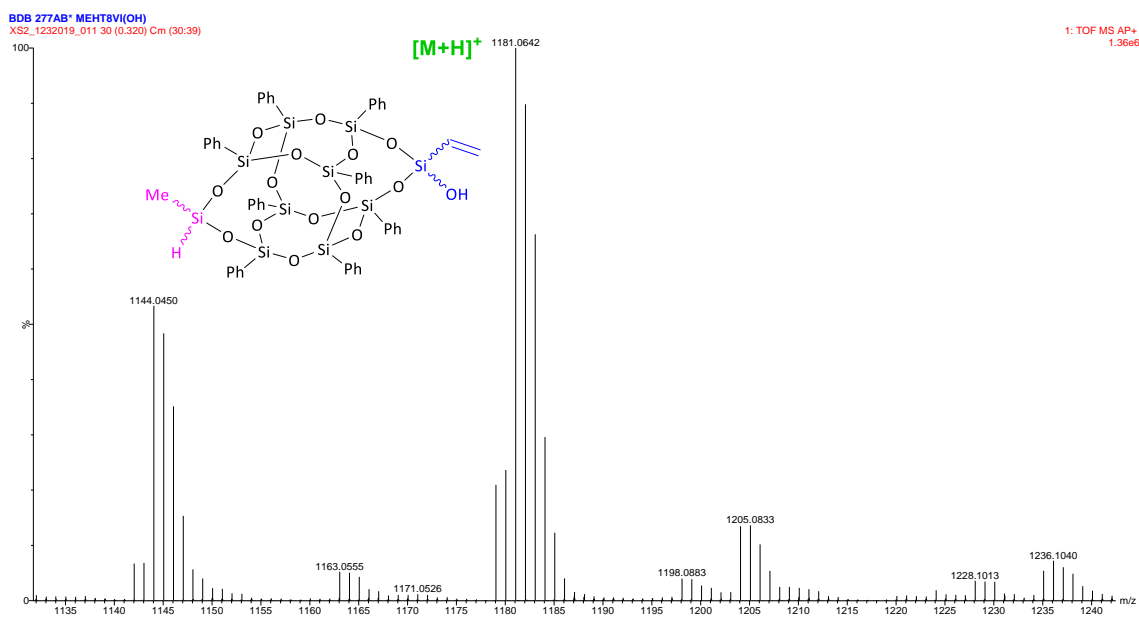


Figure 2-52: Mass Spec of AB **6g**

19-methyl-1,3,5,7,11,13,15,17-octaphenyl-9-vinyl-2,4,6,8,10,12,14,16,18,20,21,22,
23,24-tetradecaoxa-1,3,5,7,9,11,13,15,17,19-decasilapentacyclo[11.7.1.13,11.15,
17.17,15]tetracosan-9-ol (**6h**)

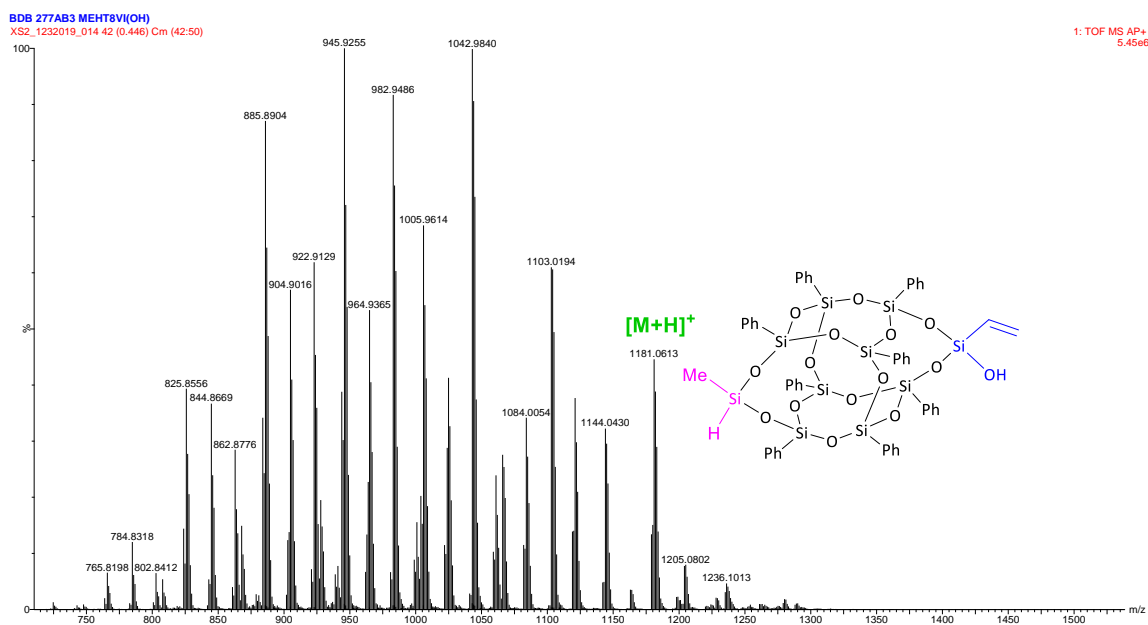


Figure 2-53: Mass Spec of AB 6h

(1*r*,3*R*,11*s*,13*S*)-9-isopropyl-19-methyl-1,3,5,7,11,13,15,17-octaphenyl-19-vinyl-2,4,6,8,10,12,14,16,18,20,21,22,23,24-tetradeca-oxa-1,3,5,7,9,11,13,15,17,19-decasila-pentacyclo[11.7.1.13,11.15,17.17,15]tetracosan-9-ol (**6i**)

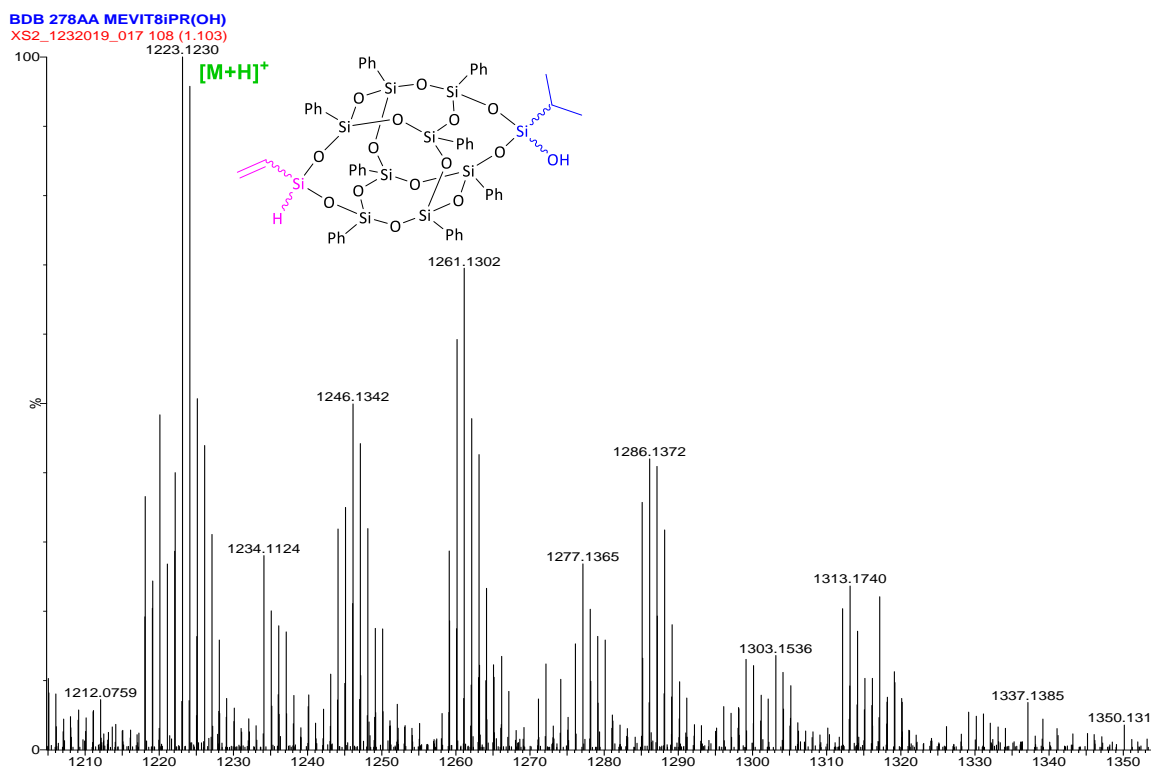


Figure 2-54: Mass Spec of AB 6i

Copies of X-Ray Crystallographic Data

Crystallographic data for the three crystal structures reported in this manuscript have been deposited with the Cambridge Crystallographic Data Centre as supplementary publication no. CCDC-1843217 for $\text{C}_{62}\text{H}_{54}\text{B}_2\text{O}_{16}\text{Si}_8$ (**2a**), 1823844 for $\text{C}_{60}\text{H}_{50}\text{B}_2\text{O}_{14}\text{Si}_8$ (**2b**) and 1850462 $\text{C}_{62}\text{H}_{54}\text{B}_2\text{O}_{14}\text{Si}_8$ (**2c**) Copies of the data can be obtained free of charge via the CCDC Website.

Table 2-6: Crystal Data and Structure Refinement for Compounds 2A - 2C

CCDC	1843217	1823844	1850462
Formula	C ₆₂ H ₅₄ B ₂ O ₁₆ Si ₈	C ₆₀ H ₅₀ B ₂ O ₁₄ Si ₈	C ₆₂ H ₅₄ B ₂ O ₁₄ Si ₈
Dcalc./ g cm ⁻³	1.345	1.376	1.359
ρ /mm ⁻¹	2.135	0.245	2.173
Formula Weight	1301.39	1241.34	1269.39
Colour	colourless	colourless	colourless
Shape	needle	hexagonal_plate	cube
Size/mm ³	0.42×0.11×0.04	0.22×0.19×0.14	0.18×0.17×0.09
T/K	173(2)	173(2)	173(2)
Crystal System	monoclinic	triclinic	triclinic
Space Group	P21/c	P-1	P-1
<i>a</i> /Å	24.7461(3)	13.0387(9)	13.2208(2)
<i>b</i> /Å	22.7525(4)	13.2083(9)	13.2988(2)
<i>c</i> /Å	11.4396(2)	19.4033(14)	19.7225(3)
<i>a</i> /°	90	76.7490(10)	76.1452(8)
<i>b</i> /°	93.6260(10)	78.4840(10)	76.4917(10)
<i>g</i> /°	90	68.2650(10)	69.0621(9)
<i>V</i> /Å ³	6428.01(18)	2997.0(4)	3102.26(8)
<i>Z</i>	4	2	2
<i>Z'</i>	1	1	1
Wavelength/Å	1.541838	0.710730	1.541838
Radiation type	CuK _α	MoK _α	CuK _α
<i>Q</i> _{min} /°	1.789	1.684	2.339
<i>Q</i> _{min} /°	72.196	25.386	70.996
Measured Refl.	44545	29082	29282
Independent Refl.	12430	10990	11139
Reflections with <i>I</i> >	-	-	9463 2(<i>I</i>)
Reflections Used	7168	6867	-
<i>R</i> _{int}	0.1278	0.0626	0.0306
Parameters	795	784	822
Restraints	0	0	0
Largest Peak	0.390	0.554	0.379
Deepest Hole	-0.322	-0.434	-0.304
GooF	0.985	1.055	1.029
<i>wR</i> ₂ (all data)	0.1490	0.1728	0.0940
<i>wR</i> ₂	0.1213	0.1444	0.0886
<i>R</i> ₁ (all data)	0.1208	0.0961	0.0426
<i>R</i> ₁	0.0577	0.0594	0.0342

Table 2-7: Bond Lengths in Å for CCDC 1843217

Atom	Atom	Length/Å
Si1A	O1A	1.598(3)
Si1A	O4A	1.613(3)
Si1A	O5A	1.613(3)
Si1A	C8A	1.851(4)
Si2A	O4A	1.610(3)
Si2A	O6A	1.620(3)
Si2A	O7A	1.613(3)
Si2A	C14A	1.841(4)
Si3A	O5A ¹	1.615(3)
Si3A	O6A	1.599(3)
Si3A	O8A	1.612(3)
Si3A	C20A	1.843(5)
Si4A	O2A	1.610(3)
Si4A	O7A ¹	1.619(3)
Si4A	O8A	1.623(3)
Si4A	C26A	1.842(4)
O1A	B1A	1.335(6)
O2A	B1A	1.358(6)
O3A	C4A	1.372(5)
O3A	C7A	1.440(7)
O5A	Si3A ¹	1.615(3)
O7A	Si4A ¹	1.619(3)
C1A	C2A	1.395(6)
C1A	C6A	1.418(6)
C1A	B1A	1.555(6)
C2A	C3A	1.387(6)
C3A	C4A	1.389(6)
C4A	C5A	1.388(7)
C5A	C6A	1.374(6)
C8A	C9A	1.390(6)
C8A	C13A	1.375(7)
C9A	C10A	1.389(6)
C10A	C11A	1.382(7)
C11A	C12A	1.358(7)
C12A	C13A	1.387(7)
C14A	C15A	1.374(6)
C14A	C19A	1.405(6)
C15A	C16A	1.384(7)
C16A	C17A	1.369(8)
C17A	C18A	1.371(7)
C18A	C19A	1.376(7)
C20A	C21A	1.391(7)
C20A	C25A	1.395(7)

Atom	Atom	Length/Å
C21A	C22A	1.394(7)
C22A	C23A	1.369(9)
C23A	C24A	1.379(9)
C24A	C25A	1.376(7)
C26A	C27A	1.401(6)
C26A	C31A	1.389(6)
C27A	C28A	1.366(7)
C28A	C29A	1.382(7)
C29A	C30A	1.375(7)
C30A	C31A	1.388(6)
Si1B	O1B	1.614(3)
Si1B	O4B	1.617(3)
Si1B	O5B	1.611(3)
Si1B	C8B	1.842(4)
Si2B	O4B	1.617(3)
Si2B	O6B	1.611(3)
Si2B	O7B	1.608(3)
Si2B	C14B	1.839(4)
Si3B	O5B ²	1.614(3)
Si3B	O6B	1.609(3)
Si3B	O8B	1.617(3)
Si3B	C20B	1.847(4)
Si4B	O2B	1.603(3)
Si4B	O7B ²	1.616(3)
Si4B	O8B	1.616(3)
Si4B	C25B	1.852(4)
O1B	B1B	1.357(6)
O2B	B1B	1.363(6)
O3B	C4B	1.369(5)
O3B	C7B	1.407(6)
O5B	Si3B ²	1.614(3)
O7B	Si4B ²	1.616(3)
C1B	C2B	1.396(6)
C1B	C6B	1.399(6)
C1B	B1B	1.558(6)
C2B	C3B	1.391(6)
C3B	C4B	1.382(6)
C4B	C5B	1.379(6)
C5B	C6B	1.406(6)
C8B	C9B	1.379(6)
C8B	C13B	1.366(7)
C9B	C10B	1.376(7)
C10B	C11B	1.340(8)
C11B	C12B	1.365(9)
C12B	C13B	1.384(8)

Table 2-7 (cont'd)

Atom	Atom	Length/Å
C14B	C15B	1.383(6)
C14B	C19B	1.393(6)
C15B	C16B	1.380(7)
C016	C20B	1.389(6)
C016	C24B	1.388(6)
C16B	C17B	1.354(9)
C17B	C18B	1.349(9)
C18B	C19B	1.378(6)
C20B	C21B	1.387(6)
C21B	C22B	1.402(6)
C22B	C23B	1.369(7)
C23B	C24B	1.377(7)
C25B	C26B	1.388(6)
C25B	C30B	1.376(6)
C26B	C27B	1.383(7)
C27B	C28B	1.368(8)
C28B	C29B	1.369(8)
C29B	C30B	1.377(7)

¹2-x,-y,1-z; ²1-x,1-y,1-z

Table 2-8: Bond Angles in ° for CCDC 1843217

Atom	Atom	Atom	Angle/°
O1A	Si1A	O4A	107.8(2)
O1A	Si1A	O5A	09.98(19)
O1A	Si1A	C8A	109.32(18)
O4A	Si1A	O5A	109.15(16)
O4A	Si1A	C8A	111.88(19)
O5A	Si1A	C8A	108.70(18)
O4A	Si2A	O6A	109.07(17)
O4A	Si2A	O7A	110.70(17)
O4A	Si2A	C14A	107.91(18)
O6A	Si2A	C14A	110.33(18)
O7A	Si2A	O6A	106.65(16)
O7A	Si2A	C14A	112.16(18)
O5A ¹	Si3A	C20A	107.70(17)
O6A	Si3A	O5A ¹	108.70(17)
O6A	Si3A	O8A	109.50(16)
O6A	Si3A	C20A	110.71(19)
O8A	Si3A	O5A ¹	108.94(16)
O8A	Si3A	C20A	111.23(19)
O2A	Si4A	O7A ¹	111.01(17)
O2A	Si4A	O8A	108.15(17)
O2A	Si4A	C26A	108.03(17)
O7A ¹	Si4A	O8A	110.67(16)
O7A ¹	Si4A	C26A	109.62(18)
O8A	Si4A	C26A	109.30(18)
B1A	O1A	Si1A	170.7(3)
B1A	O2A	Si4A	152.4(3)
C4A	O3A	C7A	117.3(4)
Si2A	O4A	Si1A	150.6(2)
Si1A	O5A	Si3A ¹	146.3(2)
Si3A	O6A	Si2A	157.5(2)
Si2A	O7A	Si4A ¹	144.3(2)
Si3A	O8A	Si4A	150.8(2)
C2A	C1A	C6A	116.9(4)
C2A	C1A	B1A	120.9(4)
C6A	C1A	B1A	122.2(4)
C3A	C2A	C1A	122.6(4)
C2A	C3A	C4A	118.4(4)
O3A	C4A	C3A	123.1(5)
O3A	C4A	C5A	115.6(4)
C5A	C4A	C3A	121.2(4)
C6A	C5A	C4A	119.5(4)
C5A	C6A	C1A	121.5(4)

Atom	Atom	Atom	Angle/°
C9A	C8A	Si1A	120.9(3)
C13A	C8A	Si1A	121.1(4)
C13A	C8A	C9A	117.9(4)
C10A	C9A	C8A	121.6(5)
C11A	C10A	C9A	118.6(5)
C12A	C11A	C10A	120.5(4)
C11A	C12A	C13A	120.4(5)
C8A	C13A	C12A	121.0(5)
C15A	C14A	Si2A	121.0(4)
C15A	C14A	C19A	116.5(4)
C19A	C14A	Si2A	122.4(3)
C14A	C15A	C16A	122.3(5)
C17A	C16A	C15A	119.8(5)
C16A	C17A	C18A	119.9(5)
C17A	C18A	C19A	120.1(5)
C18A	C19A	C14A	121.5(5)
C21A	C20A	Si3A	120.4(4)
C21A	C20A	C25A	118.3(5)
C25A	C20A	Si3A	121.0(4)
C20A	C21A	C22A	119.9(6)
C23A	C22A	C21A	120.6(6)
C22A	C23A	C24A	120.2(6)
C25A	C24A	C23A	119.6(6)
C24A	C25A	C20A	121.4(6)
C27A	C26A	Si4A	120.5(3)
C31A	C26A	Si4A	122.3(4)
C31A	C26A	C27A	117.3(4)
C28A	C27A	C26A	121.9(5)
C27A	C28A	C29A	119.9(5)
C30A	C29A	C28A	119.7(5)
C29A	C30A	C31A	120.2(5)
C30A	C31A	C26A	121.0(5)
O1A	B1A	O2A	121.5(4)
O1A	B1A	C1A	120.7(4)
O2A	B1A	C1A	117.7(4)
O1B	Si1B	O4B	109.46(17)
O1B	Si1B	C8B	110.34(18)
O4B	Si1B	C8B	108.09(18)
O5B	Si1B	O1B	107.99(16)
O5B	Si1B	O4B	110.12(15)
O5B	Si1B	C8B	110.83(17)
O4B	Si2B	C14B	111.79(17)
O6B	Si2B	O4B	108.22(17)
O6B	Si2B	C14B	107.46(17)
O7B	Si2B	O4B	109.20(15)

Table 2-8 (cont'd)

Atom	Atom	Atom	Angle/°
O7B	Si2B	O6B	109.90(15)
O7B	Si2B	C14B	110.24(18)
O5B ²	Si3B	O8B	108.44(15)
O5B ²	Si3B	C20B	110.40(16)
O6B	Si3B	O5B ²	107.59(15)
O6B	Si3B	O8B	110.15(16)
O6B	Si3B	C20B	109.71(17)
O8B	Si3B	C20B	110.49(17)
O2B	Si4B	O7B ²	108.94(17)
O2B	Si4B	O8B	110.27(16)
O2B	Si4B	C25B	110.73(18)
O7B ²	Si4B	O8B	109.51(15)
O7B ²	Si4B	C25B	109.64(17)
O8B	Si4B	C25B	107.73(17)
B1B	O1B	Si1B	143.0(3)
B1B	O2B	Si4B	165.0(3)
C4B	O3B	C7B	117.9(4)
Si2B	O4B	Si1B	146.4(2)
Si1B	O5B	Si3B ²	153.9(2)
Si3B	O6B	Si2B	145.35(18)
Si2B	O7B	Si4B ²	162.2(2)
Si4B	O8B	Si3B	144.57(19)
C2B	C1B	C6B	117.3(4)
C2B	C1B	B1B	121.9(4)
C6B	C1B	B1B	120.6(4)
C3B	C2B	C1B	121.5(4)
C4B	C3B	C2B	119.8(4)
O3B	C4B	C3B	115.0(4)
O3B	C4B	C5B	124.3(4)
C5B	C4B	C3B	120.7(4)
C4B	C5B	C6B	119.0(4)
C1B	C6B	C5B	121.6(4)
C9B	C8B	Si1B	120.5(3)

C13B	C8B	Si1B	122.6(4)
C13B	C8B	C9B	116.7(5)
C10B	C9B	C8B	121.6(5)
C11B	C10B	C9B	120.8(6)
C10B	C11B	C12B	119.1(6)
C11B	C12B	C13B	120.3(6)
C8B	C13B	C12B	121.4(6)
C15B	C14B	Si2B	123.2(4)
C15B	C14B	C19B	116.3(4)
C19B	C14B	Si2B	120.4(3)
C16B	C15B	C14B	121.4(5)
C24B	C016	C20B	121.5(4)
C17B	C16B	C15B	120.4(6)
C18B	C17B	C16B	120.1(5)
C17B	C18B	C19B	120.0(6)
C18B	C19B	C14B	121.7(5)
C016	C20B	Si3B	120.4(3)
C21B	C20B	Si3B	121.3(3)
C21B	C20B	C016	118.1(4)
C20B	C21B	C22B	120.5(4)
C23B	C22B	C21B	119.9(5)
C22B	C23B	C24B	120.6(5)
C23B	C24B	C016	119.3(5)
C26B	C25B	Si4B	119.3(3)
C30B	C25B	Si4B	122.6(4)
C30B	C25B	C26B	117.8(4)
C27B	C26B	C25B	121.1(5)
C28B	C27B	C26B	119.4(5)
C27B	C28B	C29B	120.5(5)
C28B	C29B	C30B	119.7(5)
C25B	C30B	C29B	121.4(5)
O1B	B1B	O2B	123.2(4)
O1B	B1B	C1B	118.0(4)
O2B	B1B	C1B	118.8(4)

¹2-x,-y,1-z; ²1-x,1-y,1-z

Table 2-9: Hydrogen Fractional Atomic Coordinates ($\times 10^4$) and Equivalent Isotropic Displacement Parameters ($\text{\AA}^2 \times 10^3$) for CCDC 1843217. U_{eq} is defined as 1/3 of the trace of the orthogonalised U_{ij} .

Atom	x	y	z	U_{eq}
H2A	9395	1192	195	46
H3A	8890	1696	-1274	53
H5A	7590	1657	724	54
H6A	8096	1154	2176	48
H7AA	7812	2368	-2812	136
H7AB	8202	1807	-2694	136
H7AC	8400	2425	-2157	136
H9A	8277	1678	4376	51
H10A	7401	2026	4597	59
H11A	6759	1394	5333	65
H12A	6990	444	5842	79
H13A	7857	93	5580	67
H15A	9435	2024	6022	70
H16A	9538	2942	6892	94
H17A	9990	3031	8725	88
H18A	10326	2200	9695	79
H19A	10242	1286	8811	54
H21A	11031	1577	6776	74
H22A	11690	2307	7102	99
H23A	12269	2541	5662	103
H24A	12206	2046	3876	90
H25A	11570	1306	3554	67
H27A	10803	1489	1842	55
H28A	11352	1804	415	74
H29A	11613	1150	-1018	78
H30A	11294	188	-1037	71
H31A	10737	-132	402	56
H2B	6508	3432	2466	60
H3B	6838	2639	1436	65
H5B	6027	1512	3423	50
H6B	5661	2315	4400	45
H7BA	6821	723	1552	88
H7BB	6232	893	1949	88
H7BC	6745	928	2870	88
H9B	5063	2772	7059	58
H10B	4575	2115	8111	78
H11B	3653	2057	7819	102
H12B	3208	2665	6445	147
H13B	3695	3315	5352	103
H15B	2993	4553	4095	74
H016	5623	6194	1478	50

Table 2-9 (cont'd)

Atom	x	y	z	Ueq
H16B	2213	4428	2891	105
H17B	2265	4140	974	101
H18B	3094	4015	212	89
H19B	3882	4192	1360	61
H21B	4268	5247	720	48
H22B	4149	5734	-1089	60
H23B	4766	6440	-1596	65
H24B	5495	6688	-304	65
H26B	6542	5702	2767	66
H27B	7419	5995	2410	87
H28B	8144	5389	2964	84
H29B	8000	4494	3858	76
H30B	7126	4199	4193	58

Table 2-10: Bond Lengths in Å for CDCC 1823844

Atom	Atom	Length/Å
Si1	O1	1.599(3)
Si1	O3	1.619(2)
Si1	O4	1.607(2)
Si1	C7	1.838(4)
Si2	O3	1.611(2)
Si2	O5	1.616(2)
Si2	O6	1.617(2)
Si2	C13	1.836(4)
Si3	O2 ¹	1.621(2)
Si3	O5	1.610(2)
Si3	O7	1.622(3)
Si3	C19	1.842(4)
Si4	O4	1.621(2)
Si4	O6 ¹	1.620(2)
Si4	O7	1.619(2)
Si4	C25	1.828(4)
O1	B1	1.364(5)
O2	Si3 ¹	1.621(2)
O2	B1	1.377(5)
O6	Si4 ¹	1.620(2)
B1	C1	1.554(5)
C1	C2	1.385(5)
C1	C6	1.395(5)
C2	C3	1.386(5)
C3	C4	1.366(7)
C4	C5	1.355(8)
C5	C6	1.394(6)
C7	C8	1.388(5)
C7	C12	1.385(5)
C8	C9	1.373(6)
C9	C10	1.381(7)
C10	C11	1.358(7)
C11	C12	1.382(6)
C13	C14	1.397(5)
C13	C18	1.396(5)
C14	C15	1.370(6)
C15	C16	1.366(6)
C16	C17	1.366(6)
C17	C18	1.368(5)
C19	C20	1.399(5)
C19	C24	1.392(5)
C20	C21	1.390(5)
C21	C22	1.375(5)

Atom	Atom	Length/Å
C22	C23	1.380(5)
C23	C24	1.377(5)
C25	C26	1.397(5)
C25	C30	1.392(5)
C26	C27	1.382(5)
C27	C28	1.376(6)
C28	C29	1.371(6)
C29	C30	1.383(5)
Si5	O9	1.602(3)
Si5	O10	1.597(3)
Si5	O11	1.608(3)
Si5	C37	1.845(4)
Si6	O10	1.615(3)
Si6	O12	1.612(2)
Si6	O13	1.615(3)
Si6	C43	1.845(4)
Si7	O11 ²	1.614(3)
Si7	O12	1.618(2)
Si7	O14	1.610(3)
Si7	C49	1.823(4)
Si8	O8	1.607(3)
Si8	O13 ²	1.614(3)
Si8	O14	1.608(3)
Si8	C55	1.841(4)
O8	B2	1.373(5)
O9	B2	1.356(5)
O11	Si7 ²	1.614(3)
O13	Si8 ²	1.614(3)
B2	C31	1.547(6)
C31	C32	1.364(5)
C31	C36	1.375(6)
C32	C33	1.382(6)
C33	C34	1.339(7)
C34	C35	1.344(7)
C35	C36	1.384(7)
C37	C38	1.379(6)
C37	C42	1.398(5)
C38	C39	1.378(6)
C39	C40	1.345(8)
C40	C41	1.363(7)
C41	C42	1.383(6)
C43	C44	1.365(5)
C43	C48	1.388(5)
C44	C45	1.399(6)
C45	C46	1.357(6)

Table 2-10 (cont'd)

Atom	Atom	Length/Å
C46	C47	1.367(6)
C47	C48	1.384(5)
C49	C50	1.528(10)
C49	C50A	1.455(10)
C49	C54	1.340(14)
C49	C54A	1.292(15)
C50	C51	1.395(12)
C50A	C51A	1.400(12)
C51	C52	1.372(14)
C51A	C52A	1.308(15)
C52	C53	1.399(19)
C52A	C53A	1.348(18)
C53	C54	1.375(18)
C53A	C54A	1.385(19)
C55	C56	1.399(5)
C55	C60	1.389(5)
C56	C57	1.379(5)
C57	C58	1.372(6)
C58	C59	1.367(6)
C59	C60	1.390(5)

¹1-x,1-y,2-z; ²-x,2-y,1-z

Table 2-11: Bond Angles in ° for CDCC
1823844

Atom	Atom	Atom	Angle/°
O1	Si1	O3	108.08(14)
O1	Si1	O4	10.32(14)
O1	Si1	C7	110.94(15)
O3	Si1	C7	108.91(15)
O4	Si1	O3	109.44(13)
O4	Si1	C7	109.13(15)
O3	Si2	O5	109.05(13)
O3	Si2	O6	108.37(13)
O3	Si2	C13	112.28(14)
O5	Si2	O6	107.92(13)
O5	Si2	C13	109.61(15)
O6	Si2	C13	109.51(15)
O2 ¹	Si3	O7	108.60(13)
O2 ¹	Si3	C19	108.46(14)
O5	Si3	O2 ¹	108.67(13)
O5	Si3	O7	109.33(13)
O5	Si3	C19	111.04(15)
O7	Si3	C19	110.68(14)
O4	Si4	C25	109.67(15)
O6 ¹	Si4	O4	108.82(13)
O6 ¹	Si4	C25	109.72(15)
O7	Si4	O4	110.40(13)
O7	Si4	O6 ¹	108.31(12)
O7	Si4	C25	109.89(15)
B1	O1	Si1	157.5(3)
B1	O2	Si3 ¹	136.9(2)
Si2	O3	Si1	150.84(17)
Si1	O4	Si4	154.12(17)
Si3	O5	Si2	158.92(17)
Si2	O6	Si4 ¹	140.59(16)
Si4	O7	Si3	145.11(16)
O1	B1	O2	120.4(3)
O1	B1	C1	120.1(3)
O2	B1	C1	119.4(3)
C2	C1	B1	121.8(4)
C2	C1	C6	117.8(4)
C6	C1	B1	120.3(4)
C1	C2	C3	120.8(4)
C4	C3	C2	120.4(5)
C5	C4	C3	120.1(5)
C4	C5	C6	120.5(5)
C5	C6	C1	120.4(4)
C8	C7	Si1	120.9(3)

Atom	Atom	Atom	Angle/°
C12	C7	Si1	120.7(3)
C12	C7	C8	117.9(4)
C9	C8	C7	121.6(4)
C8	C9	C10	119.8(5)
C11	C10	C9	119.0(4)
C10	C11	C12	121.8(5)
C11	C12	C7	119.9(4)
C14	C13	Si2	123.6(3)
C18	C13	Si2	120.0(3)
C18	C13	C14	116.4(4)
C15	C14	C13	120.7(4)
C16	C15	C14	121.2(4)
C15	C16	C17	119.8(4)
C16	C17	C18	119.5(4)
C17	C18	C13	122.5(4)
C20	C19	Si3	121.4(3)
C24	C19	Si3	121.7(3)
C24	C19	C20	116.9(3)
C21	C20	C19	121.7(3)
C22	C21	C20	119.5(4)
C21	C22	C23	120.1(4)
C24	C23	C22	120.1(4)
C23	C24	C19	121.7(4)
C26	C25	Si4	121.3(3)
C30	C25	Si4	121.9(3)
C30	C25	C26	116.8(3)
C27	C26	C25	121.8(4)
C28	C27	C26	119.7(4)
C29	C28	C27	120.2(4)
C28	C29	C30	119.9(4)
C29	C30	C25	121.7(4)
O9	Si5	O11	107.35(15)
O9	Si5	C37	110.88(16)
O10	Si5	O9	110.27(16)
O10	Si5	O11	110.76(14)
O10	Si5	C37	108.41(16)
O11	Si5	C37	109.19(16)
O10	Si6	O13	108.61(15)
O10	Si6	C43	111.27(15)
O12	Si6	O10	108.88(13)
O12	Si6	O13	109.95(14)
O12	Si6	C43	108.34(15)
O13	Si6	C43	109.78(15)
O11 ²	Si7	O12	107.87(14)
O11 ²	Si7	C49	111.48(18)

Table 2-11 (cont'd)

Atom	Atom	Atom	Angle/°
O12	Si7	C49	109.14(18)
O14	Si7	O11 ²	109.01(15)
O14	Si7	O12	107.68(13)
O14	Si7	C49	111.52(17)
O8	Si8	O13 ²	109.58(14)
O8	Si8	O14	108.88(14)
O8	Si8	C55	110.53(16)
O13 ²	Si8	C55	109.37(15)
O14	Si8	O13 ²	108.80(15)
O14	Si8	C55	109.65(15)
B2	O8	Si8	142.6(3)
B2	O9	Si5	158.4(3)
Si5	O10	Si6	160.10(19)
Si5	O11	Si7 ²	153.91(19)
Si6	O12	Si7	138.67(16)
Si8 ²	O13	Si6	152.60(19)
Si8	O14	Si7	155.16(18)
O8	B2	C31	119.1(3)
O9	B2	O8	121.4(3)
O9	B2	C31	119.4(3)
C32	C31	B2	122.2(4)
C32	C31	C36	115.2(4)
C36	C31	B2	122.5(4)
C31	C32	C33	123.3(4)
C34	C33	C32	120.1(5)
C33	C34	C35	118.5(5)
C34	C35	C36	121.6(5)
C31	C36	C35	121.2(5)
C38	C37	Si5	122.3(3)
C38	C37	C42	116.6(4)
C42	C37	Si5	121.0(3)
C39	C38	C37	121.3(5)
C40	C39	C38	121.0(5)
C39	C40	C41	120.1(5)
C40	C41	C42	119.7(5)
C41	C42	C37	121.4(5)
C44	C43	Si6	121.1(3)
C44	C43	C48	117.4(4)
C48	C43	Si6	121.4(3)
C43	C44	C45	120.8(4)
C46	C45	C44	120.6(4)
C45	C46	C47	119.9(4)
C46	C47	C48	119.2(4)
C47	C48	C43	122.0(4)

Atom	Atom	Atom	Angle/°
C50	C49	Si7	115.2(4)
C50A	C49	Si7	116.8(5)
C54	C49	Si7	130.7(6)
C54	C49	C50	112.0(7)
C54A	C49	Si7	124.7(7)
C54A	C49	C50A	115.2(8)
C51	C50	C49	120.0(8)
C51A	C50A	C49	119.4(9)
C52	C51	C50	120.3(10)
C52A	C51A	C50A	121.3(10)
C51	C52	C53	120.7(9)
C51A	C52A	C53A	117.6(12)
C54	C53	C52	117.6(11)
C52A	C53A	C54A	123.0(15)
C49	C54	C53	127.5(12)
C49	C54A	C53A	121.6(13)
C56	C55	Si8	118.6(3)
C60	C55	Si8	124.1(3)
C60	C55	C56	117.2(3)
C57	C56	C55	121.8(4)
C58	C57	C56	119.5(4)
C59	C58	C57	120.2(4)
C58	C59	C60	120.3(4)
C55	C60	C59	120.8(4)

¹1-x,1-y,2-z; ²-x,2-y,1-z

Table 2-12: Hydrogen Fractional Atomic Coordinates ($\times 10^4$) and Equivalent Isotropic Displacement Parameters ($\text{\AA}^2 \times 10^3$) for CCDC 1823844. U_{eq} is defined as 1/3 of the trace of the orthogonalised U_{ij} .

Atom	x	y	z	U_{eq}
H2	3063	9469	7708	56
H3	3104	10617	6604	87
H4	4565	10098	5713	118
H5	5961	8412	5899	114
H6	5915	7210	6987	73
H8	5019	5574	7090	59
H9	5445	4668	6127	86
H10	6988	3044	6083	82
H11	7972	2284	7048	79
H12	7552	3170	8023	58
H14	4544	3283	8100	51
H15	4291	1915	7669	73
H16	3818	494	8436	76
H17	3638	404	9661	67
H18	3870	1770	10106	51
H20	6545	1791	9090	41
H21	7580	220	8580	48
H22	8997	-1176	9156	50
H23	9418	-973	10217	53
H24	8349	554	10746	45
H26	8784	5142	8397	47
H27	10665	4909	8116	57
H28	11888	3867	8946	56
H29	11223	3098	10065	58
H30	9343	3327	10349	49
H32	5004	8128	3489	80
H33	6880	7114	3371	95
H34	7703	5991	4348	92
H35	6646	5952	5444	163
H36	4769	6985	5577	115
H38	2696	5979	6192	93
H39	3033	4695	7227	109
H40	2749	5246	8305	91
H41	2053	7111	8378	77
H42	1645	8424	7352	59
H44	1174	12282	6426	62
H45	1387	12864	7424	87
H46	691	12201	8554	64
H47	-207	10925	8709	58
H48	-383	10314	7720	56
H50	-261	13928	5135	78
H50A	-1003	13916	3865	81

Table 2-12 (cont'd)

Atom	x	y	z	Ueq
H51	-8	15636	4679	85
H51A	-732	15589	3303	85
H52	1182	15835	3638	81
H52A	1001	15697	3082	81
H53	1881	14440	2921	68
H53A	2410	14261	3599	78
H54	1749	12734	3424	61
H54A	2183	12606	4165	101
H56	469	11663	2785	50
H57	728	12815	1718	60
H58	2521	12663	1164	64
H59	4038	11281	1632	64
H60	3794	10138	2716	54

Table 2-13: Bond Lengths in Å for CCDC 1850462

Atom	Atom	Length/Å
Si1	O2	1.6169(13)
Si1	O3	1.6159(13)
Si1	O5 ¹	1.6098(13)
Si1	C8	1.8507(18)
Si2	O3	1.6162(13)
Si2	O4	1.6256(12)
Si2	O7 ¹	1.6156(13)
Si2	C14	1.841(2)
Si3	O4	1.6143(14)
Si3	O5	1.6163(13)
Si3	O6	1.6146(12)
Si3	C20	1.8437(17)
Si4	O1	1.6100(13)
Si4	O6	1.6223(13)
Si4	O7	1.6126(13)
Si4	C26	1.8421(18)
O1	B1	1.362(3)
O2	B1	1.366(3)
C1	C2	1.398(3)
C1	C6	1.391(3)
C1	B1	1.559(2)
C2	C3	1.398(3)
C3	C4	1.379(4)
C4	C5	1.390(4)
C4	C7	1.514(3)
C5	C6	1.385(3)
C8	C9	1.402(3)
C8	C13	1.399(3)
C9	C10	1.387(3)
C10	C11	1.381(3)
C11	C12	1.381(3)
C12	C13	1.390(3)
C14	C15	1.398(3)
C14	C19	1.396(3)
C15	C16	1.379(4)
C16	C17	1.378(4)
C17	C18	1.377(4)
C18	C19	1.386(3)
C20	C21	1.395(3)
C20	C25	1.385(3)
C21	C22	1.386(3)
C22	C23	1.377(4)
C23	C24	1.368(4)

Atom	Atom	Length/Å
C24	C25	1.389(3)
C26	C27	1.398(3)
C26	C31	1.396(3)
C27	C28	1.383(3)
C28	C29	1.381(4)
C29	C30	1.377(3)
C30	C31	1.387(3)
Si5	O8	1.6165(14)
Si5	O10	1.6063(15)
Si5	O13 ²	1.6155(14)
Si5	C39	1.8483(19)
Si6	O10	1.6101(15)
Si6	O11	1.6153(14)
Si6	O12	1.6195(13)
Si6	C45	1.838(2)
Si7	O12	1.6148(12)
Si7	O13	1.6145(15)
Si7	O14	1.6190(14)
Si7	C51	1.8493(18)
Si8	O9	1.6072(16)
Si8	O11 ²	1.6164(14)
Si8	O14	1.6105(14)
Si8	C57	1.8486(19)
O8	B2	1.370(3)
O9	B2	1.352(3)
C32	C33	1.391(3)
C32	C37	1.387(3)
C32	B2	1.552(3)
C33	C34	1.384(3)
C34	C35	1.368(3)
C35	C36	1.377(4)
C35	C38	1.506(3)
C36	C37	1.385(4)
C39	C40	1.392(3)
C39	C44	1.404(3)
C40	C41	1.391(3)
C41	C42	1.378(4)
C42	C43	1.374(4)
C43	C44	1.393(3)
C45	C46	1.395(5)
C45	C46A	1.560(5)
C45	C50	1.324(5)
C45	C50A	1.337(5)
C46	C47	1.386(6)
C46A	C47A	1.396(6)

Table 2-13 (cont'd)

Atom	Atom	Length/Å
C47	C48	1.359(11)
C47A	C48A	1.366(10)
C48	C49	1.366(10)
C48A	C49A	1.388(9)
C49	C50	1.372(7)
C49A	C50A	1.384(8)
C51	C52	1.395(3)
C51	C56	1.389(3)
C52	C53	1.391(3)
C53	C54	1.379(3)
C54	C55	1.382(3)
C55	C56	1.393(3)
C57	C58	1.394(3)
C57	C62	1.396(3)
C58	C59	1.386(3)
C59	C60	1.372(4)
C60	C61	1.374(4)
C61	C62	1.395(3)

¹1-x,-y,2-z; ²-x,1-y,1-z

Table 2-14: Bond Angles in ° for CCDC 1850462

Atom	Atom	Atom	Angle/°
O2	Si1	C8	108.34(7)
O3	Si1	O2	108.56(7)
O3	Si1	C8	109.69(8)
O5 ¹	Si1	O2	108.65(7)
O5 ¹	Si1	O3	110.09(7)
O5 ¹	Si1	C8	111.45(8)
O3	Si2	O4	108.62(7)
O3	Si2	C14	109.58(8)
O4	Si2	C14	109.67(7)
O7 ¹	Si2	O3	110.52(7)
O7 ¹	Si2	O4	108.40(7)
O7 ¹	Si2	C14	110.01(8)
O4	Si3	O5	108.27(7)
O4	Si3	O6	107.99(7)
O4	Si3	C20	109.37(8)
O5	Si3	C20	109.14(8)
O6	Si3	O5	108.89(7)
O6	Si3	C20	113.07(7)
O1	Si4	O6	108.24(7)
O1	Si4	O7	110.73(7)
O1	Si4	C26	110.80(8)
O6	Si4	C26	108.17(7)
O7	Si4	O6	109.85(7)
O7	Si4	C26	109.01(8)
B1	O1	Si4	151.40(13)
B1	O2	Si1	143.99(13)
Si1	O3	Si2	150.75(9)
Si3	O4	Si2	140.19(8)
Si1 ¹	O5	Si3	157.38(9)
Si3	O6	Si4	151.34(9)
Si4	O7	Si2 ¹	153.32(10)
C2	C1	B1	121.59(18)
C6	C1	C2	117.41(18)
C6	C1	B1	120.93(18)
C1	C2	C3	120.7(2)
C4	C3	C2	121.1(2)
C3	C4	C5	118.30(19)
C3	C4	C7	121.1(2)
C5	C4	C7	120.6(2)
C6	C5	C4	120.8(2)
C5	C6	C1	121.6(2)
C9	C8	Si1	120.90(14)
C13	C8	Si1	121.88(14)

Atom	Atom	Atom	Angle/°
C13	C8	C9	117.21(17)
C10	C9	C8	121.38(18)
C11	C10	C9	120.1(2)
C12	C11	C10	119.95(19)
C11	C12	C13	119.93(19)
C12	C13	C8	121.45(19)
C15	C14	Si2	121.16(16)
C19	C14	Si2	121.38(16)
C19	C14	C15	117.4(2)
C16	C15	C14	121.1(2)
C17	C16	C15	120.5(2)
C18	C17	C16	119.7(2)
C17	C18	C19	120.1(2)
C18	C19	C14	121.3(2)
C21	C20	Si3	119.35(14)
C25	C20	Si3	122.89(14)
C25	C20	C21	117.68(17)
C22	C21	C20	121.4(2)
C23	C22	C21	119.5(2)
C24	C23	C22	120.2(2)
C23	C24	C25	120.3(2)
C20	C25	C24	120.9(2)
C27	C26	Si4	121.05(15)
C31	C26	Si4	119.98(14)
C31	C26	C27	118.30(17)
C28	C27	C26	120.8(2)
C29	C28	C27	119.9(2)
C30	C29	C28	120.4(2)
C29	C30	C31	120.0(2)
C30	C31	C26	120.7(2)
O1	B1	O2	121.78(16)
O1	B1	C1	120.04(17)
O2	B1	C1	118.18(17)
O8	Si5	C39	110.41(9)
O10	Si5	O8	108.30(8)
O10	Si5	O13 ²	108.65(9)
O10	Si5	C39	111.24(9)
O13 ²	Si5	O8	109.37(8)
O13 ²	Si5	C39	108.84(8)
O10	Si6	O11	108.53(8)
O10	Si6	O12	107.46(7)
O10	Si6	C45	110.77(10)
O11	Si6	O12	109.23(8)
O11	Si6	C45	111.96(9)
O12	Si6	C45	108.78(8)

Table 2-14 (cont'd)

Atom	Atom	Atom	Angle/°
O12	Si7	O14	109.80(7)
O12	Si7	C51	107.76(8)
O13	Si7	O12	109.49(7)
O13	Si7	O14	108.68(7)
O13	Si7	C51	109.11(8)
O14	Si7	C51	111.96(8)
O9	Si8	O11 ²	107.07(8)
O9	Si8	O14	110.87(8)
O9	Si8	C57	110.95(9)
O11 ²	Si8	C57	108.36(8)
O14	Si8	O11 ²	110.98(8)
O14	Si8	C57	108.59(8)
B2	O8	Si5	140.62(15)
B2	O9	Si8	163.59(16)
Si5	O10	Si6	154.42(10)
Si6	O11	Si8 ²	152.04(10)
Si7	O12	Si6	141.03(8)
Si7	O13	Si5 ²	148.89(10)
Si8	O14	Si7	163.75(10)
C33	C32	B2	120.73(18)
C37	C32	C33	116.0(2)
C37	C32	B2	123.3(2)
C34	C33	C32	122.3(2)
C35	C34	C33	120.9(2)
C34	C35	C36	117.7(2)
C34	C35	C38	121.0(2)
C36	C35	C38	121.3(2)
C35	C36	C37	121.6(2)
C36	C37	C32	121.5(2)
C40	C39	Si5	124.41(16)
C40	C39	C44	118.02(19)
C44	C39	Si5	117.53(16)
C41	C40	C39	120.9(2)
C42	C41	C40	120.0(2)
C43	C42	C41	120.5(2)
C42	C43	C44	119.9(2)
C43	C44	C39	120.7(2)
C46	C45	Si6	117.0(2)
C46A	C45	Si6	117.7(2)
C50	C45	Si6	118.8(2)
C50	C45	C46	121.3(3)
C50A	C45	Si6	131.2(3)
C50A	C45	C46A	111.1(3)
C47	C46	C45	117.1(4)

Atom	Atom	Atom	Angle/°
C47A	C46A	C45	120.7(4)
C48	C47	C46	119.8(5)
C48A	C47A	C46A	121.0(5)
C47	C48	C49	121.0(6)
C47A	C48A	C49A	119.5(8)
C48	C49	C50	119.1(6)
C50A	C49A	C48A	120.1(8)
C45	C50	C49	120.0(5)
C45	C50A	C49A	127.7(5)
C52	C51	Si7	121.38(14)
C56	C51	Si7	120.69(14)
C56	C51	C52	117.89(17)
C53	C52	C51	121.21(19)
C54	C53	C52	120.0(2)
C53	C54	C55	119.7(2)
C54	C55	C56	120.2(2)
C51	C56	C55	121.01(19)
C58	C57	Si8	120.76(17)
C58	C57	C62	117.82(19)
C62	C57	Si8	121.27(16)
C59	C58	C57	121.2(2)
C60	C59	C58	120.1(3)
C59	C60	C61	120.2(2)
C60	C61	C62	120.1(3)
C61	C62	C57	120.7(2)
O8	B2	C32	116.76(18)
O9	B2	O8	122.3(2)
O9	B2	C32	120.95(18)

¹1-x,-y,2-z; ²-x,1-y,1-z

Table 2-15: Hydrogen Fractional Atomic Coordinates ($\times 10^4$) and Equivalent Isotropic Displacement Parameters ($\text{\AA}^2 \times 10^3$) for CCDC 1850462. U_{eq} is defined as 1/3 of the trace of the orthogonalised U_{ij}

Atom	x	y	z	U_{eq}
H2	5472.33	2326.14	6841.24	42
H3	5069.34	3522.87	5788.71	54
H5	2678.34	5666.91	6898.42	47
H6	3023.42	4453.26	7942.55	37
H7A	3730.98	6121.1	5507.75	87
H7B	2742.43	5669.69	5550.22	87
H7C	3938.97	5091.66	5147.28	87
H9	1723.92	4305.69	9298.6	37
H10	685.44	5885.49	9763.15	44
H11	1065.1	6184.68	10780.78	43
H12	2490.68	4897.75	11335.36	42
H13	3535.7	3313.04	10873.76	33
H15	738.61	1617.16	9742.36	47
H16	-1127.97	1871.61	10043.43	63
H17	-1843.75	1062.59	11143.89	58
H18	-678.29	-3.64	11951.14	54
H19	1193.49	-244.98	11663.81	39
H21	3812.79	-3171.07	10047.08	46
H22	3640.03	-4509.88	9547.49	68
H23	3943.31	-4362.31	8321.11	71
H24	4425.49	-2897.52	7601.42	64
H25	4569.72	-1538.65	8096.03	41
H27	5125.04	481.73	7083.98	34
H28	5529.54	-594.71	6221.69	49
H29	6897.94	-2288.37	6306.44	57
H30	7863.18	-2915.2	7251.62	51
H31	7460.23	-1850.69	8123.03	36
H33	5005.83	3457.58	3525.16	44
H34	6802.25	2328.48	3336.72	50
H36	6311.42	515.63	5244.53	90
H37	4522.19	1659.67	5449.85	73
H38A	8140.77	478.62	3657.45	83
H38B	8001.39	-126.26	4462.78	83
H38C	8394.45	930.55	4260.51	83
H40	3843.41	5338.95	2756.93	48
H41	4114.44	6451.74	1664.28	60
H42	2615.48	7647.47	1148.51	58
H43	844.52	7696.52	1692.11	52
H44	559.16	6549.53	2769.77	42
H46	-175.24	8597.18	3441.09	43
H46A	-92.49	8978.78	5108.92	41
H47	429.72	10119.8	2921.37	55

Table 2-15 (cont'd)

Atom	x	y	z	Ueq
H47A	407.37	10556.91	4666.36	54
H48	1852.59	10313.15	3309.13	61
H48A	1523.73	10740.89	3581.47	60
H49	2651.99	9064.48	4228.02	77
H49A	2191.51	9313.98	2928.52	77
H50	2034.67	7572.9	4739.02	57
H50A	1744.96	7748.92	3346.16	59
H52	-257.85	5142.88	7702.74	42
H53	-105.48	5784.39	8664.32	51
H54	497.96	7290.48	8477.22	54
H55	944.08	8156.64	7324.97	55
H56	762.95	7535.34	6362.11	42
H58	2731.27	1065.54	6244.47	50
H59	3134.45	-149.54	7285.12	67
H60	2735.46	489.6	8344.81	68
H61	1915.54	2344.74	8374.31	63
H62	1495.31	3578.73	7334.88	46

REFERENCES

REFERENCES

- (1) Ye, Q.; Zhou, H.; Xu, J. Cubic Polyhedral Oligomeric Silsesquioxane Based Functional Materials: Synthesis, Assembly, and Applications. *Chem. Asian J.* **2016**, *11*, 1322.
- (2) Hartmann-Thompson, C. Polyhedral Oligomeric Silsesquioxanes in Electronics and Energy Applications. *Adv.Silicon Sci.* **2011**, 247–325.
- (3) Calabrese, C.; Liotta, L. F.; Giacalone, F.; Gruttadauria, M.; Aprile, C. Supported Polyhedral Oligomeric Silsesquioxane-Based (POSS) Materials as Highly Active Organocatalysts for the Conversion of CO₂. *ChemCatChem* **2019**, *11*, 560–567.
- (4) Li, Y.; Dong, X.-H.; Zou, Y.; Wang, Z.; Yue, K.; Huang, M.; Liu, H.; Feng, X.; Lin, Z.; Zhang, W.; Zhang, W.-B.; Cheng, S. Z. D. *Polymer* **2017**, *125*, 303.
- (5) Carraher, C. E., Jr.; Currell, B.; Pittman, C. U., Jr.; Sheats, J.; Zeldin, M. *Inorganic and Metal-Containing Polymeric Materials*; Springer Science & Business Media, **2012**.
- (6) Dong, F.; Lu, L.; Ha, C. Silsesquioxane-Containing Hybrid Nanomaterials: Fascinating Platforms for Advanced Applications. *Macromol. Chem. Phys.* **2019**, *220*, 1800324.
- (7) Mohamed, M. G.; Kuo, S.-W. Polybenzoxazine/Polyhedral Oligomeric Silsesquioxane (POSS) Nanocomposites. *Polymers* **2016**, *8*, 225.
- (8) Li, G., Wang, L., Ni, H. *et al.* Polyhedral Oligomeric Silsesquioxane (POSS) Polymers and Copolymers: A Review. *J. Inorg. Organomet Polym.* **2001**, *11*, 123–154.
- (9) Tegou, E.; Bellas, V.; Gogolides, E.; Argitis, P. Polyhedral oligomeric silsesquioxane (POSS) acrylate copolymers for microfabrication: properties and formulation of resist materials. *Microelectron. Eng.* **2004**, *238*, 73-74.
- (10) Phillips, S. H.; Haddad, T. S.; Tomczak, S. Developments in nanoscience: polyhedral oligomeric silsesquioxane (POSS)-polymers *J. Curr. Opin. Solid State Mater. Sci.* 2004, *8*, 21–29.
- (11) Zhou, H.; Ye, Q.; Xu, J. Polyhedral oligomeric silsesquioxane-based hybrid materials and their applications. *Mater. Chem. Front.* **2017**, *1*, 212–230.
- (12) Lichtenhan, J.; Otonari, Y. A.; Carr, M. J. Linear Hybrid Polymer Building Blocks: Methacrylate-Functionalized Polyhedral Oligomeric Silsesquioxane Monomers and Polymers. *Macromolecules* **1995**, *28*, 8435–8437.
- (13) Haddad, T. S.; Lichtenhan, J. D. Hybrid Organic–Inorganic Thermoplastics: Styryl-Based Polyhedral Oligomeric Silsesquioxane Polymers. *Macromolecules* **1996**, *29*, 7302–7304.

- (14) Mather, P. T.; Jeon, H. G.; Romo-Uribe, A.; Haddad, T. S.; Lichtenhan, J. D. Mechanical Relaxation and Microstructure of Poly(norbornyl-POSS) Copolymers. *Macromolecules* **1999**, *32*, 1194–1203.
- (15) Li, Z.; Kong, J.; Wang, F.; He, C. Polyhedral oligomeric silsesquioxanes (POSSs): an important building block for organic optoelectronic materials. *J. Mater. Chem.* **2017**, *5*, 5283–5298.
- (16) Leu, C.-M.; Chang, Y.-T.; Wei, K.-H. Synthesis and Dielectric Properties of Polyimide-Tethered Polyhedral Oligomeric Silsesquioxane (POSS) Nanocomposites via POSS-diamine. *Macromolecules* **2003**, *36*, 9122–9127.
- (17) Morimoto, Y.; Watanabe, K.; Ootake, N.; Inagaki, J. I.; Yoshida, K.; Ohguma, K. Silsesquioxane Derivatives and Process for Production Thereof. 20040249103A1 **2004**.
- (18) Lee, D. W.; Kawakami, Y. Incompletely Condensed Silsesquioxanes: Formation and Reactivity. *Polym. J.* **2007**, *39*, 230–238.
- (19) Hoque, M. A.; Kakihana, Y.; Shinke, S.; Kawakami, Y. Polysiloxanes with Periodically Distributed Isomeric Double-Decker Silsesquioxane in the Main Chain. *Macromolecules* **2009**, *42*, 3309–3315.
- (20) Vogelsang, D. F.; Dannatt, J. E.; Schoen, B. W.; Maleczka, R. E., Jr; Lee, A. Phase Behavior of *cis-trans* Mixtures of Double-Decker Shaped Silsesquioxanes for Processability Enhancement. *ACS Appl. Nano Mater.* **2019**, *2*, 1223–1231.
- (21) Liu, Y.; Takeda, N.; Ouali, A.; Unno, M. Synthesis, Characterization, and Functionalization of Tetrafunctional Double-Decker Siloxanes. *Inorg. Chem.* **2019**, *58*, 4093–4098.
- (22) Wei, K.; Wang, L.; Li, L.; Zheng, S. Synthesis and characterization of bead-like poly(*N*-isopropylacrylamide) copolymers with double decker silsesquioxane in the main chains. *Polym. Chem.* **2015**, *6*, 256–269.
- (23) Liu, N.; Wei, K.; Wang, L.; Zheng, S. Organic–inorganic polyimides with double decker silsesquioxane in the main chains. *Polym. Chem.* **2016**, *7*, 1158–1167.
- (24) Wu, S.; Hayakawa, T.; Kakimoto, M.-A.; Oikawa, H. Synthesis and Characterization of Organosoluble Aromatic Polyimides Containing POSS in Main Chain Derived from Double-Decker-Shaped Silsesquioxane. *Macromolecules* **2008**, *41*, 3481–3487.
- (25) Ul-Islam, S.; Butola, B. S. *Advanced Functional Textiles and Polymers: Fabrication, Processing and Applications*; Wiley, **2019**.
- (26) Hao, J.; Wei, Y.; Chen, B.; Mu, J. Polymerization of polyhedral oligomeric silsesquioxane (POSS) with perfluoro-monomers and a kinetic study. *RSC Adv.* **2017**, *7*, 10700–10706.

- (27) Žak, P.; Delaude, L.; Dudziec, B.; Marciniec, B. N-Heterocyclic carbene-based ruthenium-hydride catalysts for the synthesis of unsymmetrically functionalized double-decker silsesquioxanes. *Chem. Commun.* **2018**, 54, 4306–4309.
- (28) Vogelsang, D. F.; Dannatt, J. E.; Maleczka, R. E.; Lee, A. Separation of asymmetrically capped double-decker silsesquioxanes mixtures. *Polyhedron* **2018**, 155, 189–193.
- (29) COSMO-V1.61 - Software for the CCD Detector Systems for Determining Data Collection Parameters, Bruker axs, Madison, WI **2000**.
- (30) Dolomanov, O. V.; Bourhis, L. J.; Gildea, R. J.; Howard, J. A. K.; Puschmann, H.; Olex2: A complete structure solution, refinement and analysis program, *J. Appl. Cryst.* **2009**, 42, 339-341.
- (31) Sheldrick, G.M., A short history of ShelX, *Acta Cryst.* **2008**, A64, 339-341.
- (32) Sheldrick, G.M., ShelXT-Integrated space-group and crystal-structure determination, *Acta Cryst.* **2015**, A71, 3-8.
- (33) Software for the Integration of CCD Detector System Bruker Analytical X-ray Systems, Bruker axs, Madison, WI (after **2013**).

CHAPTER 3.0: Synthesis of Incompletely Condensed Asymmetrically Functionalized Double-Decker Shaped Silsesquioxane Disilanol 'Bird Nest-Shaped Silsesquioxanes'

3.1 INTRODUCTION

Incompletely condensed silsesquioxanes constitute a class of organosilicon hybrid materials with exceptional physico-chemical properties not realized from pure organic and inorganic compounds.^{1–13} They are generally three-dimensional cage-like nanostructures with free transformable moieties that are amenable to numerous functional groups (**Figure 3-1**). The structural arrangement of atoms/groups in these compounds makes them ideal precursors for several applications including their utility as ligands in catalysis, as drug delivery agents in medicine and as fillers for the synthesis of telechelic, hemitelechelic and beads-on-chain composite architectures. The tetrafunctional, trifunctional and various bifunctional analogues are known.^{14–18}

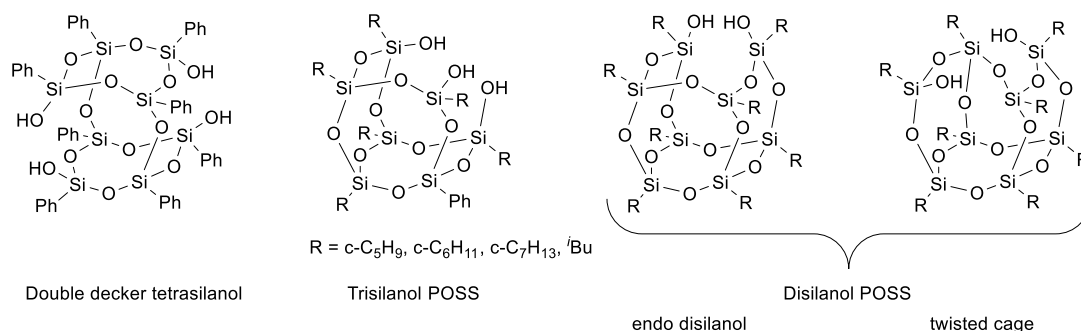
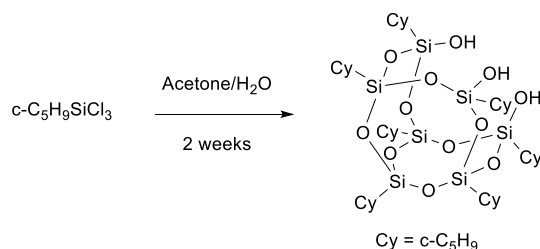


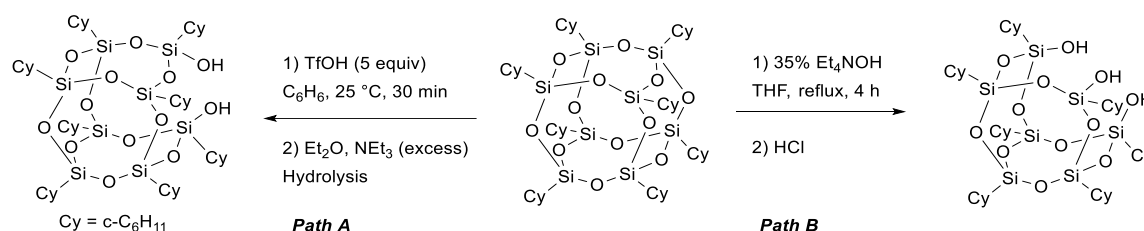
Figure 3-1: Representative Incompletely Condensed Silsesquioxanes

These compounds can be accessed from both monomeric trifunctional organo chloro/alkoxy silanes⁵ (**Scheme 3-1**) or from the fully condensed POSS cages under both acidic^{7,19,20} (**Scheme 3-2 Path A**) and basic⁸ (**Scheme 3-2 Path B**) conditions.

Scheme 3-1: Hydrolysis of cyclopentyltrichlorosilane into heptacyclopentyl POSS trisilanol



Scheme 3-2: Selective cleavage of completely condensed octacyclohexyl silsesquioxane for the synthesis of octacyclohexyl POSS disilanol (**Path A**) and heptacyclohexyl POSS trisilanol (**Path B**)



Credit for the synthesis of such compounds from fully condensed precursors is given to Feher and coworkers for developing not only the first synthetic modification of these cages via selective cleavage of one Si-O-Si linkage but also for demonstrating various other routes that have led to the increased pool of incompletely condensed POSS compounds. In their seminal report, Feher and coworkers disclosed that the treatment of cubic silsesquioxanes of the $\text{R}_8\text{Si}_8\text{O}_{12}$ type with strong acids (HX) afforded open cage structures, which upon hydrolysis yielded the $\text{R}_8\text{Si}_8\text{O}_{11}(\text{OH})_2$ frameworks.⁷

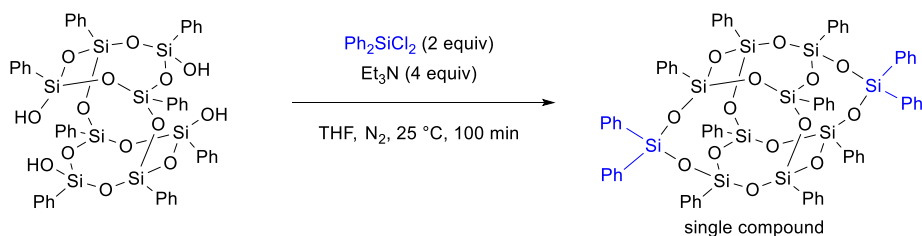
Such POSS scaffolds are flexible starting materials for the synthesis of a wide range of functional silsesquioxane and metallasilsesquioxane frameworks.^{2,8,21,22} Prior to

their work, only a handful of synthetically useful incompletely condensed POSS cages bearing bulky organic groups were known and these were solely obtained from the hydrolytic condensation of trifunctional silanes.²³ However, with the discoveries^{8,10,20} that fully-condensed $[\text{RSiO}_{3/2}]_n$ frameworks can undergo selective cleavage by strong acids and bases, a wide range of novel incompletely-condensed frameworks were obtained. Compared to other nanoparticles, their unique thermal stability, chemical/oxidative resistance, low dielectric constant and mechanical properties have found applications in polymer and material sciences. More applications emerged after the discovery of the double-decker oligomeric silsesquixane in 2004.^{14,21–26}

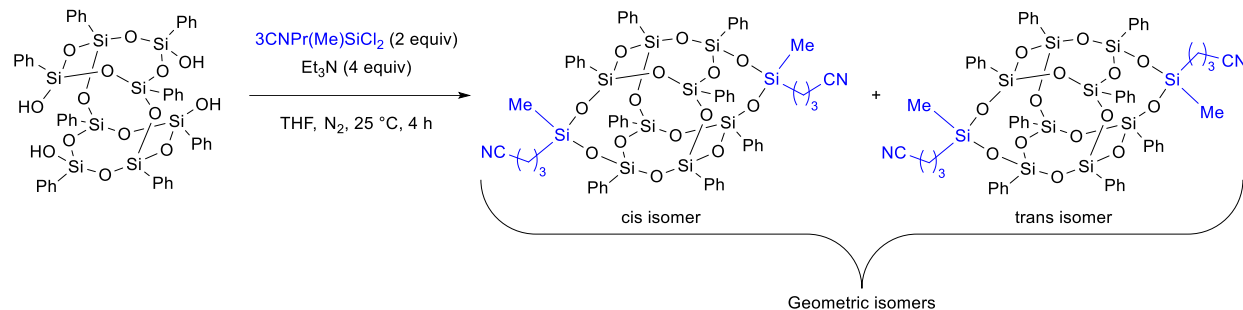
3.2 Modifications of Incompletely Condensed POSS Cages

There are quite a good number of transformations that have been conducted on various incompletely condensed POSS compounds leading to the generation of new functional materials for various applications. The symmetric tetrafunctional double decker has for instance been modified into fully condensed bifunctional siloxanes using suitable chlorosilanes. Depending on the type of capping agent used, products obtained from the side-capping can either be a single compound (**Scheme 3-3**) or one that displays geometric isomerism (**Schemes 3-4**).^{15,27–33}

Scheme 3-3: Condensation of $\text{DDSQ}(\text{OH})_4$ with diphenyldichlorosilane

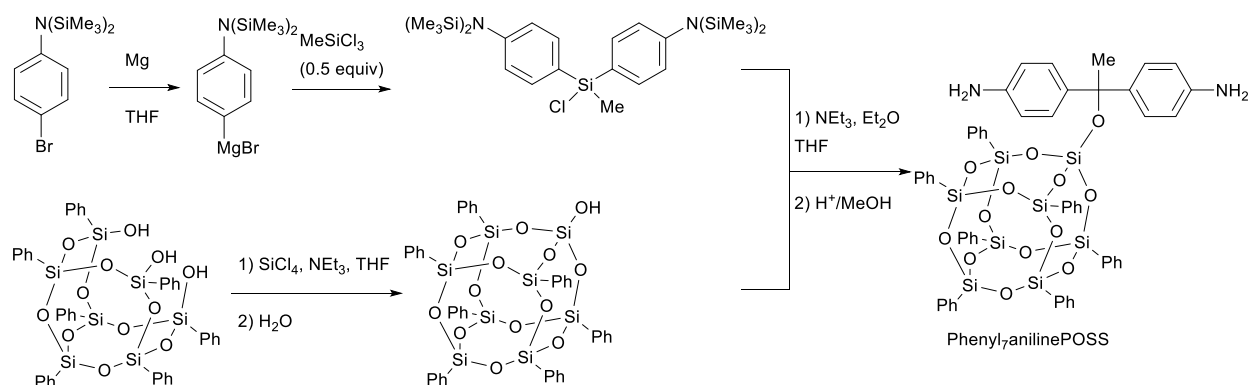


Scheme 3-4: Condensation of DDSQ(OH)₄ with 3-cyanopropyl(methyl)dichlorosilane



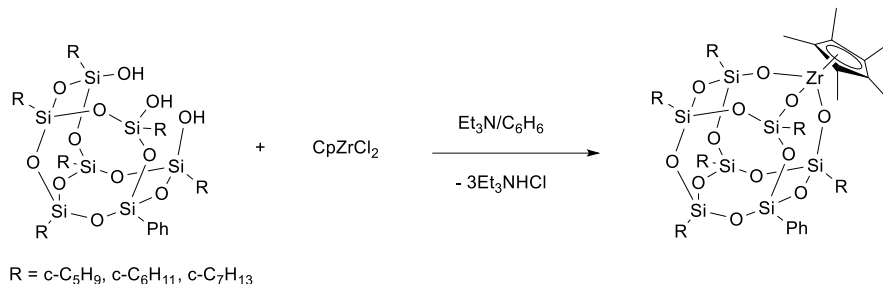
The cis/trans forms have been isolated by various groups and shown to display different properties like solubility and melting temperatures.^{34,35} Similarly, incompletely condensed trisilanols have been modified via corner-capping with various reactive groups leading to condensed structures with complete control over the functionalized POSS architecture (**Scheme 3-5**).

Scheme 3-5: Synthesis of difunctional POSS, phenyl₇anilinePOSS from heptaphenylPOSS trisilanol



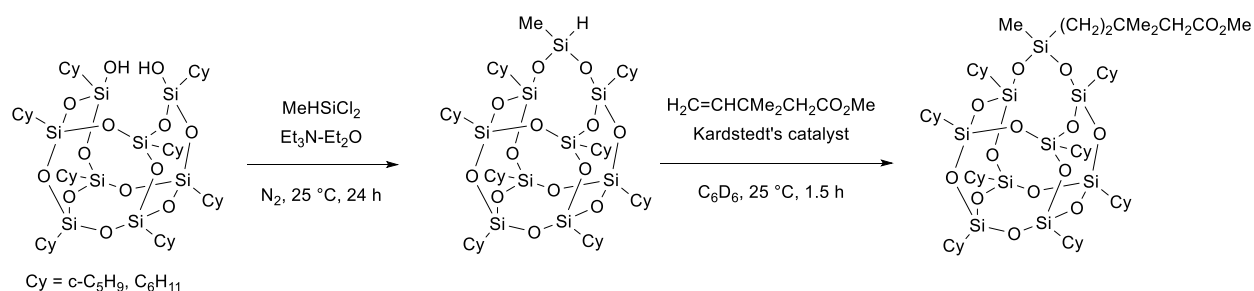
Metal-bearing POSS structures are also obtained via similar corner-capping approaches (**Scheme 3-6**)^{36–38}

Scheme 3-6: Condensation of trisilanol POSS for the synthesis of metallasilsesquioxane



Difunctional POSS precursors have also been transformed into various derivatives via the addition of unique difunctional organic groups to generate materials with properties that are distinct from those of the constituent reactants (**Scheme 3-7**). Like other incompletely condensed POSS cages, such modified POSS-based functional materials also impact intrinsic properties including thermal stability and mechanical properties on the nanocomposite.

Scheme 3-7: Functionalization of POSS endo disilanol with MeHSiCl₂ and subsequent hydrosilylation



3.2.1 Tetrafunctional Polyhedral Oligomeric Silsesquioxanes and their Derivatives

The tetrafunctional POSS frameworks generally come in three forms; the half cube with the basic molecular composition of $\text{R}_4\text{T}_4(\text{OH})_4$,^{39,40} the homologated analogue with $\text{R}_6\text{T}_6(\text{OH})_4$ and the unique double-decker bearing two well-defined cyclic

tetraphenylsiloxane decks linked together by two oxygen atoms with the four drooping functional groups symmetrically arranged in pairs on opposite ends (**Figure 3-2**).¹⁴

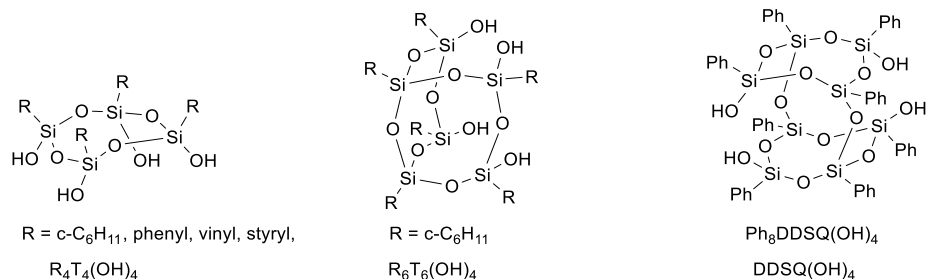


Figure 3-2: Tetrafunctional Polyhedral Oligomeric Silsesquioxanes

These cage-like silsesquioxanes have been obtained from both the monomeric trifunctional chloro/alkoxy silane and the cubic POSS precursors. However, among them, the symmetric nature of $\text{DDSQ}(\text{OH})_4$ with its rigid three-dimensional framework bearing phenyl coronae is particularly interesting. The well-defined assembly of the atoms accords this compound the molecular flexibility for easy functionalization via side-capping. By virtue of its size and structure, transformation affords macromolecular frameworks that are useful for a myriad of applications. The modified materials have a low dielectric constant and excellent thermal and oxidative stability, good optical and mechanical properties.^{31,41–49}

The growing appeal for these properties on composite materials makes the double-decker oligomeric silsesquioxane tetrasilanol the most explored of the tetrafunctional polyhedral oligomeric silsesquioxanes. Whereas research opportunities keep growing for the synthesis of novel symmetrically functionalized condensed POSS templates, the silsesquioxane bearing two distinct reactive functionalities could be an even more intriguing molecular template. We recently reported a route (Chapter 2) using protecting group strategies with aryl boronic acid to selectively mask two silanols on the

DDSQ(OH)₄. Even though this technique was superior to prior routes, it suffered from the generation of unwanted symmetric byproduct. One way we envisioned to address this limitation was to isolate either the monoborylated DDSQ diol or the one-side silylated DDSQ(OH)₂. In this study, we developed a route that yields the POSS disilanol equivalent with some modifications to our previous protocol. The disilanols synthesized in this study offered the asymmetrically capped products in excellent yields upon post functionalization. Their architecture also makes them ideal precursors for modifying solid supports like carbon fibres.

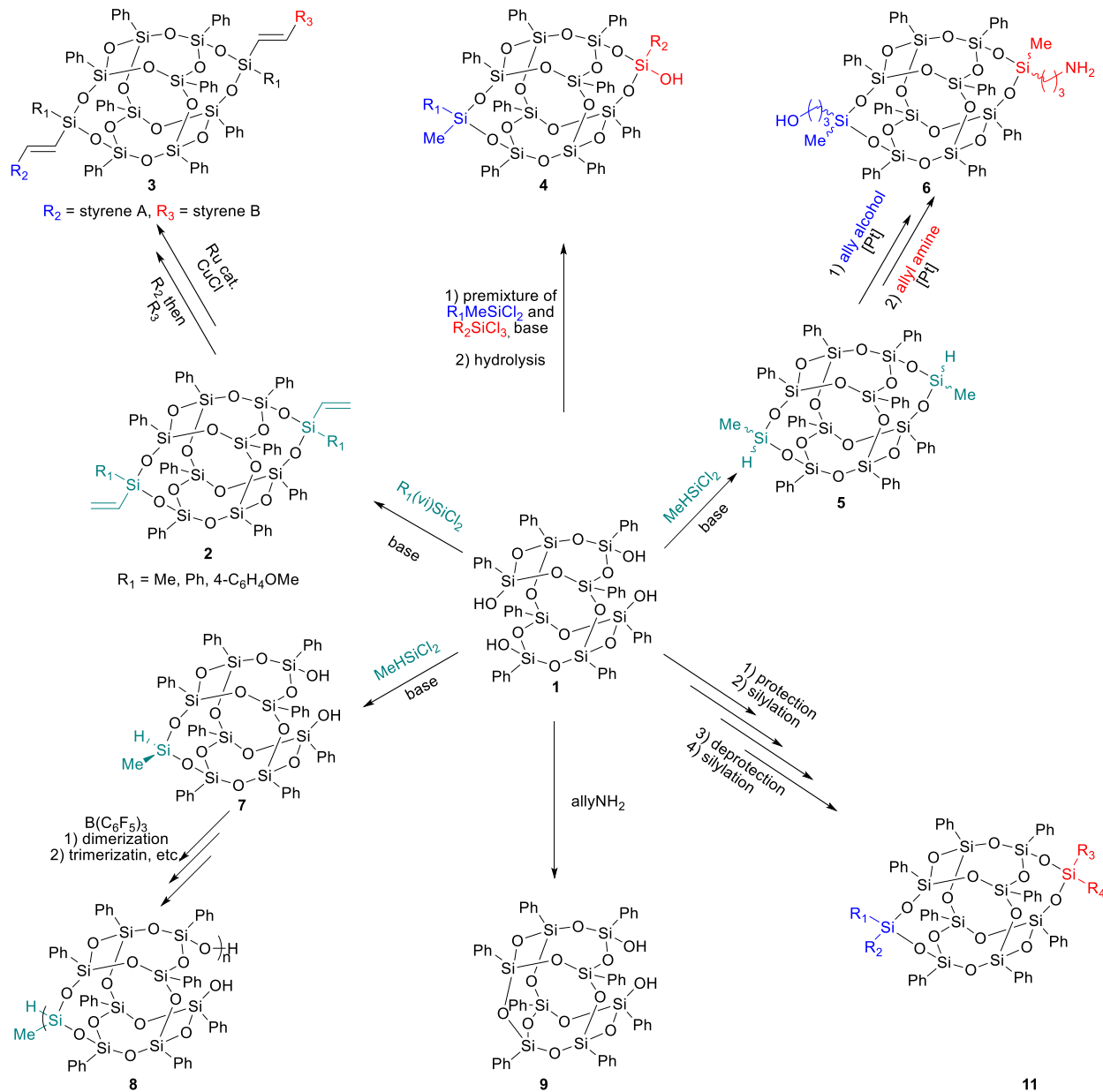
3.2.2 Asymmetrically Functionalized DDSQs

Until recently, functionalized DDSQs were exclusively the closed bifunctional siloxanes that are often incorporated into the polymer backbone as ‘beads-on-a-chain’.^{27,44,45,50–53} The well-defined architecture of the double-decker precursor allows their transformation into diverse functional macromers ideal for post functional elaboration. From an application viewpoint, the post functionalized derivatives are limited to linking identical polymers on either side of the functionalized cages.

Even though siloxanes bridging polymers in this manner have shown to reinforce the composite properties such as strength, modulus, dielectric properties, oxidative resistance, flammability and glass transition temperature (T_g),^{27,54,55} attempts to cluster analogous POSS linkers that are able to link dissimilar polymers has been a long-standing challenge. One way to overcome this problem is to destroy the symmetry in DDSQ(OH)₄ by transforming it into the asymmetrically functionalized equivalent. Whilst formation of symmetric bi-functional DDSQs appears simple, the selective reactivity of the silanols in DDSQ against different capping agents remains a serious challenge. The few

modification strategies known to date are via O-silylation, hydrosilylation and O-borylation of the silanol groups with chlorosilanes and boronic acids respectively to afford either closed T_8D_2 ^{32,49,56} or T_8D_2 ^{57,58} or open polymeric⁵⁸ siloxane frameworks. An illustration of some of these strategies is shown in **Scheme 3-8**. These preliminary discoveries laid the platform for the resulting siloxanes to be grafted to the backbone of two different polymer matrices.^{32,49,56} One route currently undergoing development in our laboratory involves accessing condensed asymmetric DDSQs via controlled hydrosilylation of bi-functionalized cages. The Marciniak group also reported a Grubb's catalyzed metathesis of a pre-functionalized DDSQ cage.⁵⁶ Our group also recently reported two routes for the synthesis of these type of POSS cages; one involving addition of a premixture of different capping/coupling agents to $DDSQ(OH)_4$ ³² and the other, a protecting group strategy.⁴⁹

Scheme 3-8: Known routes into asymmetrically functionalized DDSQs



These developments opened the avenue to a new class of POSS cages that have potential to modulate the performance of the POSS/polymer composite by regulating the motions of the dissimilar polymeric matrices to which these cages are anchored. Unfortunately, all these approaches have their associated limitations. The hydrosilylation pathway, still under development in our lab is restricted to prefucionalized

MeHSiDDSQSiMeH and allyl-containing reagents for elaboration; the metathesis route by Zac et al. is limited to a pre-functionalized symmetric $R(vi)SiDDSQSiR(vi)$, styryl coupling partners; the chlorosilane pre-mixture path is restrained by its requirement of a trichlorosilane as a second coupling partner and the generation of a large amount of unwanted symmetrically functionalized DDSQs; and lastly, the boronic acid course, requires multiple steps and also generates symmetric products to ~8%.

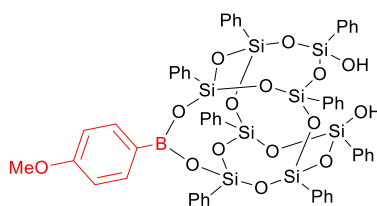
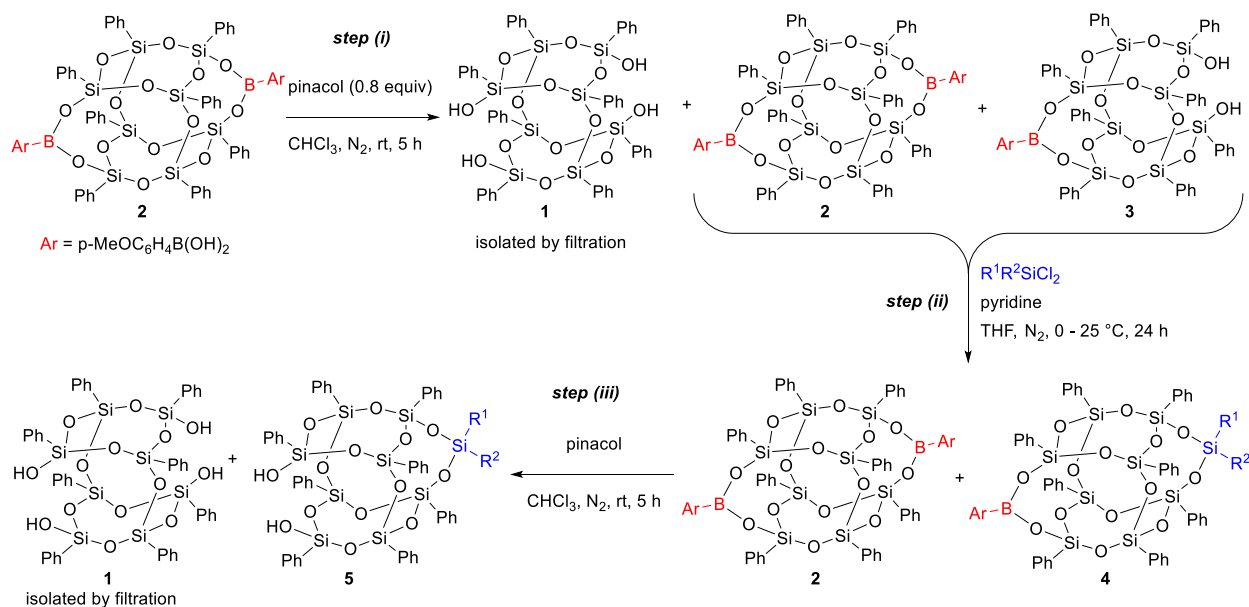


Figure 3-3: Monoborylated DDSQ(OH)₂

Efforts to improve the latter protocol via various attempts to isolate the key monoborylated DDSQ(OH)₂ (**Figure 3-3**) have been unsuccessful to date. However, we modified our previous strategy to enable us isolate the asymmetric T₈D₁ monosilylated DDSQ(OH)₂ after the first silylation. Herein, we present for the first time a strategy to modify DDSQ(OH)₄ for the selective synthesis of asymmetric monosilylated DDSQ(OH)₂. Such functionalized DDSQs are versatile precursors for the efficient synthesis of a wide range of asymmetric DDSQs, several metallasilsesquioxanes and ligands for solid supports. The starting material in this study is the bisborylated DDSQ which is obtained from the DDSQ(OH)₄. The approach herein referred to as the “reverse approach” consists of three steps, viz. (i) selective deprotection, (ii) silylation and finally (iii) global deprotection. The bis-borylated ester is first subjected to partial deborylation, then silylated with an appropriate di-/tri-chlorosilane and the resulting crude mixture finally exposed to global deborylation affording the targeted monosilylated DDSQ disilanol

(**Scheme 3-9**). Illustrations of their synthetic utility as model precursors for the synthesis of completely condensed asymmetrically functionalized DDSQs afforded excellent yields.

Scheme 3-9: Synthetic route into $R^1R^2SiDDSQ(OH)_2$ (5**)**



It is worth mentioning here that in steps (i) and (iii), DDSQ(OH)_4 (**1**) is isolated and used to synthesize more bisborylated DDSQ starting material. Unlike our previously reported protocol “the forward approach”,⁴⁹ this strategy yields more of the key intermediate monoborylated DDSQ (**3**) (mono:bis-boronate ester $\sim 1:2$) and is free from adventitious boronic acid that may alter the composition of the crude in step 1.

3.3 Results and Discussions

3.3.1 Optimization of (p-MeOC₆H₄B)₂DDSQ(OH)₂ (**3**)

Scheme 3-10: Optimal deborylation of **2** with pinacol for the synthesis of **3**

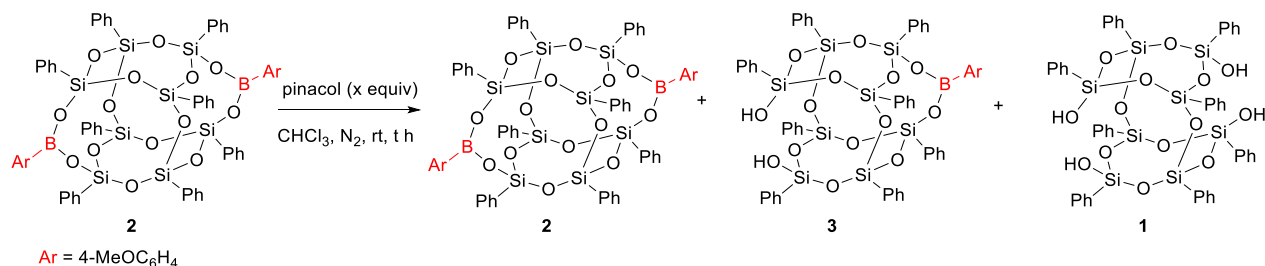


Table 3-1: Optimization for the partial deborylation of (p-MeOC₆H₄B)₂DDSQ (**2**) for the synthesis of monoborylated DDSQ diol (**3**)

Entry	2 (mmol)	pinacol (equiv)	time (h)	filtrate (g)	¹ H-NMR ratio		Amount (mmol)		DDSQ(OH) ₄ (1) (mmol)
					2	3	2	3	
1	0.25	0.5	3	0.14	4.36	1	0.076	0.034	0.10
2	0.25	0.8	3	0.16	3.01	1	0.077	0.051	0.09
3	0.25	0.8	5	0.21	2.70	1	0.096	0.071	0.06
4	0.25	1.0	2	0.17	4.22	1	0.091	0.043	0.07
5	0.25	1.0	3	0.18	2.93	1	0.085	0.054	0.09
6	0.25	1.5	1	0.17	2.62	1	0.077	0.059	0.11
7	0.25	1.5	2	0.15	3.13	1	0.073	0.047	0.11
8	0.25	1.5	3	0.14	3.66	1	0.072	0.040	0.19

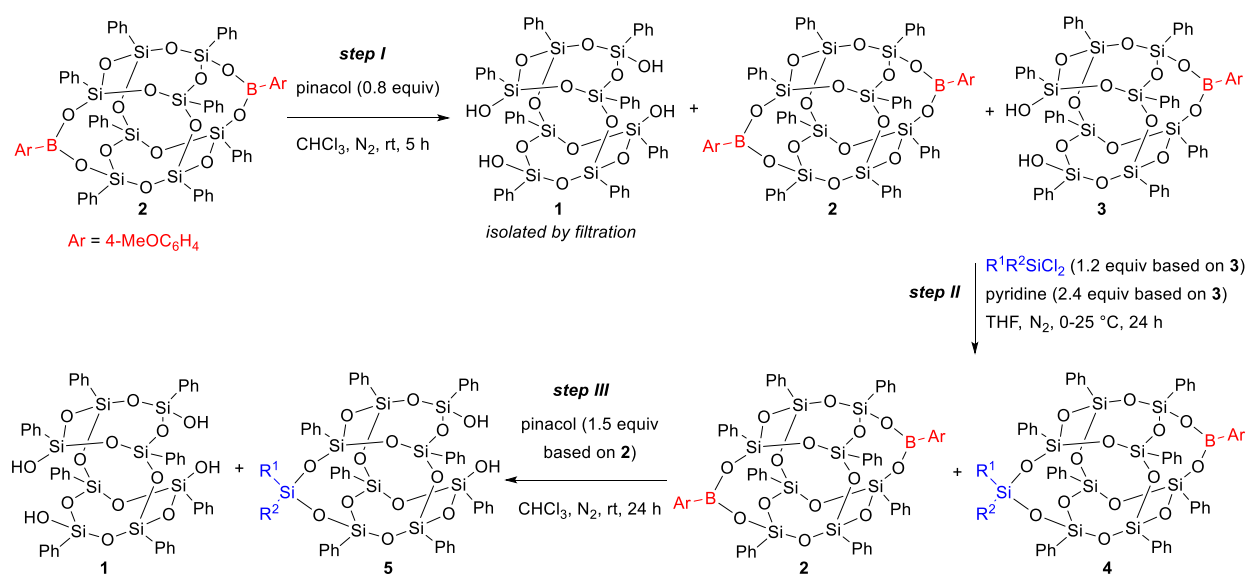
Reaction conditions: 0.25 mmol **2**, pinacol (x equiv). Residue from crude mixture is pure **1** obtained after filtration. Amounts of **2** and **3** were determined from ¹H-NMR.

Selective deborylation with varying amounts of pinacol at different reaction times never exclusively afford the target monoborylated DDSQ(OH)₂ (**3**). In all cases, a product mixture consisting of the partially deborylated DDSQ (**3**), the completely deborylated cage (**1**) and some starting materials (**2**) were obtained. Even though **1** can be separated from this mixture due to its poor solubility in chloroform, attempts to isolate **3** from **2** using various techniques has been unsuccessful. Interesting though, good nmr ratios of 2:3 was obtained with good throughputs using conditions in entries 3, 5 and 6. Conditions in entry

3 were deemed optimal because of the high ratio of 2:3 (0.096 mmol:0.071 mmol) and because these conditions afforded the highest throughput (0.21 g) of product that could be taken to the next step. With this route, symmetric AA in negligible amounts could only arise from adventitious **1** that may have escaped during the filtration process (solubility of **1** in CHCl_3 = 5.8 mg/mL).

3.3.2 Substrate Scope

Scheme 3-11: Synthesis of asymmetrically functionalized $\text{R}^1\text{R}^2\text{SiDDSQ}(\text{OH})_2$ (**5**)



All reactions were monitored using ^1H , ^{11}B , and ^{29}Si spectroscopy. The target $\text{R}^1\text{R}^2\text{SiDDSQ}(\text{OH})_2$ were further purified by flash chromatography using ethylacetate:hexane (1:9) as the eluting solvent.

Table 3-2: Substrate scope for the synthesis of asymmetric monosilylated DDSQ(OH)₂ (**5**)

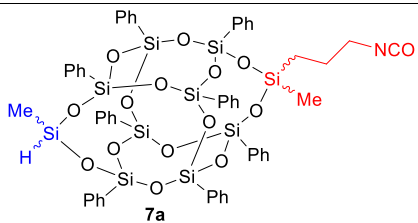
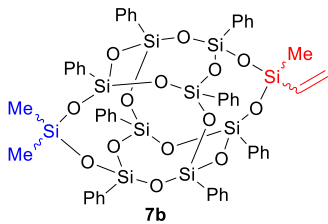
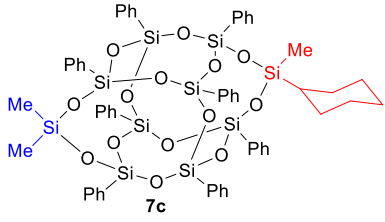
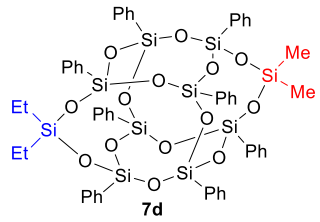
Entry	Intermediates			Deborylation 1	Total ^b 1	R ¹ R ² SiCl ₂	Yield (%) ^c	
	3	2	1				R ₁ R ₂ SiDDSQ(OH) ₂ (5)	R ₁ R ₂ SiDDSQR ₁ R ₂ (6)
1	0.31	0.45	0.13	0.28	0.41	MeHSiCl ₂	5a ; 0.16 mmol, 52%	6a ; 0.034 mmol, 4%
2	0.26	0.38	0.17	0.26	0.43	Me ₂ SiCl ₂	5b ; 0.15 mmol, 58%	6b ; 0.034 mmol, 4%
3	0.27	0.40	0.18	0.18	0.36	Et ₂ SiCl ₂	5c ; 0.14 mmol, 52%	6c ; 0.032 mmol, 4%
4	0.28	0.39	0.17	0.26	0.43	Me(3CNPr)SiCl ₂	5d ; 0.14 mmol, 51%	6d ; 0.041 mmol, 5%
5	0.29	0.40	0.19	0.27	0.46	Me(vi)SiCl ₂	5e ; 0.18 mmol, 61%	6e ; 0.033 mmol, 4%
6	0.19	0.52	0.16	0.18	0.34	Allyl(Me)SiCl ₂	5f ; 0.11 mmol, 58%	6f ; 0.040 mmol, 6%
7	0.29	0.42	0.18	0.23	0.41	MeSiCl ₃	5g ; 0.16 mmol, 55%	6g ; 0.034 mmol, 4%
8	0.27	0.51	0.17	0.23	0.40	ⁱ PrSiCl ₃	5h ; 0.16 mmol, 58%	6h ; 0.040 mmol, 5%

Conditions: ^aReactions were run on 1 mmol scale of **2**, ^btotal amount of **1** generated in steps I and III, ^cyields of **5** are based on **3**, ^dyields of **6** are obtained after subtracting the amount of **1** generated from 1 mmol of **2** in step 1.

The yields of **5** are calculated based on the amount of **3** obtained in step 1, and those for **6**, after subtracting the amount of **1** obtained in this same step from the starting material (**2**). It is noteworthy that the recovery of **1** is crucial as this material can always be used to make the bis-boronate DDSQ ester (**2**). The strategy is amenable to a wide range of capping agents affording moderate to high yields of **5** (Table 3-2). The spectral data for all functionalized **5** shows resonances that are in agreement with the proposed structures and the high-resolution mass spectrometry are in excellent agreement with the calculated theoretical masses (Appendix).

3.3.3 Transformation of Monosilylated DDSQ diol into Condensed Asymmetric DDSQs (7)

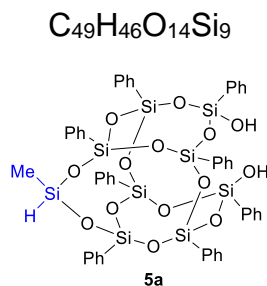
Table 3-3: Post Functionalization of asymmetric monosilylated DDSQ(OH)₂ (**5**) into Completely Condensed Asymmetric DDSQs of the D₂T₈ Type

Entry	$R^1R^2SiDDSQ(OH)_2$ (5)	$R^3R^4SiCl_2$	$R^1R^2SiDDSQSIR^3R^4$ (7)	Yield (%) ^c
1	5a	Me(PrNCO)SiCl ₂	 7a	0.081 mmol, 81%
2	5b	Me(vinyl)SiCl ₂	 7b	0.100 mmol, 100%
3	5b	Me(cyclohex)SiCl ₂	 7c	0.072 mmol, 72%
4	5c	Me ₂ SiCl ₂	 7d	0.071 mmol, 71%

Conditions: Reactions were run on 0.1 mmol scale of **5**, Yields of **7** are obtained after washing the crude with hexanes and pentanes without further purifications.

3.3.4 Spectral Data for Asymmetric R¹R²DDSQ(OH)₂

15-Methyl-1,3,5,7,9,11,13,17-octaphenyl-2,4,6,8,10,12,14,16,18,19,20,21-dodecaoxa-1,3,5,7,9,11,13,15,17-nonasilatetracyclo[9.7.1.15,17.17,13]henicosane-3,9-diol (5a)



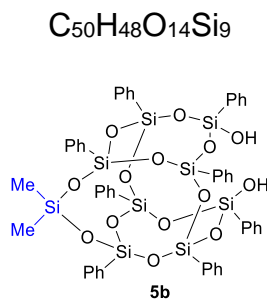
This product was isolated as a white solid in 52% yield (0.16 mmol). mp 189–192 °C.

¹H NMR (500 MHz, CDCl₃) δ (ppm) 7.53 – 7.14 (m, 40H), 5.06 (s, 2H), 4.97 (q, J = 1.6 Hz, 1H), 0.36 (d, J = 1.6 Hz, 3H).

¹³C NMR (126 MHz, CDCl₃) δ (ppm) 134.24, 134.10, 134.07, 134.06, 133.90, 131.46, 130.88, 130.71, 130.59, 130.48, 130.43, 127.86, 127.80, 127.65, 127.62, 0.61.

²⁹Si NMR (99 MHz, CDCl₃) δ (ppm) -32.83, -68.57, -77.94, -79.06, -79.25.

15,15-Dimethyl-1,3,5,7,9,11,13,17-octaphenyl-2,4,6,8,10,12,14,16,18,19,20,21-dodecaoxa-1,3,5,7,9,11,13,15,17-nonasilatetracyclo[9.7.1.15,17.17,13]henicosane-3,9-diol (5b)



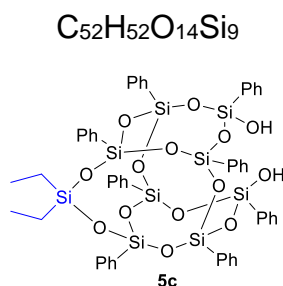
This product was isolated as a white solid in 58% yield (0.15 mmol). mp 179–182 °C.

¹H NMR (500 MHz, CDCl₃) δ (ppm) 7.52 – 7.14 (m, 40H), 5.04 (s, 2H), 0.29 (s, 6H).

^{13}C NMR (126 MHz, CDCl_3) δ (ppm) 134.22, 134.08, 133.89, 131.96, 130.85, 130.80, 130.61, 130.36, 130.33, 127.80, 127.75, 127.62., 0.51.

^{29}Si NMR (99 MHz, CDCl_3) δ (ppm) -16.48, -68.63, -78.65, -79.30.

15,15-Diethyl-1,3,5,7,9,11,13,17-octaphenyl-2,4,6,8,10,12,14,16,18,19,20,21-dodeca-oxa-1,3,5,7,9,11,13,15,17-nonasilatetracyclo[9.7.1.15,17.17,13]henicosane-3,9-diol (5c)



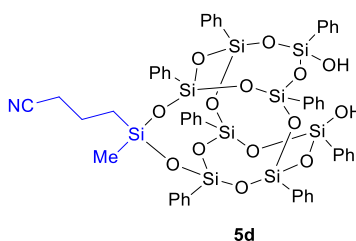
This product was isolated as a white solid in 52% yield (0.14 mmol). mp 147–150 °C.

^1H NMR (500 MHz, CDCl_3) δ (ppm) 7.51 – 7.13 (m, 40H), 0.98 (t, J = 7.9 Hz, 6H), 0.70 (q, J = 8.0 Hz, 4H).

^{13}C NMR (126 MHz, CDCl_3) δ (ppm) 134.26, 134.23, 134.13, 134.12, 134.10, 134.07, 134.03, 133.90, 133.86, 132.05, 130.91, 130.88, 130.60, 130.43, 130.34, 130.28, 127.80, 127.78, 127.75, 127.71, 127.68, 127.63, 127.61, 6.89, 6.32.

^{29}Si NMR (99 MHz, CDCl_3) δ (ppm) -16.80, -68.69, -78.91, -79.37.

4-(3,9-Dihydroxy-15-methyl-1,3,5,7,9,11,13,17-octaphenyl-2,4,6,8,10,12,14,16,18,19,20,21-dodecaoxa-1,3,5,7,9,11,13,15,17-nonasilatetracyclo[9.7.1.15,17.17,13]henicosan-15-yl)butanenitrile (**5d**).



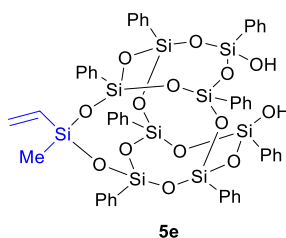
This product was isolated as a white solid in 51% yield (0.14 mmol). mp 128–131 °C.

^1H NMR (500 MHz, CDCl_3) δ (ppm) 7.52 – 7.12 (m, 40H), 5.20 (s, 2H), 2.25 (m, 2H), 1.81 – 1.59 (m, 2H), 0.84 (ddd, J = 8.4, 6.1, 2.8 Hz, 2H), 0.34 (s, 3H).

^{13}C NMR (126 MHz, CDCl_3) δ (ppm) 134.22, 134.14, 134.11, 134.04, 134.03, 133.95, 133.80, 131.50, 130.70, 130.55, 130.47, 127.94, 127.90, 127.87, 127.85, 127.81, 127.74, 127.74, 127.68, 127.62, 20.03, 19.41, 16.12.

^{29}Si NMR (99 MHz, CDCl_3) δ (ppm) -19.19, -68.59, -78.37, -79.18 (d, J = 3.7 Hz).

15-Methyl-1,3,5,7,9,11,13,17-octaphenyl-15-vinyl-2,4,6,8,10,12,14,16,18,19,20,21-dodecaoxa-1,3,5,7,9,11,13,15,17-nonasilatetracyclo[9.7.1.15,17.17,13]henicosane-3,9-diol (**5e**)



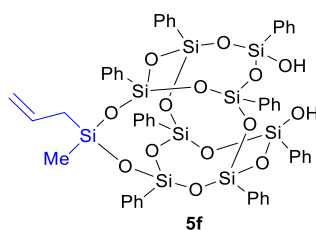
This product was isolated as a white solid in 61% yield (0.18 mmol). mp 148–150 °C.

^1H NMR (500 MHz, CDCl_3) δ (ppm) 7.54 – 7.17 (m, 40H), 6.18 – 6.09 (m, 1H), 6.01 – 5.89 (m, 2H), 0.38 – 0.34 (m, 3H).

^{13}C NMR (126 MHz, CDCl_3) δ (ppm) 134.49, 134.22, 134.08, 133.92, 131.75, 130.87, 130.73, 130.64, 130.39, 127.82, 127.75, 127.63, 127.58, -1.20.

^{29}Si NMR (99 MHz, CDCl_3) δ (ppm) -31.37, -68.61, -78.45, -79.28 (d, $J = 1.7$ Hz).

15-Allyl-15-methyl-1,3,5,7,9,11,13,17-octaphenyl-2,4,6,8,10,12,14,16,18,19,20,21-decaoxa-1,3,5,7,9,11,13,15,17-nonasilatetracyclo[9.7.1.15,17.17,13]henicosane-3,9-diol
(5f)



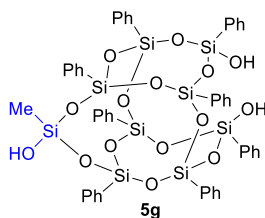
This product was isolated as a white solid in 58% yield (0.11 mmol). mp 183–186 °C.

^1H NMR (500 MHz, CDCl_3) δ (ppm) 7.52 – 7.15 (m, 40H), 5.76 (ddt, $J = 16.9, 10.1, 8.0$ Hz, 1H), 5.03 (s, 2H), 4.85 (dq, $J = 17.0, 1.6$ Hz, 1H), 4.75 (ddt, $J = 10.2, 2.2, 1.1$ Hz, 1H), 1.83 – 1.68 (m, 2H), 0.29 (s, 3H).

^{13}C NMR (126 MHz, CDCl_3) δ (ppm) 134.22, 134.07, 133.93, 132.66, 131.73, 130.82, 130.74, 130.73, 130.64, 130.40, 130.37, 127.81, 127.74, 127.63, 114.84, 24.53, -1.66.

^{29}Si NMR (99 MHz, CDCl_3) δ (ppm) -22.00, -68.64, -78.69, -79.30 (d, $J = 2.5$ Hz).

15-Methyl-1,3,5,7,9,11,13,17-octaphenyl-2,4,6,8,10,12,14,16,18,19,20,21-dodecaoxa-1,3,5,7,9,11,13,15,17-nonasilatetracyclo[9.7.1.15,17.17,13]henicosane-3,9,15-triol (5g)



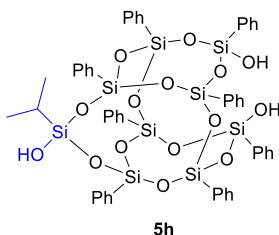
This product was isolated as a white solid in 55% yield (0.16 mmol). mp 193–196 °C.

^1H NMR (500 MHz, CDCl_3) δ (ppm) 7.58 – 7.12 (m, 40H), 0.34 (s, 3H).

^{13}C NMR (126 MHz, CDCl_3) δ (ppm) 134.22, 134.11, 134.09, 134.07, 134.04, 134.03, 134.00, 133.95, 130.70, 130.61, 130.58, 130.54, 130.52, 130.49, 127.87, 127.86, 127.83, 127.82, 127.72, 127.69, 127.67, 127.64, -3.87, -3.90.

^{29}Si NMR (99 MHz, CDCl_3) δ (ppm) -54.05 (1Si), -68.54 (2Si), -78.72 (2Si), -79.02 (2Si), -79.12 (2Si).

15-Isopropyl-1,3,5,7,9,11,13,17-octaphenyl-2,4,6,8,10,12,14,16,18,19,20,21-dodecaoxa-1,3,5,7,9,11,13,15,17-nonasilatetracyclo[9.7.1.15,17.17,13]henicosane-3,9,15-triol (5h)



This product was isolated as a white solid in 58% yield (0.16 mmol). mp 164–167 °C.

^1H NMR (500 MHz, CDCl_3) δ (ppm) 7.54 – 7.07 (m, 40H), 5.52 (s, 2H), 1.03 (d, $J = 1.6$ Hz, 6H), 0.88 (ddt, $J = 11.6, 9.9, 4.6$ Hz, 1H).

^{13}C NMR (126 MHz, CDCl_3) δ (ppm) 134.16, 134.13, 134.08, 134.04, 134.00, 133.93, 131.38, 130.69, 130.65, 130.62, 130.58, 130.44, 130.42, 130.40, 127.83, 127.78, 127.72, 127.68, 127.63, 127.59, 16.87, 11.97.

^{29}Si NMR (99 MHz, CDCl_3) δ (ppm) -55.95, -68.72, -79.02, -79.14, -79.27.

3.3.5 Structural Characterization by ^{29}Si NMR Spectroscopy

Characterization of the product cages was based on identifying chemically equivalent silicon atoms in the structures displayed. Color coding/numbers on the silicon atoms is used to match the various silicons in the proposed structure to that of the resonances in the spectra.

5a C₄₉H₄₆O₁₄Si₉

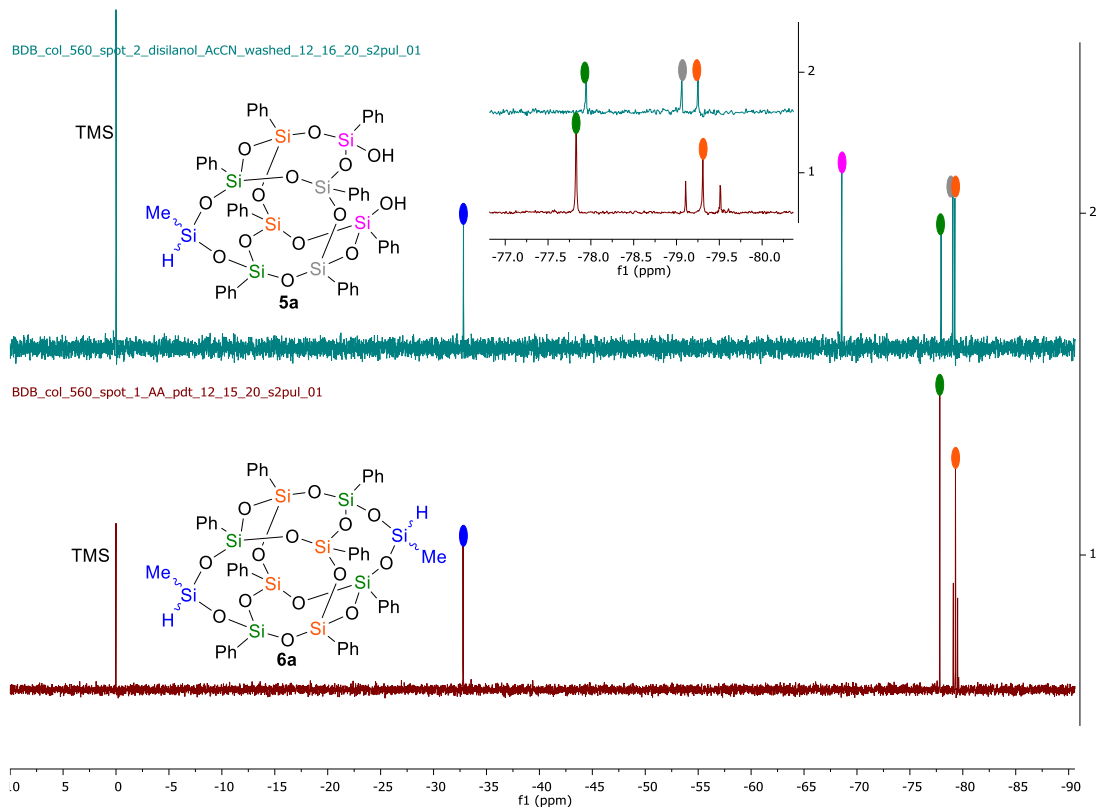
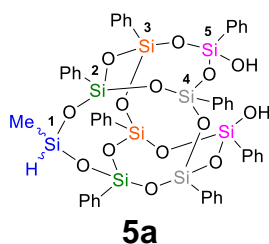


Figure 3-4: Stacked ²⁹Si NMR of AB diol **5a** and AA **6a**

Figure 3-4 is the stacked spectra for symmetric Me(H)SiDDSQSiMe(H) (**6a**) (bottom) and the asymmetric Me(H)SiDDSQ diol (**5a**) (top). Spectra for **5a** displays five (5) peaks characteristic of the five chemically different Si atoms in the structure; one D-silicon and four different pairs of T-silicons. Symmetric **6a** shows three chemically equivalent Si atoms (two D-silicons and two different sets of four T-silicons) with the triplet resonance at -79 ppm indicating the cis/trans configurations of the two D-silicons relative

to the internal silicons (purple). The unique peak at δ -68 ppm (top) is characteristic of the silanol silicons (Si#5) in **5a**.

5b C₅₀H₄₈O₁₄Si₉

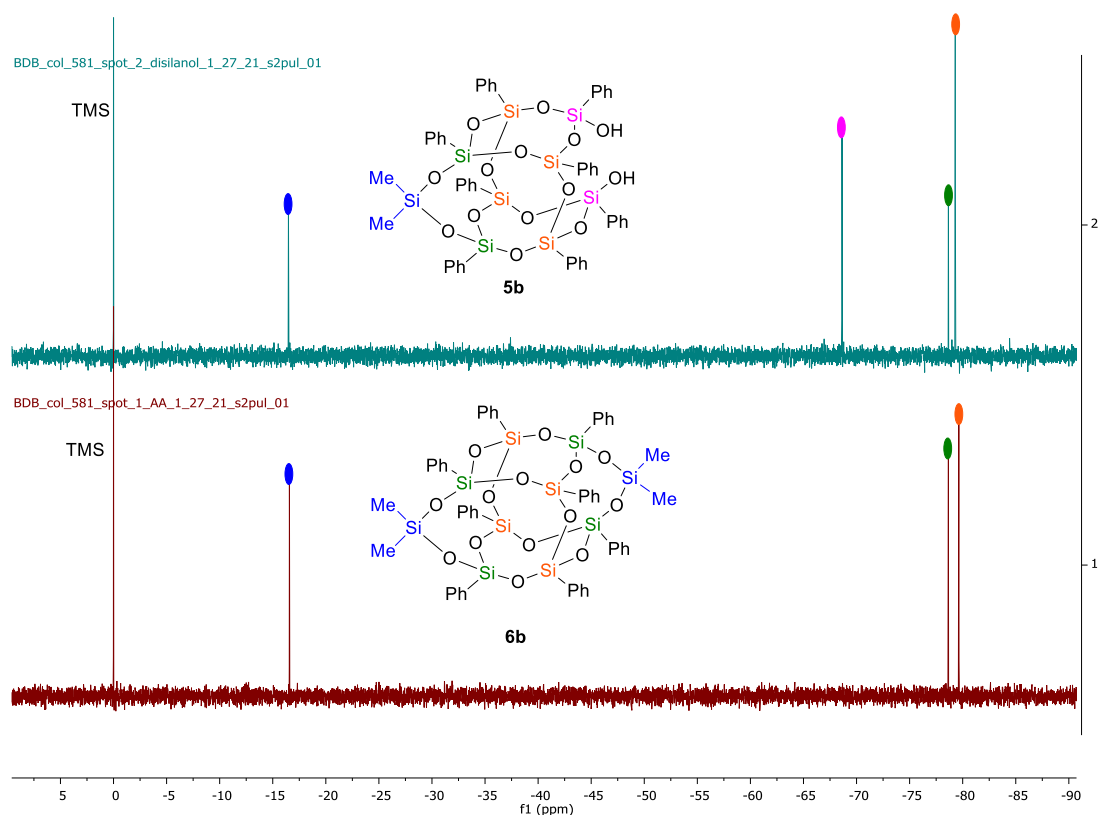
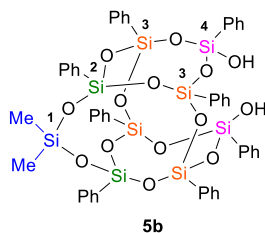


Figure 3-5: Stacked ²⁹Si NMR of AB diol **5b** and AA **6b**

Figure 3-5 gives the stacked ²⁹Si NMR spectra for asymmetric Me₂SiDDSQ(OH)₂ (**5b**) (top) and symmetric Me₂SiDDSQSiMe₂ **6b** (bottom). **5b** shows four different sets of silicon atoms; one D-silicon (Si#1) and three sets of chemically equivalent silicons (Si#2, Si#3 and Si#4). Symmetric **6b** displays 3 different sets of silicons; two D-silicons (blue),

the four silicons next to the D-silicons (green) and the four internal silicons (purple). The unique resonance at δ -69 ppm denotes the two silanol silicons (Si#4) in **5b**.

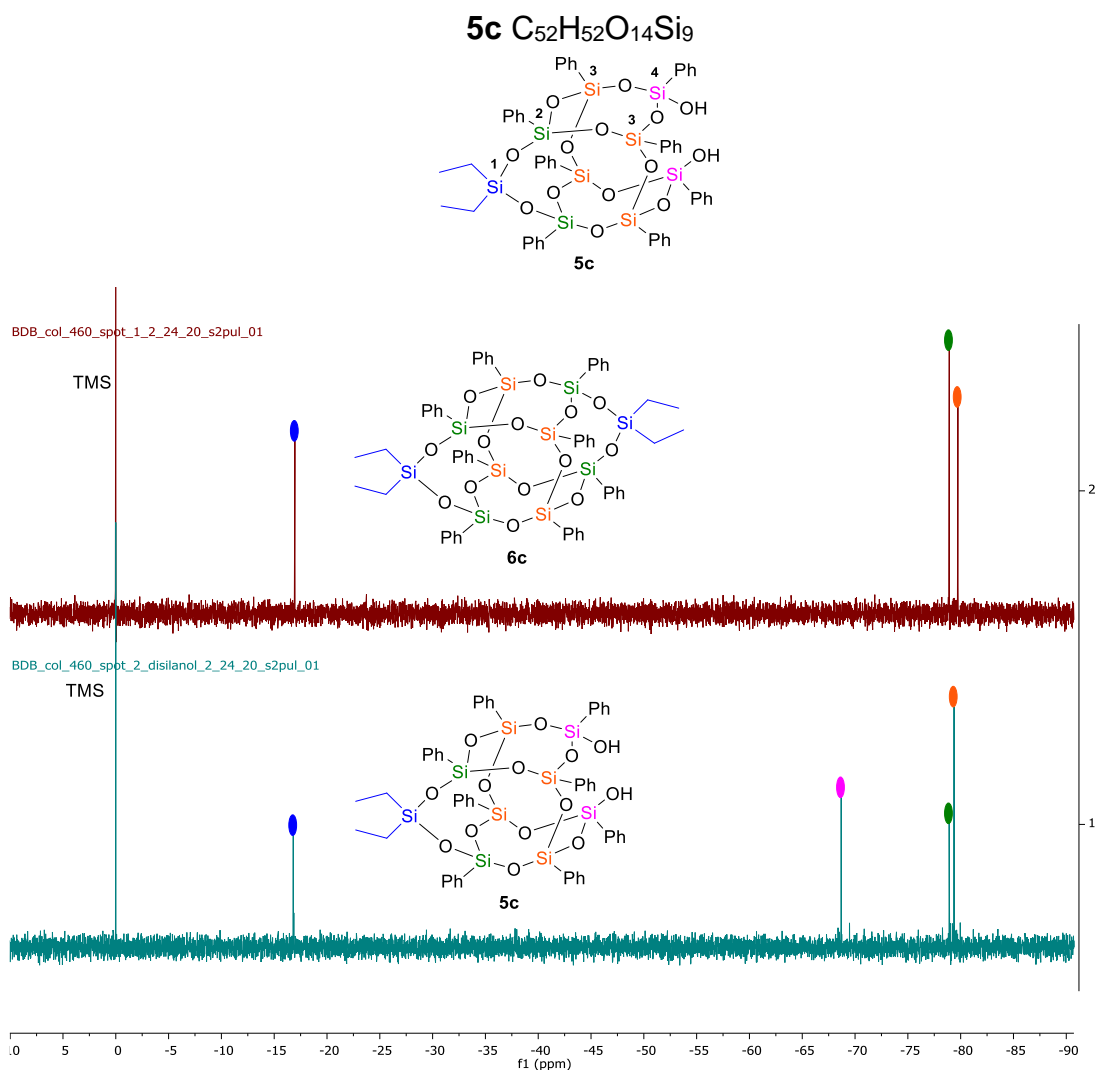


Figure 3-6: Stacked ²⁹Si NMR of AB diol **5c** and AA **6c**

Figure 3-6, the stacked ²⁹Si NMR spectra for asymmetric Et₂SiDDSQ(OH)₂ (**5c**) (bottom) and symmetric Et₂SiDDSQSiEt₂ **6c** (bottom). There are four chemically equivalent silicons in **5c** corresponding to the four different signals in the spectra (bottom) with the matching color codes. The symmetric analogue, **6c** (top), has three different silicons; two D-silicons (blue) and two sets of T-silicons (green and purple). The unique peak at δ -68 ppm denotes the two silanol silicons in **5c** (Si#4, bottom) shows four different

sets of silicon atoms; one D-silicon (Si#1) and three sets of chemically equivalent silicons (Si#2, Si#3 and Si#4). Symmetric **6c** displays three different sets of silicons; two D-silicons (blue), the four silicons next to the D-silicons (green) and the four internal silicons (purple). The unique resonance at δ -69 ppm denotes the two silanol silicons (Si#4) in **5c**.

5d C₅₃H₅₁NO₁₄Si₉

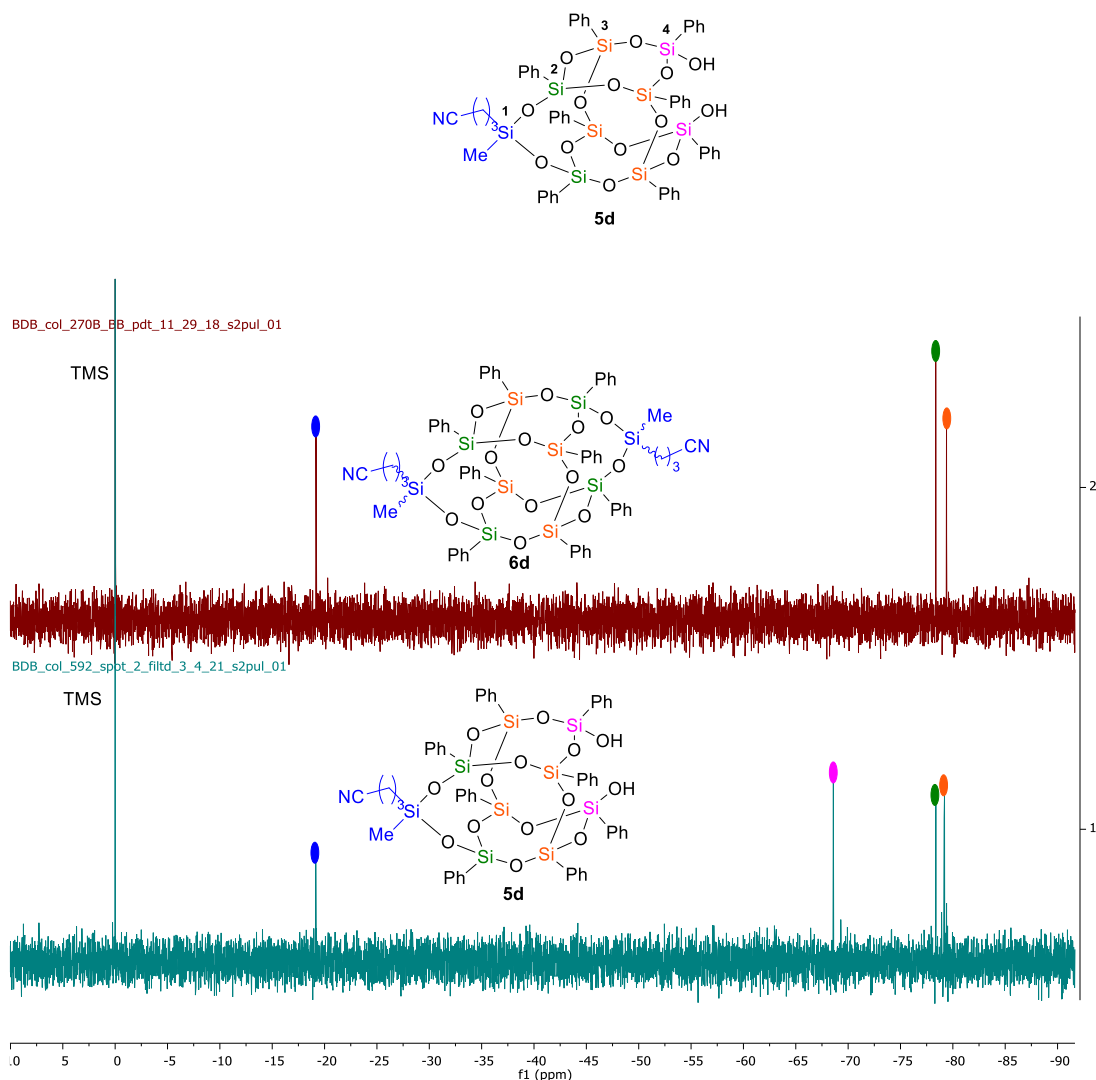


Figure 3-7: Stacked ²⁹Si NMR of AB diol **5d and AA **6d****

Figure 3-7, the stacked ²⁹Si NMR spectra for asymmetric (3CNPr)(Me)SiDDSQ(OH)₂ (**5d**) (bottom) and symmetric (3CNPr)(Me)SiDDSQSi(3CNPr)(Me) **6d** (top). **5d** has four chemically equivalent silicons;

one D-silicon (Si#1) and three sets of T-silicons (Si#2, Si#3 and Si#4) corresponding to the resonances in the spectra (bottom). **6d** on the other hand (top) has three signals: two D-silicons (blue) and two sets of T-silicons (green and purple). However, unlike **6d**, **5d** shows a unique peak at δ -68 ppm corresponding to the two silanol silicons on **5d**.

5e C₅₁H₄₈OSi₉

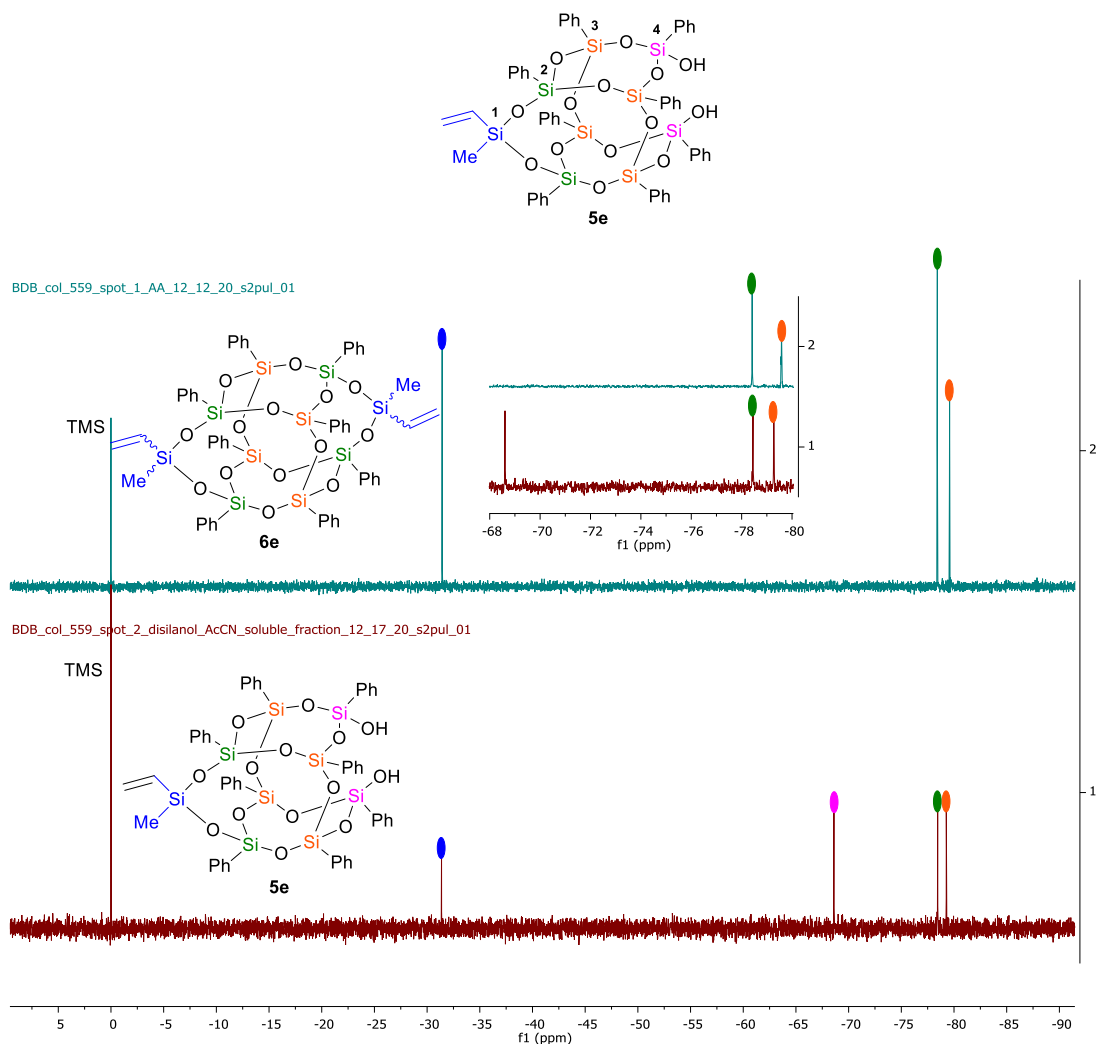


Figure 3-8: Stacked ²⁹Si NMR of AB diol **5e** and AA **6e**

Figure 3-8, the stacked ²⁹Si NMR spectra for asymmetric Me(vinyl)SiDDSQ(OH)₂ (**5e**) (bottom) and symmetric Me(vinyl)SiDDSQSiMe(vinyl) **6e** (top). There are four

chemically equivalent silicons in **5e** corresponding to the four different signals in the spectra (bottom) with the matching color codes. The symmetric analogue, **6e** (top), has three different silicons; two D-silicons (blue) and two sets of T-silicons (green and purple). The T-silicon signal at δ -79 ppm (purple) is a triplet denoting the cis/trans configuration of the two D-silicons relative to the internal silicons (purple). The unique peak at δ -68 ppm denotes the two silanol silicons in **5e** (Si#4, bottom).

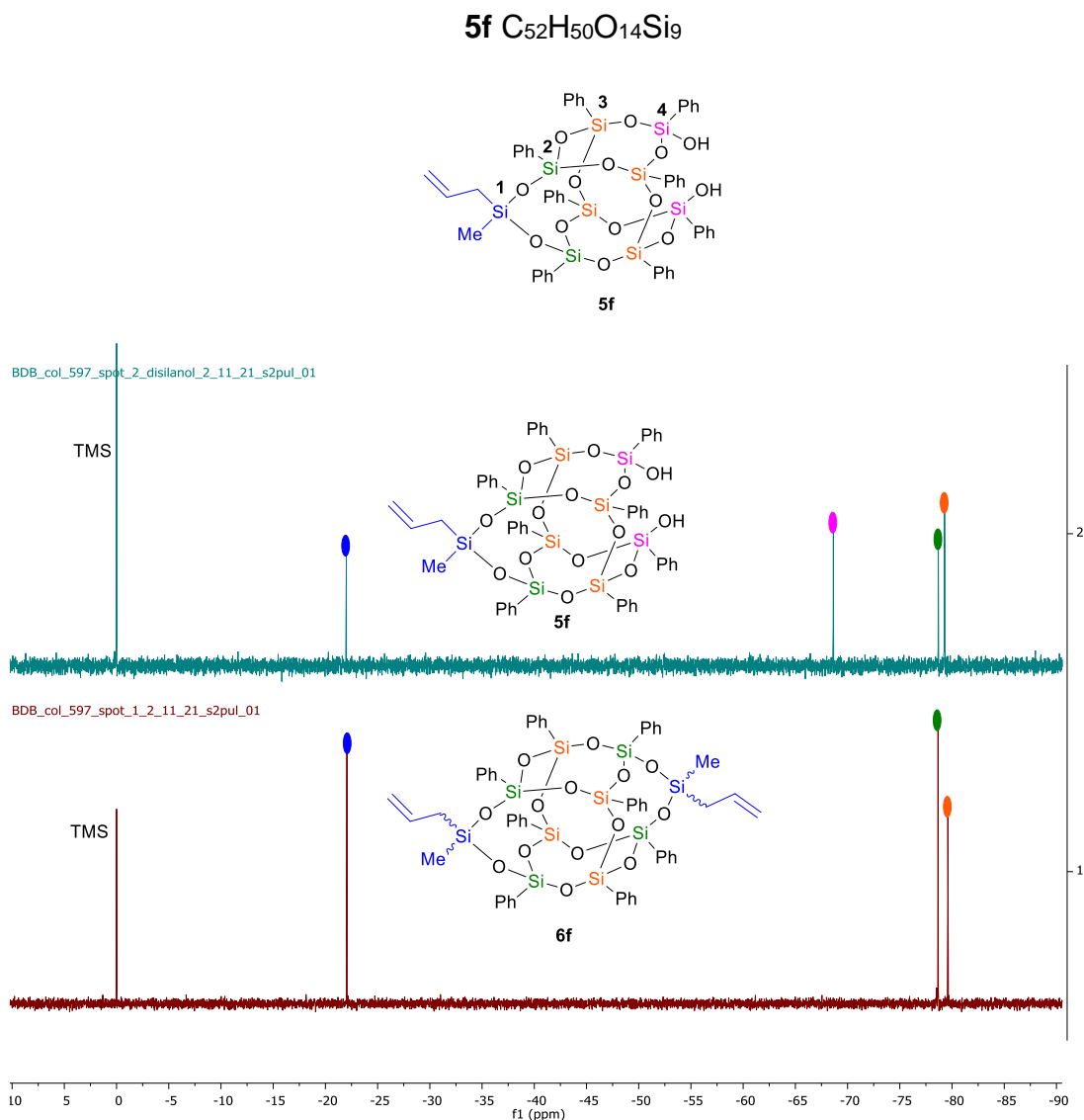


Figure 3-9: Stacked ²⁹Si NMR of AB diol **5f** and AA **6f**

Figure 3-9 is the stacked ^{29}Si NMR spectra for asymmetric (allyl)(Me)SiDDSQ(OH) $_2$ (**5f**) (top) and symmetric (allyl)(Me)SiDDSQSi(allyl)(Me) **6f** (bottom). **5f** has four chemically equivalent silicons; one D-silicon (Si#1) and three sets of T-silicons (Si#2, Si#3 and Si#4) corresponding to the resonances in the spectra (top). Unlike **5f**, **6f** (bottom) has three signals: two D-silicons (blue) and two sets of T-silicons (green and purple). However, **5f** shows a unique peak at δ -68 ppm corresponding to the two silanol silicons on the structure.

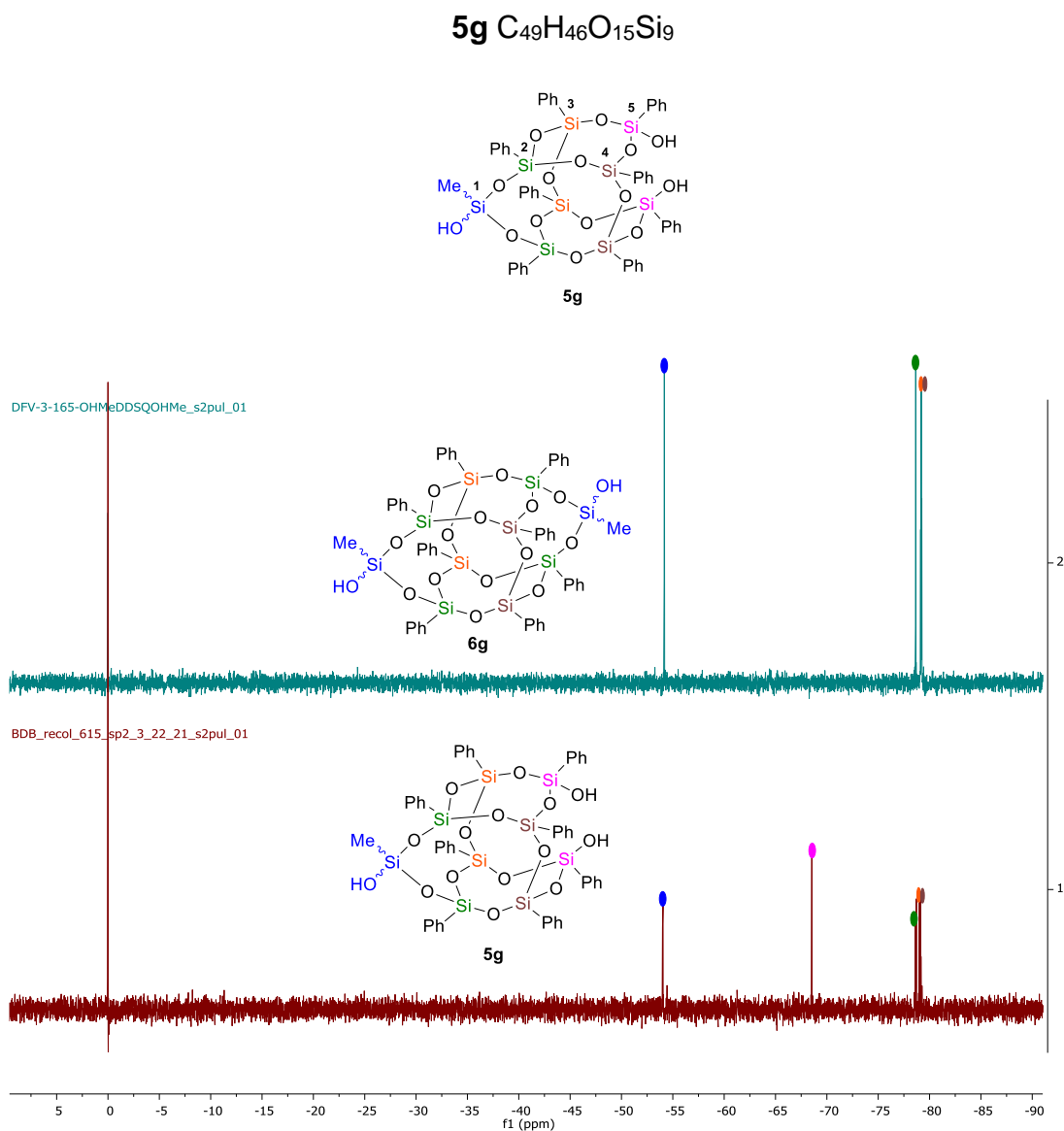


Figure 3-10: Stacked ^{29}Si NMR of AB diol **5g and AA **6g****

Figure 3-10 shows the ^{29}Si NMR spectra for symmetric (Me)(OH)SiDDSQSi(OH)(Me) **6g** (top) stacked with that for the asymmetric (Me)(OH)SiDDSQ(OH) $_2$ (**5g**) (bottom). **5g** exhibits five Si resonances, all of which are T-silicons. All resonances are upfield shifted in the T-silicon region, with the most downfield signal at -54.05 ppm being the bridging silicon having the Me and OH group. (blue, Si#1), and the signal at -68.54 ppm denoting the two silanol silicons (pink, Si#5). Si#2 (green) are the two T-silicons next to Si#1. The remaining signals in the 78.70 – 79.15 ppm range are two sets of chemically equivalent silicons (2 x Si#3, red and 2 x Si#4, purple) depending on the orientation of the groups on Si#1. On the other hand, **6g** (top) has four unique signals; all being T-silicons: Two bridging silicon (blue) for the resonance at -54.22, four green silicons at -78.64 ppm, and two sets of internal silicons (red and purple) in the -79.12 to -79.24 range with silicons consistent to the cis/trans conformation on the blue silicons.

5h C₅₁H₅₀O₁₅Si₉

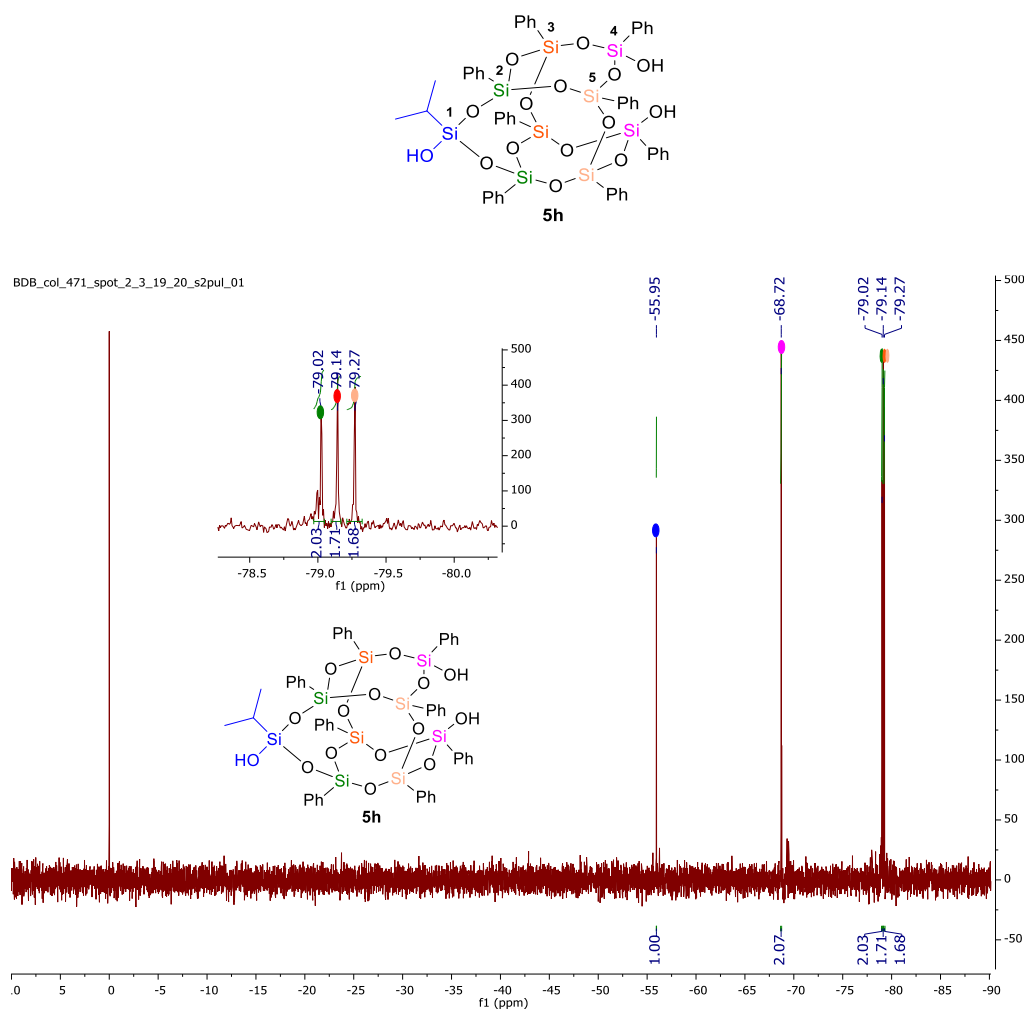


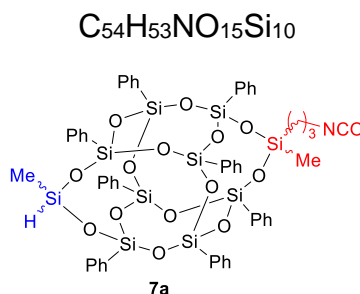
Figure 3-11: ²⁹Si NMR of AB diol **5h**

Figure 3-11 is the ²⁹Si NMR spectra of asymmetric (Me)(OH)SiDDSQ(OH)₂ (**5h**). **5h** has five Si resonances, all of which are T-silicons. Like **5g** which also has exclusively T-silicons, all resonances are relatively upfield shifted. Si#1 (blue), the most downfield signal at -55.95 ppm is the bridging silicon having the *i*Pr and OH group. The signal at -68.72 ppm denotes the two silanol silicons (pink, Si#5). Si#2 (green) at -79.02 ppm is the bridging T-silicons next to Si#1. The remaining signals at -79.14 (Si#3, red) and 79.27

(Si#5, light red) ppm are the four interchangeable innermost silicons relative to the orientation of the ¹Pr and OH substituents on Si#1.

3.3.6 NMR and Mass Spectral Data for Condensed Asymmetric D2T8 Silsesquioxanes

9-(3-Isocyanatopropyl)-9,19-dimethyl-1,3,5,7,11,13,15,17-octaphenyl-2,4,6,8,10,12,14,16,18,20,21,22,23,24-tetradeca-1,3,5,7,9,11,13,15,17,19-decasilapentacyclo[11.7.1.13,11.15,17.17,15]tetracosane (7a)



This product was isolated as a white solid (81%). mp 196-199 °C.

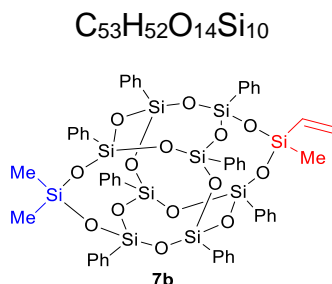
¹H NMR (500 MHz, CDCl₃) δ (ppm) 7.55 – 7.18 (m, 40H), 4.98 (p, J = 1.6 Hz, 1H), 3.13 (t, J = 6.8 Hz, 2H), 1.67 (ddt, J = 11.2, 8.3, 6.8 Hz, 2H), 0.78 – 0.72 (m, 2H), 0.37 (t, J = 1.5 Hz, 3H), 0.31 (s, 3H).

¹³C NMR (126 MHz, CDCl₃) δ (ppm) 134.03, 134.01, 134.00, 133.98, 133.92, 133.83, 131.52, 130.49, 130.47, 130.42, 127.88, 127.86, 127.83, 127.72, 127.69, 127.65, 127.64, 45.34, 24.87, 13.76, 0.62, 0.20, -0.89.

²⁹Si NMR (99 MHz, CDCl₃) δ (ppm) -18.30 (1Si), -32.87 (1Si), -77.93 (2Si), -78.41 (2Si), -79.31 (d, J = 3.0 Hz, 2Si), -79.51 (d, J = 3.1 Hz, 2Si).

LC/MS QTof: exact mass for C₅₄H₅₄NO₁₅Si₁₀ [M+H]⁺ calculated m/z 1236.1181 found m/z 1236.1089

9,9,19-Trimethyl-1,3,5,7,11,13,15,17-octaphenyl-19-vinyl-2,4,6,8,10,12,14,16,18,20,21,22,23,24-tetradecaoxa-1,3,5,7,9,11,13,15,17,19-decasilapentacyclo[11.7.1.13,11.15,17.17,15]tetracosane (7b)



This product was isolated as a white solid (100%). mp 250–253 °C.

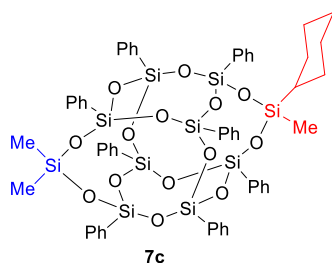
1H NMR (500 MHz, $CDCl_3$) δ (ppm) 7.55 – 7.16 (m, 40H), 6.15 (dd, $J = 20.2, 15.0$ Hz, 1H), 6.04 – 5.87 (m, 2H), 0.37 (s, 3H), 0.30 (s, 6H).

^{13}C NMR (126 MHz, $CDCl_3$) δ (ppm) 145.64, 141.70, 134.46, 134.05, 134.03, 133.94, 133.90, 132.08, 131.89, 130.98, 130.37, 130.35, 130.31, 127.79, 127.65, 127.60, 127.36, -1.17.

^{29}Si NMR (99 MHz, $CDCl_3$) δ (ppm) -16.54 (1Si), -31.42 (1Si), -78.43 (2Si), -78.63 (2Si), -79.61 (d, $J = 1.3$ Hz, 4Si).

LC/MS QTof: exact mass for $C_{53}H_{52}NaO_{14}Si_{10}$ $[M+Na]^+$ calculated m/z 1215.0942 found m/z 1216.0813

9-Cyclohexyl-9,19,19-trimethyl-1,3,5,7,11,13,15,17-octaphenyl-2,4,6,8,10,12,14,16,18,20,21,22,23,24-tetradecaoxa-1,3,5,7,9,11,13,15,17,19-decasilapentacyclo[11.7.1.13,11.15,17.17,15]tetracosane (**7c**)



This product was isolated as a white solid (72%). mp 273–276 °C.

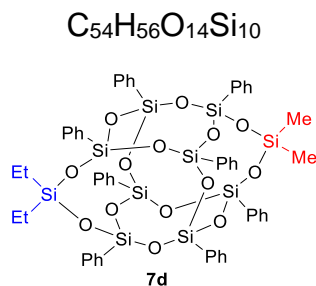
^1H NMR (500 MHz, CDCl_3) δ (ppm) 7.63 – 7.12 (m, 40H), 1.76 (d, $J = 12.8$ Hz, 6H), 1.15 (dd, $J = 39.4, 10.0$ Hz, 4H), 0.83 (d, $J = 12.6$ Hz, 1H), 0.37 – 0.26 (m, 6H), 0.24 (s, 3H).

^{13}C NMR (126 MHz, CDCl_3) δ (ppm) 134.05, 134.03, 133.94, 132.19, 132.14, 131.14, 131.08, 130.27, 127.76, 127.74, 127.61, 127.59, 27.45, 26.70, 26.30, -3.03.

^{29}Si NMR (99 MHz, CDCl_3) δ (ppm) -16.72 (1Si), -18.90 (1Si), -78.69 (2Si), -78.93 (2Si), -79.64 (2Si), -79.74 (2Si).

LC/MS QTof: exact mass for $\text{C}_{53}\text{H}_{53}\text{O}_{14}\text{Si}_{10}$ $[\text{M}+\text{H}]^+$ calculated m/z 1249.1748 found m/z 1249.1677

9,9-Diethyl-19,19-dimethyl-1,3,5,7,11,13,15,17-octaphenyl-2,4,6,8,10,12,14,16,18,20,21,22,23,24-tetradecaoxa-1,3,5,7,9,11,13,15,17,19-decasilapentacyclo[11.7.1.13,11.15,17.17,15]tetracosane (**7d**)



This product was isolated as a white solid (71%). mp 263–268 °C.

1H NMR (500 MHz, $CDCl_3$) δ (ppm) 7.55 – 7.17 (m, 40H), 1.00 (t, J = 7.9 Hz, 6H), 0.70 (q, J = 7.9 Hz, 4H), 0.30 (s, 6H).

^{13}C NMR (126 MHz, $CDCl_3$) δ (ppm) 134.02, 133.93, 133.92, 132.19, 131.12, 130.32, 130.28, 127.78, 127.76, 127.62, 6.90, 6.33, 0.54.

^{29}Si NMR (99 MHz, $CDCl_3$) δ (ppm) -16.64 (1Si), -16.88 (1Si), -78.66 (2Si), -78.91 (2Si), -79.69 (4Si).

3.3.7 Structural Characterization of Completely Condensed Asymmetric D₂T₈ Silsesquioxanes by ²⁹Si NMR Spectroscopy

9-(3-Isocyanatopropyl)-9,19-dimethyl-1,3,5,7,11,13,15,17-octaphenyl-2,4,6,8,10,12,14,16,18,20,21,22,23,24-tetradeca-oxa-1,3,5,7,9,11,13,15,17,19-decasilapentacyclo[11.7.1.13,11.15,17.17,15]tetracosane (**7a**)

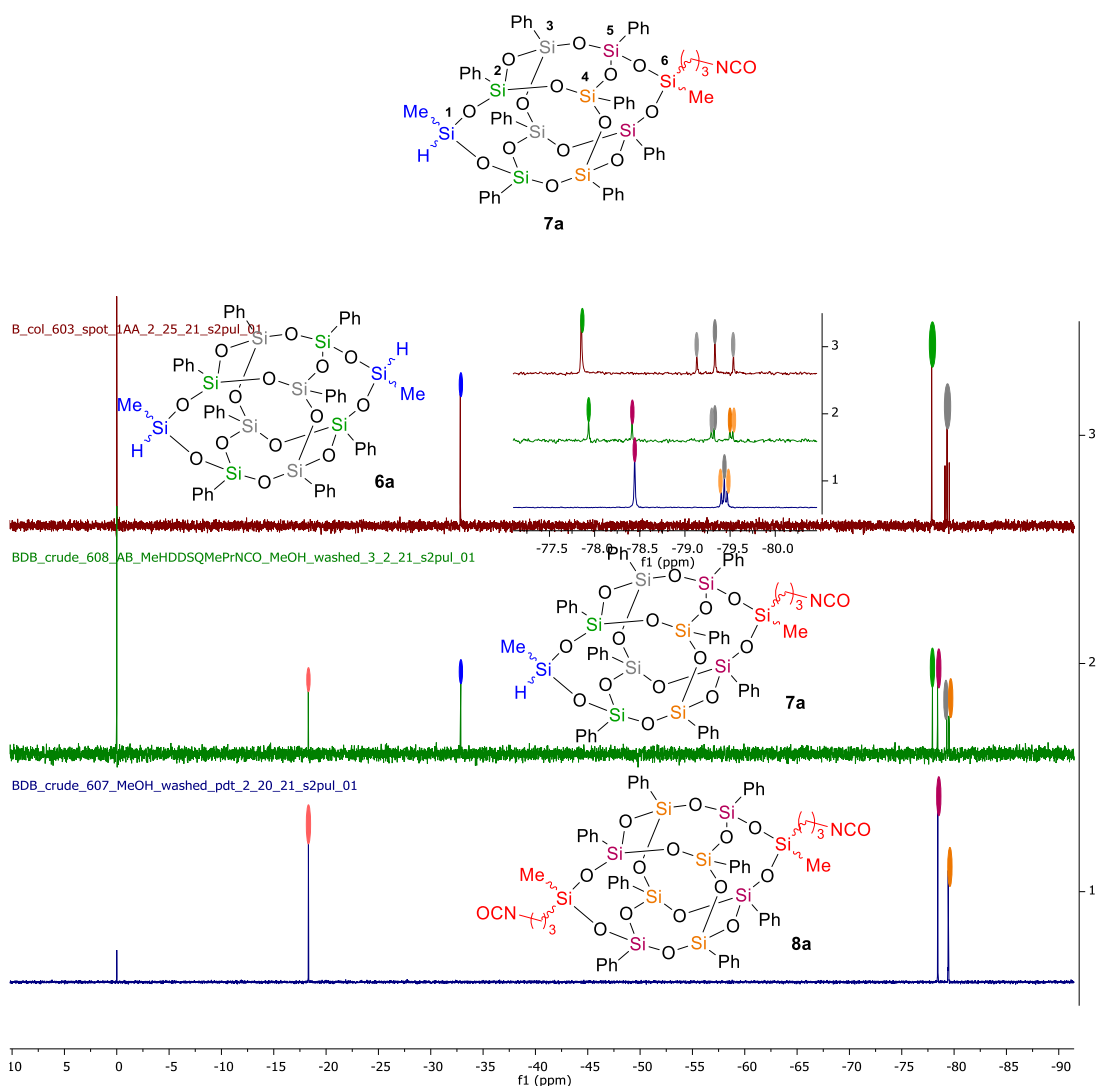


Figure 3-12: ²⁹Si NMR of **7a** stacked with its symmetric AA and BB

Figure 3-12 shows the ²⁹Si NMR spectra of asymmetric **7a** (middle) stacked with its symmetric counterparts; Me(H)SiDDSQSi(H)Me (**5a**) (top) and

PrNCO)(Me)SiDDSQSi(Me)(PrNCO) (bottom). **7a** has six (6) chemically equivalent Si-atoms corresponding to the six resonances in its spectra (middle). This structure has two D-silicons and 4 x 2 T-silicons with signals in the spectra consistent with these atoms. The D-silicon at δ -18 ppm (red, Si#6) is the Si bearing the (PrNCO)(Me) groups and that at δ -32 ppm (blue, Si#1) is the one with the (Me)(H) groups. T-silicons (Si#2 and Si#5) at δ -78 and -78.4 ppm are the T-silicons next to Si#1 and Si#6 respectively. **7a** was isolated as a mixture of its cis/trans forms and so the environments of the internal silicons (Si#3 and Si#4) can change based on the orientation of the substituents on the capping sites (Si#1 and Si#6) as is seen in the signals between the -79.00 to -79.80 ppm region. Thus, the doublet peak at -79.30 ppm (2Si) denotes Si#3 and that at -79.60 ppm (2Si) are the silicon atoms denoted as Si#4.

9,9,19-trimethyl-1,3,5,7,11,13,15,17-octaphenyl-19-vinyl-2,4,6,8,10,12,14,16,18,20,21,22,23,24-tetradeca-1,3,5,7,9,11,13,15,17,19-decasilapentacyclo[11.7.1.13,11.15,17.17,15]tetracosane (**7b**)

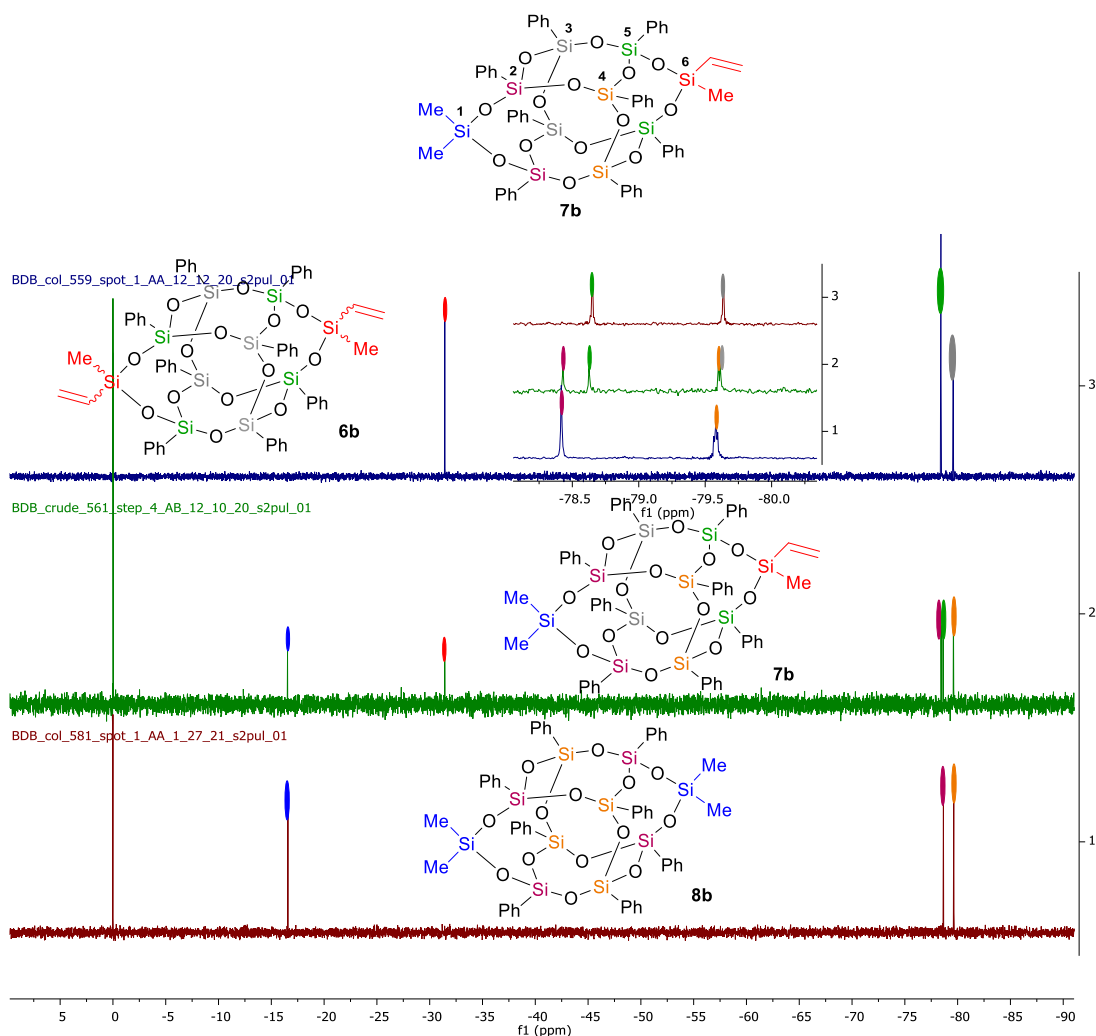


Figure 3-13: Stacked ^{29}Si NMR of AA, AB and BB (**7b**)

Figure 3-13 shows the stacked spectra of asymmetric **7b** (middle) with its symmetric counterparts; Me(vinyl)SiDDSQSi(vinyl)Me (**6b**) (top) and Me₂SiDDSQSiMe₂. **7b** has six chemically different Si atoms consistent with the resonances in its spectra (middle). Like in **7a**, asymmetric **7b** has two distinct D-silicons with a shift at -16.58 ppm typical of D-silicons with two Me groups (Si#1, blue) and one at -32.50 ppm symbolic of

the Si with the Me and vinyl substituents (Si#6, red). Si#2 (purple) and Si#5 (green) are the silicons next to Si#1 and Si#6 respectively. The remaining silicons (Si#3 and Si#4) are the internal T-silicons with δ 79.55 (purple) for cis orientation of both the two Me groups on Si#1 and Si#6 relative to Si#3 and the one with δ 79.60 for the D-silicons with Me and vinyl groups facing Si#4.

9-Cyclohexyl-9,19,19-trimethyl-1,3,5,7,11,13,15,17-octaphenyl-2,4,6,8,10,12,14,16,18,20,21,22,23,24-tetradecaoxa-1,3,5,7,9,11,13,15,17,19-decasilapentacyclo[11.7.1.13,11.15,17.17,15]tetracosane (**7c**)

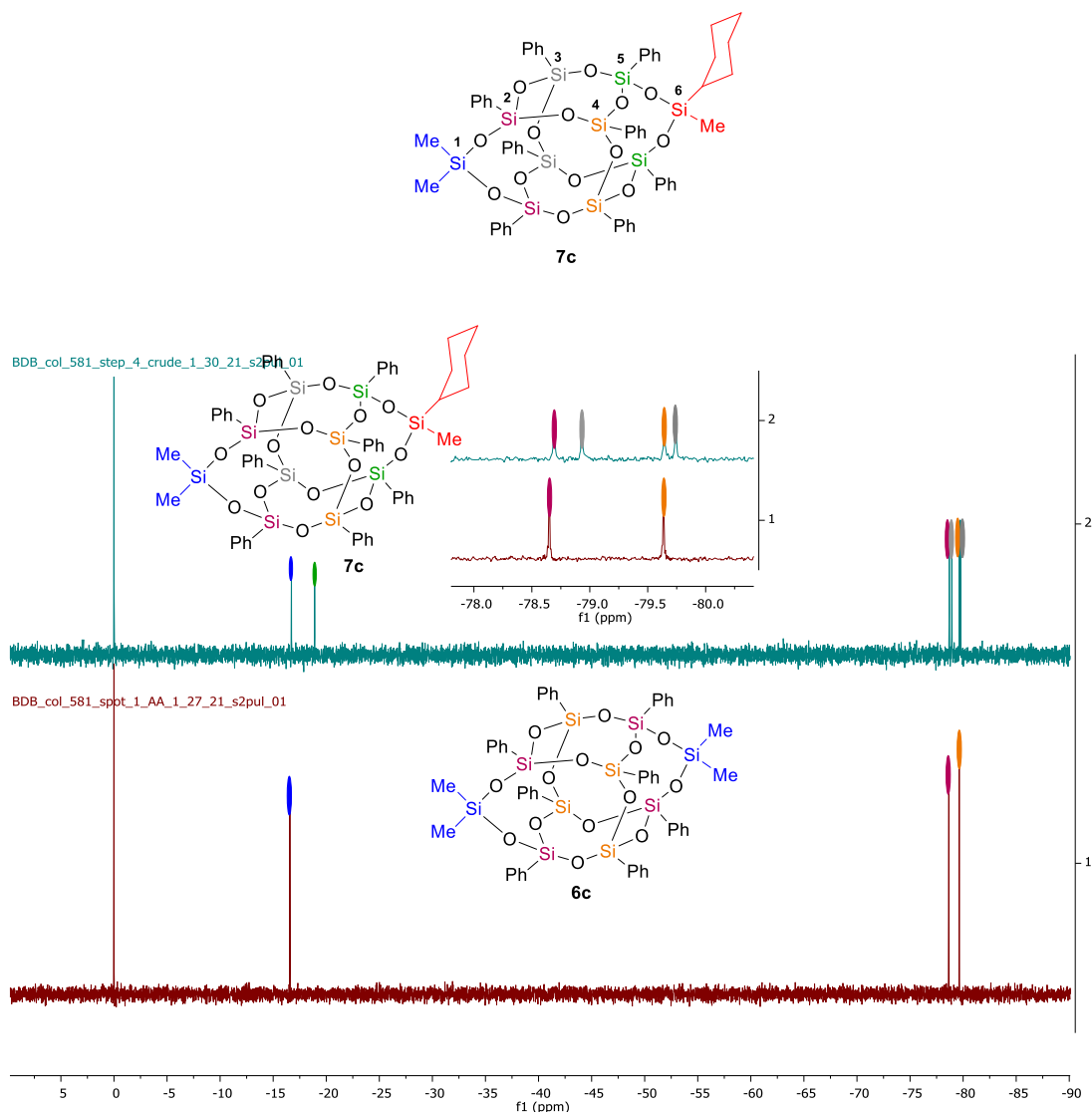


Figure 3-14: Stacked ^{29}Si NMR of AA and BB (**7c**)

Figure 3-14 is the stacked spectra asymmetric **7c** (top) and symmetric $\text{Me}_2\text{SiDDSQSiMe}_2$. **6c**. **7c** has six chemically different Si atoms, two D-silicons and 4 x 2 sets of T-silicons. Signal at -16.58 ppm is identical to the D-silicon with two methyl substituents (blue, Si#1) and the one at -18.38 ppm is symbolic of the D-silicon with the

cyclohexyl and methyl groups (red, Si#6). Si#2 (purple) and Si#5 (green) are the T-silicons next to Si#1 and Si#6 respectively. The internal signal with δ -79.65 (orange, Si#4) are the two T-silicons on the same face with the two methyl substituents on the capping D-silicons and the one at δ 79.75 (grey, Si#3) are for the two T-silicons having the same orientation with the Me and cyclohexyl substituents on the capping D-silicons.

9,9-Diethyl-19,19-dimethyl-1,3,5,7,11,13,15,17-octaphenyl-2,4,6,8,10,12,14,16,18,20,21,22,23,24-tetradeca-1,3,5,7,9,11,13,15,17,19-decasilapentacyclo[11.7.1.13,11.15,17.17,15]tetracosane (**7d**)

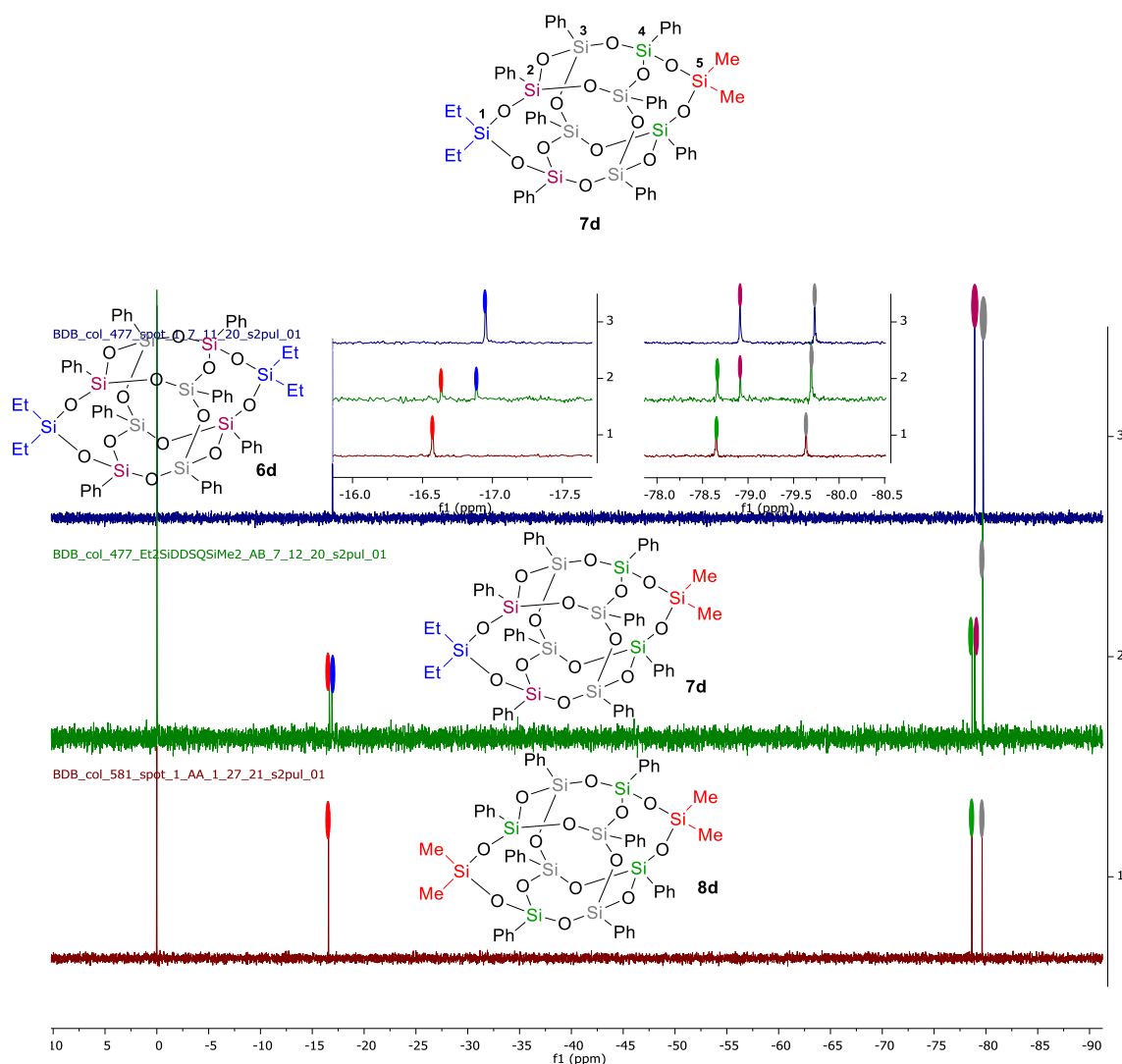


Figure 3-15: Stacked ^{29}Si NMR of AA, AB(**7d**) and BB

Figure 3-15 is the stacked spectra asymmetric **7d** (middle), symmetric $\text{Et}_2\text{SiDDSQSiEt}_2$ (**6d**) (top) and symmetric $\text{Me}_2\text{SiDDSQSiMe}_2$ (**8d**) (bottom). **7d** has five chemically different Si atoms, two D-silicons with resonances at -16.78 ppm for Si#1 (blue) bearing the two ethyl groups and the other at -16.58 ppm for the one with two

methyl groups (Si#5, red). The remaining six silicons are T-silicons with the resonances at -78.60 ppm for the two Si#4 (green) next to D-silicon Si#5, δ 78.80 for the other two Si#3 (purple) next to Si#1, δ 79.65 for the four internal silicons (Si#3, grey).

3.4 Conclusion

This protocol discloses a strategically novel approach into partially condensed bis-capped monosilylated double-decker shaped silsesquixanes. By strategically using boronic acid to mask two silanol groups, a wide range of bifunctional DDSQs were obtained in good to high yields. About 50 % of the clean starting material was recovered upon deborylation in the first and second steps. These unique monosilylated DDSQ scaffolds are interesting synthetic precursors for a variety of functional materials including condensed asymmetric DDSQs, ligands in catalysis, surface modifiers, and nano-medicine carriers. An illustration of the post-modification of these cages for the synthesis of condensed asymmetrically functionalized DDSQs afforded excellent yields of the pure targets. With this approach, formation of unwanted BB products is completely evaded, and no further purifications of the D₂T₈ POSS cages are required. However, even though the route is amenable to a broad range of substrates, capping the DDSQ(OH)₄ with dicyclohexyldichlorosilane was unsuccessful, probably due to increasing steric at the α -carbon of the cyclohexyl ring. Further investigations to reasonably account for this challenge is ongoing in our laboratory.

3.5 Experimental Details

3.5.1 Materials and Methods

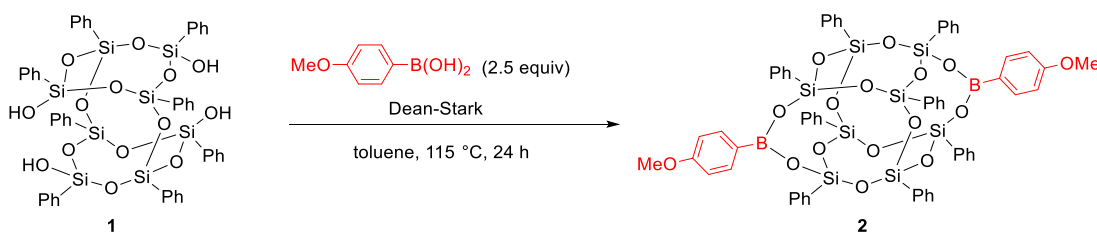
All reactions were carried out with dry solvents under a nitrogen atmosphere using standard techniques except otherwise stated. DDSQ(OH)₄ was obtained from Hybrid

Plastics. Pyridine, ethyl acetate, hexanes, acetonitrile, methanol, and isopropanol were used as received. THF was distilled over benzophenone and sodium metal at a temperature of 50 °C under nitrogen prior to use. Glassware was oven dried. Reactions were monitored by thin-layer chromatography (TLC) on silica gel plates or a Hydrion Insta-Chek pH 0-14 and. ^1H , ^{11}B , ^{13}C , and ^{29}Si NMR spectra were acquired on an Agilent DirectDrive2 500 MHz NMR spectrometer equipped with a OneProbe operating at 500 MHz for ^1H NMR, 160 MHz for ^{11}B NMR, 126 MHz for ^{13}C NMR, and 99 MHz for ^{29}Si NMR CDCl_3 and recorded at 25 °C. ^1H -NMR spectra were recorded with 8 scans, a relaxation delay of 1 s, and a pulse angle of 45° and referenced to tetramethylsilane in CDCl_3 (0.00 ppm). ^{13}C -NMR spectra were collected with 254 scans, a relaxation delay of 0.1 s, and a pulse angle 45°. ^{29}Si NMR spectra were recorded with either 256 or 512 scans, a relaxation delay of 12 s and a pulse angle of 45°. Thin-layer chromatography (TLC) was performed on plates of EMD 250- μm silica 60-F254. High-resolution mass spectroscopy was performed with APCI mass spectra recorded on a Finnigan LCQ Deca (ThermoQuest) technologies with LC/MS/MS (quadrupole/time-of-flight) and Waters Xevo G2-XS UPLC/MS/MS inert XL MSD with SIS Direct Insertion Probe. Melting points for all products were measured with a Thomas HOOVER capillary uni-melt melting point apparatus and are uncorrected. X-ray diffraction measurements were performed on a Stoe IPDS2 or a Bruker-AXS SMART APEX 2 CCD diffractometer using graphite-monochromated Mo $\text{K}\alpha$ radiation. The structures were solved using direct methods (SHELXL-97) and refined by full-matrix least-squares techniques against F^2 (SHELXL-97). Cell parameters were retrieved using the SAINT (Bruker, V8.34A, after 2013) software and refined using SAINT (Bruker, V8.34A, after 2013) on 5941 reflections, 47%

of the observed reflections. Data reduction was performed using the SAINT (Bruker, V8.34A, after 2013) software which corrects for Lorentz polarization.

3.5.2 General Experimental Procedure for the Synthesis of DDSQ Bis-boronate Ester (2)

Scheme 3-12: Synthesis of 9,19-bis(4-methoxyphenyl)-1,3,5,7,11,13,15,17-octaphenyl-2,4,6,8,10,12,14,16,18,20,21,22,23,24-tetradeca-oxa-1,3,5,7,11,13,15,17-octasila-9,19-diborapentacyclo[11.7.1.13,11.15,17.17,15]tetracosane (2)



The starting material, bis-boronate ester **2**, was synthesized following a procedure we reported earlier.⁴⁹ An oven-dried 500 mL round bottom flask equipped with a magnetic stir bar was charged with DDSQ(OH)₄ **1** (10 mmol, 10.69 g) and p-MeOC₆H₄B(OH)₂ (2.2 equiv, 22 mmol). The flask was fitted with a Dean-Stark apparatus and its contents placed under a nitrogen atmosphere. Toluene (120 mL) was added, and the setup stirred over a pre-heated oil bath at a temperature of 115 °C for 24 h. The solvent was evaporated under reduced pressure, the resulting crude then was washed with isopropanol (20 mL), filtered with a filter frit and flask and dried again at reduced pressure to afford a white solid. From this product, fine crystals appropriate for crystallographic analysis were obtained from a mixture of DCM/hexanes (1:3) of the Bis-boronate esters **2** in 98% yield. The solid was characterized by ¹H, ¹³C, ¹¹B, ²⁹Si NMR X-ray crystallography and LCMS measurements. ¹H NMR (500 MHz, CDCl₃ + 1%TMS) δ 7.70 – 7.60 (m, 8H), 7.59 – 7.53 (m, 4H), 7.50 – 7.19 (m, 32H), 6.75 – 6.65 (m, 4H), 3.74 (s, 6H).

^{13}C NMR (126 MHz, CDCl_3 + 1%TMS) δ 137.68, 134.14, 134.11, 131.43, 130.62, 130.53, 130.38, 127.94, 127.68, 113.04, 55.01.

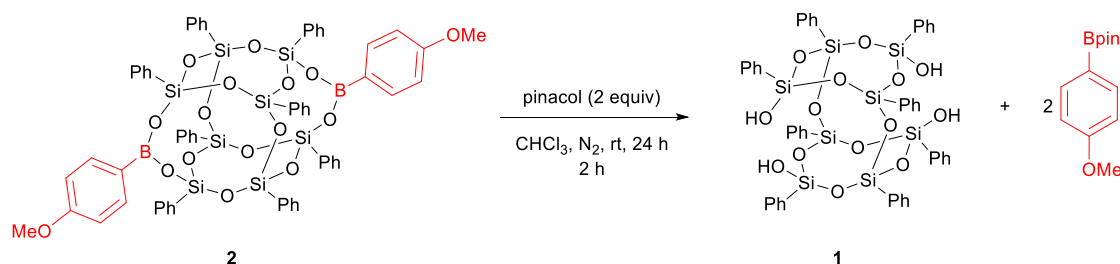
^{11}B NMR (160 MHz, CDCl_3 + 1%TMS) δ 20.09.

^{29}Si NMR (99 MHz, CDCl_3 + 1%TMS) δ -78.70, -80.45.

3.5.3 Partial Deborylation of DDSQ Bis-boronate Ester with Pinacol

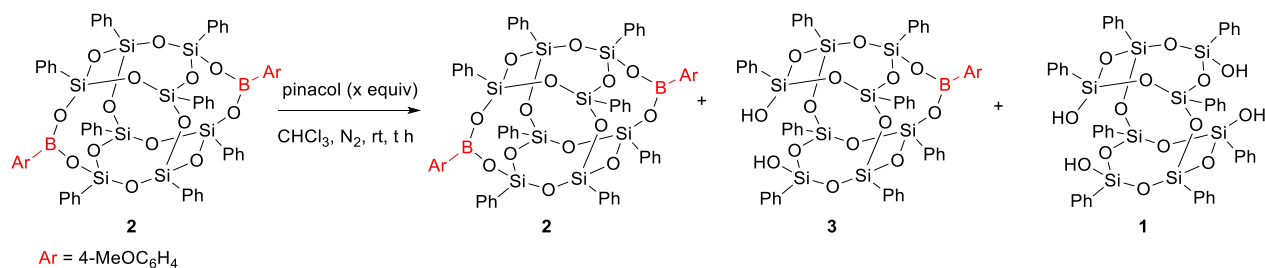
Complete transesterification of the bis-boronate ester with pinacol was described in our previous work (**Scheme 3-11**).⁴⁹

Scheme 3-13: Complete Deborylation of (p-MeOC₆H₄B)₂DDSQ (2) with Pinacol



In line with this, optimization for the synthesis of the monoborylated DDSQ disilanol was done following the same procedure with some modifications (**Scheme 3-14**).

Scheme 3-14: Partial Deborylation of (p-MeOC₆H₄B)₂DDSQ (2) with Pinacol



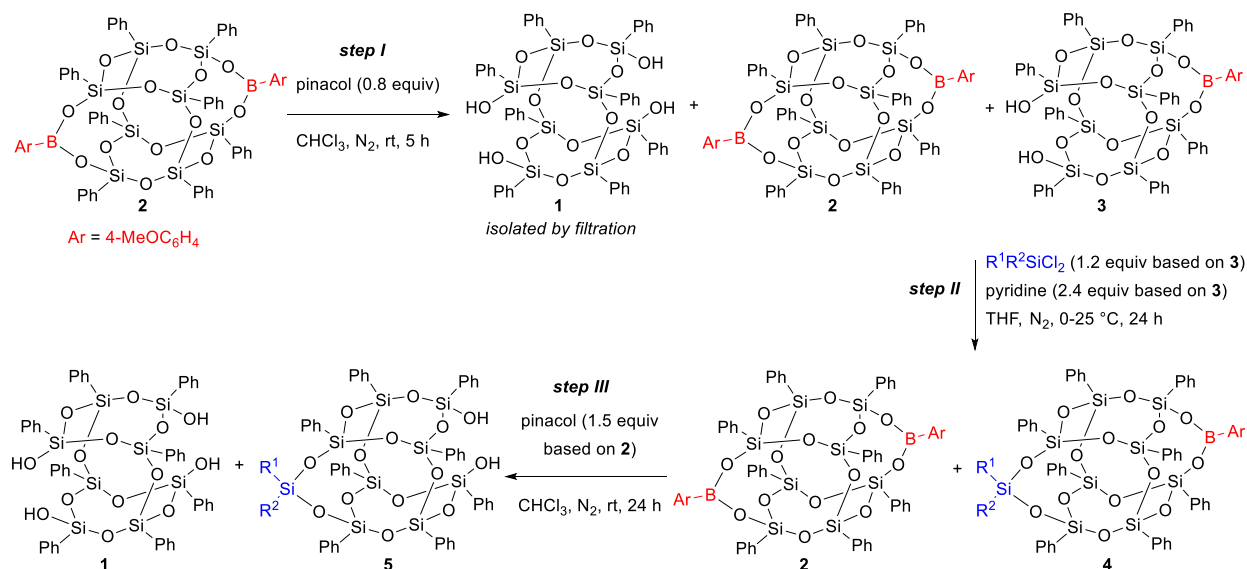
An oven-dried 50 mL round bottom flask bearing a magnetic stir bar was charged with p-MeO-C₆H₄B)₂DDSQ (**2**) (0.65 g, 0.5 mmol) and pinacol (0.8 mmol). The flask was capped with a septum, its content placed under nitrogen atmosphere and CHCl_3 (5 mL) was added to it. The reaction mixture was stirred at room temperature for 5 h (**Scheme**

3-14). The solvent was next evaporated using a rotary evaporator. The crude solid was dissolved in CHCl_3 (5 mL) and kept in a refrigerator at $-5\text{ }^\circ\text{C}$ for 5 h. The resulting heterogeneous mixture was suction filtered using a fine-frit funnel and filter flask to isolate the unreacted DDSQ tetraol. The residue was washed with CHCl_3 (2 x 5 mL), filtered, and dried in the oven at $80\text{ }^\circ\text{C}$ for 5 h. The solid 1 was analyzed by ^1H , ^{13}C , ^{11}B and ^{29}Si NMR. NMR data for the products are shown in **Appendix**. The combined filtrate was evaporated under reduced pressure to afford a white solid. This solid is a mixture of the mono- and bis-borylated cage and a trace amount of DDSQ tetraol. The combined filtrate was dried by rotary evaporation to give a white solid. The dissolution in CHCl_3 , refrigeration, filtration and rotary evaporation processes were repeated two or more times until the mixture was free of DDSQ tetraol. The final white crude obtained is a mixture of the bis- and mono-borylated cages in an approximate ratio of 2:1 (**Table 3-1**). The resulting crude product was analyzed by ^1H , ^{11}B , and ^{29}Si NMR spectroscopy. It must be mentioned that all attempts to isolate the pure mono-borylated cage were unsuccessful.

3.5.4 General Experimental Procedure for the Multi-step Synthesis of monosilylated

DDSQ diol

Scheme 3-15: Synthesis of asymmetrically functionalized monosilylated DDSQ(OH)₂



Step 1: Partial deborylation

An oven-dried 100 mL round bottom flask bearing a magnetic stir bar was charged with p-MeO-C₆H₄B₂DDSQ (**2**) (1.3 g, 1.00 mmol) and pinacol (0.8 equiv, 0.0944 g). The flask was capped with a septum, its content placed under a nitrogen atmosphere and CHCl₃ (10 mL) was added. The reaction mixture was stirred at room temperature for 5 h (**Scheme 3-15, step I**). The solvent was next evaporated using a rotary evaporator. The crude solid was then dissolved in CHCl₃ (10 mL) and kept in a refrigerator at -5 °C for 5 h. The resulting heterogeneous mixture was suction filtered using a fine-frit funnel and filter flask to isolate the generated DDSQ tetraol (**1**). The residue was washed with CHCl₃ (2 x 5 mL), filtered, and dried in the oven at 80 °C for 5 h. The combined filtrate was evaporated under reduced pressure to afford a white solid. The white solid was redissolved in CHCl₃ (10 mL), kept in a refrigerator at -5 °C for 5 h and filtered with a fine

frit funnel. This solid is a mixture of the mono- and bis-borylated cage and trace amount of DDSQ tetraol. The dissolution in CHCl_3 , refrigeration, filtration and rotary evaporation processes were repeated two or more times until the mixture was free of **1**. The resulting crude products (residue and filtrate) were analyzed by ^1H , ^{11}B , and ^{29}Si NMR spectroscopy. The final white crude obtained from the filtrate is a mixture of the bis- and mono-borylated cages in an approximate ratio of 2:1. The residue was the completely deborylated boronate ester or DDSQ tetraol (**1**). NMR data for the products are shown in **Appendix**.

Step 2: Silylation

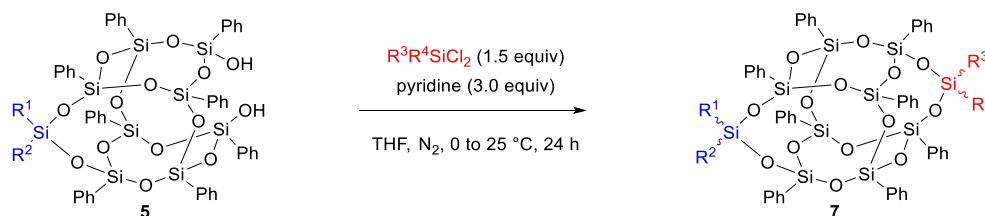
The crude filtrate mixture (**Scheme 3-15, step I**) was charged into a pre-dried 100 mL round bottom flask bearing a magnetic stir bar and sealed with a septum. The flask was purged with dry nitrogen for 30 min and THF (20 mL) was added. The flask was immersed into an ice bath and its contents stirred vigorously under nitrogen for 20 min. $\text{R}^1\text{R}^2\text{SiCl}_2$ (x mmol, 1.2 equiv. based on the mono-borylated cage) in 1 mL THF was added first followed by dropwise addition of pyridine (2x mmol, 2.4 equiv. based on the mono-borylated cage) over a period of 5 minutes. The reaction mixture was stirred at 0 °C for 4 h and at room temperature for 20 h (**Scheme 3-15, step II**). The suspension was filtered through a glass frit, the residue washed with THF (3 x 5 mL) and the solvent together with other volatiles removed from the filtrate by rotary evaporation. This crude product is a mixture of the bis-boronate DDSQ ester (**2**) and the silylated mono-boronate DDSQ ester (**4**) that forms the substrate for the next step. Reaction was followed by both ^1H , ^{13}B , and ^{29}Si NMR.

Step 3: Global Transesterification

The crude product mixture (**Scheme 3-15, step II**) was charged into a pre-dried 100 mL round bottom flask bearing a magnetic stir bar and pinacol (1.5 mmol based on the monoborylated/monosilylated DDSQ) added to it. Chloroform (10 mL) was added to the flask under nitrogen and the reaction mixture stirred vigorously at room temperature for 24 h (**Scheme 3-15, step III**). After 24 h, the resulting white suspension was filtered through a fine-fritted filter funnel. The white powdered residue was washed with chloroform (3 x 5 mL), filtered, dried in an oven at 80 °C for 5 h and characterized by ^1H and ^{29}Si NMR spectroscopy. The solvent and other volatiles were removed from the filtrate by rotary evaporation to afford a white solid or oil which was similarly characterized by ^1H , ^{11}B , ^{13}C and ^{29}Si NMR spectroscopy. Final products in step III were further purified by flash column chromatography (ethylacetate:hexanes = 1:9) and analyzed by ^1H , ^{13}C , ^{29}Si and LCMS measurement. The chromatographed products were washed with hexanes to remove the p-MeOC₆H₄Bpin. Fine crystals suitable for X-ray crystallography were obtained by crystallization from a mixture of dichloromethane:hexanes ~ 1:3. The asymmetrically functionalized DDSQ diols (**5**) synthesized in this study are listed in **Table 3-2**. Copies of NMR, mass spectra and X-ray crystal data are given in **Appendix**.

3.6 Synthetic Modifications of Monosilylated DDSQ diols (5) into Fully Condensed Asymmetric DDSQs of the D2T8 type (7)

Scheme 3-16: Synthesis of completely condensed asymmetrically functionalized D₂T₈



An oven-dried 100 mL round bottom flask bearing a magnetic stir bar was charged with the 0.5 mmol of monosilylated DDSQ diol (**5**) and capped with a septum. The flask was purged with dry nitrogen for 10 min and THF (20 mL) was added. The flask was immersed into an ice bath and the mixture stirred vigorously for 30 min under N₂. A suitable di-substituted chlorosilane bearing R groups different from those on the starting material R³R⁴SiCl₂ (1.5 equiv) in 5 mL THF was added first followed by dropwise addition of pyridine or Et₃N (3.0 equiv) over a period of 10 minutes. The reaction mixture was stirred at 0 °C for 1 h and at room temperature for 23 h. The suspension was filtered through a glass frit funnel, the residue washed with THF (3 x 5 mL) and the solvent together with other volatiles removed from the filtrate by rotary evaporation. This crude product is washed with hexanes (2 x 10 mL) and then pentane (10 mL). The solvent was evaporated at reduced pressure to afford the pure fully condensed D₂T₈ asymmetric DDSQ in good to excellent yields. Products were analyzed directly by ¹H, ¹³C, ²⁹Si and LCMS measurement without further purifications. A list of the asymmetrically functionalized D₂T₈ DDSQs are listed in **Table 3-3**. Copies of the NMR and mass spectra are given in **Appendix** and X-ray crystallographic data in **Appendix**.

APPENDIX

**Copies of NMR and Mass Spectra – Bis-boronate Ester and Asymmetrically
Silylated DDSQ Diol**

*9,19-Bis(4-methoxyphenyl)-1,3,5,7,11,13,15,17-octaphenyl-2,4,6,8,10,12,14,16,18,20,
21,22,23,24-tetradecaoxa-1,3,5,7,11,13,15,17-octasila-9,19-diborapentacyclo[11.7.1.
13, 11.15,17.17,15]tetracosane (2a)*

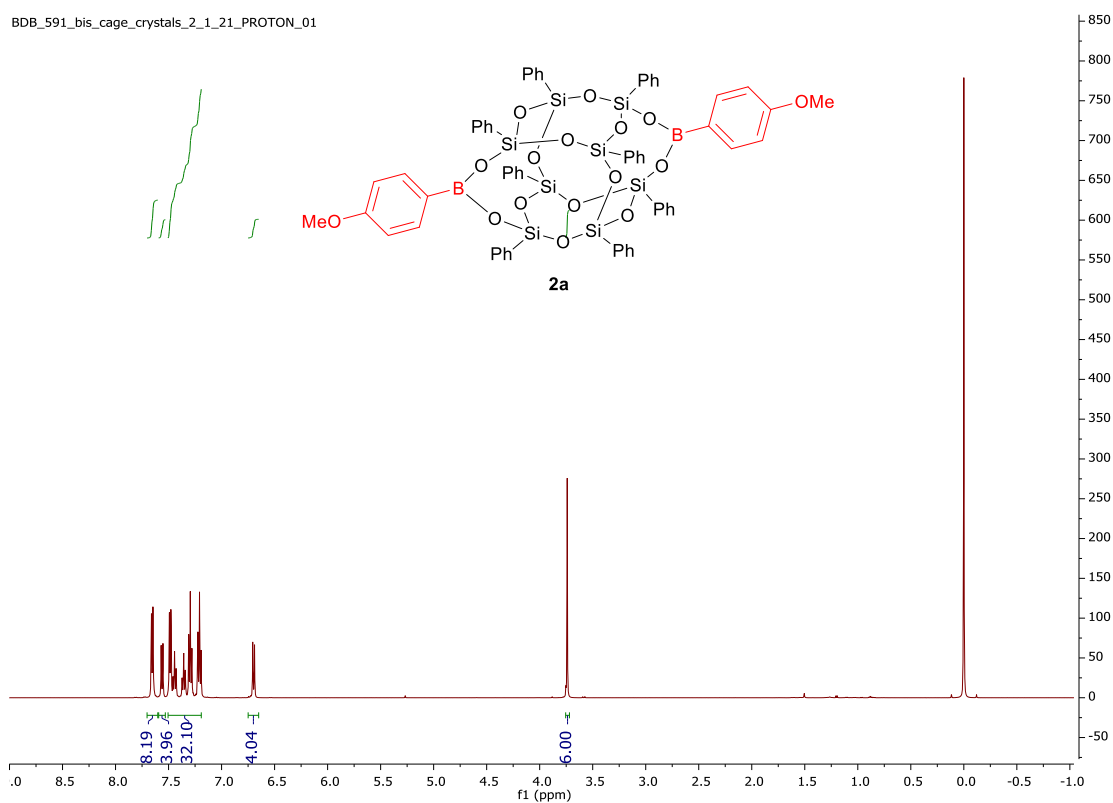


Figure 3-16: ^1H NMR of **2a** (CDCl₃ + 1%TMS, 500 MHz)

BDB_591_bis_cage_crystals_2_1_21_CARBON_01

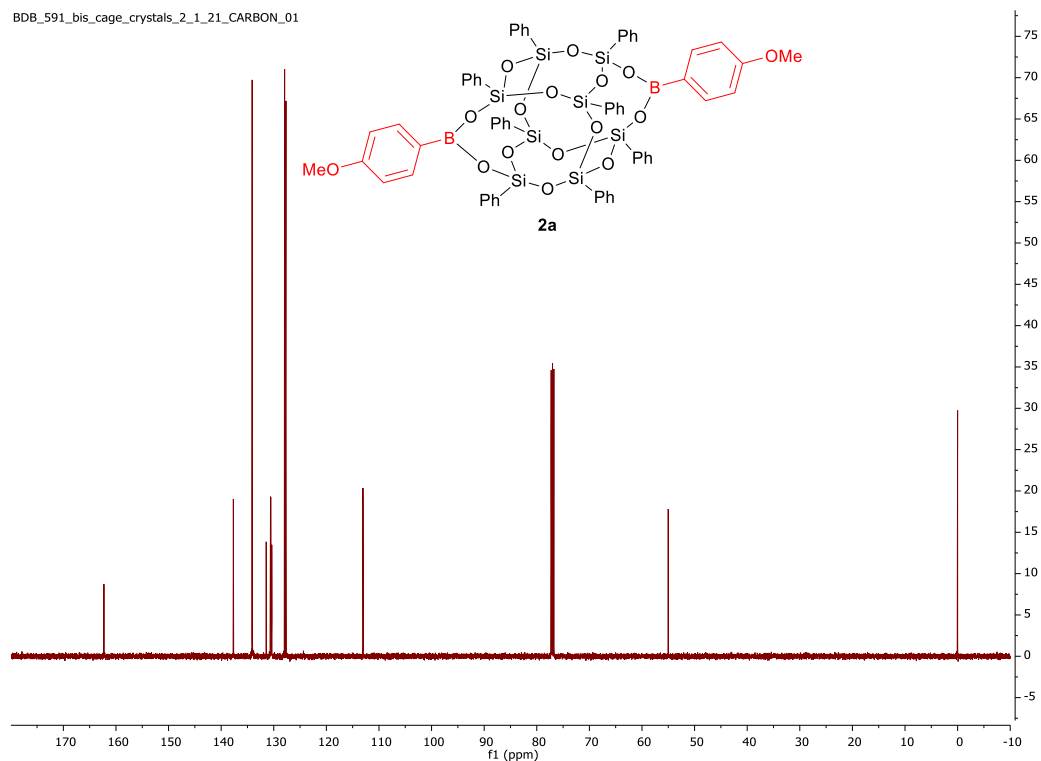


Figure 3-17: ^{13}C NMR of **2a** (CDCl_3 + 1%TMS, 126 MHz)

BDB_591_bis_cage_crystals_2_1_21_s2pul_01

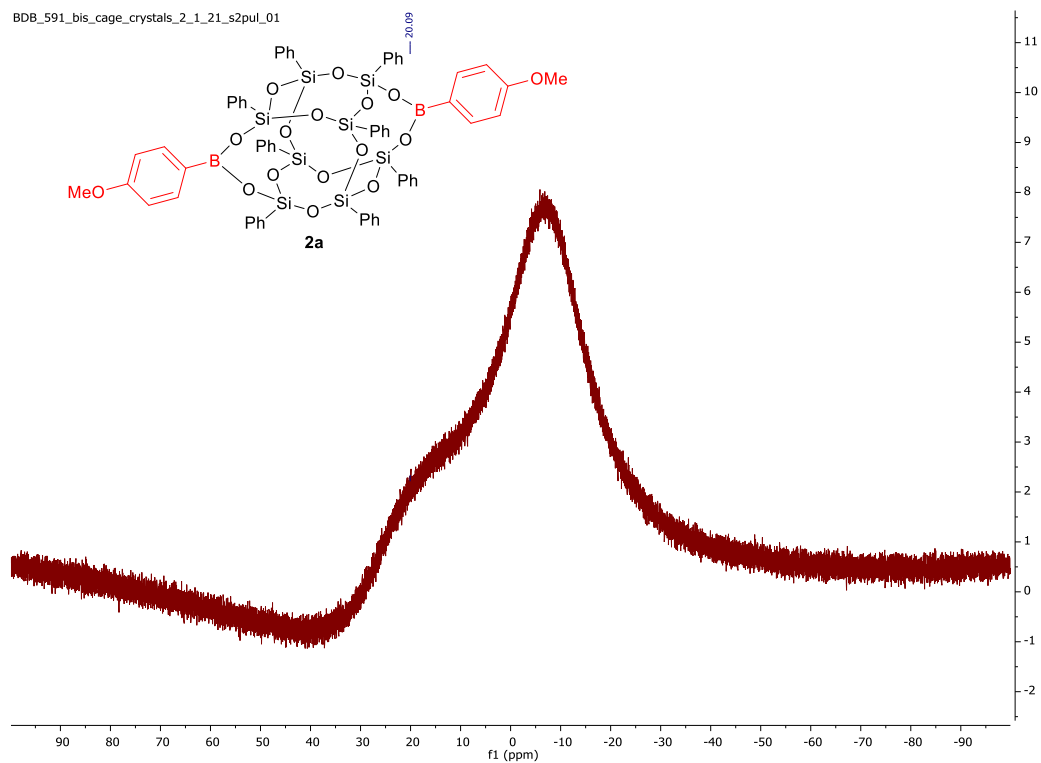


Figure 3-18: ^{11}B NMR of **2a** (CDCl_3 + 1%TMS, 160 MHz)

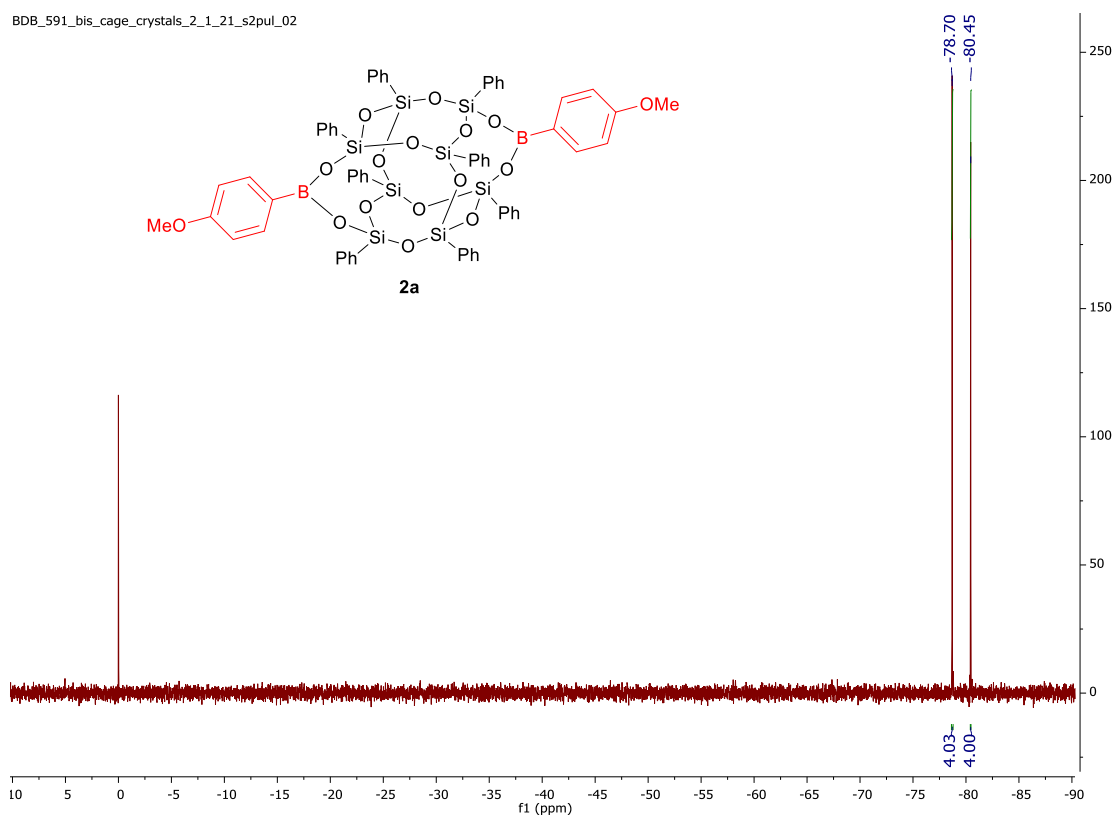


Figure 3-19: ^{29}Si NMR of **2a** (CDCl₃ + 1%TMS, 99 MHz)

15-Methyl-1,3,5,7,9,11,13,17-octaphenyl-2,4,6,8,10,12,14,16,18,19,20,21-dodecaoxa-1,3,5,7,9,11,13,15,17-nonasilatetracyclo[9.7.1.15,17.17,13]henicosane-3,9-diol (5a)

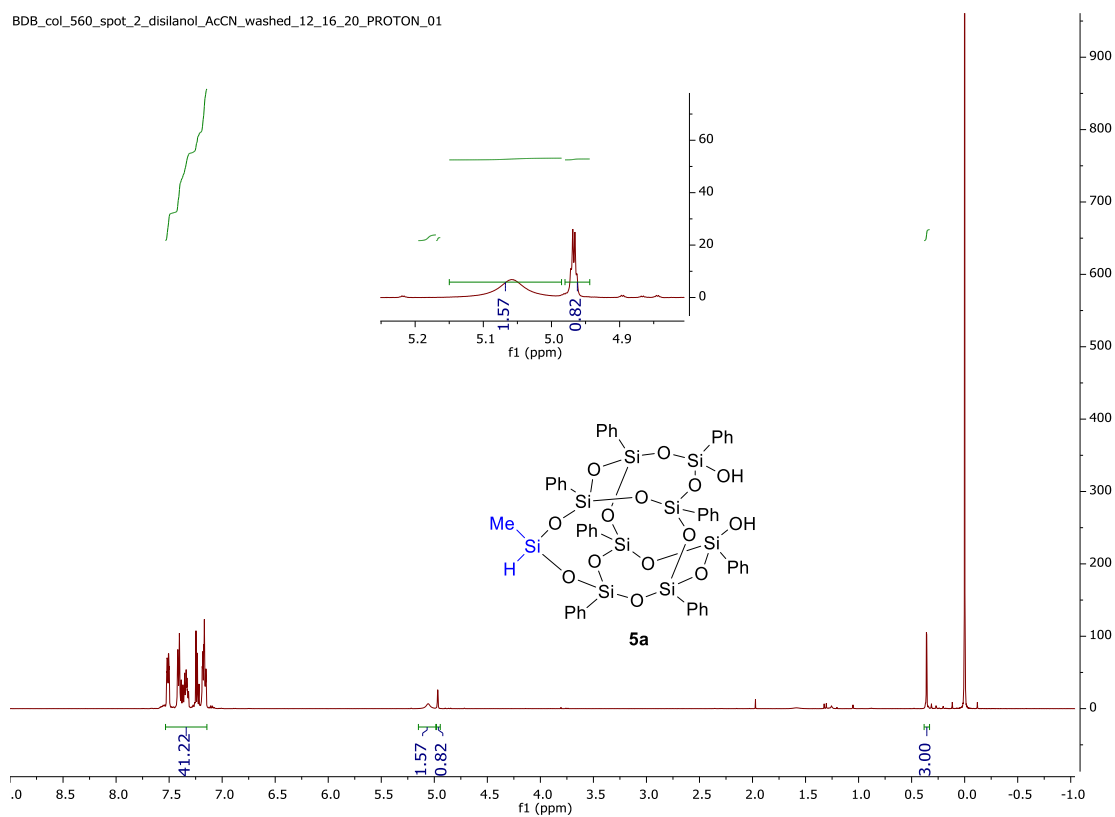


Figure 3-20: ^1H NMR of **5a** (CDCl₃ + 1% TMS, 500 MHz)

BDB_col_560_spot_2_ABdiol_12_18_20_CARBON_01

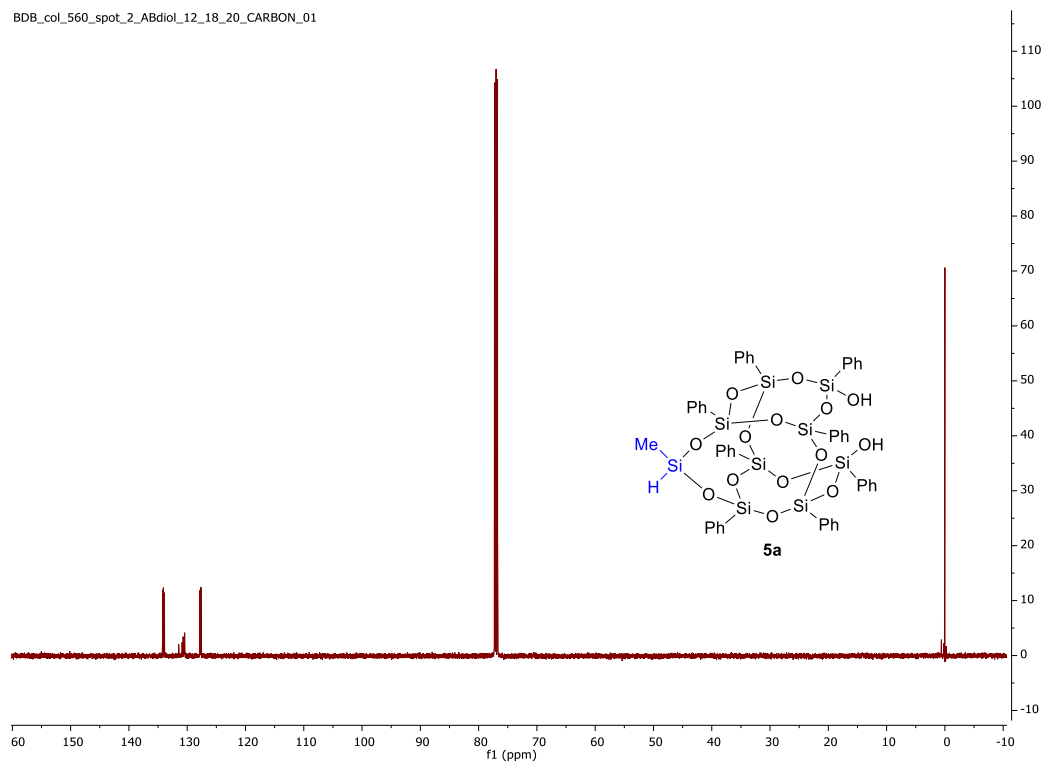


Figure 3-21: ^{13}C NMR of 5a (CDCl_3 + 1%TMS, 126 MHz)

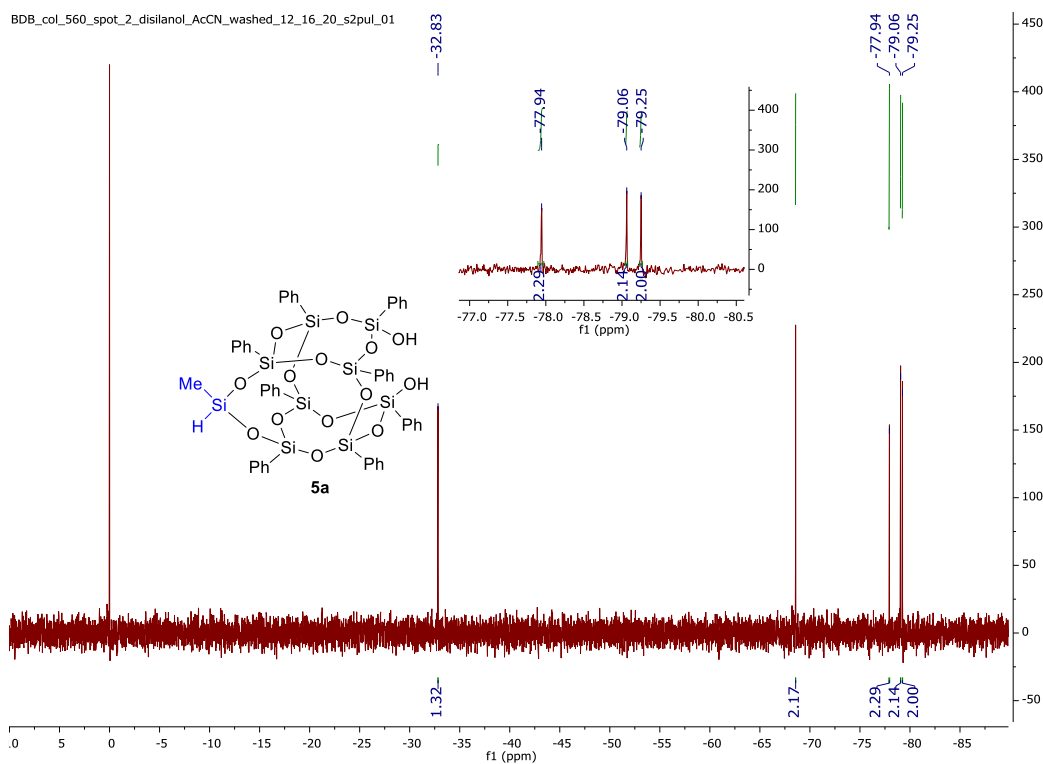


Figure 3-22: ^{29}Si NMR of 5a (CDCl_3 + 1%TMS, 99 MHz)

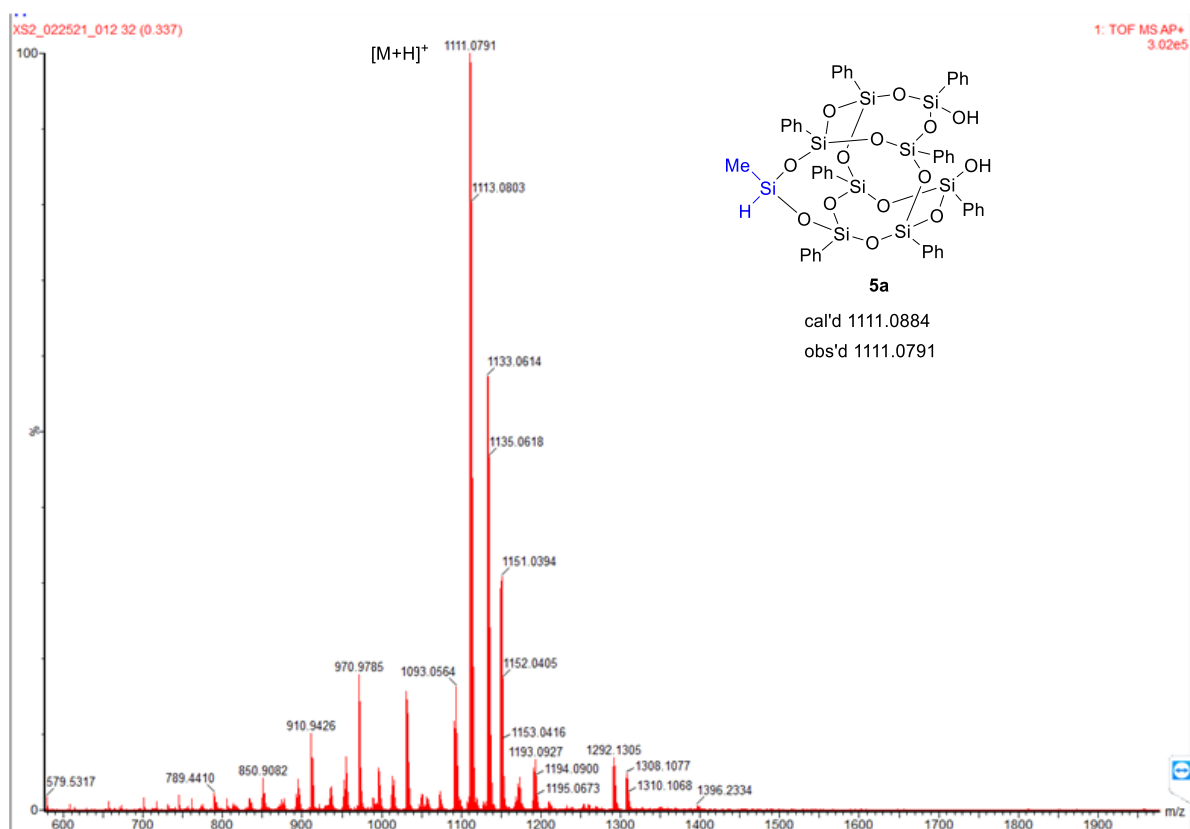


Figure 3-23: Mass spec of **5a**

15,15-dimethyl-1,3,5,7,9,11,13,17-octaphenyl-2,4,6,8,10,12,14,16,18,19,20,21-dodecaoxa-1,3,5,7,9,11,13,15,17-nonasilatetracyclo[9.7.1.15,17.17,13]henicosane-3,9-diol
(5b)

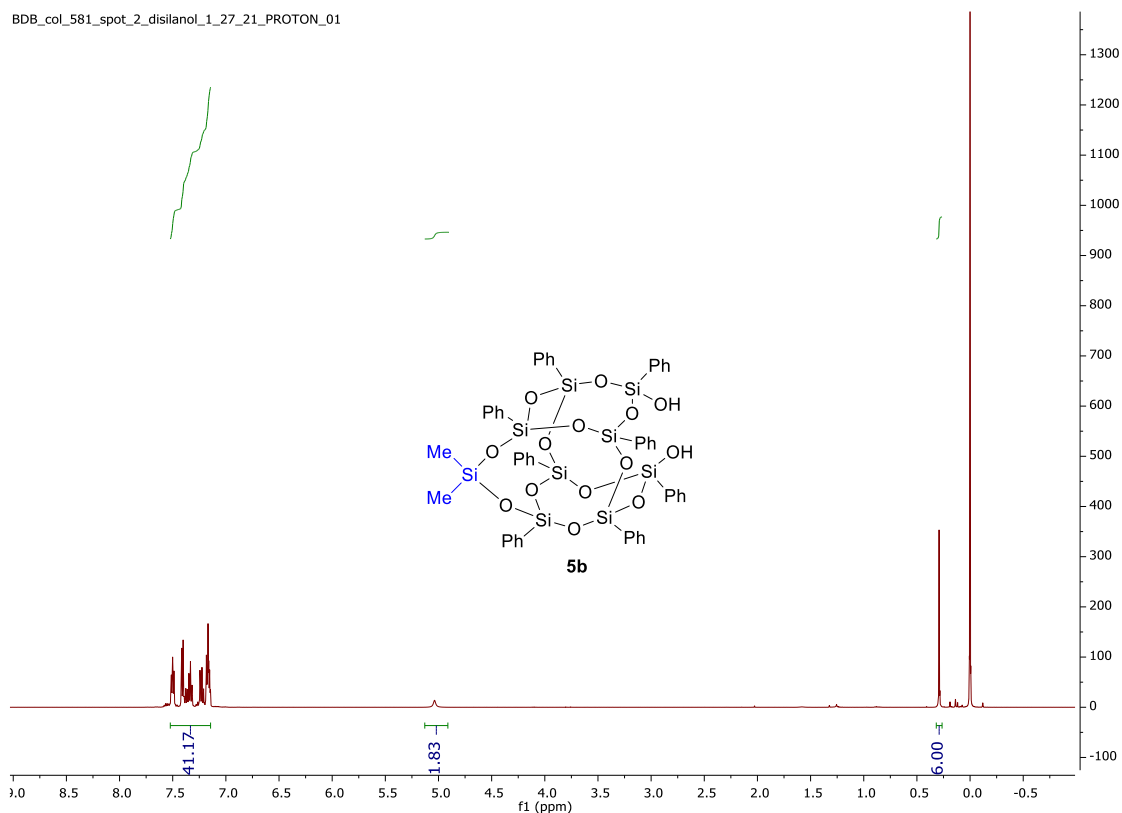
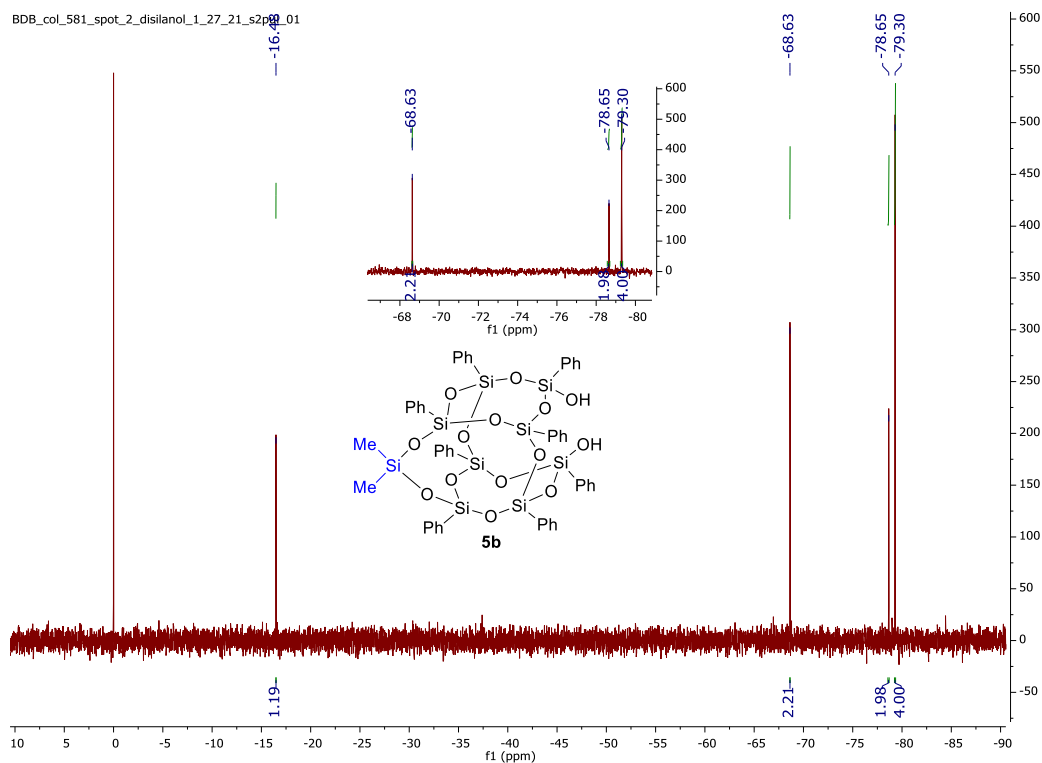
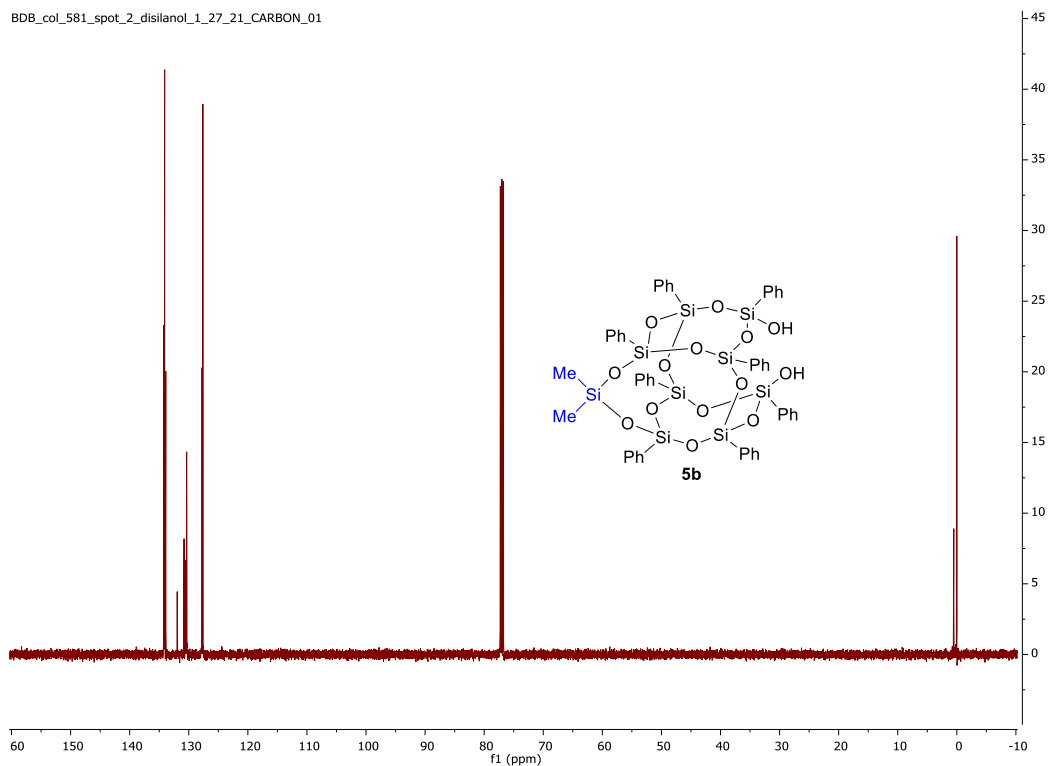


Figure 3-24: ^1H NMR of **5b** ($\text{CDCl}_3 + 1\% \text{TMS}$, 500 MHz)



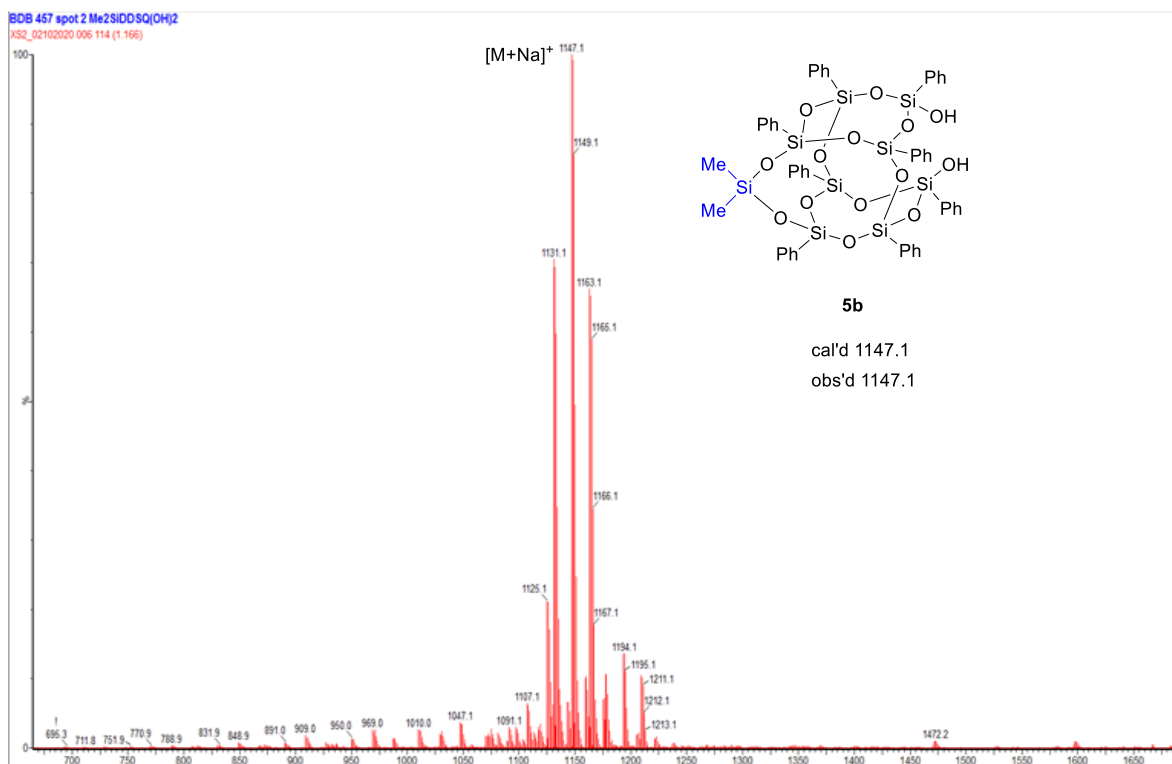


Figure 3-27: Mass spec of **5b**

15,15-diethyl-1,3,5,7,9,11,13,17-octaphenyl-2,4,6,8,10,12,14,16,18,19,20,21-dodeca-oxa-1,3,5,7,9,11,13,15,17-nonasilatetracyclo[9.7.1.15,17.17,13]henicosane-3,9-diol.

(5c)

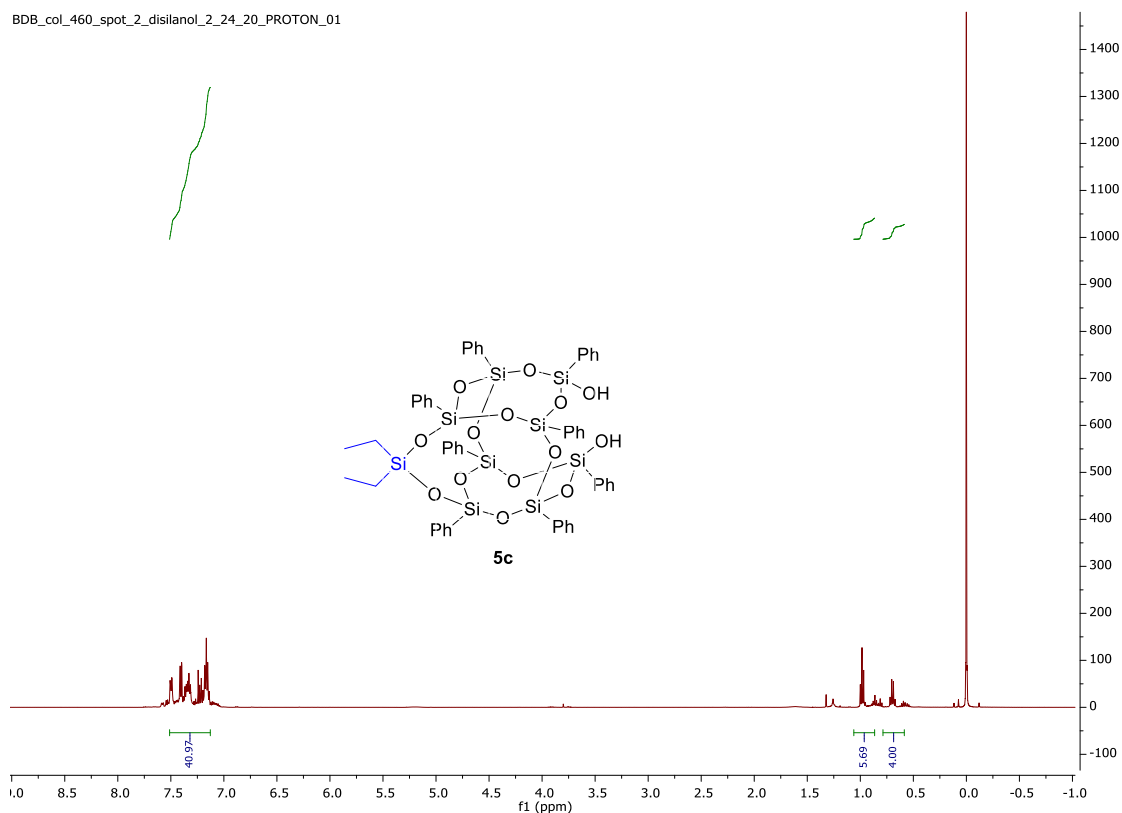


Figure 3-28: ^1H NMR of **5c** (CDCl_3 + 1%TMS, 500 MHz)

BDB_col_460_spot_2_disilanol_2_24_20_CARBON_01

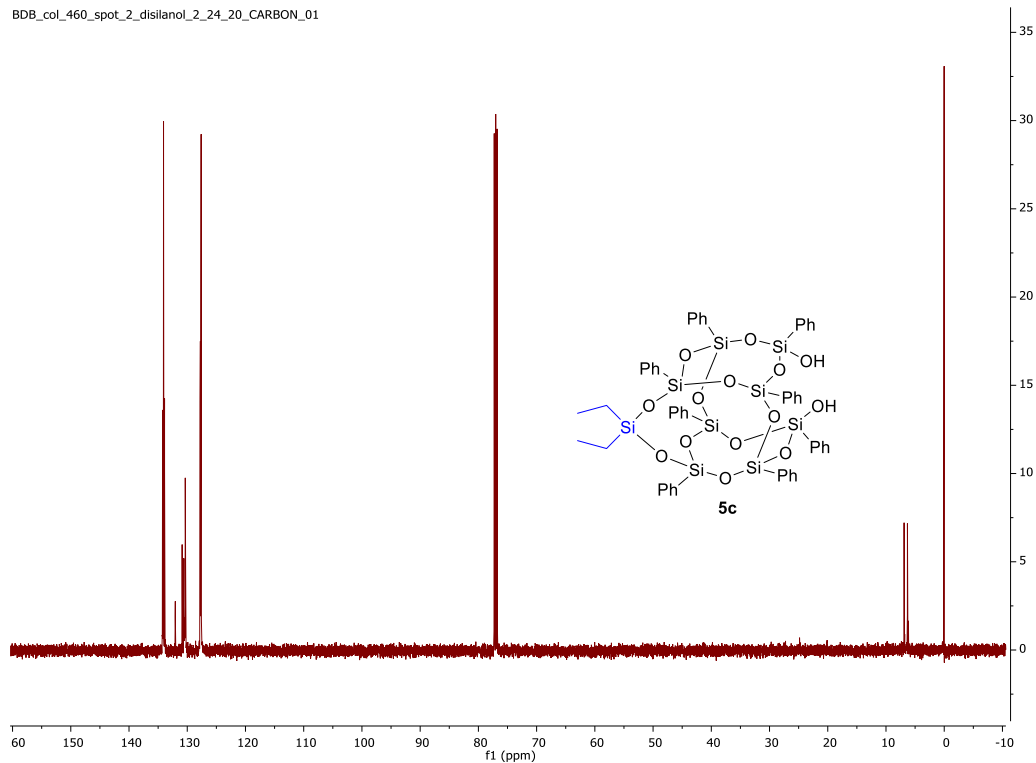


Figure 3-29: ^{13}C NMR of **5c** (CDCl_3 + 1%TMS, 126 MHz)

BDB_col_460_spot_2_disilanol_2_24_20_s2p001

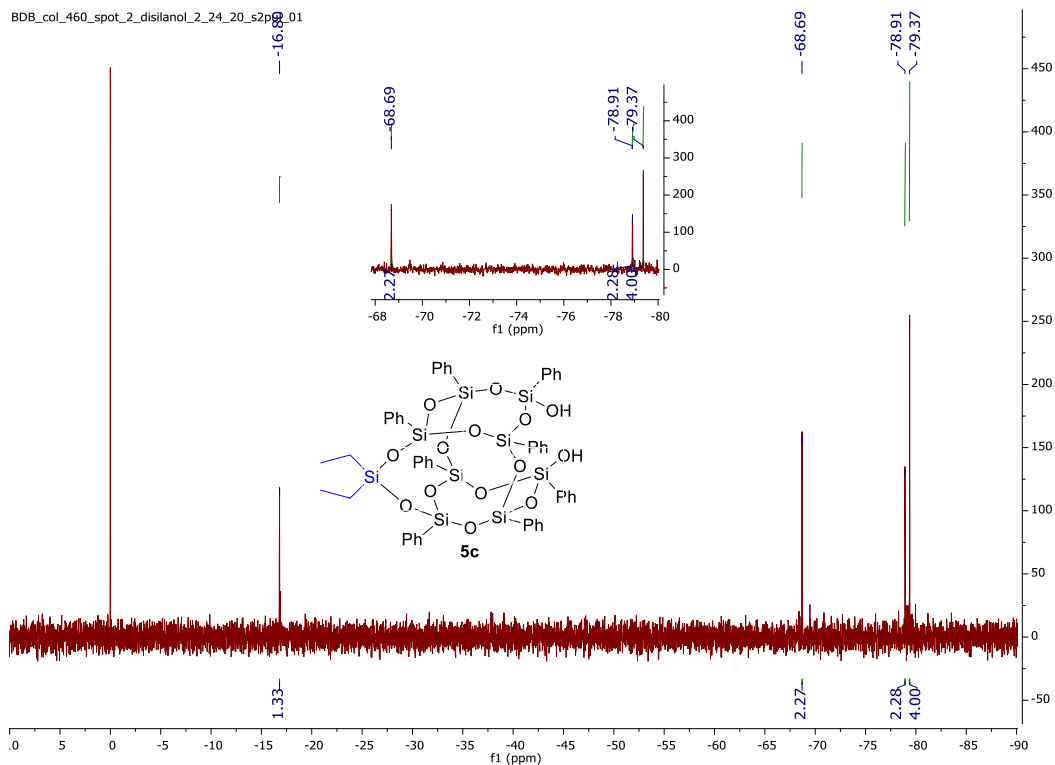


Figure 3-30: ^{29}Si NMR of **5c** (CDCl_3 + 1%TMS, 99 MHz)

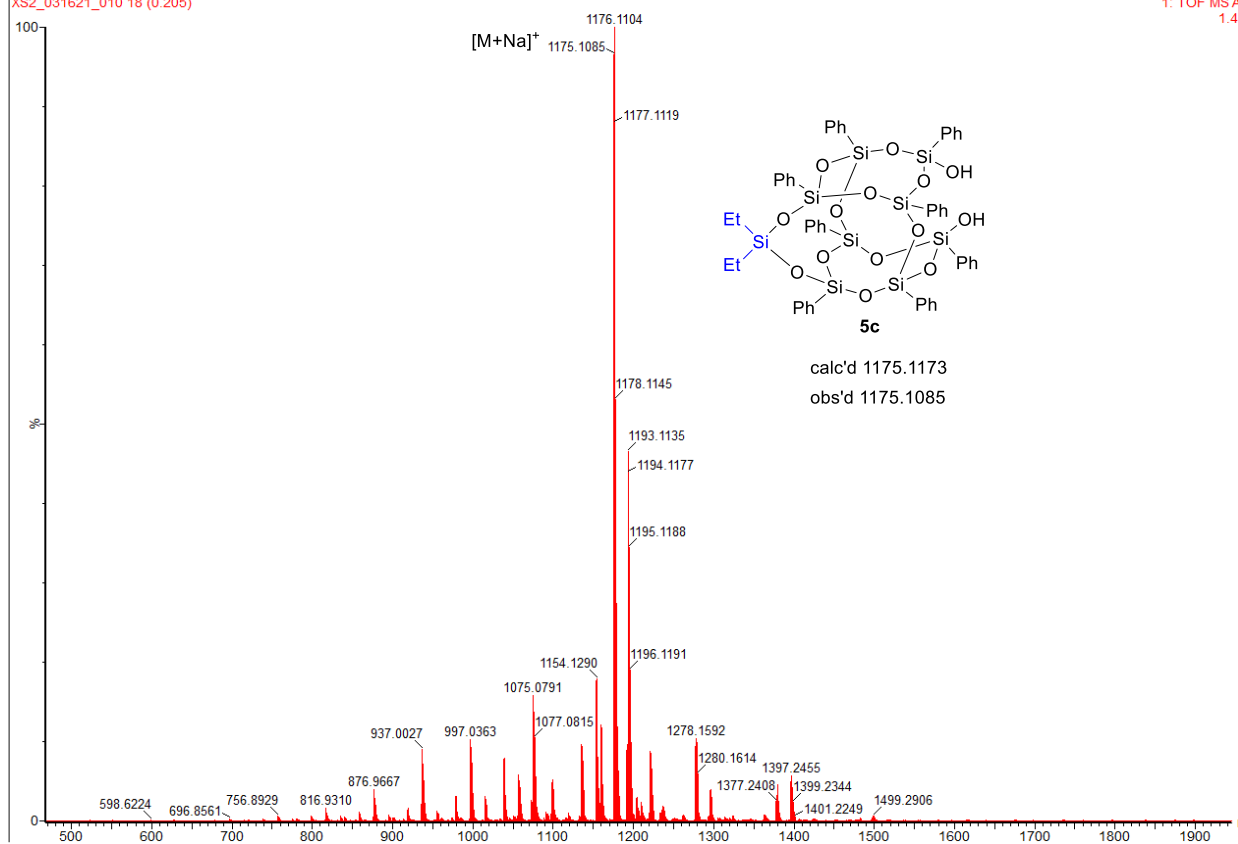


Figure 3-31: Mass spec of 5c

4-(3,9-Dihydroxy-15-methyl-1,3,5,7,9,11,13,17-octaphenyl-2,4,6,8,10,12,14,16,18,19,20,21-dodecaoxa-1,3,5,7,9,11,13,15,17-nonasilatetracyclo[9.7.1.15,17.17,13]henicosan-15-yl)butanenitrile. (**5d**)

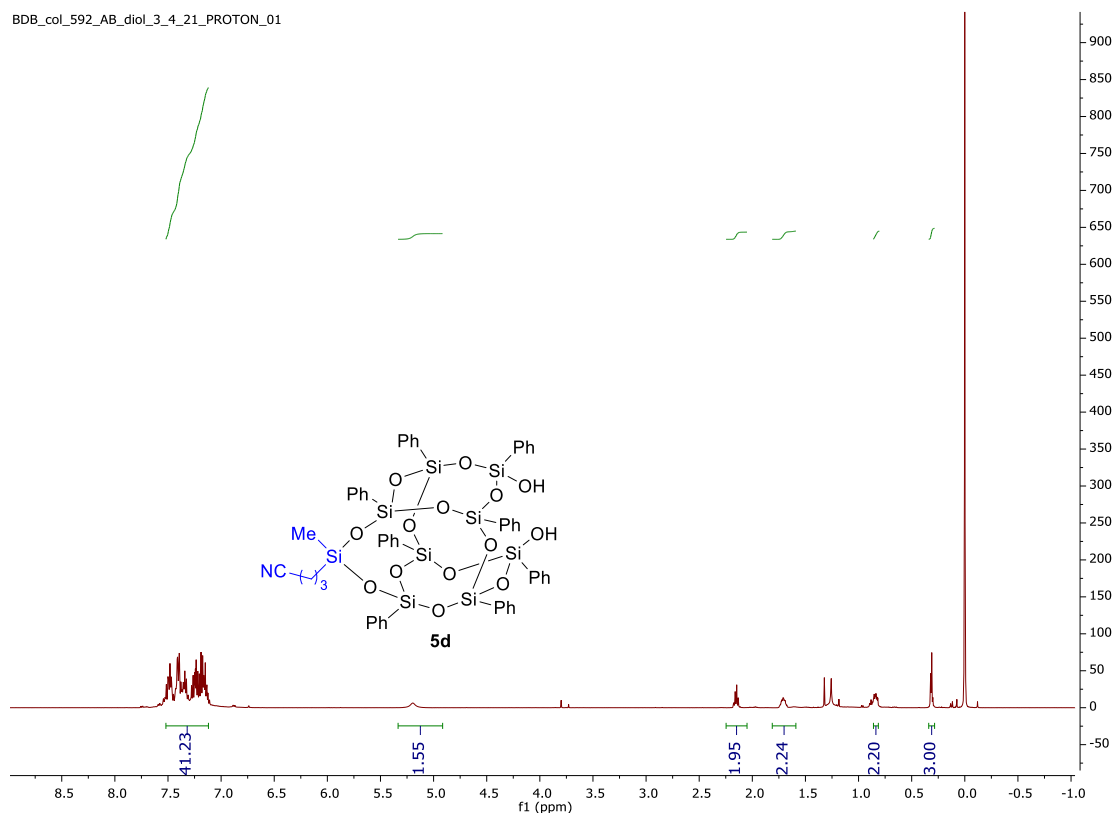
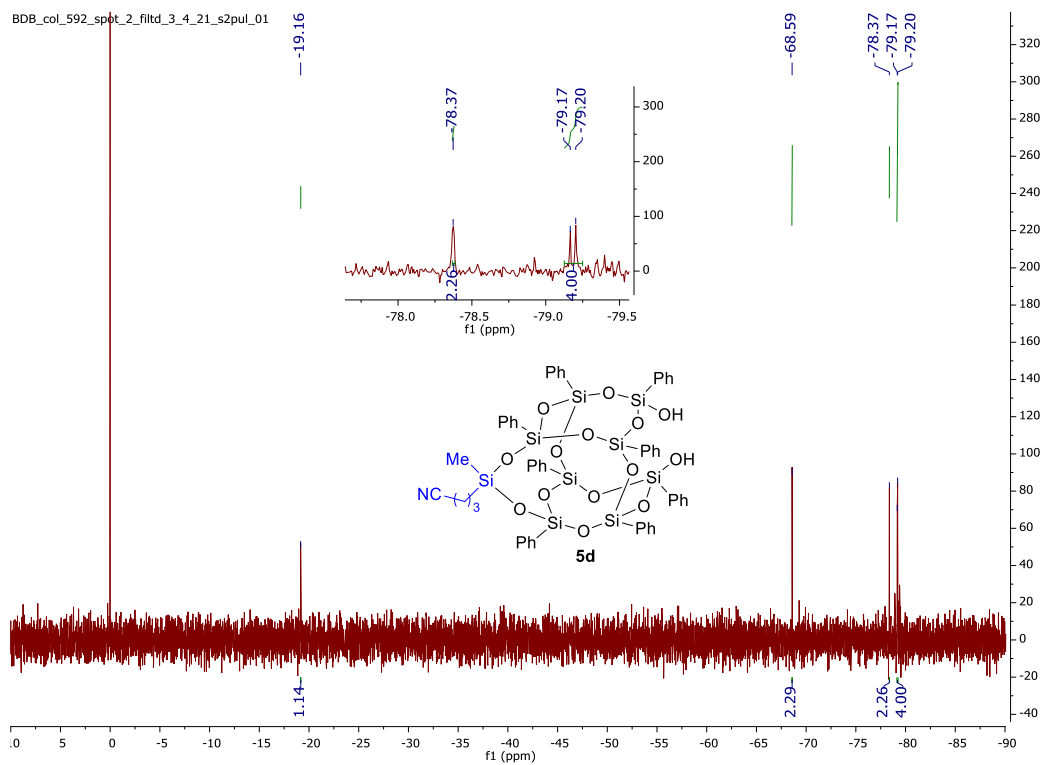
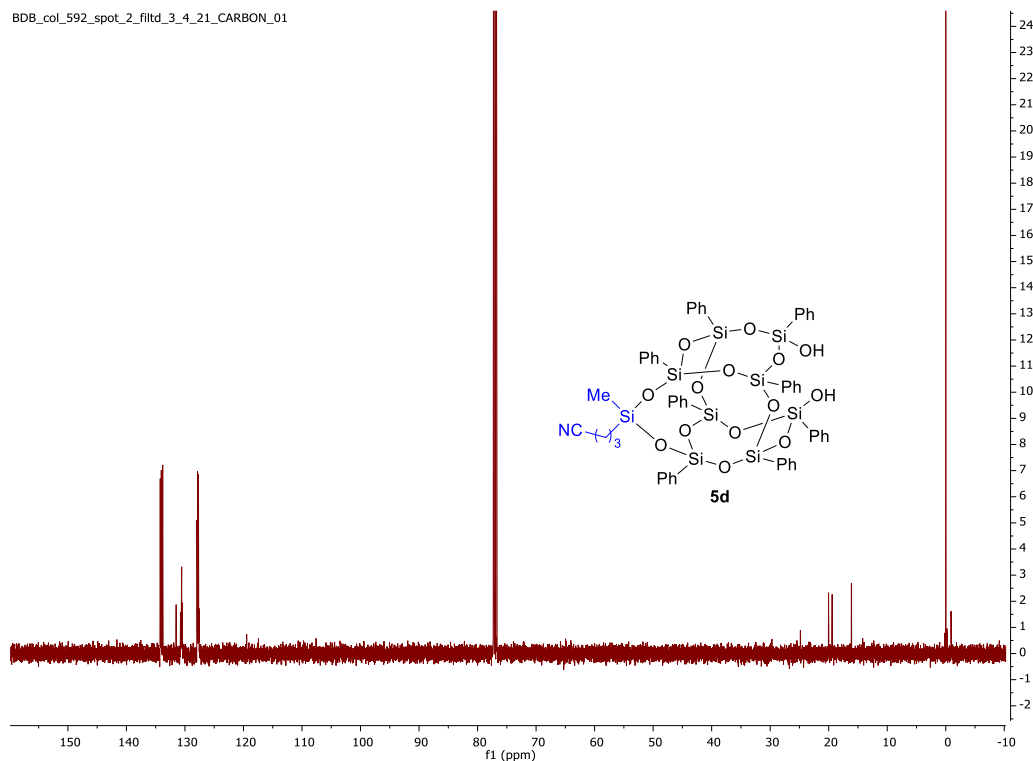


Figure 3-32: ¹H NMR of **5d** (CDCl₃ + 1%TMS, 500 MHz)



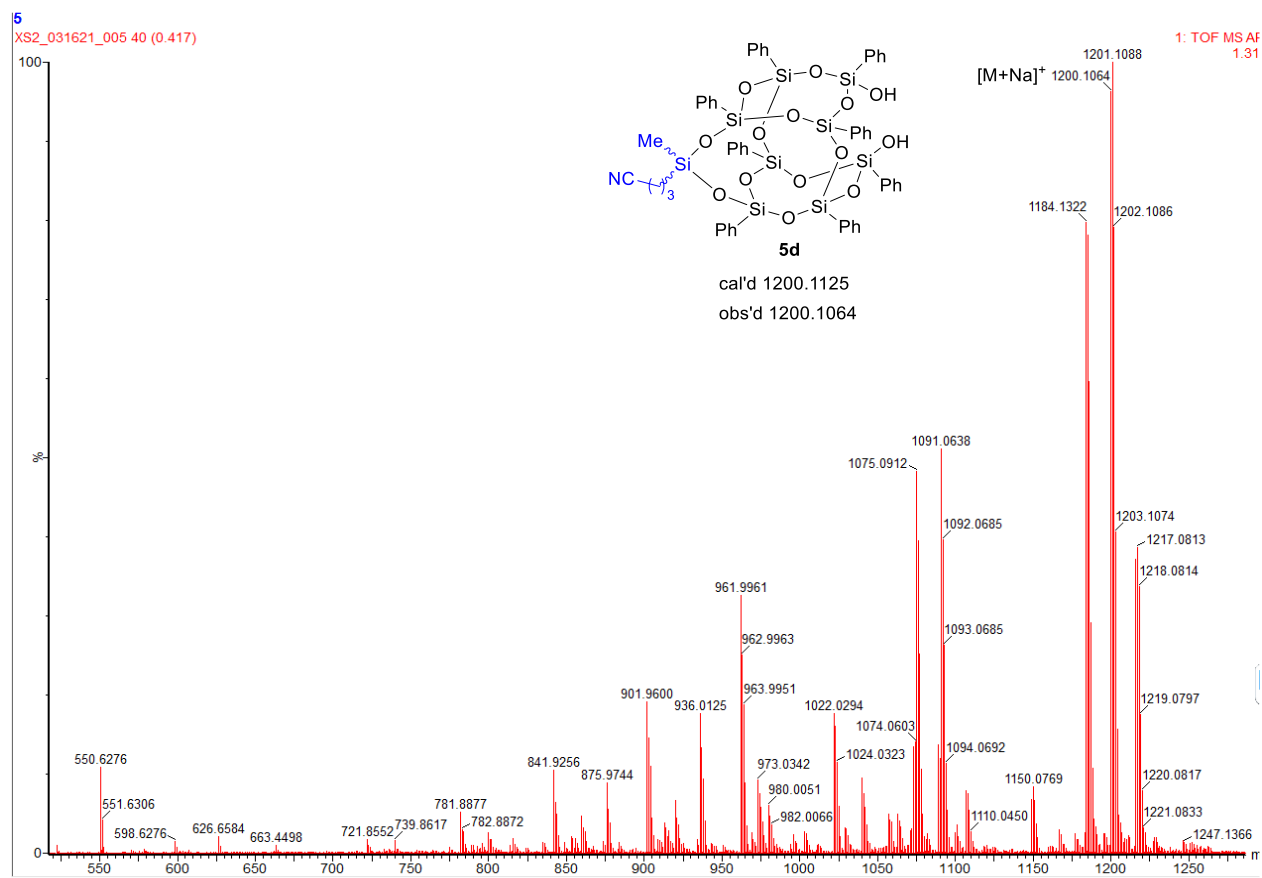


Figure 3-35: Mass spec of 5d

15-Methyl-1,3,5,7,9,11,13,17-octaphenyl-15-vinyl-2,4,6,8,10,12,14,16,18,19,20,21-dodecaoxa-1,3,5,7,9,11,13,15,17-nonasilatetracyclo[9.7.1.15,17.17,13]henicosane-3,9-diol
(**5e**)

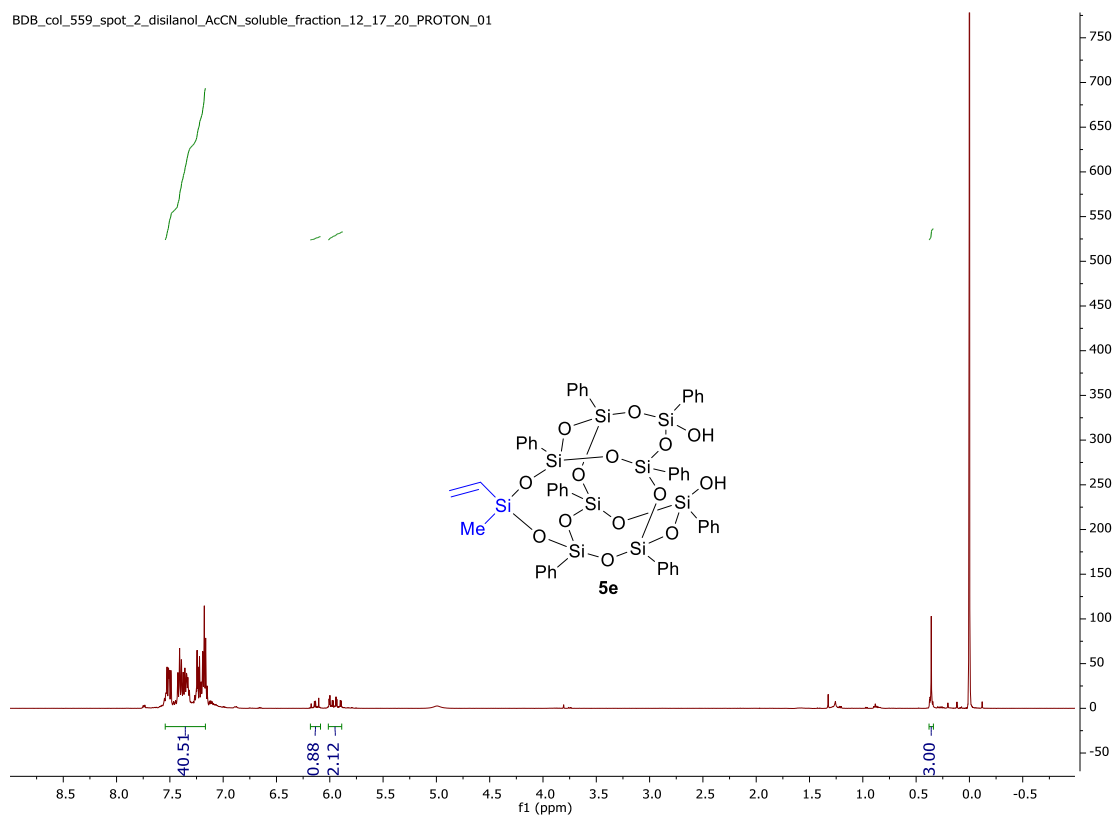


Figure 3-36: ¹H NMR of **5e** (CDCl₃ + 1%TMS, 500 MHz)

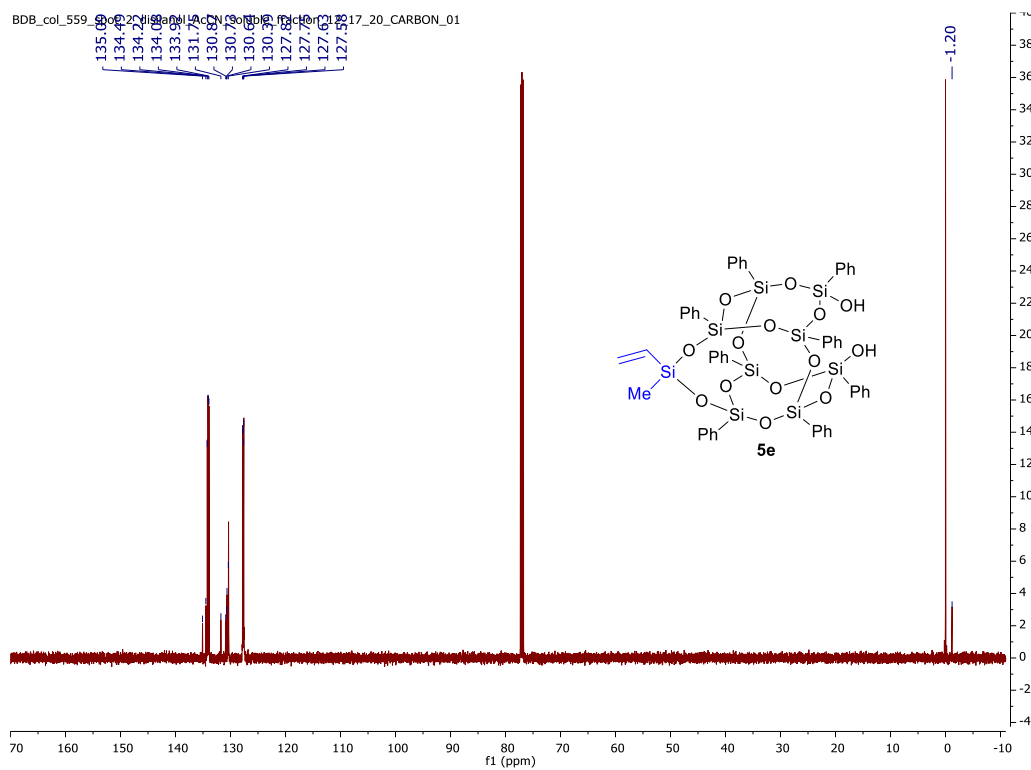


Figure 3-37: ^{13}C NMR of **5e** (CDCl_3 + 1%TMS, 126 MHz)

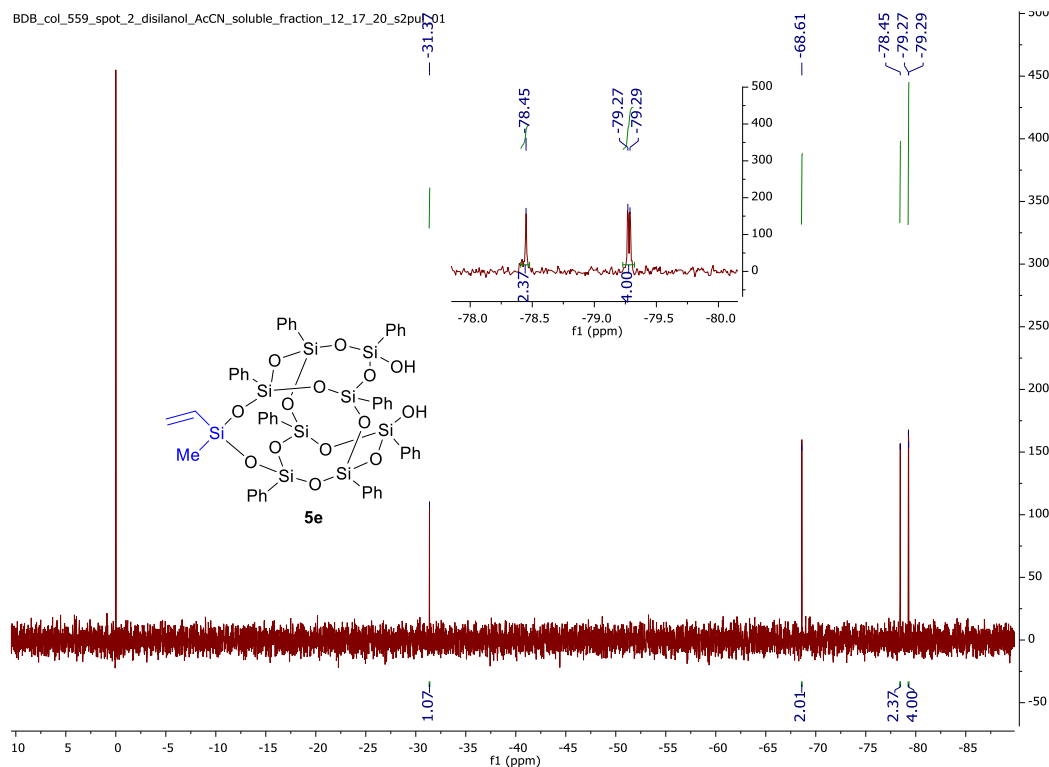


Figure 3-38: ^{29}Si NMR of **5e** (CDCl_3 + 1%TMS, 99 MHz)

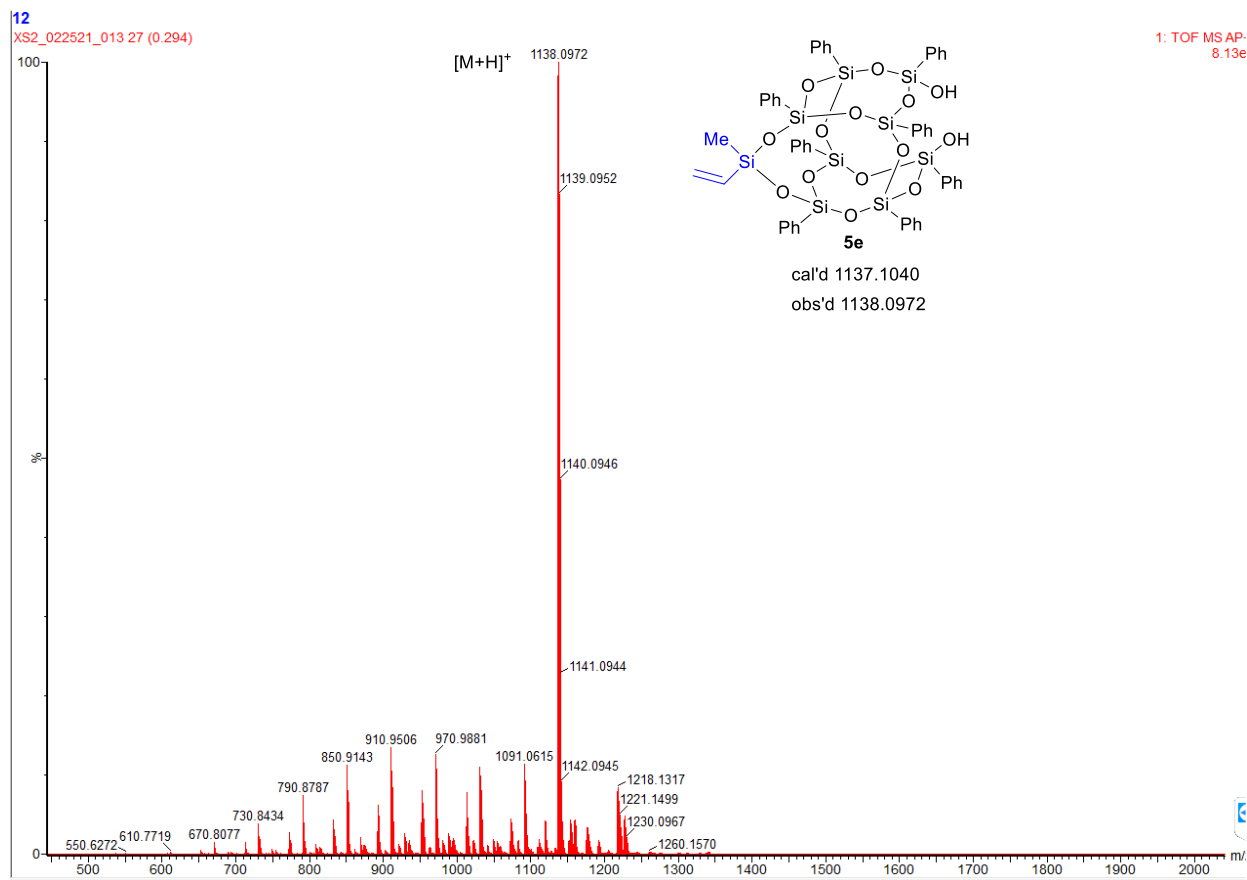


Figure 3-39: Mass spec of **5e**

15-Allyl-15-methyl-1,3,5,7,9,11,13,17-octaphenyl-2,4,6,8,10,12,14,16,18,19,20,21-dodecaoxa-1,3,5,7,9,11,13,15,17-nonasilatetracyclo[9.7.1.15,17.17,13]henicosane-3,9-diol (**5f**)

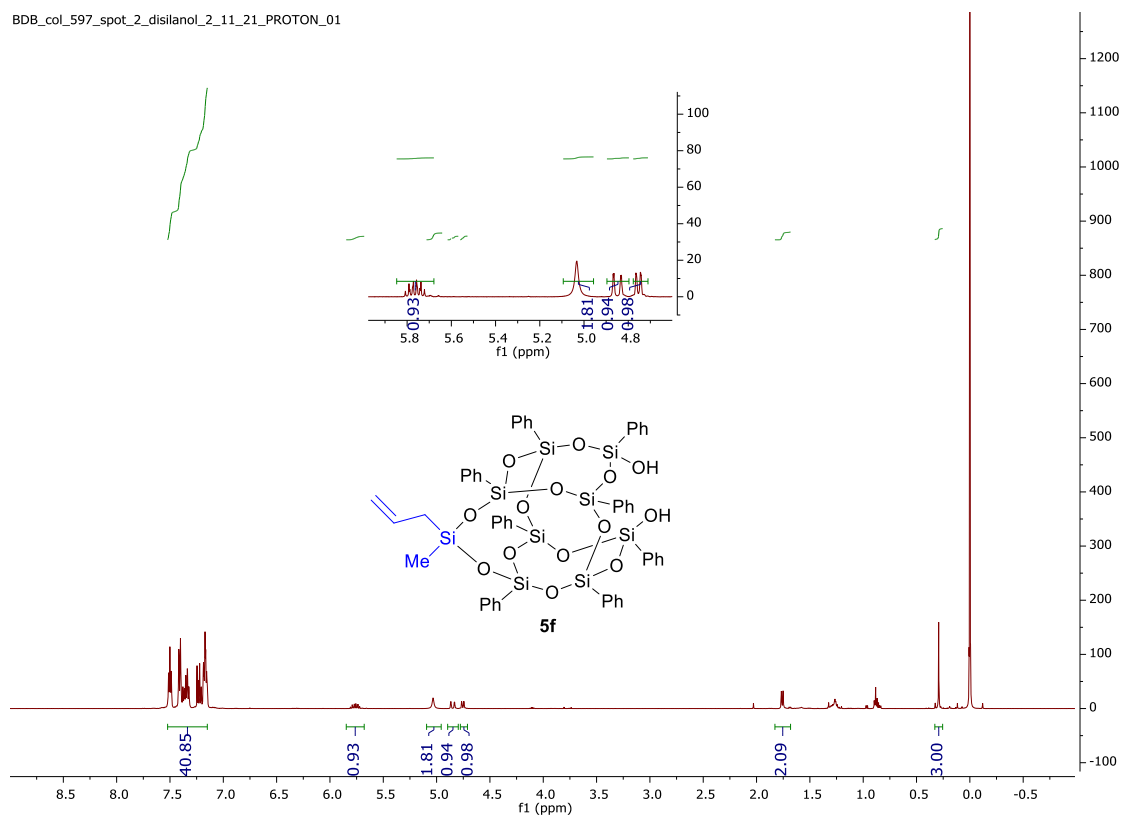


Figure 3-40: ^1H NMR of **5f** ($\text{CDCl}_3 + 1\% \text{TMS}$, 500 MHz)

BDB_col_597_spot_2_disilanol_2_11_21_CARBON_01

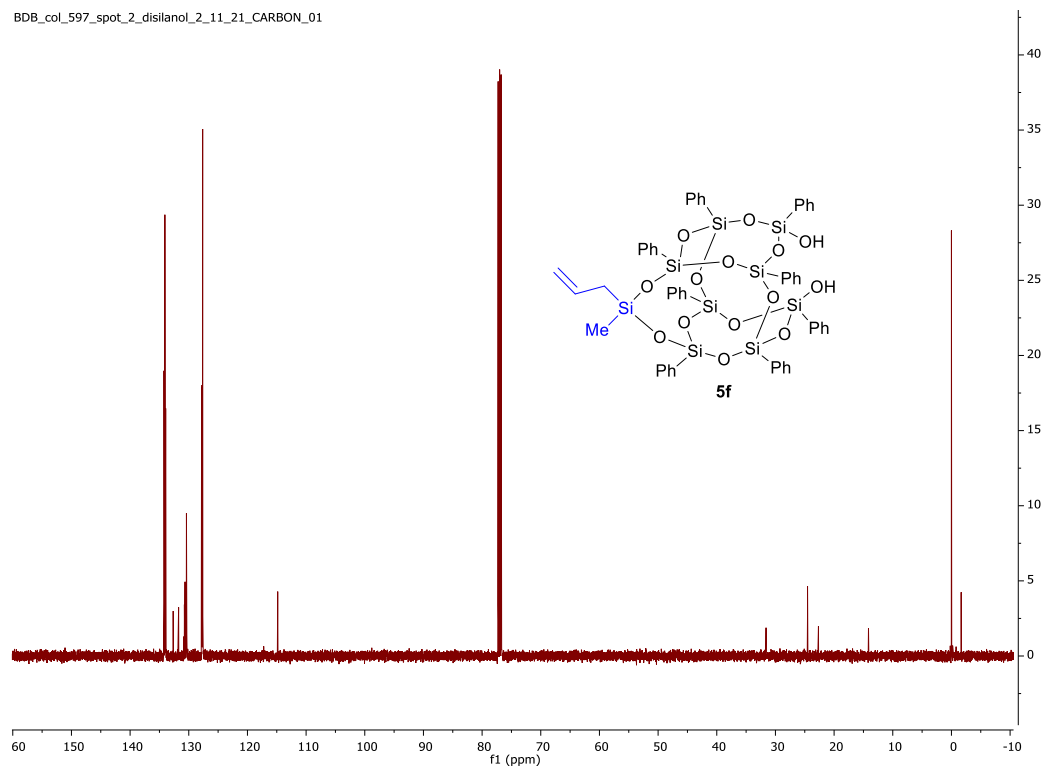


Figure 3-41: ^{13}C NMR of **5f** (CDCl_3 + 1%TMS, 126 MHz)

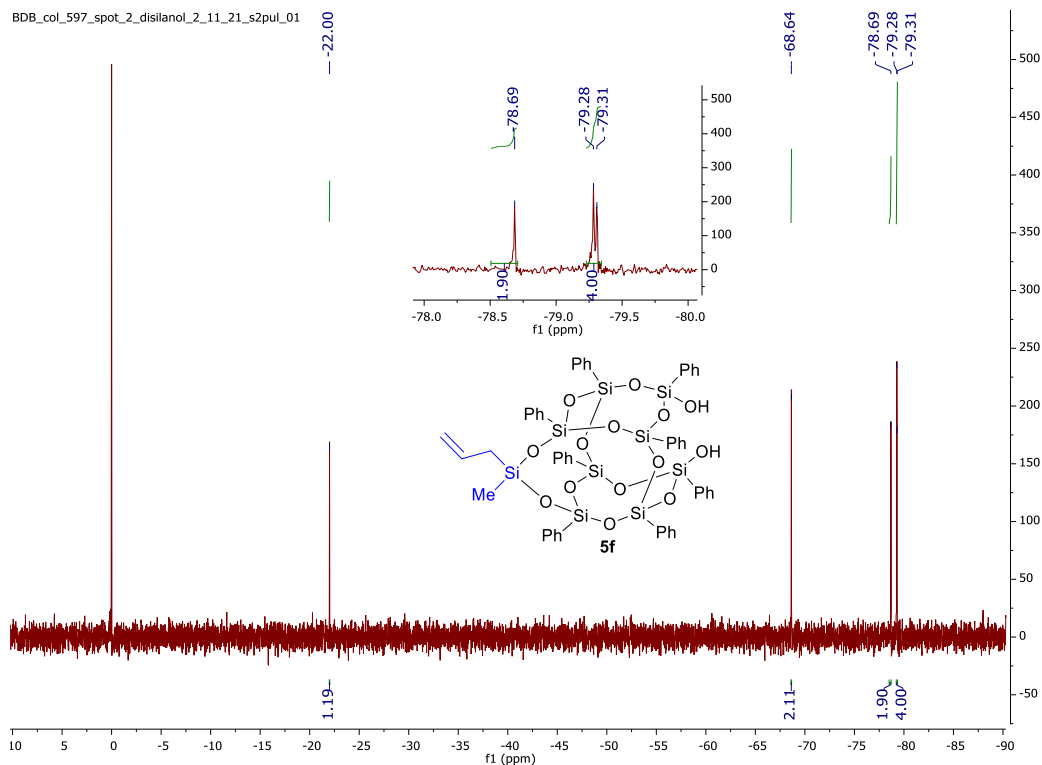


Figure 3-42: ^{29}Si NMR of **5f** (CDCl_3 + 1%TMS, 99 MHz)

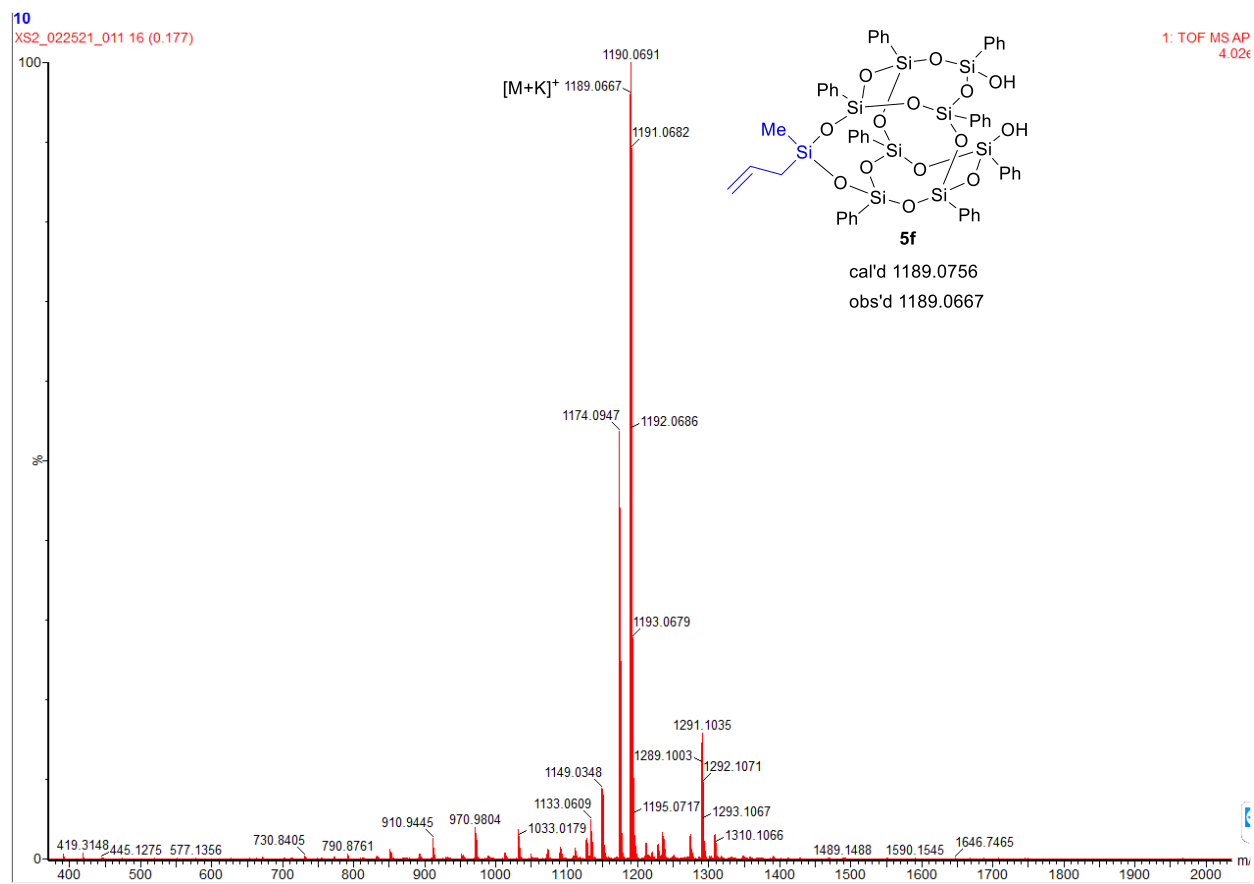


Figure 3-43: Mass spec of 5f

15-Methyl-1,3,5,7,9,11,13,17-octaphenyl-2,4,6,8,10,12,14,16,18,19,20,21dodecaoxa-1,3,5,7,9,11,13,15,17-nonasilatetracyclo[9.7.1.15,17.17,13]henicosane-3,9,15-triol (5g)

$C_{49}H_{46}O_{15}Si_9$

BDB_recol_615_sp2_3_22_21_PROTON_01

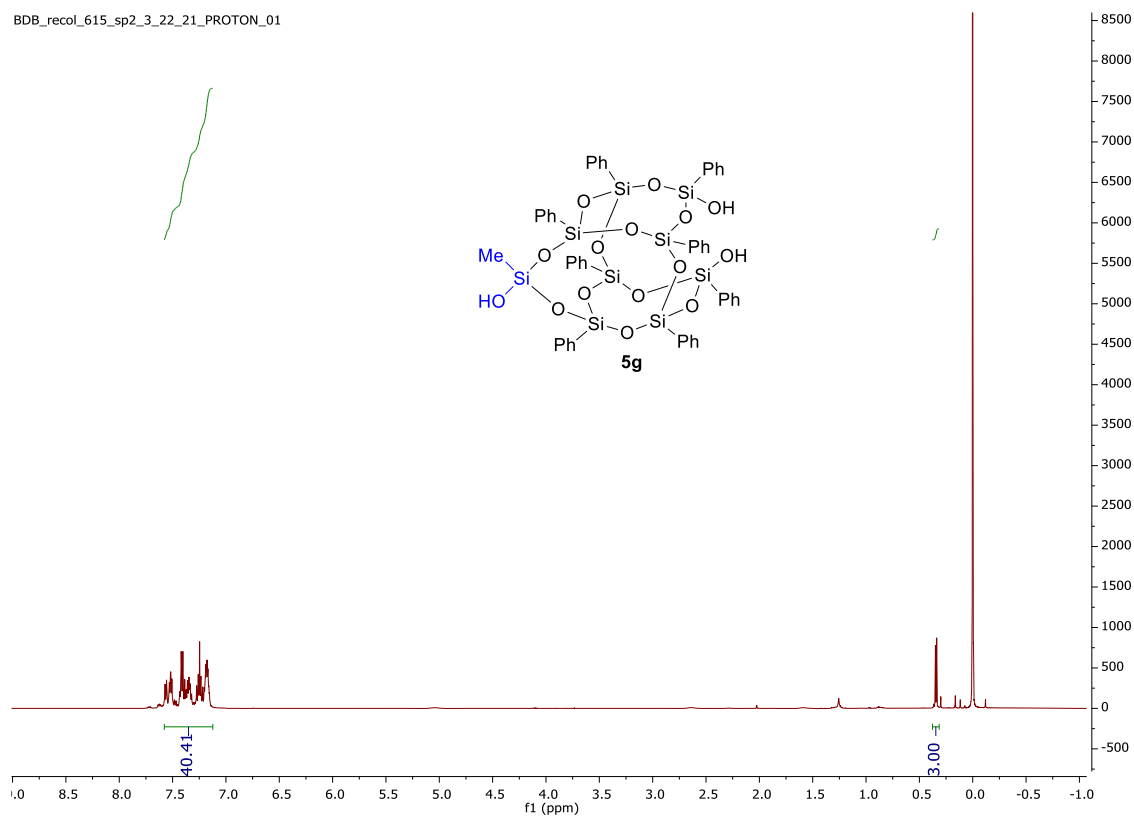
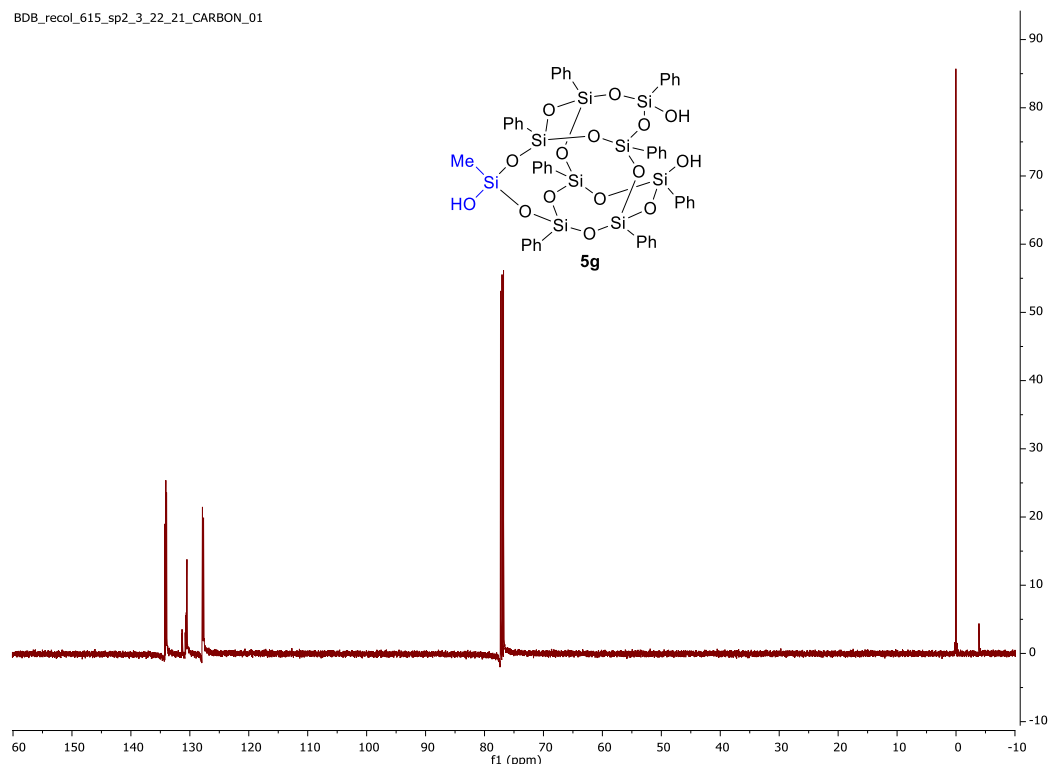
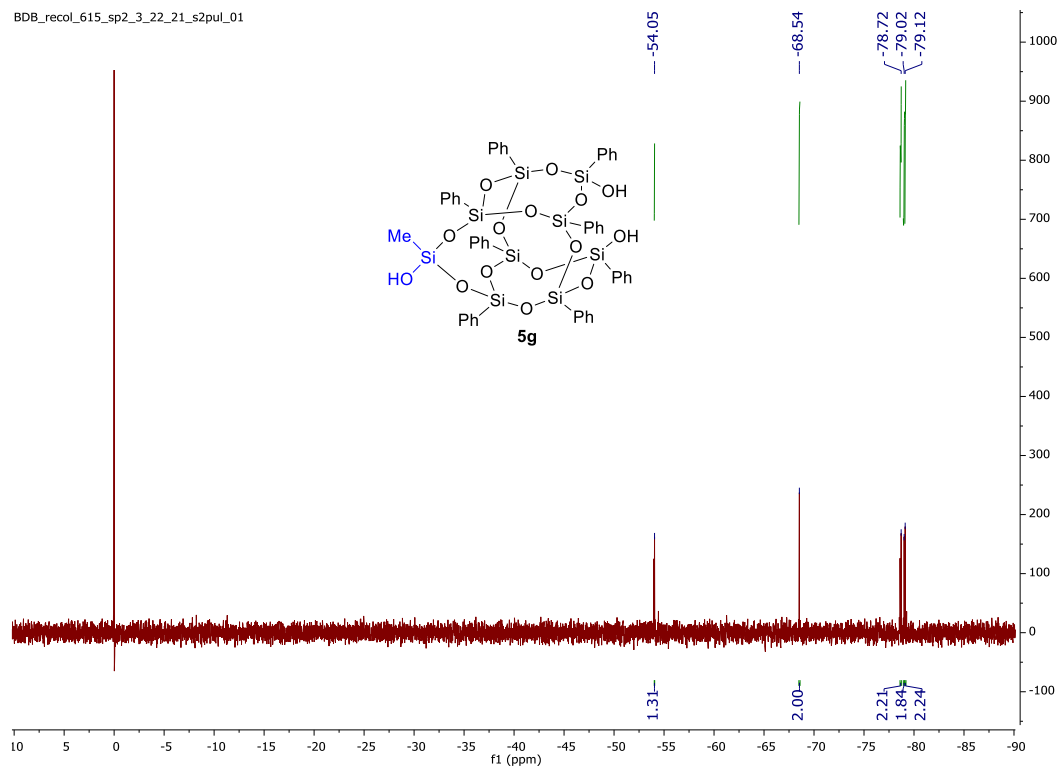


Figure 3-44: 1H NMR of **5g** ($CDCl_3$ + 1%TMS, 500 MHz)

BDB_recol_615_sp2_3_22_21_CARBON_01



BDB_recol_615_sp2_3_22_21_s2pul_01



*15-Isopropyl-1,3,5,7,9,11,13,17-octaphenyl-2,4,6,8,10,12,14,16,18,19,20,21-dodeca-
oxa-1,3,5,7,9,11,13,15,17-nonasilatetracyclo[9.7.1.15,17.17,13]henicosane-3,9,15-triol*
(**5h**)

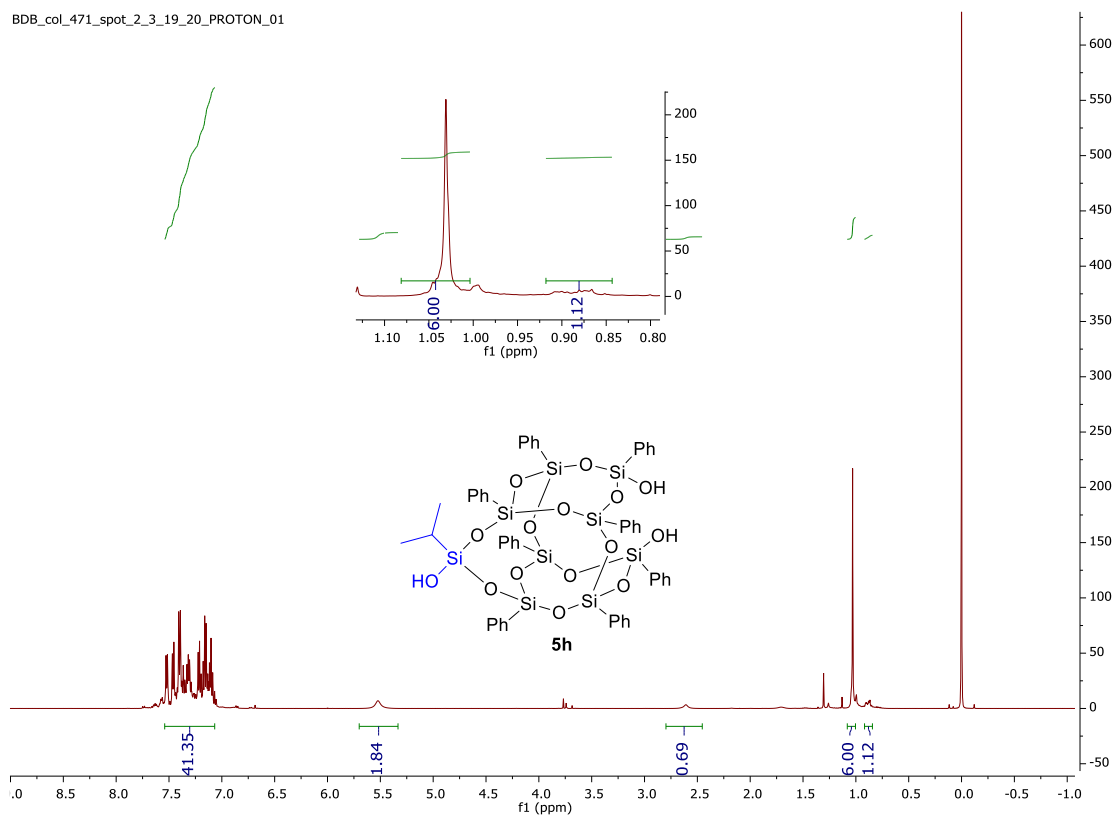


Figure 3-47: ^1H NMR of **5h** (CDCl_3 + 1%TMS, 500 MHz)

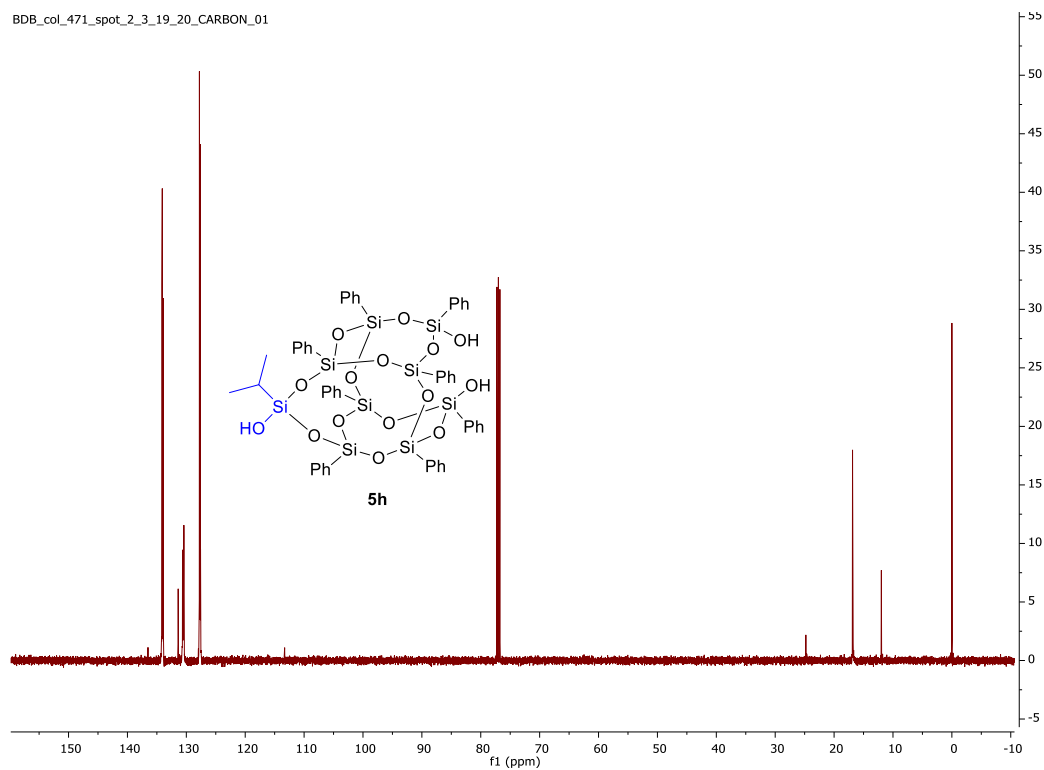


Figure 3-48: ¹³C NMR of **5h** (CDCl₃ + 1%TMS, 126 MHz)

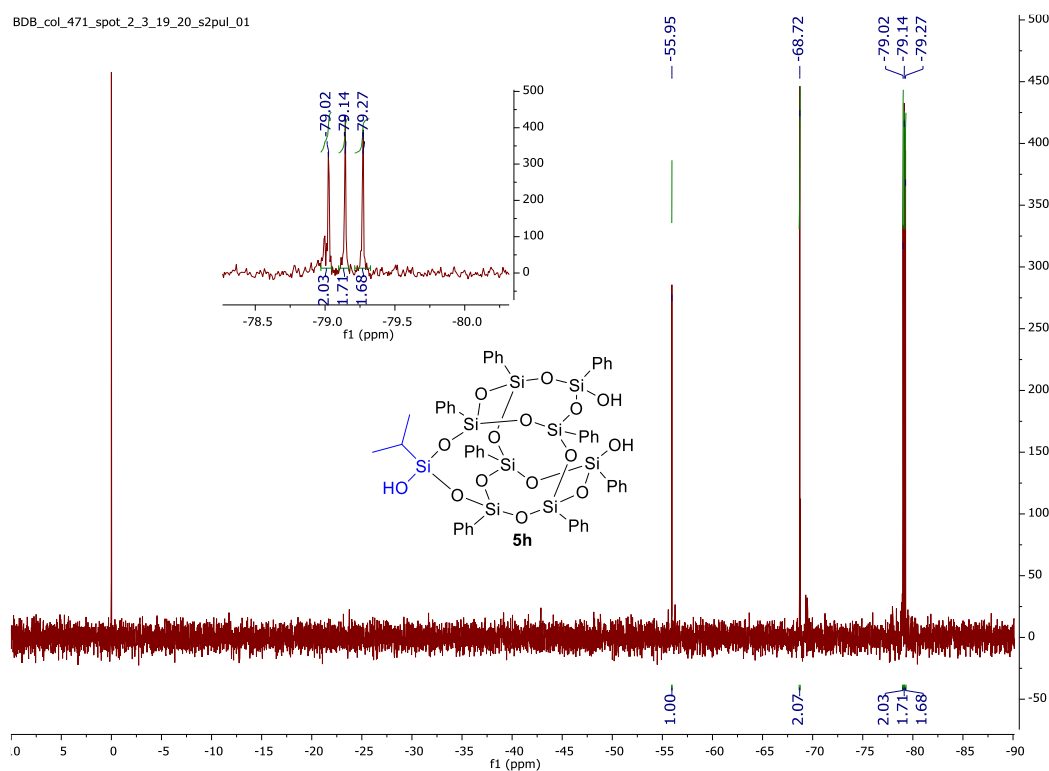


Figure 3-49: ²⁹Si NMR of **5h** (CDCl₃ + 1%TMS, 99 MHz)

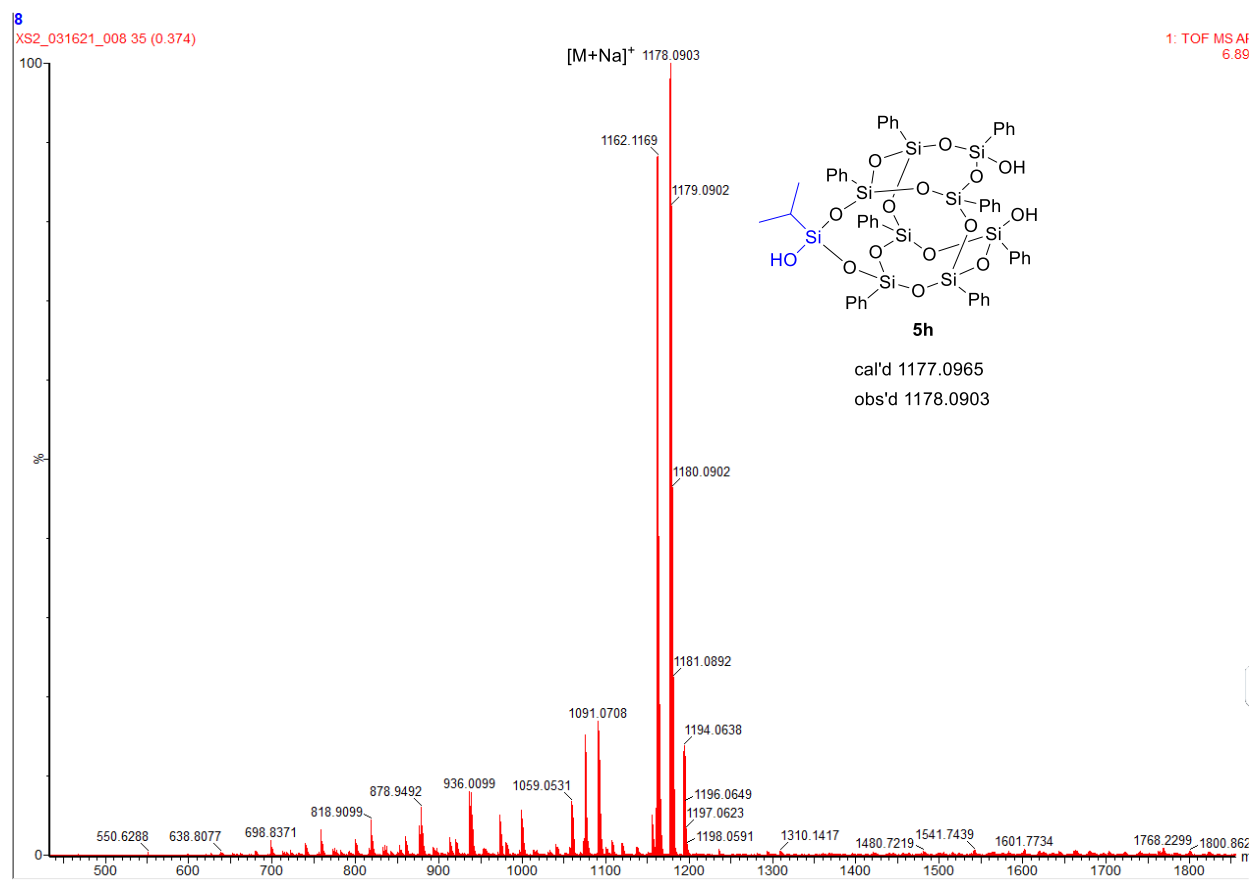


Figure 3-50: Mass spec of 5h

Single X-Ray Crystallographic Data of 5

Table 3-4: Crystal Data and Structure Refinement for Asymmetric DDSQ Diols **5a**, **5b**, **5e** and **5f**

	5a	5b	5e	5f
CCDC	2064703	2052368	1986063	-
Formula	C _{49.5} H ₄₇ Cl _{0.5} O ₁₄ Si ₉	C _{50.5} H ₅₀ O _{14.5} Si ₉	C ₅₁ H ₄₈ O ₁₄ Si ₉	C _{51.57} H _{50.57} O ₁₄ Si ₉
$D_{calc}/\text{g cm}^{-3}$	1.379	1.390	1.398	1.359
μ/mm^{-1}	2.821	2.619	2.634	2.543
Formula Weight	1136.40	1141.71	1137.70	1147.17
Colour	colourless	colourless	colourless	colourless
Shape	needle	needle	needle	needle
Size/mm ³	0.27×0.07×0.05	0.44×0.07×0.03	0.25×0.05×0.04	0.35×0.21×0.15
T/K	100.0(4)	101(2)	100.00(10)	100.01(10)
Crystal System	monoclinic	monoclinic	monoclinic	monoclinic
Space Group	$P2_1/c$	$P2_1/c$	$P2_1/c$	$P2_1/c$
$a/\text{\AA}$	10.86380(10)	10.84639(7)	11.04925(11)	10.90427(11)
$b/\text{\AA}$	25.5534(3)	25.56527(16)	14.90570(19)	26.0236(3)
$c/\text{\AA}$	19.7196(2)	19.68348(14)	32.8348(3)	19.8193(2)
$\alpha/^\circ$	90	90	90	90
$\beta/^\circ$	91.7170(10)	92.0317(6)	91.5123(9)	94.2165(10)
$\gamma/^\circ$	90	90	90	90
$V/\text{\AA}^3$	5471.84(10)	5454.62(6)	5405.90(10)	5608.86(11)
Z	4	4	4	4
Z'	1	1	1	1
Wavelength/ \AA	1.54184	1.54184	1.54184	1.54184
Radiation type	Cu K_α	Cu K_α	Cu K_α	Cu K_α
$\theta_{min}/^\circ$	2.831	2.834	2.692	2.807
$\theta_{max}/^\circ$	77.004	77.115	77.372	80.173
Measured Refl's.	33813	73347	41543	45620
Indep't Refl's	10231	11423	11055	11532
Refl's $I \geq 2 \sigma(I)$	9188	10309	9379	10109
R_{int}	0.0329	0.0420	0.0405	0.0380
Parameters	683	688	734	736
Restraints	3	0	1	0
Largest Peak	0.780	0.537	0.810	0.454
Deepest Hole	-0.806	-0.912	-0.775	-0.564
GooF	1.018	1.065	1.041	1.065
wR_2 (all data)	0.1154	0.1250	0.1344	0.1106
wR_2	0.1124	0.1217	0.1287	0.1073
R_1 (all data)	0.0460	0.0495	0.0606	0.0444
R_1	0.0417	0.0446	0.0515	0.0388

15-Methyl-1,3,5,7,9,11,13,17-octaphenyl-2,4,6,8,10,12,14,16,18,19,20,21-dodecaoxa-1,3,5,7,9,11,13,15,17-nonasilatetracyclo[9.7.1.15,17.17,13]henicosane-3,9-diol (**5a**)

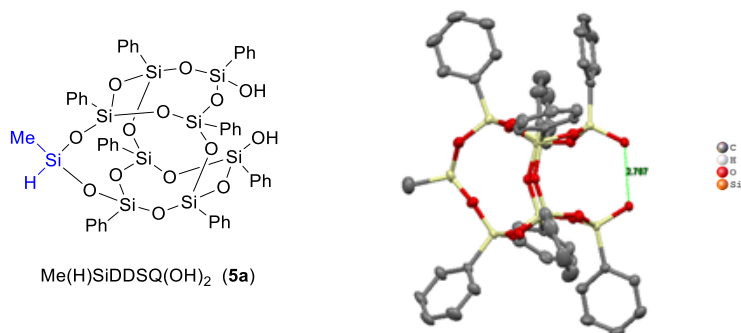


Figure 3-51: Single Crystal Structure of **5a** (Displacement ellipsoid contour probability drawn at 50%)

CCDC 2064703 contains the supplementary crystallographic data for **5a**. The data can be obtained free of charge from The Cambridge Crystallographic Data Centre via www.ccdc.cam.ac.uk/structures. There is a single molecule in the asymmetric unit, which is represented by the reported sum formula. In other words: Z is 4 and Z' is 1.

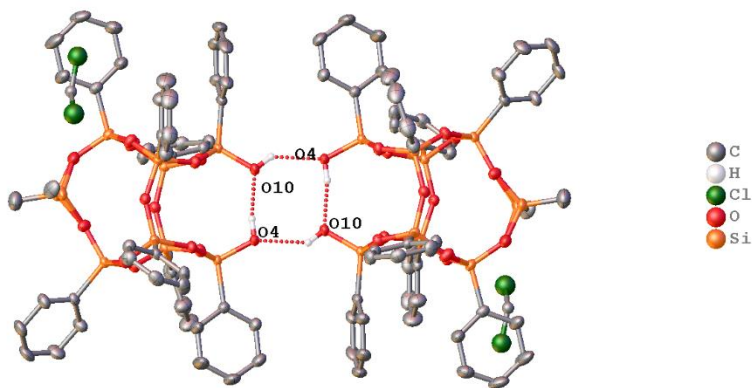


Figure 3-52: The following hydrogen bonding interactions with a maximum D-D distance of 2.9 Å and a minimum angle of 120 ° are present in **5a**: O4–O10: 2.767 Å, O10–O4₁: 2.738 Å

15,15-Dimethyl-1,3,5,7,9,11,13,17-octaphenyl-2,4,6,8,10,12,14,16,18,19,20,21-dodecaoxa-1,3,5,7,9,11,13,15,17-nonasilatetracyclo[9.7.1.15,17.17,13]henicosane-3,9-diol
(**5b**)

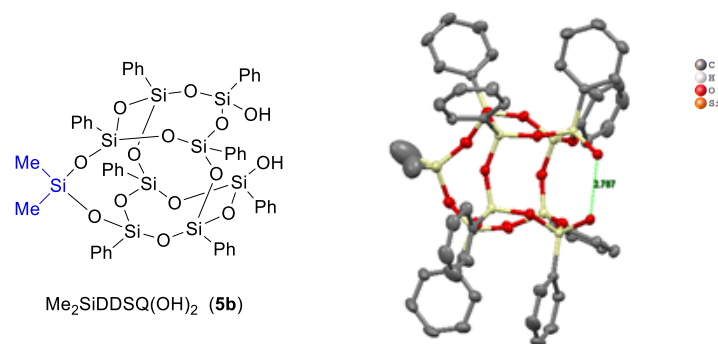


Figure 3-53: Single Crystal Structure of **5b** (Displacement ellipsoid contour probability drawn at 50%)

CCDC 2052368 contains the supplementary crystallographic data for **5b**. The data can be obtained free of charge from The Cambridge Crystallographic Data Centre via www.ccdc.cam.ac.uk/structures. There is a single molecule in the asymmetric unit, which is represented by the reported sum formula. In other words: Z is 4 and Z' is 1.

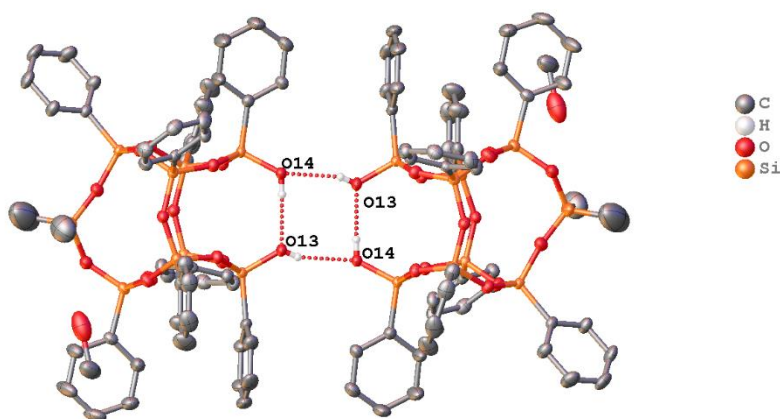


Figure 3-54: The following hydrogen bonding interactions with a maximum D-D distance of 3.1 Å and a minimum angle of 110 ° are present in REN1220D: O13–O14₁: 2.741 Å, O14–O13: 2.767 Å

15-Methyl-1,3,5,7,9,11,13,17-octaphenyl-15-vinyl-2,4,6,8,10,12,14,16,18,19,20,21-dodecaoxa-1,3,5,7,9,11,13,15,17-nonasilatetracyclo[9.7.1.15,17.17,13]henicosane-3,9-diol (5e)

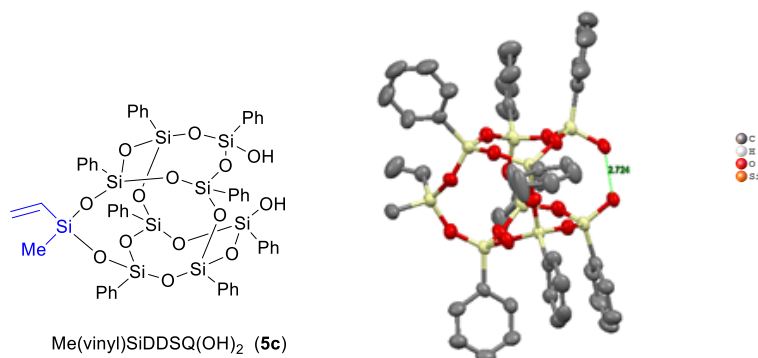


Figure 3-55: Single Crystal Structure of **5e** (Displacement ellipsoid contour probability drawn at 50%)

CCDC 1986063 contains the supplementary crystallographic data for this paper. The data can be obtained free of charge from The Cambridge Crystallographic Data Centre via www.ccdc.cam.ac.uk/structures. There is a single molecule in the asymmetric unit, which is represented by the reported sum formula. In other words: Z is 4 and Z' is 1.

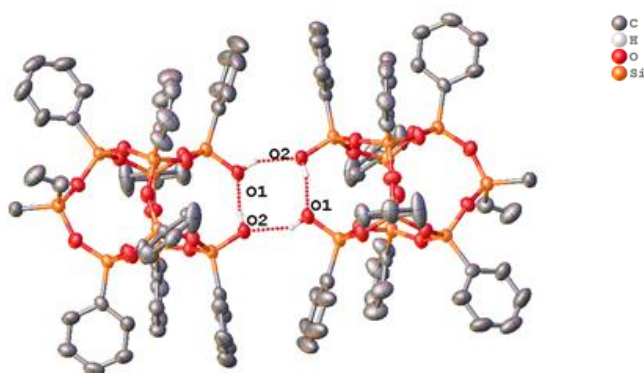


Figure 3-56: The following hydrogen bonding interactions with a maximum D-D distance of 2.9 Å and a minimum angle of 120 ° are present in **5e**: O1–O2₁: 2.721 Å, O2–O1: 2.724 Å

15-Allyl-15-methyl-1,3,5,7,9,11,13,17-octaphenyl-2,4,6,8,10,12,14,16,18,19,20,21-dodecaoxa-1,3,5,7,9,11,13,15,17-nonasilatetracyclo[9.7.1.15,17.17,13]henicosane-3,9-diol (5f)

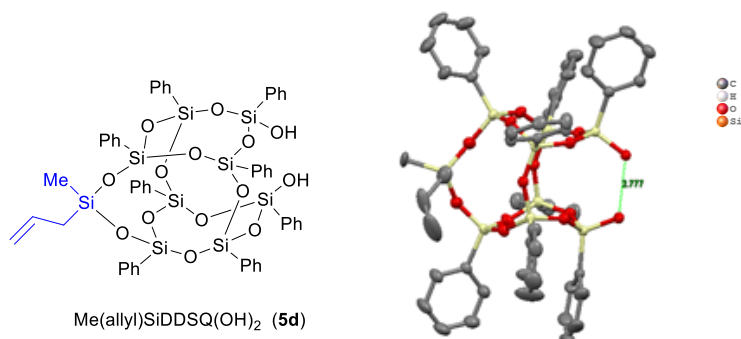


Figure 3-57: Single Crystal Structure of **5f** (Displacement ellipsoid contour probability drawn at 50%)

Crystal structure for **REM221BB** does not clearly determine if this is dimethyl, diAllyl or methyl-Allyl substituted on the Si atom. X-ray Diffraction model suggests mixture but need more chemical information to know for sure. There is a single molecule in the asymmetric unit, which is represented by the reported sum formula. In other words: Z is 4 and Z' is 1.

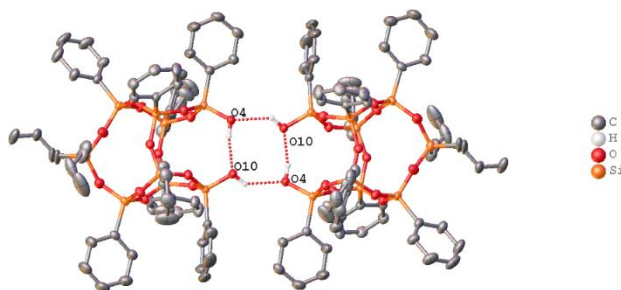


Figure 3-58: The following hydrogen bonding interactions with a maximum D-D distance of 2.9 Å and a minimum angle of 120 ° are present in REM221BB: O4–O10: 2.777 Å, O10–O4₁: 2.787 Å

NMR and Mass Spectra of Completely Condensed Asymmetric D₂T₈
Silsesquioxanes

9-(3-Isocyanatopropyl)-9,19-dimethyl-1,3,5,7,11,13,15,17-octaphenyl-2,4,6,8,10,12,14,16,18,20,21,22,23,24-tetradecaoxa-1,3,5,7,9,11,13,15,17,19-decasilapentacyclo-[11.7.1. 13,11.15,17.17,15]tetracosane. (**7a**)

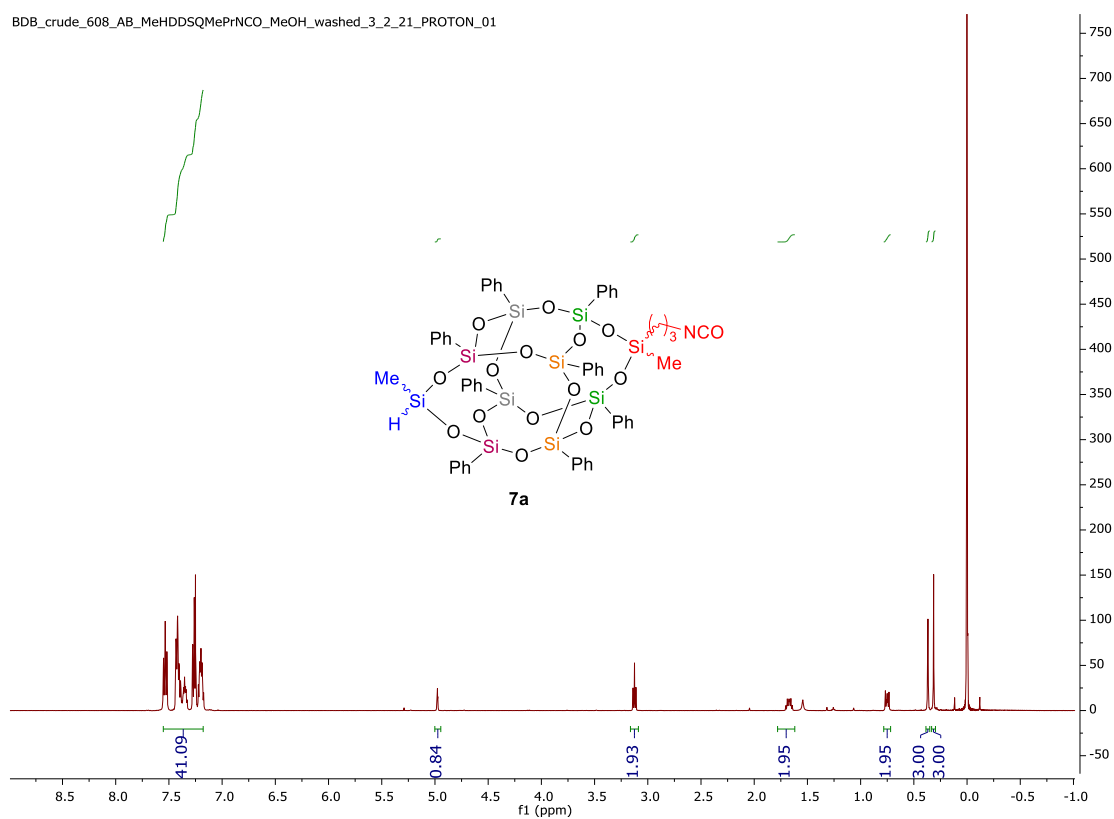


Figure 3-59: ¹H NMR (CDCl₃ + 1%TMS, 500 MHz)

BDB_crude_608_AB_MeHDDSQMePrNCO_MeOH_washed_3_2_21_CARBON_01

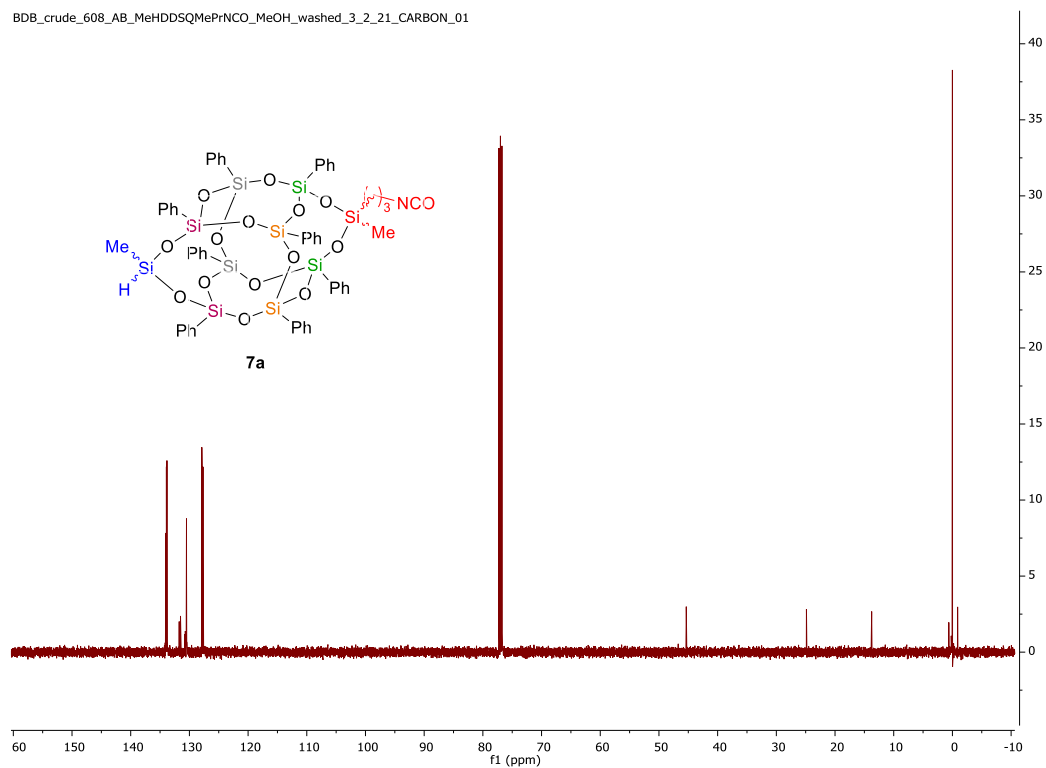


Figure 3-60: ^{13}C NMR (CDCl_3 + 1%TMS, 126 MHz)

BDB_crude_608_AB_MeHDDSQMePrNCO_MeOH_washed_3_2_21_s2pul_01

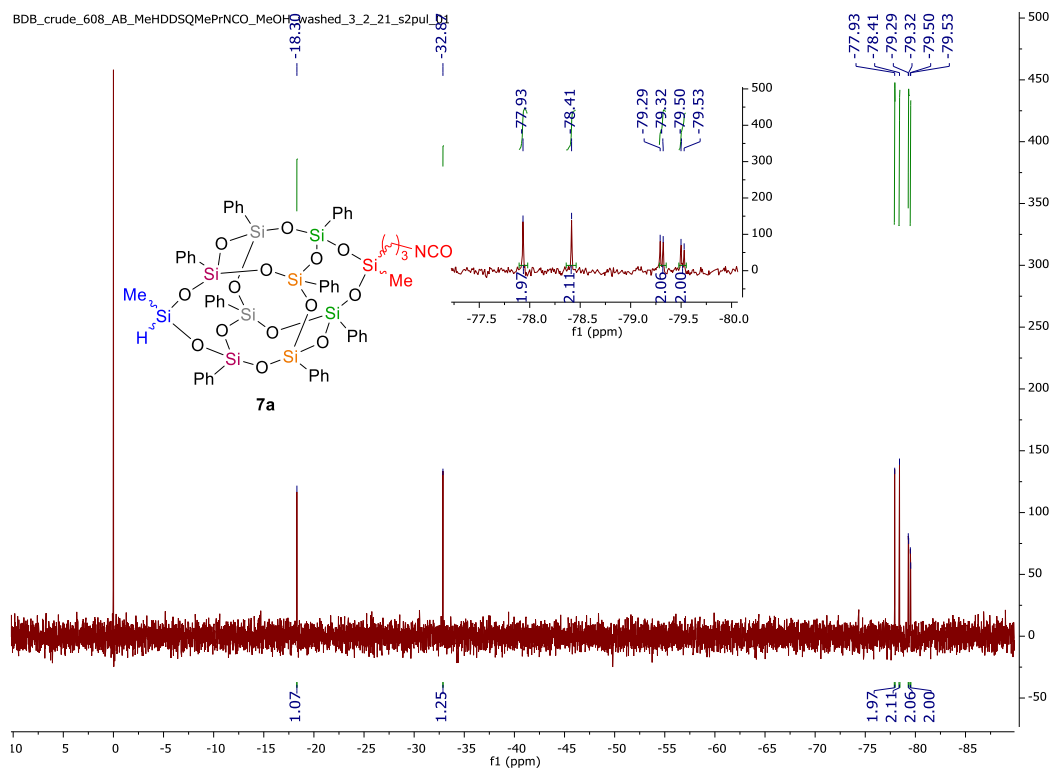


Figure 3-61: ^{29}Si NMR (CDCl_3 + 1%TMS, 99 MHz)

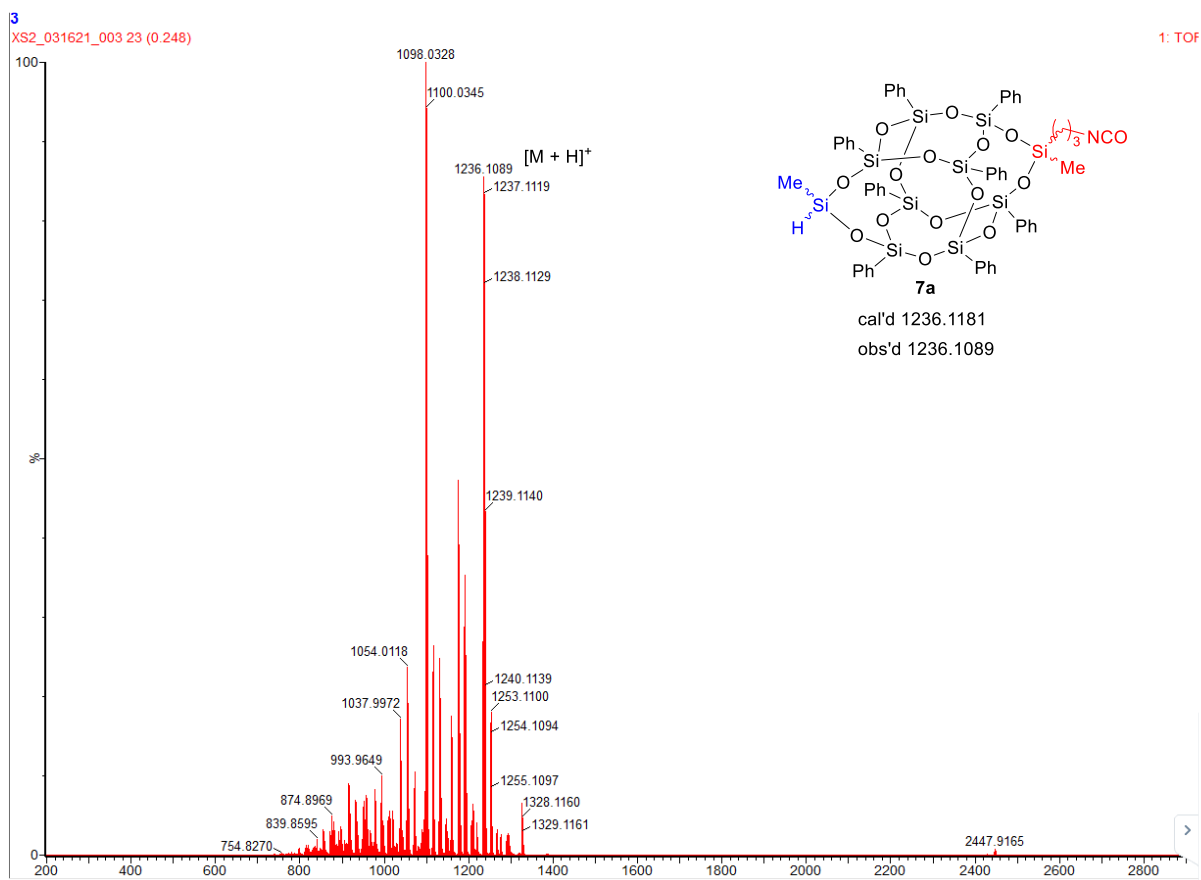


Figure 3-62: Mass spec of 7a

9,9,19-Trimethyl-1,3,5,7,11,13,15,17-octaphenyl-19-vinyl-2,4,6,8,10,12,14,16,18,20,21,22,23,24-tetradeca-1,3,5,7,9,11,13,15,17,19-decasilapentacyclo[11.7.1.13,11.15,17.17,15]tetracosane. (**7b**)

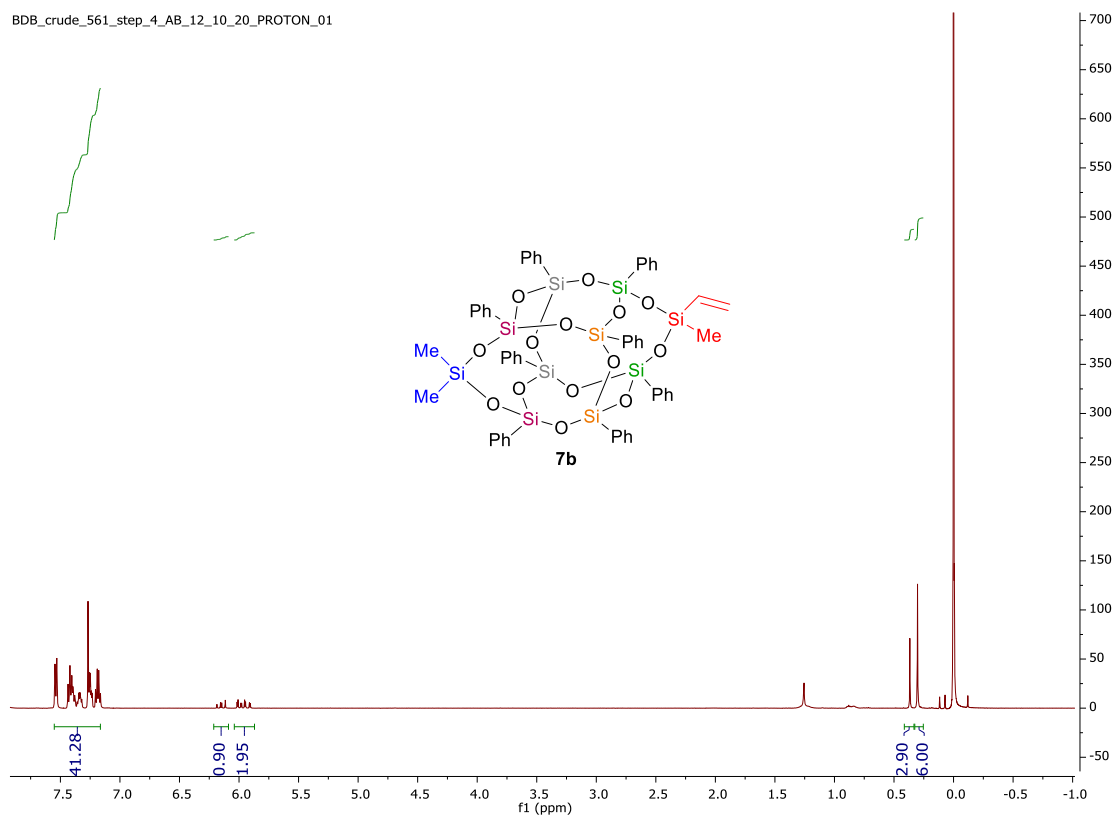
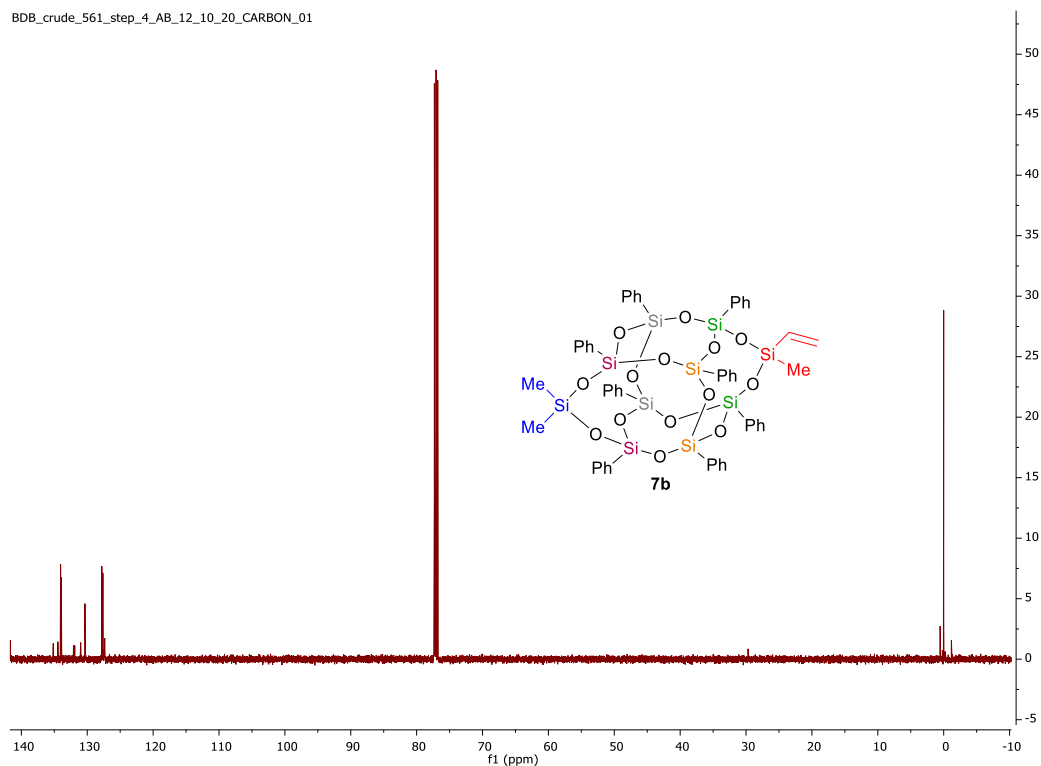
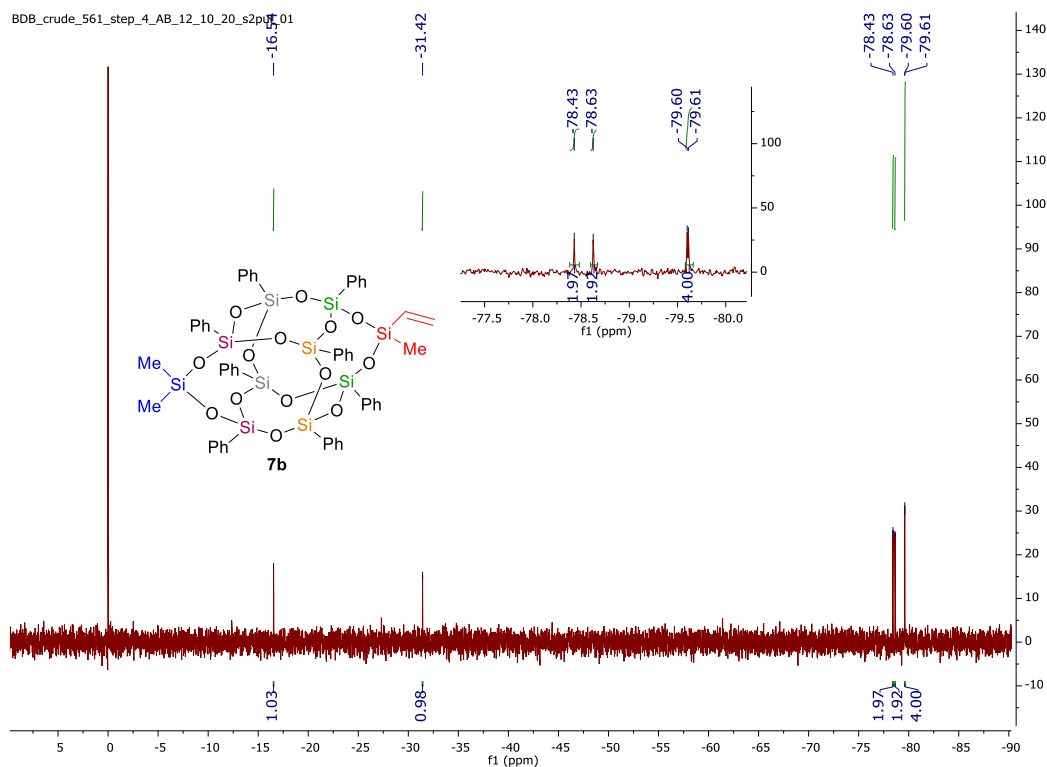


Figure 3-63: ^1H NMR (CDCl₃ + 1%TMS, 500 MHz)

BDB_crude_561_step_4_AB_12_10_20_CARBON_01



BDB_crude_561_step_4_AB_12_10_20_s2p01



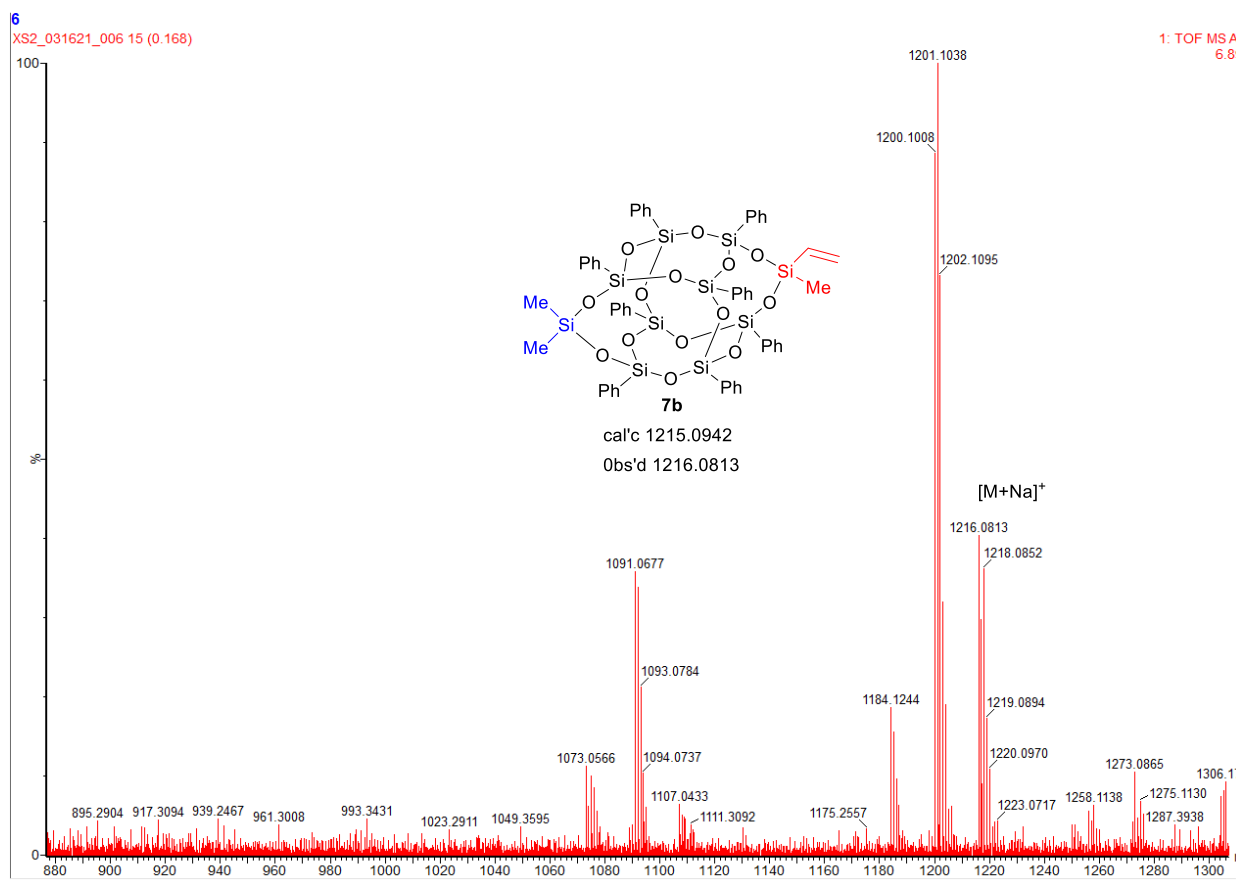


Figure 3-66: Mass spec of **7b**

9-cyclohexyl-9,19,19-trimethyl-1,3,5,7,11,13,15,17-octaphenyl-2,4,6,8,10,12,14,16,18,20,21,22,23,24-tetradeca-oxa-1,3,5,7,9,11,13,15,17,19-decasilapentacyclo[11.7.1.1.3,11.1.5,17,15]tetracosane (**7c**)

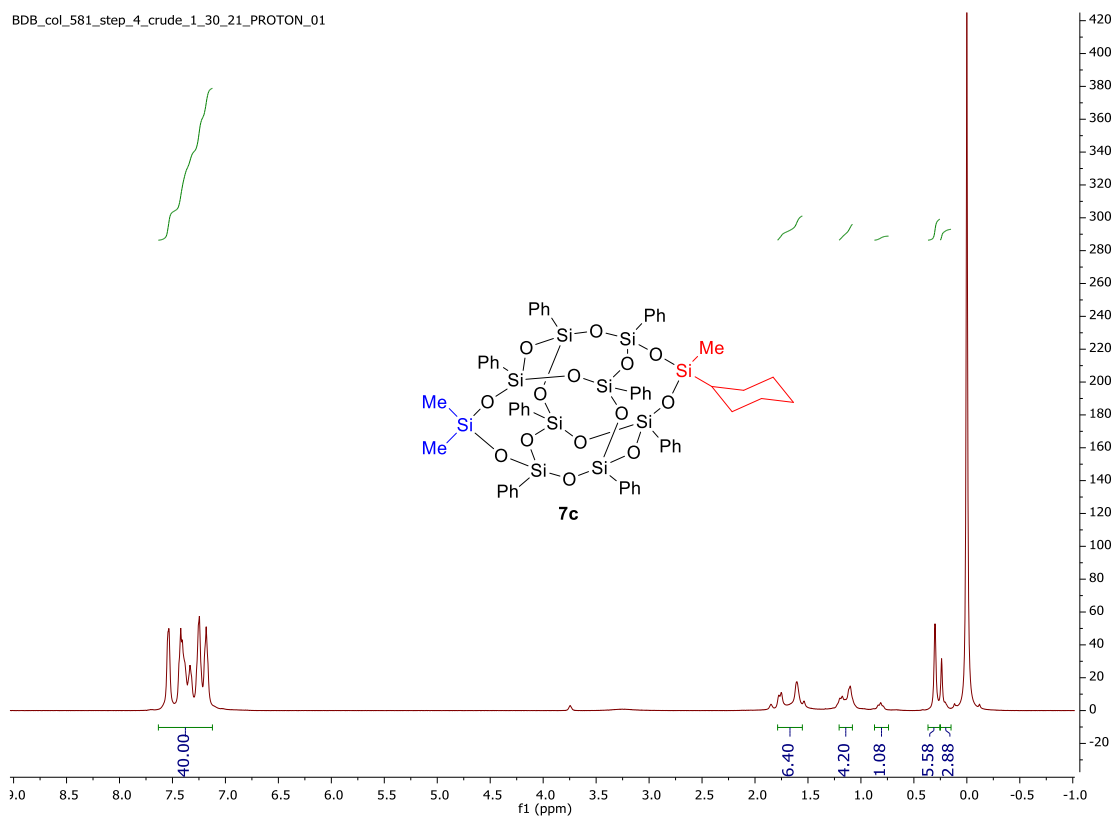


Figure 3-67: ^1H NMR (CDCl₃ + 1%TMS, 500 MHz)

BDB_col_581_step_4_crude_1_30_21_CARBON_01

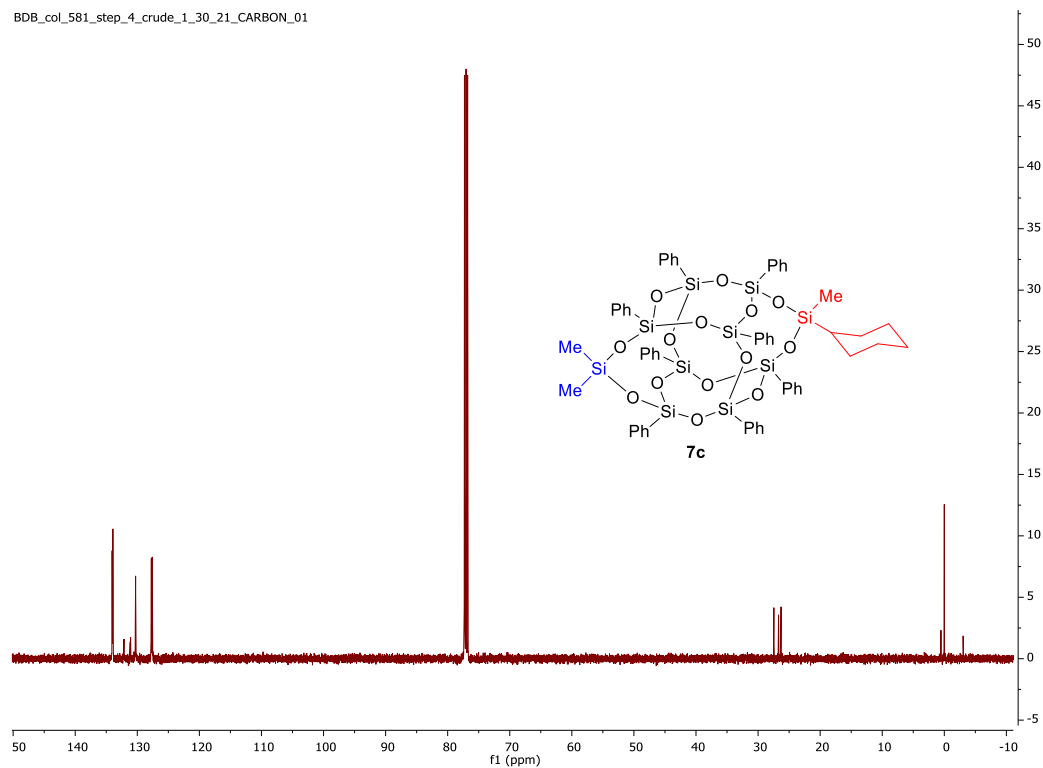


Figure 3-68: ^{13}C NMR (CDCl_3 + 1%TMS, 126 MHz)

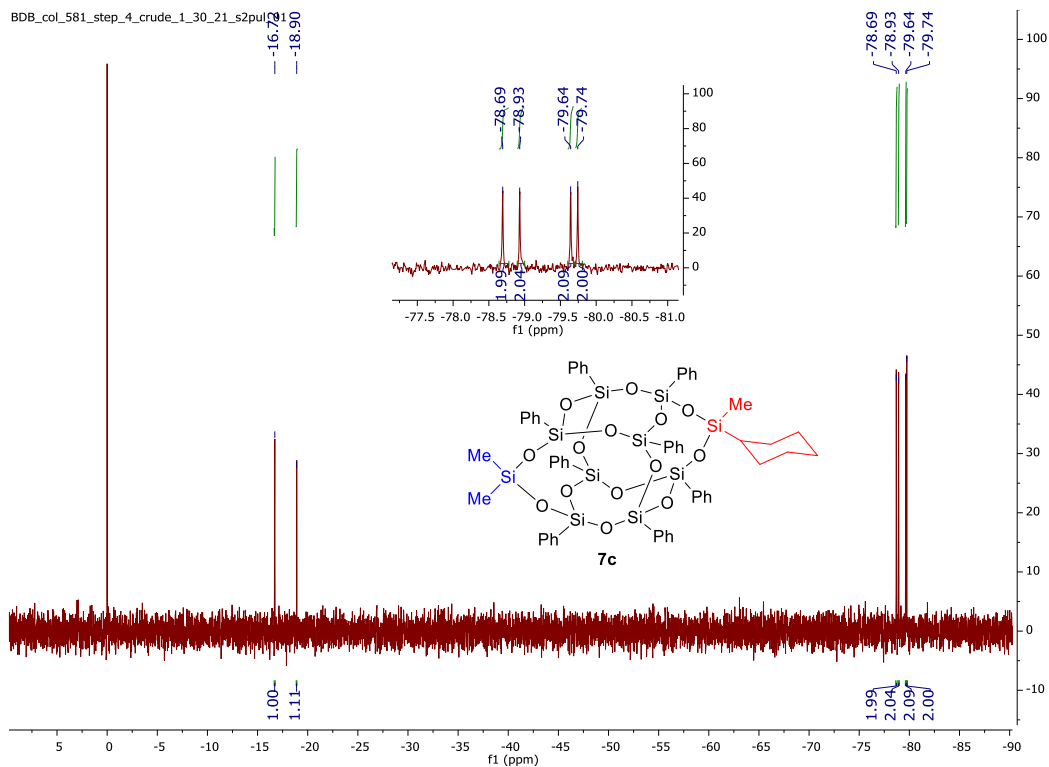


Figure 3-69: ^{29}Si NMR (CDCl_3 + 1%TMS, 99 MHz)

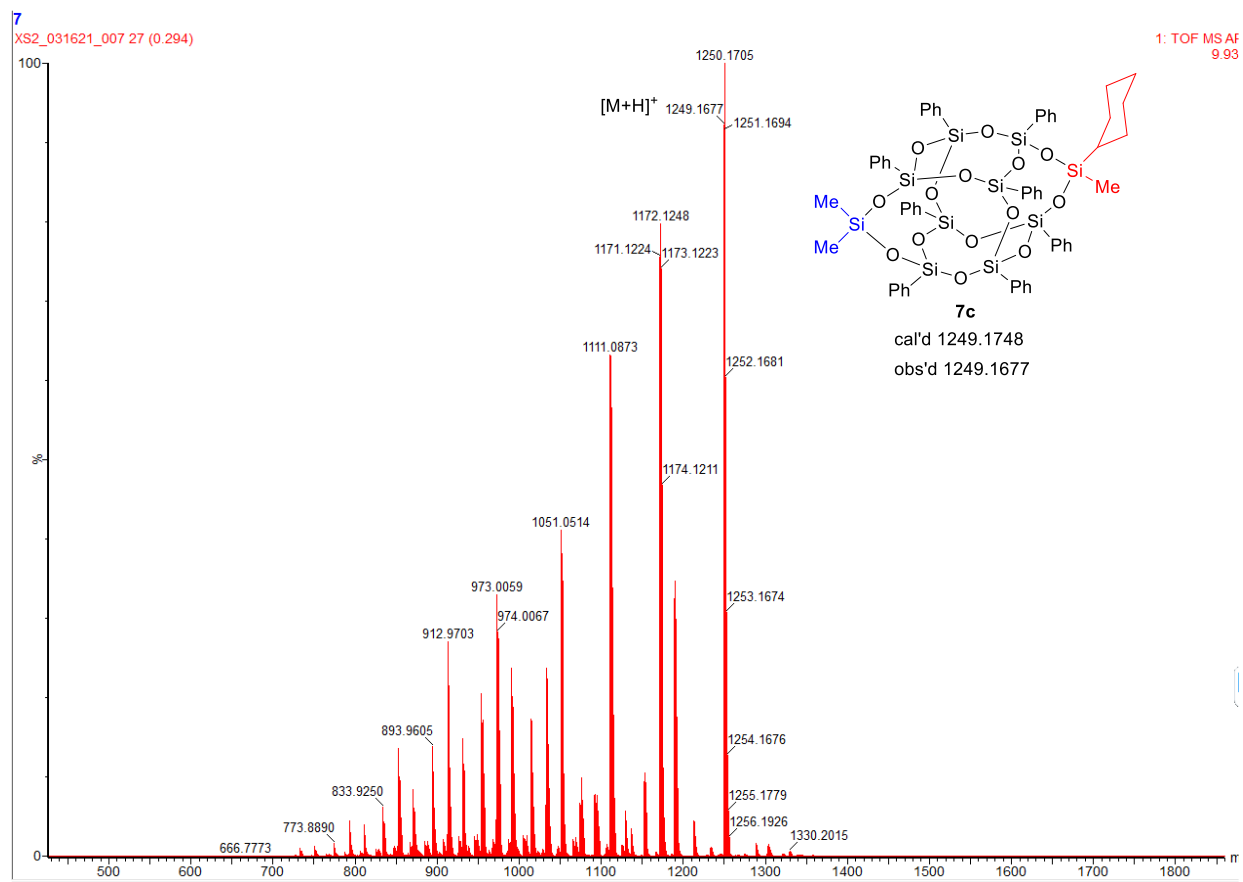


Figure 3-70: Mass spec of **7c**

9,9-Diethyl-19,19-dimethyl-1,3,5,7,11,13,15,17-octaphenyl-2,4,6,8,10,12,14,16,18,20,
21,22,23,24-tetradeca-1,3,5,7,9,11,13,15,17,19-decasilapentacyclo[11.7.1.13,
11.15, 17.17,15]tetracosane (**7d**)

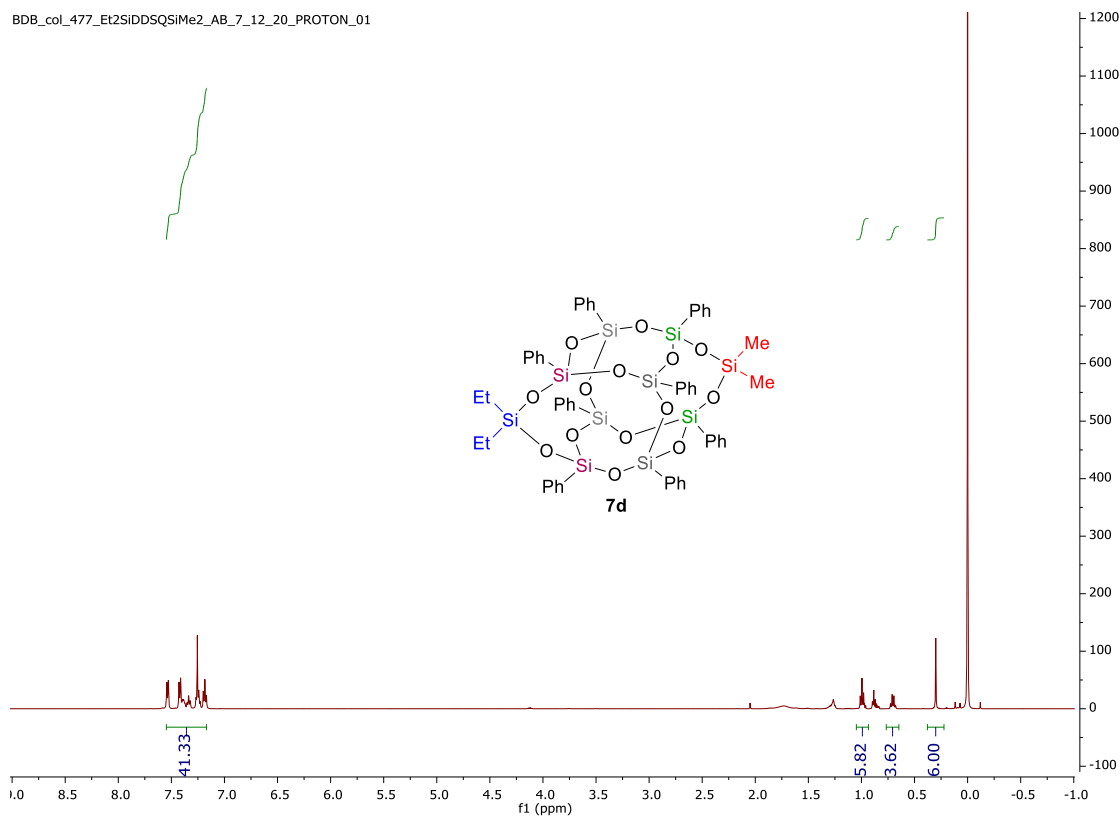


Figure 3-71: ^1H NMR (CDCl₃ + 1%TMS, 500 MHz)

BDB_col_477_Et2SIDDSSiMe2_AB_7_12_20_CARBON_01

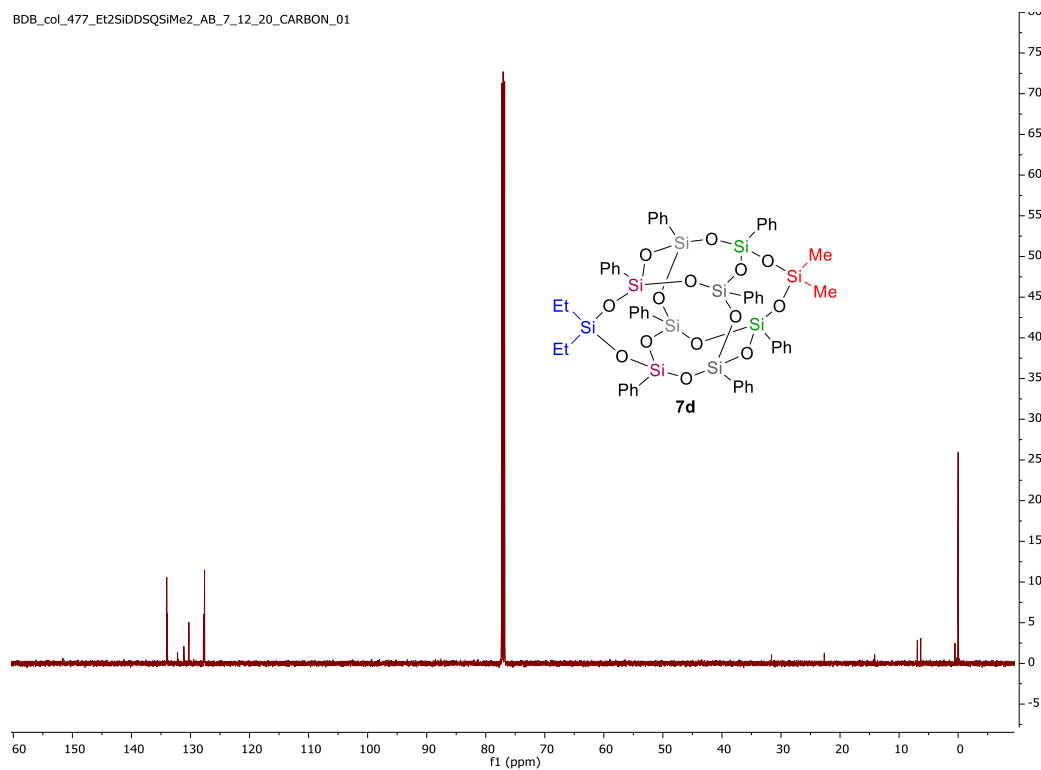


Figure 3-72: ¹³C NMR (CDCl₃ + 1%TMS, 126 MHz)

BDB_col_477_Et2SIDDSSiMe2_AB_7_12_20_SILICON_01

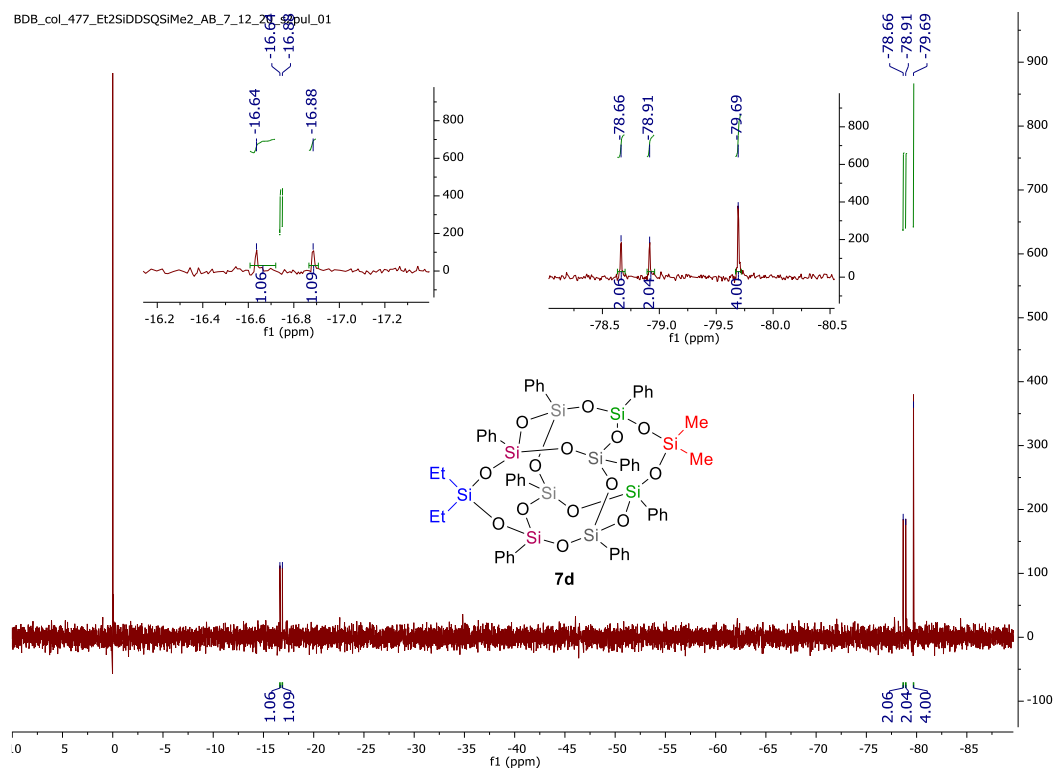


Figure 3-73: ²⁹Si NMR (CDCl₃ + 1%TMS, 99 MHz)

Characteristic Single Crystal Structure of Compounds 7

9-(3-isocyanatopropyl)-9,19-dimethyl-1,3,5,7,11,13,15,17-octaphenyl-2,4,6,8,10,12,14,16,18,20,21,22,23,24-tetradeca-oxa-1,3,5,7,9,11,13,15,17,19-decasilapentacyclo[11.7.1.13,11.15,17.17,15]tetracosane (**7a**)

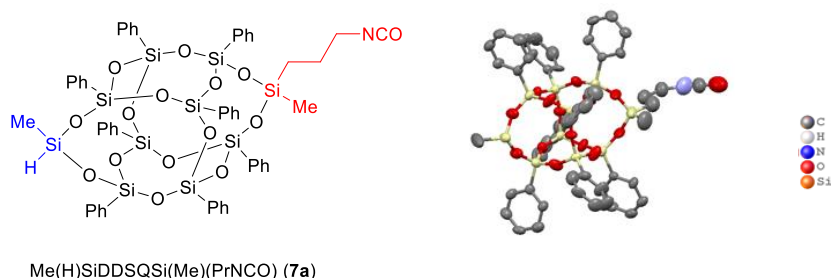


Figure 3-74: Single Crystal Structure of **7a** (Displacement ellipsoid contour probability drawn at 50%)

CCDC 2073474 contains the supplementary crystallographic data for **7a**. The data can be obtained free of charge from The Cambridge Crystallographic Data Centre via www.ccdc.cam.ac.uk/structures. The value of Z' is 0.5. This means that only half of the formula unit is present in the asymmetric unit, with the other half consisting of symmetry equivalent atoms. The Flack parameter was refined to 0.30(8). Determination of absolute structure using Bayesian statistics on Bijvoet differences using the Olex2 results in 0.35(3).

Table 3-5: Crystal Data and Structure Refinement for Asymmetric DDSQ **7a**

Compound 7a	REM321B	Compound 7a	REM321B
Formula	C ₅₄ H ₅₈ NO ₁₅ Si ₁₀	Z	2
CCDC	2073474	Z'	0.5
Dcalc./ g cm ⁻³	1.389	Wavelength/Å	1.54184
m/mm ⁻¹	2.649	Radiation type	Cu Kα
Formula Weight	1241.91	$\theta_{min}/^\circ$	3.791
Colour	colourless	$\theta_{max}/^\circ$	76.306
Shape	block	Measured Refl's.	10468
Size/mm ³	0.12×0.10×0.10	Indep't Refl's	4310
T/K	100.00(10)	Refl's I≥2 σ(I)	3732
Crystal System	monoclinic	R _{int}	0.0336
Flack Parameter	0.30(8)	Parameters	382
Hoofit Parameter	0.35(3)	Restraints	11
Space Group	Im	Largest Peak	0.627
a/Å	10.0891(4)	Deepest Hole	-0.846
b/Å	20.9814(8)	GooF	1.056
c/Å	14.0991(6)	wR ₂ (all data)	0.1737
α/°	90	wR ₂	0.1643
β/°	95.784(4)	R ₁ (all data)	0.0671
γ/°	90	R ₁	0.0589
V/Å ³	2969.4(2)		

REFERENCES

REFERENCES

- (1) Han, S.-J.; Tang, J.; Kumar, B.; Falk, A.; Farmer, D.; Tulevski, G.; Jenkins, K.; Afzali, A.; Oida, S.; Ott, J.; *et al.* High-Speed Logic Integrated Circuits with Solution-Processed Self-Assembled Carbon Nanotubes. *Nat. Nanotechnol.* **2017**, *12*, 861.
- (2) Harrison, P. G. Silicate Cages: Precursors to New Materials. *J. Organomet. Chem.* **1997**, *542*, 141–183.
- (3) Feher, F. J.; Newman, D. A.; Walzer, J. F. Silsesquioxanes as Models for Silica Surfaces. *J. Am. Chem. Soc.* **1989**, *111*, 1741–1748.
- (4) Feher, F. J.; Terroba, R.; Ziller, J. W. Base-Catalyzed Cleavage and Homologation of Polyhedral Oligosilsesquioxanes. *Chem. Commun.* **1999**, *0*, 2153–2154.
- (5) Feher, F. J.; Budzichowski, T. A.; Blanski, R. L.; Weller, K. J.; Ziller, J. W. Facile Syntheses of New Incompletely Condensed Polyhedral Oligosilsesquioxanes: [(c-C₅H₉)₇Si₇O₉(OH)₃], [(c-C₇H₁₃)₇Si₇O₉(OH)₃], and [(c-C₇H₁₃)₆Si₆O₇(OH)₄]. *Organometallics* **1991**, *10*, 2526–2528.
- (6) Feher, F. J.; Soulivong, D.; Nguyen, F.; Ziller, J. W. A New Route to Heterosilsesquioxane Frameworks. *Angew. Chem. Int. Ed Engl.* **1998**, *37*, 2663–2666.
- (7) Feher, F. J.; Soulivong, D.; Nguyen, F. Practical Methods for Synthesizing Four Incompletely Condensed Silsesquioxanes from a Single R₈Si₈O₁₂ Framework. *Chem. Commun.* **1998**, 1279–1280.
- (8) Feher, F. J.; Terroba, R.; Ziller, J. W. A New Route to Incompletely-Condensed Silsesquioxanes: Base-Mediated Cleavage of Polyhedral Oligosilsesquioxanes. *Chem. Commun.* **1999**, 2309–2310.
- (9) Abbenhuis, H. C. L.; Krijnen, S.; van Santen, R. A. Modelling the Active Sites of Heterogeneous Titanium Epoxidation Catalysts Using Titanium Silasequioxanes: Insight into Specific Factors That Determine Leaching in Liquid-Phase Processes. *Chem. Commun.* **1997**, 331–332.
- (10) Feher, F. J.; Wyndham, K. D.; Baldwin, R. K.; Soulivong, D.; Ziller, J. W.; Lichtenhan, J. D.; Lichtenhan, J. D. Methods for Effecting Monofunctionalization of (CH₂=CH)₈Si₈O₁₂. *Chem. Commun.* **1999**, 1289–1290.
- (11) Liu, H.; Kondo, S.-I.; Tanaka, R.; Oku, H.; Unno, M. Erratum to “A Spectroscopic Investigation of Incompletely Condensed Polyhedral Oligomeric Silsesquioxanes (POSS-Mono-OI, POSS-Diol and POSS-Triol): Hydrogen-Bonded Interaction and Host–guest Complex” *J. Organomet. Chem.* **2008**, *693*, 1301–1308. *J. Organomet. Chem.* **2010**, *695*, 642.

- (12) Chandrasekhar, V.; Boomishankar, R.; Nagendran, S. Recent Developments in the Synthesis and Structure of Organosilanol. *Chem. Rev.* **2004**, *104*, 5847–5910.
- (13) Feher, F. J. Controlled Cleavage of $R_8Si_8O_{12}$ Frameworks: A Revolutionary New Method for Manufacturing Precursors to Hybrid Inorganic–organic Materials. *Chem. Commun.* **1998**, 399–400.
- (14) Morimoto, Y.; Watanabe, K.; Ootake, N.; Inagaki, J. I.; Yoshida, K.; Ohguma, K. Silsesquioxane Derivatives and Process for Production Thereof. 20040249103A1, 2004.
- (15) Lee, D. W.; Kawakami, Y. Incompletely Condensed Silsesquioxanes: Formation and Reactivity. *Polym. J.* **2007**, *39*, 230–238.
- (16) Harada, A.; Koge, S.; Ohshita, J.; Kaneko, Y. Preparation of a Thermally Stable Room Temperature Ionic Liquid Containing Cage-Like Oligosilsesquioxane with Two Types of Side-Chain Groups. *Bull. Chem. Soc. Jpn.* **2016**, *89*, 1129–1135.
- (17) Bagheri, H.; Soofi, G.; Javanmardi, H.; Karimi, M. A 3D Nanoscale Polyhedral Oligomeric Silsesquioxanes Network for Microextraction of Polycyclic Aromatic Hydrocarbons. *Mikrochim. Acta* **2018**, *185*, 418.
- (18) Li, Z.; Yang, R. Synthesis, Characterization, and Properties of a Polyhedral Oligomeric Octadiphenylsulfonylsilsesquioxane. *J. Appl. Polym. Sci.* **2014**, *131*.
- (19) Feher, F.; Ziller, J.; Others. A New Route to Incompletely Condensed Silsesquioxanes: Acid-Mediated Cleavage and Rearrangement of $(C-C_6H_{11})_6Si_6O_9$ to $C_2-[(C-C_6H_{11})_6Si_6O_8X_2]$. *Chem. Commun.* **1999**, 1705–1706.
- (20) Feher, F. J.; Soulivong, D.; Nguyen, F. Practical Methods for Synthesizing Four Incompletely Condensed Silsesquioxanes from a Single $R_8Si_8O_{12}$ Framework. *Chem. Commun.* **1998**, 1279–1280.
- (21) Zhang, W.; Li, X.; Yang, R. Flame Retardancy Mechanisms of Phosphorus-Containing Polyhedral Oligomeric Silsesquioxane (DOPO-POSS) in Polycarbonate/acrylonitrile-Butadiene-Styrene Blends. *Polym. Adv. Technol.* **2012**, *23*, 588–595.
- (22) Fina, A.; Monticelli, O.; Camino, G. POSS-Based Hybrids by Melt/reactive Blending. *J. Mater. Chem.* **2010**, *20*, 9297–9305.
- (23) Huo, L.; Wu, X.; Tian, C.; Gao, J. Thermal, Mechanical, and Electrical Properties of Alkyd-Epoxy Resin Nanocomposites Modified with 3-Glycidyloxypropyl-POSS. *Polym. Plast. Technol. Eng.* **2018**, *57*, 371–379.
- (24) Kowalewska, A. Self-Assembling Polyhedral Silsesquioxanes - Structure and Properties. *Curr. Org. Chem.* **2017**, *21*, 1243–1264.

- (25) Bilyachenko, A. N.; Kulakova, A. N.; Levitsky, M. M.; Petrov, A. A.; Korlyukov, A. A.; Shul'pina, L. S.; Khrustalev, V. N.; Dorovatovskii, P. V.; Vologzhanina, A. V.; Tsareva, U. S.; *et al.* Unusual Tri-, Hexa-, and Nonanuclear Cu(II) Cage Methylsilsesquioxanes: Synthesis, Structures, and Catalytic Activity in Oxidations with Peroxides. *Inorg. Chem.* **2017**, *56*, 4093–4103.
- (26) Wheeler, P. A.; Fu, B. X.; Lichtenhan, J. D.; Weitao, J.; Mathias, L. J. Incorporation of Metallic POSS, POSS Copolymers, and New Functionalized POSS Compounds into Commercial Dental Resins. *J. Appl. Polym. Sci.* **2006**, *102*, 2856–2862.
- (27) Wei, K.; Wang, L.; Li, L.; Zheng, S. Synthesis and Characterization of Bead-like Poly(N -Isopropylacrylamide) Copolymers with Double Decker Silsesquioxane in the Main Chains. *Polym. Chem.* **2015**, *6*, 256–269.
- (28) Walczak, M.; Januszewski, R.; Majchrzak, M.; Kubicki, M.; Dudziec, B.; Marciniec, B. Unusual Cis and Trans Architecture of Dihydrofunctional Double-Decker Shaped Silsesquioxane and Synthesis of Its Ethyl Bridged π -Conjugated Arene Derivatives. *New J. Chem.* **2017**, *41*, 3290–3296.
- (29) Schoen, B. W.; Lira, C. T.; Lee, A. Separation and Solubility of Cis and Trans Isomers in Nanostructured Double-Decker Silsesquioxanes. *J. Chem. Eng. Data* **2014**, *59*, 1483–1493.
- (30) Schoen, B. W.; Holmes, D.; Lee, A. Identification and Quantification of Cis and Trans Isomers in Aminophenyl Double-Decker Silsesquioxanes Using ^1H - ^{29}Si gHMBC NMR: Quantification of Cis and Trans Isomers in Double-Decker Silsesquioxanes. *Magn. Reson. Chem.* **2013**, *51*, 490–496.
- (31) Vogelsang, D. F.; Dannatt, J. E.; Schoen, B. W.; Maleczka, R. E., Jr; Lee, A. Phase Behavior of Cis--Trans Mixtures of Double-Decker Shaped Silsesquioxanes for Processability Enhancement. *ACS Appl. Nano Mater.* **2019**, *2*, 1223–1231.
- (32) Vogelsang, D. F.; Dannatt, J. E.; Maleczka, R. E.; Lee, A. Separation of Asymmetrically Capped Double-Decker Silsesquioxanes Mixtures. *Polyhedron* **2018**, *155*, 189–193.
- (33) Vogelsang, D. F.; Maleczka, R. E.; Lee, A. HPLC Characterization of Cis and Trans Mixtures of Double-Decker Shaped Silsesquioxanes. *Silicon Chem.* **2019**, *11*, 5–13.
- (34) Schoen, B. W. Aminophenyl Double Decker Silsesquioxanes: Spectroscopic Elucidation, Physical and Thermal Characterization, and Their Applications. **2013**.
- (35) Moore, L. M. J.; Zavala, J. J.; Lamb, J. T.; Reams, J. T.; Yandek, G. R.; Guenther, A. J.; Haddad, T. S.; Ghiassi, K. B. Bis-Phenylethynyl Polyhedral Oligomeric Silsesquioxanes: New High-Temperature, Processable Thermosetting Materials. *RSC Adv.* **2018**, *8*, 27400–27405.

- (36) Feher, F. J.; Weller, K. J. Synthesis and Characterization of Labile Spherosilicates: $[(\text{Me}_3\text{SnO})_8\text{Si}_8\text{O}_{12}]$ and $[(\text{Me}_4\text{SbO})_8\text{Si}_8\text{O}_{12}]$. *Inorg. Chem.* **1991**, *30*, 880–882.
- (37) Abbenhuis, H. C. L. Advances in Homogeneous and Heterogeneous Catalysis with Metal-Containing Silsesquioxanes. *Chem.--Eur. J.* **2000**, *6*, 25–32.
- (38) Zhang, L.; Abbenhuis, H. C. L.; Gerritsen, G.; Bhriain, N. N.; Pieter C M; Mezari, B.; Han, W.; van Santen, R. A.; Yang, Q.; Li, C. An Efficient Hybrid, Nanostructured, Epoxidation Catalyst: Titanium Silsesquioxane–Polystyrene Copolymer Supported on SBA-15. *Chem. Eur. J.* **2007**, *13*, 1210–1221.
- (39) Ronchi, M.; Pizzotti, M.; Biroli, A. O.; Macchi, P.; Lucenti, E.; Zucchi, C. Synthesis and Structural Characterization of Functionalized Cyclotetrasiloxane Rings $[\text{4-RC}_6\text{H}_4\text{Si}(\text{O})\text{OR}']_4$ ($\text{R} = \text{Cl, Br, CHCH}_2, \text{CH}_2\text{Cl}$; $\text{R}' = \text{Na, SiMe}_3$) as Scaffolds for the Synthesis of Models of a Silica Bound Monolayer of Fluorescent or Second Order NLO Active Organic Chromophores. *J. Organomet. Chem.* **2007**, *692*, 1788–1798.
- (40) Cordes, D. B.; Lickiss, P. D. Preparation and Characterization of Polyhedral Oligosilsesquioxanes. In *Applications of Polyhedral Oligomeric Silsesquioxanes*; Hartmann-Thompson, C., Ed.; Springer Netherlands: Dordrecht, **2011**, 47–133.
- (41) Dudziec, B.; Marciniak, B. Double-Decker Silsesquioxanes: Current Chemistry and Applications. *Curr. Org. Chem.* **2017**, *21*, 2794–2813.
- (42) Xu, S.; Zhao, B.; Wei, K.; Zheng, S. Organic-Inorganic Polyurethanes with Double Decker Silsesquioxanes in the Main Chains: Morphologies, Surface Hydrophobicity, and Shape Memory Properties. *J. Polym. Sci. Part B: Polym. Phys.* **2018**, *56*, 893–906.
- (43) Ayandele, E.; Sarkar, B.; Alexandridis, P. Polyhedral Oligomeric Silsesquioxane (POSS)-Containing Polymer Nanocomposites. *Nanomaterials* **2012**, *2*, 445–475.
- (44) Laine, R. M.; Roll, M. F. Polyhedral Phenylsilsesquioxanes. *Macromolecules* **2011**, *44*, 1073–1109.
- (45) Jiang, Q.; Zhang, W.; Hao, J.; Wei, Y.; Mu, J.; Jiang, Z. A Unique “cage–cage” Shaped Hydrophobic Fluoropolymer Film Derived from a Novel Double-Decker Structural POSS with a Low Dielectric Constant. *J. Mater. Chem.* **2015**, *3*, 11729–11734.
- (46) Wu, S.; Hayakawa, T.; Kikuchi, R.; Grunzinger, S. J.; Kakimoto, M.-A.; Oikawa, H. Synthesis and Characterization of Semiaromatic Polyimides Containing POSS in Main Chain Derived from Double-Decker-Shaped Silsesquioxane. *Macromolecules* **2007**, *40*, 5698–5705.
- (47) Hoque, M. A.; Kakihana, Y.; Shinke, S.; Kawakami, Y. Polysiloxanes with Periodically Distributed Isomeric Double-Decker Silsesquioxane in the Main Chain. *Macromolecules* **2009**, *42*, 3309–3315.

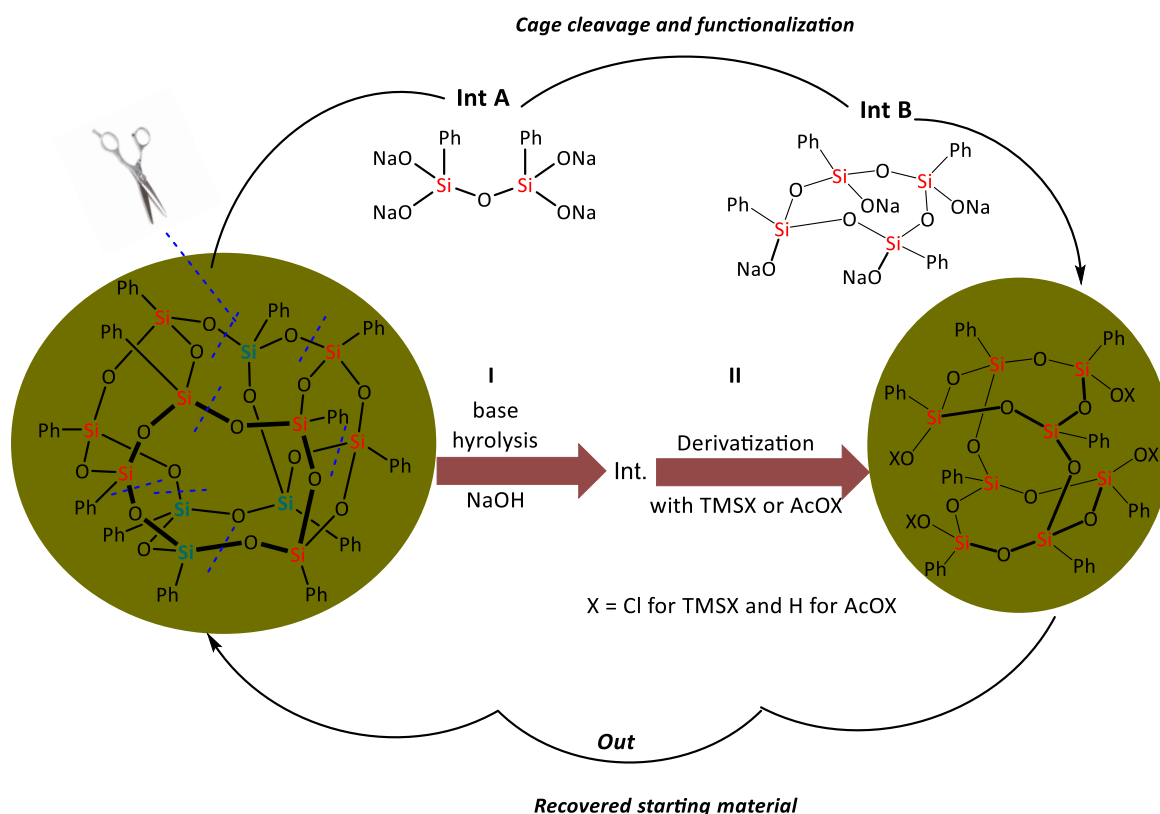
- (48) Endo, H.; Takeda, N.; Unno, M. Synthesis and Properties of Phenylsilsesquioxanes with Ladder and Double-Decker Structures. *Organometallics* **2014**, *33*, 4148–4151.
- (49) Barry, B.-D.; Dannatt, J. E.; King, A. K.; Lee, A.; Maleczka, R. E., Jr. A General Diversity Oriented Synthesis of Asymmetric Double-Decker Shaped Silsesquioxanes. *Chem. Commun.* **2019**, *55*, 8623–8626.
- (50) Dudziec, B.; Żak, P.; Marciniec, B. Synthetic Routes to Silsesquioxane-Based Systems as Photoactive Materials and Their Precursors. *Polymers* **2019**, *11*.
- (51) Haddad, T.; Mabry, J.; Yandek, G.; Vij, V. Peripherally Aromatic Silsesquioxanes Featuring Reactive Functionality: Synthesis and Applications US8981140, **2015**.
- (52) Liu, N.; Wei, K.; Wang, L.; Zheng, S. Organic–inorganic Polyimides with Double Decker Silsesquioxane in the Main Chains. *Polym. Chem.* **2016**, *7*, 1158–1167.
- (53) Mohamed, M. G.; Kuo, S. W. Functional Polyimide/Polyhedral Oligomeric Silsesquioxane Nanocomposites. *Polymers* **2018**, *11*.
- (54) Kickelbick, G. Hybrid Materials - Past, Present and Future, **2014**.
- (55) Kickelbick, G. Silsesquioxanes. *Struct. Bond.* **2013**, 1–28.
- (56) Żak, P.; Delaude, L.; Dudziec, B.; Marciniec, B. N-Heterocyclic Carbene-Based Ruthenium-Hydride Catalysts for the Synthesis of Unsymmetrically Functionalized Double-Decker Silsesquioxanes. *Chem. Commun.* **2018**, *54*, 4306–4309.
- (57) Kunthom, R.; Takeda, N.; Unno, M. Synthesis and Characterization of Unsymmetrical Double-Decker Siloxane (Basket Cage). *Molecules* **2019**, *24*, 4252.
- (58) Tian, K.; Luh, T.-Y.; Wang, X.; Hao, C.; Yang, X.; Li, Z.; Lai, G. Caterpillar-Shaped Polysilsesquioxanes. *Chem. Commun.* **2019**, *55*, 2613–2615.

Chapter 4.0: Base-Promoted Hydrolysis of Dodecaphenyl Silsesquioxane into Partially Condensed Octaphenyl Silsesquioxane

Badru-Deen Barry,^a Andre Lee ^{*b} and Robert E. Maleczka Jr.^{*a}. (Manuscript under preparation)

4.1 Abstract

Hydrolysis of dodecaphenylsilsesquioxane ($\text{Ph}_{12}\text{T}_{12}$) with aq. NaOH affords an intermediate, which upon derivatization with TMSCl gives a 'double-decker' shaped silsesquioxane. Time-resolved mass spectroscopic studies indicates $\text{Ph}_{12}\text{T}_{12}$ is transformed to the partially condensed octaphenyl T_8 . This is the first report of $\text{Ph}_{12}\text{T}_{12}$ as a precursor to a partially condensed lower cage framework.



Parts of this chapter is under preparation for publication in *Green Chemistry*.

4.2 Introduction

Fully condensed oligomeric silsesquioxanes can form nanosized model organosilicon compounds with a well-defined 3D inner siloxy cage, having a general formula $(\text{RSiO}_{3/2})_n$, where $n = 6, 8, 10, 12, 14$, etc.¹⁻⁷ The peripheral organic moieties, R, on the silicon vertices promote miscibility and hence allow for synthetic elaboration.^{1,8-12} Cage-like silsesquioxanes come in two variations; (i) completely condensed cages,^{3,8,13-16} e.g. **1** and **2** and (ii) their partially condensed counterparts **3** and **4** (Figure 4.1).¹⁷⁻²⁰

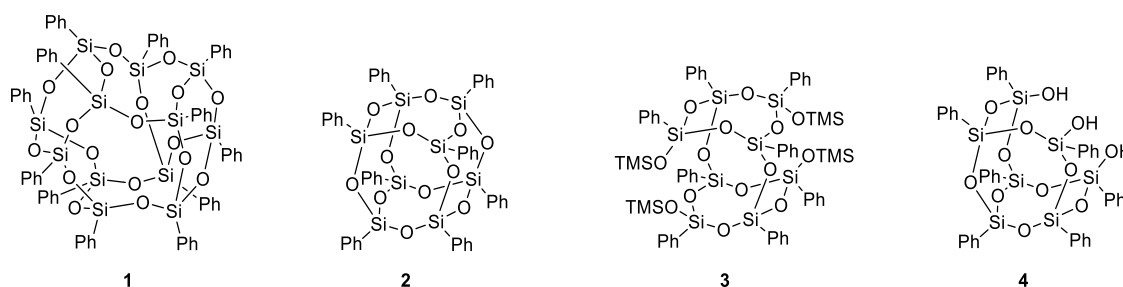


Figure 4-1: Structures of cage-like Silsesquioxanes - dodecaphenylT₁₂ (**1**), octaphenylT₈ (**2**), tetrakis(trimethylsilyl)octaphenylT₈ (**3**), and heptaphenylT₇ triol (**4**)

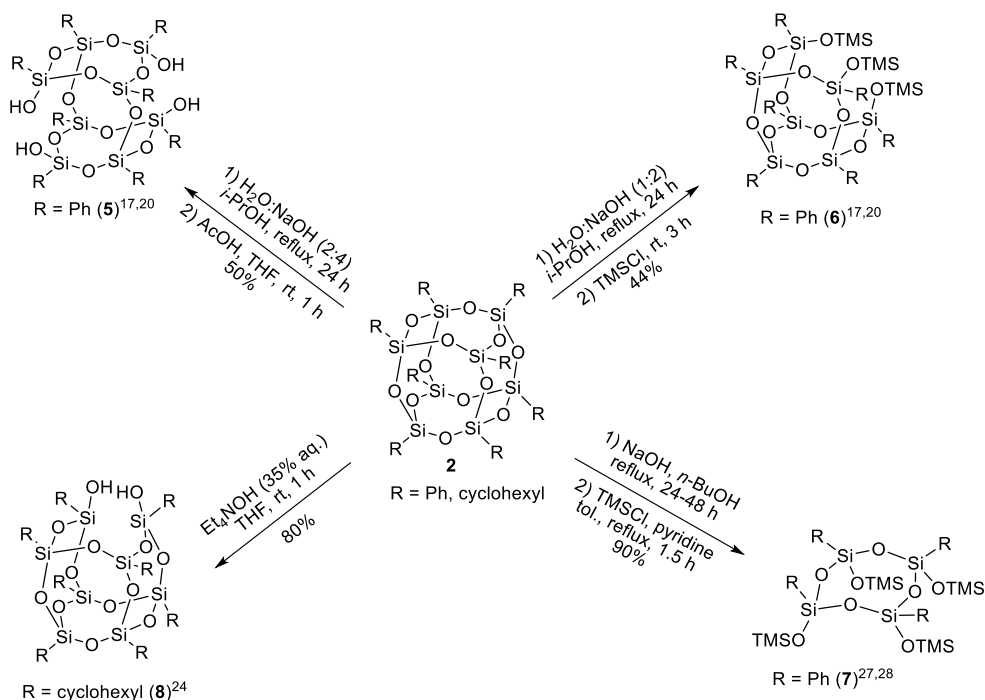
Even though both classes of compounds are pivotal building blocks for the synthesis of advanced inorganic-organic materials, the latter category is more interesting because the structures allow tunability for a range of engineering applications.^{3,10,21-23}

Several groups have cleaved completely condensed silsesquioxanes (SQ) to obtain different types of partially condensed cages (**Scheme 4.1**). Feher et al.¹⁹ reported acid¹⁹ and base²⁴ promoted partial cleavage of fully condensed $[\text{RSiO}_{3/2}]_n$ frameworks and further illustrated the manipulation of the resulting functional groups for use as precursors to inorganic-organic hybrid materials. Li and Kawakami²⁰ also reported the formation of partially condensed double-decker shaped octaphenyl silsesquioxane

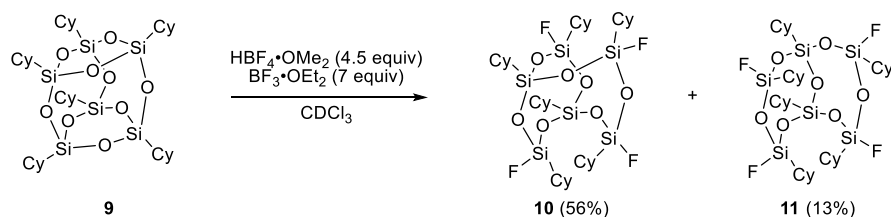
(DDSQ) from the hydrolysis of the completely condensed precursor **2**. Half cubes have also been obtained from the base hydrolysis of cubic octasilsesquioxanes.^{27, 28} For instance, Laine et al.²⁸ demonstrated the formation and transformation of the sodium phenylsiloxanolate half cube into well-defined bi-functional “Janus” cubes by directly treating a methanol solution of the salt with MeSiCl₃ followed by acid hydrolysis.

Scheme 4-1: Prior strategies for the partial cleavage of completely condensed (a) octaphenylT₈, (b) hexacyclohexylT₆

(a) Selected strategies for the cleavage of octaphenylT₈



(b) Cleavage of completely condensed hexacyclohexylT₆¹⁹



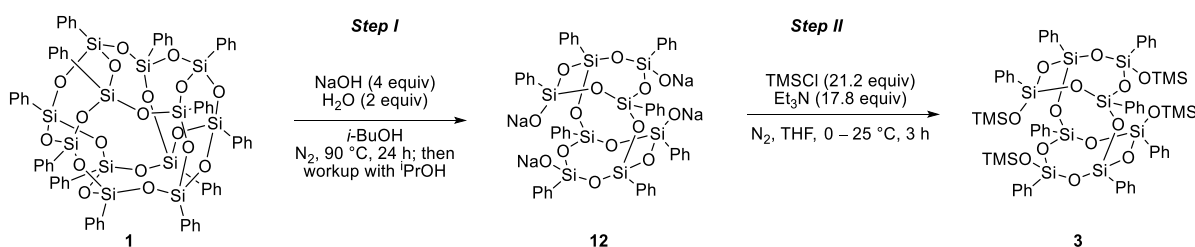
Rikowski and Marsmann²⁸ disclosed that various functional octasilsesquioxanes can undergo base catalyzed rearrangement of the cage into the higher deca- and dodeca-

analogues. Similar analogues were also reported by Ervithayasuporn et al. via the nucleophilic reaction of condensed octa-functional silsesquioxanes with substituted sodium phenoxide salts.⁶ However, to date, all syntheses of partially condensed polyhedral oligomeric silsesquioxane cages from completely condensed precursors started with T₆ or T₈ silsesquioxanes and none from condensed T₁₀ or T₁₂.^{5,19,20,24}

4.3 Research Hypothesis

Stimulated by the foregoing lacuna, and prior art on the hydrolysis of completely condensed octaphenylT₈ to yield the double-decker tetrasodium derivative,²⁰ we hypothesized that reacting completely condensed Ph₁₂T₁₂ (**1**) with NaOH could affect the selective fissure of Si-O-Si bonds. Were this to be realized, opening and/or reorganization of the cage architecture could afford discreet partially condensed products. To test this idea, Ph₁₂T₁₂ (**1**) was treated with four equivalents of aqueous NaOH in isobutanol at 90 °C for 24 h.²⁰ To aid in the identification of the reaction products, we silylated the crude reaction product with TMSCl (**Scheme 4.2**).

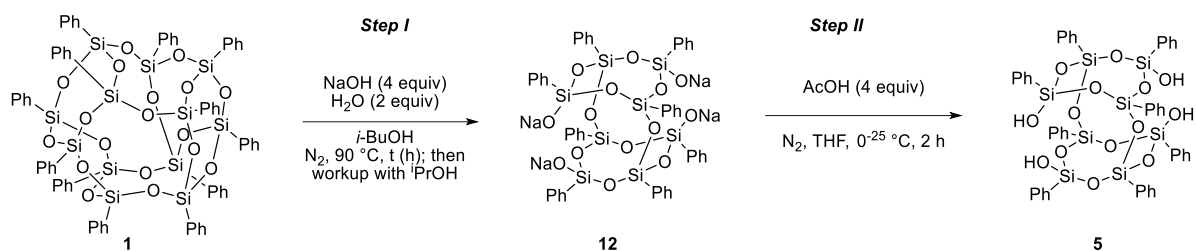
Scheme 4-2: Hydrolysis of Ph₁₂T₁₂ (**1**) for the synthesis of 5,11,14,17-tetrakis(trimethylsilyl)octaphenyltetracyclo[7.3.3.3^{3;7}]octasilsesquioxane (**3**)



This sequence resulted in the generation of a material that crystallized from hexanes at –30 °C. To our surprise, characterization of this material by ¹H, ¹³C, and ²⁹Si NMR spectroscopy, MS, and single-crystal X-ray indicated that the product was 5,11,14,17-tetrakis(trimethylsilyl)octaphenyltetracyclo[7.3.3.3^{3;7}]octasilsesquioxane (**3**).¹⁷

To better understand the process of affording **3** from Ph₁₂T₁₂ (**1**), we conducted a time-course experiment. With that information in hand, we next sought to isolate the more useful double-decker octaphenyl silsesquioxanetetraol (**5**) by protonating the resultant hydrolysis intermediate in step 1 (**Scheme 4.3**) with AcOH.¹⁷

Scheme 4-3: Base cleavage of **1** with NaOH followed by acid hydrolysis of intermediate **12** with AcOH to give **5**

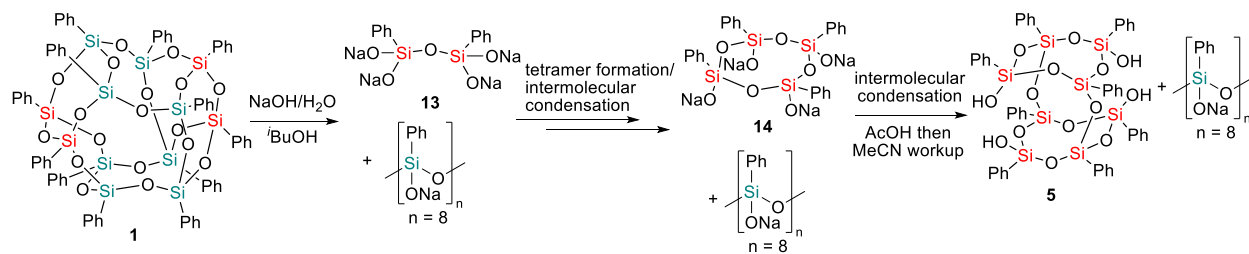


Detailed synthetic procedures, isolations and characterization techniques for all products synthesized here are described in the experimental section below.

4.4 Proposed Reaction Mechanism for the Formation of Double-decker Octaphenyl silsesquioxanetetraol (**5**)

Based on the structure of **1** and our experimental data, we suggest **5** results from first the cleavage of two Si–O–Si bonds in **1** to give linear (PhSi(ONa)₂)₂O (**13**) fragments, which dimerizes to afford the tetrameric cyclic *sym-cis* tetraphenyl tetrasiloxane species **14**. Intermolecular condensation of **14** would result in **5** (**Scheme 4.4**).

Scheme 4-4: Proposed route to **5** from **1**

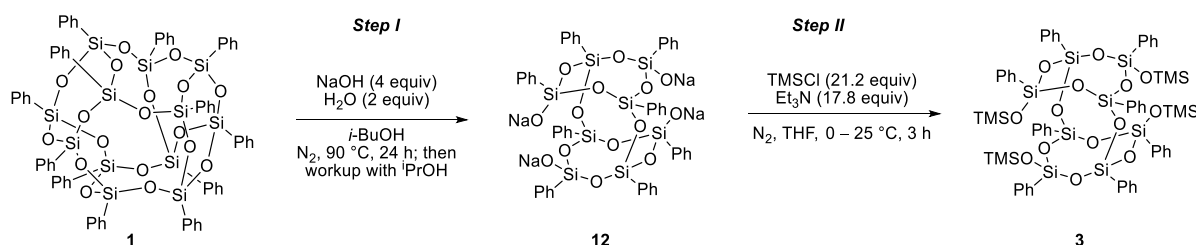


This proposal agrees with the kinetic and mechanistic studies conducted by the Hwang group¹⁴ with $\text{PhSi}(\text{OMe})_3$ as a precursor. They detected the transient $(\text{PhSi}(\text{OH})_2)\text{O}$ species and its subsequent disappearance due to formation of **1** by ^{29}Si NMR. In our case, formation of $(\text{PhSiO})_4(\text{OH})_2(\text{ONa})_2$ (**14**), which could result from the dimerization of **13** is supported by mass spectrometric data obtained for $(\text{PhSiO})_4(\text{OTMS})_4$ during the time-course experiments (**Table 4.1**) on the cleavage of **1**.

In conclusion, we have established a new route to the lower, highly symmetrical, partially condensed double-decker shaped octaphenyl silsesquioxane framework starting with dodecaphenyl T_{12} ($\text{Ph}_{12}\text{T}_{12}$). Mass spectral data from a time-resolved study point to early formation of a tetracyclosiloxane as a key intermediate for the formation of the ‘double-decker’ shaped silsesquioxane. This result demonstrates the first use of dodecaphenyl T_{12} as precursor to the lower functionalized partially condensed octaphenyl T_8 frameworks.⁴ Results and Discussions

4.4.1 Hydrolysis of $\text{Ph}_{12}\text{T}_{12}$ (**1**) into $[(\text{PhSiO})_8(\text{O})_2(\text{OTMS})_4]$ (**3**)

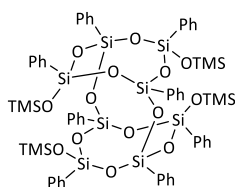
Scheme 4-5: Synthesis of 5,11,14,17-tetrakis(trimethylsilyl)octaphenyltetracyclo- [7.3.3.-3^{3,7}]octasilsesquioxane $[(\text{PhSiO})_8(\text{O})_2(\text{OTMS})_4]$ (**3**) from $\text{Ph}_{12}\text{T}_{12}$ (**1**)



Following the sequence of reactions outlined in **Scheme 4.5**, a white solid was generated that crystallized at $-30\text{ }^{\circ}\text{C}$ overnight. To our surprise, characterization of this material by ^1H , ^{13}C , and ^{29}Si NMR spectroscopy, MS, and single-crystal X-ray indicated

that the product was 5,11,14,17-tetrakis(trimethylsilyl)octaphenyl-tetracyclo[7.3.3.-3^{3,7}]octasilsesquioxane (**3**). Moreover, based on moles of **1**, as opposed to silicon equivalents, **3** was formed in 89% yield (1.87 g, 1.38 mmol). Yields are calculated based on the starting material that reacted (i.e. after subtracting the recovered Ph₁₂T₁₂). However, it is worth mentioning that a white suspension was obtained prior to the recrystallization step. This solid in the organic phase separated by filtration using a fine frit funnel was shown to be the unreacted dodecaphenylT₁₂ **1** based on proton and silicon NMR.

5,11,14,17-tetrakis(trimethylsilyl)octaphenyltetracyclo[7.3.3.-3^{3,7}]octasilsesquioxane
 $[(PhSiO)_8(O)_2(OTMS)_4]$ **3**



Chemical Formula: C₆₀H₇₄O₁₄Si₁₂

This product is a white crystalline solid. mp 225 – 228

¹H NMR (500 MHz, CDCl₃ + 1% TMS) δ (ppm) 7.47 – 7.43 (m, 8H), 7.38 – 7.08 (m, 32H).

¹³C NMR (126 MHz, CDCl₃ + 1% TMS) δ (ppm) 134.34, 133.59, 131.78, 130.08, 129.71, 127.42, 1.90.

²⁹Si NMR (99 MHz, CDCl₃ + 1% TMS) δ (ppm) 10.53 (4Si), -76.09 (4Si), -78.92 (4Si).

4.4.2 Time-course Study for the Hydrolysis of **1** into **3**

Scheme 4-6: Time-course analysis for the synthesis of **3** from **1**

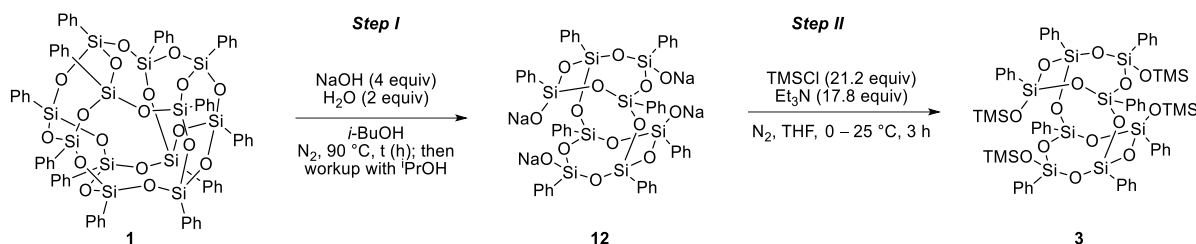


Table 4-1: LCMS-G2-XS QToF time course analysis of data for selected intermediates obtained from the hydrolysis of **1** followed by silylation with TMSCl

Compound	time	Relative	m/z [M + H] ⁺		m/z [M + NH ₄] ⁺		m/z [M + Na] ⁺	
		Int. (%)	(Calc'd)	(Found)	(Calc'd)	(Found)	(Calc'd)	(Found)
Ph ₁₂ T ₁₂ (1)	0 h	100	1549.11	1549.13	1566.14	1567.12	1571.09	1571.12
Ph ₁₂ T ₁₂ (1)	1 h	100	1549.11	1549.13	1566.14	1567.12	1571.09	1571.12
Ph ₁₂ T ₁₂ (1)	2 h	89	1549.11	1549.13	1566.14	1566.12	1571.09	1571.12
[(PhSiO) ₄ (OTMS) ₄] (7)	2 h	11	858.25	858.97	—	—	—	—
Ph ₁₂ T ₁₂ (1)	4 h	45	1549.11	1549.13	1566.14	1566.12	1571.09	1571.12
[(PhSiO) ₈ (O) ₂ (OTMS) ₄] (3)	4 h	54	1357.25	1357.24	1374.28	1374.27	—	—
[(PhSiO) ₄ (OTMS) ₄] (7)	4 h	1	—	—	859.25	858.96	863.20	863.15
Ph ₁₂ T ₁₂ (1)	8 h	41	1549.11	1549.08	—	—	—	—
[(PhSiO) ₈ (O) ₂ (OTMS) ₄] (3)	8 h	58	—	—	1374.28	1374.99	1379.24	1379.61
[(PhSiO) ₄ (OTMS) ₄] (7)	8 h	1	841.22	841.18	859.25	858.96	863.20	862.84
Ph ₁₂ T ₁₂ (1)	16 h	7	1549.11	1549.08	1566.14	1567.25	1571.09	1570.24
[(PhSiO) ₈ (O) ₂ (OTMS) ₄] (3)	16 h	90	1357.25	1357.13	—	—	1571.09	1570.24
[(PhSiO) ₄ (OTMS) ₄] (7)	16 h	3	841.22	840.95	859.25	858.96	863.20	861.95
Ph ₁₂ T ₁₂ (1)	24 h	2	1549.11	1549.08	1566.14	1567.25	1571.09	1571.12
[(PhSiO) ₈ (O) ₂ (OTMS) ₄] (3)	24 h	96	1357.25	1357.14	—	—	1379.24	1379.23
[(PhSiO) ₄ (OTMS) ₄] (7)	24 h	2	841.22	840.95	859.25	858.96	—	—
Ph ₁₂ T ₁₂ (1)	36 h	2	1549.11	1549.08	1566.14	1566.07	—	—
[(PhSiO) ₈ (O) ₂ (OTMS) ₄] (3)	36 h	95	1357.25	1357.24	1374.28	1374.99	1379.24	380.23
[(PhSiO) ₄ (OTMS) ₄] (7)	36 h	3	841.22	840.95	859.25	858.96	—	—
Ph ₁₂ T ₁₂ (1)	48 h	6	1549.11	1549.08	1566.14	1567.10	—	—
[(PhSiO) ₈ (O) ₂ (OTMS) ₄] (3)	48 h	91	1357.25	1357.24	1374.28	1374.90	1379.24	1380.23
[(PhSiO) ₄ (OTMS) ₄] (7)	48 h	3	841.22	840.95	859.25	858.96	863.20	861.95
Ph ₁₂ T ₁₂ (1)	72 h	3	1549.11	1549.08	—	—	1571.09	1571.01
[(PhSiO) ₈ (O) ₂ (OTMS) ₄] (3)	72 h	94	1357.25	1357.24	1374.28	1374.99	1379.24	380.23
[(PhSiO) ₄ (OTMS) ₄] (7)	72 h	3	841.22	840.95	859.25	858.96	—	—

Atomic pressure chemical ionization mass spectrometry (APCI MS) was used to monitor reaction progress. This analysis showed the loss of **1** being met with an increase in the formation of **3**. Notably, the mass spectral data indicated $(\text{PhSiO})_4(\text{OTMS})_4$ (**7**) as an intermediate species prior to the formation of **3**. **Table 4.2** details the presence of these selected species at different reaction times. This table gives the MS data of selected species for the hydrolysis and silylation of **1** at various time intervals.

Table 4-2: Relative intensity of Species in Table 4.1 expressed as a percentage

		Time (h)/Relative Intensity (%)										
Entry	Species	0	1	2	4	8	16	24	36	48	72	
1	Ph ₁₂ T ₁₂ (1)	100	100	89	45	41	7	2	2	6	3	
2	[(PhSiO) ₄ (OTMS) ₄] (7)	0	0	11	1	1	3	2	3	3	3	
3	[(PhSiO) ₈ (O) ₂ (OTMS) ₄] (3)	0	0	0	54	58	90	96	95	91	94	

A graphical plot of this data showing the consumption of **1** and formation of **3** is shown in **Figure 4.2**

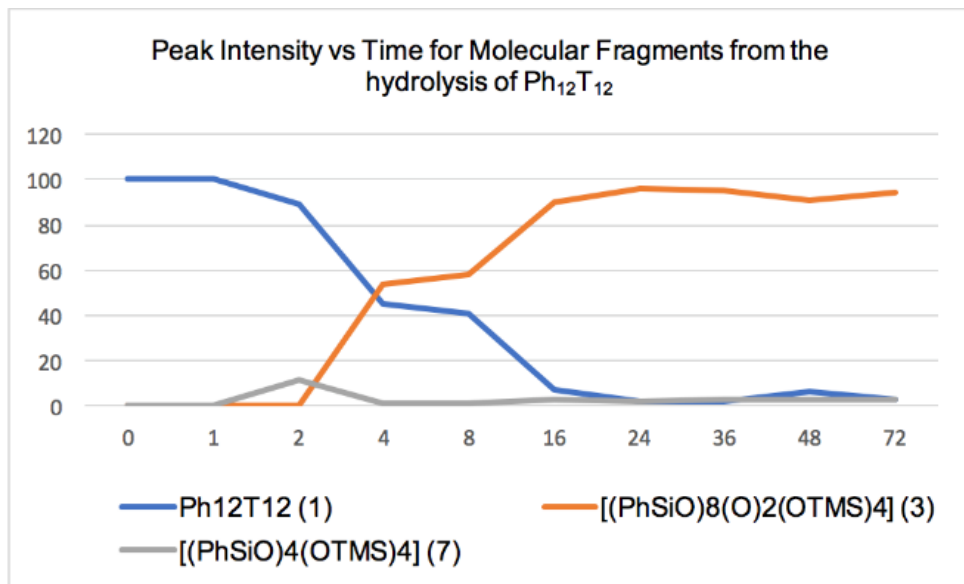


Figure 4-2: Graph of relative intensity (%) vs hydrolysis time

At the 2-hour point, APCI-MS indicated the presence of **1** and **7** but provided no evidence for the presence of **3**. Compound **3** was first detected at the 4- and 8-hour time points. By the 16-hour time point, the mass peak for **3** was predominant. In practice, the optimal yield of **3** was 89% and obtained when silylation occurred after the base hydrolysis of **1** had run for 48 h (**Table 4.2**).

Table 4-3: Synthesis of $[(\text{PhSiO})_8(\text{O})_2(\text{OTMS})_4]$ (**3**) from $\text{Ph}_{12}\text{T}_{12}$ (**1**)

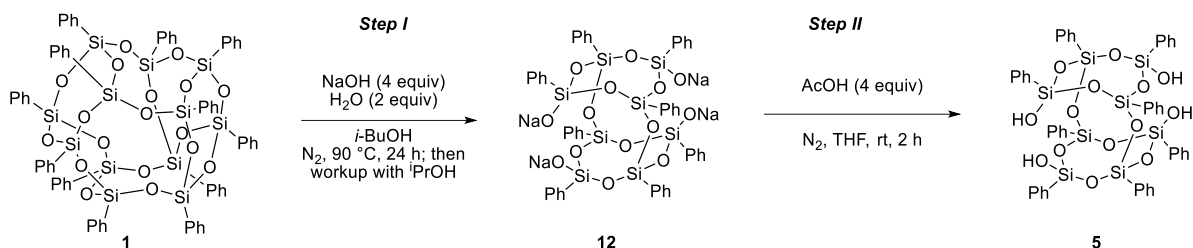
Entry	starting 1 (mmol)	recovered 1 (mmol)	reacted 1 (mmol)	hydrolysis (time/h)	3 (mmol) ^b	Resinous product (g)	Loss in mass	Yield (%) ^c
1	2	1.04 (0.67)	2.06 (1.33)	16	0.98 (0.72)	1.13	0.34	54
2	2	0.63 (0.41)	2.47 (1.59)	24	1.70 (1.25)	0.66	0.50	78
3	2	0.70 (0.45)	2.40 (1.55)	48	1.87 (1.38)	0.58	0.34	89
4	2	0.54 (0.35)	2.56 (1.65)	72	1.28 (0.94)	1.30	0.37	57

^aReaction done in two consecutive steps; hydrolysis with NaOH to give intermediate (**12**) which was treated with TMSCl. ^bAmount of **3** isolated. ^cYields are calculated based on mmols of reacted **1**.

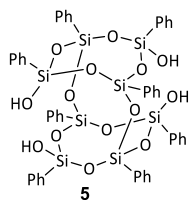
After product isolation, characterization by ^1H , ^{13}C , and ^{29}Si NMR spectroscopy, MS, and single-crystal X-ray diffraction analysis with X-ray refinement parameters for **3** are consistent with the literature.²⁰ This result indicates that the NaOH hydrolysis of **1** affords the double-decker octaphenyl silsesquioxanetetraol tetrasodium salt **12** (**Figure 4.2**) as the **Scheme 4.5** intermediate. It is noteworthy here that order than MS, other spectroscopic data did not show evidence of any rearrangement for shorter hydrolysis time. However, despite the early detection of **3** from the mass spectral data, isolation of pure **3** was achieved for the silylation of all hydrolyzed intermediates from 16-72 h (**Table 4.3**). It should be noted that the APCI-MS data were only a measure of the soluble product. Indeed, insoluble solids remained in the reaction and once isolated proved to be unreacted **1**, as judged by ^1H , ^{13}C , ^{29}Si NMR and mass spectral data (**Appendix**).

4.4.3 Synthesis of [(PhSiO)₈(O)₂(OH)₄] (5) from Ph₁₂T₁₂ (1)

Scheme 4-7: Synthesis of **5** from **1**



Following neutralization with AcOH and filtration of the insoluble material, MeCN was added. The addition of MeCN caused a precipitation. That precipitate proved to be 5,11,14,17-tetra(hydro)octaphenyltetracyclo[7.3.3.-3^{3;7}]octasilsesquioxane (**5**). The amount of **5** isolated represented a 61% yield from **1**. The product was characterized by ¹H, ¹³C and ²⁹Si NMR, X-ray crystallography and APCI+ QToF LCMS Measurements.



Chemical Formula: C₄₈H₄₄O₁₄Si₈

This product is a white solid.

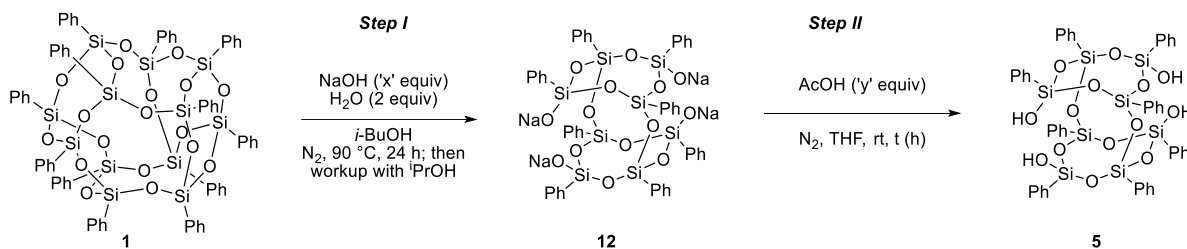
¹H NMR (500 MHz, CDCl₃ + 1% TMS) δ 7.60 – 7.51 (m, 8H), 7.47 – 7.28 (m, 16H), 7.18 (dt, *J* = 25.2, 7.6 Hz, 16H)

¹³C NMR (126 MHz, CDCl₃ + 1% TMS) δ 134.23, 132.32, 131.53, 130.40, 127.78, 127.53

²⁹Si NMR (99 MHz, CDCl₃ + 1% TMS) δ -69.08 (4Si), -79.26 (4Si).

4.4.4 Condition Screening Results for the Synthesis of (PhSiO)₈(O)₂(OH)₄ **5** from Ph₁₂T₁₂ (**1**)

Scheme 4-8: Optimal Conditions for the Synthesis of (PhSiO)₈(O)₂(OH)₄ (**5**)



Results of efforts to optimize the yield of **5** are given in **Table 4.4**.

Table 4-4: Hydrolysis of **12** with Acetic Acid^a

Entry	Starting 1 (mmol)	Recv'd 1 (mmol)	Reacted 1 (mmol)	NaOH (equiv)	Isolated 12 (g)	AcOH (equiv)	time (h)	Isolated 5 ^b (mmol)	Isolated resin ^c (g)
1	1	0.23	0.77	4	1.57	8	1	0.47 (61%)	0.55
2	2	0.37	1.63	4	3.04	4	2	1.08 (66%)	0.77
3	2	0.36	1.64	4	2.57	6	2	0.82 (50%)	1.04
4	2	trace	2.00	6	3.18	8	1	0.57 (29%)	1.61
5^d	1	0.30	0.70	4	1.60	4	2	0.51 (73%)	0.62

^aReaction conditions: Ph₁₂T₁₂ (**1**), NaOH, H₂O, *i*-BuOH, 90 °C 24 h. The hydrolysis step was done with AcOH and work up with MeCN. ^b%Yields of **5** are calculated based on moles of Reacted **1**. ^cResin from MeCN solution. ^dInsoluble solid recombined with fresh **1**.

The results from the acid hydrolysis show that optimal conditions for the formation of **5** are those listed in **entry 2, Table 4.4**. However, this yield (66%) did not compare to the optimal 89% yield observed for the silylated product **3**. This is due to **5** being slight solubility in MeCN (solubility in MeCN at 25 °C = 1.32 x 10⁻²g/10 mL) and thus lost to the filtrate. Indeed, mass spectral analysis of the filtrate confirmed the presence of **5**. The filtrate also contained a resinous material. Though the exact structure of this product was

not established, mass spectral data and DOSY NMR suggested a resinous oligomer. This would not be surprising as **1** is made up of two pairs of fused cyclic tetrasiloxanes and fused cyclic pentasiloxanes.^{6,26} Subjection of such an oligomer to base hydrolysis could conceivably afford cage structures. Unfortunately, the material remained as a resin when treated with aqueous NaOH. In contrast, when the insoluble solid obtained prior to the MeCN treatment was recombine with fresh **1** and then subjected to the NaOH conditions, **5** was obtained (**Table 4.3**, entry 5) in 73% yield. This confirmed that this insoluble material is unreacted **1**.

4.5 Single Crystal X-ray Structures

Crystallographic structures for compound **3** (CCDC-299794) was reported by Lee and Kawakami based on single crystal X-ray. The same group reported a powder XRD structure for compound **5**.²⁰ In our specific case, the structure of compound **5** (CCDC-1901262) was resolved based on single crystal X-ray crystallography. Data for these crystal structures obtained in our lab and used in this manuscript have been deposited with the Cambridge Crystallographic Data Centre as supplementary publication number CCDC-1912552 for C₆₀H₇₆O₁₄Si₁₂ (**3**) and CCDC-1901262 for C₅₆H₆₀O₁₆Si₈ (**5**). Copies of the data can be obtained free of charge via the CCDC Website (www.ccdc.cam.ac.uk/structures).

xane (C₆₀H₇₆O₁₄Si₁₂) (**3**)



(Displacement ellipsoid contour probability drawn at 50%)



reported sum (Z is 4 and Z' is 1)



Figure 4-5: Packing diagram of 3

5,11,14,17-Tetra(hydro)octaphenyltetracyclo[7.3.3.-3³;7]octasilsesquioxane
($C_{48}H_{44}O_{14}Si_8$) (**5**)

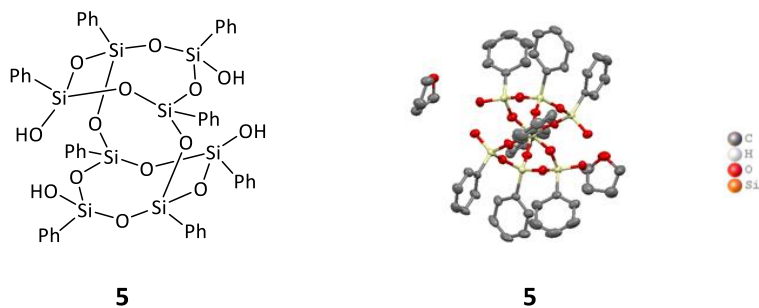


Figure 4-6: Compound **5** with two THF molecules co-crystallized per molecule of interest
(Displacement ellipsoid contour probability drawn at 50%)

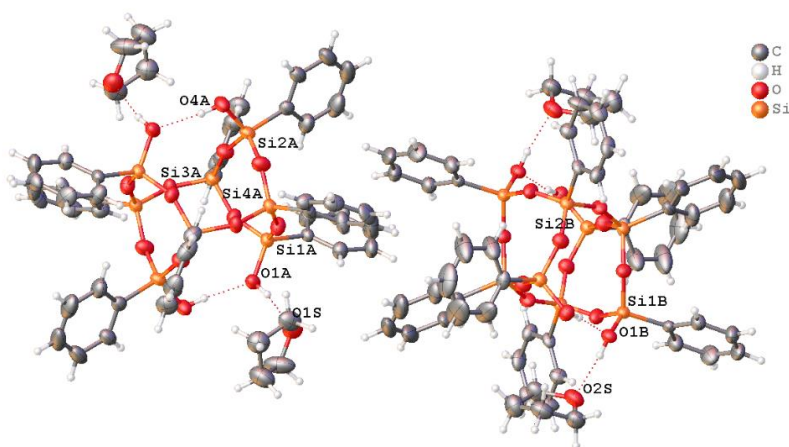


Figure 4-7: Single molecule of **5** in the asymmetric unit, which is represented by the reported sum formula (Z is 2 and Z' is 1)

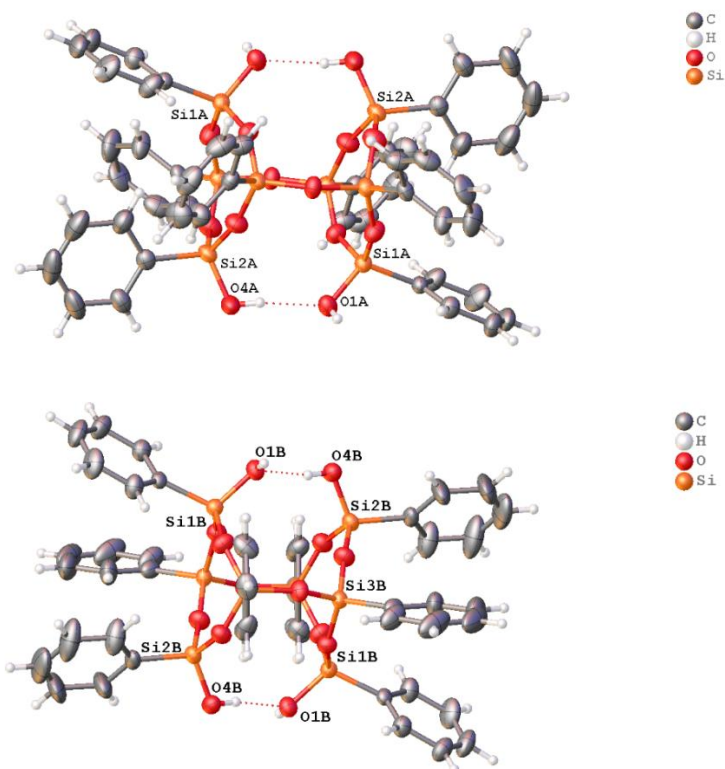


Figure 4-8: Hydrogen bonding interactions in **5**

The following hydrogen bonding interactions with a maximum D-D distance of 2.9 Å and a minimum angle of 120 ° are present in 5,11,14,17-tetra(hydro)octaphenyltetracyclo[7. 3.3.-3^{3;7}]octasilsesquioxane (**5**): O1A–O1S: 2.645 Å, O4A–O1A_1: 2.782 Å, O1B–O2S: 2.647 Å, O4B–O1B_2: 2.743 Å.

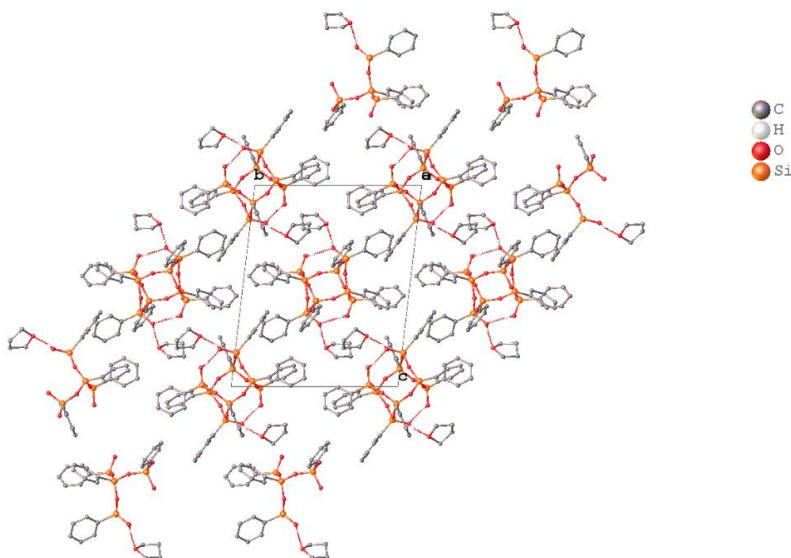


Figure 4-9: Packing diagram of 5,11,14,17-tetra(hydro)octaphenyltetracyclo[7.3.3.-3^{3;7}]octasilsesquioxane (**5**)

Notes: Jonathan E Dannatt is thanked for his significant contributions to this project during our silicon group meetings.

4.6 Experimental Section

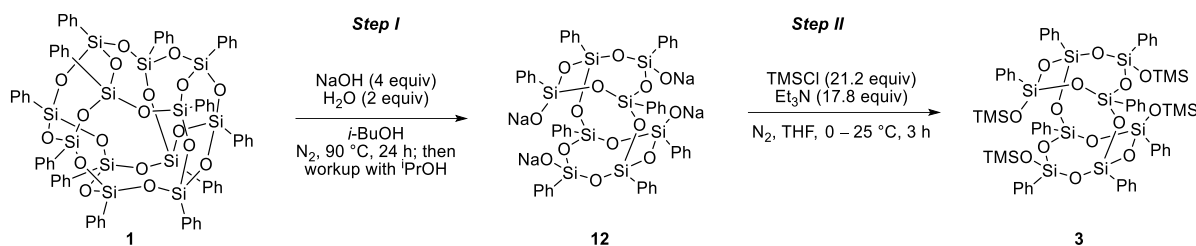
4.6.1 Materials and Methods

All reactions were carried out with dry solvents under a nitrogen atmosphere using standard techniques except otherwise stated. DodecaphenylIT₁₂ was obtained from Hybrid Plastics. Triethylamine (Et₃N) was distilled over calcium hydride before use. Ethyl acetate, hexanes, diethyl ether, acetonitrile, methanol, isopropanol, isobutanol, and acetic acid were used as received. THF was distilled over benzophenone and sodium metal at a temperature of 50 °C under nitrogen prior to use. Glassware was oven dried. Reactions were monitored thin-layer chromatography (TLC) on silica gel plates or a Hydrion Insta-Chek pH pH 0-14 and. ¹H, ¹³C, and ²⁹Si NMR spectra were acquired on an Agilent DirectDrive2 500 MHz NMR spectrometer equipped with a OneProbe operating

at 500 MHz for ^1H NMR, 126 MHz for ^{13}C NMR, and 99 MHz for ^{29}Si NMR CDCl_3 or toluene- d_8 and recorded at 25 °C. ^1H -NMR spectra were recorded with 8 scans, a relaxation delay of 1 s, and a pulse angle of 45° and referenced to tetramethylsilane in CDCl_3 (0.00 ppm). ^{13}C -NMR spectra were collected with 254 scans, a relaxation delay of 0.1 s, and a pulse angle 45°. ^{29}Si NMR spectra were recorded with either 256 or 512 scans, a relaxation delay of 12 s and a pulse angle of 45°. Thin-layer chromatography (TLC) was performed on plates of EMD 250- μm silica 60-F254. High-resolution mass spectroscopy was performed with APCI mass spectra recorded on a Finnigan LCQ Deca (ThermoQuest) technologies with LC/MS/MS (quadrupole/time-of-flight) and Waters Xevo G2-XS UPLC/MS/MS inert XL MSD with SIS Direct Insertion Probe. Melting points for all products were measured with a Thomas HOOVER capillary uni-melt melting point apparatus and are uncorrected. X-ray diffraction measurements were performed on a Stoe IPDS2 or a Bruker-AXS SMART APEX 2 CCD diffractometer using graphite-monochromated $\text{Mo K}\alpha$ radiation. The structures were solved using direct methods (SHELXL-97) and refined by full-matrix least-squares techniques against F^2 (SHELXL-97). Cell parameters were retrieved using the SAINT (Bruker, V8.34A, after 2013) software and refined using SAINT (Bruker, V8.34A, after 2013) on 5941 reflections, 47% of the observed reflections. Data reduction was performed using the SAINT (Bruker, V8.34A, after 2013) software which corrects for Lorentz polarization.

4.6.1.1 Synthesis of 5,11,14,17-tetrakis(trimethylsilyl)octaphenyltetracyclo[7.3.3.3^{3,7}]octasilsesquioxane (**3**) from DodecaphenylT₁₂ [Ph₁₂T₁₂] (**1**)

Scheme 4-9: Hydrolysis of Ph₁₂T₁₂ (**1**) for the synthesis of 5,11,14,17-tetrakis(trimethylsilyl)octaphenyltetracyclo[7.3.3.3^{3,7}]octasilsesquioxane (**3**)



Step I: Hydrolysis of Ph₁₂T₁₂ (1**) with NaOH.**

Hydrolysis of dodecaphenylT₁₂ (**1**) was carried out under basic conditions following the literature procedure described by Kawakami and Li with slight modifications.²⁰ Into a 100 mL round bottom flask equipped with a stir bar was charged with Ph₁₂T₁₂ (**1**) (2 mmol, 3.17 g) and NaOH (8 mmol, 4 equiv, 0.32 g). The flask was sealed with a septum, its contents placed under a nitrogen atmosphere, and charged with isobutanol (30 mL). Next, water (4 mmol, 2 equiv, 0.075 mL) was added. The reaction flask was placed in a pre-heated oil bath at 90 °C and then the reaction mixture was stirred for 24 h. The flask was cooled to room temperature and the heterogeneous mixture filtered through a fine frit filter funnel. The residue was washed several times with isopropanol and dried in an oven at 105 °C for 5 h. The dried white solid (**12**) was next silylated (*Step II*) with TMSCl and characterized.

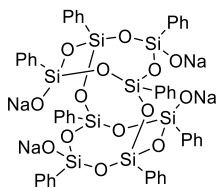


Figure 4-10: 5,11,14,17-tetra(sodio)octaphenyltetracyclo[7.3.3.3^{3,7}]octasilsesquioxanolate (**12**)

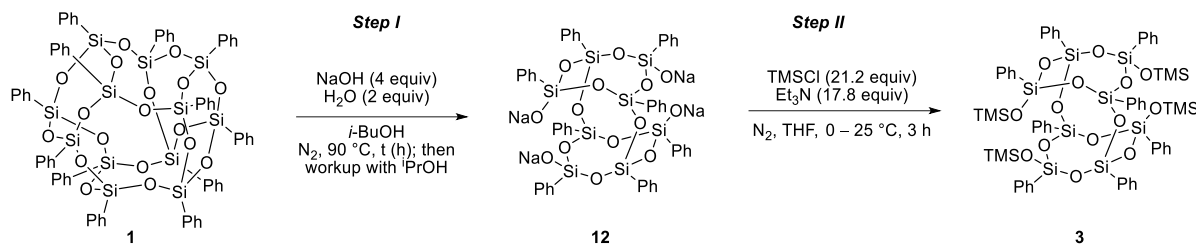
Step II: Silylation of Intermediate (**12**) into 5,11,14,17-tetrakis(trimethylsilyl)octaphenyltetracyclo[7.3.3.-3^{3,7}]octasilsesquioxane [(PhSiO)₈(O)₂(OTMS)₄] (**3**).

A 100 mL oven-dried round bottom flask containing the white product (**12**) obtained from the hydrolysis of 2 mmol of Ph₁₂T₁₂ (*step 1 above*) was equipped with a magnetic stirrer and its contents placed under a nitrogen atmosphere. The flask was placed in an ice bath and charged with THF (20 mL). TMSCl (5.38 mL, 42.4 mmol, 21.2 equiv based on mmol of Ph₁₂T₁₂) and triethylamine (Et₃N) (4.96 mL, 35.6 mmol, 17.8 equiv based on mmol of Ph₁₂T₁₂) were added to flask and the reaction mixture stirred vigorously at room temperature for 3 h. Deionized water (20 mL) was added, and the reaction mixture was further stirred for 10 min before being extracted with hexanes (3 x 10 mL). The insoluble solid in the organic phase was separated by filtration using a fine frit funnel. This solid (0.63 g, 0.41 mmol) proved to be the unreacted dodecaphenylT₁₂ (**1**) based on proton and silicon NMR. To the hexanes filtrate was added *n*-hexane (40 mL) and the solution left to stand in a -30 °C refrigerator overnight. The precipitated solid was filtered off and dried at reduced pressure to afford 1.70 g (1.25 mmol, 79% yield based on recovered **1**) of pure 5,11,14,17-tetrakis(trimethylsilyl)octaphenyltetracyclo[7.3.3.-3^{3,7}]octasilsesquioxane [(PhSiO)₈(O)₂(OTMS)₄] (**3**) as a white crystalline solid (mp 225–228 °C). Note: Yields are calculated based on the starting material. Products are characterized by ¹H,

^{13}C , ^{29}Si NMR, X-ray crystallography, APCI+ QToF LCMS. Analytical results are provided in **Appendix** (NMR, X-ray crystallography and mass spectral data).

4.6.1.2. Time-course Study for the Hydrolysis of **1** followed by TMS Capping to Afford **3**

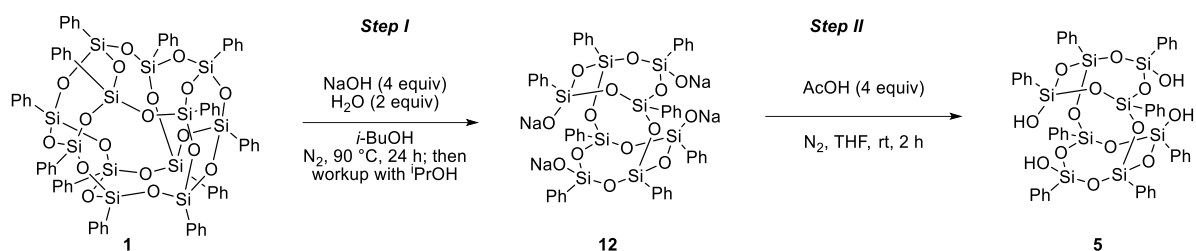
Scheme 4-10: Time-course study for the synthesis of **3** from **1**



Ten 100 mL round bottom flasks containing **1** (1 mmol), NaOH (4 equiv), H₂O (2 equiv) and isobutanol (15 mL) were subjected to the base hydrolysis procedure described in **Step I** of **section 4.6.1.1**. These individual reactions were stopped at ten different time points; 0 h, 1 h, 2 h, 4 h, 8 h, 16 h, 24 h, 36 h, 48 h and 72 h respectively. The resulting white precipitates (**12**) were filtered through a fine frit funnel, washed several times with 2-propanol, and the residues dried in an oven at 105 °C for 5 h. Product identification was done by converting the intermediates into their TMS derivatives as described in **Step II** (**Section 4.6.1.1**). The individual products were analyzed by ^1H , ^{13}C , ^{29}Si NMR and MS (**Table 4.1**).

4.6.1.3 Synthesis of 5,11,14,17-Tetra(hydro)octaphenyltetracyclo[7.3.3.3^{3;7}.7]octasilsesquioxane [(PhSiO)₈(O)₂(OH)₄] **5 from Dodecaphenyl Silsesquioxane [Ph₁₂T₁₂] **1****

Scheme 4-11: Base hydrolysis of [Ph₁₂T₁₂] **1** for the synthesis of [(PhSiO)₈(O)₂(OH)₄] **5**



Step I: Hydrolysis of Ph₁₂T₁₂ **1 with NaOH**

See *step 1*, section 4.4.1.1 above.

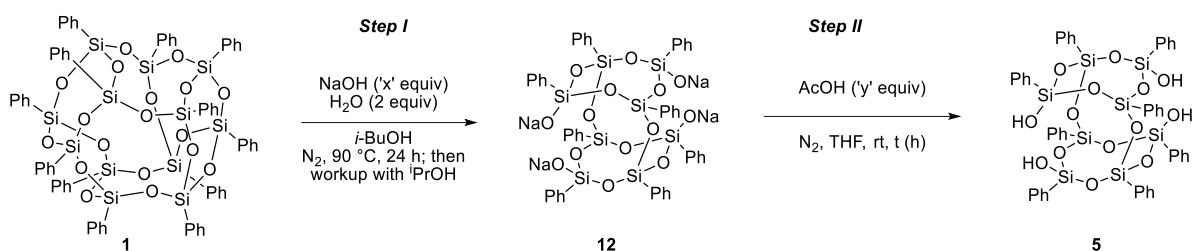
Step II: Acid Hydrolysis of Int I with AcOH

Acetic acid (0.48 g, 8 mmol) was added dropwise to a THF (20 mL) dispersion of **12** (obtained from the hydrolysis in *step I*) under nitrogen atmosphere. The reaction mixture was stirred at room temperature for 1 h. The solution was next neutralized with saturated aqueous sodium hydrogen carbonate (10 mL) and washed with deionized water (20 mL). The mixture was extracted with Et₂O (3 x 10 mL) and the heterogenous organic layer was filtered with a fine frit funnel. The residue was dried in an oven at 105 °C for 5 h and analyzed by ¹H, ¹³C, ²⁹Si NMR and APCI+ QToF LCMS Measurements. Results from these analyses showed that the residue was the unreacted Ph₁₂T₁₂ (**1**). The filtrate was dried over anhydrous magnesium sulfate, filtered and the solvent evaporated under reduced pressure. The resulting solid was washed with acetonitrile from which a white insoluble solid was isolated as pure (PhSiO)₈(O)₂(OH)₄ **5** in 0.50 g (0.47 mmol, 61%). Yields were calculated based on the exact amount of **1** that reacted (i.e after deducting

the amount of recovered **1**). The product was characterized by ^1H , ^{13}C and ^{29}Si NMR, X-ray crystallography and APCI+ QToF LCMS Measurements (**Appendix**).

4.6.1.4 Screening Conditions for the Synthesis of $(\text{PhSiO})_8(\text{O})_2(\text{OH})_4$ **3** from **1**

Scheme 4-12: Optimization for the synthesis of $(\text{PhSiO})_8(\text{O})_2(\text{OH})_4$ (**5**)



Step I: Hydrolysis of $\text{Ph}_{12}\text{T}_{12}$ **1** with NaOH

See *step 1*, section 4.4.1.1 above for experimental procedure. Cleavage of **1** with NaOH was done following the procedure outlined in *step I* of section 4.4.1.1 except that the amounts of NaOH used were varied (**Table 4.3**).

Step II: Acid Hydrolysis of Int-I with AcOH

Acid hydrolysis of the intermediate from *step I*, section 4.4.1.1 above was carried out with AcOH following procedure as outlined in *step II of section 4.4.1.3*. A series of reactions were run with varied amounts of **1**, NaOH, AcOH and reaction time. Results from this screening are shown in **Table 4.3**.

APPENDIX

Copies of ^1H , ^{13}C , ^{29}Si NMR Spectra

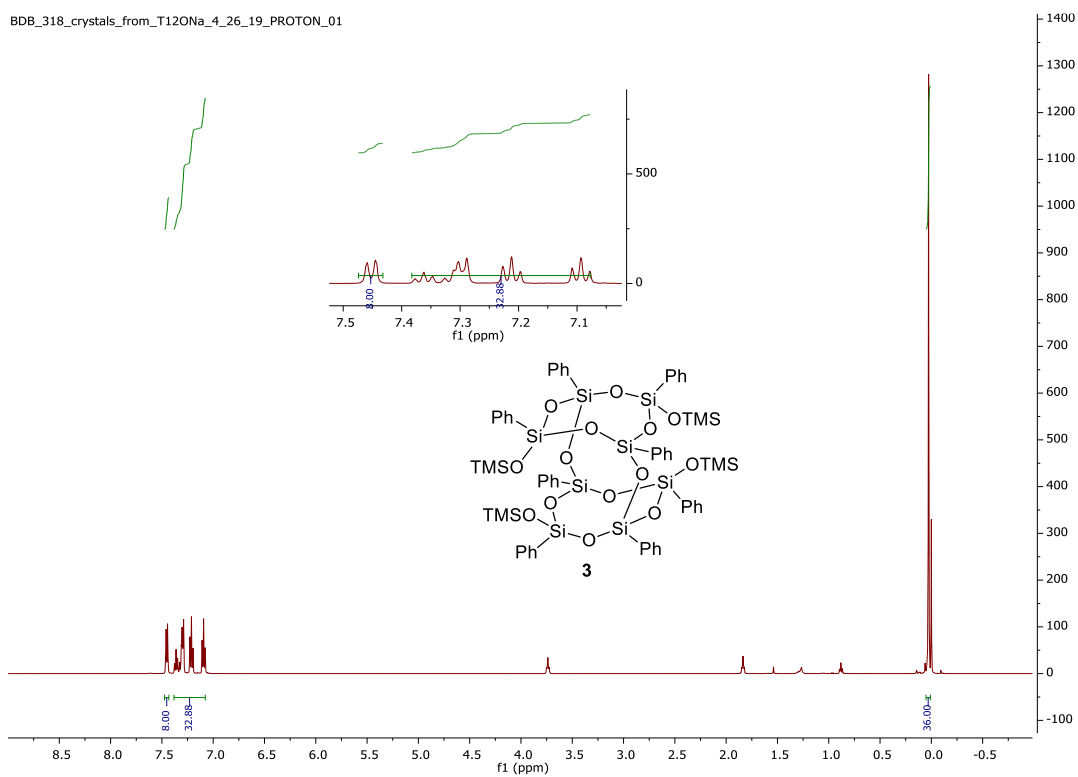


Figure 4-11: ^1H NMR of **3** (500 MHz, CDCl_3)

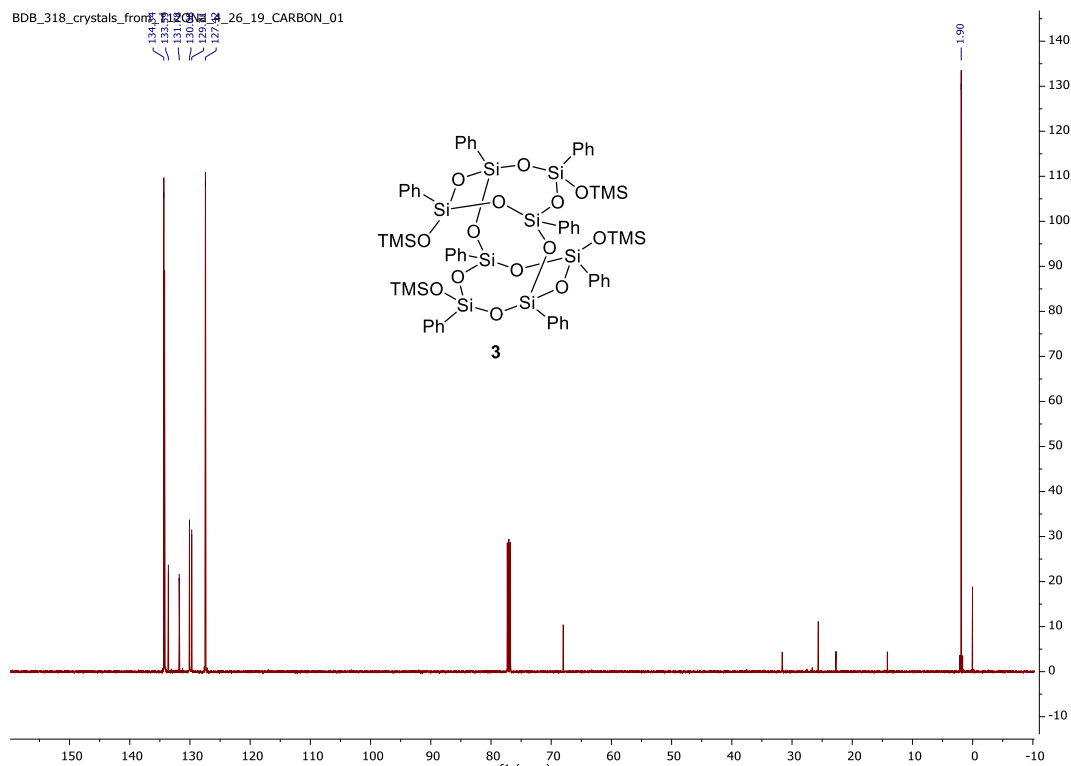


Figure 4-12: ^{13}C NMR of **3** (126 MHz, CDCl_3)

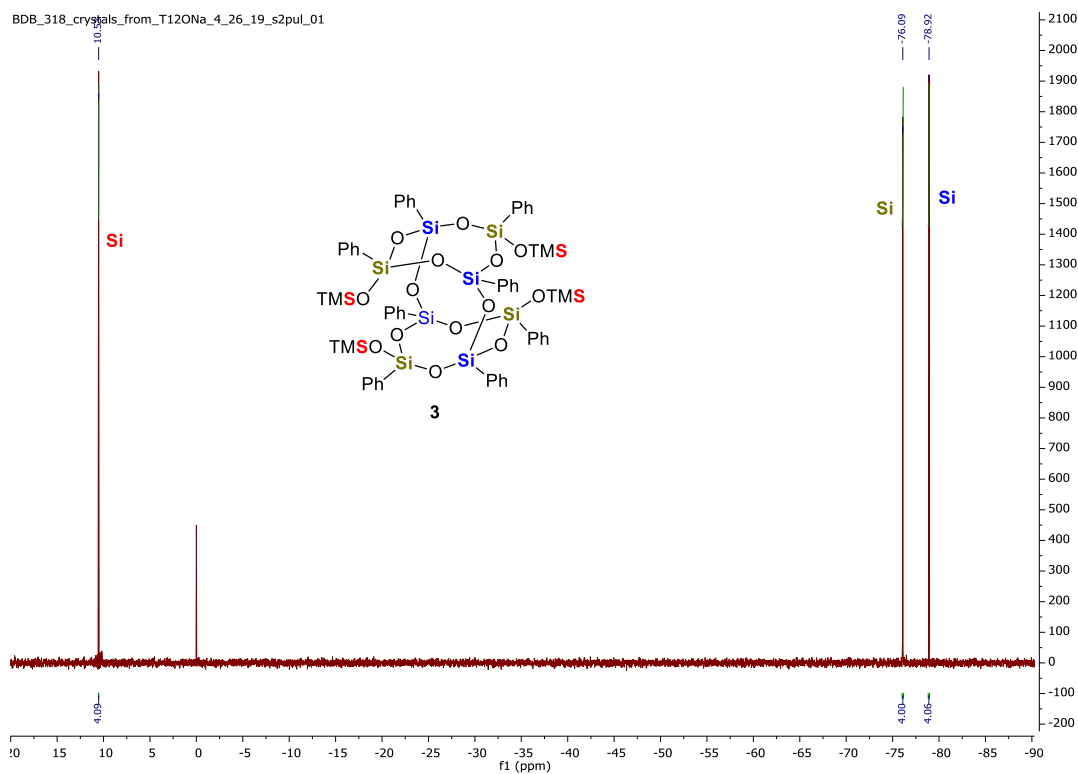


Figure 4-13: ^{29}Si NMR of **3** (99 MHz, CDCl_3)

BDB_401_AcCN_insol_pdt_T8OH_11_14_19_PROTON_01

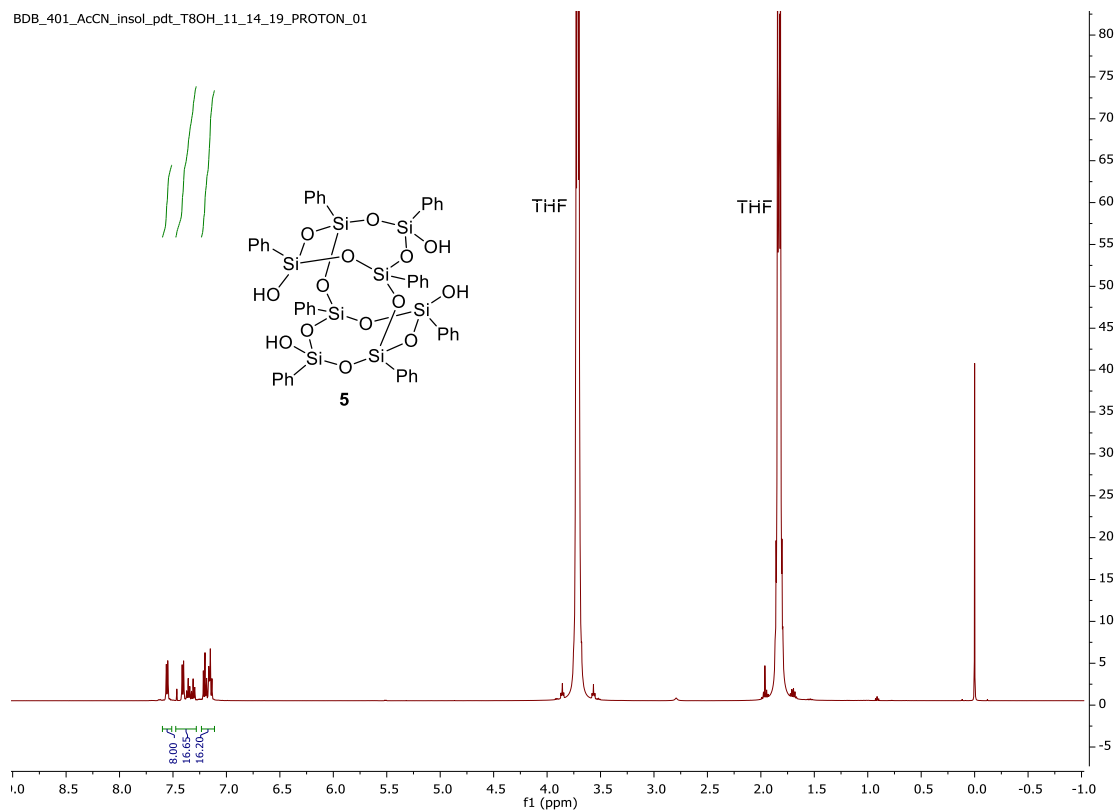


Figure 4-14: ¹H NMR of **5** (500 MHz, CDCl₃)

BDB_401_AcCN_insol_pdt_T8OH_11_14_19_CARBON_01

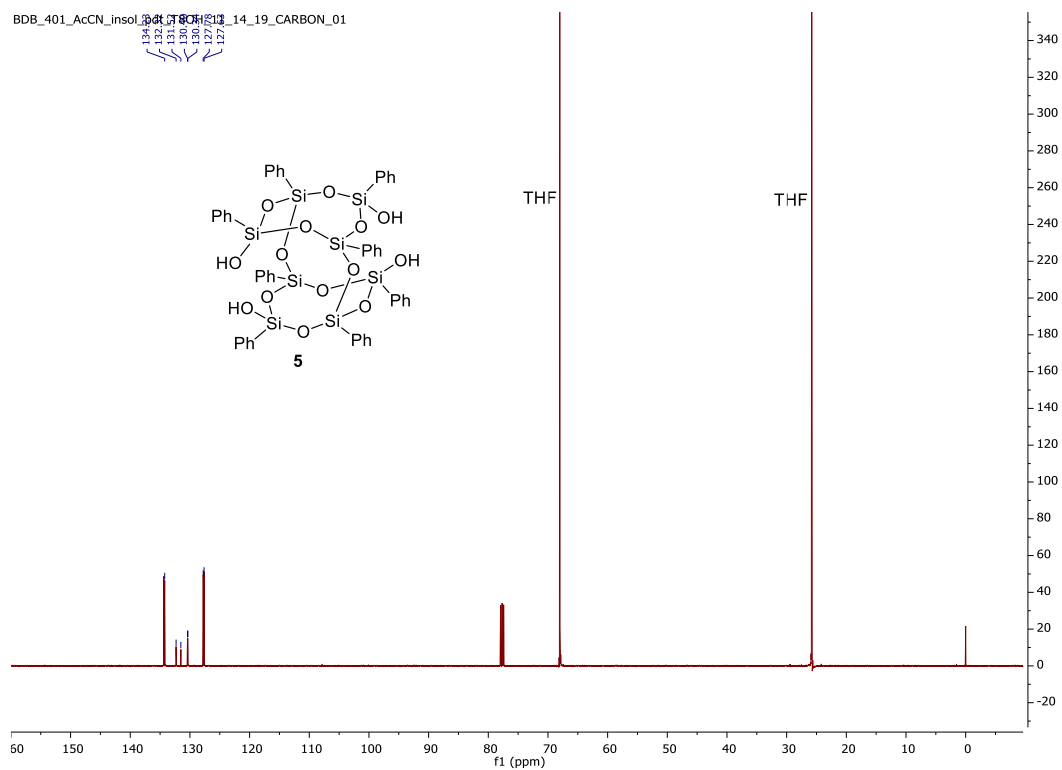


Figure 4-15: ¹³C NMR of **5** (126 MHz, CDCl₃)

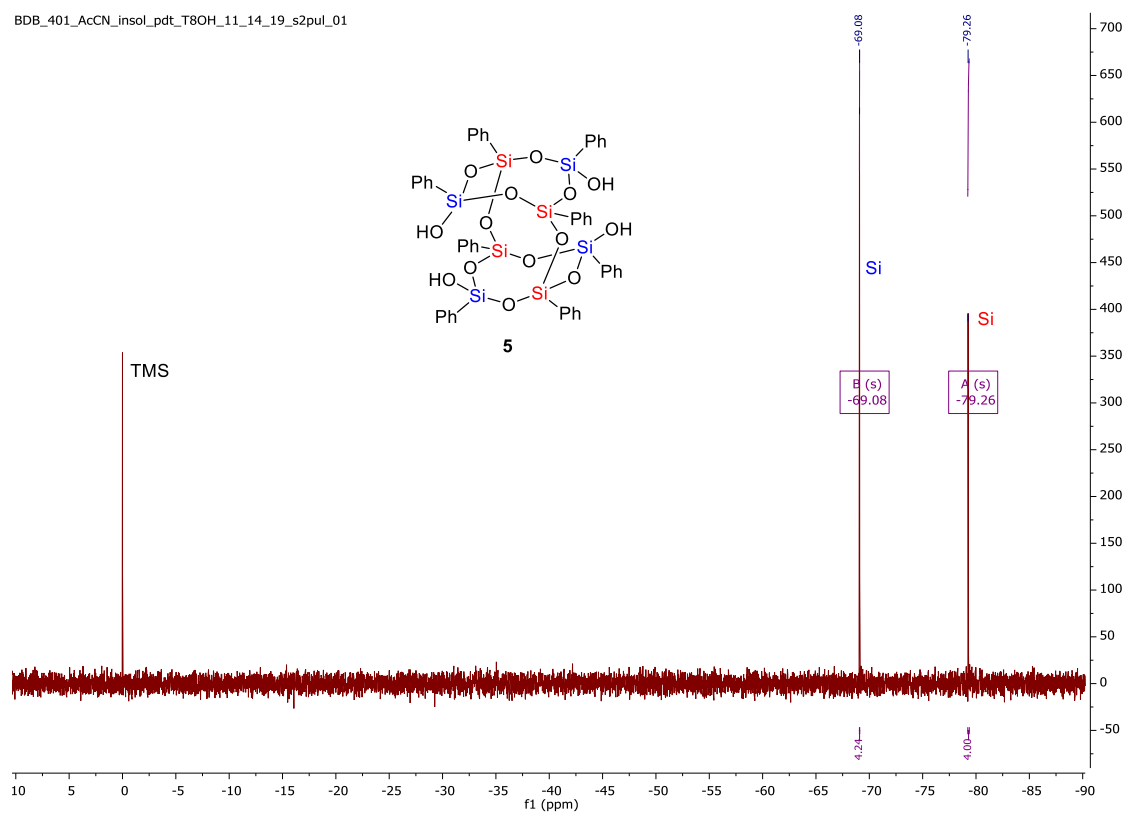


Figure 4-16: ^{29}Si NMR of **5** (99 MHz, CDCl_3)

Spectral Data from Time-Course Experiment

¹H NMR (500 MHz, Chloroform-*d*) δ 7.46 – 7.07 (m, 40H), 0.08 (s, 36H).

BDB_347_16h_xtals_from_-30deg_8_11_19_PROTON_01

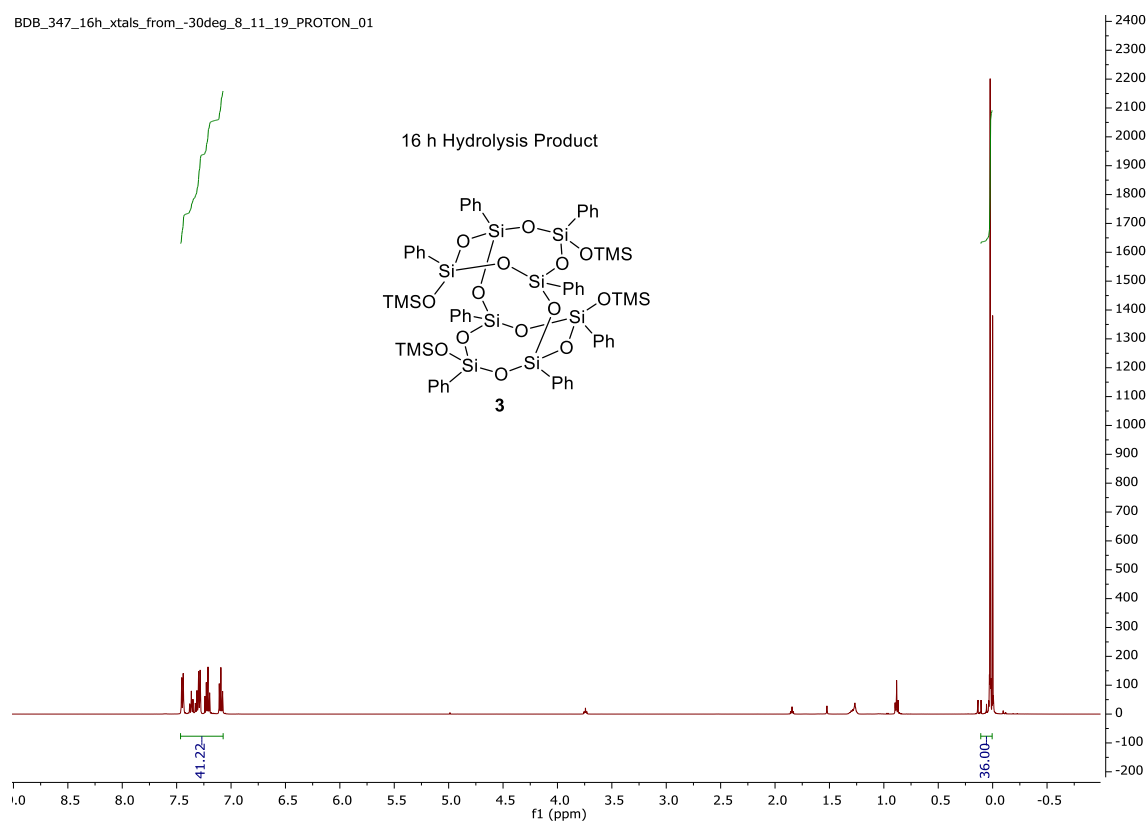


Figure 4-17: ^1H NMR of **3** – 16h (500 MHz, CDCl_3)

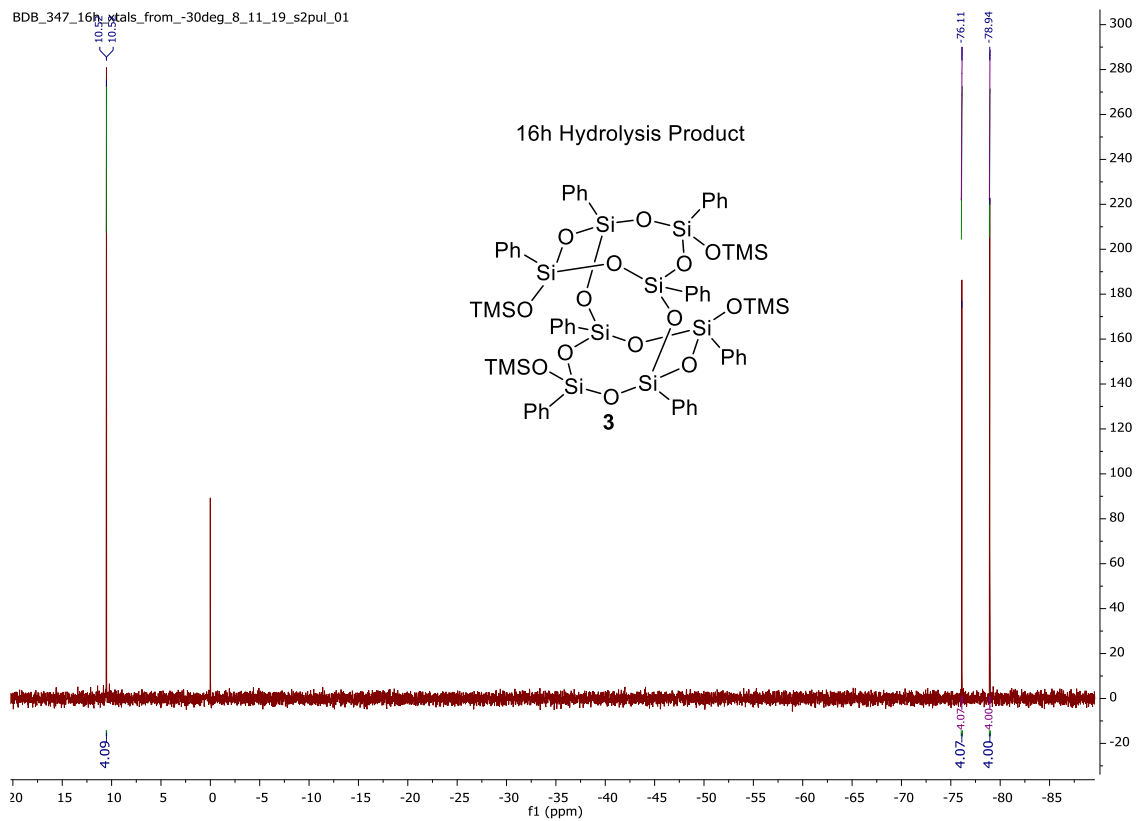
²⁹Si NMR (99 MHz, Chloroform-*d*) δ 10.54 – 10.50, -76.11, -78.94.

Figure 4-18: ^{29}Si NMR of **3** – 16h (99 MHz, CDCl_3)

^1H NMR (500 MHz, Chloroform- d) δ 7.46 – 7.07 (m, 40H), 0.06 (s, 36H).

BDB_367J_T8OTMS_xtals_from_T12ONa_24h_rxn_10_6_19_PROTON_01

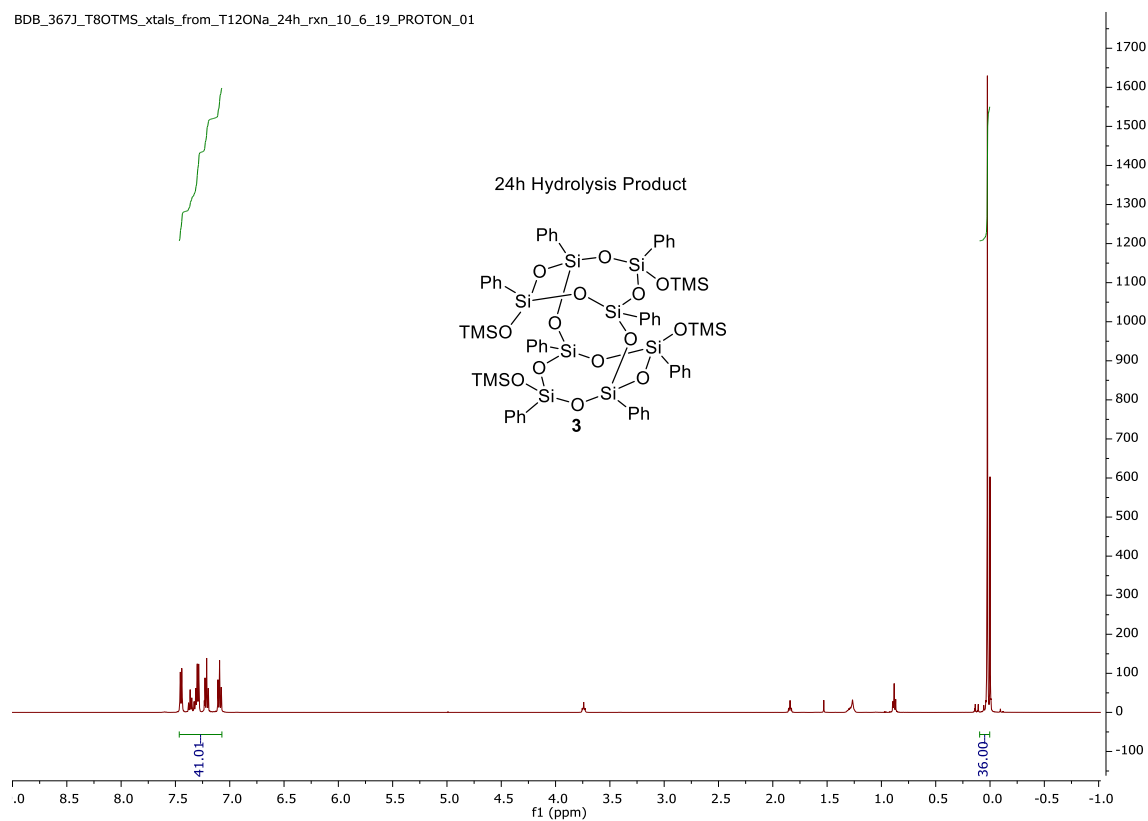


Figure 4-19: ^1H NMR of **3** – 24h (500 MHz, CDCl_3)

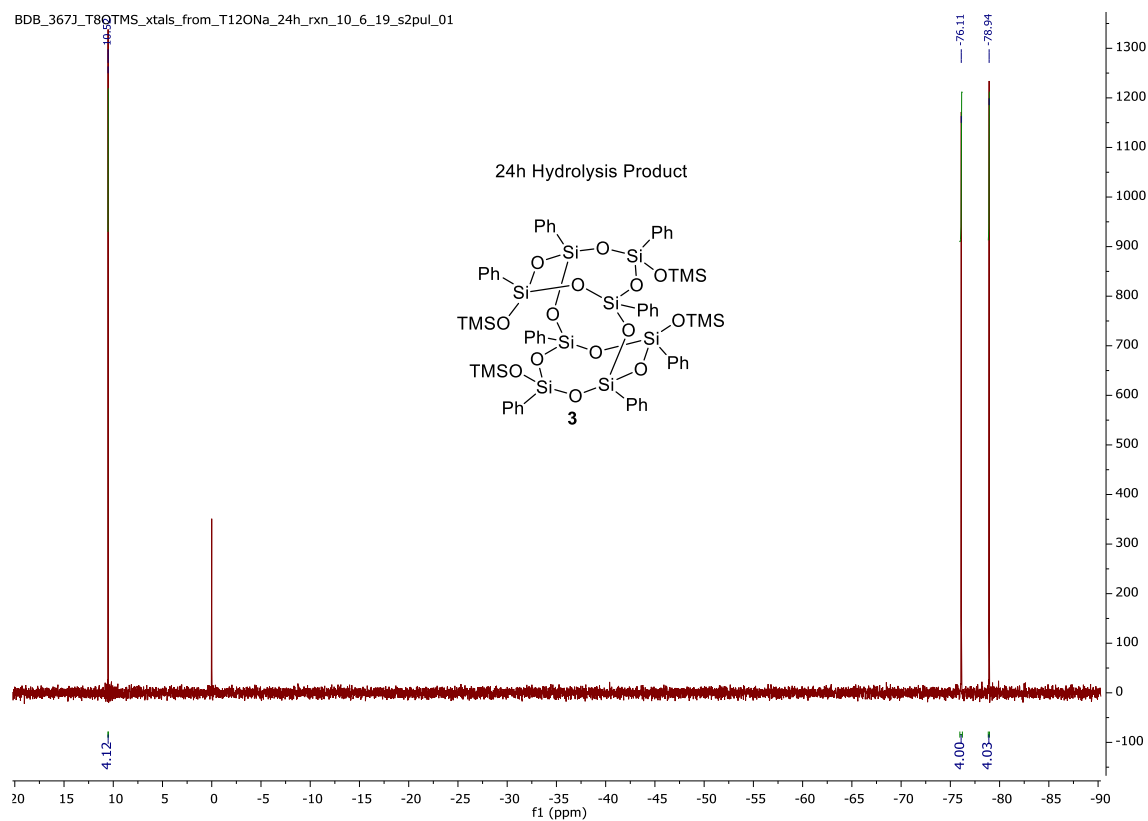
²⁹Si NMR (99 MHz, Chloroform-*d*) δ 10.52, -76.11, -78.94.

Figure 4-20: ^{29}Si NMR **3** – 24h (99 MHz, CDCl_3)

^1H NMR (500 MHz, Chloroform- d) δ 7.46 – 7.07 (m, 40H), 0.06 (s, 36H).

BDB_371_T12OTMS_crystals_36_h_hydrolysis_10_9_19_PROTON_01

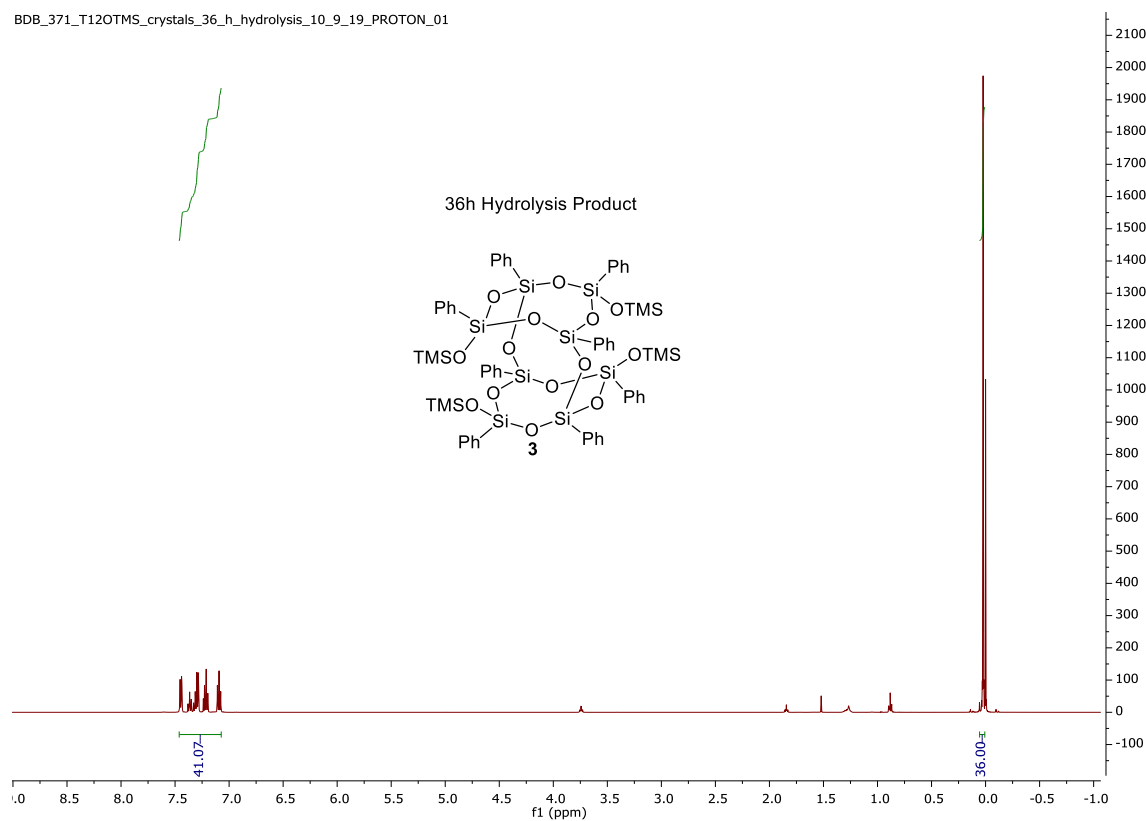


Figure 4-21: ^1H NMR **3** – 36h (500 MHz, CDCl_3)

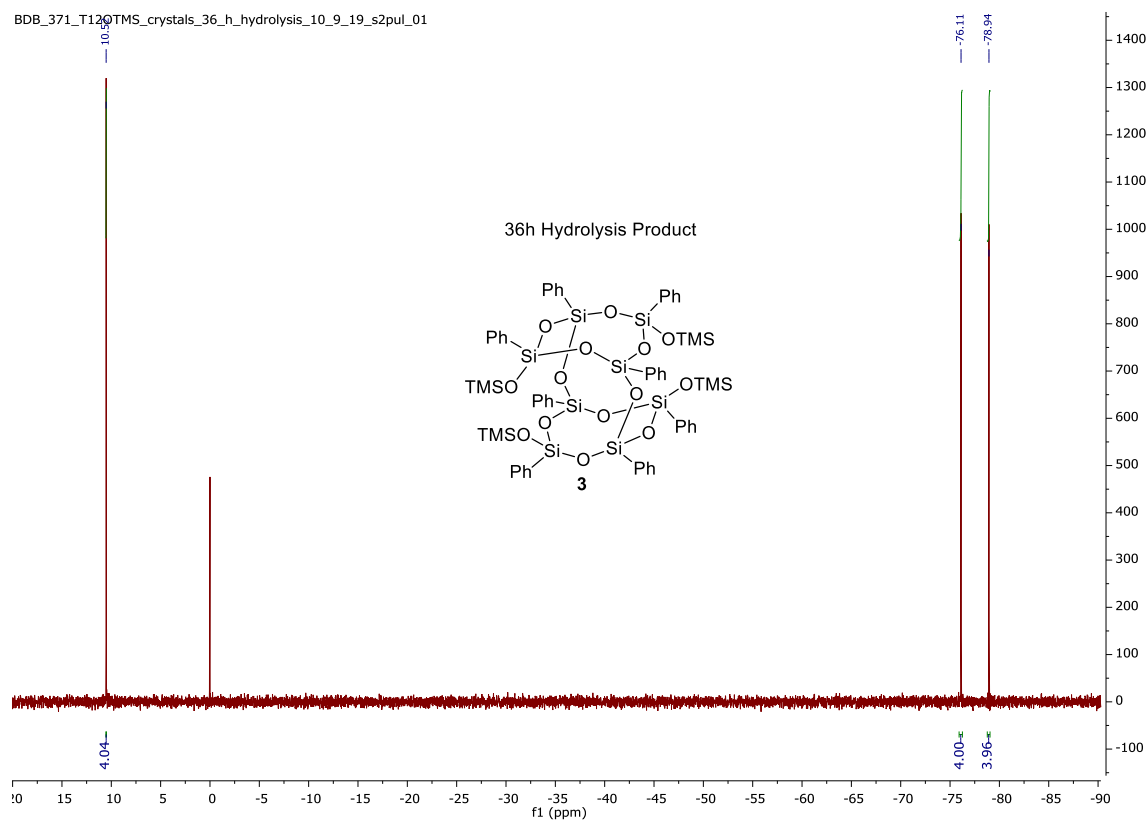
²⁹Si NMR (99 MHz, Chloroform-*d*) δ 10.52, -76.11, -78.94.

Figure 4-22: ^{29}Si NMR **3** – 36h (99 MHz, CDCl_3)

^1H NMR (500 MHz, Chloroform- d) δ 7.46 – 7.08 (m, 40H), 0.06 (s, 36H).

BDB_373_T12OTMS_48h_crystals_10_13_19_PROTON_01

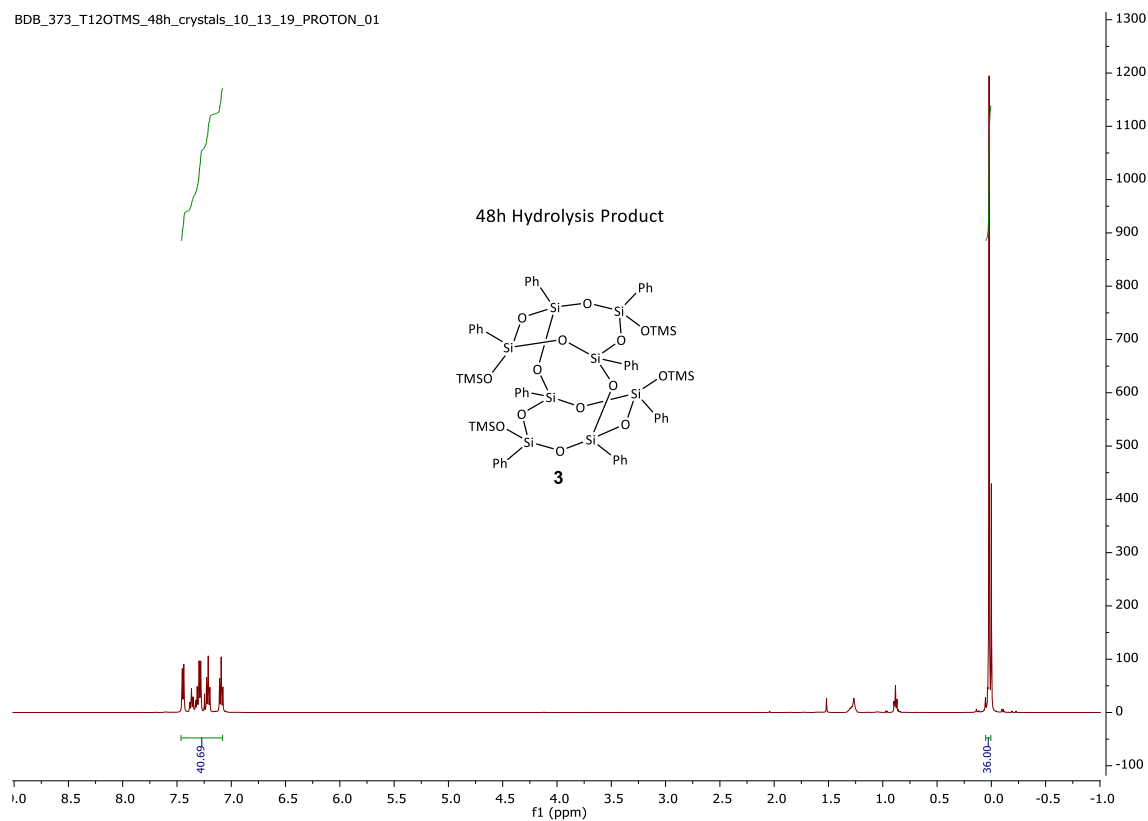


Figure 4-23: ^1H NMR **3** – 48h (500 MHz, CDCl_3)

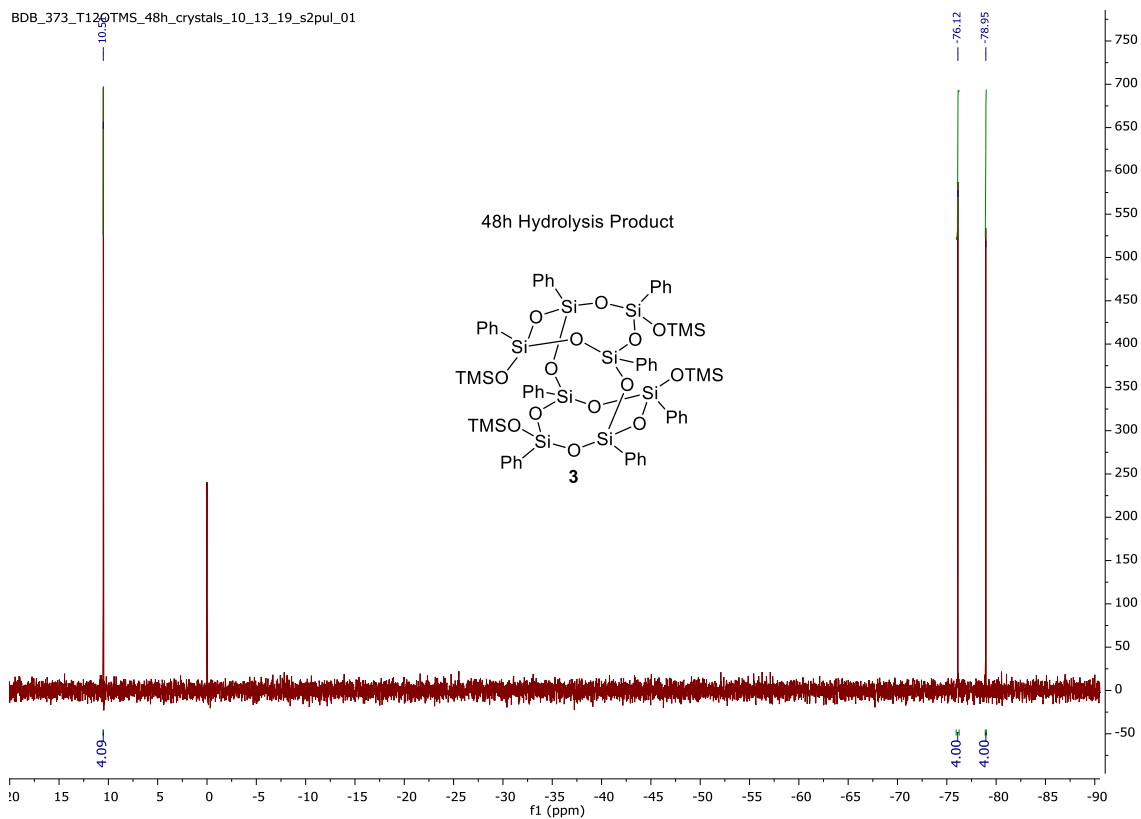
²⁹Si NMR (99 MHz, Chloroform-*d*) δ 10.51, -76.12, -78.95.

Figure 4-24: ^{29}Si NMR **3** – 48h (99 MHz, CDCl_3)

^1H NMR (500 MHz, Chloroform- d) δ 7.47 – 7.07 (m, 41H), 0.06 (s, 36H).

BDB_371_T12OTMS_crystals_72_h_hydrolysis_10_9_19_PROTON_01

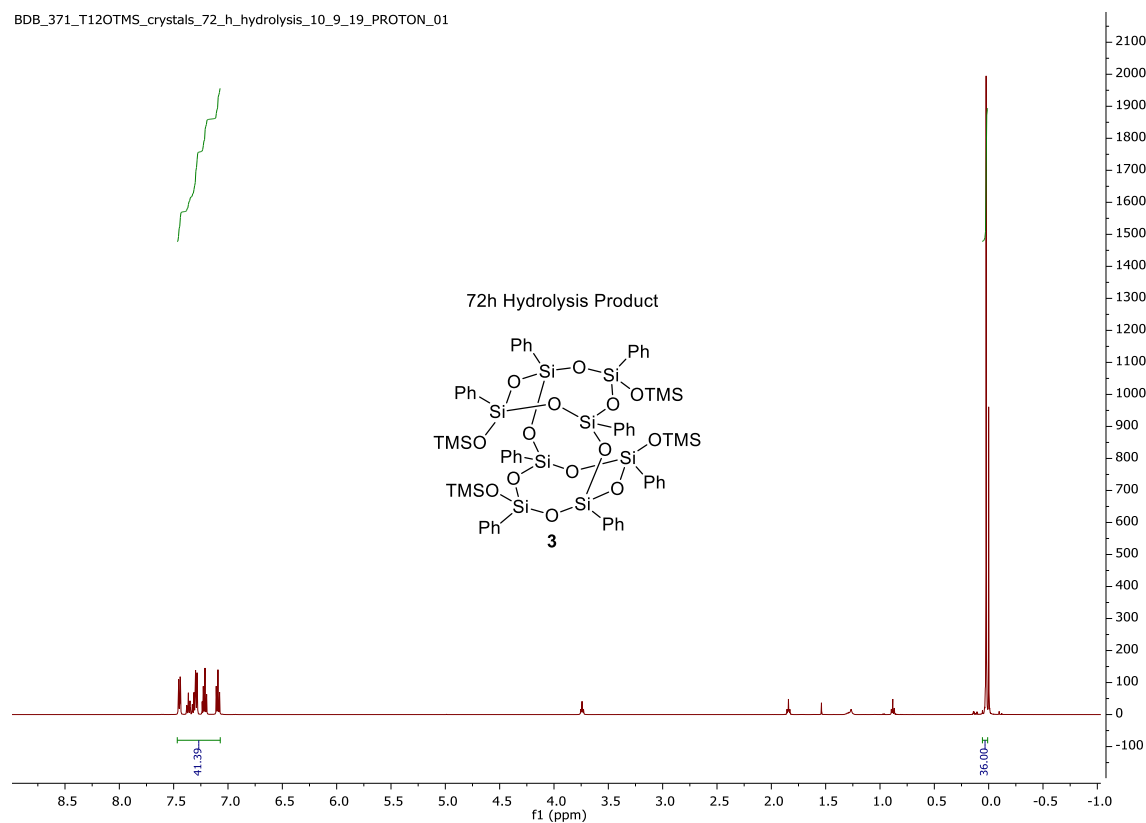


Figure 4-25: ^1H NMR **3** – 72h (500 MHz, CDCl_3)

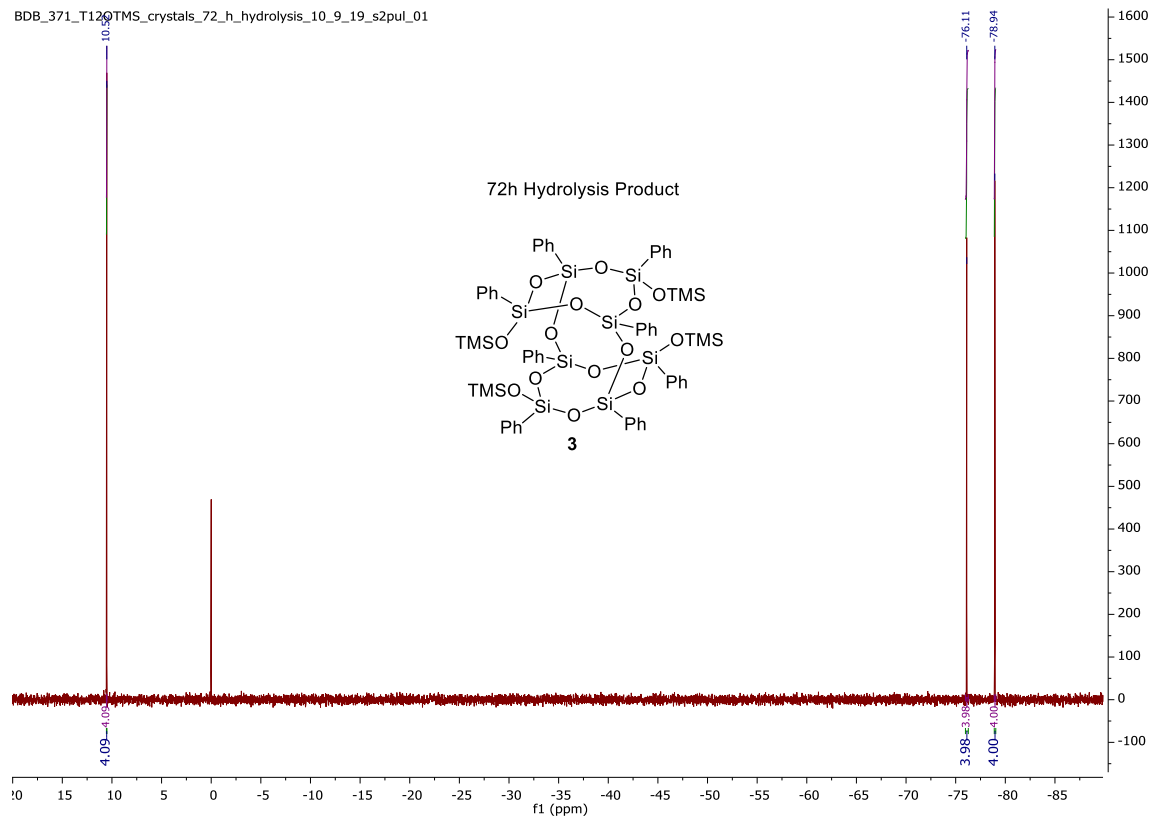
²⁹Si NMR (99 MHz, Chloroform-*d*) δ 10.52, -76.11, -78.94.

Figure 4-26: ^{29}Si NMR 3 – 72h (99 MHz, CDCl_3)

Stacked ^1H NMR of 5,11,14,17-tetrakis(trimethylsilyl)octaphenyltetracyclo[7.3.3.- $3^{3,7}$]octasilsesquioxane (**3**) from 16 to 72 Hydrolysis of **1**

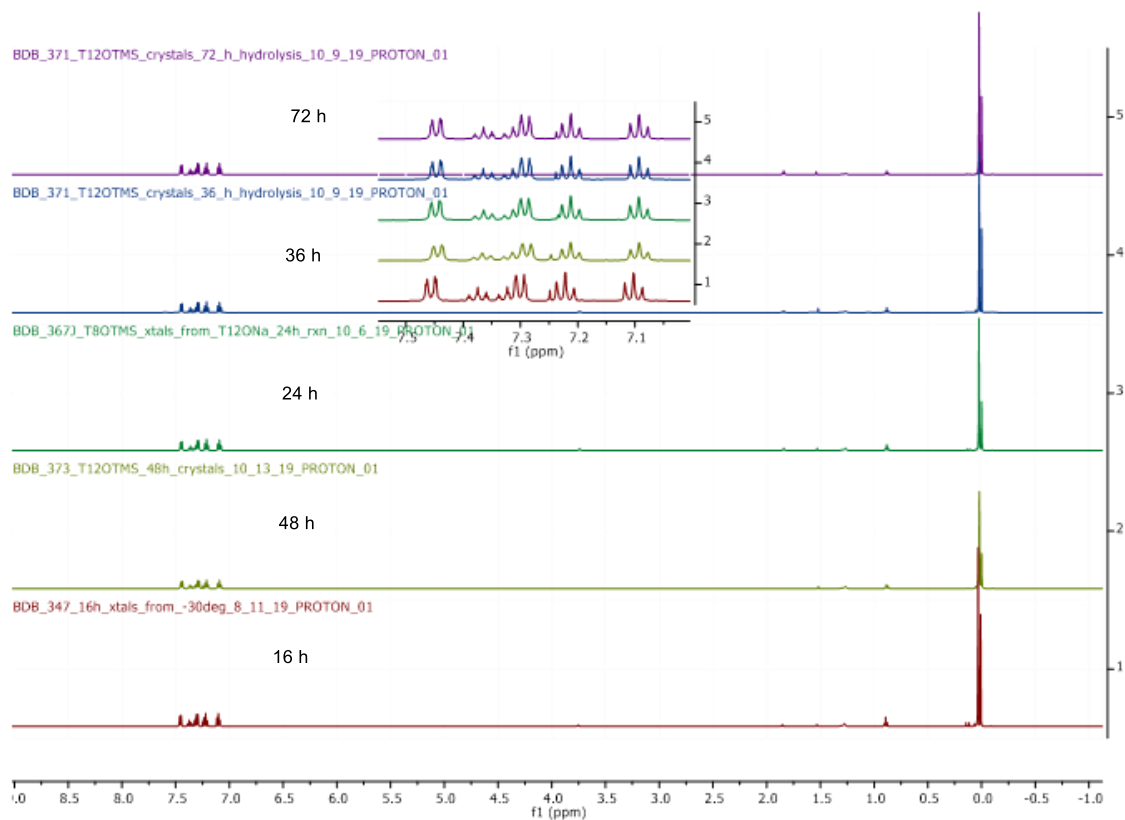


Figure 4-27: Stacked ^1H NMR of 5,11,14,17-tetrakis(trimethylsilyl)octaphenyltetracyclo[7.3.3.- $3^{3,7}$]octasilsesquioxane (**3**) from 16 to 72 Hydrolysis of **1** (500 MHz, CDCl_3)

Stacked ^{29}Si NMR of 5,11,14,17-tetrakis(trimethylsilyl)octaphenyltetracyclo[7.3.3.- $3^{3,7}$]octasilsesquioxane (**3**) from 16 to 72 Hydrolysis of **1**

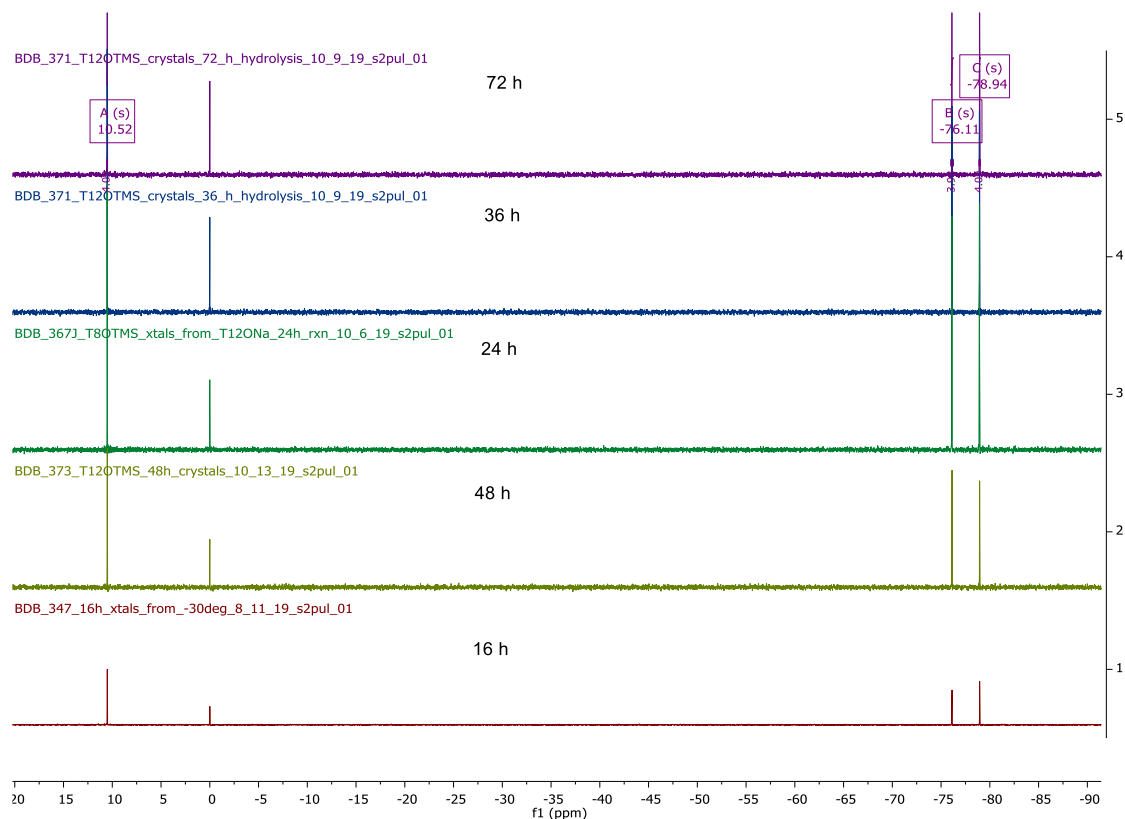


Figure 4-28: Stacked ^{29}Si NMR of 5,11,14,17-tetrakis(trimethylsilyl)octaphenyltetracyclo[7.3.3.- $3^{3,7}$]octasilsesquioxane (**3**) from 16 to 72 Hydrolysis of **1** (99 MHz, CDCl_3)

¹H and ²⁹Si NMR of Commercial Dodecaphenylsilsesquioxane (Ph₁₂T₁₂) (1)

¹H NMR (500 MHz, Toluene-*d*₈) δ 8.15 – 7.84 (m, 24H), 7.40 – 7.17 (m, 36H).

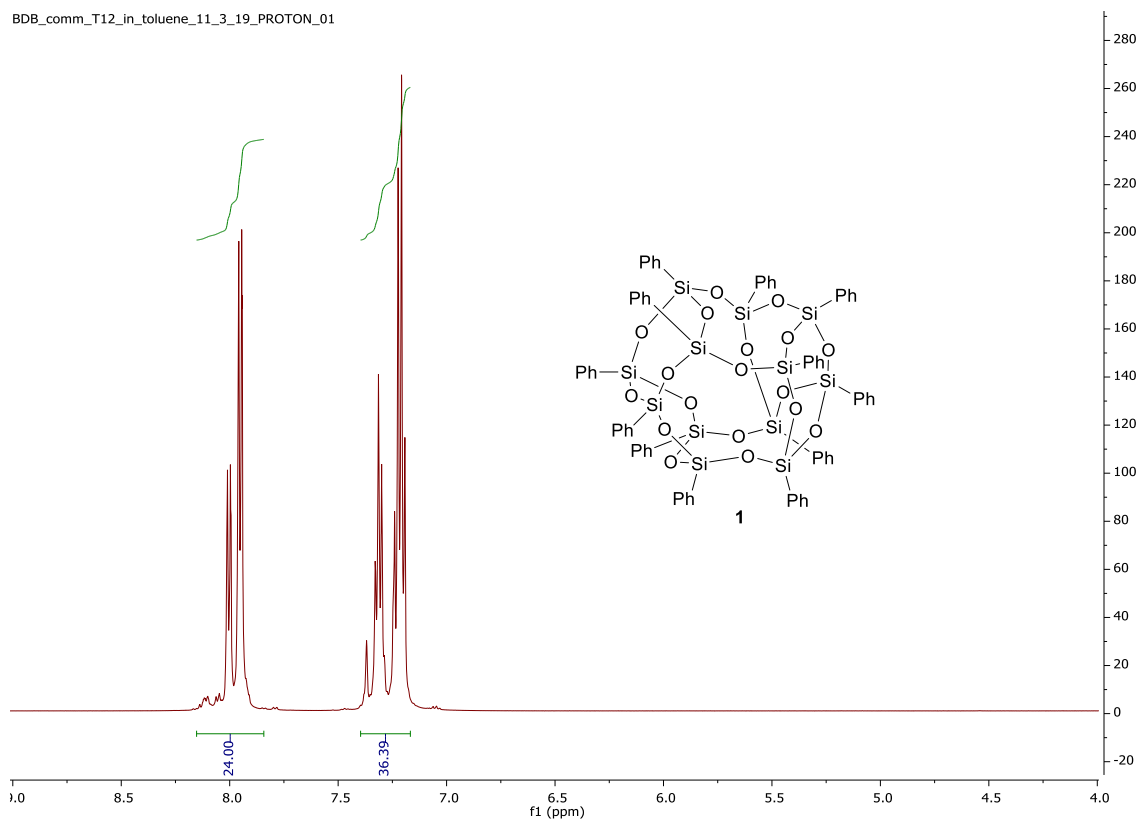


Figure 4-29: ¹H NMR of commercial **1** (500 MHz, Toluene-*d*₈)

^{29}Si NMR (99 MHz, Toluene- d_8) δ -73.63, -75.77

BDB_comm_T12_in_toluene_11_3_19_s2pul_01

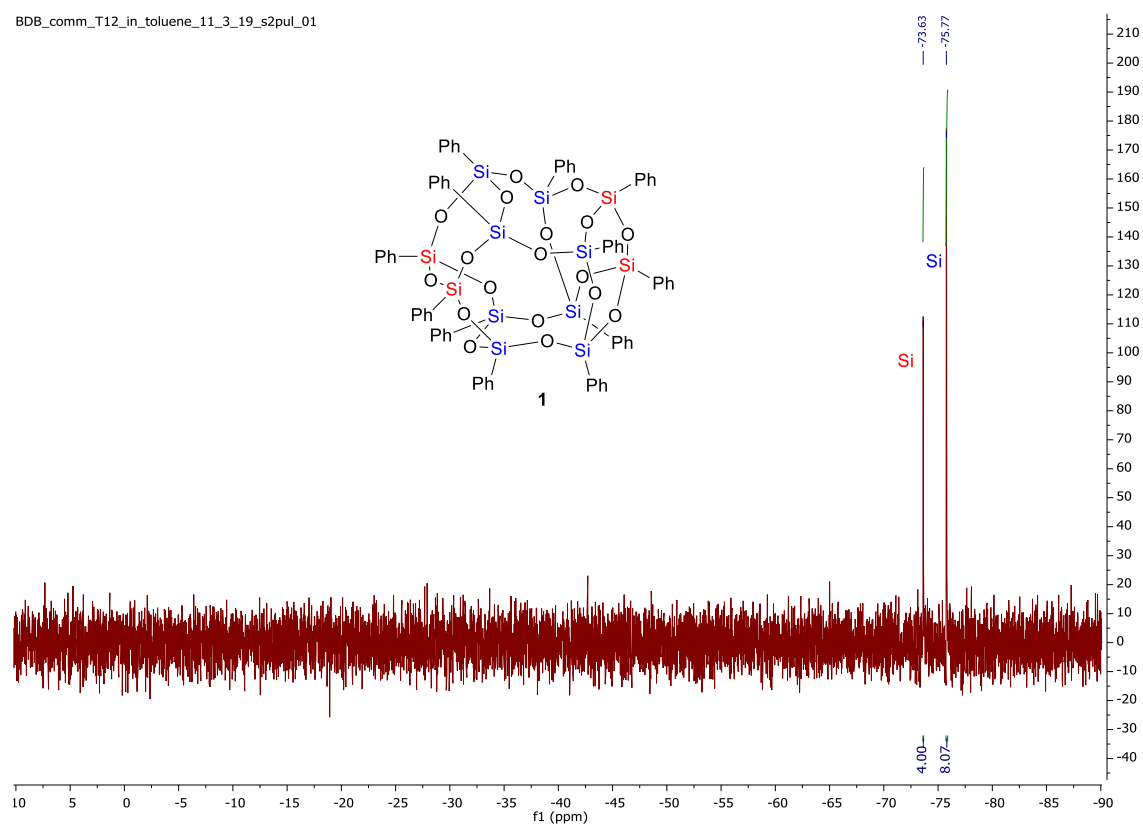


Figure 4-30: ^{29}Si NMR of commercial 1 (99 MHz, CDCl_3)

Recovered $\text{Ph}_{12}\text{T}_{12}$ (1) from the hydrolysis of 1 with NaOH

^1H NMR (500 MHz, Toluene- d_8) δ 8.21 – 7.74 (m, 24H), 7.38 – 7.19 (m, 36H).

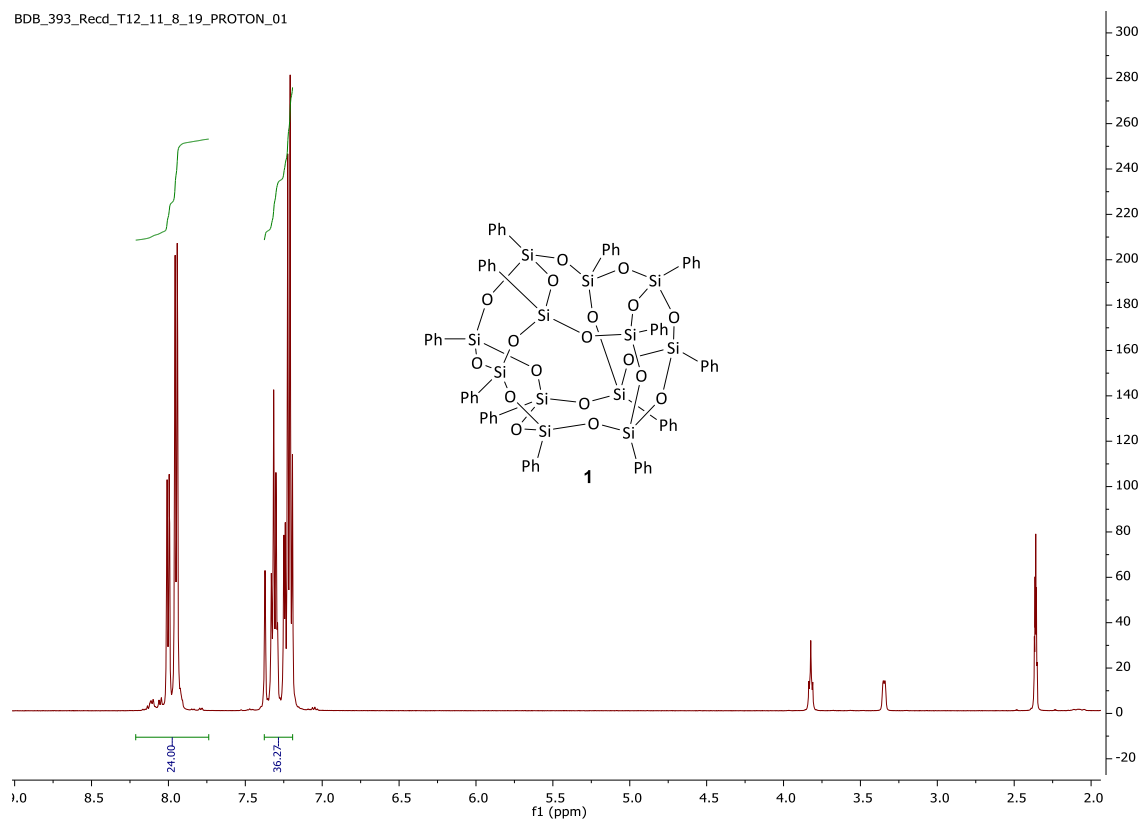


Figure 4-31: ^1H NMR of recovered 1 (500 MHz, Toluene- d_8)

^{29}Si NMR (99 MHz, Toluene- d_8) δ -73.63, -75.77.

BDB_393_Recd_T12_11_8_19_s2pul_01

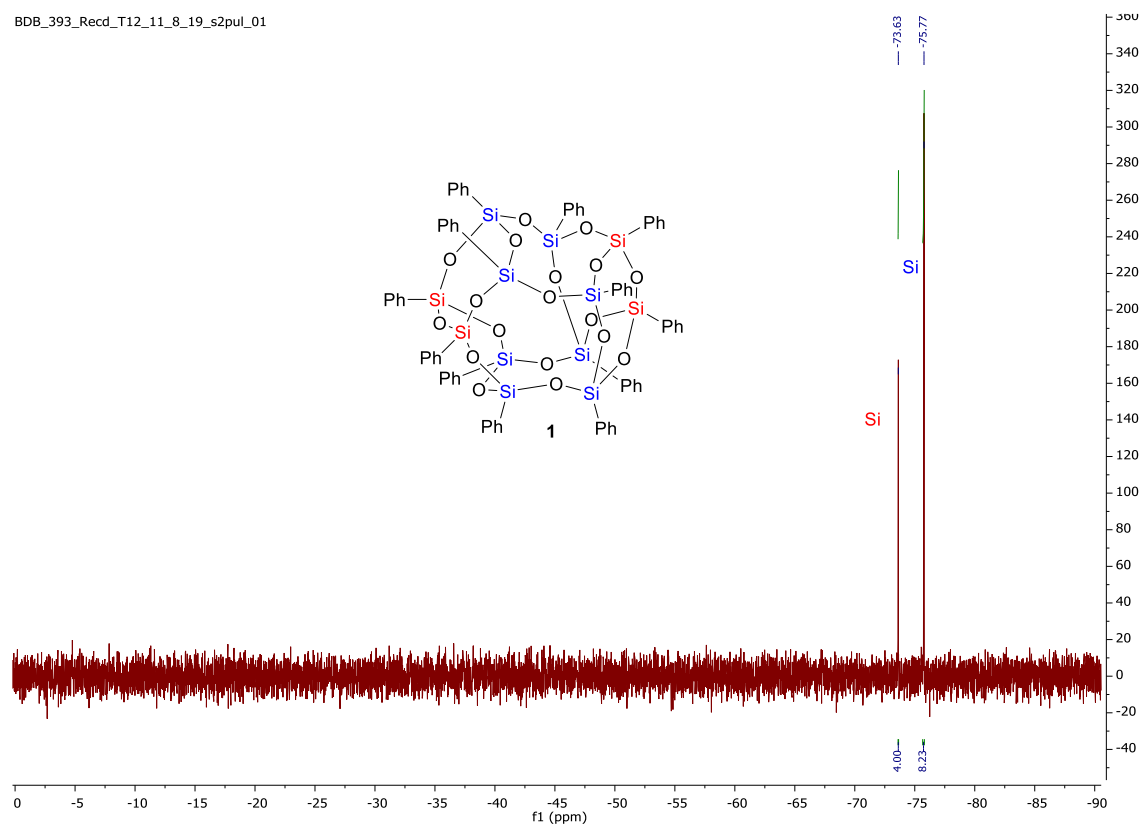


Figure 4-32: ^{29}Si NMR of recovered **1** (99 MHz, CDCl_3)

Stacked ^1H NMR of Commercial $\text{Ph}_{12}\text{T}_{12}$ (**1**) and Recovered $\text{Ph}_{12}\text{T}_{12}$ (**1**)

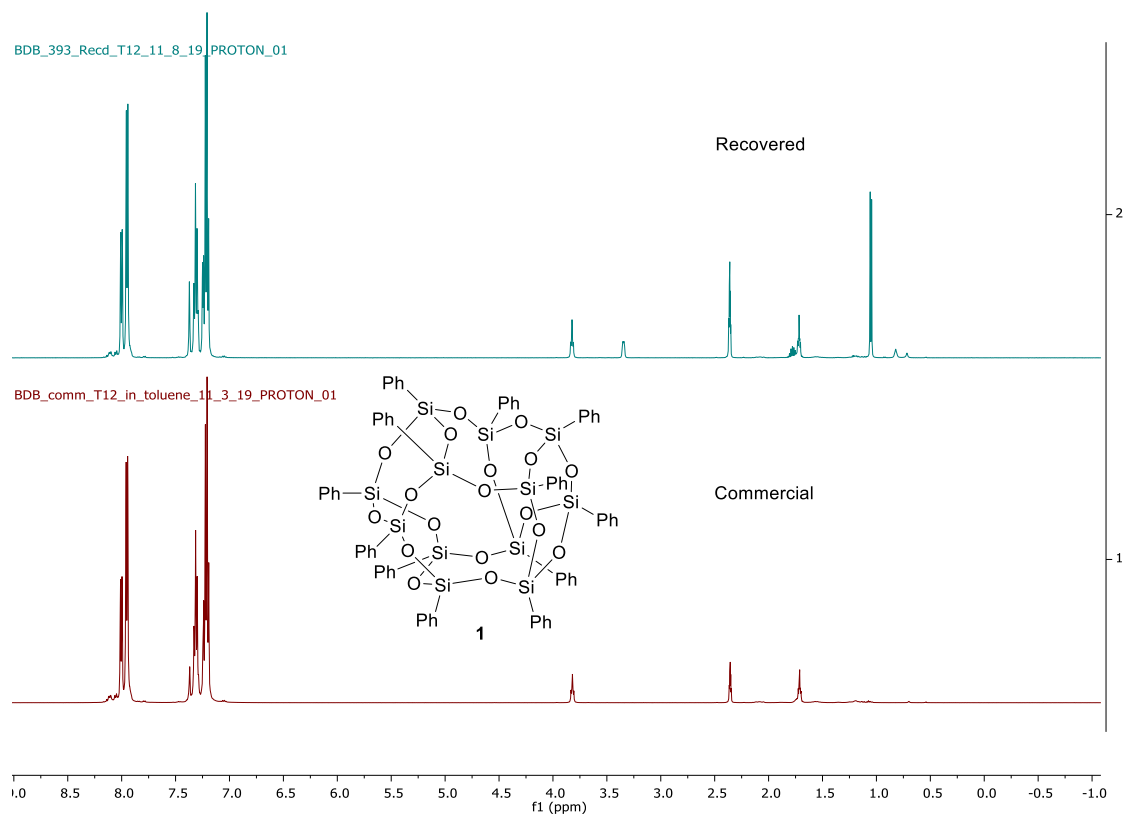


Figure 4-33: Stacked ^1H NMR of Commercial $\text{Ph}_{12}\text{T}_{12}$ (**1**) and Recovered $\text{Ph}_{12}\text{T}_{12}$ (**1**) (500 MHz, Toluene- d_8)

Stacked ^{29}Si NMR of Commercial $\text{Ph}_{12}\text{T}_{12}$ (1) and Recovered $\text{Ph}_{12}\text{T}_{12}$ (1)

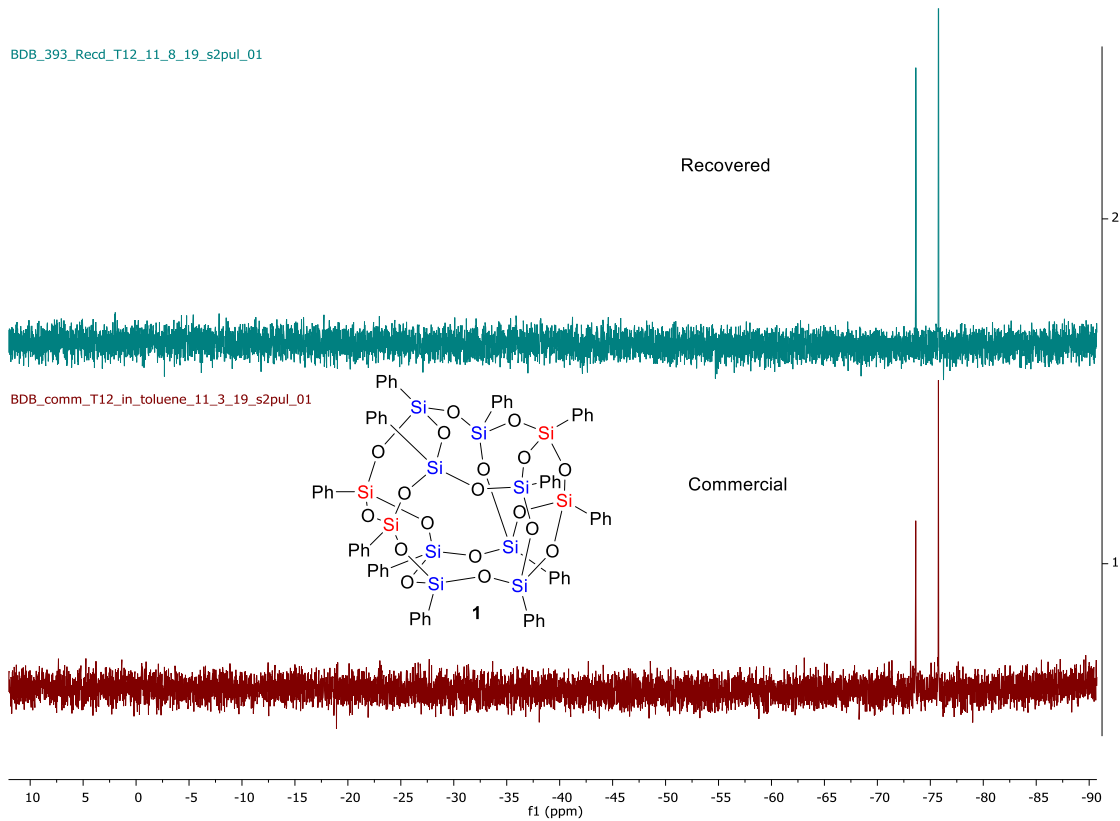


Figure 4-34: Stacked ^{29}Si NMR of Commercial $\text{Ph}_{12}\text{T}_{12}$ (1) and Recovered $\text{Ph}_{12}\text{T}_{12}$ (1)
(99 MHz, CDCl_3)

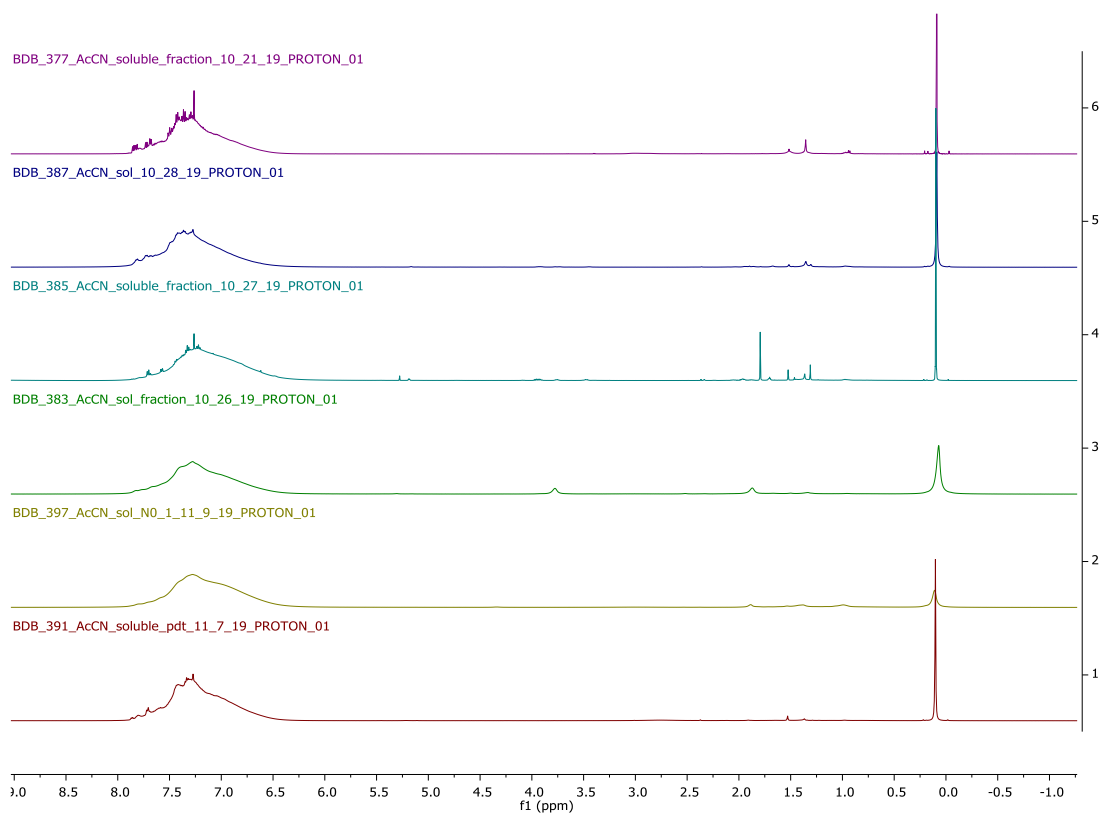


Figure 4-35: Stacked ^1H NMR of Resinous product from the acid hydrolysis of intermediate salt (**12**) (500 MHz, CDCl_3)

The aromatic protons in the 6.5–8.0 ppm is attributed to phenyl groups.³ The peaks in this region are broader due to a higher molecular weight suggesting that the material could be a resin from $\text{Ph}_{12}\text{T}_{12}$.

*Stacked ^{29}Si NMR of Resinous product from the acid hydrolysis of intermediate salt **12***

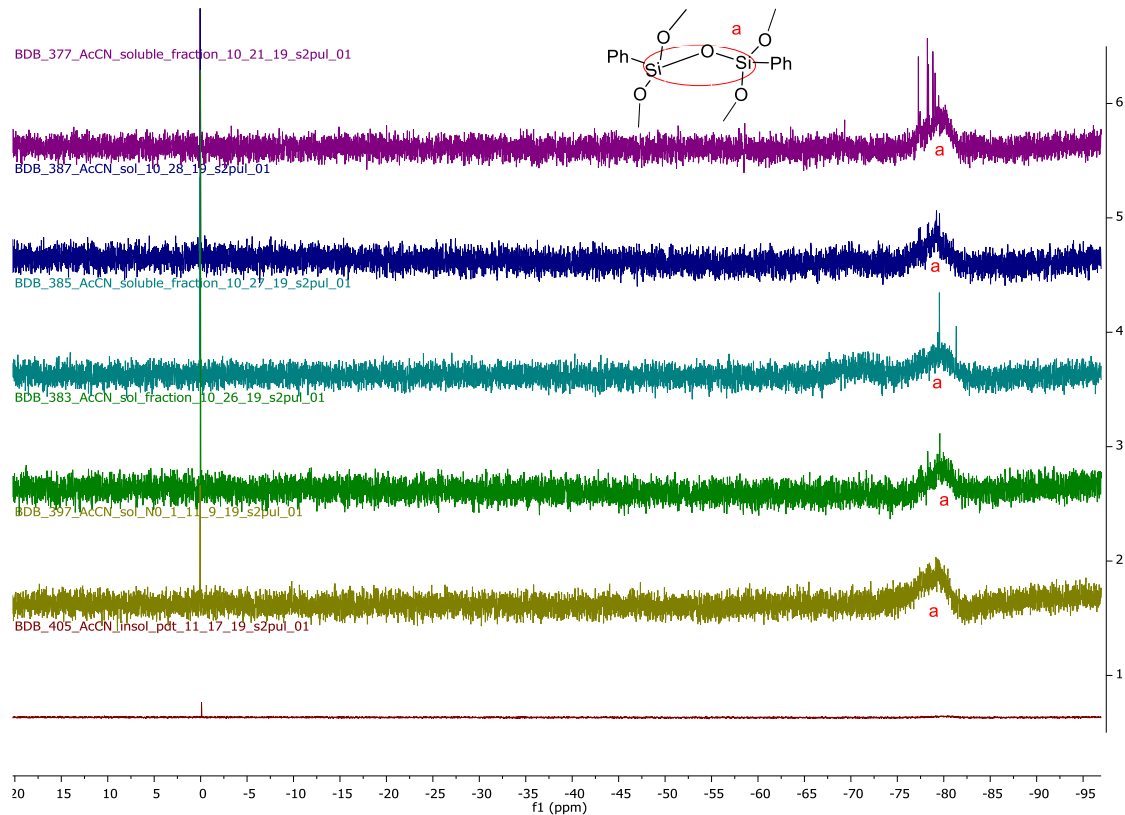


Figure 4-36: Stacked ^{29}Si NMR of Resinous product from the acid hydrolysis of intermediate salt **12** (99 MHz, CDCl_3)

The broad siloxane peak centered about -80 ppm is characteristic of the T3 unit $\text{Ph-Si}(\text{O-Si-})_3$ denoting a polysilsesquioxane fragment.^{3,4} The sharp peaks between -77 and -79 ppm are ascribed to some fully condensed siloxane structures lost into the MeCN solvent.

DOESY NMR Spectra of resinous product.

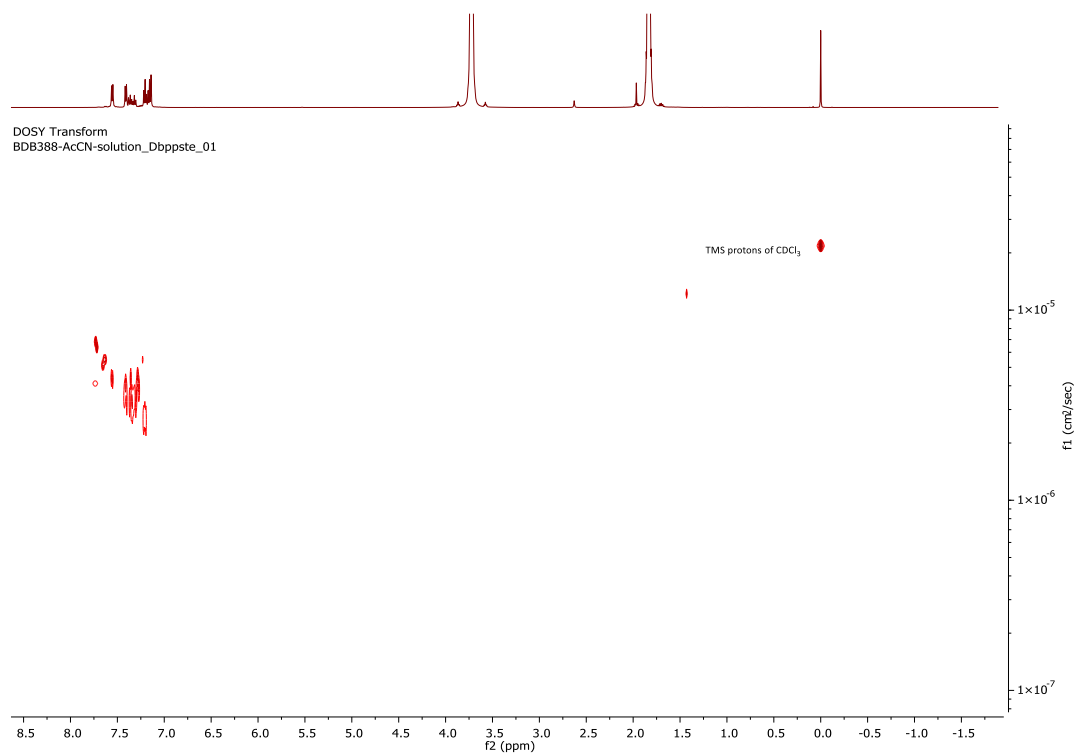


Figure 4-37: DOESY NMR Spectra of resinous product (500 MHz, CDCl₃)

DOSY Spectra for 5,11,14,17-tetrakis(trimethylsilyl)octaphenyltetracyclo[7.3.3.-
3^{3,7}]octasilsesquioxane (**3**).

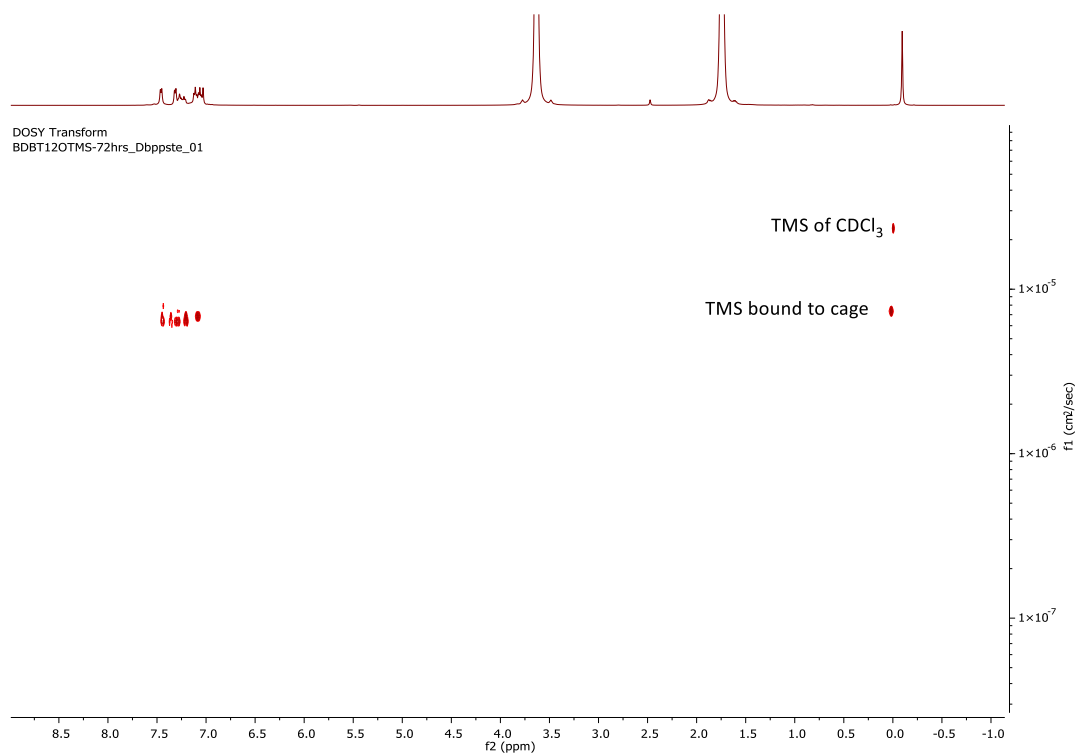


Figure 4-38: DOSY Spectra for 5,11,14,17-tetrakis(trimethylsilyl)octaphenyltetracyclo-
[7.3.3.-3^{3,7}]octasilsesquioxane (**3**) (500 MHz, CDCl₃)

Selected Mass Spectra

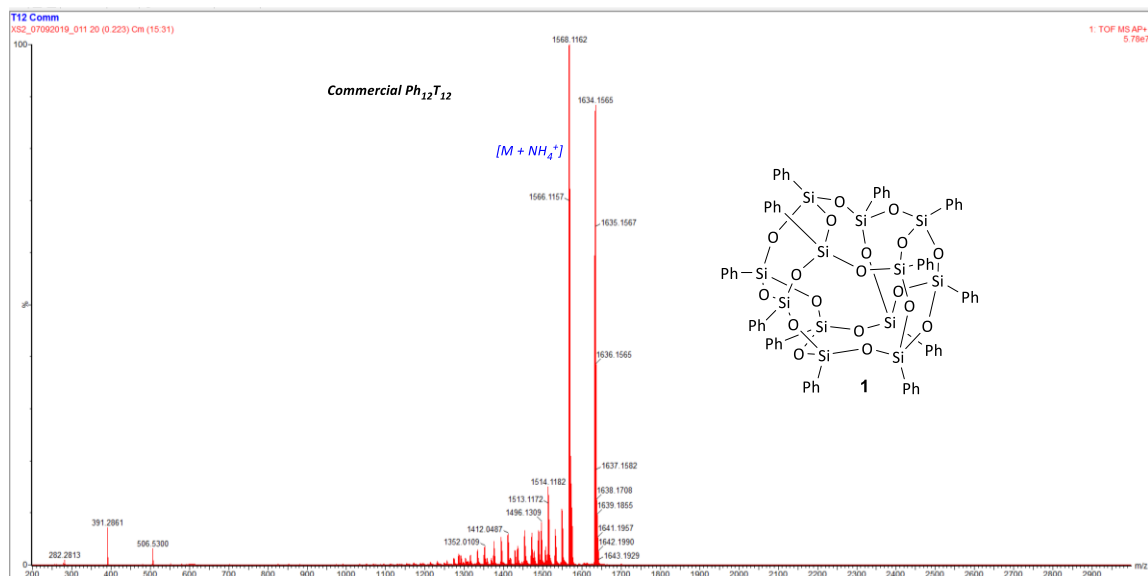


Figure 4-39: Commercial Ph₁₂T₁₂ (1)

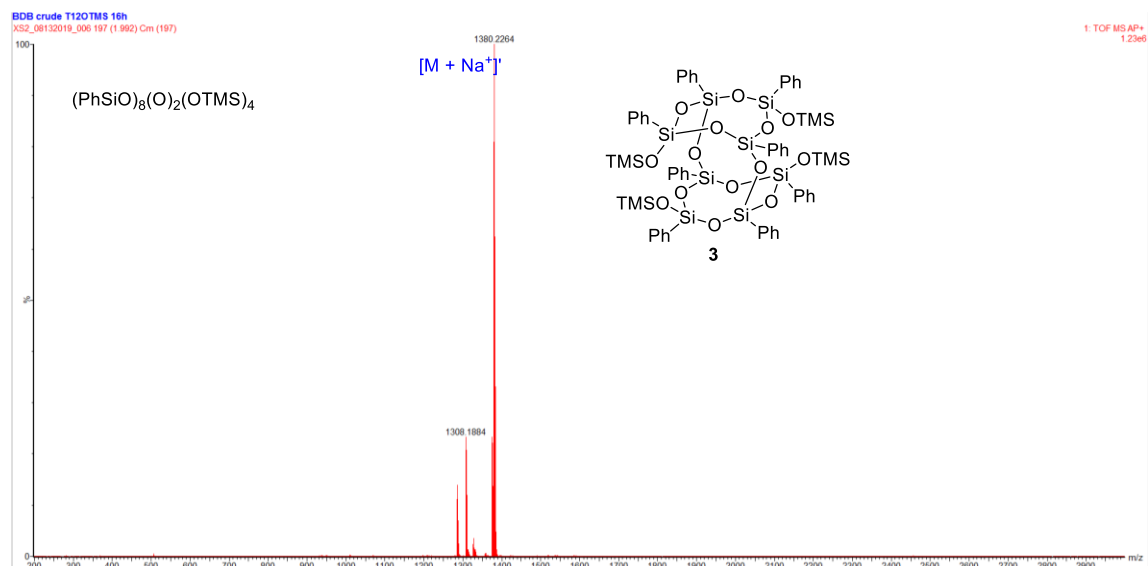


Figure 4-40: 5,11,14,17-tetrakis(trimethylsilyl)octaphenyltetracyclo[7.3.3.-3^{3,7}]octasilsequioxane (**3**) from 16 h hydrolyzed **12**

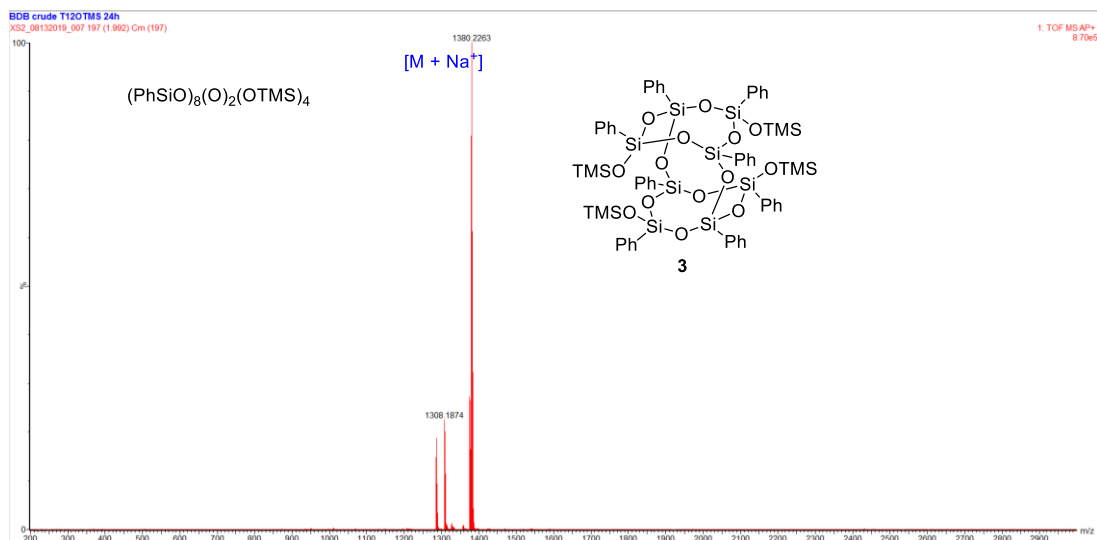


Figure 4-41: 5,11,14,17-tetrakis(trimethylsilyl)octaphenyltetracyclo[7.3.3.-3^{3,7}]octasilses-quioxane (**3**) from 24 h hydrolyzed **12**

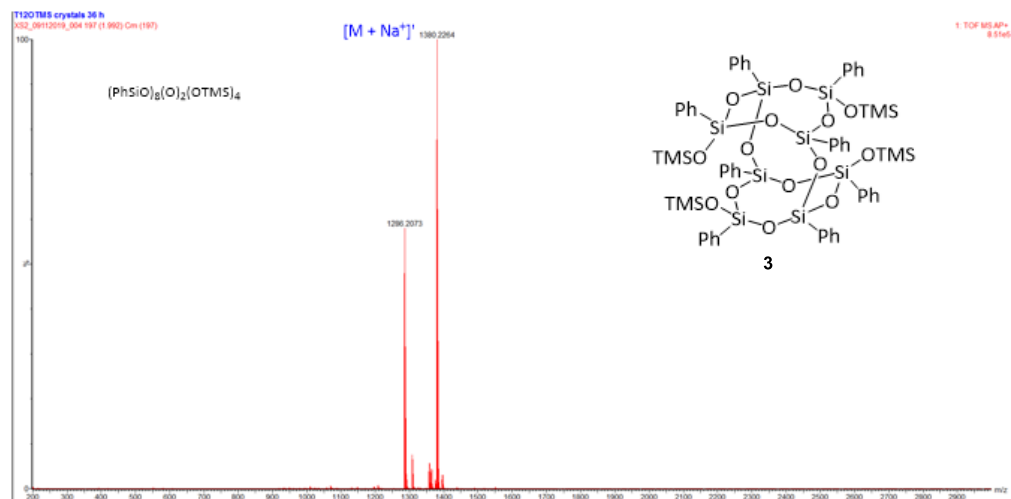


Figure 4-42: 5,11,14,17-tetrakis(trimethylsilyl)octaphenyltetracyclo[7.3.3.-3^{3,7}]octasilses-quioxane (**3**) from 36 h hydrolyzed **12**

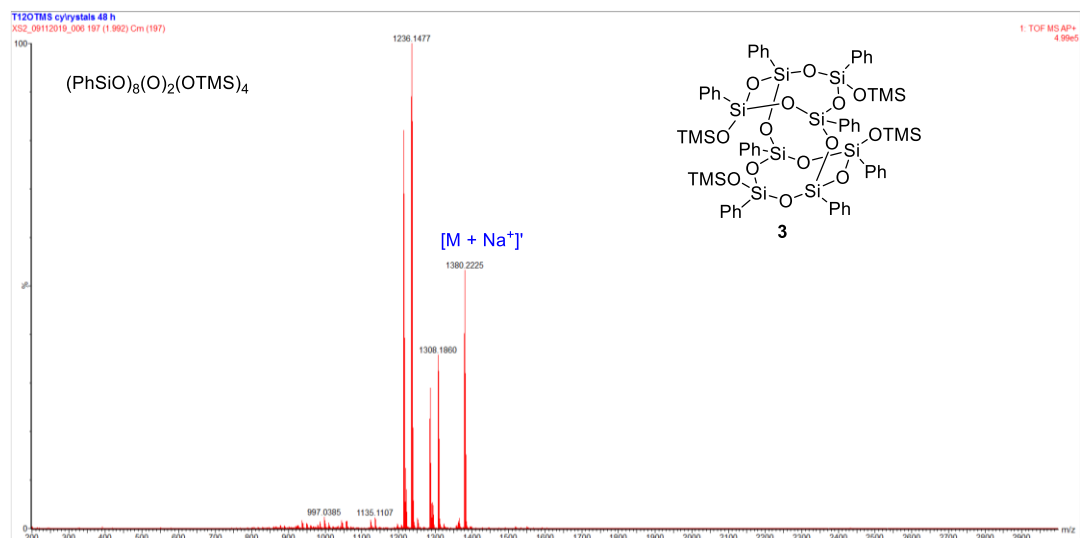


Figure 4-43: 5,11,14,17-tetrakis(trimethylsilyl)octaphenyltetracyclo[7.3.3.-3^{3,7}]octasilsesquioxane (**3**) from 48 h hydrolyzed **12**

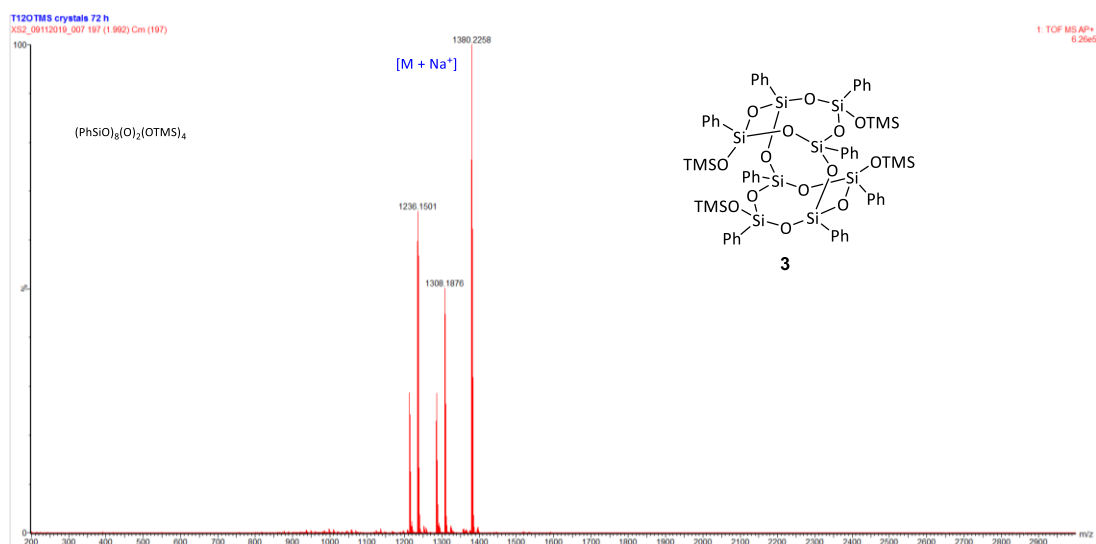


Figure 4-44: 5,11,14,17-tetrakis(trimethylsilyl)octaphenyltetracyclo[7.3.3.-3^{3,7}]octasilsesquioxane (**3**) from 72 h hydrolyzed **12**

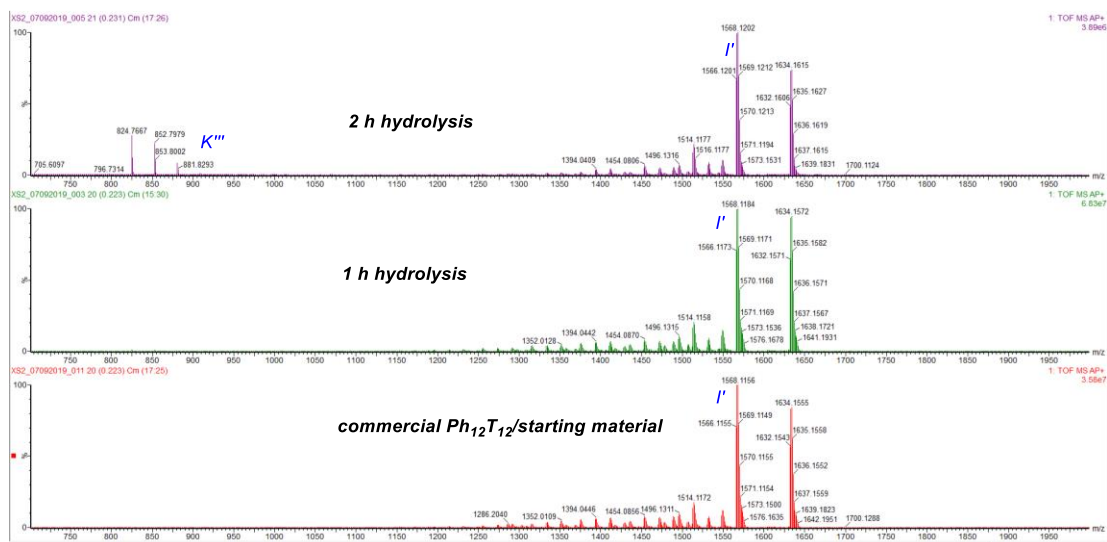


Figure 4-45: MS Spectra for 0 – 2 h hydrolyzed 12

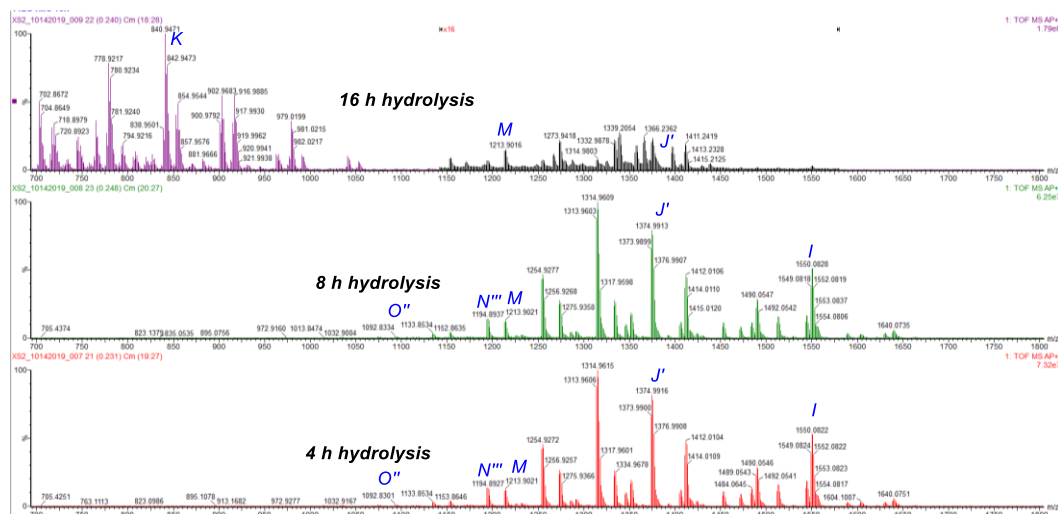
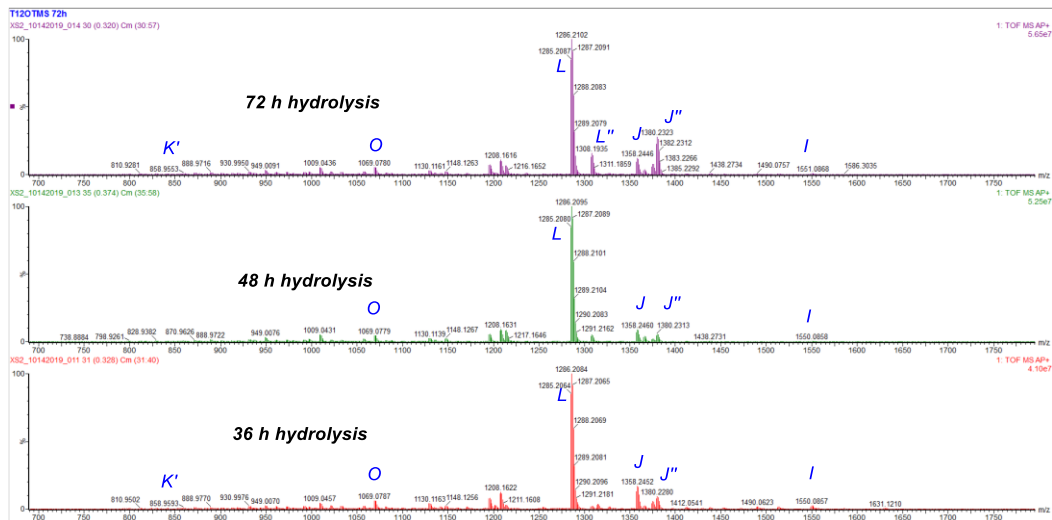


Figure 4-46: MS Spectra for 4 – 8 h hydrolyzed 12

$I = [\text{Ph}_{12}\text{T}_{12} + \text{H}^+]$, $I' = [\text{Ph}_{12}\text{T}_{12} + \text{NH}_4^+]$, $I'' = [\text{Ph}_{12}\text{T}_{12} + \text{Na}^+]$, $I''' = [\text{Ph}_{12}\text{T}_{12} + \text{K}^+]$
 $J = [(\text{PhSiO})_8(\text{O})_2(\text{OTMS})_4 + \text{H}^+]$, $J' = [(\text{PhSiO})_8(\text{O})_2(\text{OTMS})_4 + \text{NH}_4^+]$, $J'' = [(\text{PhSiO})_8(\text{O})_2(\text{OTMS})_4 + \text{Na}^+]$, $J''' = [(\text{PhSiO})_8(\text{O})_2(\text{OTMS})_4 + \text{K}^+]$
 $K = [(\text{PhSiO})_4(\text{OTMS})_4 + \text{H}^+]$, $K' = [(\text{PhSiO})_4(\text{OTMS})_4 + \text{NH}_4^+]$, $K'' = [(\text{PhSiO})_4(\text{OTMS})_4 + \text{Na}^+]$, $K''' = [(\text{PhSiO})_4(\text{OTMS})_4 + \text{K}^+]$
 $L = [(\text{PhSiO})_8(\text{O})_2(\text{OH})(\text{OTMS})_3 + \text{H}^+]$, $L' = [(\text{PhSiO})_8(\text{O})_2(\text{OH})(\text{OTMS})_3 + \text{NH}_4^+]$, $L'' = [(\text{PhSiO})_8(\text{O})_2(\text{OH})(\text{OTMS})_3 + \text{Na}^+]$, $L''' = [(\text{PhSiO})_8(\text{O})_2(\text{OH})(\text{OTMS})_3 + \text{K}^+]$
 $M = [(\text{PhSiO})_8(\text{O})_2(\text{OH})_2(\text{OTMS})_2 + \text{H}^+]$, $M' = [(\text{PhSiO})_8(\text{O})_2(\text{OH})_2(\text{OTMS})_2 + \text{NH}_4^+]$, $M'' = [(\text{PhSiO})_8(\text{O})_2(\text{OH})_2(\text{OTMS})_2 + \text{Na}^+]$, $M''' = [(\text{PhSiO})_8(\text{O})_2(\text{OH})_2(\text{OTMS})_2 + \text{K}^+]$
 $N = [(\text{PhSiO})_8(\text{O})_2(\text{ONa})_4 + \text{H}^+]$, $N' = [(\text{PhSiO})_8(\text{O})_2(\text{ONa})_4 + \text{NH}_4^+]$, $N'' = [(\text{PhSiO})_8(\text{O})_2(\text{ONa})_4 + \text{Na}^+]$, $N''' = [(\text{PhSiO})_8(\text{O})_2(\text{ONa})_4 + \text{K}^+]$
 $O = [(\text{PhSiO})_8(\text{O})_2(\text{OH})_4 + \text{H}^+]$, $O' = [(\text{PhSiO})_8(\text{O})_2(\text{OH})_4 + \text{NH}_4^+]$, $O'' = [(\text{PhSiO})_8(\text{O})_2(\text{OH})_4 + \text{Na}^+]$, $O''' = [(\text{PhSiO})_8(\text{O})_2(\text{OH})_4 + \text{K}^+]$



X-ray crystallographic data

Table 4-5: Crystal and Experimental Data for 5,11,14,17-tetrakis(trimethylsilyl)-octaphenyltetracyclo[7.3.3.-3^{3,7}]octasilsesquioxane (**3**) (CCDC 299794^a)

Compound	5,11,14,17-tetrakis(trimethylsilyl)octaphenyltetracyclo[7.3.3.-3 ^{3,7}]octasilsesquioxane (3)
$D_{calc.}/\text{g cm}^{-3}$	1.239
μ/mm^{-1}	2.317
Formula Weight	1502.49
Color	colourless
Shape	block
Size/ mm^3	0.41×0.30×0.22
T/K	173(2)
Crystal System	monoclinic
Space Group	$P2_1/n$
$a/\text{\AA}$	12.8512(2)
$b/\text{\AA}$	18.5351(5)
$c/\text{\AA}$	16.9170(3)
$\alpha/^\circ$	90
$\beta/^\circ$	91.2150(10)
$\gamma/^\circ$	90
$V/\text{\AA}^3$	4028.69(14)
Z	2
Z'	0.5
Wavelength/ \AA	1.541838
Radiation type	$\text{CuK}\alpha$
$\theta_{min}/^\circ$	3.538
$\theta_{max}/^\circ$	68.573
Measured Refl.	13317
Independent Refl.	13317
Reflections with $I > 2(I)$	11099
R_{int}	.
Parameters	440
Restraints	0
Largest Peak	0.631
Deepest Hole	-0.535
GooF	1.087
wR_2 (all data)	0.1878
wR_2	0.1750
R_1 (all data)	0.0737
R_1	0.0603

^aCrystallographic data are those obtained in this study but the CDCC number is that from Kawakami and Lee.²⁰

Table 4-6: Crystal and Experimental Data for 5,11,14,17-tetra(hydro)octaphenyl tetracyclo[7.3.3.-3^{3;7}]octasilsesquioxane (C₄₈H₄₄O₁₄Si₈) (**5**)

Compound	5,11,14,17-Tetra(hydro)octaphenyltetracyclo[7.3.3.-3 ^{3;7}]octasilsesquioxane (5)
CCDC	1901262
Formula	C ₅₆ H ₆₀ O ₁₆ Si ₈
<i>D</i> _{calc.} / g cm ⁻³	1.339
μ/mm ⁻¹	2.238
Formula Weight	1213.76
Color	colourless
Shape	needle
Size/mm ³	0.28×0.10×0.04
<i>T</i> /K	173(2)
Crystal System	triclinic
Space Group	<i>P</i> -1
<i>a</i> /Å	10.9096(2)
<i>b</i> /Å	15.1731(3)
<i>c</i> /Å	18.3358(3)
<i>α</i> /°	83.1970(10)
<i>β</i> /°	88.0820(10)
<i>γ</i> /°	88.1450(10)
<i>V</i> /Å ³	3010.88(10)
<i>Z</i>	2
<i>Z'</i>	1
Wavelength/Å	1.541838
Radiation type	CuK _α
<i>θ</i> _{min} /°	2.428
<i>θ</i> _{max} /°	72.185
Measured Refl.	45542
Independent Refl.	11525
Reflections with <i>I</i> > 2(<i>I</i>)	7020
<i>R</i> _{int}	0.1531
Parameters	725
Restraints	0
Largest Peak	0.543
Deepest Hole	-0.414
GooF	1.013
<i>wR</i> ₂ (all data)	0.1589
<i>wR</i> ₂	0.1338
<i>R</i> ₁ (all data)	0.1140
<i>R</i> ₁	0.0594

Table 4-7: Bond Lengths in Å for 5,11,14,17-tetra(hydro)octaphenyltetracyclo[7.3.3.-33;7]octasilsesquioxane (5)

Atom	Atom	Length (Å)
Si1A	O1A	1.631(3)
Si1A	O2A	1.613(3)
Si1A	O6A ¹	1.618(3)
Si1A	C0AA	1.839(4)
Si2A	O3A	1.620(3)
Si2A	O4A	1.613(3)
Si2A	O7A ¹	1.619(3)
Si2A	C6AA	1.852(4)
Si3A	O2A	1.622(3)
Si3A	O3A	1.600(3)
Si3A	O5A	1.606(3)
Si3A	C2BA	1.848(4)
Si4A	O5A	1.608(3)
Si4A	O6A	1.611(3)
Si4A	O7A	1.612(3)
Si4A	C00S	1.847(4)
C0AA	C1AA	1.384(6)
C0AA	C5AA	1.392(6)
C0BA	C1BA	1.384(7)
C0BA	C9AA	1.378(8)
C00S	C012	1.377(6)
C00S	C015	1.394(6)
C1AA	C2AA	1.401(6)
C01B	C01I	1.367(7)
C01B	C01O	1.358(7)
C1BA	C6AA	1.387(6)
C01I	C015	1.390(6)
C01O	C012	1.407(7)
C2AA	C3AA	1.371(7)
C2BA	C3BA	1.398(6)
C2BA	C7BA	1.381(6)
C3AA	C4AA	1.361(7)
C3BA	C4BA	1.393(6)
C4AA	C5AA	1.393(6)
C4BA	C5BA	1.379(8)
C5BA	C6BA	1.354(7)
C6AA	C7AA	1.404(6)
C6BA	C7BA	1.390(7)
C7AA	C8AA	1.382(7)
C8AA	C9AA	1.381(9)
Si1B	O1B	1.621(3)
Si1B	O2B	1.624(3)
Si1B	O7B ²	1.618(3)

Table 4-7 (cont'd)

Atom	Atom	Length (Å)
Si1B	C1A	1.844(4)
Si2B	O3B	1.620(3)
Si2B	O4B	1.606(3)
Si2B	O6B ²	1.628(3)
Si2B	C7A	1.843(4)
Si3B	O2B	1.619(3)
Si3B	O3B	1.602(3)
Si3B	O5B	1.605(3)
Si3B	C13A	1.859(4)
Si4B	O5B	1.615(3)
Si4B	O7B	1.613(3)
Si4B	C19A	1.837(4)
C1A	C2A	1.394(6)
C1A	C6A	1.397(6)
C2A	C3A	1.393(6)
C3A	C4A	1.382(7)
C4A	C5A	1.368(7)
C5A	C6A	1.381(6)
C7A	C8A	1.383(7)
C7A	C12A	1.394(7)
C8A	C9A	1.398(8)
C9A	C10A	1.373(10)
C10A	C11A	1.369(10)
C11A	C12A	1.379(7)
C13A	C14A	1.385(7)
C13A	C18A	1.385(7)
C14A	C15A	1.385(7)
C15A	C16A	1.378(10)
C16A	C17A	1.368(10)
C17A	C18A	1.410(7)
C19A	C20A	1.396(6)
C19A	C24A	1.398(6)
C20A	C21A	1.390(6)
C21A	C22A	1.375(7)
C22A	C23A	1.372(7)
C23A	C24A	1.386(6)
O1S	C1S	1.435(6)
O1S	C4S	1.423(7)
C1S	C2S	1.483(8)
C2S	C3S	1.511(8)
C3S	C4S	1.485(8)

Table 4-8: Bond Angles in ° for 5,11,14,17-tetra(hydro)octaphenyltetracyclo[7.3.3.-33;7]octasilsesquioxane (5)

Atom	Atom	Atom	Angle (°)
O1A	Si1A	C0AA	112.23(17)
O2A	Si1A	O1A	105.51(15)
O2A	Si1A	O6A ¹	111.33(15)
O2A	Si1A	C0AA	110.80(17)
O6A ¹	Si1A	O1A	109.87(16)
O6A ¹	Si1A	C0AA	107.18(16)
O3A	Si2A	C6AA	109.33(18)
O4A	Si2A	O3A	109.95(16)
O4A	Si2A	O7A ¹	109.97(18)
O4A	Si2A	C6AA	108.95(18)
O7A ¹	Si2A	O3A	108.39(16)
O7A ¹	Si2A	C6AA	110.24(18)
O2A	Si3A	C2BA	111.61(17)
O3A	Si3A	O2A	109.26(16)
O3A	Si3A	O5A	109.59(16)
O3A	Si3A	C2BA	109.92(18)
O5A	Si3A	O2A	107.61(15)
O5A	Si3A	C2BA	108.81(17)
O5A	Si4A	O6A	110.25(16)
O5A	Si4A	O7A	108.38(16)
O5A	Si4A	C00S	107.60(17)
O6A	Si4A	O7A	110.06(16)
O6A	Si4A	C00S	110.08(18)
O7A	Si4A	C00S	110.42(17)
Si1A	O2A	Si3A	150.4(2)
Si3A	O3A	Si2A	163.0(2)
Si3A	O5A	Si4A	153.4(2)
Si4A	O6A	Si1A ¹	153.3(2)
Si4A	O7A	Si2A ¹	149.0(2)
C1AA	C0AA	Si1A	123.3(3)
C1AA	C0AA	C5AA	118.1(4)
C5AA	C0AA	Si1A	118.7(3)
C9AA	C0BA	C1BA	120.6(5)
C012	C00S	Si4A	123.5(3)
C012	C00S	C015	117.6(4)
C015	C00S	Si4A	118.8(3)
C0AA	C1AA	C2AA	120.6(5)
C01O	C01B	C01I	121.2(5)
C0BA	C1BA	C6AA	121.0(5)
C01B	C01I	C015	118.8(5)
C01B	C01O	C012	119.9(5)

Table 4-8 (cont'd)

Atom	Atom	Atom	Angle (°)
C3AA	C2AA	C1AA	119.8(5)
C3BA	C2BA	Si3A	121.3(3)
C7BA	C2BA	Si3A	121.6(3)
C7BA	C2BA	C3BA	117.1(4)
C4AA	C3AA	C2AA	120.7(4)
C4BA	C3BA	C2BA	120.7(5)
C3AA	C4AA	C5AA	119.8(5)
C5BA	C4BA	C3BA	120.0(5)
C0AA	C5AA	C4AA	121.1(4)
C6BA	C5BA	C4BA	120.3(5)
C1BA	C6AA	Si2A	122.0(3)
C1BA	C6AA	C7AA	118.2(4)
C7AA	C6AA	Si2A	119.7(3)
C5BA	C6BA	C7BA	119.7(5)
C8AA	C7AA	C6AA	120.0(5)
C2BA	C7BA	C6BA	122.2(5)
C9AA	C8AA	C7AA	121.2(6)
C0BA	C9AA	C8AA	118.9(5)
C00S	C012	C01O	120.6(5)
C01I	C015	C00S	121.9(4)
O1B	Si1B	O2B	104.20(14)
O1B	Si1B	C1A	111.67(17)
O2B	Si1B	C1A	110.98(16)
O7B ²	Si1B	O1B	111.21(15)
O7B ²	Si1B	O2B	110.92(15)
O7B ²	Si1B	C1A	107.90(17)
O3B	Si2B	O6B ²	108.00(15)
O3B	Si2B	C7A	110.53(17)
O4B	Si2B	O3B	109.46(16)
O4B	Si2B	O6B ²	111.49(16)
O4B	Si2B	C7A	108.32(18)
O6B ²	Si2B	C7A	109.06(19)
O2B	Si3B	C13A	111.65(17)
O3B	Si3B	O2B	109.17(15)
O3B	Si3B	O5B	109.57(16)
O3B	Si3B	C13A	109.82(19)
O5B	Si3B	O2B	107.97(15)
O5B	Si3B	C13A	108.64(18)
O5B	Si4B	C19A	109.32(16)
O6B	Si4B	O5B	109.22(15)
O6B	Si4B	O7B	110.68(15)
O6B	Si4B	C19A	110.06(17)
O7B	Si4B	O5B	109.27(16)
O7B	Si4B	C19A	108.27(17)

Table 4-8 (cont'd)

Atom	Atom	Atom	Angle (°)
Si3B	O2B	Si1B	146.72(18)
Si3B	O3B	Si2B	167.1(2)
Si3B	O5B	Si4B	155.21(19)
Si4B	O6B	Si2B ²	144.03(19)
Si4B	O7B	Si1B ²	149.74(19)
C2A	C1A	Si1B	122.5(3)
C2A	C1A	C6A	117.7(4)
C6A	C1A	Si1B	119.9(3)
C3A	C2A	C1A	121.1(4)
C4A	C3A	C2A	119.3(5)
C5A	C4A	C3A	120.5(4)
C4A	C5A	C6A	120.1(5)
C5A	C6A	C1A	121.2(4)
C8A	C7A	Si2B	121.4(4)
C8A	C7A	C12A	118.0(4)
C12A	C7A	Si2B	120.7(4)
C7A	C8A	C9A	121.3(6)
C10A	C9A	C8A	118.8(7)
C11A	C10A	C9A	121.0(6)
C10A	C11A	C12A	119.9(7)
C11A	C12A	C7A	121.0(6)
C14A	C13A	Si3B	120.4(4)
C14A	C13A	C18A	118.7(4)
C18A	C13A	Si3B	120.8(4)
C13A	C14A	C15A	122.0(6)
C16A	C15A	C14A	118.3(6)
17A	C16A	C15A	121.6(5)
C16A	C17A	C18A	119.4(6)
C13A	C18A	C17A	119.8(6)
C20A	C19A	Si4B	121.7(3)
C20A	C19A	C24A	117.1(4)
C24A	C19A	Si4B	121.1(3)
C21A	C20A	C19A	121.5(4)
C22A	C21A	C20A	119.7(4)
C23A	C22A	C21A	120.2(4)
C22A	C23A	C24A	120.3(5)
C23A	C24A	C19A	121.2(4)
C4S	O1S	C1S	106.8(4)
O1S	C1S	C2S	105.0(4)
C1S	C2S	C3S	102.0(5)
C4S	C3S	C2S	103.3(5)
C5S	C6S	C7S	103.9(4)

¹1-x,1-y,1-z; ²-x,2-y,2-z

Table 4-9: Hydrogen Fractional Atomic Coordinates ($\times 10^4$) and Equivalent Isotropic Displacement Parameters ($\text{\AA}^2 \times 10^3$) for 5,11,14,17-tetra(hydro)octaphenyltetracyclo [7.3.3.-3^{3;7}]octasilsesquioxane (**5**). U_{eq} is defined as 1/3 of the trace of the orthogonalised U_{ij}

Atom	x	y	z	U_{eq}
H1A	4555.44	4990.65	2757.58	54
H4A	6551.4	4018.68	6578.17	60
H0BA	8563.17	430.43	6312.28	79
H1AA	3312.2	2342.31	3922.91	57
H01B	-1747.43	5915.8	7143.67	66
H1BA	8118.58	1916.35	6424.62	54
H01I	-1531.02	5077.63	6167.07	60
H01O	-70.31	6525.63	7597.44	77
H2AA	3290.7	1040.03	3347.79	72
H3AA	4532.78	901.61	2314.87	61
H3BA	1242.08	3149.68	4927.78	50
H4AA	5796.42	2035.04	1844.59	58
H4BA	67.48	1887.28	5217.45	66
H5AA	5846.61	3328.67	2418.06	48
H5BA	879.23	647.78	5930.3	70
H6BA	2818.08	676.04	6385.93	70
H7AA	5646.85	1982.02	4816.92	61
H7BA	3997.48	1926.96	6100.59	56
H8AA	6101.12	493.04	4720.37	85
H9AA	7584.54	-284.29	5446.17	90
H012	1877.79	6374.44	7027.09	58
H015	406.31	4895.87	5614.73	50
H1B	350.66	11237	7911.04	49
H4B	-1605.04	8424.38	11168.95	52
H2A	-1153.79	9075.56	7336.24	51
H3A	-783.61	8321.46	6305.69	70
H4AB	1230.54	8076.6	5891.55	66
H5A	2858.38	8492.06	6539.12	58
H6A	2501.97	9240	7562.72	47
H8A	-1225.21	6346.38	10422.81	93
H9A	-1572.43	5095.27	9826.1	129
H10A	-2514.42	5282.31	8697.84	115
H11A	-3013.66	6687.03	8134.88	111
H12A	-2623.67	7929.2	8709.37	81
H14A	899.13	7235.77	8958.05	71
H15A	2036.07	5978.42	8692.84	97
H16A	4041.2	5779.58	9090.44	105
H17A	4924.26	6819.32	9717.3	98
H18A	3742.62	8066.16	10021.59	67
H20A	4781.37	10277.05	10575.04	46

Table 4-9 (cont'd)

Atom	x	y	z	U_{eq}
H21A	6591.13	9826.28	11169.34	56
H22A	6505.63	9026.49	12332.51	55
H23A	4623.85	8671.41	12898.81	58
H24A	2812.75	9087.4	12300.42	46
H1SA	7111.46	5778.75	1745.11	76
H1SB	6716.28	5562.96	2600.05	76
H2SA	6796.81	7168.88	2072.46	79
H2SB	5640.17	6874.28	2608.03	79
H3SA	4600.03	7422.58	1584.78	94
H3SB	5699.85	7153.41	1036.87	94
H4SA	3808.73	6107.29	1647.95	104
H4SB	4687.07	5946.06	953.39	104
H5SA	-1274.97	12214.5	8512.18	72
H5SB	-2186.69	12571.88	7864.9	72
H6SA	-947.49	13631.76	8603.98	78
H6SB	-1537.69	13950.12	7818.78	78
H7SA	485.5	14174.66	7498.21	71
H7SB	951.51	13365.31	8085.29	71
H8SA	-172.08	13230.14	6711.43	68
H8SB	1050.13	12707.29	7014.88	68

Table 4-10: Hydrogen Bond information for 5,11,14,17-tetra(hydro)octaphenyltetra-cyclo[7.3.3.-3^{3,7}]octasilsesquioxane (**5**)

D	H	A	d(D-H) (Å)	d(H-A) (Å)	d(D-A) (Å)	D-H-A (°)
O1A	H1A	O1S	0.84	1.82	2.645(5)	168.6
O4A	H4A	O1A ¹	0.84	1.95	2.782(4)	172.1
O1B	H1B	O2S	0.84	1.84	2.647(4)	161.2
O4B	H4B	O1B ²	0.84	1.91	2.743(4)	169.5

¹1-x,1-y,1-z; ²-x,2-y,2-z

REFERENCES

REFERENCES

- (1) Tanaka, K.; Chujo, Y. Advanced Functional Materials Based on Polyhedral Oligomeric Silsesquioxane (POSS). *J. Mater. Chem.*, **2012**, 22, 1733–1746.
- (2) Kawakami, Y.; Kataoka, K.; Hagiwara, T. React. Funct. Polym. **2007**, 67, 1103–1104.
- (3) Ayandele, E.; Sarkar, B.; Alexandridis, P. Polyhedral Oligomeric Silsesquioxane (POSS)-Containing Polymer Nanocomposites. *Nanomaterials* **2012**, 2, 445–475.
- (4) Unno, M.; Suto, A.; Takada, K.; Matsumoto, H. Synthesis of Ladder and Cage Silsesquioxanes from 1,2,3,4-Tetrahydroxycyclotetrasiloxane. *Bull. Chem. Soc. Jpn.* **2000**, 73, 215–220.
- (5) Laine, R. M.; Roll, M. F. Polyhedral Phenylsilsesquioxanes. *Macromolecules* **2011**, 44, 1073–1109.
- (6) Chimjarn, S.; Kunthom, R.; Chancharone, P.; Sodkhomkhum, R.; Sangtrirutnugul, P.; Ervithayasuporn, V. Synthesis of Aromatic Functionalized Cage-Rearranged Silsesquioxanes (T₈, T₁₀, and T₁₂) via Nucleophilic Substitution Reactions. *Dalton Trans.* **2015**, 44, 916–919.
- (7) Kannan, R. Y.; Salacinski, H. J.; Odlyha, M.; Butler, P. E.; Seifalian, A. M. The Degradative Resistance of Polyhedral Oligomeric Silsesquioxane Nanocore Integrated Polyurethanes: An in Vitro Study. *Biomaterials* **2006**, 27, 1971–1979.
- (8) Haddad, T. S.; Lichtenhan, J. D. Hybrid Organic–Inorganic Thermoplastics: Styryl-Based Polyhedral Oligomeric Silsesquioxane Polymers. *Macromolecules* **1996**, 29, 7302–7304.
- (9) Katoh, R.; Imoto, H.; Naka, K. One-Pot Strategy for Synthesis of Open-Cage Silsesquioxane Monomers. *Polym. Chem.* **2019**, 10, 2223–2229.
- (11) Wu, S.; Hayakawa, T.; Kikuchi, R.; Grunzinger, S. J.; Kakimoto, M.-A.; Oikawa, H. Synthesis and Characterization of Semiaromatic Polyimides Containing POSS in Main Chain Derived from Double-Decker-Shaped Silsesquioxane. *Macromolecules* **2007**, 40, 5698–5705.
- (12) Barry, B.-D.; Dannatt, J. E.; King, A. K.; Lee, A.; Maleczka, R. E. A General Diversity Oriented Synthesis of Asymmetric Double-Decker Shaped Silsesquioxanes. *Chem. Commun.* **2019**, 55, 8623–8626.
- (12) Vogelsang, D. F.; Dannatt, J. E.; Schoen, B. W.; Maleczka, R. E.; Lee, A. Phase Behavior of cis–trans Mixtures of Double-Decker Shaped Silsesquioxanes for Processability Enhancement. *ACS Appl. Nano Mater.* **2019**, 2, 1223–1231.

- (13) Furgal, J. C.; Jung, J. H.; Clark, S.; Goodson, T.; Laine, R. M. Beads on a Chain (BoC) Phenylsilsesquioxane (SQ) Polymers via F⁻ Catalyzed Rearrangements and ADMET or Reverse Heck Cross-Coupling Reactions: Through Chain, Extended Conjugation in 3-D with Potential for Dendronization. *Macromolecules* **2013**, *46*, 7591–7604.
- (14) Lee, A. S.; Choi, S.-S.; Lee, H. S.; Baek, K.-Y.; Hwang, S. S. A New, Higher Yielding Synthetic Route towards Dodecaphenyl Cage Silsesquioxanes: Synthesis and Mechanistic Insights. *Dalton Trans.* **2012**, *41*, 10585.
- (15) Agaskar, P. A.; Klemperer, W. G. The Higher Hydridospherosiloxanes: Synthesis and Structures of H_nSi_nO_{1.5n} (n = 12, 14, 16, 18). *Inorganica Chim. Acta* **1995**, *229*, 355–364.
- (16) Cordes, D. B.; Lickiss, P. D.; Rataboul, F. Recent Developments in the Chemistry of Cubic Polyhedral Oligosilsesquioxanes. *Chem. Rev.* **2010**, *110*, 2081–2173.
- (17) Lee, D. W.; Kawakami, Y. Incompletely Condensed Silsesquioxanes: Formation and Reactivity. *Polym. J.* **2007**, *39*, 230–238.
- (18) Ye, M.; Wu, Y.; Zhang, W.; Yang, R. Synthesis of Incompletely Caged Silsesquioxane (T7-POSS) Compounds via a Versatile Three-Step Approach. *Res. Chem. Intermed.* **2018**, *44*, 4277–4294.
- (19) Feher, F. J.; Soulivong, D.; Lewis, G. T. Facile Framework Cleavage Reactions of a Completely Condensed Silsesquioxane Framework. *J. Am. Chem. Soc.* **1997**, *119*, 11323–11324.
- (20) Li, Z.; Kawakami, Y. Formation of Incompletely Condensed Oligosilsesquioxanes by Hydrolysis of Completely Condensed POSS via Reshuffling. *Chem. Lett.* **2008**, *37*, 804–805.
- (21) Wu, S.; Hayakawa, T.; Kakimoto, M.-A.; Oikawa, H. Synthesis and Characterization of Organosoluble Aromatic Polyimides Containing POSS in Main Chain Derived from Double-Decker-Shaped Silsesquioxane. *Macromolecules* **2008**, *41*, 3481–3487.
- (22) Leu, C.-M.; Chang, Y.-T.; Wei, K.-H. Synthesis and Dielectric Properties of Polyimide-Tethered Polyhedral Oligomeric Silsesquioxane (POSS) Nanocomposites via POSS-Diamine. *Macromolecules* **2003**, *36*, 9122–9127.
- (23) Fina, A.; Monticelli, O.; Camino, G. POSS-Based Hybrids by Melt/reactive Blending. *J. Mater. Chem.* **2010**, *20*, 9297–9305.
- (24) Kickelbick, G. Hybrid Materials - Past, Present and Future, 2014.
- (25) Feher, F. J.; Terroba, R.; Ziller, J. W. A New Route to Incompletely-Condensed Silsesquioxanes: Base-Mediated Cleavage of Polyhedral Oligosilsesquioxanes. *Chem. Commun.* **1999**, 2309–2310.

- (26) Asuncion, M. Z.; Ronchi, M.; Abu-Seir, H.; Laine, R. M. Synthesis, Functionalization and Properties of Incompletely Condensed “half Cube” Silsesquioxanes as a Potential Route to Nanoscale Janus Particles. *C. R. Chimie* **2010**, *13*, 270–281.
- (27) Shchegolikhina, O.; Pozdniakova, Y.; Antipin, M.; Katsoulis, D.; Auner, N.; Herrschaft, B. Synthesis and Structure of Sodium Phenylsiloxanolate. *Organometallics*, **2000**, *19*, 1077–1082.
- (28) Rikowski, E.; Marsmann, H. C. Cage-Rearrangement of Silsesquioxanes. *Polyhedron* **1997**, *16*, 3357–3361.
- (29) Wagner, T.; Foundling, S.; Bauer, C. A SMART Move. The Bruker AXS Integrated System for Protein Data Collection. *Acta Cryst.* **2000**, *56*, s220–s220.
- (30) Dolomanov, O. V.; Bourhis, L. J.; Gildea, R. J.; Howard, J. A. K.; Puschmann, H. OLEX2: A Complete Structure Solution, Refinement and Analysis Program. *J. Appl. Crystal.*, **2009**, *42*, 339–341.
- (31) Beck, T.; Krasauskas, A.; Gruene, T.; Sheldrick, G. M. A Magic Triangle for Experimental Phasing of Macromolecules. *Acta Cryst.* **2008**, *64*, 1179–1182.
- (32) Sandler, C.; Overson, G. B.; Black, C. A.; Rocabado, G. A.; Howard, B. R. Use of the Bruker AXS SMART BREEZETM System for Macromolecular X-Ray Data Collection.
- (33) Morawetz, K. Diffraction on a Barrier. Oxford Scholarship Online, **2018**.

Chapter 5.0: De novo construction of Double-Decker Shaped Silsesquioxanes with Modifiable Surface Functionalities

5.1 Introduction

There is a growing demand for novel hybrid materials with the double-decker shaped architecture that can inspire new technological applications in chemistry and engineering. With the extensive research efforts reported so far,^{1,2} the only known double decker is the octaphenyl double-decker shaped silsesquioxane (DDSQ).^{3–5} In the past several years, this cage has been functionalized in diverse ways on its open ends leading to the generation of condensed symmetric and asymmetric DDSQs.^{6–11} The development of methodologies that can mimic this nanocage, particularly those bearing transformable groups as the silica coronae, would be intriguing molecular templates that may afford tunable multifunctional nanocomposites through modifications of its sides and surfaces. Such molecular designs are promising precursors in materials and polymer chemistry for the generation of linear POSS/polymer composites and the formation of 3D networks. To actualize such a vision, the manipulation of trifunctional silanes or caged silsesquioxanes decorated with transformable organic peripherals on the silicon vertices should be explored.

Generally, cage silsesquioxanes bearing various silica coronae have been obtained from the hydrolytic condensation of trifunctional silanes, and various benzyltrimethyl- ammonium hydroxide (BzTMAH) or tetrabutylammonium fluoride (TBAF) catalyzed condensation reactions.^{2,12–20} Lately, cages with reactive functionalities on the silicon vertices have attracted interest for surface functionalization and for their plausible utility as precursors to various incompletely condensed nanohybrid functional

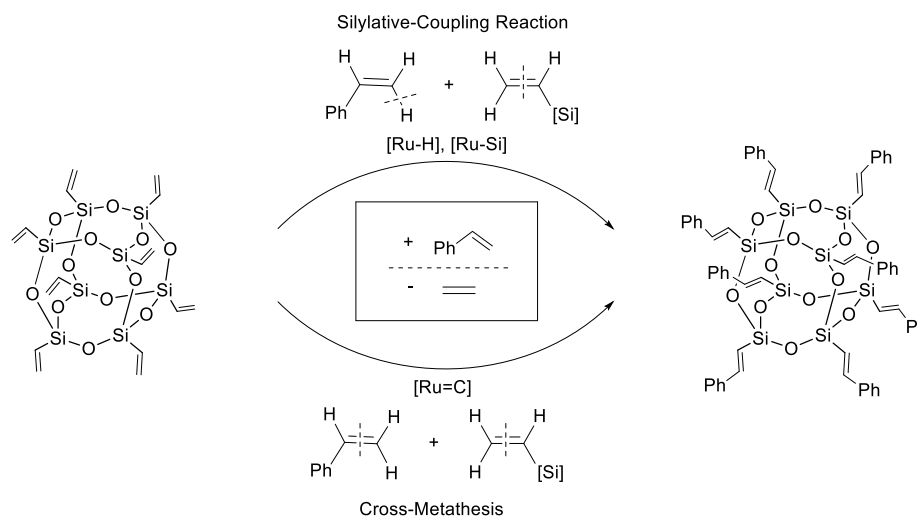
materials.^{21–31} Reactive POSS cages bearing ortho-, meta- and para- functional moieties on the phenyl groups are quite promising candidates^{32–37} for the generation of 3D composites. Thus, part of our efforts to design hybrid functional nanoparticles was to explore possible routes for the synthesis of DDSQs with defined symmetry and surface functionalities that are based on peripherals other than phenyl.

Inspired by the works of the Ohgum and Kawakami groups on the synthesis of the octaphenyl double-decker shaped silsesquioxane,^{3,4} and the recent report by the Unno group on the assembly of styryl-functionalized T_n cages, we envisioned that a DDSQ with styryl or halophenyl functionalities as coronae could be quite interesting. Such double-decker shaped silsesquioxanes, if realized, would enable a wide range of corner capping and surface modifications that could afford nanobuilding materials with superior properties. To fabricate such compounds, our efforts were focused on obtaining the incompletely condensed octafunctional double-decker oligomeric silsesquioxanes trimmed on the silicon vertices with styryl and 4-bromophenyl motifs. Such molecular frameworks will offer multifunctional sites for modification into more interesting classes of nano-precursors with perfect symmetry. Thus, we intended to either directly assemble the substituted phenylDDSQ(OH)₄ from the monomeric chloro/alkoxysilane or from the controlled cleavage of the fully condensed substituted octafunctional POSS. The unhindered substituent on the phenyl moiety and the free silanol groups will provide the necessary molecular design for multi functionalization using various chemistries including epoxidation, hydrosilylation, thioetherification, polymerization, and other reactions typical of alkenes and cross-coupling reactions into a variety of products for various applications.

5.1.1 Styrenyl functionalized Polyhedral Oligomeric Silsesquioxanes

The direct synthesis of POSS cages with styryl and styrenyl substituents has been a longstanding challenge. Lately however, several groups have reported indirect procedures to access styrenyl POSS. For instance, Itami, et al. reported the synthesis of octastyrenyl POSS via the transformation of a pre-assembled octavinylsilsesquioxane (octavinylT₈) using both a ruthenium carbene complexed–silylative coupling and cross-metathesis with various substituted styrenes (**Scheme 5-1**).^{38,39}

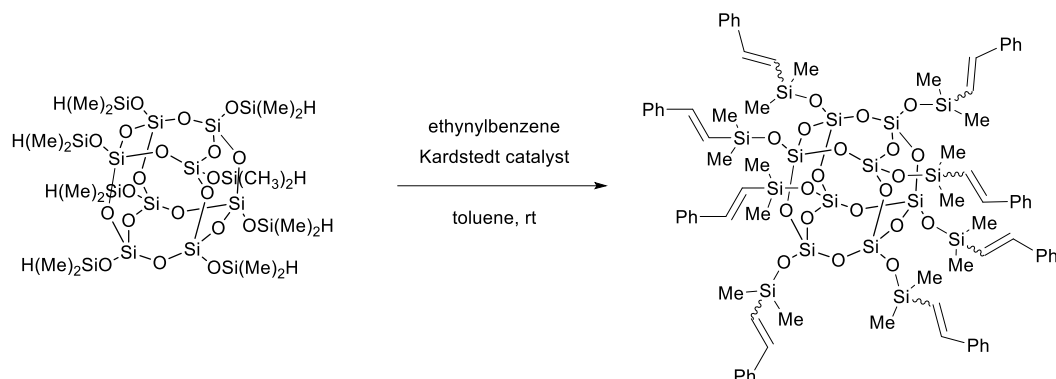
Scheme 5-1: Silylative coupling and cross metathesis of octavinylT₈ with styrenes



The resultant POSS cage is an octastyrenyl POSS in which the styrene is bound onto the POSS core via the alkenyl moiety.

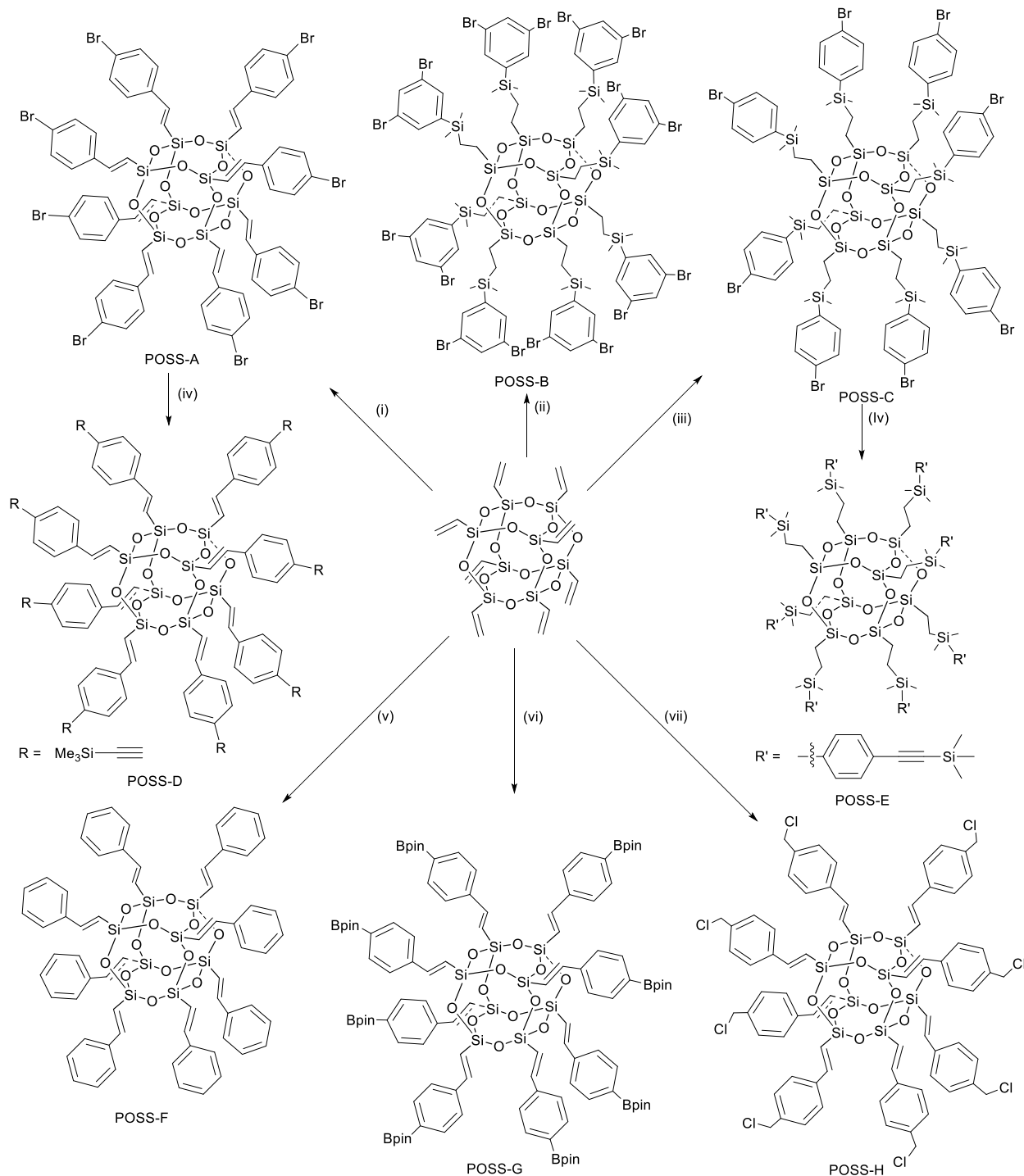
Starting with a terminal aryl alkyne, the Ye group also reported the synthesis of an octastyrenyl POSS from the hydrosilylation of an octasilanePOSS (POSS-OSi(Me)₂H) with ethynylbenzene. A rigid octastyrenyl POSS with alkenylsilane linkages was obtained from the treatment of an equimolar ratio of [Si-H]:[C≡C] = (1:1) (**Scheme 5-2**).⁴⁰

Scheme 5-2: Hydrosilylation of POSS-OSi(Me)₂H with ethynylbenzene



The Cole-Hamilton group in 2008 disclosed a myriad of techniques for the elaboration of octavinylsilsesquioxane into various functionalized cubic octastyrenyl- and octastyrethynyl-silsesquioxanes. A demonstration of the versatility of their work was illustrated by the successful modification of all eight peripheral vinyl groups in octavinylT₈ using various techniques including the palladium catalyzed Heck coupling, ruthenium catalyzed cross metathesis, Karstedt's catalyzed hydrosilylation and Sonogashira coupling reactions (**Scheme 5-3**) therein designated as POSS-A through H.⁴¹

Scheme 5-3: Elaboration of OctavinylIT₈ for the synthesis of a variety of POSS



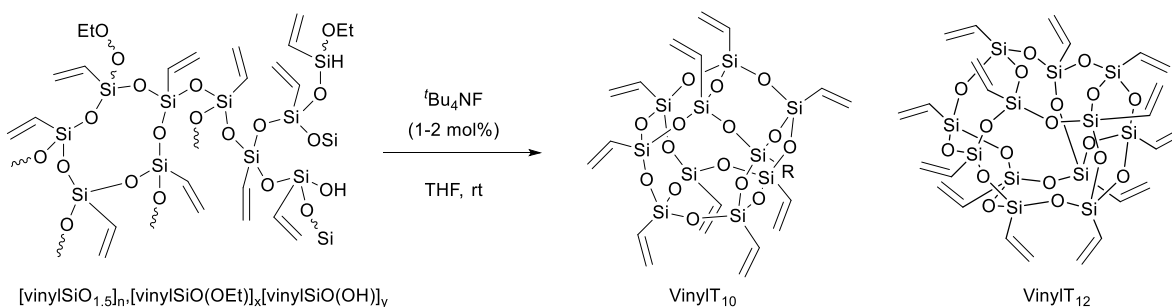
Reaction conditions: (i) 4-bromostyrene, Grubbs' catalyst (1st gen., 4 mol%), CH₂Cl₂; (ii) (3,5-dibromophenyl)dimethylsilane, Karstedt's catalyst (75 μL), Et₂O; (iii) 4-bromophenyl(dimethyl)silane, Karstedt's catalyst (75 μL), Et₂O; (iv) trimethylsilylacetylene, [Pd(PPh₃)₂Cl₂] (78 mol%), CuI (1.59 equiv), PPh₃, Et₃N/THF; (v)

iodobenzene, [Pd(OAc)₂] (40 mol%), PPh₃, Et₃N/THF; (vi) 4-(4,4,5,5-tetramethyl-1,3,2-dioxaborolan-2-yl)styrene, Grubbs' catalyst (1st gen., 6 mol%), CH₂Cl₂; (vii) 4-vinylbenzyl chloride, Grubbs' catalyst (1st gen. 3 mol%), CH₂Cl₂.

The presence of olefinic, acetylenic, chloro, bromo or Bpin groups in these functional compounds make them ideal nanobuilding blocks for further transformation into novel interesting materials with useful chemical and mechanical properties. In contrast to a protocol reported by the Laine group for the iron-catalyzed synthesis of brominated POSS, this procedure allows for the precise number and location of bromine atoms per unit molecule. Octafunctionalized POSS trimmed with aryl borate groups ideal for Suzuki cross coupling were also obtained (**Scheme 5-3, (iv)**).

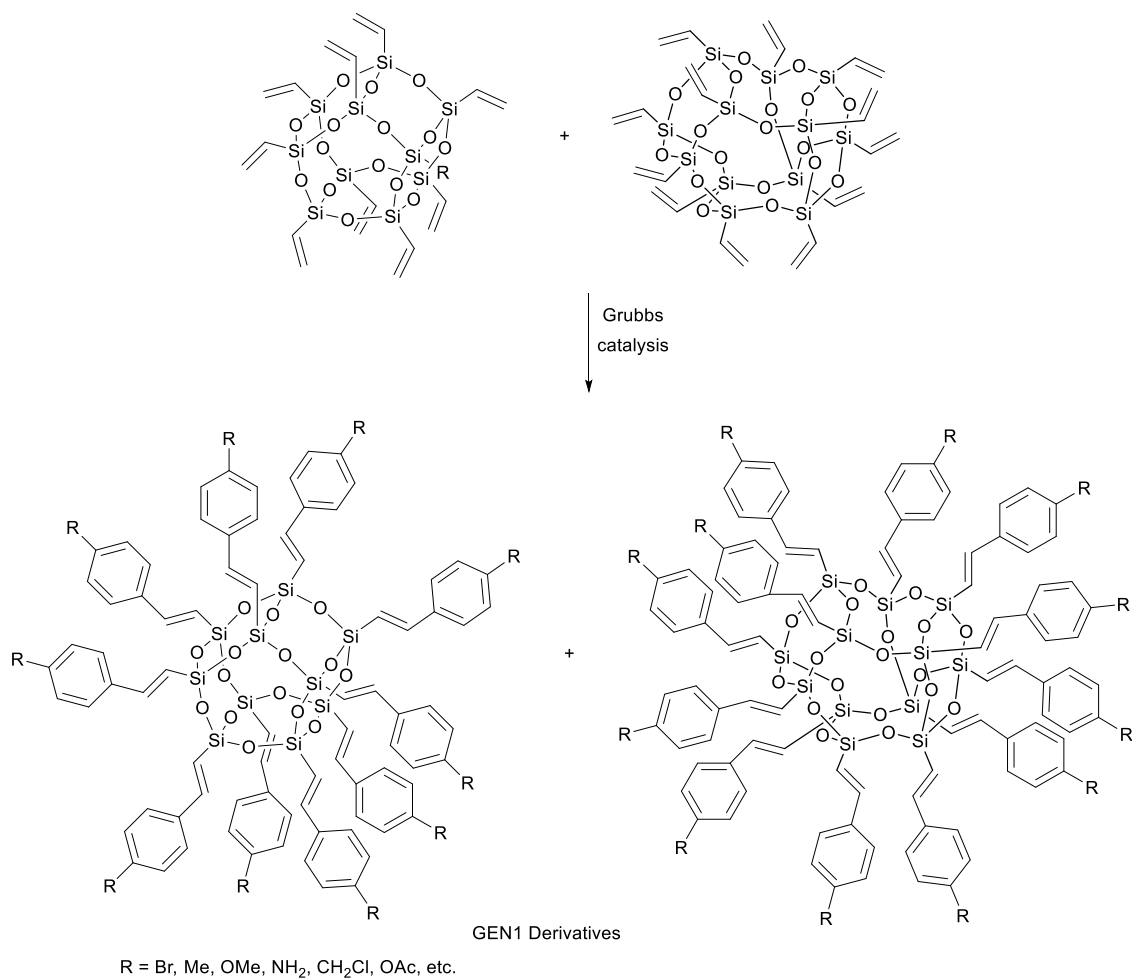
Styrenyl functionalized POSSs have also been obtained from vinyl substituted polysilsesquioxanes, $-\text{[vinylSiO}_{1.5}\text{]}_n-$. For instance, the Laine group reported a fluoride ion catalyzed rearrangement of oligomeric and polymeric polyvinylsilsesquioxanes (PVS) in THF^{44,45} for the synthesis of a mixture of T₁₀, T₁₂ and T₁₄ vinyl functionalized cages (**Scheme 5-4**).

Scheme 5-4: Fluoride catalyzed rearrangement of polysilsesquioxanes to mixed T₁₀ and T₁₂ isomers



Elaboration of these cages by metathesis with p-R-styrene afforded the styrenyl analogues therein referred to as the generation 1 compounds (GEN1) (**Scheme 5-5**).⁴⁴

Scheme 5-5: Metathesis of mixed VinylIT₁₀ and VinylIT₁₂ for the synthesis of styrenylIT_{10/12} cages



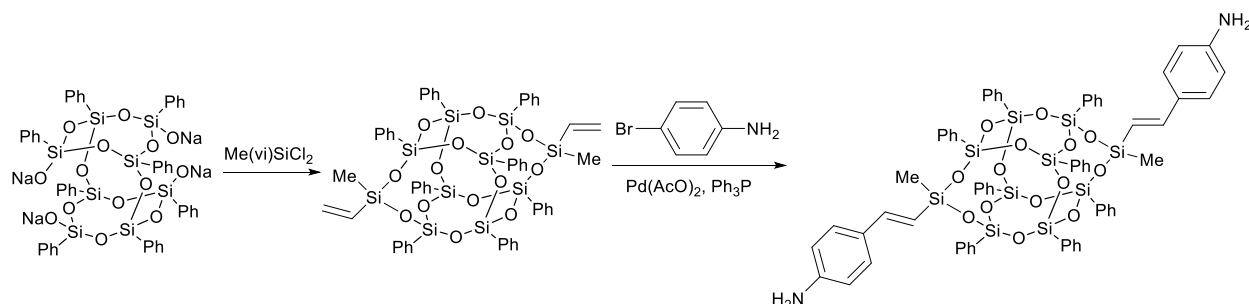
Further modification of these cages via Heck reaction with p-substituted-styrenes gave the p-substituted-stilbenevinylIT_{10/12} GEN2 derivatives in excellent yields.

5.1.2 Corner-capping DDSQ(OH)₄ with styrenyl and styryl groups

Attempts have also been made to functionalize DDSQ(OH)₄ with styryl and styrenyl groups, but these transformations have so far been limited to the open ends of the cage. For instance, pre-functionalized divinyl(Me)DDSQs have been transformed into styrenyl DDSQs by various groups. The Zheng group in 2016 introduced styrenyl groups

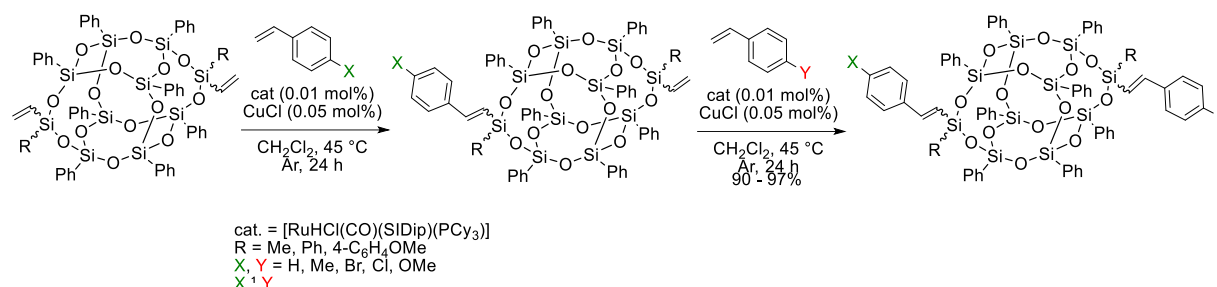
onto the $\text{DDSQ}(\text{OH})_4$ indirectly via a Heck coupling reaction of a pre-fabricated 3,13-divinyloctaphenyl double decker silsesquioxane (3,13-divinyl DDSQ) with 4-bromoaniline (**Scheme 5-6**).⁴³ The precursor, 3,13-divinyloctaphenyl double decker silsesquioxane (3,13-divinyl DDSQ) was obtained from the silylation of octaphenyldicyclooctasiloxane tetrasodium silanolate with methylvinylchlorosilane.

Scheme 5-6: Synthesis of 3,13-dianilino DDSQ from phenyltrimethoxysilane



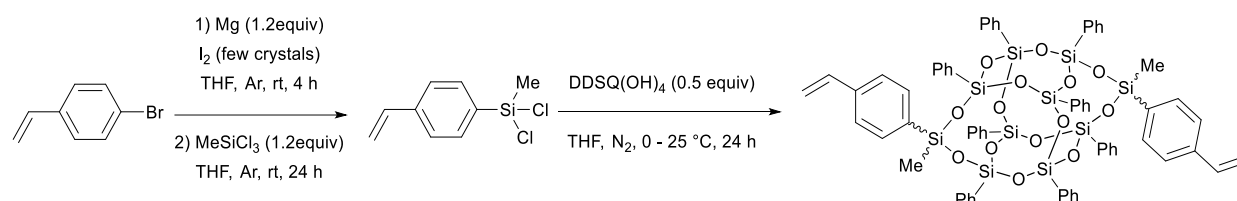
Recently, Zac et al.^{9,46} reported a ruthenium catalyzed metathesis of divinyl-capped DDSQs with several substituted styrenes for the synthesis of asymmetrically functionalized styrenyl D_2T_8 silsesquioxanes (**Scheme 5-7**). The $[\text{RuHCl}(\text{CO})(\text{NHC})(\text{PCy}_3)]$ in the presence of CuCl was highly efficient with exclusive (E)-selective silylative coupling of various para-substituted styrenes and the divinylDDSQ. However, in this work, the styryl group was grafted to the cage by the vinyl moiety affording a condensed DDSQ with hindered ethynyl groups.

Scheme 5-7: Synthesis of asymmetric styrenylDDSQs from the silylative coupling of divinylDDSQ with substituted styrenes



Lately our laboratory was able to corner cap DDSQ(OH)₄ with a pre-synthesized styryl(Me)SiCl₂ providing a D₂T₈ DDSQ with unhindered styryl groups for the first time (**Scheme 5-8**). Even with this development, the system only afforded a condensed styryl functionalized D₂T₈ DDSQ with unhindered vinyl groups for post-modification.

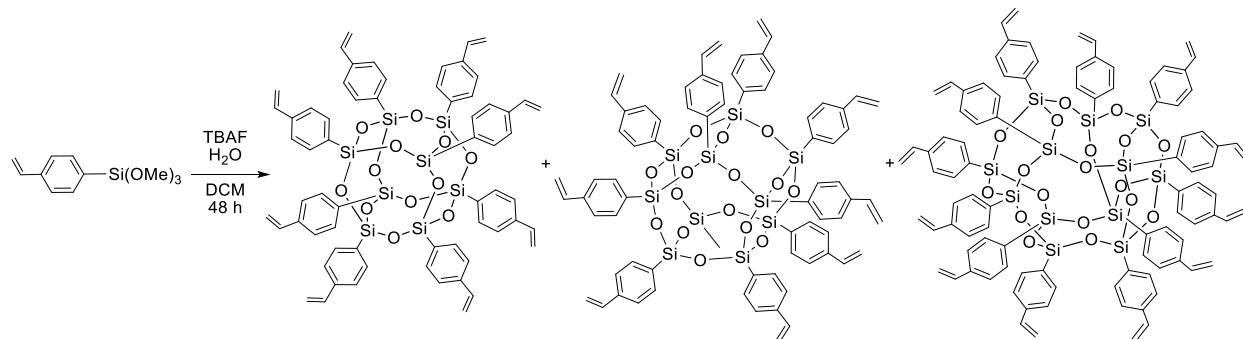
Scheme 5-8: Synthesis of [(styryl(Me))₂DDSQ]



5.1.3 Styryl functionalized Polyhedral Oligomeric Silsesquioxanes

Until the latest work by Unno and coworkers in 2020,⁴⁷ styryl decorated cages linked to the T_n POSS via the phenyl group were unknown (**Scheme 5-9**). However, several groups have reported the successful synthesis of monofunctionalized styryl POSS via corner-capping of a trisilanol POSS⁴⁸ and by Grubbs' catalyzed metathesis of a pre-monofunctionalized vinyl POSS with substituted styrenes,⁴⁹ the styryl T_n garnished systems with unhindered vinylic groups have the advantage of making the vinylic moiety easily accessible for further modifications.

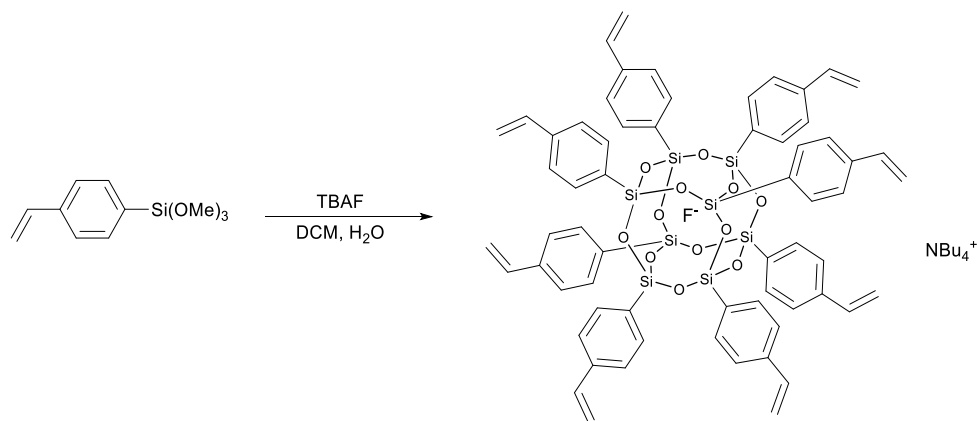
Scheme 5-9: Route to styryl-functionalized T_n cage silsesquioxanes



Like other POSS cages, the well-defined structures of styryl T_n POSS make them potential nano-linkers to polymer matrices with good thermal and oxidative stabilities. Their benignity and nano-structural dimensions (approximately 3 Å) could equally make them effective templates as nanocarriers in medicine, catalysis, and electronics. The sterically unhindered styryl group provides the opportunity for post-modifications and/or their utility as synthons for the synthesis of 3D cross-linked polymers.

Styryl functionalized POSS cages with an encapsulated fluoride ion (T₈-F) in the siloxy core has also been reported by Man and coworkers (**Scheme 5-10**).⁵⁰ The fluoride ion was extracted from the cage using various approaches, in most cases leading to improved yields of the T₈ compound.^{14,16,50,51}

Scheme 5-10: Synthesis of styryl-functionalised T₈-F Cage



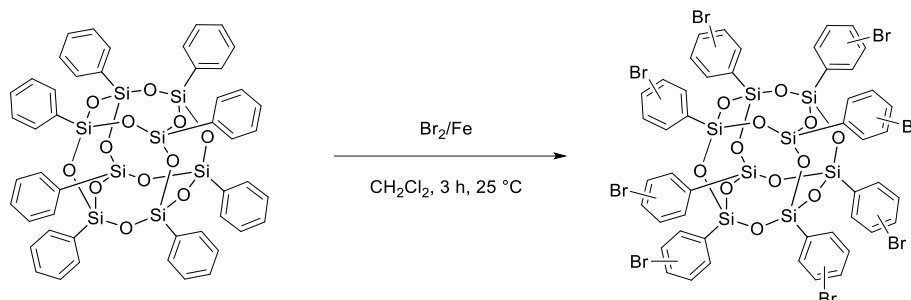
Some common approaches include dissolution of the cage in THF followed by stirring in the presence of either LiCl or CaCl₂, or washing with a saturated solution of CaCl₂, or addition of CaCl₂ to the reaction mixture prior to workup to sequester the fluoride anion by the Ca²⁺.

Post-functionalizations of this material via metathesis, silylative coupling, Heck coupling, thiol-ene click reactions, etc. have offered more useful products that find applications in catalysis,^{52,53} optical materials^{54,55} and coatings.⁵⁶ Based on literature reports, alkoxysilanes with electron-donating sp³-hybridized organic groups will only give T₈ cages without entrapped fluoride whereas those with electron withdrawing sp³ or sp² hybridized groups affords T₈-F compound.^{47,50,57,58} Interestingly further attempts to modify these cages have remained a challenge. However, other POSS cages with entrapped fluoride ions are known. The Bassindale's group for instance, reported the first successful encapsulation of a fluoride ion in the void of a cubic octaphenyl-functionalized POSS.⁵⁹

5.1.4 p-Bromophenyl functionalized Polyhedral Oligomeric Silsesquioxanes

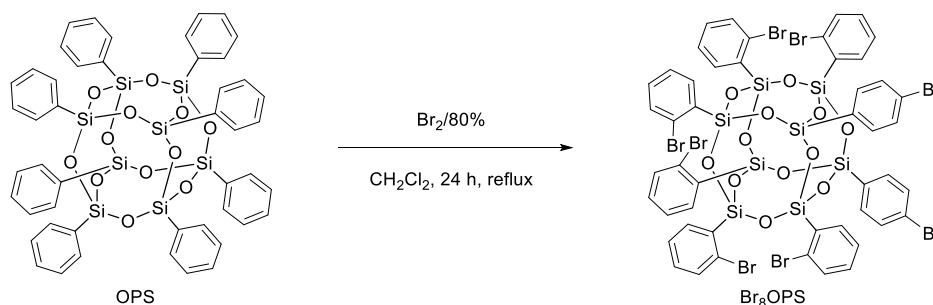
Cubic brominated octaphenyl silsesquioxanes have been obtained from the monomeric alkoxysilane and from the bromination of octaphenyl POSS using Br₂/Fe. The iron catalyzed route with molecular bromine reported by the Brick et al. is controlled by the reaction stoichiometry.⁶⁰ The process is complicated and, depending on the reaction stoichiometry, can lead to a mixture of multibrominated-phenyl substitution products. The initial bromination occurs at the para position of the phenyl groups followed by subsequent intramolecular rearrangement that affords the 2,5-dibrominated species as the major product (**Scheme 5-11**). Such brominated T₈ POSS can undergo various coupling reactions to generate a range of inorganic-organic nanohybrid materials.

Scheme 5-11: Synthesis of Brominated Octaphenylsilsesquioxanes (Br_xOPS), x = the average number of bromines per molecule



Further exploration of this chemistry by way of manipulating reaction parameters such as choice of catalyst, temperature, concentration and order of reagents addition led this same group to discover a better route for the synthesis of octa-, hexadeca- and tetraicosa-brominated octaphenylsilsesquioxane, $[\text{PhSiO}_{1.5}]_8$ or OPS.⁶¹ Two mechanisms have been proposed for these 3-D brominated cages; one with an external catalyst and the other without. They observed that even in the absence of a Lewis catalyst, OPS can auto-catalyze its bromination in DCM to give a high selective ortho:para brominated cage of 85:15 (**Scheme 5-12**).

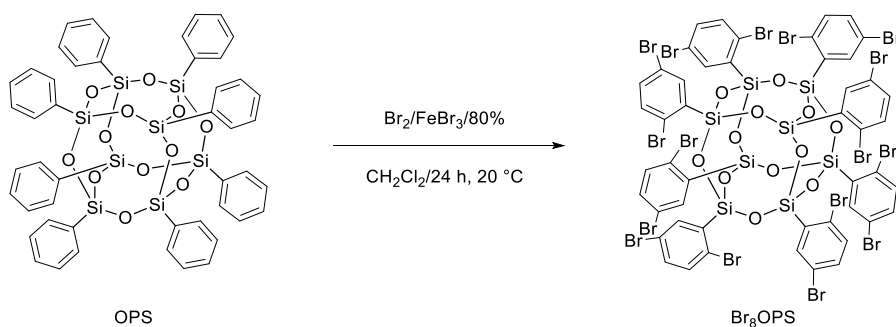
Scheme 5-12: Selective self-catalyzed bromination of octa(phenyl)silsesquioxane (OPS) for the selective synthesis of octabrominated OPS



To account for this surprising bromination of the unactivated phenyl groups, they opined that the cage, being electrophilic forms a complex with molecular bromine. This

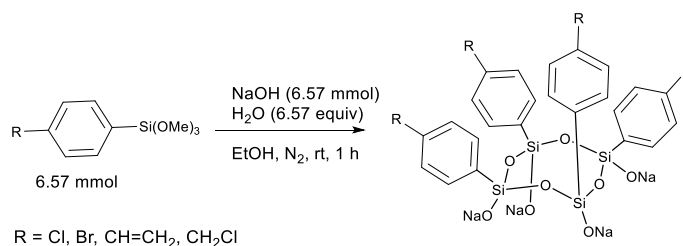
results in the polarization of the Br₂ with the partially positive bromine (Br^{δ+}) being proximal to the ortho position relative to the silicon atom which in turn promotes the bromination at the *ortho* position of the phenyl groups. However, if the bromination is done for a prolonged reaction time or in the presence of a Lewis acid catalyst, the doubly, or multiply brominate Br₁₆OPS (**Scheme 5-13**) and Br₂₄OP silsesquioxanes are formed.

Scheme 5-13: Synthesis of octa(dibromophenyl)silsesquioxane



Half-cube p-substituted phenyl cyclosiloxanes have also been reported by several groups including the Zucchi and Shchegolikhina groups. Ronchi et al for example,⁶² reported the synthesis of a generation of functionalized sodium para-substituted phenylcyclotetrasiloxanates that are potential silica supports to second order NLO active or fluorescent organic chromophores (**Scheme 5-14**).

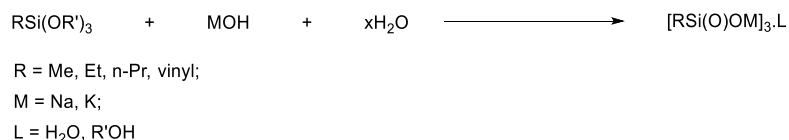
Scheme 5-14: Synthesis of sodium cyclotetrasiloxanates from para-substituted phenyltriethoxysilane



The single crystal structures of the trimethylsiloxy derivatives of these 2D scaffolds have all phenyl rings in a cis orientation. Interestingly, this same group was faced with

challenges in their efforts to obtain similar scaffolds following the route reported by Shchegolikhina et al. for alkyl and vinyl trialkoxysilane derivatives (**Scheme 5-15**).⁶³

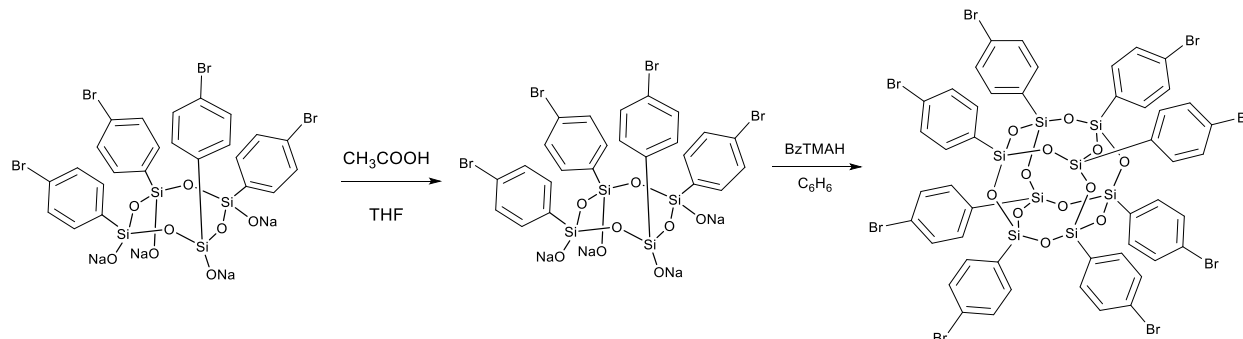
Scheme 5-15: Synthesis of sodium and potassium cyclosiloxanates based on trisiloxanolate cycles with vinyl and alkyl substituents



The complex mixture of oligomers and resinous materials obtained using para-substituted phenyltriethoxysilane as starting material in the Shchegolikhina approach was ascribed to the sensitivity of cyclotetrasiloxane rings to reaction conditions such as amount of water, nature of solvent, and base content that could affect their separation due to solubility.

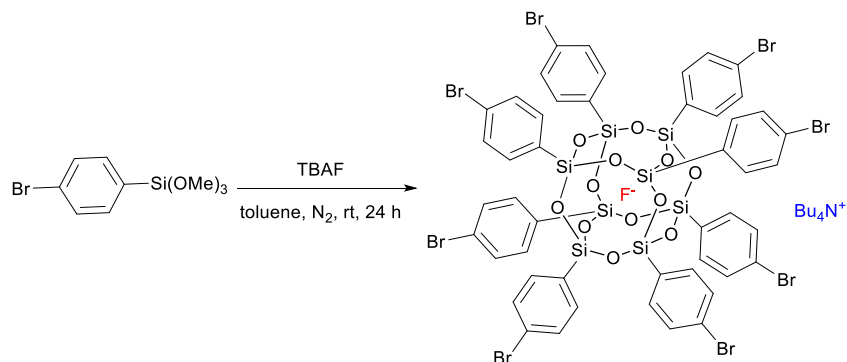
Picking up from the efforts of Ronchi and Shchegolikhina⁶³ and also the pioneering art of Brown for the synthesis of the first tetraphenyltetrasiloxanetetraol⁶⁴ the Kawakami group elaborated on the sodium 4-bromophenylcyclotetrasiloxanates half cube for the synthesis of pure cubic octa(4-bromo-substituted phenyl)octasilsesquioxane.¹⁸ Thus acidification of sodium 4-bromophenylcyclotetrasiloxanolate with acetic acid followed by treatment of the resulting condensate in benzene with benzyltrimethylammonium hydroxide (BzTMAH) afforded pure crystalline 4-bromo-substituted phenylsilsesquioxane (**Scheme 5-16**).¹⁸

Scheme 5-16: Synthesis of Br-T₈ from all-cis-Br-T₄-tetraol



This route is quite unique from the standpoint that the precise location of the transformable group (i.e. the Br atom) in the cage is known, and unlike previously reported procedures where the brominated products are obtained from bromination of octaphenylsilsesquioxane. An alternative route to this was a procedure reported by Taylor et al. involving the TBAF catalyzed synthesis of the fluoride-encapsulated brominated octasilsesquioxane cage (**Scheme 5-17**).¹⁴ In that report, both the synthesis of the fluoride encapsulated octasilsesquioxane cages and methods for the migration of the fluoride anion out of the cage using strong acids and lithium salts without distorting the cage architecture was disclosed.

Scheme 5-17: Synthesis of tetra-*n*-butylammonium octa(para-bromophenyl)octasilsesquioxane fluoride



Despite these tremendous advances reported to date on the synthesis of these types of POSS cages, there are no reports in the literature for synthesis of the double-decker parity bearing styryl or bromophenyl substituents as pendants. Thus, with the desire to obtain a styryl or bromophenyl trimmed DDSQ(OH)₄ being our goal, we sought to develop strategies that can fabricate such compounds by either the selective and symmetric cleavage of two Si-O bond in the fully condensed POSS precursor or direct synthesis of the partially condensed cages from their respective trichloro/alkoxy silanes. Such cages, if realized, will extend post-functionalization to both its surfaces and corners.

5.2 Experimental Section

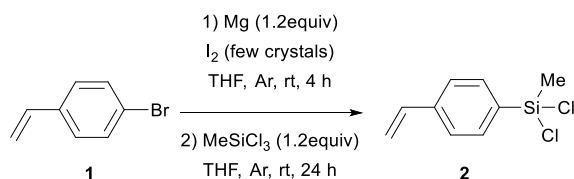
5.2.1 Materials and Methods

All reactions were carried out with dry solvents under a nitrogen atmosphere using standard techniques except otherwise stated. 4-bromophenyltrimethoxysilane was purchased from Gilest Inc. and styryltrimethoxysilane from Shin-Etsu Chemical Co. Ltd. Triethylamine (Et₃N) and toluene were distilled over calcium hydride before use. Acetic acid, hexanes, acetonitrile, methanol, isopropanol, and isobutanol were used as received. THF was distilled over benzophenone and sodium metal at a temperature of 50 °C under nitrogen prior to use. Glassware was oven dried. Reactions were monitored thin-layer chromatography (TLC) on silica gel plates or a Hydrion Insta-Chek pH pH 0-14 and. ¹H, ¹³C, ¹⁹F, and ²⁹Si NMR spectra were acquired on an Agilent DirectDrive2 500 MHz NMR spectrometer equipped with a OneProbe operating at 500 MHz for ¹H NMR, 126 MHz for ¹³C NMR, 471.82 MHz for ¹⁹F NMR, and 99 MHz for ²⁹Si NMR with CDCl₃ or acetone-d₆ and recorded at 25 °C. ¹H-NMR spectra were recorded with 8 scans, a relaxation delay of 1s, and a pulse angle of 45° and referenced to tetramethylsilane in CDCl₃ (0.00 ppm).

^{13}C -NMR spectra were collected with 254 scans, a relaxation delay of 0.1 s, and a pulse angle of 45° . ^{19}F NMR spectra were collected with 32 Scans, a relaxation delay of 25 s, and a pulse angle of 60° . ^{29}Si NMR spectra were recorded with either 256 or 512 scans, a relaxation delay of 12 s and a pulse angle of 45° . Thin-layer chromatography (TLC) was performed on plates of EMD 250- μm silica 60-F254. High-resolution mass spectroscopy was performed with APCI mass spectra recorded on a Finnigan LCQ Deca (ThermoQuest) technologies with LC/MS/MS (quadrupole/time-of-flight) and Waters Xevo G2-XS UPLC/MS/MS inert XL MSD with SIS Direct Insertion Probe. Melting points for all products were measured with a Stuart SMP30 melting point apparatus and are uncorrected. X-ray diffraction measurements were performed on a Stoe IPDS2 or a Bruker-AXS SMART APEX 2 CCD diffractometer using graphite-monochromated $\text{Mo K}\alpha$ radiation. The structures were solved using direct methods (SHELXL-97) and refined by full-matrix least-squares techniques against F^2 (SHELXL-97). Cell parameters were retrieved using the SAINT (Bruker, V8.34A, after 2013) software and refined using SAINT (Bruker, V8.34A, after 2013) on 5941 reflections, 47% of the observed reflections. Data reduction was performed using the SAINT (Bruker, V8.34A, after 2013) software which corrects for Lorentz polarization.

5.2.1.1 Synthesis of dichloro(methyl)(4-vinylphenyl)silane (**2**) from 4-bromostyrene (**1**)

Scheme 5-18: Synthesis of dichloro(methyl)(4-vinylphenyl)silane (**2**) via Grignard



Magnesium powder (0.58 g, 24 mmol) was added onto an oven dried 100 mL two-necked round bottom bearing a stir bar and fitted with a dropping funnel. The flask was dried under vacuum (1 mmHg) and filled with pure argon. The magnesium was activated with a few crystals of I₂ and THF (10 mL) was added to the flask. The mixture was placed in an ice bath, stirred continuously and a few drops of 4-bromostyrene added to allow the exothermic reaction to occur slowly. Once the system returned to room temperature, the remaining 4-bromostyrene making the total volume of 2.61 mL (3.66 g, 20 mmol) was added slowly through the dropping funnel to prevent polymerization (**Scheme 5-18, step 1**). The reaction was allowed to react under the inert Ar atmosphere and at room temperature for 4 h. An aliquot of the crude quenched with MeOH and analyzed by GC/MS showed full conversion of **1** into the Grignard product. Into another pre-heated 100 mL round bottom flask equipped with a stir bar and an argon atmosphere was added freshly distilled MeSiCl₃ (2.82 mL, 24 mmol) in 10 mL THF. The Grignard solution prepared above was next cannulated dropwise over a period of 20 minutes into the flask bearing the MeSiCl₃ (**Scheme 5-18, step 2**). The mixture was left to stir at room temperature for 24 h at which time GC/MS showed full conversion into **2**. This product was isolated as a colorless oil in 77% yield (1.8 mL, 15.4 mmol).

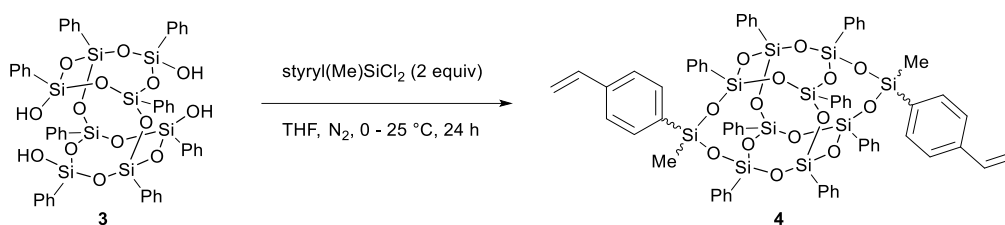
^1H NMR (500 MHz, CDCl_3 + 1% TMS) δ (ppm): 7.71 – 7.65 (m, 2H), 7.48 – 7.45 (m, 2H), 6.80 – 6.62 (m, 2H), 5.86 – 5.81 (m, 1H), 5.34 (dd, J = 10.9, 0.8 Hz, 1H), 1.01 (s, 3H).

^{13}C NMR (126 MHz, CDCl_3 + 1% TMS) δ (ppm) 140.66, 136.16, 133.34, 126.04, 125.86, 116.06, 5.53.

^{29}Si NMR (99 MHz, CDCl_3 + 1% TMS) δ (ppm) 18.50 (1Si)

5.2.1.2 Synthesis of $[[(\text{styryl})(\text{Me})]_2\text{DDSQ}]$ from $\text{DDSQ}(\text{OH})_4$ (**3**) and $\text{styryl}(\text{Me})\text{SiCl}_2$ (**2**)

Scheme 5-19: Capping of $\text{DDSQ}(\text{OH})_4$ (**3**) with dichloro(methyl)(4-vinylphenyl)silane (**2**)



$\text{DDSQ}(\text{OH})_4$ (1.05 g, 1.0 mmol) was charged into a pre-dried 100 mL round bottom flask bearing a magnetic stir bar and sealed with a septum. The flask was purged with dry nitrogen and THF (10 mL) was added. The flask was immersed into an ice bath and $\text{styryl}(\text{Me})\text{SiCl}_2$ (0.23 mL, 2 equiv) in 3 mL THF was added followed by dropwise addition of pyridine (0.32 mL, 4 equiv). The reaction mixture was stirred at 0 °C for 2 h and at room temperature for 22 h (**Scheme 5-19**). The suspension was filtered through a glass frit, the residue washed with THF (3 x 5 mL) and the solvent together with other volatiles removed from the filtrate by rotary evaporation. This crude was further purified by flash column chromatography with ethylacetate/hexane:1/3 to give a white solid. The product was isolated as a white solid in 38% yield (0.53 g, 0.39 mmol) and was analyzed by ^1H , ^{13}C , ^{29}Si , single X-ray crystallography and LCMS measurement. mp 265 – 268 °C.

^1H NMR (500 MHz, CDCl_3 + 1% TMS) δ (ppm) ^1H NMR (500 MHz, Chloroform-*d*) δ 7.62 – 7.03 (m, 41H), 6.80 – 6.55 (m, 2H), 5.85 – 5.63 (m, 2H), 5.35 – 5.18 (m, 2H), 0.51 (d, J = 5.3 Hz, 6H).

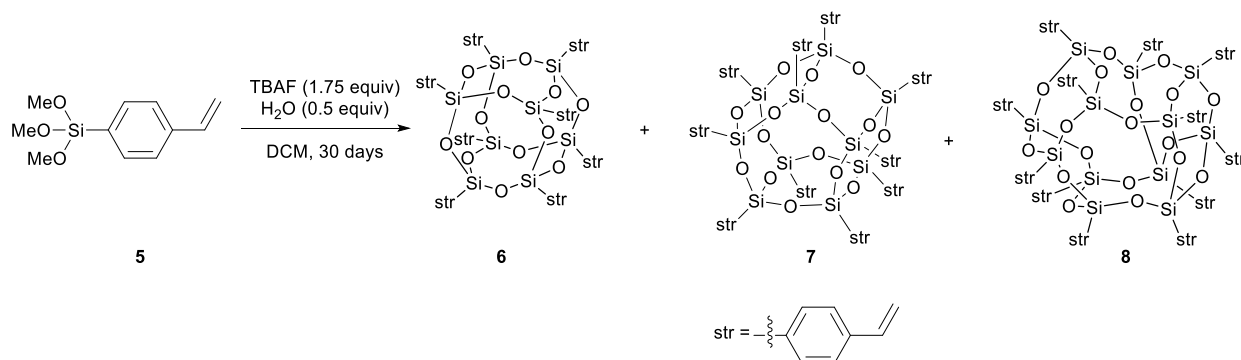
^{13}C NMR (126 MHz, CDCl_3 + 1% TMS) δ (ppm) 136.90, 134.31, 134.17, 133.82, 131.97, 131.30, 130.37, 127.87, 127.78, 127.56, 127.49, 125.71, 114.58, -0.41

^{29}Si NMR (99 MHz, CDCl_3 + 1% TMS) δ (ppm) -30.87 (2Si), -78.40 (4Si), -79.21 (1Si), -79.57 (2Si), -79.84 (1Si).

LCMS (APCI) m/z calcd for $\text{C}_{66}\text{H}_{60}\text{KO}_{14}\text{Si}_{10}^+$ $[\text{M} + \text{K}]^+$ 1395.1307, obs'd 1395.1235

5.2.2 Synthesis of T_n styryl Silsesquioxanes

Scheme 5-20: Synthesis of sty_8T_8 (**6**), $\text{sty}_{10}\text{T}_{10}$ (**7**) and $\text{sty}_{12}\text{T}_{12}$ (**8**) from styryltrimethoxy-silane (**5**)



In an oven-dried round bottom flask equipped with a stir bar was added a solution of trimethoxy(4-vinylphenyl)silane (3.7 mL, 17.5 mmol) in DCM (400 mL). The flask was placed over a pre-heated oilbath at $30\text{ }^\circ\text{C}$ and water (160 μL , 8.75 mmol, 0.5 equiv) was added followed by dropwise addition of TBAF solution in THF (10 mL, 10 mmol). After 48 h reaction time, anhydrous CaCl_2 (1.2 g, 11 mmol) was then added to the solution and stirred for a further 16 h (**Scheme 5-20**). The resulting crude reaction mixture was filtered, washed three times with water (3 x 100 mL), and dried over anhydrous Na_2SO_4 . The

solvent was removed by rotary evaporation affording a crude reaction mixture containing styryl- T_8 , T_{10} and T_{12} cage Silsesquioxanes. Products were further purified by flash column chromatography using dichloromethane/hexane:1/4.

Octastyryl silsesquioxane (sty₈T₈) (6):

This product was isolated as a white solid in 10% yield (0.26g, 0.21 mmol). mp > 400 °C,

^1H NMR (500 MHz, CDCl_3 + 1% TMS) δ (ppm) 7.73 – 7.69 (m, 16H), 7.42 – 7.39 (m, 16H), 6.70 (dd, J = 17.6, 10.9 Hz, 8H), 5.80 (dd, J = 17.6, 0.9 Hz, 8H), 5.29 (dd, J = 10.8, 0.9 Hz, 8H).

^{13}C NMR (126 MHz, CDCl_3 + 1% TMS) δ (ppm) 139.77, 136.66, 134.47, 129.47, 125.68, 115.06.

^{29}Si NMR (99 MHz, CDCl_3 + 1% TMS) δ (ppm) -78.31 (8Si).

LCMS (Qtof) calculated for $\text{C}_{64}\text{H}_{57}\text{O}_{12}\text{Si}_8$ $[\text{M} + \text{H}]^+$ 1241.1999, found 1241.1703.

Decastyryl silsesquioxane (sty₁₀T₁₀) (7):

This product was isolated as a white solid in 11% yield (0.29 g, 0.19 mmol). mp > 400 °C.

^1H NMR (500 MHz, CDCl_3 + 1% TMS) δ (ppm) 7.57 (d, J = 7.7 Hz, 16H), 7.30 (d, J = 7.7 Hz, 16H), 6.67 (dd, J = 17.6, 10.9 Hz, 8H), 5.76 (d, J = 17.6 Hz, 8H), 5.26 (d, J = 10.9 Hz, 8H).

^{13}C NMR (126 MHz, CDCl_3 + 1% TMS) δ (ppm) 139.53, 136.69, 134.41, 129.90, 125.55, 114.90.

^{29}Si NMR (99 MHz, CDCl_3 + 1% TMS) δ (ppm) -79.68 (10Si).

LCMS (APCI) m/z calcd for $\text{C}_{80}\text{H}_{70}\text{NaO}_{15}\text{Si}_{10}^+$ $[\text{M} + \text{Na}]^+$ 1573.2300, obs'd 1573.2207

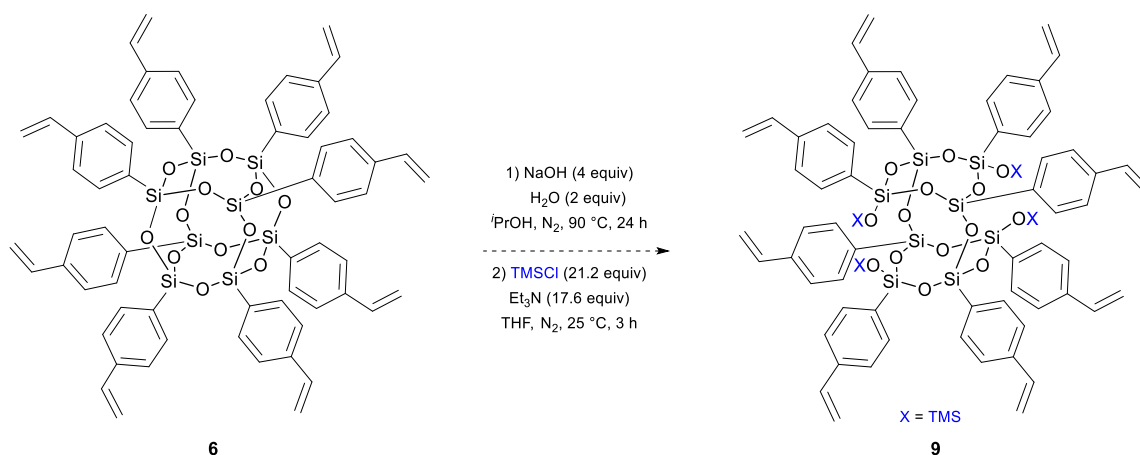
Dodecastyryl silsesquioxane (sty₁₂T₁₂) (8):

This product was not isolated as a pure compound.

5.2.3 Synthesis of 5,11,14,17-tetrakis((trimethylsilyl)oxy)-1,3,5,7,9,11,14,17-octakis(4-vinylphenyl)-2,4,6,8,10,12,13,15,16,18-decaoxa-1,3,5,7,9,11,14,17-octasilatricyclo[7.3.3.3^{3,7}]octadecane (9)

Step 1: Attempted cleavage of octastyrylsilsesquioxane (sty₈T₈) (6) for the synthesis of sodium 1,3,5,7,9,11,14,17-octakis(4-vinylphenyl)-2,4,6,8,10,12,13,15,16,18-decaoxa-1,3,5,7,9,11,14,17-octasilatricyclo[7.3.3.3^{3,7}]octadecane-5,11,14,17-tetrakis(olate)

Scheme 5-21: Hydrolysis of sty₈T₈ with sodium hydroxide



Step 1: Synthesis of from [(stySiO)₈(ONa)₄] (9) from octastyryl₈T₈ (6)

To a 100 mL round bottom flask equipped with a stir bar was added styryl₈T₈ (0.05 g, 0.04 mmol) and NaOH (0.064 g, 4 equiv). The reaction mixture was placed under nitrogen and 15 mL of iso-propanol added. Next 0.0014 mL (2 equiv) of water was added, and the mixture stirred at 70 °C for 24 h. The resulting white precipitate was filtered, washed several times with 2-propanol and dried under vacuum at 70 °C for 24 h. Product identification was done by derivatizing the siloxanolate intermediate to the TMS derivative and characterized by ¹H, ¹³C, ²⁹Si NMR and MS.

Step 2: Synthesis of tetrakis(trimethylsilyl) octastyrylsilsesquioxane [(stySiO)₈(OTMS)₄] (9) from [(stySiO)₈(ONa)₄]

The intermediate obtained from the NaOH hydrolysis of the octastyrylsilsesquioxane (**Scheme 5-21, step 1**) was charged into a 100 mL oven-dried round bottom flask equipped with a magnetic stirrer. The flask was purged with nitrogen gas for 30 minutes and THF (20 mL) added to it. Trimethylchlorosilane (0.092 g, 0.11 mL, 21.2 equiv) was then added followed by dropwise addition of triethylamine (0.071 g, 0.10 mL, 17.6 equiv) for 1 minute (**Scheme 5-21, step 2**). The reaction mixture was stirred at room temperature for 3 h. Deionized water (5 mL) was added to dissolve any NaCl produced and to hydrolyze unreacted Me₃SiCl. The organic layer was separated by means of a separating funnel, *n*-hexane (5 mL) was added, and the organic layer repeatedly washed with deionized water. *n*-Hexane (20 mL) was added to this solution which was then kept in a freezer at -30 °C overnight. However, the ¹H NMR obtained for this product shows that the product is a mixture of compounds.

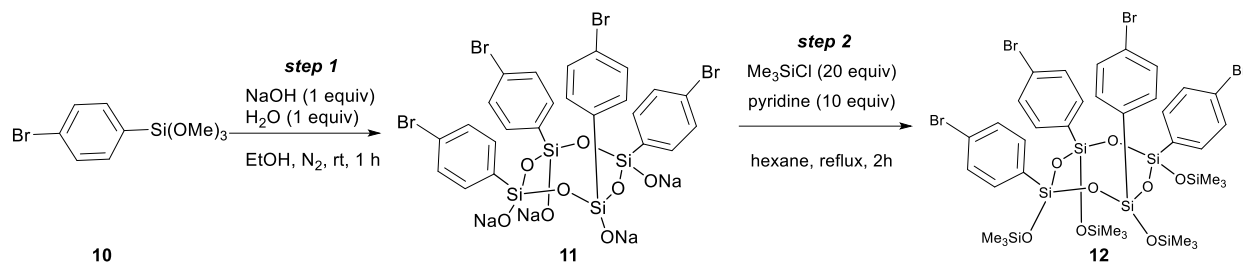
¹H NMR (500 MHz, CDCl₃ + 1% TMS) δ (ppm) 7.58 – 7.50 (m, 7H), 7.49 – 7.43 (m, 8H), 7.38 – 7.30 (m, 6H), 7.30 – 7.27 (m, 8H), 6.70 (ddd, *J* = 17.7, 10.9, 9.1 Hz, 8H), 5.83 – 5.71 (m, 8H), 5.29 – 5.22 (m, 8H), 0.07 (s, 28H), 0.05 (s, 32H).

¹³C NMR (126 MHz, CDCl₃ + 1% TMS) δ (ppm) 137.03, 134.26, 125.24, 114.05, 1.70.

²⁹Si NMR (99 MHz, CDCl₃ + 1% TMS) δ (ppm) 9.08, -79.94, -90.14.

5.2.4 Synthesis of 2,4,6,8-tetrakis(4-bromophenyl)-2,4,6,8-tetrakis((trimethylsilyl)oxy)-1,3,5,7,2,4,6,8-tetraoxatetrasilocane

Scheme 5-22: Synthesis of 2,4,6,8-tetrakis(4-bromophenyl)-2,4,6,8-tetrakis((trimethylsilyl)oxy)-1,3,5,7,2,4,6,8-tetraoxatetrasilocane (**12**) from the sodium hydroxide hydrolysis of 4-bromophenyltrimethoxysilane (**10**)



Step 1: Controlled alkaline hydrolysis of *p*-bromophenyltrimethoxysilane (10**)**

To a mixture of EtOH (4.4 mL), NaOH (0.263 g, 6.57 mmol, 1 equiv) and H₂O (0.118 g, 0.12 mL, 6.67 mmol, 1 equiv) was added (4-BrC₆H₄)Si(OMe)₃ (1.82 g, 6.57 mmol). The reaction mixture was stirred under a nitrogen stream for about an hour when the solvent volume reduced to half (**Scheme 22, step 1**). The resulting white precipitate was washed and centrifuged three times with anhydrous n-hexane and dried in vacuo to afford crude sodium 4-bromophenylcyclotetrasiloxanolate as a white solid in 24% yield (1.51 g, 1.58 mmol).

Step 2: Synthesis of 2,4,6,8-tetrakis(4-bromophenyl)-2,4,6,8-tetrakis((trimethylsilyl)oxy)-1,3,5,7,2,4,6,8-tetraoxatetrasilocane (12**) from Sodium 4-bromophenylcyclotetrasiloxanolate (**11**)**

To a 100 mL round bottom flask containing the sodium salt (**11**) (0.62 g, 0.65 mmol) above in anhydrous hexanes (60 mL) was added Me₃SiCl (1.65 mL, 13.0 mmol, 20 equiv) and pyridine (0.55 mL, 6.5 mmol, 10 equiv). The suspension was refluxed for 2 h under

a nitrogen atmosphere and after cooling to room temperature, the pyridinium salt was filtered off and washed with deionized water until the mixture is chloride free. The mixture was dried over MgSO₄, filtered and the solvent removed by rotary evaporation to afford the crude product as an oil in 71% yield (0.54 g, 0.46 mmol). This crude product was characterized by ¹H, ¹³C and ²⁹Si NMR.

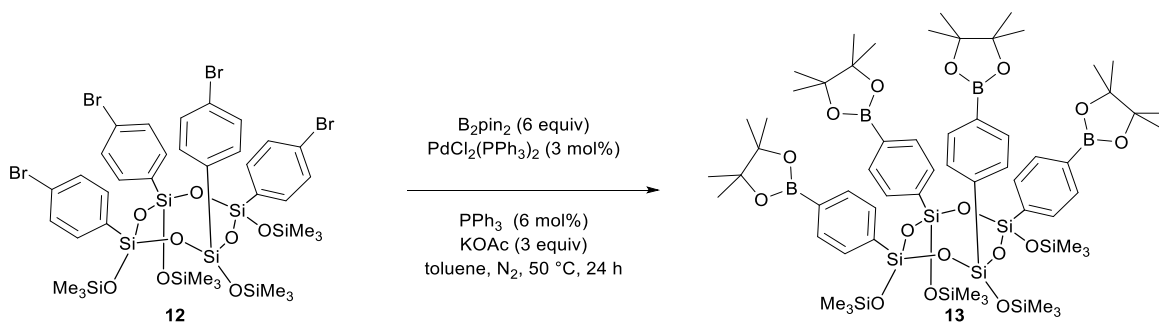
¹H NMR (500 MHz, CDCl₃ + 1% TMS) δ (ppm) 7.31 – 7.28 (m, 8H), 7.13 – 7.09 (m, 8H), 0.17 (s, 36H).

¹³C NMR (126 MHz, CDCl₃ + 1% TMS) δ (ppm) 135.27 (2C), 131.52 (1C), 130.85 (2C), 125.08 (1C), 1.78 (12C).

²⁹Si NMR (99 MHz, CDCl₃ + 1% TMS) δ (ppm) 11.59 (4Si), -79.97 (4Si).

5.2.5 Borylation of [4-BrC₆H₄Si(OTMS)]₄

Scheme 5-23: Synthesis of 2,4,6,8-tetrakis(4-(4,4,5,5-tetramethyl-1,3,2-dioxaborolan-2-yl)phenyl)-2,4,6,8-tetrakis((trimethylsilyl)oxy)-1,3,5,7,2,4,6,8-tetraoxatetrasilocane

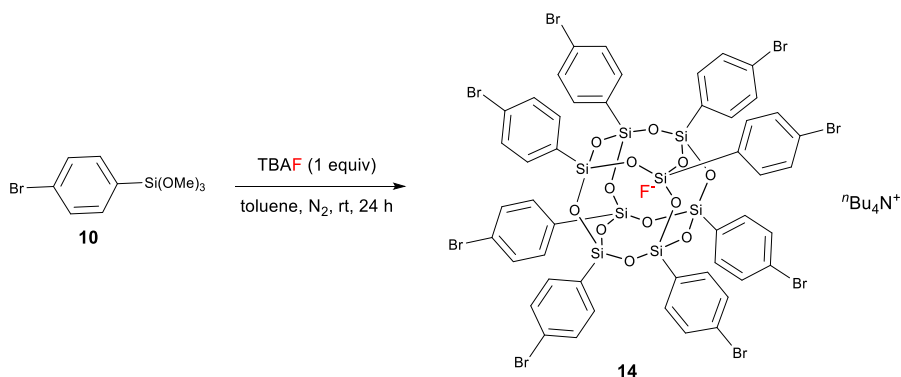


Onto a flask equipped with a magnetic stirrer in a glove box was added PdCl₂(PPh₃)₂ (3 mol%), Ph₃P (6 mol%), KOAc (3 equiv), bis(pinacolato)diboron (6 equiv), toluene (6 mL), and 2,4,6,8-tetrakis(4-bromophenyl)-2,4,6,8-tetrakis((trimethylsilyl)oxy)-1,3,5,7,2,4,6,8-tetraoxatetrasilocane (**12**) (0.20 g, 0.17 mmol). The mixture was placed over a preheated mantle at 50 °C and stirred for 12 h.⁶² The mixture was left to cool to room temperature and then extracted three times with water and benzene. The combined

organic layer washed with brine and dried over anhydrous MgSO_4 . The crude pinacolyl boronate (**13**) (0.18 g, 0.13 mmol, 76%) was then analyzed by ^1H , ^{11}B , ^{13}C and ^{29}Si NMR. ^1H NMR (500 MHz, CDCl_3 + 1% TMS) δ (ppm) 7.25 (t, J = 7.5 Hz, 8H), 7.18 – 7.15 (m, 8H), 2.35 (s, 11H), 1.36 – 1.31 (m, 12H), 1.26 (s, 48H), 0.17 (t, J = 6.7 Hz, 12H). ^{11}B NMR (160 MHz, CDCl_3 + 1% TMS) δ (ppm) 22.27. ^{29}Si NMR (99 MHz, CDCl_3 + 1% TMS) δ (ppm) 10.80 (4Si), -79.99 (4Si).

5.2.6 Synthesis of tetra-*n*-butylammonium octa(4-bromophenyl)octasilsesquioxane fluoride

Scheme 5-24: Synthesis of fluoride ion entrapped octa(4-bromophenyl)octasilsesquioxane (**14**)



Octa(para-bromophenyl)octasilsesquioxane with an entrapped fluoride anion was synthesized following the procedure developed by Taylor et al.¹⁴ using 4-bromophenyltrimethoxysilane. A 100 mL round bottom flask bearing a magnetic stirrer was sealed with a septum and purged with N_2 gas for 20 min. 4-Bromophenyltrimethoxysilane (2.77 g, 10 mmol, 2 equiv) and toluene (40 mL) were then added and the reaction mixture stirred for a further 20 minutes. Next tetra-*n*-butylammonium fluoride (5.0 mL of 1 M solution in THF with 5% water, 1 equiv). was added and the mixture stirred at room temperature (**Scheme 5-24**). After 24 h reaction

time, the solvent was evaporated with a rotary evaporator and the resulting brown liquid was further dried under vacuum at a temperature of 80 °C and a pressure of 70 mbar for 20 minutes to afford a yellow solid. The solid was further purified by flash column chromatography on silica gel (acetone/hexane: 3/7) to afford a white solid in 0.88 g (37 % yield). mp > 400 °C.

^1H NMR (500 MHz, Acetone- d_6) δ (ppm) 7.75 – 7.62 (m, 16H), 7.59 – 7.45 (m, 16H), 3.46 – 3.39 (m, 8H), 1.81 (tt, J = 8.1, 6.2 Hz, 8H), 1.43 (h, J = 7.4 Hz, 8H), 0.97 (t, J = 7.4 Hz, 12H).

^{13}C NMR (126 MHz, Acetone- d_6) δ (ppm) 135.90, 135.51, 130.58, 123.61, 58.44, 19.50, 12.98.

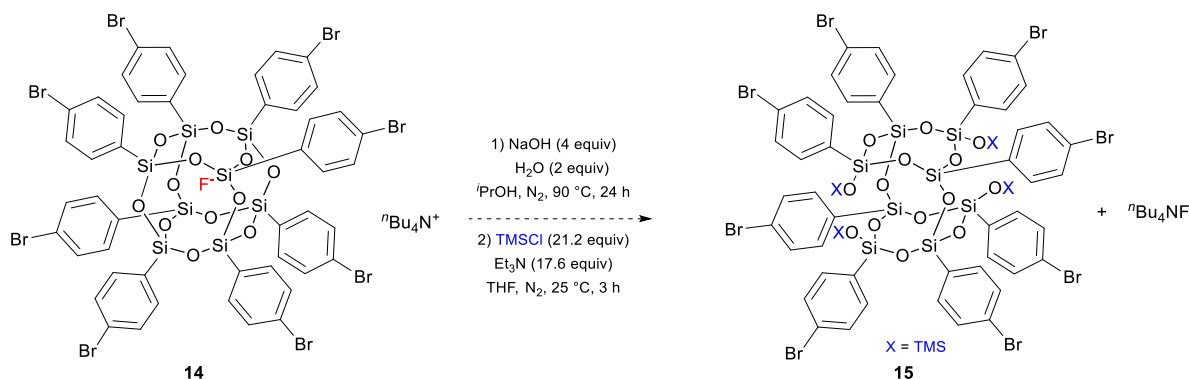
^{19}F NMR (470 MHz, Acetone- d_6) δ -27.28.

^{29}Si NMR (99 MHz, Acetone- d_6) δ -80.82.

5.2.7 Synthesis of 1,3,5,7,9,11,14,17-octakis(4-bromophenyl)-5,11,14,17-tetrakis((trimethylsilyl)oxy)-2,4,6,8,10,12,13,15,16,18-decaoxa-1,3,5,7,9,11,14,17-octasilatricyclo[7.3.3.3^{3,7}]octadecane

Step 1: Attempted cleavage of tetra-n-butylammonium octa(p-bromophenyl)octasilsesquioxanolate fluoride with sodium hydroxide

Scheme 5-25: Cleavage of **14** for the synthesis of 1,3,5,7,9,11,14,17-octakis(4-bromophenyl)-5,11,14,17-tetrakis((trimethylsilyl)oxy)-2,4,6,8,10,12,13,15,16,18-decaoxa-1,3,5,7,9,11,14,17-octasilatricyclo[7.3.3.3^{3,7}]octadecane (**15**)



To a 100 mL round bottom flask equipped with a stir bar was added (4-BrC₆H₄)₈T₈ (0.50 g, 0.30 mmol) and NaOH (0.048 g, 4 equiv). The reaction mixture was placed under nitrogen and 24 mL of iso-butanol added. Next 0.01 mL (2 equiv) of water was added, and the mixture stirred at 90 °C for 24 h (**Scheme 5-25**). The resulting white precipitate was filtered, washed several times with 2-propanol and dried under vacuum at 70 °C for 24 h. Product identification was done by derivatizing the sodium salt to the [(p-BrC₆H₄)₈(SiO)₈(OTMS)₄] and characterized by ¹H, ¹³C, ²⁹Si NMR and MS.

Step 2: Synthesis of tetrakis(trimethylsilyl) octa(p-bromophenyl)silsesquioxane [(p-BrC₆H₄)₈(SiO)₈(OTMS)₄] from [(p-BrC₆H₄)₈(SiO)₈(ONa)₄]

The intermediate obtained from the NaOH hydrolysis of 14 (**Scheme 5-25, step 1**) above was charged into a 100 mL oven-dried round bottom flask equipped with a magnetic stirrer. The flask was purged with nitrogen gas for 30 minutes and THF (20 mL) added to it. Trimethylchlorosilane (21.2 equiv) was then added followed by dropwise addition of triethylamine (17.6 equiv) for 1 minute (**Scheme 5-25, step 2**). The reaction mixture was stirred at room temperature for 3 h. Deionized water (5 mL) was added to dissolve any NaCl produced and to hydrolyze unreacted Me₃SiCl. The organic layer was separated by means of a separating funnel. *n*-Hexane (5 mL) was added, and the organic layer repeatedly washed with deionized water. *n*-Hexane (20 mL) was added to this solution, and the solution left standing at -30 °C in a refrigerator overnight. The precipitated solid was filtered off and dried at reduced pressure to afford a white impure solid (0.43 g) that was characterized by ¹H, ¹³C and ²⁹Si NMR.

¹H NMR (500 MHz, CDCl₃ + 1%TMS) δ 7.62 – 7.57 (m, 16H), 7.45 – 7.38 (m, 16H), 2.45 – 2.36 (m, 8H), 1.20 (p, *J* = 7.3 Hz, 8H), 1.15 – 1.06 (m, 8H), 0.90 (t, *J* = 7.2 Hz, 12H).

¹³C NMR (126 MHz, CDCl₃) δ 135.99, 135.63, 130.49, 123.80, 23.57, 19.64, 13.65.

²⁹Si NMR (99 MHz, CDCl₃) δ -81.45.

APPENDIX

Copies of GC/MS, MS, ^1H , ^{11}B , ^{13}C , ^{19}F and ^{29}Si NMR Spectra

GC/MS for styrene

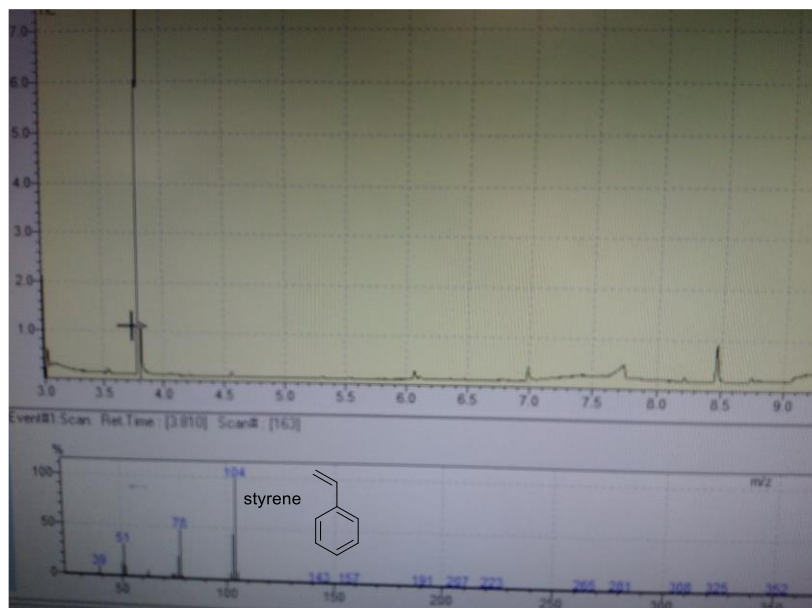


Figure 5-1: GC/MS – styrene

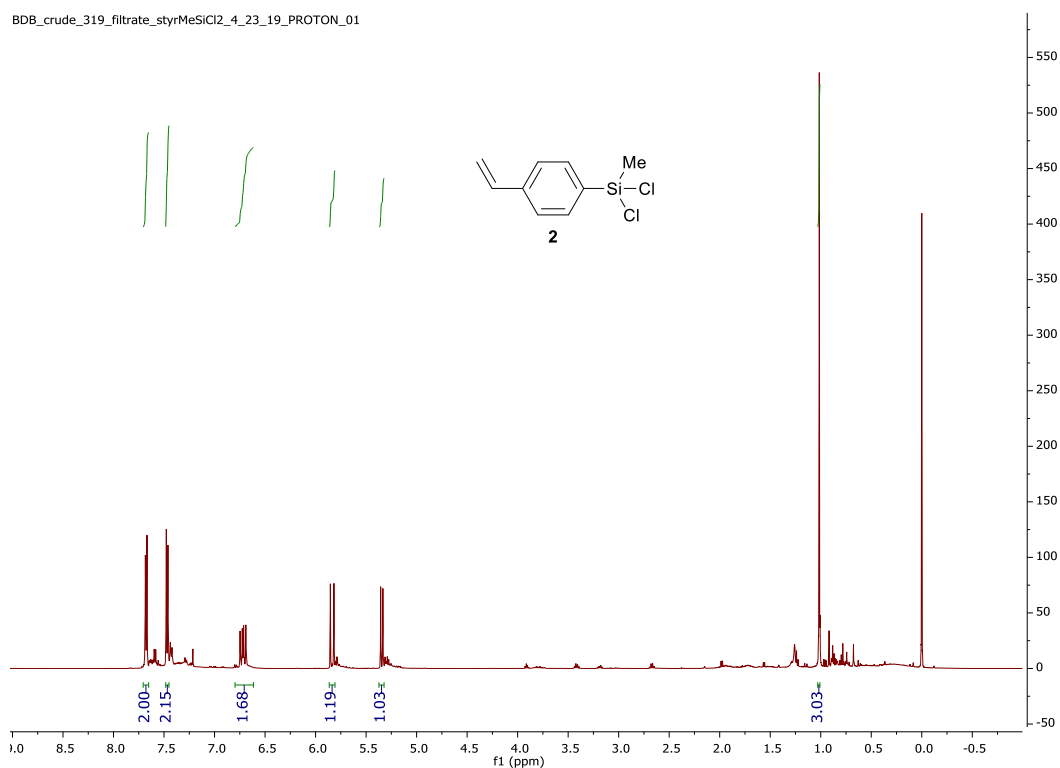


Figure 5-2: ^1H NMR of **2 (CDCl_3 + 1%TMS, 500 MHz)**

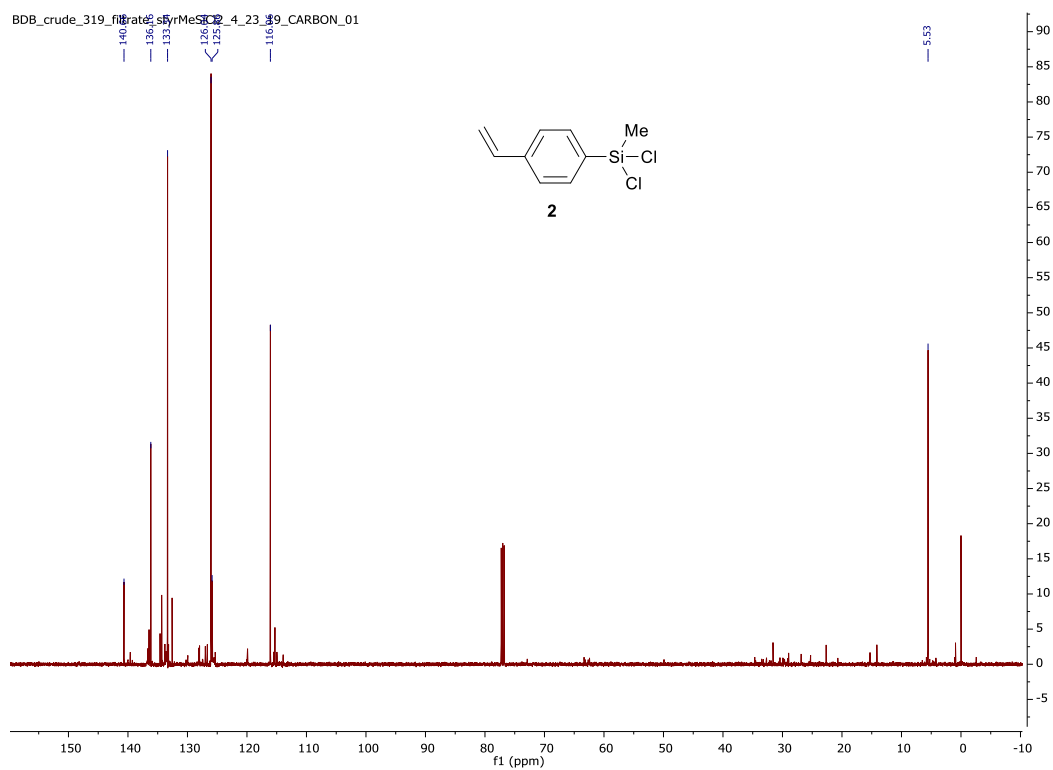


Figure 5-3: ¹³C NMR of **2** (CDCl₃ + 1%TMS, 126 MHz)

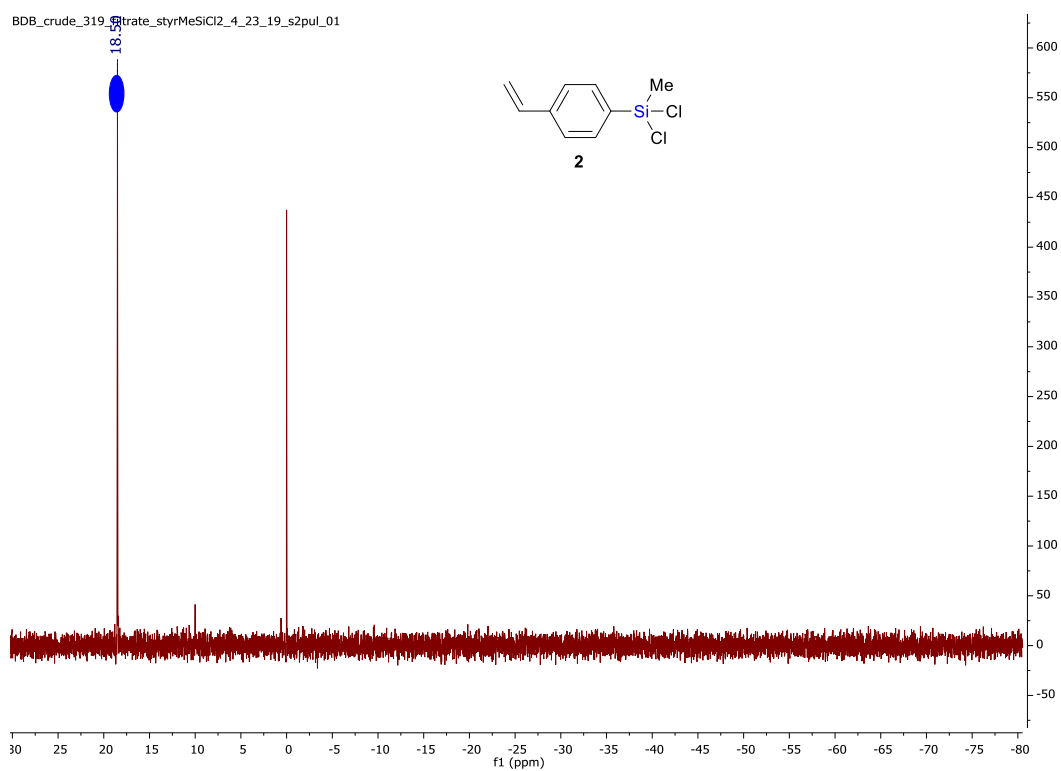


Figure 5-4: ²⁹Si NMR of **2** (99 MHz, CDCl₃)

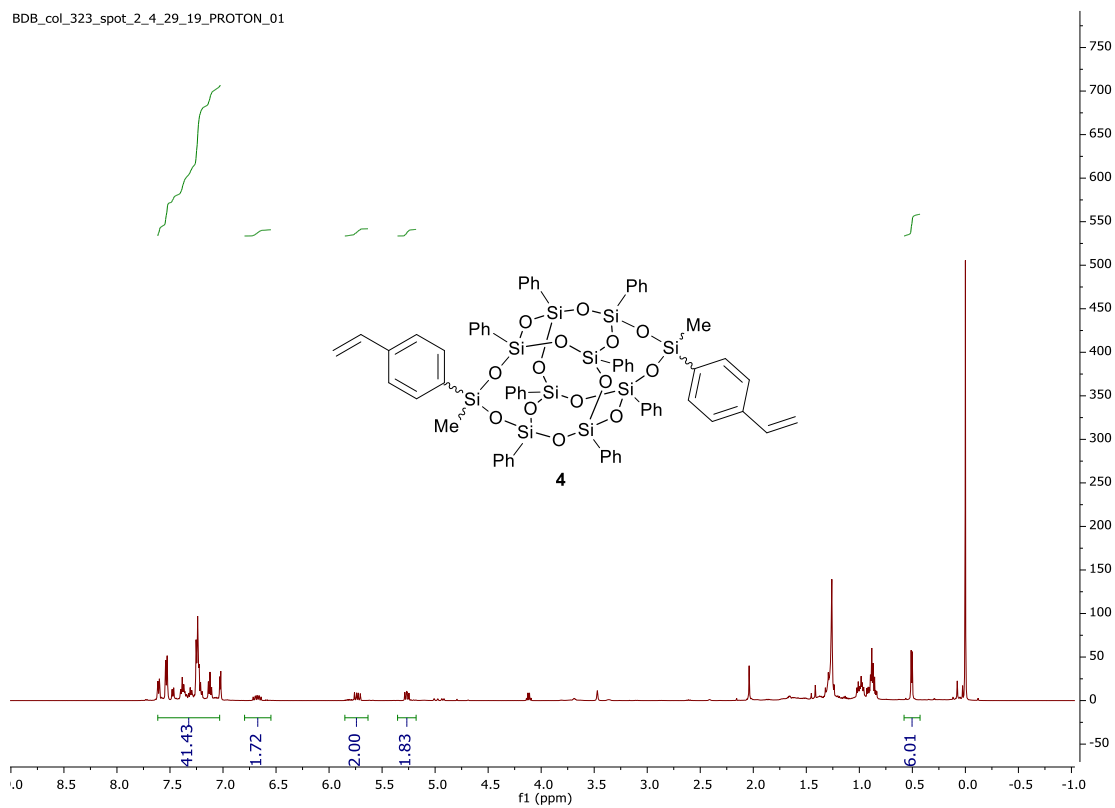


Figure 5-5: ^1H NMR of 4 (CDCl_3 + 1% TMS, 500 MHz)

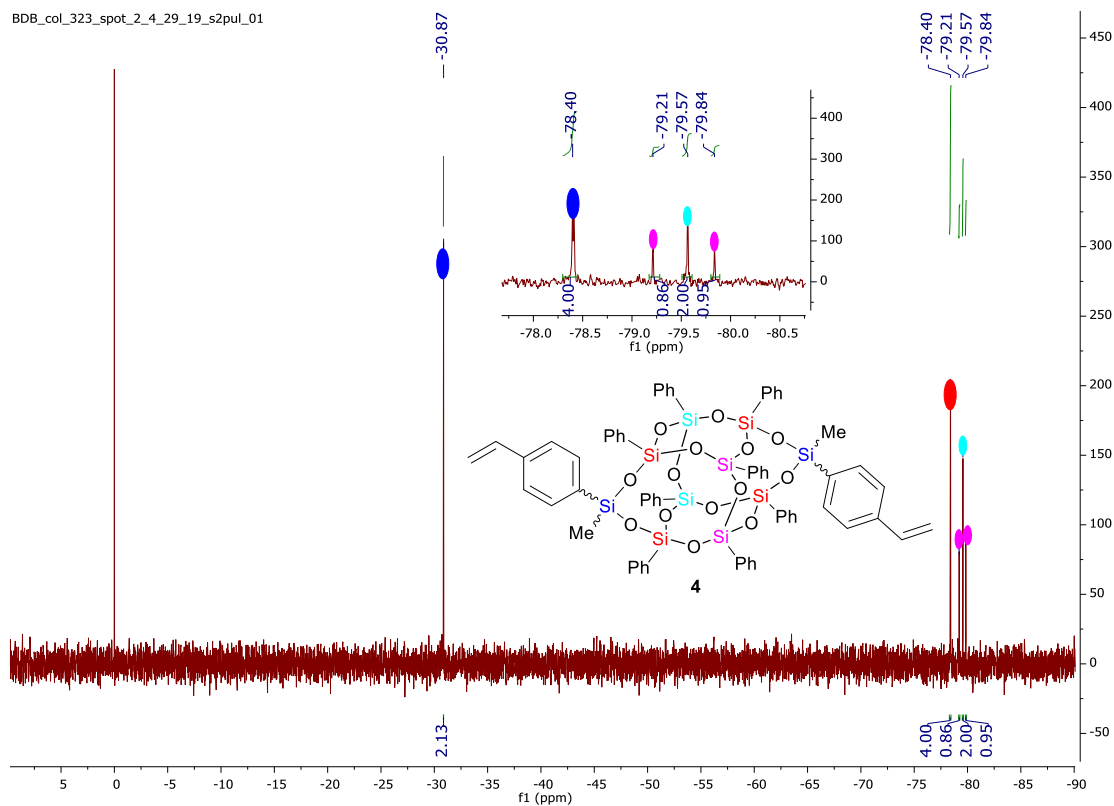


Figure 5-6: ^{29}Si NMR of **4** (99 MHz, CDCl_3)

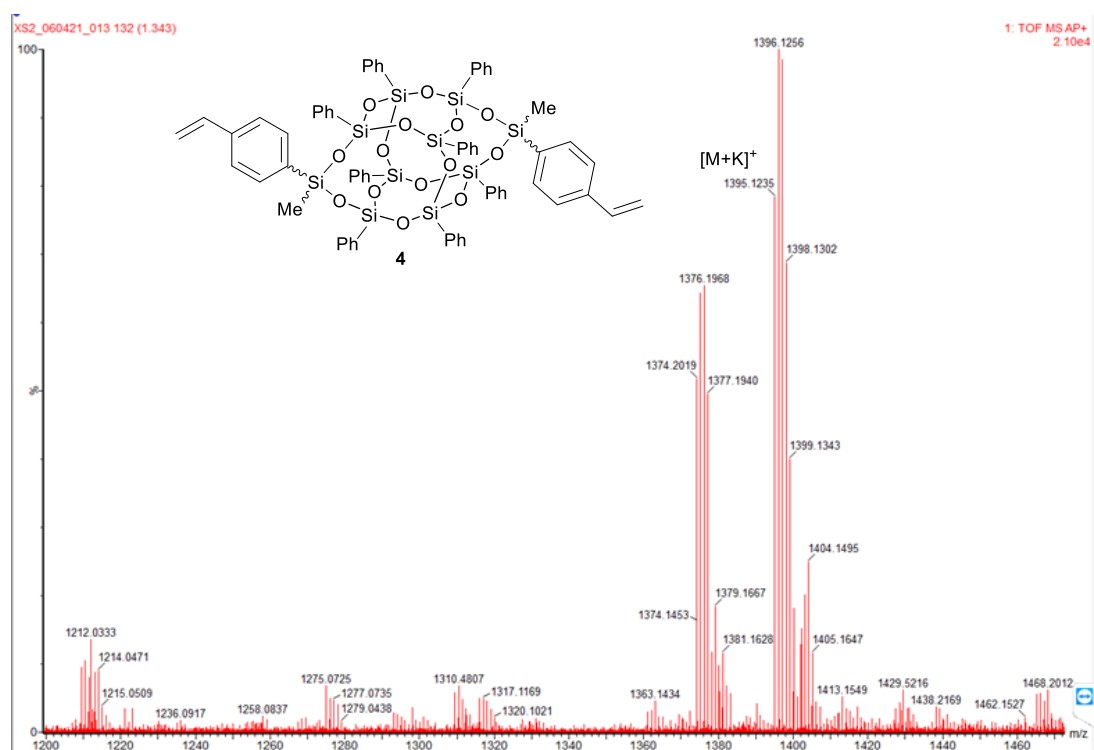


Figure 5-7: Mass spec of **4**

BDB_col_635 sty8T8_5_20_21_PROTON_01

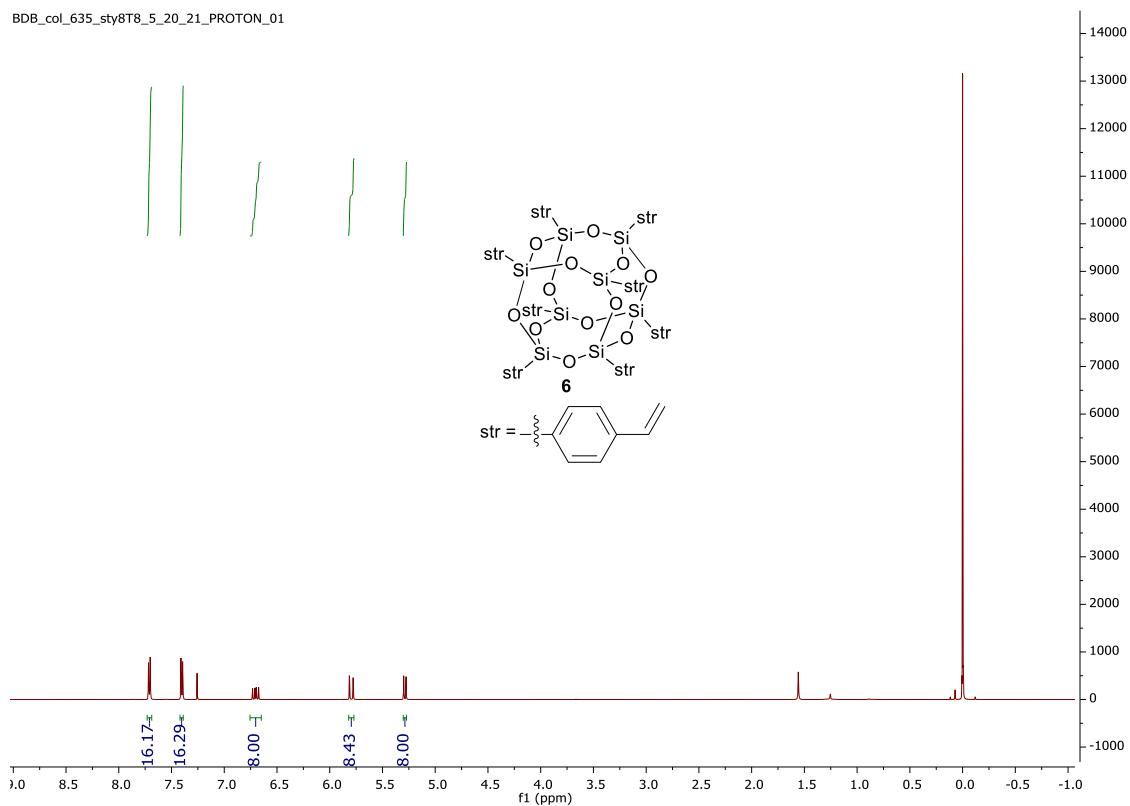


Figure 5-8: ^1H NMR of 6 (CDCl_3 + 1%TMS, 500 MHz)

BDB_col_635 sty8T8_5_20_21_13C_NMR_01

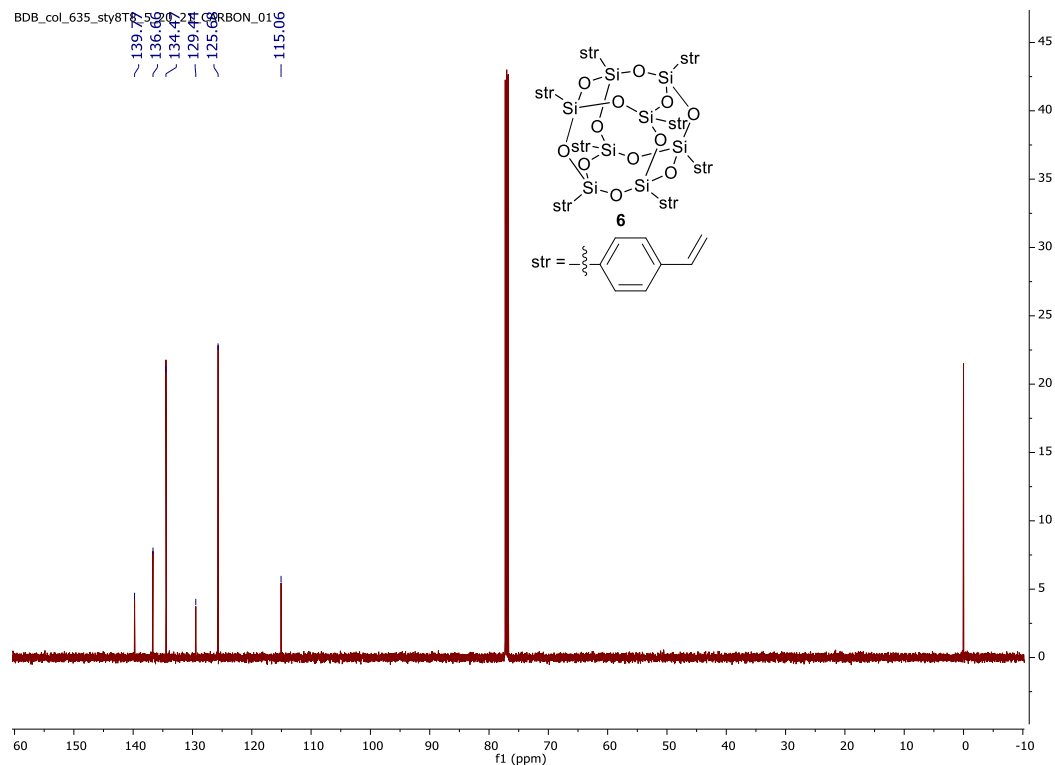


Figure 5-9: ^{13}C NMR of 6 (CDCl_3 + 1%TMS, 126 MHz)

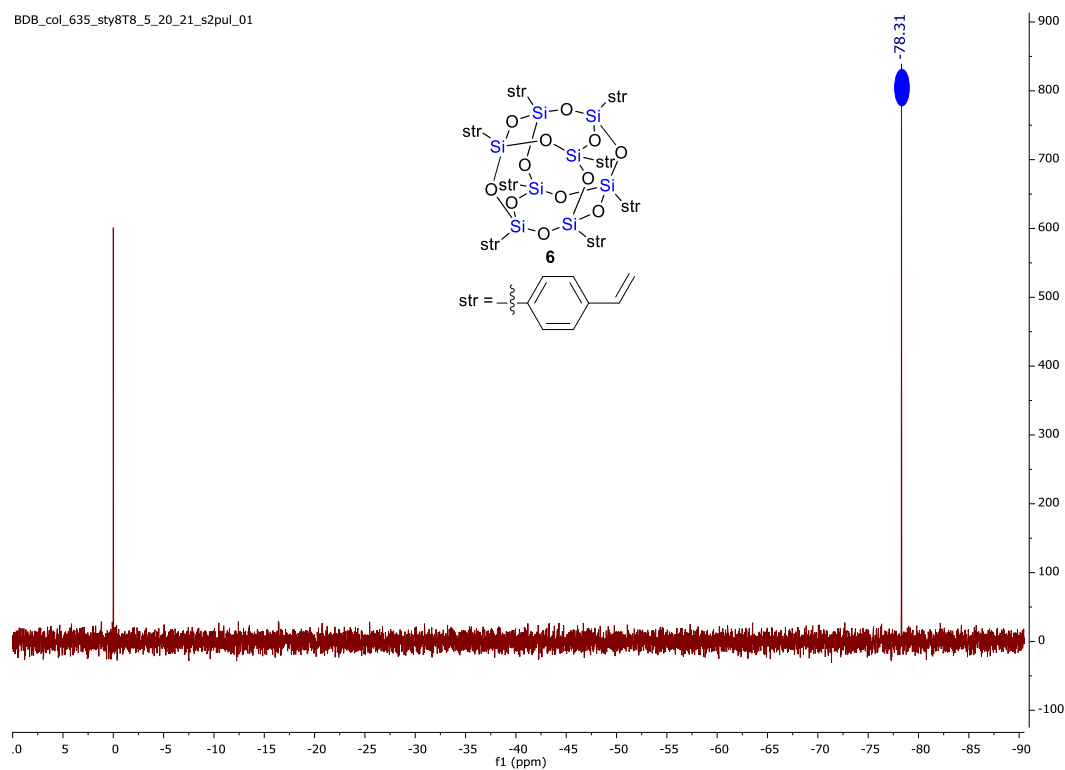


Figure 5-10: ^{29}Si NMR of **6** (99 MHz, CDCl_3)

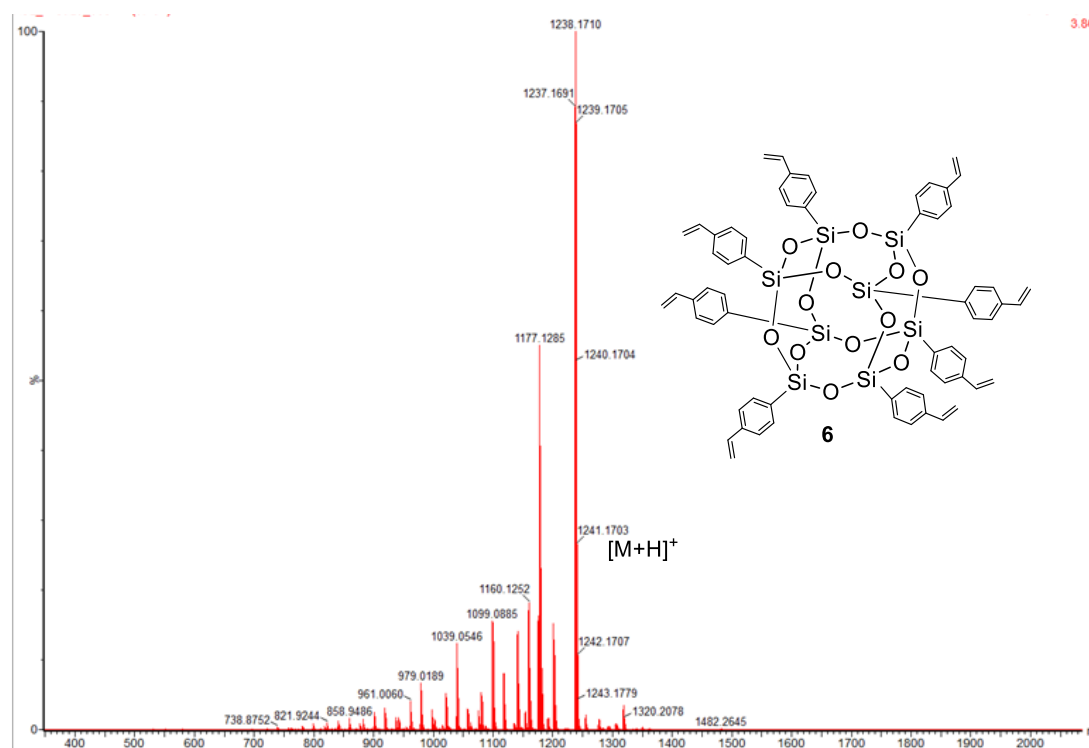


Figure 5-11: Mass spec of **6**

BDB_col_635_sty10T10_5_20_21_PROTON_01

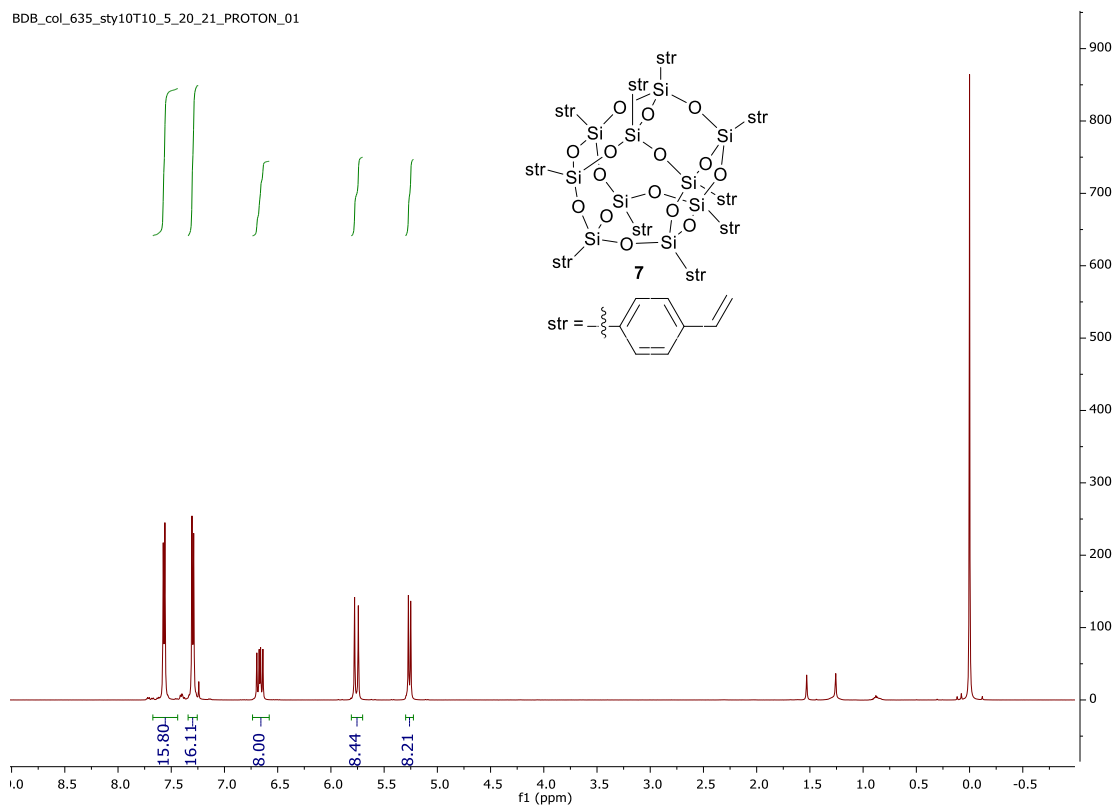


Figure 5-12: ^1H NMR of 7 (CDCl_3 + 1%TMS, 500 MHz)

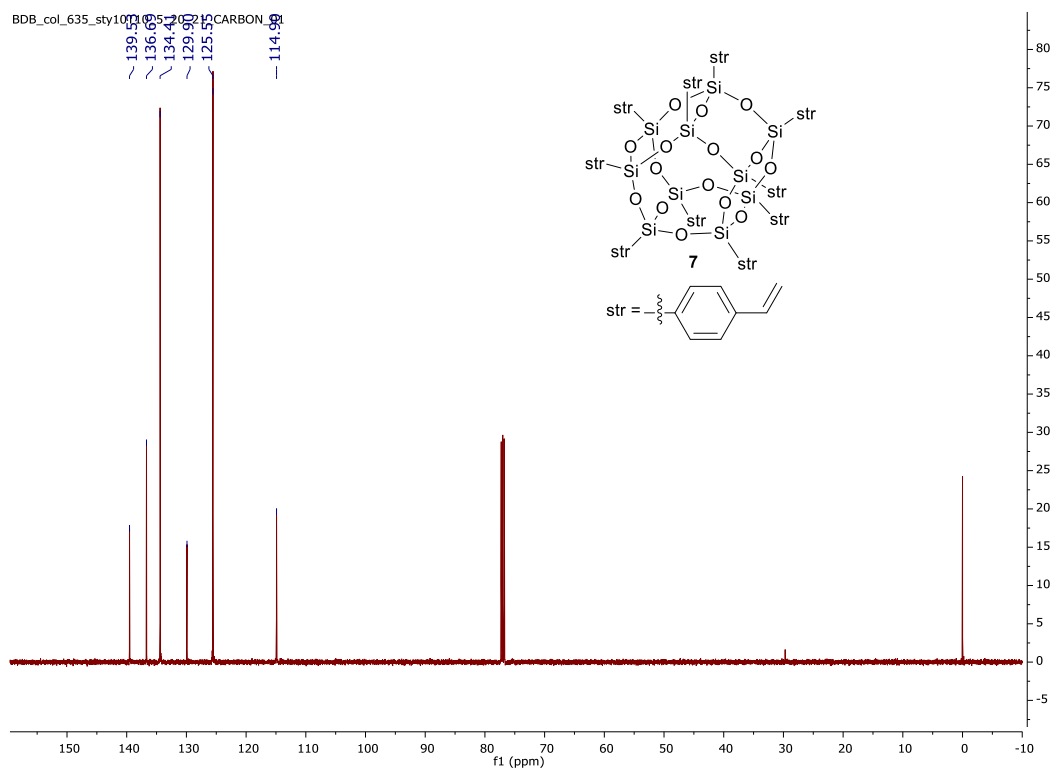


Figure 5-13: ^{13}C NMR of 7 (CDCl_3 + 1%TMS, 126 MHz)

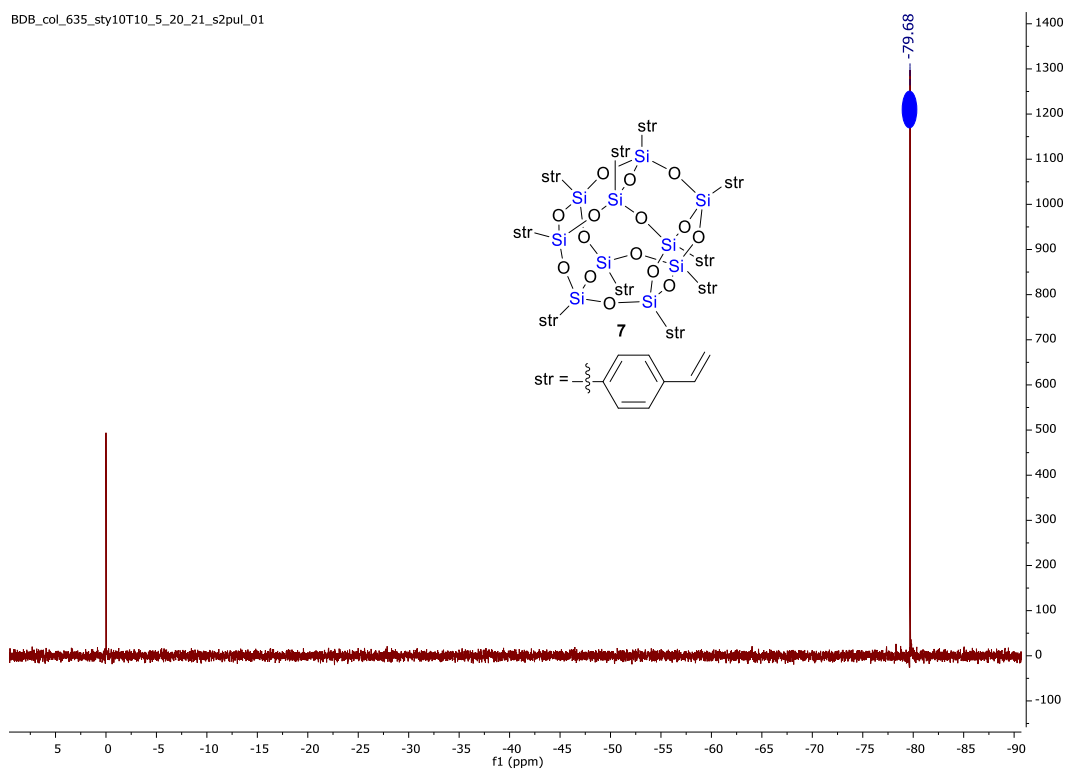


Figure 5-14: ^{29}Si NMR of 7 (99 MHz, CDCl_3)

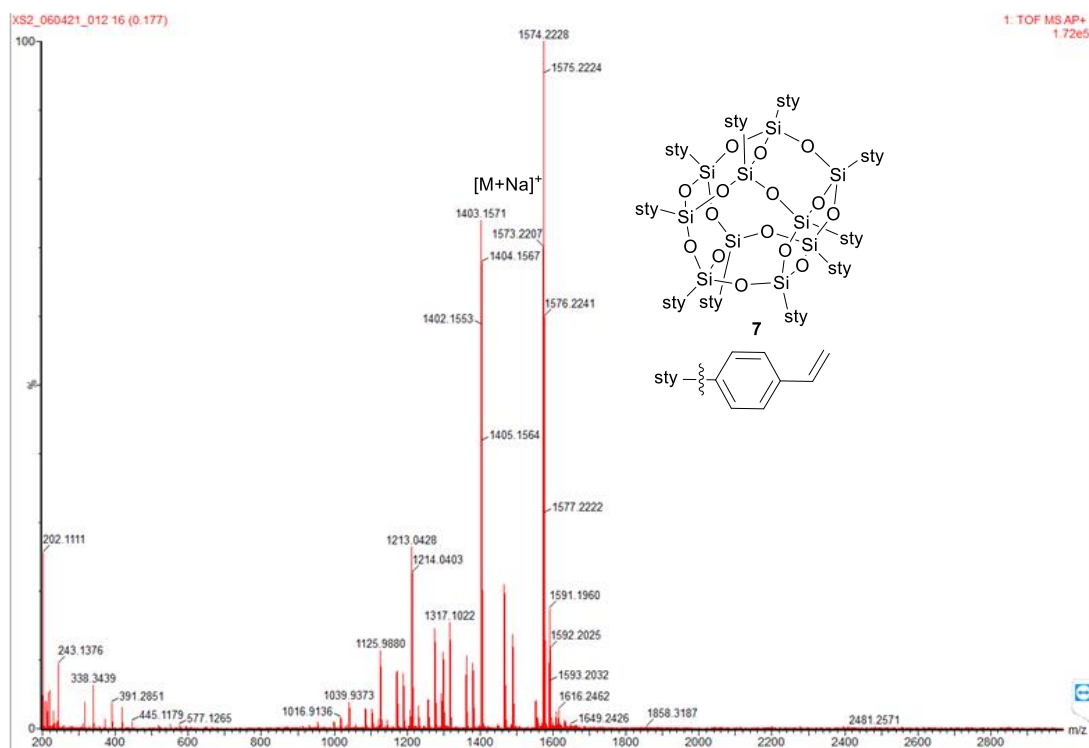


Figure 5-15: Mass spec of 7

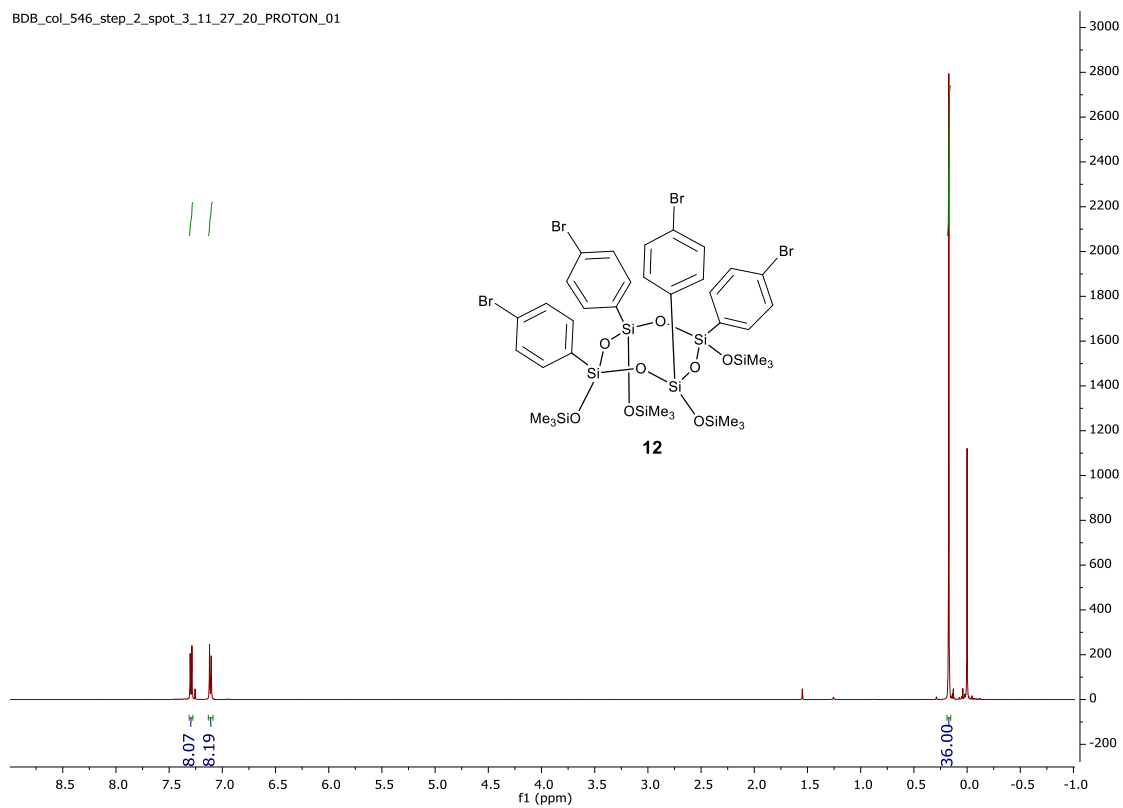


Figure 5-16: ^1H NMR of **12** ($\text{CDCl}_3 + 1\% \text{TMS}$, 500 MHz)

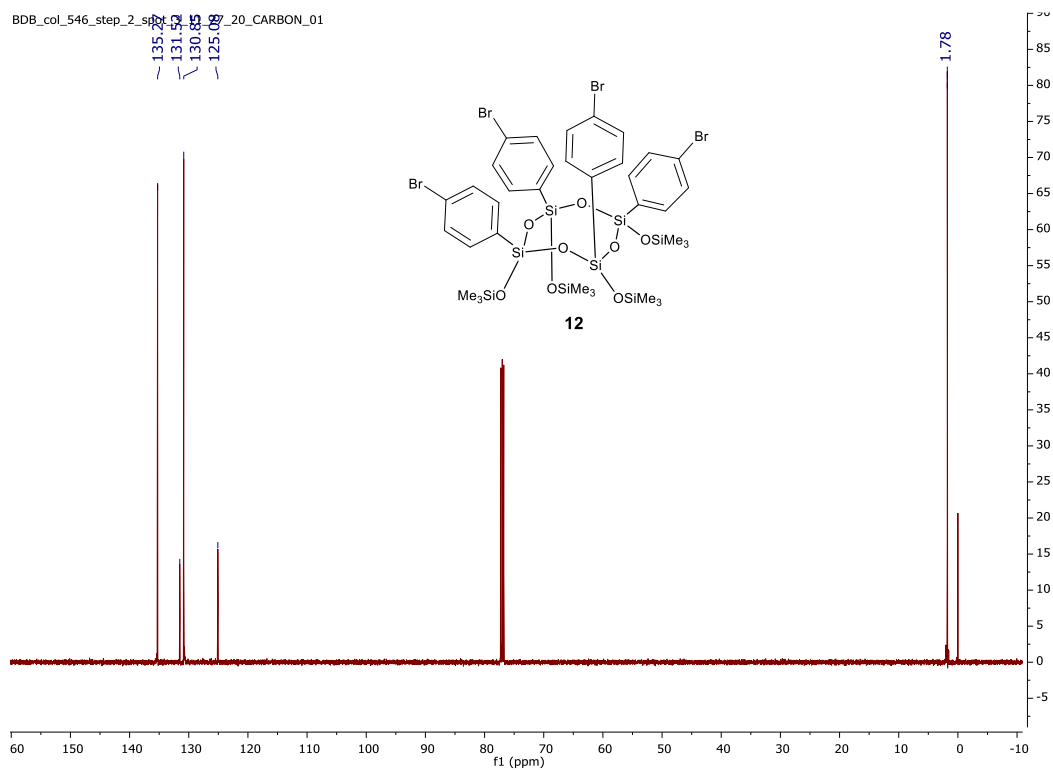


Figure 5-17: ^{13}C NMR of 12 (CDCl_3 + 1%TMS, 126 MHz)

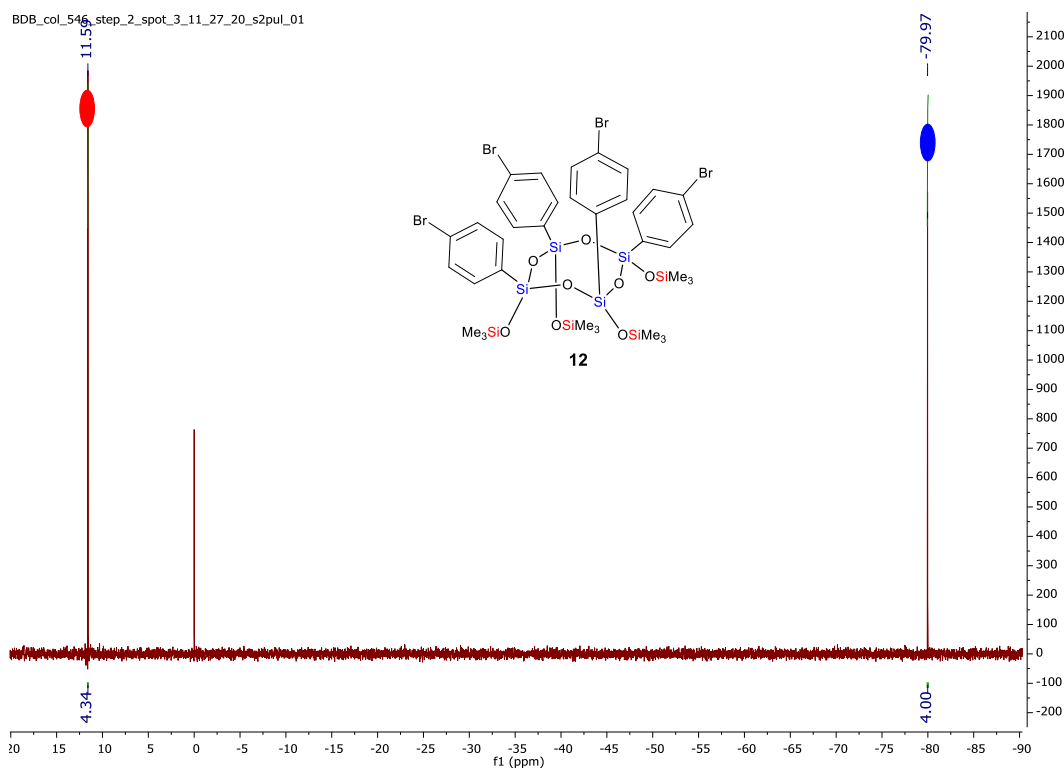


Figure 5-18: ^{29}Si NMR of 12 (99 MHz, CDCl_3)

BDB_crude_578_borylated_4BrPhT4OTMS_1_16_21_PROTON_01

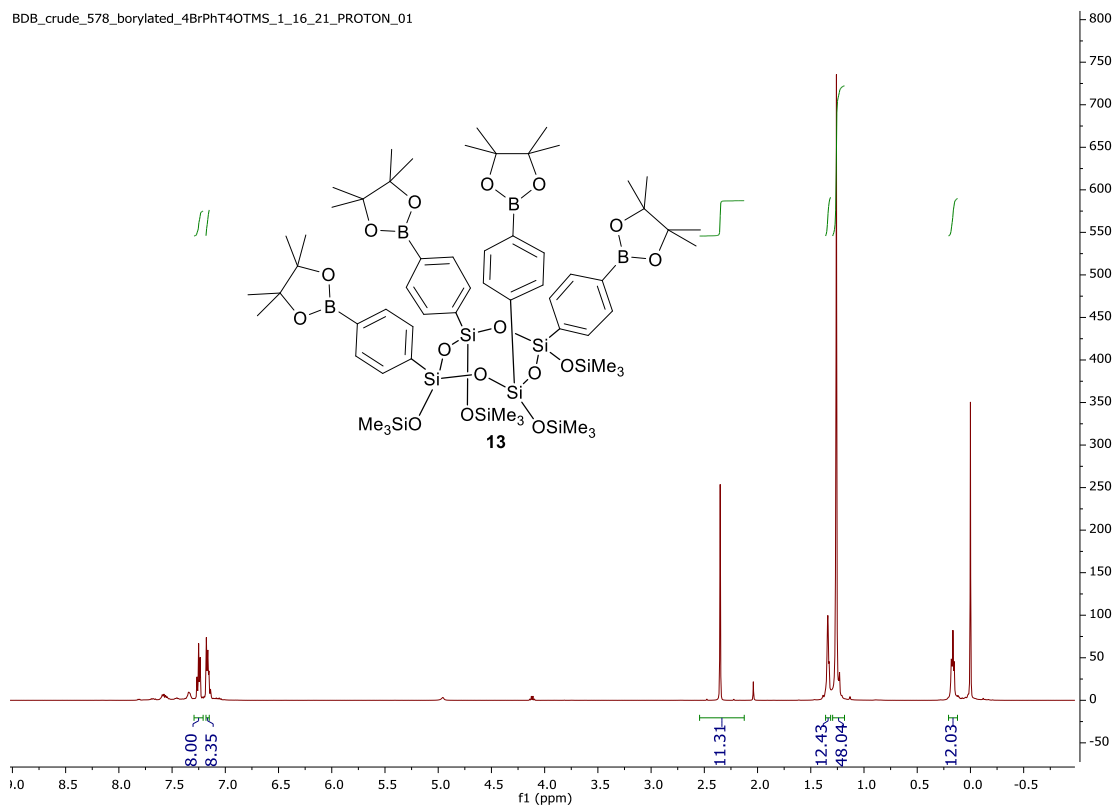


Figure 5-19: ¹H NMR of **13** (CDCl₃ + 1%TMS, 500 MHz)

BDB_crude_578_borylated_4BrPhT4OTMS_1_16_21_s2pul_01

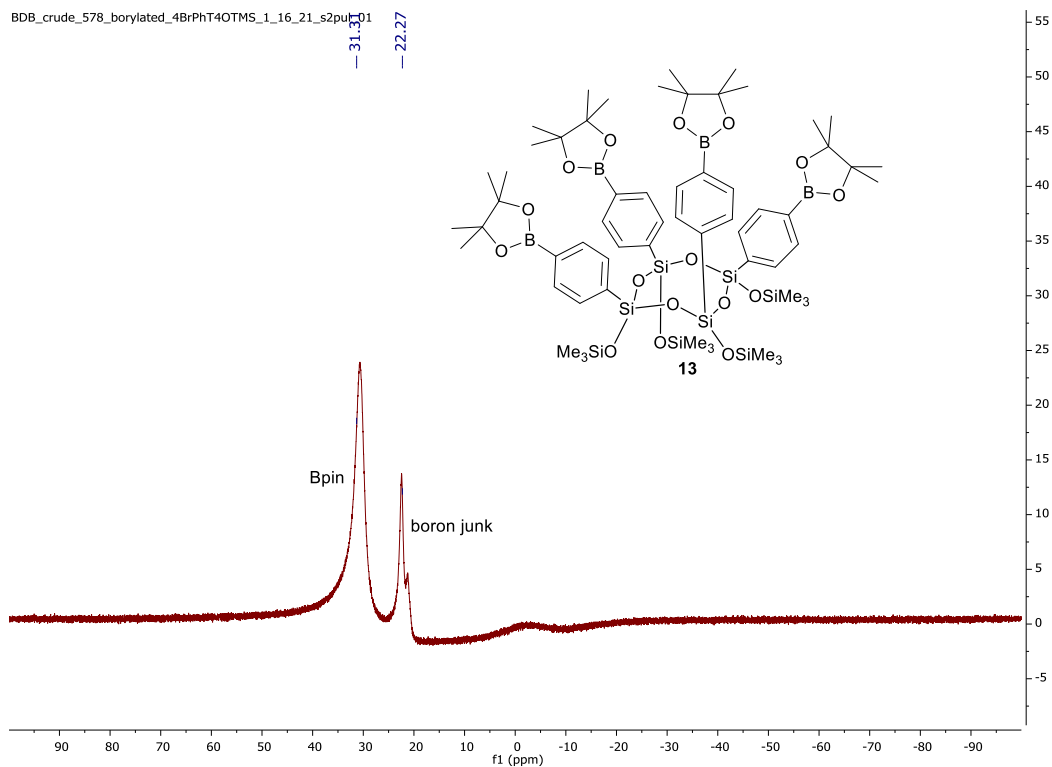


Figure 5-20: ¹¹B NMR of **13** (CDCl₃ + 1%TMS, 160 MHz)

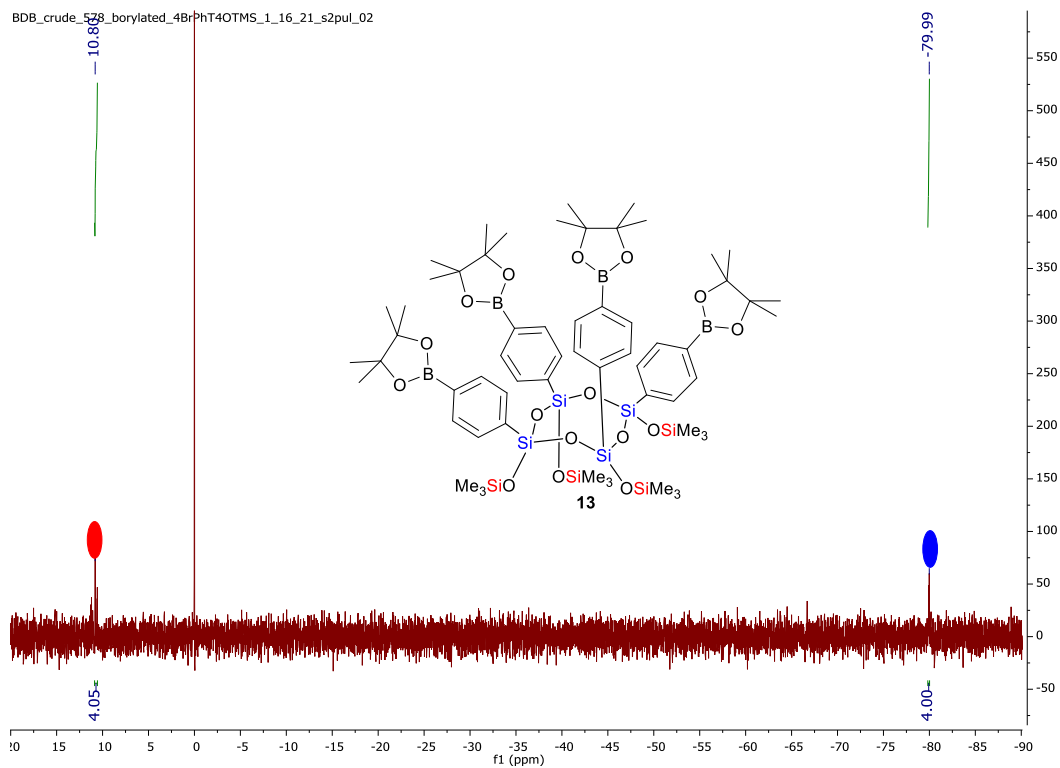


Figure 5-21: ²⁹Si NMR of **13** (99 MHz, CDCl₃)

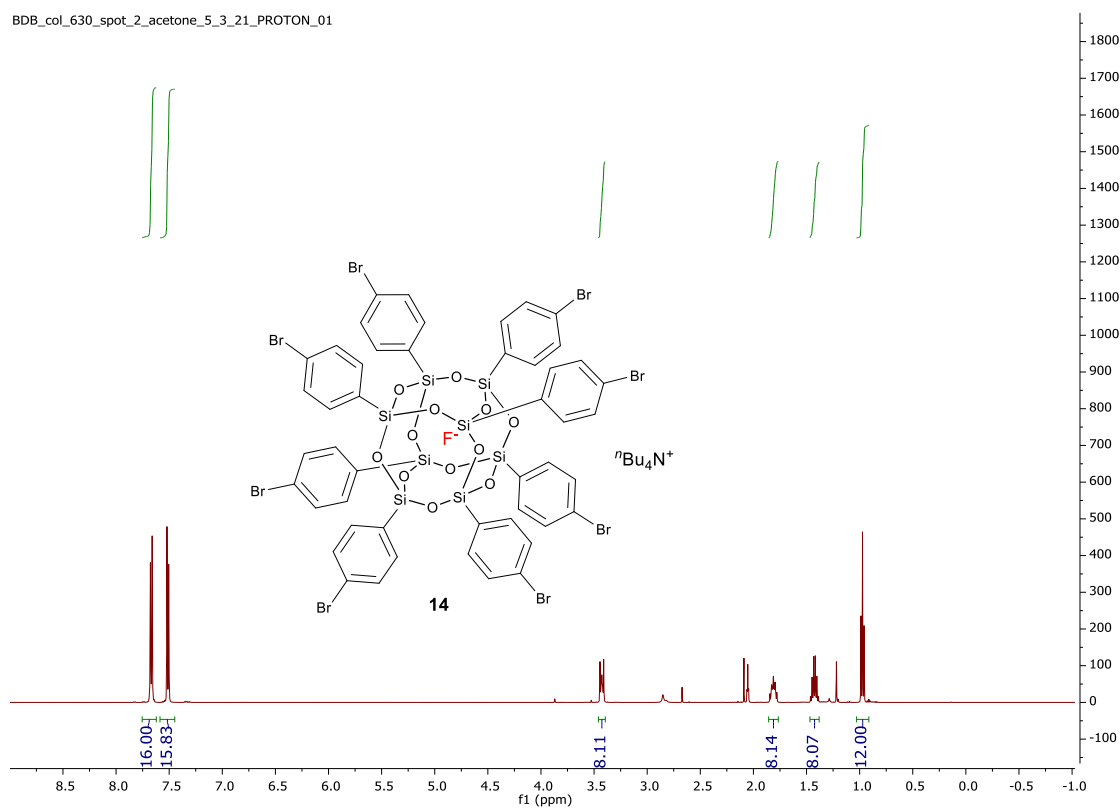


Figure 5-22: ¹H NMR of **14** (Acetone-*d*₆, 500 MHz)

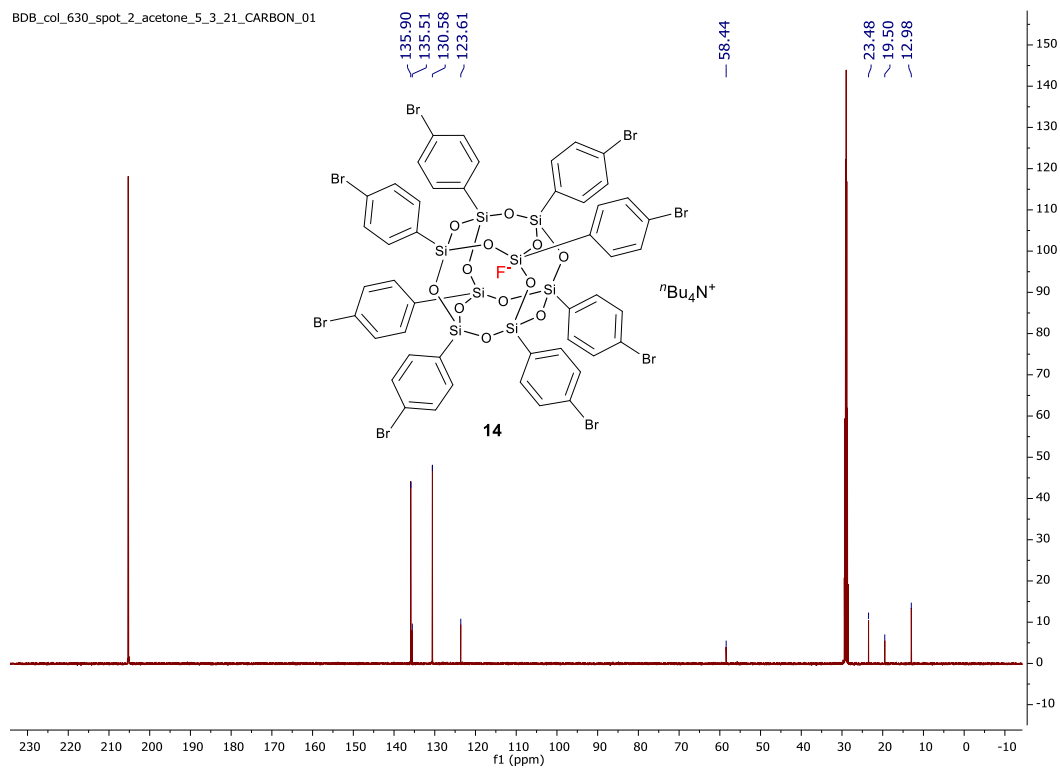


Figure 5-23: ^{13}C NMR of **14** (126 MHz, Acetone- d_6)

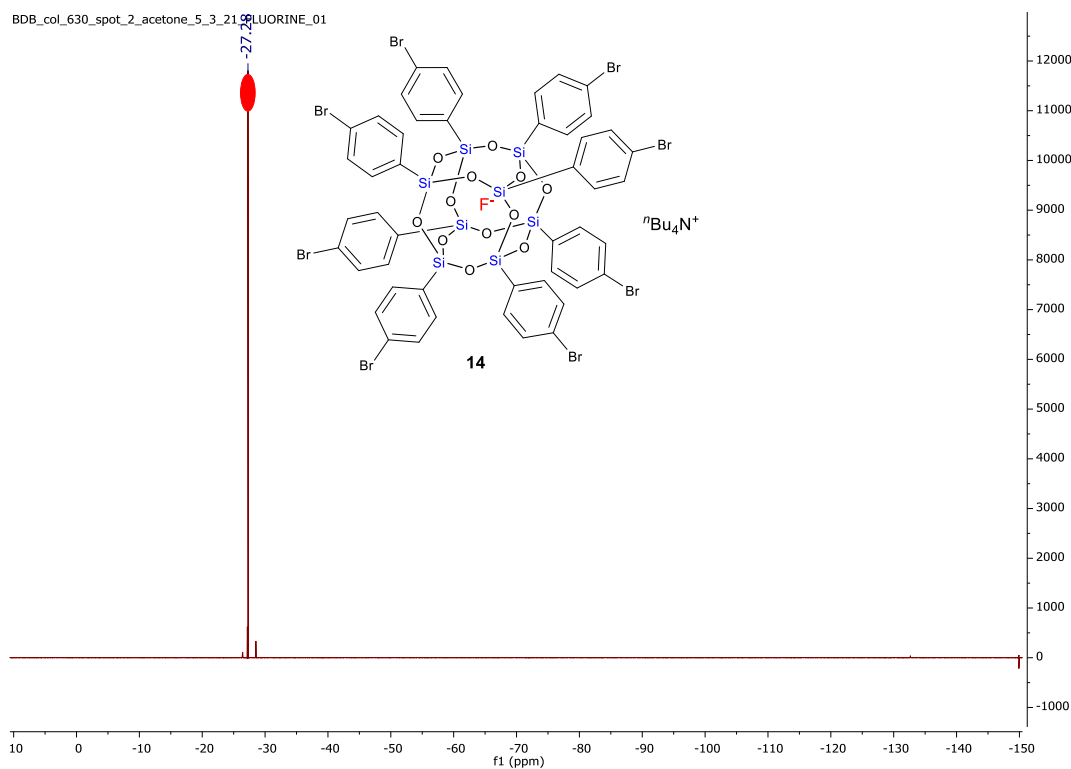


Figure 5-24: ^{19}F NMR of **14** (Acetone- d_6 , 471 MHz)

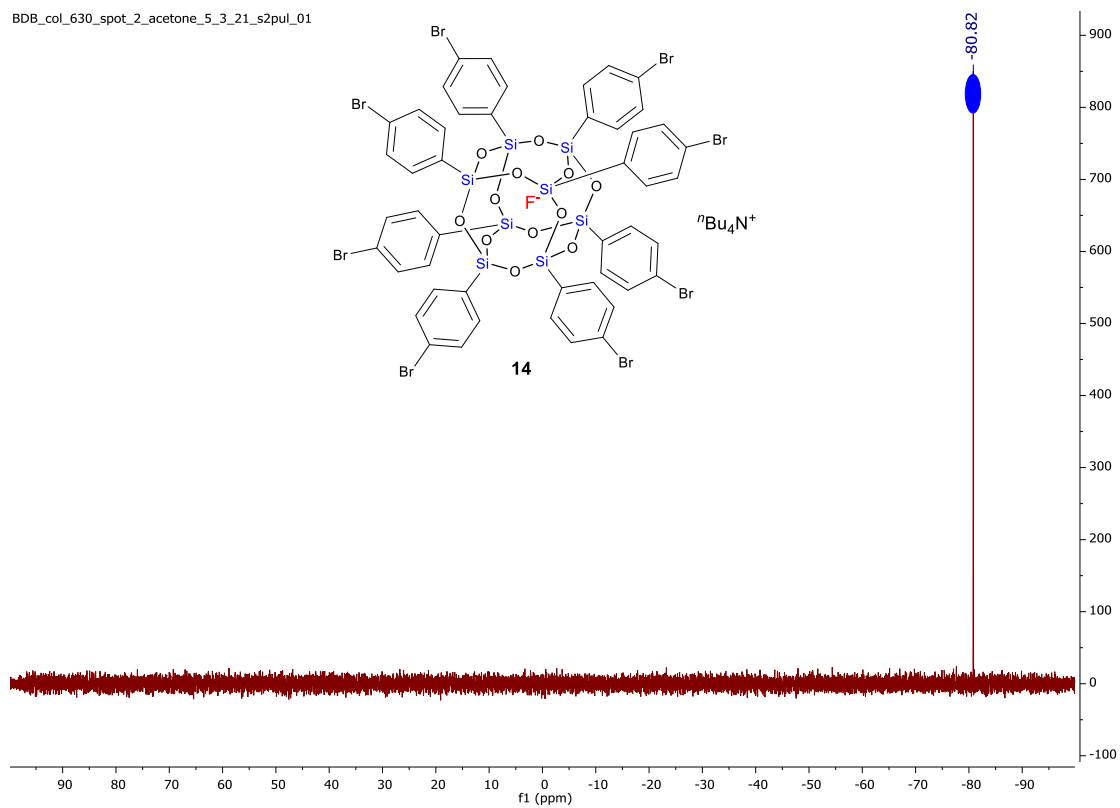


Figure 5-25: ^{29}Si NMR of **14** (Acetone- d_6 , 99 MHz)

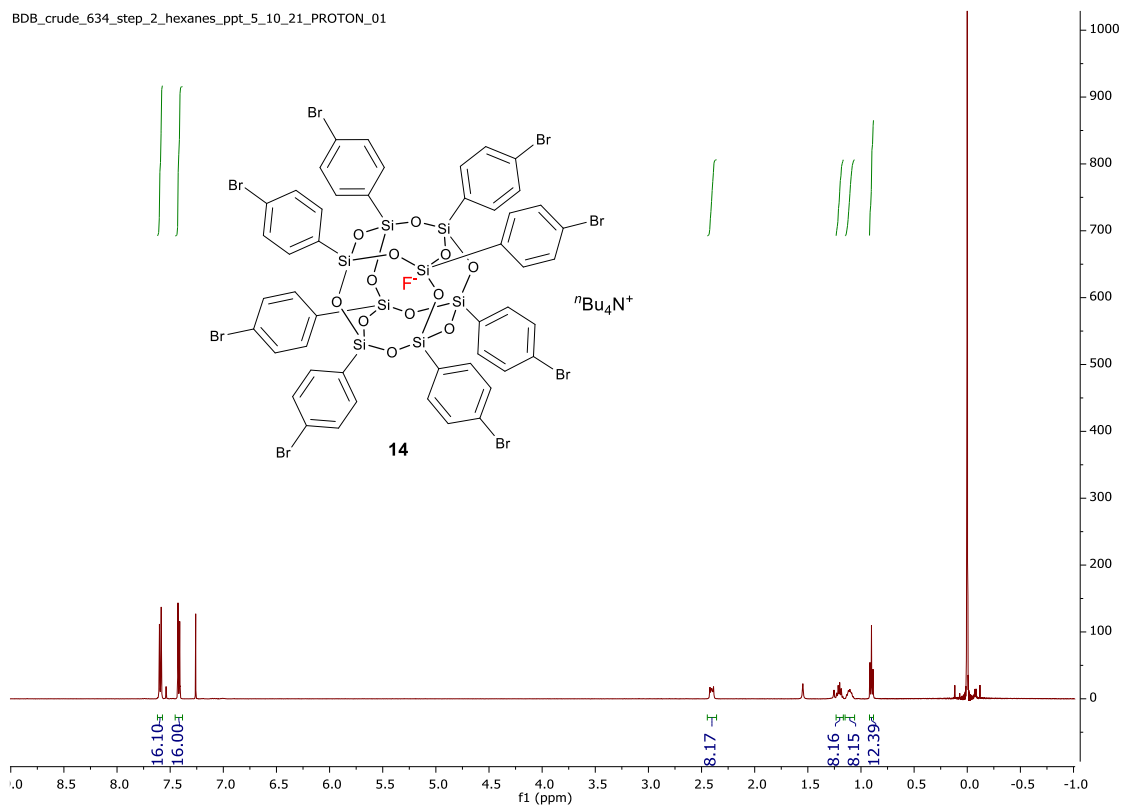


Figure 5-26: ^1H NMR of **14** (CDCl₃ + 1%TMS, 500 MHz)

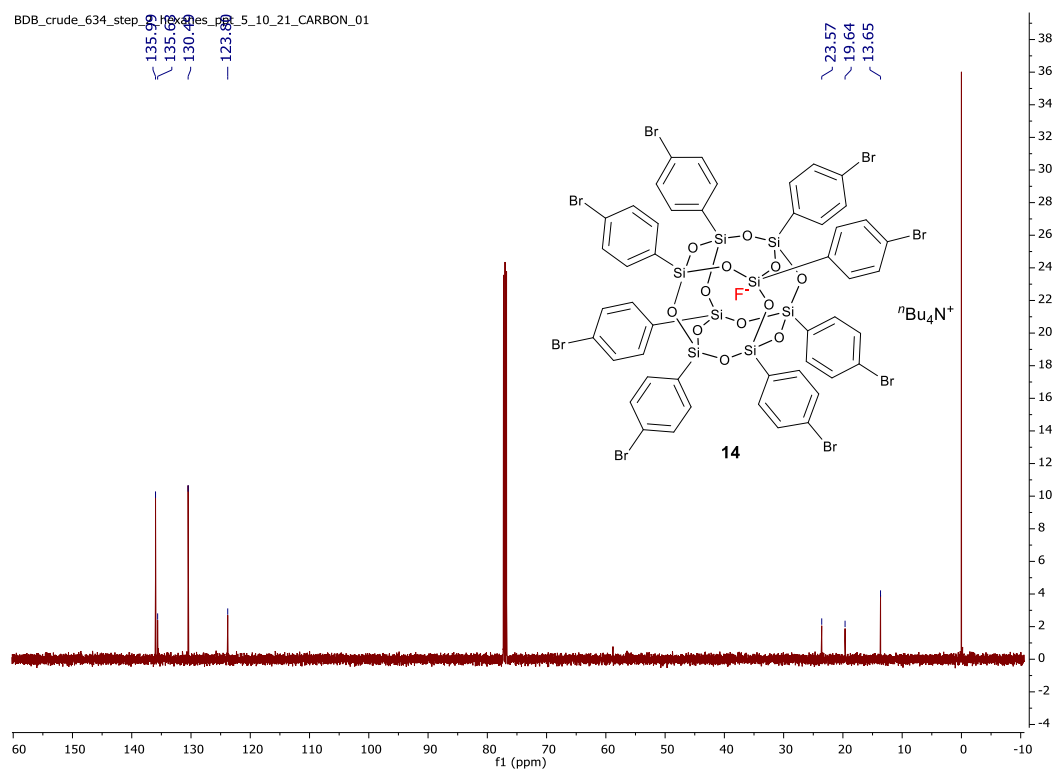


Figure 5-27: ^{13}C NMR of **14** (CDCl₃ + 1%TMS, 500 MHz)

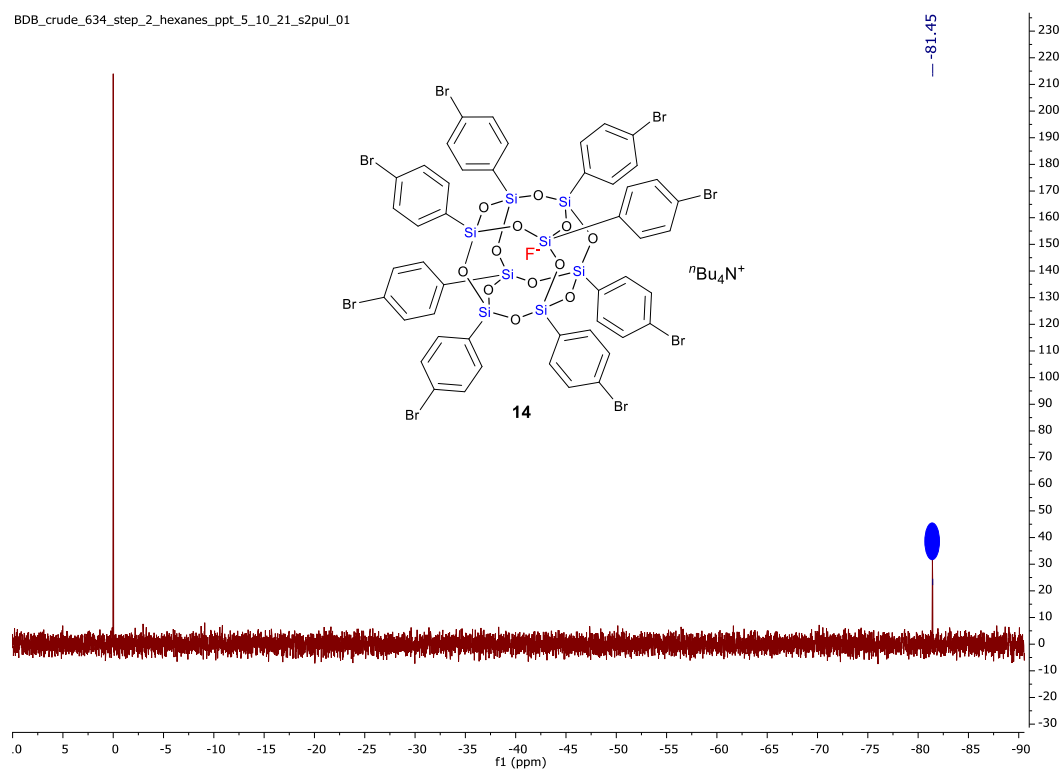


Figure 5-28: ^{29}Si NMR of **14** (CDCl_3 + 1%TMS, 99 MHz)

Table 5-1: Crystal and Experimental Data for 9,19-dimethyl-1,3,5,7,11,13,15,17-octaphenyl-9,19-bis(4-vinylphenyl)-2,4,6,8,10,12,14,16,18,20,21,22,23,24-tetradeca-oxa-1,3,5,7,9,11,13,15,17,19-decasilapentacyclo[11.7.1.13,11.15,17.17,15]tetracosane (**4**)

Compound	9,19-dimethyl-1,3,5,7,11,13,15,17-octaphenyl-9,19-bis(4-vinylphenyl)-2,4,6,8,10,12,14,16,18,20,21,22,23,24-tetradeca-oxa-1,3,5,7,9,11,13,15,17,19-decasilapentacyclo[11.7.1.13,11.15,17.17,15]tetracosane (4)	Compound	9,19-dimethyl-1,3,5,7,11,13,15,17-octaphenyl-9,19-bis(4-vinylphenyl)-2,4,6,8,10,12,14,16,18,20,21,22,23,24-tetradeca-oxa-1,3,5,7,9,11,13,15,17,19-decasilapentacyclo[11.7.1.13,11.15,17.17,15]tetracosane (4)
Formula	C ₆₆ H ₆₀ O ₁₄ Si ₁₀	Z	4
CCDC	1917847	Z'	0.5
$D_{calc}/\text{g cm}^{-3}$	1.334	Wavelength/Å	0.710730
μ/mm^{-1}	0.257	Radiation type	Mo K α
Formula Weight	1358.04	$\theta_{min}/^\circ$	1.541
Colour	colourless	$\theta_{max}/^\circ$	26.068
Shape	block	Measured Refl's.	57273
Size/mm ³	0.15×0.15×0.08	Indep't Refl's	6699
T/K	173(2)	Refl's with I >	3832
Crystal System	monoclinic	R _{int}	0.0777
Space Group	C2/c	Parameters	416
a/Å	20.926(2)	Restraints	1
b/Å	17.074(2)	Largest Peak	0.457
c/Å	18.972(2)	Deepest Hole	-0.244
$\alpha/^\circ$	90	GooF	1.046
$\beta/^\circ$	93.806(2)	wR_2 (all data)	0.2246
$\gamma/^\circ$	90	wR_2	0.1875
V/Å ³	6764.0(14)	R_1 (all data)	0.1154
		R_1	0.0701

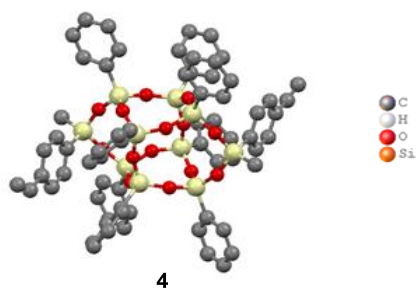
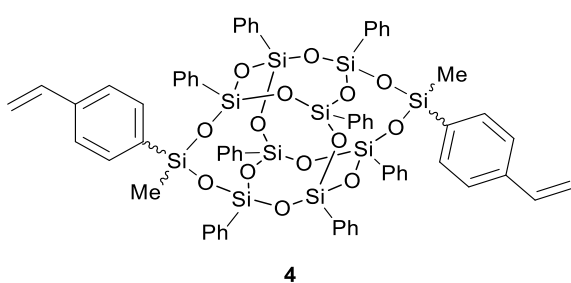


Figure 5-29: Crystal Structure of **4**

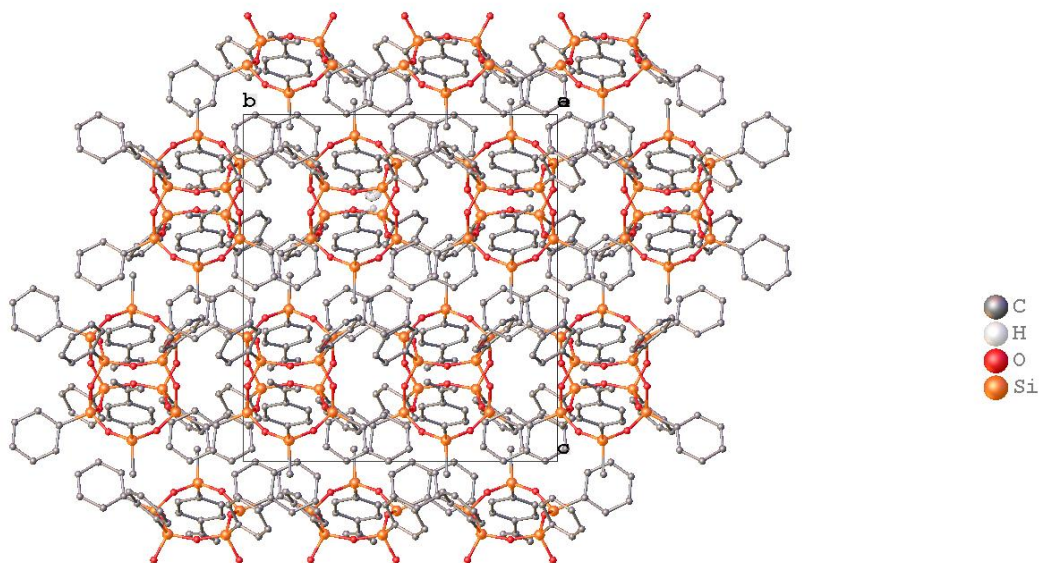


Figure 5-30: Packing diagram of 9,19-dimethyl-1,3,5,7,11,13,15,17-octaphenyl-9,19-bis(4-vinylphenyl)-2,4,6,8,10,12,14,16,18,20,21,22,23,24-tetradeca-oxa-1,3,5,7,9,11,13,15,17,19-decasilapentacyclo[11.7.1.13,11.15,17.17,15]tetracosane (**4**) (Displacement ellipsoid contour probability drawn at 50%)

The value of Z' is 0.5. This means that only half of the formula unit is present in the asymmetric unit, with the other half consisting of symmetry equivalent atoms.

CCDC 1917847 contains the supplementary crystallographic data for **4**. The data can be obtained free of charge from The Cambridge Crystallographic Data Centre via www.ccdc.cam.ac.uk/structures.

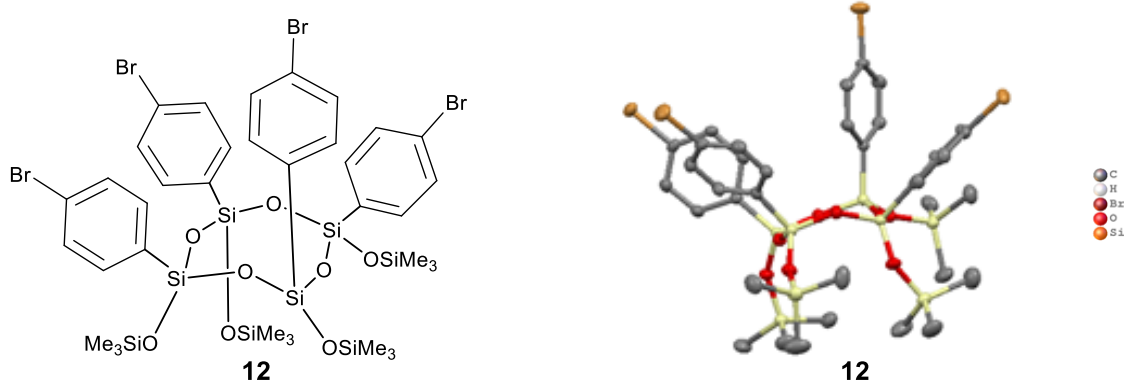


Figure 5-31: Crystal Structure of 12

Table 5-2: Crystal and Experimental Data for 2,4,6,8-tetrakis(4-bromophenyl)-2,4,6,8-tetrakis(trimethylsilyloxy)-1,3,5,7,2,4,6,8-tetraoxatetrasilocane⁶⁵⁻⁶⁷

Compound	2,4,6,8-tetrakis(4-bromophenyl)-2,4,6,8-tetrakis(trimethylsilyloxy)-1,3,5,7,2,4,6,8-tetraoxatetrasilocane	Compound	2,4,6,8-tetrakis(4-bromophenyl)-2,4,6,8-tetrakis(trimethylsilyloxy)-1,3,5,7,2,4,6,8-tetraoxatetrasilocane
Formula	C ₃₆ H ₅₂ Br ₄ O ₈ Si ₈	Z	4
CCDC	2051116	Z'	1
D_{calc} /g cm ⁻³	1.501	Wavelength/Å	0.71073
μ /mm ⁻¹	3.374	Radiation type	Mo K α
Formula Weight	1157.13	$\theta_{min}/^\circ$	2.075
Colour	colourless	$\theta_{max}/^\circ$	31.008
Shape	block	Measured Refl's.	52991
Size/mm ³	0.34×0.23×0.15	Indep't Refl's	13005
T/K	100.00(10)	Refl's $I \geq 2 \sigma(I)$	10246
Crystal System	monoclinic	R _{int}	0.0352
Space Group	P21/c	Parameters	517
a/Å	21.9089(4)	Restraints	0
b/Å	21.0688(4)	Largest Peak	0.726
c/Å	11.14916(18)	Deepest Hole	-0.645
$\alpha/^\circ$	90	GooF	1.020
$\beta/^\circ$	95.7991(16)	wR ₂ (all data)	0.0784
$\gamma/^\circ$	90	wR ₂	0.0735
V/Å ³	5120.04(16)	R ₁ (all data)	0.0527
		R ₁	0.0340

There is a single molecule in the asymmetric unit, which is represented by the reported sum formula. In other words: Z is 4 and Z' is 1.⁶⁵⁻⁶⁷

CCDC 2051116 contains the supplementary crystallographic data for this

structure. The data can be obtained free of charge from The Cambridge Crystallographic Data Centre via www.ccdc.cam.ac.uk/structures.

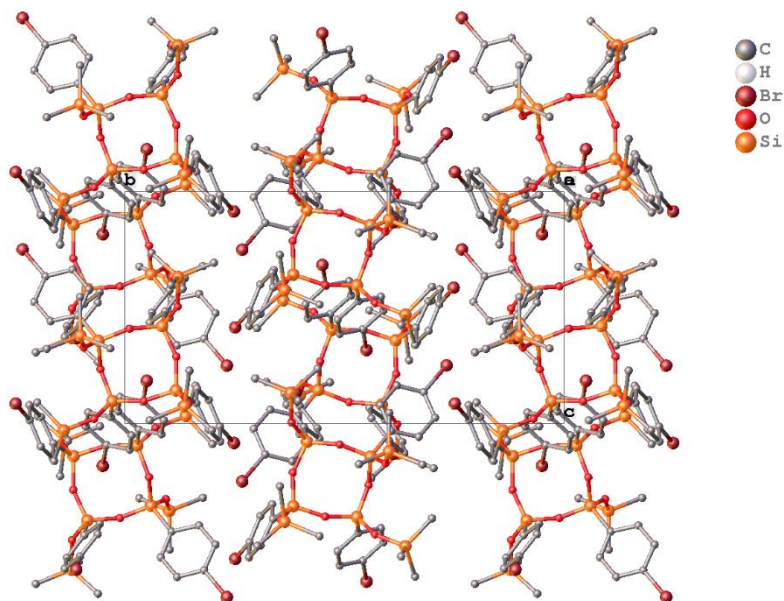


Figure 5-32: Packing diagram of 2,4,6,8-tetrakis(4-bromophenyl)-2,4,6,8-tetrakis((tri-methylsilyl)oxy)-1,3,5,7,2,4,6,8-tetraoxatetrasilocane

REFERENCES

REFERENCES

- (1) Pakjamsai, C.; Kawakami, Y. Tendency of Loop Formation of Oligosilsesquioxanes Obtained from (4-Substituted Phenyl) Trimethoxysilane Catalyzed by Benzyltrimethylammonium Hydroxide. *Polym. J.* **2004**, 36, 455–464.
- (2) Pakjamsai, C.; Kawakami, Y. Study on Effective Synthesis and Properties of Ortho-Alkyl-Substituted Phenyl Octasilsesquioxane. *Designed Monomers and Polymers*. **2005**, 423–435.
- (3) Morimoto, Y.; Watanabe, K.; Ootake, N.; Inagaki, J. I.; Yoshida, K.; Ohguma, K. Silsesquioxane Derivatives and Process for Production Thereof. US20040249103A1.
- (4) Li, Z.; Kawakami, Y. Formation of Incompletely Condensed Oligosilsesquioxanes by Hydrolysis of Completely Condensed POSS via Reshuffling. *Chem. Lett.* **2008**, 37, 804–805.
- (5) Lee, D. W.; Kawakami, Y. Incompletely Condensed Silsesquioxanes: Formation and Reactivity. *Polym. J.* **2007**, 39, 230–238.
- (6) Vogelsang, D. F.; Dannatt, J. E.; Schoen, B. W.; Maleczka, R. E.; Lee, A. Phase Behavior of cis–trans Mixtures of Double-Decker Shaped Silsesquioxanes for Processability Enhancement. *ACS Appl. Nano Mater.* **2019**, 1223–1231.
- (7) Liu, Y.; Takeda, N.; Ouali, A.; Unno, M. Synthesis, Characterization, and Functionalization of Tetrafunctional Double-Decker Siloxanes. *Inorg. Chem.* **2019**, 58, 4093–4098.
- (8) Wei, K.; Wang, L.; Li, L.; Zheng, S. Synthesis and Characterization of Bead-like poly(N-Isopropylacrylamide) Copolymers with Double Decker Silsesquioxane in the Main Chains. *Polym. Chem.* **2015**, 256–269.
- (9) Žak, P.; Delaude, L.; Dudziec, B.; Marciniec, B. N-Heterocyclic Carbene-Based Ruthenium-Hydride Catalysts for the Synthesis of Unsymmetrically Functionalized Double-Decker Silsesquioxanes. *Chem. Commun.* **2018**, 54, 4306–4309.
- (10) Vogelsang, D. F.; Dannatt, J. E.; Maleczka, R. E.; Lee, A. Separation of Asymmetrically Capped Double-Decker Silsesquioxanes Mixtures. *Polyhedron* **2018**, 155, 189–193.
- (11) Barry, B.-D.; Dannatt, J. E.; King, A. K.; Lee, A.; Maleczka, R. E., Jr. A General Diversity Oriented Synthesis of Asymmetric Double-Decker Shaped Silsesquioxanes. *Chem. Commun.* **2019**, 55, 8623–8626.

- (12) Pakjamsai, C.; Kawakami, Y. Tendency of Loop Formation of Oligosilsesquioxanes Obtained from (4-Substituted Phenyl)trimethoxysilane Catalyzed by Benzyltrimethylammonium Hydroxide in Benzene. *Polym. J.* **2004**, 36, 455–464.
- (13) Bassindale, A. R.; Liu, Z.; MacKinnon, I. A.; Taylor, P. G.; Yang, Y.; Light, M. E.; Horton, P. N.; Hursthouse, M. B. A Higher Yielding Route for T8 Silsesquioxane Cages and X-Ray Crystal Structures of Some Novel Spherosilicates. *Dalton Trans.* **2003**, 2945–2949.
- (14) Taylor, P. G.; Bassindale, A. R.; El Aziz, Y.; Pourny, M.; Stevenson, R.; Hursthouse, M. B.; Coles, S. J. Further Studies of Fluoride Ion Entrapment in Octasilsesquioxane Cages; X-Ray Crystal Structure Studies and Factors That Affect Their Formation. *Dalton Trans.* **2012**, 2048–2059.
- (15) Bassindale, A. R.; Chen, H.; Liu, Z.; MacKinnon, I. A.; Parker, D. J.; Taylor, P. G.; Yang, Y.; Light, M. E.; Horton, P. N.; Hursthouse, M. B. A Higher Yielding Route to Octasilsesquioxane Cages Using Tetrabutylammonium Fluoride, Part 2: Further Synthetic Advances, Mechanistic Investigations and X-Ray Crystal Structure Studies into the Factors That Determine Cage Geometry in the Solid State. *J. Organomet. Chem.* **2004**, 689, 3287–3300.
- (16) Aziz, Y. E.; El Aziz, Y.; Bassindale, A. R.; Taylor, P. G.; Horton, P. N.; Stephenson, R. A.; Hursthouse, M. B. Facile Synthesis of Novel Functionalized Silsesquioxane Nanostructures Containing an Encapsulated Fluoride Anion. *Organometallics* **2012**, 31, 6032–6040.
- (17) Kawakami, Y.; Yamaguchi, K.; Yokozawa, T.; Serizawa, T.; Hasegawa, M.; Kabe, Y. Higher Polyhedral Silsesquioxane (POSS) Cage by Amine-Catalyzed Condensation of Silanols and Related Siloxanes. *Chem. Lett.* **2007**, 36, 792–793.
- (18) Tateyama, S.; Kakihana, Y.; Kawakami, Y. Cage Octaphenylsilsesquioxane from Cyclic Tetrasiloxanetetraol and Its Sodium Salt. *J. Organomet. Chem.* **2010**, 695, 898–902.
- (19) Lichtenhan, J. D.; Vu, N. Q.; Carter, J. A. *Macromol.*, 1993, 26, 2141; Lichtenhan, J. D.; Gilman, J. W.; Ismail, I. M. K.; Burmeister, M. *J. Chem. Mater* **1996**, 8, 1250.
- (20) Ervithayasuporn, V.; Wang, X.; Kawakami, Y. Synthesis and Characterization of Highly Pure Azido-Functionalized Polyhedral Oligomeric Silsesquioxanes (POSS). *Chem. Commun.* **2009**, 34, 5130–5132.
- (21) Feher, F. J. Polyhedral Oligometallasilsesquioxanes (POMSS) as Models for Silica-Supported Transition-Metal Catalysts. Synthesis and Characterization of $(\text{C}_5\text{Me}_5)\text{Zr}[(\text{Si}_7\text{O}_{12})(\text{c-C}_6\text{H}_{11})_7]$. *J. Am. Chem. Soc.* **1986**, 108, 3850–3852.
- (22) Haddad, T. S.; Lichtenhan, J. The Incorporation of Transition Metals into Polyhedral Oligosilsesquioxane Polymers. *J. Inorg. Organomet. Polym.* **1995**, 5, 237–246.

- (23) Mantz, R. A.; Jones, P. F.; Chaffee, K. P.; Lichtenhan, J. D.; Gilman, J. W.; Ismail, I. M. K.; Burmeister, M. J. Thermolysis of Polyhedral Oligomeric Silsesquioxane (POSS) Macromers and POSS–Siloxane Copolymers. *Chem. Mater.* **1996**, 1250–1259.
- (24) Sellinger, A.; Laine, R. M. Silsesquioxanes as Synthetic Platforms. 3. Photocurable, Liquid Epoxides as Inorganic/Organic Hybrid Precursors. *Chem. Mater.* **1996**, 8, 1592–1593.
- (25) Laine, R. M.; Zhang, C.; Sellinger, A.; Viculis, L. Polyfunctional Cubic Silsesquioxanes as Building Blocks for Organic/inorganic Hybrids. *Appl. Organomet. Chem.* **1998**, 12, 715–723.
- (26) Zheng, L.; Waddon, A. J.; Farris, R. J.; Coughlin, E. B. X-Ray Characterizations of Polyethylene Polyhedral Oligomeric Silsesquioxane Copolymers. *Macromolecules* **2002**, 35, 2375–2379.
- (27) Waddon, A. J.; Zheng, L.; Farris, R. J.; Coughlin, E. B. Nanostructured Polyethylene-POSS Copolymers: Control of Crystallization and Aggregation. *Nano Lett.* **2002**, 2, 1149–1155.
- (28) Wright, M. E.; Schorzman, D. A.; Feher, F. J.; Jin, R.-Z. Synthesis and Thermal Curing of Aryl-Ethynyl-Terminated coPOSS Imide Oligomers: New Inorganic/Organic Hybrid Resins. *Chem. Mater.* **2003**, 15, 264–268.
- (29) Iacono, S. T.; Vij, A.; Grabow, W.; Smith, D. W., Jr; Mabry, J. M. Facile Synthesis of Hydrophobic Fluoroalkyl Functionalized Silsesquioxane Nanostructures. *Chem. Commun.* **2007**, 47, 4992–4994.
- (30) Laine, R. M.; Roll, M.; Asuncion, M.; Sulaiman, S.; Popova, V.; Bartz, D.; Krug, D. J.; Mutin, P. H. Perfect and Nearly Perfect Silsesquioxane (SQs) Nanoconstruction Sites and Janus SQs. *J. Sol-Gel Sci. Technol.* **2008**, 46, 335–347.
- (31) Wahab, M. A.; Mya, K. Y.; He, C. Synthesis, Morphology, and Properties of Hydroxyl Terminated-POSS/polyimide Low-Knanocomposite Films. *J. Polym. Sci. A Polym. Chem.* **2008**, 46, 5887–5896.
- (32) Korchkov, V. P.; Martynova, T. N.; Belyi, V. I. Low Temperature Dielectric Films from Octavinylsilsesquioxane. *Thin Solid Films.* **1983**, 373–376.
- (33) Blomgren, E.; O'M. Bockris, J.; Jesch, C. The adsorption of butyl, phenyl and naphthyl compounds at the interface mercury—aqueous acid solution. *J. Phys. Chem.* **1961**, 65, 2000–2010.
- (34) Choi, J.; Kim, S. G.; Laine, R. M. Organic/Inorganic Hybrid Epoxy Nanocomposites from Aminophenylsilsesquioxanes. *Macromolecules* **2004**, 37, 99–109.
- (35) Choi, J.; Tamaki, R.; Kim, S. G.; Laine, R. M. Organic/Inorganic Imide Nanocomposites from Aminophenylsilsesquioxanes. *Chem. Mater.* **2003**, 15, 3365–3375.

- (36) Nagendiran, S.; Alagar, M.; Hamerton, I. Octasilsesquioxane-Reinforced DGEBA and TGDDM Epoxy Nanocomposites: Characterization of Thermal, Dielectric and Morphological Properties. *Acta Mater.* **2010**, *58*, 3345–3356.
- (37) Asuncion, M. Z.; Laine, R. M. Silsesquioxane Barrier Materials. *Macromolecules* **2007**, *40*, 555–562.
- (38) Itami, Y.; Marciniak, B.; Kubicki, M. Functionalization of Octavinylsilsesquioxane by Ruthenium-Catalyzed Silylative Coupling versus Cross-Metathesis. *Chemistry - A European J.* **2004**, 1239–1248.
- (39) Itami, Y.; Marciniak, B.; Majchrzak, M.; Kubicki, M. Novel Organosilicon Starburst Compounds Based on Ruthenium-Catalyzed Silylative Coupling Reactions of 1,3,5-Tris(dimethylvinylsilyl)benzene. *Organometallics* **2003**, 1835–1842.
- (40) Marciniak, B.; Pietraszuk, C. Silylation of Styrene with Vinylsilanes Catalyzed by $\text{RuCl}(\text{SiR}_3)(\text{CO})(\text{PPh}_3)_2$ and $\text{RuHCl}(\text{CO})(\text{PPh}_3)_3$. *Organometallics*. **1997**, 4320–4326.
- (41) Liu, Z.; Ma, S.; Chen, L.; Xu, J.; Ou, J.; Ye, M. Porous Styryl-Linked Polyhedral Oligomeric Silsesquioxane (POSS) Polymers Used as a Support for Platinum Catalysts. *Mater. Chem. Front.* **2019**, *3*, 851–859.
- (42) Cheng, G.; Vautravers, N. R.; Morris, R. E.; Cole-Hamilton, D. J. Synthesis of Functional Cubes from Octavinylsilsesquioxane (OVS). *Org. Biomol. Chem.* **2008**, 4662–4667.
- (43) Liu, N.; Wei, K.; Wang, L.; Zheng, S. Organic–inorganic Polyimides with Double Decker Silsesquioxane in the Main Chains. *Polym. Chem.* **2016**, *7*, 1158–1167.
- (44) Jung, J. H.; Furgal, J. C.; Goodson, T.; Mizumo, T.; Schwartz, M.; Chou, K.; Vonet, J.-F.; Laine, R. M. 3-D Molecular Mixtures of Catalytically Functionalized $[\text{vinylSiO}_{1.5}]_{10}/[\text{vinylSiO}_{1.5}]_{12}$. Photophysical Characterization of Second Generation Derivatives. *Chem. Mater.* **2012**, 1883–1895.
- (45) Ronchi, M.; Sulaiman, S.; Boston, N. R.; Laine, R. M. Fluoride Catalyzed Rearrangements of Polysilsesquioxanes, Mixed Me, Vinyl T₈, Me, Vinyl T₁₀ and T₁₂ Cages. *Appl. Organomet. Chem.* **2009**, *24*, 551–557.
- (46) Żak, P.; Dudziec, B.; Kubicki, M.; Marciniak, B. Silylative Coupling versus Metathesis-Efficient Methods for the Synthesis of Difunctionalized Double-Decker Silsesquioxane Derivatives. *Chem. Eur. J.* **2014**, *20*, 9387–9393.
- (47) Laird, M.; Van der Lee, A.; Dumitrescu, D. G.; Carcel, C.; Ouali, A.; Bartlett, J. R.; Unno, M.; Man, M. W. C. Styryl-Functionalized Cage Silsesquioxanes as Nanoblocks for 3-D Assembly. *Organometallics* **2020**, *39*, 1896–1906.

- (48) Haddad, T. S.; Lichtenhan, J. D. Hybrid Organic–Inorganic Thermoplastics: Styryl-Based Polyhedral Oligomeric Silsesquioxane Polymers. *Macromolecules* **1996**, *29*, 7302–7304.
- (49) Araki, H.; Naka, K. Syntheses and Properties of Dumbbell-Shaped POSS Derivatives Linked by Luminescent π -Conjugated Units. *J. Polym. Sci. Part A: Polym. Chem.* **2012**, *50*, 4170–4181.
- (50) Laird, M.; Totée, C.; Gaveau, P.; Silly, G.; Van der Lee, A.; Carcel, C.; Unno, M.; Bartlett, J. R.; Man, M. W. C. Functionalised Polyhedral Oligomeric Silsesquioxane with Encapsulated Fluoride – First Observation of Fluxional Si...F Interactions in POSS. *Dalton Trans.* **2021**, *50*, 81–89.
- (51) Syroeshkin, M.; Wang, Y.; Dieng, M.; Gul'tyai, V.; Jouikov, V. Octaorgano Silsesquioxanes with Encapsulated Fluoride Anion, TBA(F-@T₈), as a New Class of Non-Coordinating Non-Nucleophilic Supporting Electrolytes. *ECS Trans.* **2013**, *29*–38.
- (52) Quadrelli, E. A.; Basset, J.-M. On Silsesquioxanes' Accuracy as Molecular Models for Silica-Grafted Complexes in Heterogeneous Catalysis. *Coord. Chem. Rev.* **2010**, *254*, 707–728.
- (53) Bivona, L. A.; Giacalone, F.; Carbonell, E.; Gruttadauria, M.; Aprile, C. Proximity Effect Using a Nanocage Structure: Polyhedral Oligomeric Silsesquioxane-Imidazolium Tetrachloro- Palladate Salt as a Precatalyst for the Suzuki-Miyaura Reaction in Water. *ChemCatChem*. **2016**, *8*, 1685–1691.
- (54) Prigyai, N.; Chanmungkalakul, S.; Ervithayasuporn, V.; Yodsin, N.; Jungsuttiwong, S.; Takeda, N.; Unno, M.; Boonmak, J.; Kiatkamjornwong, S. Lithium-Templated Formation of Polyhedral Oligomeric Silsesquioxanes (POSS). *Inorg. Chem.* **2019**, *58*, 15110–15117.
- (55) Williams, E.; Sellinger, A.; Pardo, D.; Tamaki, R.; Laine, R. M.; Ueno, K.; Tanabe, H.; Jabbour, G. E. Organic Light-Emitting Devices Based on Organic-Inorganic Hole Transport Material Having Nanobuilding Blocks of Octavinylsilsesquioxane. *Front. Optics* **2003**.
- (56) Kalia, S.; Pielichowski, K. Polymer/POSS Nanocomposites and Hybrid Materials: Preparation, Properties, Applications; *Springer*, **2018**.
- (57) Zhang, C.; Babonneau, F.; Bonhomme, C.; Laine, R. M.; Soles, C. L.; Hristov, H. A.; Yee, A. F. Highly Porous Polyhedral Silsesquioxane Polymers. Synthesis and Characterization. *J. Am. Chem. Soc.* **1998**, *120*, 8380–8391.
- (58) Laird, M.; Yokoyama, J.; Carcel, C.; Unno, M.; Bartlett, J. R.; Wong Chi Man, M. Sol–gel Processing of Polyhedral Oligomeric Silsesquioxanes: Nanohybrid Materials Incorporating T₈ and T₁₀ Cages. *J. Sol-Gel Sci. Technol.* **2020**, *95*, 760–770.

- (59) Bassindale, A. R.; Pourny, M.; Taylor, P. G.; Hursthouse, M. B.; Light, M. E. Fluoride-Ion Encapsulation within a Silsesquioxane Cage. *Angew. Chem.* **2003**, *115*, 3612–3614.
- (60) Brick, C. M.; Tamaki, R.; Kim, S.-G.; Asuncion, M. Z.; Roll, M.; Nemoto, T.; Ouchi, Y.; Chujo, Y.; Laine, R. M. Spherical, Polyfunctional Molecules Using Poly(bromophenylsilsesquioxane)s as Nanoconstruction Sites. *Macromolecules* **2005**, *38*, 4655–4660.
- (61) Roll, M. F.; Mathur, P.; Takahashi, K.; Kampf, J. W.; Laine, R. M. [PhSiO_{1.5}]₈ Promotes Self-Bromination to Produce [o-BrPhSiO_{1.5}]₈: Further Bromination Gives Crystalline [2,5-Br₂PhSiO_{1.5}]₈ with a Density of 2.32 G cm⁻³ and a Calculated Refractive Index of 1.7 or the Tetraicosa Bromo Compound [Br₃PhSiO_{1.5}]₈. *J. Mater. Chem.* **2011**, *21*, 11167–11176.
- (62) Ronchi, M.; Pizzotti, M.; Orbelli Biroli, A.; Macchi, P.; Lucenti, E.; Zucchi, C. Synthesis and Structural Characterization of Functionalized Cyclotetrasiloxane Rings [4-RC₆H₄Si(O)OR']₄ (R=Cl, Br, CHCH₂, CH₂Cl; R'=Na, SiMe₃) as Scaffolds for the Synthesis of Models of a Silica Bound Monolayer of Fluorescent or Second Order NLO Active Organic Chromophores. *J. Organomet. Chem.* **2007**, *692*, 1788–1798.
- (63) Pozdniakova, Y. A.; Lyssenko, K. A.; Korlyukov, A. A.; Blagodatskikh, I. V.; Auner, N.; Katsoulis, D.; Shchegolikhina, O. I. Alkali-Metal-Directed Hydrolytic Condensation of Trifunctional Phenylalkoxysilanes. *Eur. J. Inorg. Chem.* **2004**, 1253–1261.
- (64) Brown, J. F. The Polycondensation of Phenylsilanetriol. *J. Am. Chem. Soc.* **1965**, *87*, 4317–4324.
- (65) Dolomanov, O. V.; Bourhis, L. J.; Gildea, R. J.; Howard, J. A. K.; Puschmann, H. Olex2: A complete structure solution, refinement and analysis program, *J. Appl. Cryst.* **2009**, *42*, 339–341.
- (66) Sheldrick, G.M., A short history of ShelX, *Acta Cryst.* **2008**, *A64*, 339–341.
- (67) Sheldrick, G.M., Crystal structure refinement with ShelXL, *Acta Cryst.* **2015**, *71*, 3–8.

CHAPTER 6: Conclusions and Future Direction

6.1 Conclusions

This dissertation profiles several intriguing findings on the exploration of procedures for the synthesis of novel functionalized cage like silsesquioxanes. Thus, following recommendations from our group on previous studies, this research work recorded the following feats:

- Use of a protecting group approach that afforded asymmetrically functionalized double-decker shaped silsesquioxanes in good yields. In this strategy, we employed a bidentate boronic acid that benignly and selectively masked the silanol groups of the $\text{DDSQ}(\text{OH})_4$ providing a model for the functionalization with different chlorosilanes. Unlike other protecting groups which are generally challenging on deprotection, pinacol chemoselectively demasked the boronic acid without compromising the cage architecture.
- A protocol, which in close relation to the above, outlines an approach toward the synthesis of asymmetric monosilylated DDSQ disilanol $[\text{R}^1\text{R}^2\text{SiDDSQ}(\text{OH})_2]$. Such partially functionalized DDSQs are ideal molecular templates for the effective synthesis of condensed asymmetric D_2T_8 siloxanes, various metallasilsesquioxanes and for modification of solid supports. An illustration of its synthetic utility for the synthesis of the D_2T_8 siloxane is herein disclosed.
- Demonstration of the base promoted hydrolysis of cubic dodecaphenylsilsesquioxane ($\text{Ph}_{12}\text{T}_{12}$) for the synthesis of the more desirable and highly symmetrical 'double-decker' shaped silsesquioxane. Whereas other research groups have recorded the synthesis of higher cage frameworks starting from lower

cage Silsesquioxanes, this work serves as the first report of the conversion of dead-end $\text{Ph}_{12}\text{T}_{12}$ into the partially condensed double-decker shaped silsesquioxane tetraol $[\text{DDSQ}(\text{OH})_4]$.

- Progress on the synthesis of novel ‘double-decker’ shaped Silsesquioxanes bearing transformable silicon coronal groups. In this work, efforts were directed to cages with styryl or bromophenyl groups that could provide avenues for multifunctionalization on the sides and surfaces.

6.2 Future Directions

Our desire to explore strategies for the synthesis and modifications of siloxanes keeps growing as some realizations are met. Thus, the recommendations made herein are in no way exhaustive but based on our materials’ development drive, the achievements and challenges faced during this study. Even though a considerable progress is recorded, the following proposals are thought-provoking:

- Exploration of an atom-economic and non-protecting group route for the synthesis of asymmetrically functionalized D_2T_8 ‘double-decker’ shaped silsesquioxanes. Based on preliminary results from our investigations, the use of solvents in which the $\text{DDSQ}(\text{OH})_4$ has very poor solubility seems promising.
- Applications of the asymmetrically functionalized DDSQs as nano-linkers to two different block copolymers. Studies of the property enhancement relative to symmetric POSS/polymer composites should also be explored.
- Use of the asymmetric $\text{R}^1\text{R}^2\text{SiDDSQ}(\text{OH})_2$ as precursors in nanomedicine, catalysis and for the modification of solid supports should be given due considerations.

- Surface modification of the phenyl groups in pre-synthesized condensed D₂T₈ POSS will result to a molecular design with pendants that are ideal for the formation of 3D networks.
- Venture towards the applications of C-H borylation chemistry to functionalize the cage phenyl groups on the commercially available cubic cages or the tetrasilanolPOSS or condensed functionalized DDSQs to generate compounds that are susceptible to a variety of transformations that could result to a host of previously unexplored cages.
- Exploration of routes for the synthesis of 'double-decker shaped Silsesquioxanes that are based on other coranae order than phenyl. This area, being so nascent can be approached from either the trichloro/alkoxysilane or backward, from the selective fissure of two Si-O-Si linkages.